![EPA United States Environmental Protection Agency logo]

Characterization of Emissions from Commercial Aircraft Engines during the Aircraft Particle Emissions eXperiment (APEX) 1 to 3

Characterization of Emissions from Commercial Aircraft Engines during the Aircraft Particle Emissions eXperiment (APEX) 1 to 3

John S. Kinsey, QEP

Principal Investigator

Office of Research and Development

National Risk Management Research Laboratory

Research Triangle Park, NC 27711

EPA Review Notice

Foreword

The U.S. Environmental Protection Agency (EPA) is charged by Congress with protecting the Nation's land, air, and water resources. Under a mandate of national environmental laws, the Agency strives to formulate and implement actions leading to a compatible balance between human activities and the ability of natural systems to support and nurture life. To meet this mandate, EPA's research program is providing data and technical support for solving environmental problems today and building a science knowledge base necessary to manage our ecological resources wisely, understand how pollutants affect our health, and prevent or reduce environmental risks in the future.

The National Risk Management Research Laboratory (NRMRL) is the agency's center for investigation of technological and management approaches for preventing and reducing risks from pollution that threaten human health and the environment. The focus of the laboratory's research program is on methods and their cost-effectiveness for prevention and control of pollution to air, land, water, and subsurface resources; protection of water quality in public water systems; remediation of contaminated sites, sediments and ground water; prevention and control of indoor air pollution; and restoration of ecosystems. NRMRL collaborates with both public and private sector partners to foster technologies that reduce the cost of compliance and to anticipate emerging problems. NRMRL's research provides solutions to environmental problems by: developing and promoting technologies that protect and improve the environment; advancing scientific and engineering information to support regulatory and policy decisions; and providing the technical support and information transfer to ensure implementation of environmental regulations and strategies at the national, state, and community levels.

This publication has been produced as part of the laboratory's strategic long-term research plan. It is published and made available by EPA's Office of Research and Development to assist the user community and to link researchers with their clients.

Sally Gutierrez, Director
National Risk Management Research Laboratory

Acknowledgements

Table of Contents

List of Appendices

Appendix A   Description of the Dilution Sampling System (DSS)
Appendix B   Target Analytes and Detection Limits for SUMMA Canister Samples
Appendix C   Target Carbonyl Compounds and Detection Limits for DNPH-Impregnated Silica Gel Cartridge Samples
Appendix D   Tables for Section 8 - Particulate Matter Mass Emissions
Appendix E   Tables for Section 9 - PM Number Emissions
Appendix F   Tables for Section 10 - Particle Size Distribution and Geometric Mean Diameter
Appendix G   Tables for Section 11 - Black Carbon and PAH Emissions
Appendix H   Tables for Section 13 - Particle-Phase Chemical Composition

List of Figures

xi

List of Tables

List of Acronyms, Initializations, and Abbreviations

40CFR	Title 40 of the Code of Federal Regulations
acfm	actual ft^3/min
AEC	Aircraft Emissions Characterization
AEDC	U.S. Air Force's Arnold Engineering Development Center
AIM	Aerosol Instrument Manager
APEX	Aircraft Particle Emissions eXperiment
ARCADIS	ARCADIS U.S., Inc.
ARI	Aerodyne Research, Inc.
B&K	Brüel and Kjær
BC	black carbon
CD	compact disc
CFMI	CFM International
C/O	climb-out
CO	carbon monoxide
CO$_2$	carbon dioxide
CPC	condensation particle counter
CPU	central processing unit
DAS	data acquisition system
DEAL	Diesel Emissions Aerosol Laboratory
DFRC	Dryden Flight Research Center
DI	deionized
DMA	differential mobility analyzer
DNPH	2,4-dinitrophenylhydrazine
DQI	data quality indicator
DSS	dilution sampling system
EC	elemental carbon
EEPS	engine exhaust particle sizer
EI	emission index
EI$_M$	PM-2.5 mass emission index
EI$_N$	PM-2.5 number emission index

ELPI	electrical low pressure impactor
EPA	U.S. Environmental Protection Agency
EPC	electronically programmable control
ERG	Eastern Research Group
ESP	electrostatic precipitator
FAA	Federal Aviation Administration
FID	flame ionization detector
FPCL	Fine Particle Characterization Laboratory
GC/MS	gas chromatography/mass spectrometry
GMD	geometric mean diameter
GRE	ground run-up enclosure
GSD	geometric standard deviation
GVW	gross vehicle weight
H_2O	water
HAP	hazardous air pollutant
HEPA	High-Efficiency Particulate Air
Hg	mercury
HP	Hewlett-Packard
HPLC	high performance liquid chromatography
I/O	input/output
IC	ion chromatography
ICAO	International Civil Aviation Organization
ID	inside diameter
IR	infrared
KVM	keyboard-video-monitor
LTO	landing and take-off
MDL	method detection limit
MFC	mass flow controllers
MnO_2	manganese dioxide
MOP(s)	miscellaneous operating procedure(s)
MSD	mass selective detection
NAAQS	National Ambient Air Quality Standard

NaCl	sodium chloride
NASA	National Aeronautics and Space Administration
NERL	National Exposure Research Laboratory
NIOSH	National Institute for Occupational Safety and Health
NIST	National Institute of Standards and Technology
NMOC	nonmethane organic compound
NMVOC	nonmethane volatile organic compound
NO_X	nitrogen oxides
NRMRL	National Risk Management Research Laboratory
OC	organic carbon
OD	outside diameter
OTAQ	Office of Transportation and Air Quality
PA	photoacoustic analyzer
PAH	polycyclic aromatic hydrocarbon
PAS	photoelectric aerosol sensor
PM	particulate matter
PM-2.5	particles ≤2.5 μm in aerodynamic diameter
PQL	practical quantitation limit
PSD	particle size distribution
PTV	programmable temperature vaporizing
PUF	polyurethane foam
QA	quality assurance
QAPP	quality assurance project plan
QC	quality control
QCM	quartz crystal microbalance
R^2	correlation coefficient
R&P	Rupprecht and Patashnick
RSD	relative standard deviation
RTP	Research Triangle Park
SAE	Society of Automotive Engineers
SD	standard deviation
SIP	State Implementation Plan

SM	smoke number
SMPS	scanning mobility particle sizer
SN	smoke number
SNMOC	speciated non-methane organic compound
SOP	standard operating procedure
SUMMA	SUMMA-polished stainless steel canisters
SVOC(s)	semi-volatile organic compound(s)
T/O	take-off
TCD	thermal conductivity detector
TD	thermal desorption
TEOM	tapered element oscillating microbalance
THC	total hydrocarbons
TWA	time-weighted average
UMR	Missouri University of Science and Technology Center of Excellence
UPS	uninterruptible power supply
UV	ultraviolet
VOC	volatile organic compound
XRF	x-ray fluorescence

This page intentionally left blank.

Executive Summary

The fine particulate matter (PM) emissions from aircraft operations at large airports located in areas of the U. S. designated as non-attainment for the National Ambient Air Quality Standard (NAAQS) for PM-2.5 (particles $\leq$2.5 µm in aerodynamic diameter) are of major environmental concern. In general, the majority of the available PM emissions data for commercial aircraft engines is limited and does not completely characterize volatile components resulting from atmospheric cooling and dilution. There is, therefore, the need for a comprehensive PM emissions database for aircraft turbine engines which includes mass-based emission factors and chemical speciation data, and which also relates the PM emissions to key engine operating parameters and fuel characteristics.

To address the need for improved aircraft PM emissions data, the Aircraft Particle Emissions eXperiment (APEX) was organized in 2003. The APEX program is a major collaborative effort between the National Aeronautics and Space Administration (NASA) and a number of other research organizations including the U.S. Environmental Protection Agency's (EPA's) National Risk Management Research Laboratory (NRMRL) in Research Triangle Park, North Carolina. The objectives of the three APEX sampling campaigns (APEX-1, -2, and -3) were to update and improve emission factors (indices) and chemical source profiles for aircraft-generated fine PM and, if possible, to assess the effect of fuel properties (e.g., sulfur content) and engine operating conditions (e.g., cold vs. warm) on PM formation.

During APEX-1, -2 and -3, ground level measurements were conducted by EPA in the engine exhaust plume, primarily at a single point located a distance of 30 m behind the engine exit. The system was configured as a beveled nozzle connected to a 5-cm outside diameter (OD) polished stainless steel sampling line that ran from the plume centerline to the inlet of EPA's Diesel Emissions Aerosol Laboratory (DEAL) instrumented sampling tunnel. Thoroughly cleaned stainless steel tubing and uncontaminated fittings were used for the entire system. The sampling probe was constructed from 5-cm diameter stainless steel tubing with a tapered inlet nozzle which was attached to a rigid stand anchored to the tarmac. The exact length and configuration of the sampling line running from the probe to the DEAL depended on the engine type and sampling campaign.

The DEAL uses two centrifugal blowers, each controlled by a variable frequency drive and mass flow meter, to continuously extract 1.1 (actual) m^3 min^{-1} of sample gas from the plume. After extraction, the plume sample flows through a 5-cm diameter stainless steel sampling tube into a PM-2.5 "cut point" (i.e., particle diameter representing a 50% collection efficiency for equivalent unit density spheres ≤2.5 µm in aerodynamic diameter) virtual impactor, and then into an 8.8-m long, 15-cm inside diameter (ID) stainless steel sampling tunnel. A series of "buttonhook" stack sampling nozzles, staggered in height inside the tunnel to minimize aerodynamic interference, is used to extract samples from the tunnel. The sample flow captured by each nozzle exits the sampling tunnel through custom designed four-way flow splitters that direct the flow from the tunnel to the various instruments. Either grounded stainless steel or conductive

silicone rubber lines connect the instruments to the appropriate sample splitter. A similar sampling system was also used for determination of the ambient background.

The DEAL was outfitted and configured to accommodate the sample collection and continuous monitoring requirements of the APEX monitoring plan. Both continuous monitoring and time-integrated sampling were conducted during the three APEX campaigns for both particle- and gas-phase air pollutants. Continuous monitoring was conducted for PM mass and number concentration, particle size distribution, black carbon, particle surface polycyclic aromatic hydrocarbons, carbon dioxide, carbon monoxide (APEX-1), total volatile organic compounds (APEX-1), plume temperature and velocity (APEX-2), and ambient wind speed/direction. Time-integrated sampling was also performed for PM mass concentration (Teflon filter), total volatile PM (i.e., Teflon filter sampling downstream of a thermal denuder), elemental/organic carbon, speciated semivolatile organic compounds, speciated water-soluble ions, elemental composition, gas-phase nonmethane volatile organic compounds, and gas-phase carbonyls.

Emission indices (factors) were calculated from the experimental data in terms of mass (or number) of pollutant per mass of fuel burned using a carbon balance involving the percent carbon in the fuel determined by fuel analysis and the concentration of carbon dioxide measured in the sample stream (note that CO and total hydrocarbons are generally insignificant compared to CO_2). The experimental data are always presented in terms of the engine fuel flow recorded during each test, but sometimes are shown relative to nominal percent rated thrust for ease of comparison between different engine types.

There was a total of 24 tests conducted during the three APEX campaigns. A CFM56-2C1 engine mounted on a DC-8 airframe was used throughout the nine APEX-1 tests to investigate the effects of fuel composition on emissions at various power settings. Three types of fuel were used: a base fuel (JP-8 or Jet-A1), a high-sulfur fuel (JP-8 doped with approximately four times the sulfur content of the base fuel), and a higher-aromatic JP-8.

During APEX-2 and -3, each engine was run with the available Jet-A fleet fuel it would use during normal commercial operations. The same engine family used during APEX-1, the CFM56 mounted on B737 airframes, was also included in all four APEX-2 tests and two of the eleven APEX-3 tests. These tests provided further characterization of the fine particulate emissions from these widely-used jet engines.

Five additional turbine engines of various sizes were also studied in APEX-3. These additional turbine engines included a General Electric CJ610-8ATJ turbojet (in use on a Lear Model 25), Rolls Royce AE3007A1E and AE3007A1P mixed turbofans (in use on the Embraer ERJ145), a Pratt and Whitney PW4158 turbofan (in use on the Airbus A300), and a Rolls Royce RB211-535E4-B mixed turbofan (in use on the B757).

In general, the test engines were operated at a series of steady-state power conditions which were set for the ambient conditions using the expertise of the on-site engine company representative. During APEX-1, two engine test matrices were used. The "EPA" test matrix followed the landing and take-off (LTO) cycle defined by the International Civil Aviation Organization (ICAO) to simulate aircraft emissions at an airport. This matrix consisted of approximately four repetitions of the following power settings: 26 min at idle (7% rated thrust), 0.7 min at takeoff (100%), 2.2 min at climb (85%), and 4 min at approach (30%). The "NASA" test matrix was designed to investigate the effects of engine operating parameters on particle emissions and included 11 power settings. Except for the 100 percent thrust level, where run-time was

limited to 1.5 min, approximately 10 min were provided at each power setting to allow for samples to be adequately analyzed.

For APEX-2 and -3, the engines were operated in cycles encompassing a series of steady state power settings to investigate the effects of these power settings on particle emissions. The power levels included those used during engine certification, simulated cruise, engine start/stop, and transitions between throttle settings. During these tests, the thrust was changed in a stepwise fashion from the lowest thrust level to highest under the "cold" engine condition, and then decreased in a similar fashion under the "warm" engine condition. The specific power conditions and fuel flow varied slightly by both campaign and engine type.

Based on the experimental data collected, the following conclusions were reached:

- The testing of aircraft turbine engine emissions is difficult, requiring long sampling lines with their associated high residence time and particle losses. Corrections were made for particle losses, but the impact of the long residence time has yet to be established.

- The PM mass emission index ranged from approximately 10 to 550 mg/kg of fuel burned, depending on engine and fuel type, operating power, and environmental conditions.

- For the turbofan engines tested, the relationship of EI_M (the PM-2.5 mass emission index expressed in particulate mass per kg of fuel burnt) to fuel flow (engine power) followed a characteristic U-shape with the emissions high at idle, dropping off to a minimum at mid-range power, and rising again at high engine thrust.

- The particle number emission indices observed in the program ranged from approximately $1(10)^{15}$ to $1(10)^{17}$ particles/kg of fuel burned, again depending on engine and fuel type, operating power, and environmental conditions.

- For most of the turbofan engines tested, a logarithmic relationship of EI_N (the PM-2.5 number emission index expressed in number of particles per kg of fuel burned) to fuel flow (engine power) was determined in the general form:

    $EI = m(ln\ fuel\ flow) + b$

where
    m   = slope of the regression line = $-2(10)^{15}$ to $-3(10)^{16}$
    b   = intercept of the regression line = $2(10)^{16}$ to $2(10)^{17}$

- Both EI_M and EI_N were found to increase with increasing fuel sulfur content. For EI_M, the PM emission increased linearly with fuel sulfur, whereas for EI_N, the increase appears to be more of an exponential function.

- It was also observed that engine operating temperature had a measurable effect on both EI_M and EI_N. In both cases, the emissions were slightly lower (i.e., ~8%) when the engine was warm.

- The particle size distributions of the emissions found in the study were generally unimodal and lognormally distributed with electrical mobility diameters ranging from ~3 to slightly larger than 100 nm. At higher power levels, a small accumulation mode was also observed.

- Both the geometric mean diameter (GMD) and geometric standard deviation (GSD) of the particle size distribution (PSD) also varied with engine and fuel type, thrust, and environmental conditions. The GMD ranged from approximately 10 to 30 nm (electrical mobility diameter) and the GSD ranged from 1.4 to 2.

- In general, the largest GMDs and GSDs were obtained at high power conditions. The observations suggest that the PSDs produced by the engines tested under power conditions of <30% rated thrust were unimodal and consisted of primary nuclei particles, whereas for thrust levels >85%, accumulation mode particles were formed, and the PSD curves became broader.

- A comparison of measurement techniques for PM mass, number, and size indicated significant discrepancies between instruments. Of particular note is a comparison of the EI_M obtained by the Nano-Scanning Mobility Particle Sizer (SMPS) and the time-integrated Teflon filter sampling. The filter-based method always produced higher values than the SMPS-based method and there was no linear correlation between the two techniques.

- Of the various instruments used to measure PM mass, number, and size, the SMPS appears to be the most reliable. The lack of correlation with the filter-based technique is disturbing, however, and an area worthy of further investigation.

- The emission indices for black carbon (BC) and particle surface-bound PAHs (polycyclic aromatic hydrocarbons) generally follow trends similar to EI_M discussed above except that: (1) BC was always highest at high power, and (2) fuel composition had no measureable effect on either BC or PAH emissions. Note, however, that the BC and PAH on-line measurements were highly variable and oftentimes did not track well with power changes.

- The chemical composition of the gas-phase nonmethane volatile organic compounds (NMVOCs) and carbonyls varied by engine type as measured on a time-integrated basis over all power conditions. However, significant quantities of a number of compounds listed in the Clean Air Act as hazardous air pollutants (HAPs) were found in some or all engines including formaldehyde, acetaldehyde, benzene, acrolein, toluene, and 1,3-butadiene.

- The elemental composition of the PM samples collected on Teflon filters was dominated by sulfur. In some samples, however, significant amounts of crustal elements such as silicon were also found due to the resuspension of concrete cuttings generated during installation of the sampling probes and lines.

- Sulfate was by far the most abundant water-soluble ion determined from the Teflon filter samples. Calculations of the transformation of S(IV) in the fuel to S(VI) indicate conversion rates in the range of 2 to 4%, which compare favorably to the values obtained by other investigators.

- The emission indices determined in the program for organic carbon (OC) and elemental carbon (EC) as determined from quartz filter sampling ranged from 37 to 83 mg/kg fuel for OC and 21 to 98 mg/kg fuel for EC, respectively. The ratio of EC to OC ranged from 0 to almost 2 depending on the engine type and fuel being tested.

- Over 70% of the particle-phase organic compounds, also determined from the quartz filters, consisted of *n*-alkanes and PAHs. Also, of the engines tested, the CFM56-3B1 and AE3007A1E had the highest

emission indices of total speciated organic compounds, whereas the P&W 4158 and CFM56-7B24 had the lowest.

- The results obtained in the study are at least generally comparable to the results obtained by other APEX investigators. However, a report of the APEX-3 results from the other groups has not as yet been released.

From the above conclusions, the following recommendations for future research are offered for consideration for funding:

- One major issue to be resolved in future work is the effect of the sampling system on the experimental results. These effects include both particle losses in the sampling lines, as well as the potential transformation of the aerosol from the point of collection to the point of measurement. A standardized sampling system with well-characterized performance should be employed in all future testing. Also, the issue of representative plume sampling should be addressed.

- The lack of good agreement between instruments is also a significant issue warranting additional research. Of particular importance is the lack of correlation between on-line SMPS and filter-based methods for determining EI_M.

- Although particle losses through the sampling system can be characterized using traditional aerosol science techniques [e.g., sodium chloride (NaCl) aerosol], a reliable soot calibration source is needed that is both reproducible and stable. Although work is underway under both NASA and EPA Office of Transportation and Air Quality sponsorship to develop the necessary calibration equipment, additional research and development is definitely needed in this regard.

- A reliable on-line method for the direct determination of PM mass emissions is needed. Neither the Tapered Element Oscillating Microbalance (TEOM) nor the Quartz Crystal Microbalance (QCM) appears capable of conducting these measurements in a reliable manner. The TEOM is generally not sensitive enough and the QCM produces values higher than other methods and has limited sampling times due to crystal saturation.

- The effect of fuel composition is also an area worthy of additional investigation. In particular, the further examination of the influence of sulfur and aromatics on sulfate and organic emissions is needed to assess the impact of future aviation fuels on local air quality and global climate change.

- Further work is needed in the characterization of plume aging. To date, all measurements have been performed in the near-field plume < 50 m from the engine exit. Many issues related to fence-line and neighborhood air quality need to be addressed at distances far greater than 50 m and multiple points downstream. For the plume aging tests, the instrumentation should be positioned directly in the plume to avoid problems with long sampling lines.

- Additional chemical characterization of both the gas- and particle-phase emissions by power condition is needed. The data provided are representative of all thrust levels during a particular test. However, specific data for at least the four ICAO-specified power conditions are needed in order to make a determination of the local air quality impacts from airports.

This page intentionally left blank.

1.   Introduction

1.1 Background

The fine particulate matter (PM) emissions from aircraft operations at large airports in National Ambient Air Quality Standards (NAAQS) nonattainment areas are of major environmental concern. Like diesel engines, the PM emissions generated by aircraft gas turbine engines are nanometer in size, contain a variety of toxic air pollutants, and are carbonaceous in nature. In addition, very little chemical source profile data currently exist for aircraft engines; these data are critical for use in receptor modeling, which is used during the State Implementation Plan (SIP) development process.

The fine PM generated from aircraft gas turbine engines can be classified into two major components, non-volatile and volatile PM. Non-volatile PM (or soot) is produced in the combustor and is present at engine exit temperature and pressure whereas volatile PM is formed in the near-field plume downstream of the engine through the gas-to-particle conversion of sulfur and organic gases. Total PM is the combination of both volatile and non-volatile components. In the true sense, total PM can only be characterized by sampling of the exhaust plume after natural cooling and dilution in the atmosphere. There is, however, considerable controversy as to the definition of volatile PM as it applies to both local air quality and global climate impacts.

For a new gas turbine engine used for aero-propulsion (a jet engine), the exhaust gas emissions must comply with applicable regulations promulgated by the International Civil Aviation Organization (ICAO) for unburned total hydrocarbons (THC), carbon monoxide (CO), nitrogen oxides (NO_X), and smoke number (SN). The current range of certifiable operating conditions includes four power (thrust) settings (7, 30, 85 and 100%) indicative of the landing and take-off (LTO) cycle at commercial airports. Since there is currently no emission standard for PM, ICAO is interested in setting a certification limit for this pollutant to address both local air quality and global climate issues.

In general, the majority of the available PM emissions data for commercial aircraft engines is limited and does not completely characterize volatile components resulting from atmospheric cooling and dilution. There is, therefore, a real need for a comprehensive emissions data set for aircraft turbine engines. These data need to include mass-based emission factors and chemical speciation data, which relate the PM emissions to engine operating parameters and key fuel characteristics. This data set must also consider the formation of volatile components in the near-field plume.

To address the need for better PM emissions data for aircraft, the Aircraft Particle Emissions eXperiment (APEX) was organized in 2003. The APEX program is a major collaborative effort between the National Aeronautics and Space Administration (NASA) and a number of other research organizations including the U.S. Environmental Protection Agency's (EPA) National Risk Management Research Laboratory (NRMRL) in Research Triangle Park (RTP), North Carolina. Other APEX collaborators include the Federal

Aviation Administration (FAA), the U.S. Air Force's Arnold Engineering Development Center (AEDC), California Air Resources Board, General Electric, Pratt & Whitney, Rolls-Royce, three commercial airlines, two international airports, the Missouri University of Science and Technology Center of Excellence (UMR), the University of California-Riverside, and Aerodyne Research, Inc. (ARI).

The APEX program is a high visibility, major research priority for EPA's Office of Transportation and Air Quality (OTAQ). The need for emission factors and source profiles has also been expressed by EPA Region 9 for use in air quality analyses around the Los Angeles International Airport. In addition, the program is also part of ongoing efforts by the Society of Automotive Engineers (SAE) E-31 Committee to develop a standard PM test method for aircraft engine certification as requested by ICAO. The APEX tests also support the FAA "Aircraft Emissions Characterization (AEC) Research Road Map" for commercial aircraft.

1.2   Research Objectives

The three sampling campaigns presented in this report (APEX-1, -2, and -3) focused on collecting the data necessary to update and improve emission factors (indices) and source profiles for commercial aircraft-generated PM. The specific objectives of this program were to:

- Develop PM emission factors (indices) and chemical profiles for representative commercial aircraft engines (primary objective) and

- Determine the effect of fuel properties (e.g., sulfur and aromatic content) and engine operating conditions (e.g., cold vs. warm) on the PM emissions (secondary objective).

Measurements conducted by NRMRL during APEX-1, -2 and -3 were conducted in the plume, mostly at 30 m behind the engine, and as such represent the total PM emissions present at that location. This testing was conducted using the Diesel Emissions Aerosol Laboratory (DEAL), and resulted in the first EPA-generated emission factors for commercial aircraft engines since the late 1970s. Samples extracted at other distances were analyzed by APEX collaborators.

This program was originally designed to also provide critical PM emissions data for artificially diluted exhaust (measured 1 m behind the engine) as well as for the plume after natural atmospheric dilution and cooling. This comparison of methods was conducted during the first two tests of APEX-1 using the NRMRL Dilution Sampling System (DSS). However, because of the aggressive scope of the remainder of the project, limited availability of the DSS, and the disparate results produced between the two methods in APEX-1, this portion of the study was deferred for further investigation at a future date.

1.3   Organization of this Report

This report describes three related field campaigns for characterizing the PM emissions from engines manufactured by CFM International (CFMI), General Electric, Pratt & Whitney, and Rolls Royce under the auspices of the APEX program. Engines manufactured by CFMI were tested during all three field tests. The first campaign, APEX-1, was conducted in April 2004 at NASA's Dryden Flight Research Center (DFRC) on Edwards Air Force Base (AFB), California. The second field campaign, APEX-2, was conducted in August 2005 at the Oakland International Airport in Oakland, California. The final campaign, APEX-3, was conducted in November 2005 at NASA's Glenn Research Center at the Cleveland-Hopkins International Airport in Cleveland, Ohio.

Although the APEX research team conducted collaborative testing efforts, with the data being shared among the various project participants, this document addresses only the measurements conducted by EPA-NRMRL. The fuel flow rate at each power setting (i.e., percent rated thrust) was provided to NRMRL by APEX collaborators. Also, except for the carbon content of the fuels used in APEX-2, the chemical analysis of each fuel tested was also provided by others. Meteorological data were supplied by NASA for APEX-1 and The University of Central Florida (Volpe National Transportation Center) for APEX-3. Volpe also supplied background and ambient CO_2 measurements during APEX-2 and -3. ARCADIS U.S., Inc. (ARCADIS) collected the weather data for APEX-2.

Following this introduction, Section 2 describes the test sites and engine specifications for each of the three campaigns. The experimental apparatus and testing procedures are detailed in Sections 3 and 4, respectively. Section 5 details the post-test data analysis conducted. The test matrix, fuel composition and engine operation are discussed in Section 6, and the environmental and engine operating data are provided in Section 7. Sections 8 through 13 present, respectively, the data comparison of PM mass emissions, PM number emissions, particle size distribution (PSD) and geometric mean diameter (GMD), instrumental black carbon and particle surface-bound polycyclic aromatic hydrocarbon (PAH) emissions, gas-phase chemical composition, and PM-phase chemical composition. Each data section presents a comparison of results between the three campaigns, as well as selected comparisons to other available data collected by collaborators. A discussion of quality assurance (QA) is presented in Section 14, and the conclusions of this three-part sampling campaign are found in Section 15. Finally, all experimental data will be archived either on the NASA public website (http://particles.grc.nasa.gov) and/or a suitable EPA website to be established for this purpose.

This page intentionally left blank.

2. Test Site Description and Engine Specifications

2.1 APEX-1 Site Description and Setup

The CFMI model CFM-56-2C1 jet engine, used throughout APEX-1, was mounted on a Boeing DC-8 airframe at NASA's DFRC, Edwards AFB, California. Figure 2-1 illustrates the experimental setup, located on PAD 14 at Edwards AFB. EPA extracted a sample from the centerline of the exhaust plume of the inside starboard engine at a distance of 30 m behind the engine exit plane. The location is indicated in the figure by the dot farthest from the engine with the label "3 sample rakes." The dot closest to the engine represents a 1-m probe location, and the middle dot represents a 10-m probe location. Samples extracted from these locations were analyzed by other organizations collaborating on this research campaign.
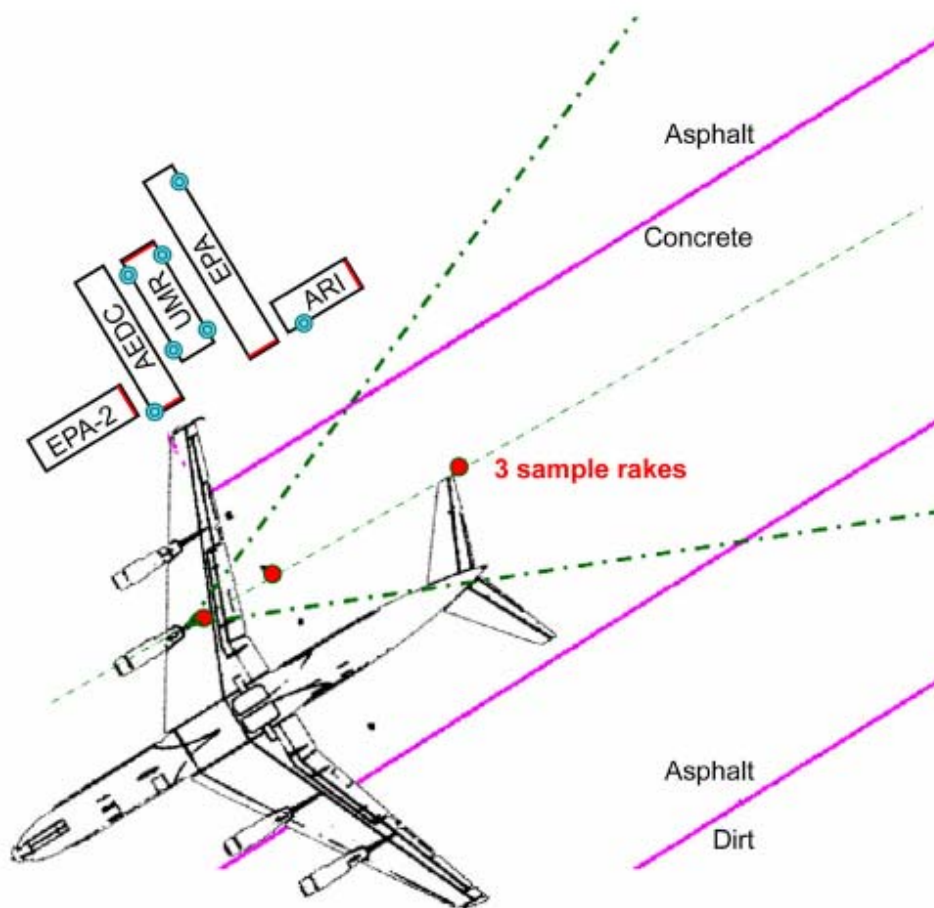
Figure 2-1.   APEX-1 experimental setup.

Although spatially-integrated, multi-point sampling is normally preferred for most emissions measurements, based on the prior experience of APEX collaborators, the DEAL's sample extraction system (described in detail in Section 3) was used to collect an air stream from a single point at the center line of the jet engine exhaust plume 30 m downstream from the engine exit. The concurrent measurement of CO_2 at this measurement location allowed the normalization of the emissions to a fuel-specific basis using a carbon balance as described in Section 5.

The sampling system was configured as a beveled nozzle connected to a 5-cm (2-in) outside diameter (OD) stainless steel tube that ran from the center of the plume (30 m behind the engine) to the inlet of the virtual impactor positioned in the DEAL trailer. The sample extraction system for the 30-m probe location consisted of the probe itself, two 90° turns (each fabricated from two 45° elbows), 18 m (60 ft) of straight tubing, and a Teflon "pop-off" valve for pressure relief at high engine power. The tubing entered the DEAL through the trailer floor and connected to the virtual impactor and the DEAL's instrumented sampling tunnel. Thoroughly cleaned 5-cm (2-in) stainless steel tubing and uncontaminated fittings were used for the entire system, from the virtual impactor to the probe. The probe, shown in Figure 2-2, was constructed from 5-cm (2-in) diameter stainless steel tubing with a tapered inlet nozzle. The probe was attached to a tripod stand that was anchored to the tarmac. Three 6-m (20-ft) pieces of the 5-cm stainless steel tubing were used for the 18-m run from the probe to the trailer.

Figure 2-2.   DEAL 30-m exhaust plume probe assembly for APEX-1.

A vertical slipjoint was fabricated to enable small height adjustments of the probe. A similar horizontal slipjoint (Figure 2-3) was located near the trailer to allow for small adjustments of the sample line length without having to relocate the trailer. Teflon gaskets and sanitary clamps were used to establish leak-tight joints at all connections (Kinsey et al., 2006a). The nozzle at the inlet of the assembly was positioned to face directly into the sample gas stream (i.e., the jet engine exhaust plume). The probe feet and the sections of tube closest to the probe were anchored to the tarmac and the remaining tube was either anchored or weighted down with sand bags. Based on the prior experience of APEX collaborators, no attempt was made to insulate the sampling line or otherwise condition the sample.

Figure 2-3.   Sample line enters DEAL floor downstream of horizontal slipjoint and two 45° bends.

Measurements were also made during APEX-1 using the dilution sampling system (DSS) which is described in Appendix A. However, the data obtained were generally inconsistent between the two tests conducted and with other APEX-1 data and, therefore, were deemed questionable and not included in any further analysis. The DSS was not used during APEX-2 or -3.

2.2   APEX-2 Site Description and Setup

During APEX-2, two CFMI model CFM56-7B24 jet engines were tested while mounted on a Boeing 737-700 airframe, and CFM56-3B1 and -3B2 jet engines were tested while mounted on a Boeing 737-300 airframe. Figure 2-4 illustrates the experimental setup, which was located inside a three-sided noise abatement enclosure, known as a ground run-up enclosure (GRE), at the Oakland International Airport in Oakland, California. As was done during APEX-1, EPA extracted a sample from the exhaust plume of the starboard engine at a distance of 30 m behind the engine exit plane. Additional probes were located at distances of 1 and 54 m behind the starboard engine. Samples extracted from these locations were analyzed by other APEX collaborators.

A plume sampling system was used to collect an air sample from the jet engine exhaust for subsequent analysis using instrumentation located in the DEAL trailer. The plume sampling system was composed of a probe located at the exhaust centerline 30 m behind the starboard engine. The probe was connected to the inlet of the virtual impactor in the DEAL by a 5-cm (2-in) OD stainless steel sampling line. The configuration of the plume sample extraction system for the 30-m probe was exactly the same configuration used during APEX-1, with one exception. The system consisted of the probe and two 90° turns (each fabricated from two 45° elbows), but there was an additional 3 m of sample line length (21 m total). This tubing entered the DEAL through the trailer floor, after which the tubing connected to the virtual impactor and the DEAL's instrumented sampling tunnel. Clean 5-cm stainless steel tubing and uncontaminated fittings were again used for the entire system from the virtual impactor to the probe. Again, the line was not insulated.
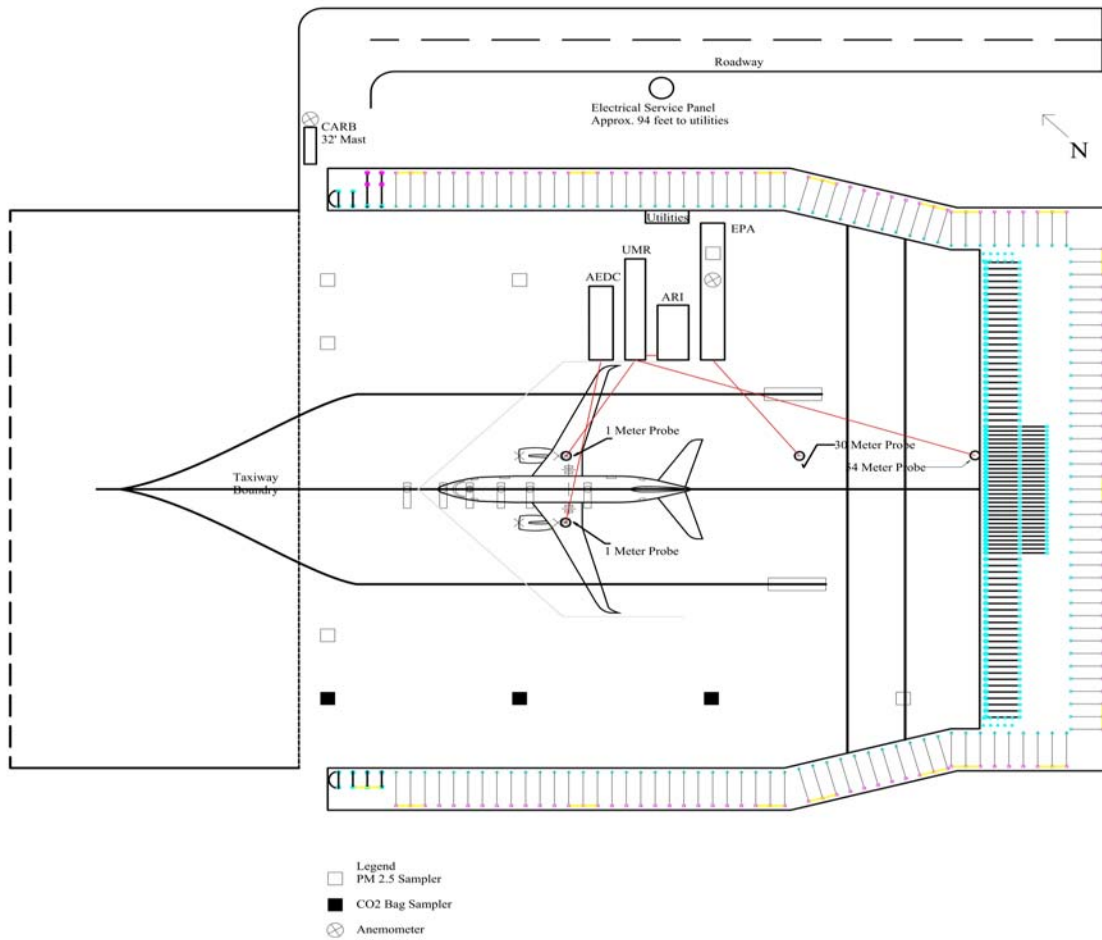
Figure 2-4.   APEX-2 experimental setup.

The 30-m probe stand used during APEX-2 is shown in Figure 2-5. The cone-shaped High-Efficiency Particulate Air (HEPA) filter fitted on the probe nozzle inlet was used in a pre-test particle leak check. An array of nine T-type thermocouples and a pitot tube mounted on the probe stand provided additional information on the structure of the plume during testing. The pitot tube and associated differential pressure cell is shown in Figure 2-5 mounted directly under the probe inlet. The thermocouple array consisted of five thermocouples mounted on the vertical member and four mounted on the horizontal member. Also shown in Figure 2-5 is the vertical slipjoint used during both APEX-1 and APEX-2 that allowed small height adjustments of the probe. The associated mounting apparatus and most of the sampling line were hard-mounted to the tarmac of the GRE using a series of drilled anchors and bolts. Outside the jet exhaust, the sampling line was secured with sand bags.

Figure 2-5.   DEAL 30-meter exhaust plume probe assembly for APEX-2.

Note: the sandbags in the photo were later replaced with anchors and bolts drilled into the tarmac up to the point that the sample line was outside the jet exhaust.

2.3   APEX-3 Site Description and Setup

During APEX-3, two CFMI model CFM56-3B1 engines, tested during APEX-2 on a Boeing 737-300 airframe, were tested again. In addition, five other jet engines of various sizes were studied. These engines included the following:

- General Electric CJ610-8ATJ turbojet on a Lear Model 25 airframe

- Rolls Royce AE3007A1E and AE3007A1/1 turbofans on Embraer ERJ-145 airframes

- Pratt and Whitney PW4158 turbofan on an Airbus A300 airframe

- Rolls Royce RB211-535E4-B turbofan on a Boeing 757 airframe.

Figure 2-6 illustrates the experimental setup at NASA's Glenn Research Center at the Cleveland-Hopkins International Airport. The aircraft engine test pad was located on the eastern extension of the airport and across the street from the NASA aircraft hangar. A chain link fence serves as a boundary between the airport property and the road to the west of the pad; the fence then continues between the airport property and the UPS distribution center and their parking lot.
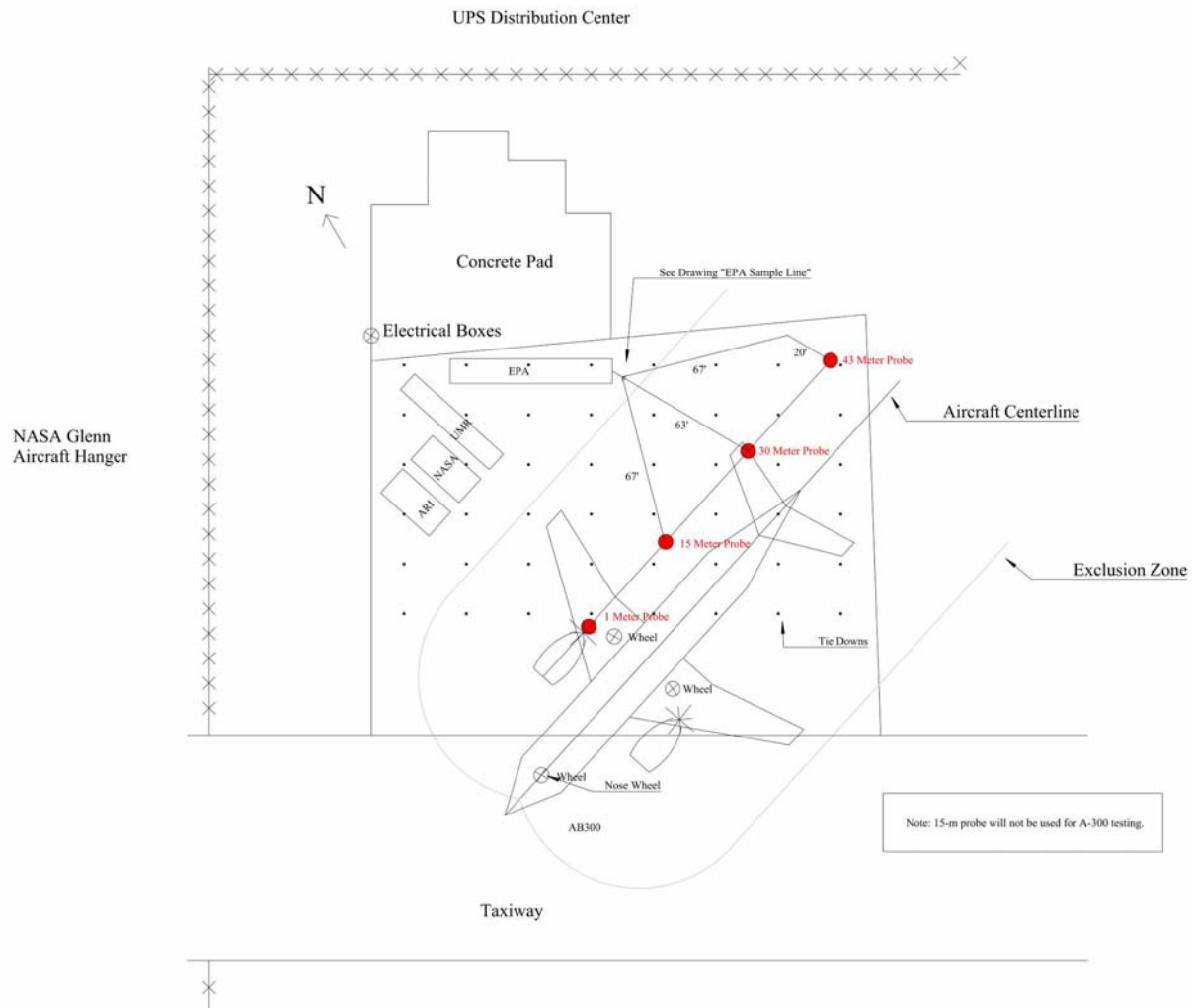
Figure 2-6.   APEX-3 experimental setup.

In APEX-3, EPA extracted a sample from the engine exhaust plume at a distance of 30 m behind the exit plane. In addition, samples were sometimes collected from either a 15-m or 43-m probe location depending on aircraft type. An additional probe was located 1 m behind the engine. Samples extracted from this location were analyzed by other organizations collaborating on this research campaign.

A plume sampling system was used to collect an air sample from the jet engine exhaust for subsequent sampling and analysis using instrumentation located in the DEAL trailer. The plume sampling system was composed of three probes located at the plume centerline 15 m, 30 m, and 43 m behind the starboard engine. In all three locations, the probe tip was a 5-cm stainless steel tube with a tapered end, identical to the probe tips used in APEX-1 (Figure 2-2) and APEX-2 (Figure 2-5).

For the APEX-3 campaign, new probe stands were specially designed for the 15-, 30-, and 43-m sampling locations. The new designs were required so that the probe tip with a large T-type thermocouple array and pitot tubes could be positioned at different heights to accommodate the various aircraft being

studied. During the first test, the probe stands were observed to be unstable and all three stands had to be removed from the test pad. Therefore, the probe stands from APEX-1 and APEX-2 were used for the 30-m location, and a second stand was fabricated from parts on-hand at the NASA Glenn machine shop. This stand was alternated between the 15- and 43-m sampling locations. The replacement probe stands were positioned on the pad and secured with anchors, allowing the testing campaign to continue. However, the replacement stands did not have the ability to raise the probe tips to always be in the center of the exhaust plume of some of the engines tested, nor could they accommodate the thermocouples and pitot tubes that were to be used to collect additional information on the structure of the plume. Like APEX-1 and -2, uninsulated, 5-cm diameter stainless steel sampling lines ran from the probe to the DEAL.

Since more than one sampling point was used during certain tests, a special valving system was developed specifically for APEX-3. This system allowed sample to flow to the DEAL as well as the NASA trailer on an as-needed basis. Figure 2-7 illustrates the valve system used for the three sampling points during APEX-3. The layout of the sample lines was previously shown in Figure 2-6. End-of–runway sampling of advected (wind transported) aircraft plumes was also attempted during APEX-3, but later abandoned due to poor wind conditions. The DEAL's "wing" probe used to extract these samples is shown in Figure 2-8.
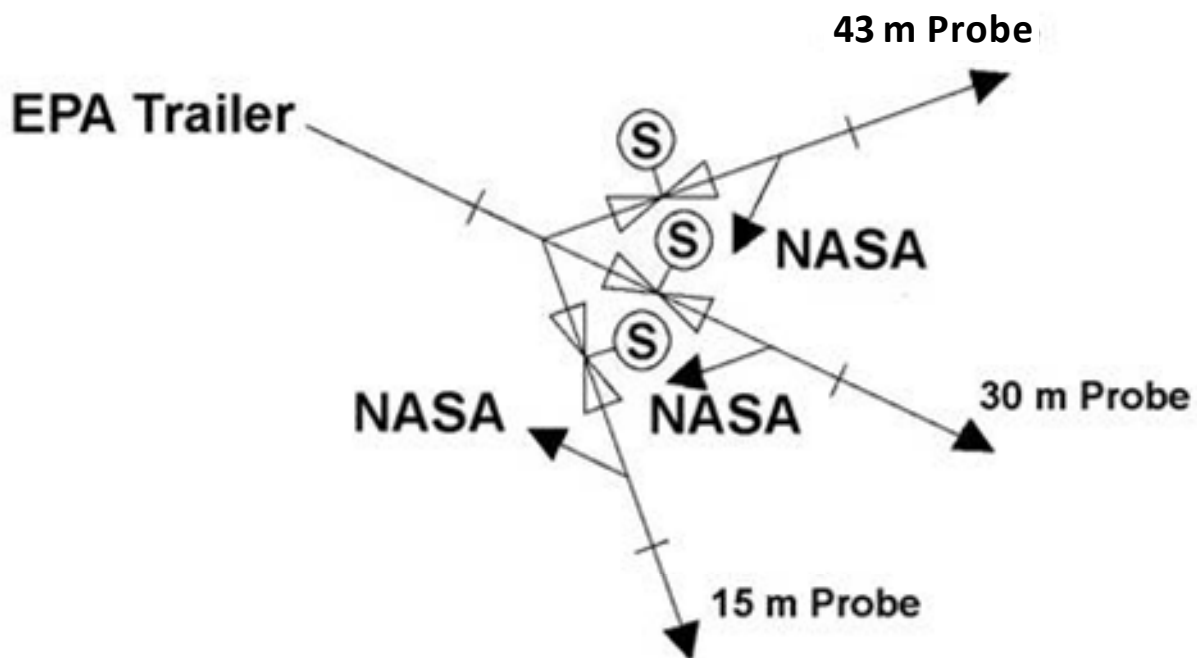
Figure 2-7.   Valve arrangement used for multi-point sampling during APEX-3.

Figure 2-8.   DEAL's "wing probe".

2.4   Engines Tested

A single engine was tested during APEX-1: a CFMI model CFM-56-2C1 mounted on a NASA-owned Boeing (formerly McDonnell-Douglas) DC-8 jet aircraft (Figure 2-9). The engines were originally installed in 1986 but had recently been rebuilt. The aircraft was located at NASA's DFRC on Edwards AFB, California. During APEX-2, three engine dash numbers of the same CFMI engine model were tested: CFM56-3B1, CFM56-3B2 and CFM56-7B24. These engines were mounted on a Boeing 737-300 (-3B1 and -3B2) and a Boeing 737-700 (-7B24) airframe, respectively. The aircraft were owned and operated by Southwest Airlines at Oakland International Airport, Oakland, California. During APEX-3, testing of the CFMI CFM56 family of engines continued. Two of the eleven tests were conducted with a model CFM56-3B1, which had been tested during APEX-2.

Figure 2-10 shows the CFM56 engines tested during the three field campaigns. This family of engines includes four fan sizes and thrusts ranging from 18,500 to 34,000 pounds, with applications in short-, medium- and long-range aircraft. The CFM-56-2 model engine first entered commercial service in 1982 on the DC-8 airframe. The CFM-56-2 engine is the predecessor of the CFM-56-3 model, which was introduced into commercial service in 1984 and which retained the core and the low pressure turbine of the earlier model. The CFM-56-7 engine was introduced into commercial service in 1997. The CFM-56 family is one of the most widely used engines in the commercial fleet.

During APEX-3, engines from three additional manufacturers were tested: General Electric, Pratt & Whitney, and Rolls Royce. Table 2-1 details the engines tested during the three campaigns.

Figure 2-9. CFMI Model CFM56-2C1 jet engine tested during APEX-1.

Figure 2-10. CFMI Model CFM56 engines: CFM56-2 (left), CFM56-3 (center), and CFM56-7 (right).

Table 2-1.   Engines Tested in APEX-1, -2 and -3

Engine[a]	Airframe	Bypass Ratio[b]	Rated Thrust[b] (kN)	ICAO Smoke Number[c]				Tail Number	Test Site/Test #
				T/O	C/O	App	Idle		
CFMI CFM56-2C1	Boeing DC-8	6	97.86	6.0	3.0	2.6	2.2	N817NA	APEX-1 / All Tests
CFMI CFM56-7B24	Boeing 737-700	5.2	107.7	12.6[d]	NA	NA	NA	N435WN; N429WN	APEX-2 / Test # 1 & 4
CFMI CFM56-3B1	Boeing 737-300	5.1	89.41	4.0	2.5	2.5	2.2	N353SW; N14324; N70330	APEX-2 / Test # 2; APEX-3 / Test # 1 & 11
CFMI CFM56-3B2	Boeing 737-300	5.1	98.3	6.0	3.0	2.5	2.2	N695SW	APEX-2 / Test # 3
General Electric CJ610-8ATJ (Turbojet) Starboard	Lear Model 25	na	13.12	NA	NA	NA	NA	—	APEX-3 / Test # 2 & 5
Rolls Royce AE3007A1E[e]	Embraer ERJ145	4.8	33.7	1.0	0	0	0	N11193	APEX-3 / Test # 3 (Starboard) & 4 (Port)
Pratt & Whitney 4158 Starboard	Airbus A300	4.6	258.0	8.1[d]	NA	NA	NA	N729FD	APEX-3 / Test # 6 & Test #7
Rolls Royce RB211-535E4-B Starboard[e]	Boeing 757-324	4.1	191.7	7.3[d]	NA	NA	NA	N75853	APEX-3 / Test # 8
Rolls Royce RB211-535E4-B Starboard[e]	Boeing 757-324	4.1	191.7	7.3[d]	NA	NA	NA	N74856	APEX-3 / Test # 9
Rolls Royce AE3007A1/1 Starboard[e]	Embraer ERJ145	4.8	34.74	1.0	0	0	0	N16927	APEX-3 / Test # 10

a. All engines are turbofan except as noted.
b. Civil Turbojet/Turbofan Specifications http://www.jet-engine.net/civtfspec.html or ICAO Databank Issue 15-C.
c. Data from ICAO Engine Emissions Databank Issue 15-C.

    T/O = take-off
    C/O = climb-out
    App = approach
    NA = not available

d. Maximum SN; no power specified.
e. These engines are internally mixed-flow turbofan engines.

3.   Experimental Apparatus

3.1   General Description

The DEAL consists of a Kenworth T-800 diesel-powered tractor and a 45-ft Great Dane trailer. General specifications of the DEAL are outlined in Table 3-1. A detailed description of the construction and operation of the DEAL and the various instruments may be found in the approved quality assurance project plan (QAPP) for each of the three studies *(*EPA, 2004; EPA, 2005a; EPA, 2005b).

Table 3-1.   Specifications of the DEAL

Vehicle Parameter	Specification
SAE Vehicle Classification	3-S2
Gross Vehicle Weight (GVW) Classification	8
Service Classification	D
Gross Train Weight or GVW	36,284 kg (80,000 lb)
Tractor Wheelbase	6.1 m (20 ft)
Length of Trailer	14 m (45 ft)
Tire Size/Type	Michelin 11R24.5 radial
Engine	2000 Detroit Diesel Series 60
Engine Displacement	12.7 L
Engine Power Output	373 kW (500 hp) @ 2100 rpm
Engine Emission Limit (Measured at West Virginia University)	0.13 g/kW·hr (0.1 g/bhp·hr)

Electric power is supplied to the trailer through two panel boxes from which individual circuits are run to various locations inside the trailer to support the power requirements of all the instruments, pumps, blowers and other equipment. The panel boxes can receive power from a conventional power source or from two 12-kW diesel-powered generators mounted to the underside of the trailer. When the DEAL is in its staging configuration, it can accept external (i.e., utility) power and additional calibration gases can be connected to the Continuous Emission Monitoring System. All instruments are supplied conditioned power via an uninterruptible power supply (UPS). Pumps and other equipment that do not contain delicate electronics do not receive conditioned power from the UPS.

For APEX-2 and -3, a rental tractor was used instead of EPA's Kenworth T-800 tractor to pull the DEAL trailer to the test site. Because the main computer operator's station used to monitor and control the sampling instruments and equipment was located in the Kenworth sleeper, a new desktop computer

station was set up inside the DEAL trailer. To simplify the electrical setup for the DEAL and the other participants during APEX-2 and -3, a single power station was designed and fabricated to make the electrical setup and tear-down more efficient for the entire research team. The electrical power skid is shown in Figure 3-1.

Figure 3-1.   Electrical power skid used during APEX-2 and APEX-3.

3.2   Sampling System

The DEAL uses two centrifugal blowers, each controlled by a variable frequency drive and mass flow meter, to continuously extract 1.1 actual m^3/min — 40 actual ft^3/min (acfm) — of sample gas from the plume. After extraction, the plume sample flows through a 5-cm diameter stainless steel sampling tube into a PM-2.5 "cut point" (i.e., particle diameter representing a 50% collection efficiency for equivalent unit density spheres ≤2.5 μm in diameter) virtual impactor, and then into an 8.8-m long, 15-cm inside diameter (ID) stainless steel sampling tunnel. A series of "buttonhook" sampling nozzles, which are staggered in height inside the tunnel to minimize aerodynamic interference, is used to extract samples from the tunnel. The sample flow captured by each nozzle exits the plume tunnel through flow splitters that direct the flow from the sampling tunnel to various instruments. The tunnel is supported from the trailer floor by columns integrated into the plume instrument rack. Conductive silicone rubber lines connect the instruments to the appropriate sample splitter.

The DEAL was outfitted and configured to accommodate the sample collection and continuous monitoring requirements of the APEX monitoring plan. Figure 3-2 is representative of the DEAL exhaust plume measurement equipment configuration used for speciated testing during the APEX campaigns. In this context, "speciated" refers to those tests designated for the determination of gas- and particle-phase chemical characteristics by time-integrated sampling.
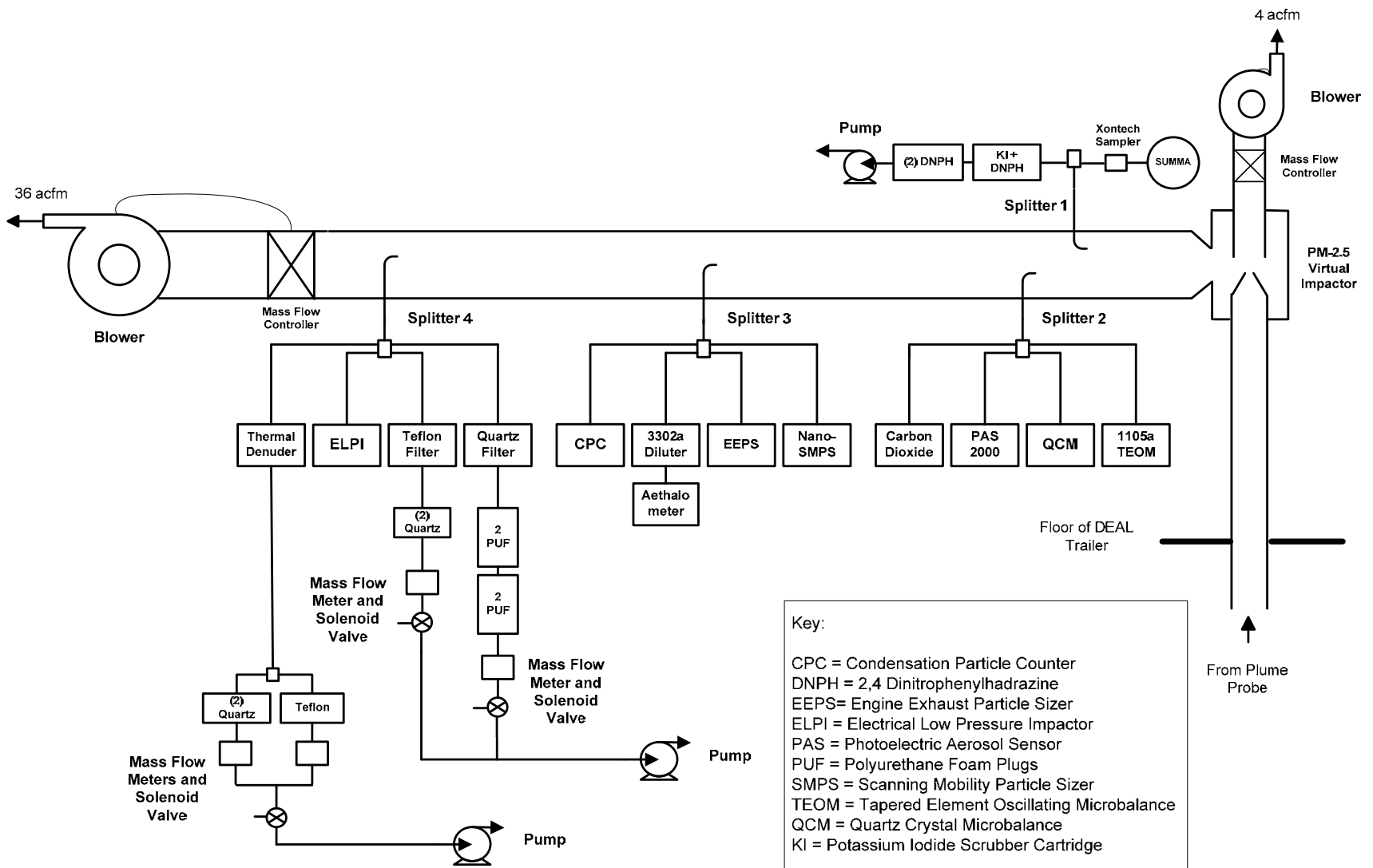
Figure 3-2. Representative DEAL exhaust plume measurement equipment configuration, speciated test.

During the three measurement campaigns, the plume sampling instrument configuration varied slightly from that shown in Figure 3-2. For APEX-1, the configuration shown changed only in that there were two instrument substitutions. On splitter 2, a tracer gas analyzer (B&K Model 1302 Photoacoustic Analyzer) was used to measure CO_2 instead of the continuous online Milton Roy Model 5300A analyzer. On splitter 3, the TSI Model 3936 (Long DMA—Differential Mobility Analyzer) Scanning Mobility Particle Sizer (SMPS) was substituted for the TSI Model 3090 Engine Exhaust Particle Sizer (EEPS). Note also that during APEX-1, the Quartz Crystal Microbalance (QCM) failed to function properly. Therefore, no data were recorded from this instrument during APEX-1.

The background was sampled by an independent sample extraction and analysis system. The background sample air enters the system through a "rain hat" to an elevated transfer line. The sample stream is then routed into two parallel PM-10/PM-2.5 (particles ≤10 μm or ≤2.5 μm in aerodynamic diameter, respectively) pre-collectors and into a sampling tunnel from which the instruments draw their sample through staggered probes and flow splitters. Figure 3-3 is representative of the DEAL background measurement equipment configured for speciated testing during the APEX campaigns.

During APEX-1, the configuration shown in Figure 3-3 changed only because there were two instrument substitutions. On splitter 1, an integrated bag sampler was used instead of the Milton Roy Model 5300A CO_2 analyzer, and the older 3934 SMPS was used instead of the 3936 (Long DMA) SMPS.

For non-speciated tests, whether for plume or background sampling, there again were only minor differences in the DEAL configuration. First, no sampling was conducted off splitter 1: the SUMMA canister and the 2,4-dinitrophenylhydrazine (DNPH) and potassium iodide (KI)-DNPH cartridges were removed. Second, during APEX-1, the dual series of polyurethane foam (PUF) cartridges was replaced with two quartz filters for both plume and background sampling. Third, during APEX-3, no sample collection media were run during the non-speciated tests.

In APEX-1, three of the nine tests were speciated. During APEX-2, all sampling equipment configurations in the DEAL were for speciated tests. Finally, six of the eleven tests conducted during APEX-3 were also speciated. Recall that the end-of-runway sampling in APEX-3 was unsuccessful due to poor wind conditions.

Tables 3-2 and 3-3 present detailed information about the sampling location of each instrument inside the DEAL for the plume and background sample tunnels, respectively, for all three APEX sampling campaigns. Any instrument substitutions or the removal of any instruments between campaigns has been reflected in this table. Note that Tables 3-2 and 3-3 also distinguish between tests in which samples were collected for speciation and tests in which no samples were collected for speciation. Table 3-4 presents descriptions of the measurement capabilities of the DEAL and is followed by descriptions of each individual instrument.
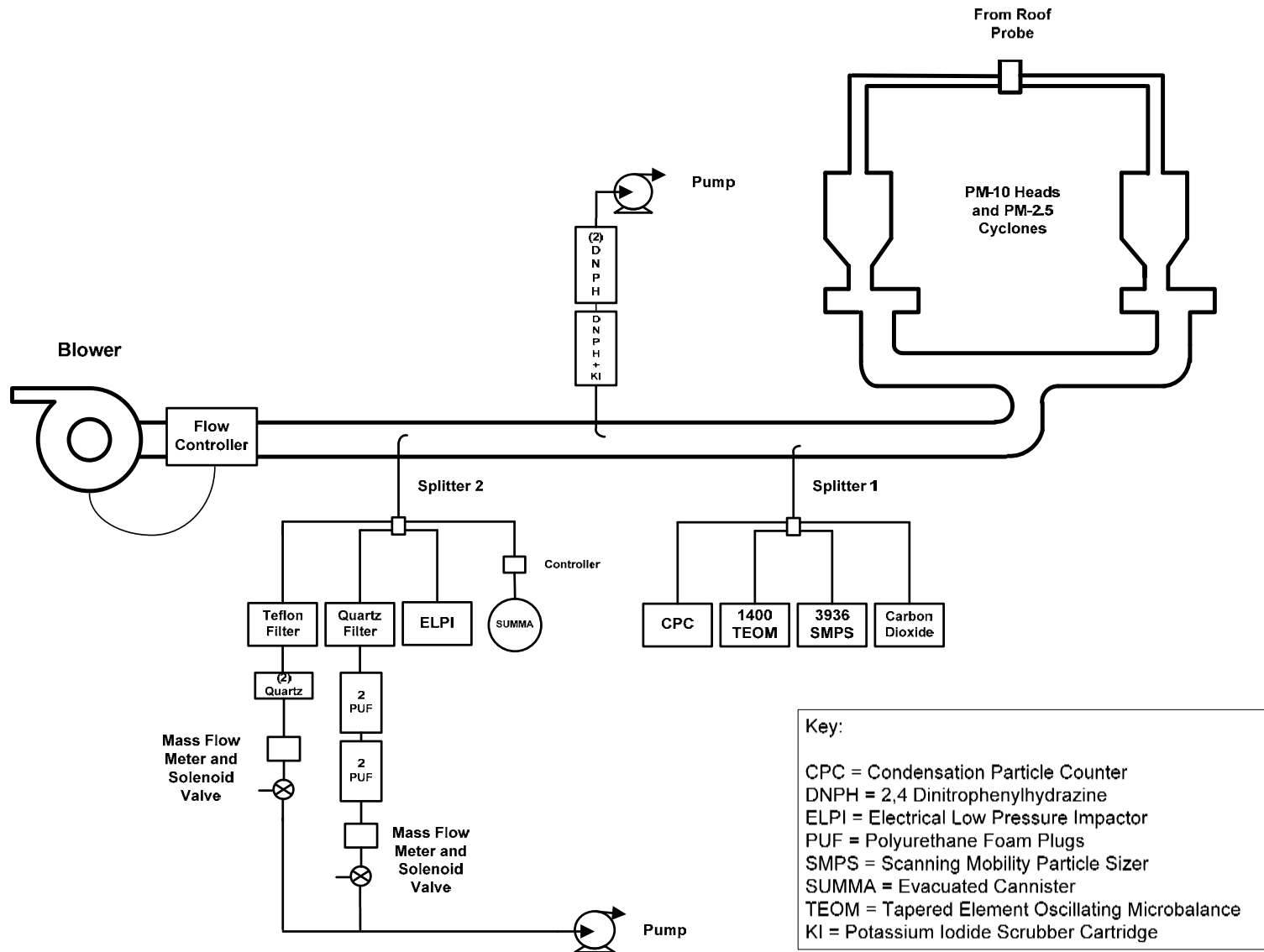
Figure 3-3. Representative DEAL background measurement equipment configuration, speciated test.

Table 3-2.   Measurement Configuration for the Plume Sample Tunnel

Campaign		Splitter 1		Splitter 2				Splitter 3					Splitter 4			
APEX	Test #	DNPH	SUMMA	CO_2	PAS 2000	QCM	1105a TEOM	CPC	Aethal-ometer	3936L SMPS	EEPS	Nano SMPS	Thermal Denuder	ELPI	Teflon + 2Q	Quartz + PUF
1	EPA-1	X	X	PA	X		X	X	X	X		X	X	X	X	X
	EPA-2	X	X	PA	X		X	X	X	X		X	X	X	X	X
	NASA-1			PA	X		X	X	X	X		X	X	X		2Q
	NASA-1a			PA	X		X	X	X	X		X	X	X		2Q
	EPA-3	X	X	PA	X		X	X	X	X		X	X	X	X	X
	NASA-2			PA	X		X	X	X	X		X	C	X	C	C2Q
	NASA-3			PA	X		X	X	X	X		X	C	X	C	C2Q
	NASA-4			PA	X		X	X	X	X		X	C	X	C	C2Q
	NASA-5			PA	X		X	X	X	X		X	C	X	C	C2Q
2	T1	X	X	X	X	X	X	X	X		X	X	X	X	X	X
	T2	C	X	X	X	X	X	X	X		X	X	C	X	C	C
	T3	C	X	X	X	X	X	X	X		X	X	C	X	C	C
	T4	X	X	X	X	X	X	X	X		X	X	X	X	X	X
3	T1			X	X	X	X	X	X		X	X		X		
	T2			X	X	X	X	X	X		X	X		X		
	T3	X	X	X	X	X	X	X	X		X	X	C	X	C	C
	T4	X	X	X	X	X	X	X	X		X	X	C	X	C	C
	T5			X	X	X	X	X	X		X	X		X		
	T6	C	X	X	X	X	X	X	X		X	X	C	X	C	C
	T7	C	X	X	X	X	X	X	X		X	X	C	X	C	C
	T8			X	X	X	X	X	X		X	X	C	X		
	T9	X	X	X	X	X	X	X	X		X	X	C	X	X	X
	T10			X	X	X	X	X	X		X	X		X		
	T11	X	X	X	X	X	X	X	X		X	X	X	X	X	X

2Q = Double quartz backup filters (NASA runs)

CPC = Condensation Particle Counter

DNPH = 2,4-Dinitrophenylhydrazine

EEPS = Engine Exhaust Particle Sizer

ELPI = Electrical Low Pressure Impactor

PA = Photoacoustic analyzer

PUF = Polyurethane foam

QCM = Quartz Crystal Microbalance

SMPS = Scanning Mobility Particle Sizer

SUMMA = SUMMA-polished stainless steel canisters

TEOM = Tapered Element Oscillating Microbalance

C = Cartridges were composited for both runs to collect sufficient sample mass (see Section 6)

Table 3-3.   Measurement Configuration for the Background Sample Tunnel

Campaign		Splitter 1						Splitter2				Splitter 3
APEX	Test #	CPC	1400 TEOM	3934 SMPS	3936L SMPS	Bag Samp.	CO2	Teflon +2Q	Quartz + PUF	ELPI	SUMMA	DNPH
1	EPA-1	X	X	X		X		X	X	X	X	X
	EPA-2	X	X	X		X		X	X	X	X	X
	NASA-1	X	X	X		X		X	2Q	X		
	NASA-1a	X	X	X		X		X	2Q	X		
	EPA-3	X	X	X		X		X	X	X	X	X
	NASA-2	X	X	X		X		C*	C2Q	X		
	NASA-3	X	X	X		X				X		
	NASA-4	X	X	X		X		C	C2Q	X		
	NASA-5	X	X	X		X				X		
2	T1	X	X		X		X	X	X	X	X	X
	T2	X	X		X		X	C	C	X	X	C
	T3	X	X		X		X			X	X	
	T4	X	X		X		X	X	X	X	X	X
3	T1	X	X		X		X			X		
	T2	X	X		X		X			X		
	T3	X	X		X		X	C	C	X	X	X
	T4	X	X		X		X			X	X	X
	T5	X	X		X		X			X		
	T6	X	X		X		X	C	C	X	X	C
	T7	X	X		X		X			X	X	
	T8	X	X		X		X			X		
	T9	X	X		X		X	X	X	X	X	X
	T10	X	X		X		X			X		
	T11	X	X		X		X	X	X	X	X	X

2Q = Double quartz backup filters (NASA runs)   PUF = Polyurethane foam

CPC = Condensation Particle Counter   QCM = Quartz Crystal Microbalance

DNPH = 2,4-Dinitrophenylhydrazine   SMPS = Scanning Mobility Particle Sizer

EEPS = Engine Exhaust Particle Sizer   SUMMA = SUMMA-polished stainless steel canisters

ELPI = Electrical Low Pressure Impactor   TEOM = Tapered Element Oscillating Microbalance

PA = Photoacoustic analyzer   * = Teflon filter *was not* composited

C = Cartridges were composited for both runs to collect sufficient sample mass (see Section 6)

Table 3-4. Measurements Performed by the DEAL during APEX-1, -2, and -3

Parameter	Sampling Location	Measurement Technique	Type of Sample	Instruments and Sampling Media
PM-2.5 mass concentration	Background	Microbalance	Continuous	Rupprecht and Patashnick Series 1400a TEOM
	Background	Gravimetric analysis	Time-integrated	47-mm Teflon filter with double quartz backup filters for collection of gas-phase "blow off" [a]
	Plume	Microbalance	Continuous	Rupprecht and Patashnick (now Thermo Electron) Series 1105a TEOM
	Plume	APEX-2 & -3: QCM	Continuous	SEMTECH Model RPM-100 particulate monitor + diluter
	Plume	Gravimetric analysis	Time-integrated	47-mm Teflon filter with double quartz backup filters[a]
Particle size distribution	Background	Low pressure cascade impactor (aerodynamic diameter)	Continuous / time-integrated	Dekati ELPI
	Background	Electrical mobility classifier/condensation nuclei counter (electrical mobility diameter)	Continuous	APEX-1: TSI Model 3934 SMPS, Model 3071 A classifier, Model 3010 CPC
				APEX-2 & -3: TSI Model 3936 SMPS (long), Model 3080 classifier, Model 3025a CPC, Model 3081 DMA
	Plume	Low-pressure cascade impactor (aerodynamic diameter)	Continuous / time-integrated	Dekati ELPI
	Plume	Electrical mobility classifier/condensation nuclei counter (electrical mobility counter)	Continuous	TSI Model 3936 SMPS (Nano). Model 3080 classifier, Model 3025a CPC, Model 3085 DMA
	Plume	APEX-1: electrical mobility classifier/condensation nuclei counter (electrical mobility counter)	Continuous	APEX-1: TSI Model 3936 SMPS (long), Model 3080 classifier, Model 3025 CPC, Model 3081 DMA
		APEX-2 & -3: electrical mobility classifier/electrometers (electrical mobility counter)		APEX-2 & -3: TSI Model 3090 EEPS + diluter
PM-2.5 number concentration[c]	Background	Condensation nuclei counter	Continuous	Model 3025a CPC
	Plume	Condensation nuclei counter	Continuous	Model 3025a CPC + diluter
Elemental carbon/organic carbon (EC/OC)	Background	Thermo-optical analysis (NIOSH Method 5040)	Time-integrated	Prefired 47 mm quartz filter
	Plume	Thermo-optical analysis (NIOSH Method 5040)	Time-integrated	Prefired 47 mm quartz filter
	Plume	Optical attenuation/UV absorption (black carbon)	Continuous	TSI 3302a Diluter +Magee Model AE-2 Aethalometer[d]
PM semivolatile organic compounds (SVOCs)	Background	GC/MS	Time-integrated	Prefired 47 mm quartz filter with 4 PUF plugs.[a]
	Background	Low-pressure cascade impactor	Time-integrated	12 aluminum foil ELPI stages + prefired quartz back-up filter[b]
	Plume	GC/MS	Time-integrated	Prefired 47 mm quartz filter with 4 PUF plugs.[a]
	Plume	Low-pressure cascade impactor	Time-integrated	12 aluminum foil ELPI stages + prefired quartz back-up filter[b]
	Plume	UV analyzer (particle surface PAHs)	Continuous	EcoChem Model PAS 2000

Parameter	Sampling Location	Measurement Technique	Type of Sample	Instruments and Sampling Media
PM volatile compounds (VOCs)	Plume	Gravimetric/thermo-optical analysis	Time-integrated	Dekati Model EKA-111 thermal denuder with parallel Teflon and double prefired quartz filters
PM inorganic water-soluble ions	Background	Ion chromatography	Time-integrated	Teflon filter
	Plume	Ion chromatography	Time-integrated	Teflon filter
PM elemental composition	Background	XRF	Time-integrated	Teflon filter
	Plume	XRF	Time-integrated	Teflon filter
APEX-1 CO, CO_2, total VOCs	Background	IR absorption	Integrated bag[e]	Brüel & Kjær Model 1302 Photoacoustic Analyzer
	Plume	IR absorption	Continuous	Brüel & Kjær Model 1302 Photoacoustic Analyzer
APEX-2 & -3 CO_2	Background	IR absorption	Continuous	Milton-Roy (CA Analytical) Model 5300A
	Plume	IR absorption	Continuous	Milton-Roy (CA Analytical) Model 5300A
Gas-phase NMOCs	Background	GC/MS/FID	Time-integrated	SUMMA-passivated canister
	Plume	GC/MS/FID	Time-integrated	SUMMA-passivated canister
Gas-phase carbonyl compounds	Background	HPLC	Time-integrated	DNPH impregnated silica gel cartridges with KI ozone scrubber cartridge
	Plume	HPLC	Time-integrated	DNPH impregnated silica gel cartridges with KI ozone scrubber cartridge
Sample temperature[f]	Plume tunnel	Thermocouple	Continuous	K-Type thermocouples; T-Type only on APEX-2 sampling probes
APEX-2 plume temperature	Plume	Thermocouples	Continuous	Multiple T-type thermocouples
APEX-2 plume velocity	Plume	Pitot tube	Continuous	Standard pitot tube plus differential pressure cell
APEX-2 wind speed/direction	Background	Propeller anemometer & wind vane	Continuous	Vaisala MAWS weather station

[a] Filter holder design per Federal Test Procedure (FTP) published in 40 Code of Federal Regulations (CFR), Part 86. "Blow off" are gas-phase semivolatile species that have been released from the particulate deposited on the primary filter by the air flow passing through the medium.

[b] Aluminum foil substrates from the ELPI were not analyzed due to insufficient mass.

[c] These measurements were redundant and these data were not used.

[d] The aethalometer measures "black" carbon which approximates elemental carbon content as determined from diesel engine testing at West Virginia University (Kinsey et al., 2006b).

[e] Post-test analysis of time-integrated Tedlar bag sample collected over the entire test period.

[f] Temperature was not monitored in sampling lines.

CPC = Condensation Particle Counter	NMOC = Nonmethane Organic Compound
DMA = Differential Mobility Analyzer	NIOSH = National Institute for Occupational Safety and Health
DNPH = 2,4-Dinitrophenylhydrazine	PAH = Polycyclic Aromatic Hydrocarbon
EEPS = Engine Exhaust Particle Sizer	PUF = Polyurethane Foam
ELPI = Electrical Low Pressure Impactor	QCM = Quartz Crystal Microbalance
FID = Flame Ionization Detector	SMPS = Scanning Mobility Particle Sizer
GC/MS = Gas Chromatography/ Mass Spectrometry	TEOM = Tapered Element Oscillating Microbalance
HPLC = High Performance Liquid Chromatography	UV = Untraviolet
IR = Infrared	XRF = X-ray Fluorescence

In addition to the above equipment, exit plane sampling was also attempted at a location of 1 m during APEX-1 using EPA's Dilution Sampling System (DSS). This system is based on the dilution stack sampler developed by Hildeman et al. (1991) and described in Appendix A. As stated previously, no useful data were obtained from the DSS and thus the measurement results are not presented in this report.

3.3   Instrumentation

3.3.1   Tapered Element Oscillating Microbalance Monitors

The Rupprecht and Patashnick (R&P) Tapered Element Oscillating Microbalance (TEOM) Series 1105 Diesel Particulate Monitor and Series 1400a Ambient Particulate Monitor incorporates a patented inertial balance that directly measures the mass collected on an exchangeable filter cartridge. The TEOM monitors the change in the natural oscillating frequency of a tapered element as additional mass collects on the filter. The sample flow passes through the filter, where PM collects, and then continues through the hollow tapered element on its way to a dynamic flow control system and vacuum pump.

The TEOM mass transducer does not normally require recalibration because it is specially designed and constructed from non-fatiguing materials. The mass calibration of the TEOM was verified before sampling using an optional Mass Calibration Verification Kit that contains a filter of known mass. A flow controller maintains the sample flow rate input by the user. TEOM Series 1105 interfaces with the multicomputer via an input/output (I/O) card, cable, and software supplied by the manufacturer, Thermo Electron, Inc. The TEOM Series 1400a monitor incorporates the same technology as the 1105a, but incorporates an internal microprocessor and data storage system.

3.3.2   Quartz Crystal Microbalance

An older instrument, which has recently been reintroduced, is the QCM. The harmonic oscillator principle used in the QCM is similar to the TEOM, except that the collected PM is actually deposited onto a crystal element using an electrostatic precipitator (ESP). Due to its high-frequency operation, the QCM exhibits far less instrumental noise than the TEOM, but the QCM also can overload in a relatively short period. To offset this problem, a dilutor was used with the instrument to extend the useful life of the crystal element. The QCM was operated and the data collected using the software provided by the manufacturer.

3.3.3   Electrical Low Pressure Impactor

The Dekati Electrical Low Pressure Impactor (ELPI) is a real-time particle size spectrometer designed for real-time monitoring of aerosol particle size distribution. The ELPI measures airborne particle size distributions (PSD) with 12 channels in the size range of 0.03 to 10 µm. The principle is based on charging, inertial classification, and electrical detection of the aerosol particles. The instrument consists primarily of a corona charger, low pressure cascade impactor, and multi-channel electrometer. The ELPI communicates with the multicomputer via a serial port using the ELPI VI software provided with the instrument. The software is used for setup and configuration and to view data.

3.3.4   Engine Exhaust Particle Sizer

The TSI Model 3090 EEPS measures the size distribution and number concentration of exhaust particle emissions in the range from 5.6 to 560 nm. The instrument continuously draws a sample of the exhaust flow into the inlet, and the particles in the flow are positively charged to a predictable level using a corona charger. These charged particles are then introduced to the measurement region near the top-center of a high-voltage electrode column surrounded by a stack of electrometers and the particles are transported

down the column in a sheath of HEPA-filtered air. A positive voltage is applied to the electrode and creates an electric field that repels the positively charged particles outward according to their electrical mobility.

Charged particles strike the respective electrometers and transfer their charge. A particle with higher electrical mobility strikes an electrometer near the top, whereas a particle with lower electrical mobility strikes an electrometer lower in the stack. This multiple detector arrangement using highly sensitive electrometers allows for simultaneous concentration measurements of multiple particle sizes.

3.3.5   Scanning Mobility Particle Sizer

The TSI Model 3934 SMPS is a system that measures the size distribution of aerosols in the size range from 10 to 1,000 nm. The particles are classified with the Model 3071A Electrostatic Classifier and their concentration is measured with the Model 3010 Condensation Particle Counter (CPC). The system communicates with the multicomputer via a serial port. The Aerosol Instrument Manager (AIM) software Version 5.2 is used for setup and configuration and to view data.

The TSI Model 3936 Long SMPS is a system that measures the size distribution of aerosols in the size range from approximately 9 nm to 1,000 nm. The particles are classified with the Model 3080 Electrostatic Classifier with a Model 3081 Long DMA, and their concentration is then measured with the Model 3025A CPC. The Long DMA is the traditional length DMA used in the older Model 3071 Electrostatic Classifier. The system communicates with the multicomputer via a serial port.

The TSI Model 3936 Nano-SMPS is a system that measures the size distribution of aerosols in the size range from 2 to 150 nm. The particles are classified with the Model 3080 Electrostatic Classifier with a Model 3085 Nano-DMA and their concentration is then measured with the Model 3025A CPC. The Nano-DMA is optimized for the size range below 20 nm. The system communicates with the multicomputer via a serial port. The AIM software Version 5.2 package is used for setup and configuration, and to view data.

3.3.6   Condensation Particle Counter

The Model 3025A CPC detects and counts particles larger than 3 nm in diameter by an optical detector after a supersaturated vapor (*n*-butyl alcohol) condenses onto the particles, causing them to grow into larger droplets. The range of particle concentrations extends from less than 0.01 to 9.99×10^4 particles/cm^3. The system communicates with the multicomputer via a serial port. The CPC LOG software developed by NRMRL was used to log the data.

3.3.7   Aethalometer

The Magee (Andersen) Model AE-2 Aethalometer measures real-time "black" carbon [i.e., elemental carbon (EC)] and is designed for fully automatic and unattended operation. The sample is collected as a spot on a roll of quartz fiber tape. An optical method is then used to measure the attenuation of a beam of light transmitted through the sample. The optical attenuation is linearly proportional to the amount of black carbon collected on the quartz fiber tape. The aethalometer communicates with the multicomputer via an analog output signal with a voltage range of 0 to 5 volts. Operation of the instrument was checked before sampling using an optical test strip.

3.3.8 Photoelectric Aerosol Sensor

The PAS 2000 Photoelectric Aerosol Sensor works on the principle of photoionization of particle surface-bound polycyclic aromatic hydrocarbons (PAH). Using an Excimer lamp, the aerosol flow is exposed to ultraviolet (UV) radiation. The Excimer lamp offers a high intensity, narrow band source of UV radiation. The wavelength of the light is chosen so that only the PAH-coated aerosols are ionized, while gas molecules and non-carbon aerosols remain neutral. The aerosol particles that have PAH molecules adsorbed on the surface emit electrons, which are subsequently removed when an electric field is applied. The remaining positively-charged particles are collected on a filter inside an electrometer, where the charge is measured. The resulting electric current establishes a signal that is proportional to the concentration of total particle-bound PAHs.

3.3.9 Tracer Gas Analyzer

The Brüel and Kjær (B&K) Model 1302 Photoacoustic Analyzer operates on the principle of infrared (IR) photoacoustic spectroscopy. A pump draws air from the sampling point through two air filters to flush out the "old" air in the measurement system and replace it with a "new" air sample, which is hermetically sealed in the analysis cell by closing the inlet and outlet valves. Light from an IR source is reflected off a mirror, passed through a mechanical chopper (which pulsates it), and then through one of the optical filters in a filter carousel. The light transmitted by the optical filter is selectively absorbed by the gas being monitored, causing the temperature of the gas to increase. Because the light is pulsating, the gas temperature increases and decreases causing an equivalent increase and decrease in the pressure of the gas (an acoustic signal) in the closed cell. Two microphones mounted in the cell wall measure this acoustic signal, which is directly proportional to the concentration of the monitored gas present in the cell.

During APEX-1, the photoacoustic analyzer was used to sample from two different sources. During testing, the analyzer recorded the results of a continuous sample of the jet engine exhaust from the plume tunnel. After the test was completed, the same instrument was used to analyze an integrated bag sample captured from the background tunnel during the test. Whether sampling from the plume tunnel or the bag sampler, the same bypass flow configuration and equipment was used to allow the instrument's internal pump to draw its own sample from a slipstream. The bypass flow system consisted of a rotameter, an external pump to overcome the negative pressure in the plume tunnel, a three-way valve to switch between the calibration line and the sample line, and a second three-way valve to switch between the bag sampler line and the plume tunnel sample line. Under all operating scenarios, the gas being introduced to the analyzer flowed through the external pump and the rotameter.

3.3.10 Thermal Denuder

The Dekati Model EKA-111 Thermodenuder is designed to remove volatile and semivolatile compounds from an exhaust sample. These compounds are known to cause variations in particle measurements through nucleation and condensation. The Thermodenuder heats the sample gas up to 250 °C and therefore vaporizes the unwanted compounds. The vaporized compounds are subsequently collected in active charcoal in the adsorber section. Since the particles in the sample have much slower diffusion speeds (less than 1/100 for 10 nm particles) than the vaporized compounds, the vaporized volatiles are collected efficiently, while the sample aerosol particles follow the gas stream lines unaffected. Chilled water driven through the cooling channels cools the sample aerosol in the adsorber.

3.3.11 Carbon Dioxide Analyzer

The Milton-Roy (CA Analytical) Model 5300A analyzer uses a technique based on the IR absorption characteristics of gases to measure gas concentration. A single beam of IR energy is modulated and passed through a sample cell containing the gas to be measured. The beam emerges attenuated by the amount of energy absorbed by the gas in the sample. Changes in the concentration of the gas result in changes in the intensity of the beam. The remaining energy in the beam is passed serially through two cavities of an IR detector, which is a mass-flow sensor filled with gas of the type to be measured. Changes in the intensity of the beam change the pressure differential between the cavities and, consequently, the balance of an electrical bridge in the detector circuit. Electronic processing of the imbalance signal is used to generate an electrical output signal proportional to the concentration of the gas measured.

3.4 Data Acquisition System

The data acquisition system (DAS) used in the DEAL consists of a multicomputer network containing up to eight CPUs, a monitor, a keyboard, and a mouse as installed in a trailer instrument rack plus a separate computer, two flat screen monitors, a keyboard, and a mouse installed in either the tractor sleeper compartment (APEX-1) or a stand-alone operator's station (APEX-2 and -3). The computer at the operator's station is networked via modem to the multicomputer to allow file access and transfers. A keyboard-video-monitor (KVM) switch also allows the operator to access and run instrument operating software on the multicomputer in the trailer. All instrument measurements are recorded on the DAS and stored as individual data files. All calculated quantities are determined post-test from the raw data as described in Section 5. A clock card is also installed in the master computer, which is used to time-synchronize the remainder of the computers. The master computer clock is set daily to an atomic clock that is traceable to the National Institute of Standards and Technology (NIST).

This page intentionally left blank.

4.   Experimental Procedures

4.1   General Sampling Approach

The exhaust plume was sampled at a location approximately 15, 30, or 43 m downstream of the engine being tested. Sampling was done at the centerline using a single probe (as described earlier). The exhaust was cooled and diluted at this location (no less than 30:1, and possibly more) so that, in most cases, no special conditioning was required for gaseous and particulate sampling. In addition to on-line analyzers, chemical source profiles were developed from time-integrated measurements. The DEAL also sampled ambient background about 1.83 m (6 ft) above the roof of the DEAL with a separate system used to continuously monitor ambient background concentrations (physical and chemical).

Ambient conditions such as wind speed and direction, temperature, and relative humidity were monitored continuously by NASA-Dryden during APEX-1, by the NRMRL team during APEX-2, and by the University of Central Florida (Volpe Center) during APEX-3.

4.2   Pre-test Procedures

4.2.1   System Cleaning and Leak Checks

Initial cleaning of the sampling tunnels and lines was conducted by power washing the internal surfaces using a dilute solution of laboratory detergent in deionized (DI) water, followed by a DI water rise. After power washing, the equipment was allowed to air dry. All port plugs were then removed from the tunnels to clean out anything that may have fallen into the cavities. Each sampling line was then capped at both ends for transport to the field.

Following the setup of each sampling system in the field, and prior to any sample collection, positive pressure system leak checks were performed on the sampling tunnel inside the DEAL. These leak checks were done by placing a cap on the end of the tunnel downstream of the virtual impactor. The cap was fitted with a 6-mm union and connected to a cylinder of compressed air that was used to pressurize the tunnel. The barb fittings on the outlet side of all of the flow splitters were removed and replaced with caps, and all the other ports were sealed. A soap and water mixture was used to detect leaks until the tunnel could maintain a positive pressure after shutting off the air cylinder.

Positive pressure sample system leak checks were also performed on the sample line upstream of the virtual impactor and up to the probe inlet. In both cases, a section of the 5-cm sample tube that connected to the virtual impactor inside the trailer was removed. The section of sample tube was then replaced with a cap that was fitted with a 6-mm union and then plumbed to a cylinder of compressed air. A rubber stopper was used to seal the probe inlet. The system was pressurized to about 260 mm mercury (Hg) and the valve to the air cylinder was shut off. If the pressure dropped to zero, the system was re-pressurized and all the uncontaminated flange joints and other fittings were checked for leaks while pressure was maintained on the system. A final check was made to ensure that pressure could be maintained.

4.2.2 Sampling Media Preparation

All sampling media were prepared in NRMRL's Fine Particle Characterization Laboratory (FPCL) before leaving for the field. Prior to and after sampling, the quartz filters and ELPI substrates shown in Table 4-1 were stored in aluminum-foil lined, plastic petri dishes inside a laboratory freezer maintained at -50 °C. The Teflon filters were stored inside plastic petri dishes, also in the -50 °C freezer. The PUF plugs were stored and transported in glass jars with Teflon-lined screw caps. Silica gel tubes impregnated with DNPH for collection of gaseous carbonyl compounds and cleaned SUMMA canisters were prepared and supplied by the analytical subcontractor, Eastern Research Group (ERG). Carbonyl sampling tubes were stored in the freezer before and after sampling and SUMMA canisters were stored under ambient conditions before and after sampling.

Table 4-1.   General Analytical Plan

Type of Analysis	Sampling Media	Analytical Method
PM-2.5 mass	47-mm Teflon filters	Gravimetric
PM-2.5 mass	Aluminum foil ELPI substrates	Gravimetric
EC/OC	47-mm prefired quartz filters	NIOSH 5040 (NIOSH, 2003)
Semivolatile Organic Compounds	47-mm prefired quartz filters	Multisolvent extraction, GC/MS or thermal desorption, GC/MS
Semivolatile Organic Compounds	PUF plugs	Multisolvent extraction, GC/MS
Semivolatile Organic Compounds	Aluminum foil ELPI substrates[a]	Thermal desorption, GC/MS
Water-soluble ions	47-mm Teflon filters	Ion chromatography (IC)
Elemental composition	47-mm Teflon filters	XRF spectroscopy
Gas-phase organics	SUMMA canisters	GC/MS, GC/FID
Gas-phase carbonyl compounds	DNPH sampling cartridges	HPLC

a. Collected, but not analyzed, due to insufficient mass

During transport and in the field laboratory, all sampling media were stored in a small portable freezer operated at a nominal temperature of approximately -20 °C. This portable freezer was also used as the primary shipping container for the sampling media to and from the sampling site (the freezer was operated on generator power en route). Carbonyl sampling tubes were stored in the freezer before and after sampling; SUMMA canisters were stored under ambient conditions before and after sampling. Although field blank samples were collected and analyzed, no special measures were taken to determine sample degradation during storage and shipment.

Sampling system leak tests were performed prior to transporting the sampling systems to the test site to assure that the systems had been cleaned properly and were leak free. A post-test plume tunnel blank test was also performed by running the entire system with a HEPA filter installed on the inlet and then immediately recovering the samples. Monitoring data for tunnel blank samples were then processed exactly like samples collected from the emission source and used to determine if any hysteresis effects were present during sample collection requiring post-test correction of the experimental data.

4.2.3 Particle Instrument Calibration

The preparation and calibration of source sampling equipment and monitoring instrumentation is essential in maintaining data quality. The instrumentation / equipment arrived at the test site pre-calibrated according to the procedures contained in the approved QAPP. Calibrated measuring devices (e.g., thermocouples, pressure transmitters, and flow meters used with the time-integrated sampling equipment) and replacement / repair of parts were also provided. In addition, the quality control (QC) checks outlined in Section 4.3.2 were performed upon arrival and before each day of sampling.

The types of calibrations performed on the PM instruments are generally limited to air flow rate and similar parameters as outlined in the applicable instrument manual. The scheduled calibrations for each instrument and the associated acceptance criterion for each are shown in Table 4-2.

4.2.4 Gas Analyzer Calibration

Both the Model 1302 Photoacoustic Analyzer and the Model 3300A CO_2 Analyzer were calibrated prior to being deployed to the field and checked daily thereafter. Table 4-3 provides the scheduled calibrations for each analyzer.

Calibration of the photoacoustic instrument is a complicated procedure that requires at least 24 hours of continuous sampling to complete. Following the manufacturers recommendations, a single-point calibration was performed for each of the three optical filters before the sampling campaign. In the case of the photoacoustic analyzer, the QC checks performed during the sampling campaign are detailed in Section 4.3.3. In the case of the Milton-Roy CO_2 Analyzer used in APEX-2 and -3, a multipoint calibration was conducted before being deployed to the field.

4.3 Field Sampling Procedures

4.3.1 Continuous Analyzer Operation

A consistent and rigorous routine was followed to ensure proper operation of all the instruments during each sampling campaign. Miscellaneous operating procedures (MOP) were developed for each instrument type as outlined in the approved QAPP. These MOPs are included here by reference (EPA, 2004; EPA, 2005a; EPA, 2005b). The specific measurement protocols used during this aircraft engine study are summarized in Table 4-4.

The first thing to be done in the daily test start-up procedure was to power on the instruments to make sure all of the clocks were time synchronized. Some instruments, such as the TEOMs, require a stabilization period for their heaters and their flows to reach their set points. Most instruments were left "on" continuously throughout the campaign since testing occurred on a daily basis. While the instruments were stabilizing, their internal clocks, as well as the master clock in the multicomputer, were synchronized with an atomic clock supplied for this purpose.

4.3.2 Instrumental Quality Control Checks

To assure proper operation of the laboratory in the field, a number of QC checks were established as shown in Table 4-5. A daily checklist was prepared for each sampling campaign; this checklist included all of the QC measures shown in Table 4-5, as well as other important instrument operating parameters. The checklist was used as part of the laboratory start-up and shut-down procedures. These checklists were then stored in a ring binder for later reference.

Table 4-2. PM Instrument Calibration Schedule

Instrument	Calibration Performed	Nominal Frequency[a]	Acceptance Criterion
R & P Series 1105a and 1400a TEOM	Main air flow audit	Before/after sampling campaign	+ 10% of set-point
R & P Series 1105a and 1400a TEOM	Mass transducer verification	Before/after sampling campaign	$K^O = \pm 2.5\%$ of factory calibration
RPM-100 QCM	Sample flow calibration	Before/after sampling campaign	± 10% of indicated value
Dekati ELPI	Single point flow audit	Before/after sampling campaign	10 ± 0.1 L/min
TSI Model 3025a CPC[b]	"Aerosol" air flow calibration	Before/after sampling campaign	0.03 ± 0.003 L/min
TSI Model 3025a CPC[b]	"Condenser" air flow calibration	Before/after sampling campaign	0.3 ± 0.03 L/min
TSI Model 3025a CPC[b]	Inlet "high" air flow audit	Before/after sampling campaign	1.5 ± 0.15 L/min
TSI Model 3080 Classifier[c]	"Sheath Air" flow calibration	Before/after sampling campaign	± 10% of set-point
TSI Model 3080 Classifier[c]	"By-Pass Air" flow calibration	Before/after sampling campaign	± 10% of set-point
TSI Model 3080 Classifier[c]	"Impactor" air flow calibration	Before/after sampling campaign	± 10% of set-point
TSI Model 3090 EEPS	Single point flow audit	Before/after sampling campaign	± 10% of set-point
Aethalometer	Sample air flow calibration	Before/after sampling campaign	± 10% of set-point
PAS 2000 PAH analyzer	Sample air flow audit	Before/after sampling campaign	2 ± 0.2 L/min
Time-integrated sampler MFCs	Air flow calibration	Multi-point before sampling; single point audit after sampling	± 10% of indicated value
Sampling tunnel MFCs (plume and background)	Air flow calibration	Multi-point before sampling; single point audit after sampling	± 10% of indicated value

a. Frequency of calibration is dependent on whether instrument was new or had recently been returned from the factory after service. In either case, the factory calibration was used and no flow calibration was performed prior to use.

b. Both alone and as part of the TSI Model 3936 SMPS.

c. Part of Model 3936 SMPS and connected to Model 3025a CPC.

MFCs = Mass flow controllers

Table 4-3. Gas Analyzer Calibration Schedule

Gas Analyzer	Type of Calibration	Frequency	Acceptance Criteria
B&K Model 1302 Photoacoustic Analyzer (APEX-1)	Single point calibration using CO and CO_2 in nitrogen and hexane in zero air	Before/after sampling campaign	± 5.0% of certified value
	Zero and span check	Daily	± 5.0% of calibrated value
Milton-Roy Model 3300A (APEX-2 & -3)	Multipoint calibration using CO_2 in nitrogen	Before/after sampling campaign	± 5.0% of certified value
	Zero and span check	Daily	± 5.0% of calibrated value

Table 4-4.   Available MOPs for On-Line Analyzers

Parameter(s) Measured	Instrument Make/Model	MOP Number
PM-2.5 mass concentration	R&P Series 1105a Tapered Element Oscillating Microbalance (TEOM)	1414
PM-2.5 mass concentration	R&P Series 1400 Tapered Element Oscillating Microbalance (TEOM)	1415
PM-2.5 mass concentration	SEMTECH Model RPM-100 Quartz Crystal Microbalance (QCM)	1425
PM-2.5 number concentration	TSI Model 3025a Condensation Particle Counter (CPC)	1412
Particle size distribution	Dekati Electrical Low Pressure Impactor (ELPI)	1413
Particle size distribution	TSI Model 3934 Scanning Mobility Particle Sizer (SMPS) equipped w/ Model 3071 Differential Mobility Analyzer	1411
Particle size distribution	TSI Model 3936 Scanning Mobility Particle Sizer (SMPS) equipped w/ Model 3081 Differential Mobility Analyzer	1412
Particle size distribution	TSI Model 3090 Engine Exhaust Particle Sizer	1426
"Black"/"blue" carbon	Magee Model AE-2 Aethalometer	1416
Surface-bound PAHs	EcoChem Model PAS 2000	1417
Carbon dioxide, Hexane, CO	Operation of B&K 1302 Gas Analyzer for Tracer Gas Measurements	1418
Carbon dioxide, Hexane, CO	Performing Zero Check of the B&K 1302 Analyzer	1419
Carbon dioxide	Milton-Roy Model 3300A	1427

Table 4-5.   Field Sampling Equipment QC Checks

Experimental Parameter	Instrument	QC Check(s)	Frequency	Acceptance Criterion
Sample Extraction / Collection System	Background and plume sampling system	Leak check sampling tunnel and instrument sample lines	Before field sampling	No indicated leak
	Background and plume sampling system	Electrical ground continuity check	Upon initial setup	"Circuit" not open
	Background and plume sampling system	Check major/minor air flow rates with Roots Meter	Before sampling campaign	± 10% of required flow
	All continuous analyzers and samplers	Establish "tunnel blank" using HEPA filter on tunnel inlets	After sampling	Record and store files for later evaluation
DAS	All instruments with digital outputs	All software running and communicating with each instrument	Before each test	No indication of faults
	All instruments with analog outputs	DASYLAB software running and instruments responding	Before each test	No "dead" signal inputs
	Master computer	Set time using atomic clock	Daily	All computers time-synchronized
CO_2 concentration	Model 1302 photoacoustic analyzer or Model 3300A IR analyzer	Zero and span checks	Twice daily	See Table 4-3
Particle mass concentration	Time-integrated samplers	Leak check	Before each test	Per 40 CFR Part 86
	Model 1105a and 1400a TEOM	Install new filter and check frequency (1105a)	Daily	< 1 (10^6) Hz/Hz with filtering "off"
		Check red fault light on front panel	Before each test	Light "off"
		Check status indicator on display (1400a only)	Before each test	Status condition "OK"
	Model RPM 100	Check status indicators on front panel	Before each test	All lights off
		Change crystal and zero instrument using inlet filter	Before each test	Instrument output ~ 20-30 $\mu g/m^3$ baseline
Particle number concentration (alone and in conjunction with an SMPS)	Model 3025a CPC	Check indicator lights for optics, condenser, saturator, liquid level, aerosol/total flow	Before each test	All lights green
		Zero instrument using inlet air filter	Daily	< 0.5 particle/cm^3
		Perform side-by-side comparison in laboratory	Before sampling campaign	± 500 particles/cm^3

Experimental Parameter	Instrument	QC Check(s)	Frequency	Acceptance Criterion
Particle size distribution	Model 3936 SMPS (including CPC)	Check polydisperse aerosol, monodisperse aerosol, and sheath air flow set points	Before each test	± 10% of set point
		Check CPC reading without voltage scanning	Before each test	< 0.5 particle/cm^3
		Check inlet impactor and clean/grease, if necessary	Daily	Document
	Dekati ELPI	Check instrument flow on display	Before each test	100 mbar ± 10%
		Zero electrometers ("All Zero") twice and leave purge pump "on" until test begins	Before each test	Document
		Check charger voltage and current	Before each test	± 10% of set point
	Model 3090 EEPS	Check for error messages on front panel display	Before each test	No errors indicated
		Zero instrument using inlet air filter	Before each test	Particle counts below detection limit on front screen
Black carbon	Aethalometer	Perform optical test using optical test strip per operating manual	Before sampling campaign	± 5% in the "test ratio"
		Check status lights on display for faults	Before each test	All lights green
PAH concentration	Photoelectric Aerosol Sensor (PAS) 2000	Check lamp intensity on display	Before each test	100 ± 5%
		Check frequency on display	Before each test	< 15 kHz
		Check air flow rate on display	Before each test	2 ± 0.2 L/min
Plume temperature (APEX-2)	T-type thermocouples	Check each by holding hand around sensor to assure instrument is responding to temperature change	Daily	Reading on DAS goes up
Plume air velocity	Pitot tubes and dP cells	Blow into pitot inlet to assure instrument response	Daily	Reading as DAS goes up
Wind direction (APEX-2)	Wind vane on meteorological station	Orient vane to North	Before sampling	± 3°

4.3.3   Gas Analyzer QC Checks

During the APEX-1 sampling campaign, the photoacoustic analyzer response was checked with certified calibration gases prior to testing using a procedure that required a minimum of 2 hours for warm up and the response check. The procedure first required that the analyzer be allowed to sample air or nitrogen for a 30-minute warm-up period before checking its response to the certified calibrations gases. Next, the analyzer response was checked while sampling one or more of the three certified calibration gases. The calibration gas was introduced as close to the analyzer inlet as possible while maintaining the inlet conditions as if the instrument were collecting a sample from the plume tunnel or the bag sampler. The analyzer is very pressure sensitive, so introducing the calibration gas under any other conditions was not an option. The analyzer response was then checked while sampling from the Tedlar bag in the background bag sampler that had been prefilled with nitrogen or one of the certified calibration gases. All calibration checks that were performed were done prior to starting a test and are listed in Table 4-6.

Table 4-6.   Photoacoustic Analyzer Response Checks Performed during APEX-1

Date	Direct Response Checks	Bag Sampler Bias Response Checks
4/20/2004	CO_2, Hexane, CO	CO_2, Hexane, CO
4/22/2004	CO_2, Hexane, CO	CO_2, Hexane, CO
4/23/2004	CO_2	--
4/24/2004	CO_2, Hexane, CO	CO_2, Hexane, CO
4/25/2004	CO_2	CO_2
4/26/2004	CO_2	CO_2
4/27/2004	CO_2	CO_2
4/28/2004	--	--
4/29/2004	CO_2	CO_2
4/30/2004	CO_2, Hexane, CO	CO_2, Hexane, CO

Table 4-3 provides the intended calibration schedule for the photoacoustic analyzer used to measure these gases. As can be seen in Table 4-6, it was not possible to perform all necessary calibration checks of the analyzer due to logistical restrictions that limited access to the DEAL either before or after the tests.

In the case of the Milton-Roy CO_2 Analyzer during APEX-2 and -3, the instrument was zeroed and spanned before and after each day's testing. In addition, the analyzer was also used to analyze bag samples collected by the University of Central Florida (VOLPE) just prior to the post-test zero and span of the instrument.

4.3.4   Time-Integrated Sampling

Sample substrates (filters, canisters, PUF, DNPH-impregnated silica gel cartridges) were prepared in advance in accordance with the number and type of samples designated in the approved QAPP. During preparation of the sample collection media, a unique laboratory identification number was provided for each type of medium listed in Table 4-1. This number was recorded in a bound laboratory notebook and kept in the permanent record for the study. At the time of loading the media into each sampler prior to each speciated test, the laboratory identification number was entered on a special media data form.

These forms list the laboratory identification number and sampling system details. These forms, as well as the samples collected in the field, were transferred to EPA's FPCL or the Eastern Research Group (ERG) laboratories upon returning from the field.

4.3.5 Documentation

A field project notebook or special data forms were used to record operational parameters of the fine particulate sampling systems. Setup and calibration of the instruments was also documented in a bound laboratory notebook or stored electronically. All test details including QC checks, engine operation, environmental conditions, observations made during sampling, etc., were also recorded either in a bound laboratory notebook, on checklists, or on log sheets, as appropriate. All such paper records were kept in a ring binder and stored as part of the study archive. All electronic data were stored on the DAS as well as archived daily on compact disc (CD).

4.4 Laboratory Analysis Procedures

Samples collected for speciated test runs included the following:

- Gas-phase nonmethane volatile organic compounds (VOC) using SUMMA-polished stainless steel canisters (ERG);

- Gas-phase carbonyl compound emissions using DNPH-impregnated silica gel cartridges (ERG);

- Gas-phase semivolatile organic compounds (SVOC) using PUF plugs as well as quartz filters;

- PM mass and particle-phase elemental/organic carbon (EC/OC), particle-phase SVOCs, elemental composition, and water soluble ions using quartz and Teflon filters plus aluminum foil ELPI substrates (collected, but not analyzed due to insufficient mass); and

- PM continuous monitoring data and selected fixed gases over the specified monitoring range.

The chemical analysis of PM samples collected in the field involved the following laboratory operations:

- Preparation of samplers and sampling array components for field deployment, including decontamination of sampling media and weighing filters;

- Maintenance of suitable records covering receipt of samples in the laboratory to final sample disposition;

- Cold storage of samples from preparation to analysis and archiving samples for possible future reanalysis; and

- Data reduction, data archiving, and reporting results.

A summary of the analytical methods used is provided in Table 4-7.

Table 4-7.   Analytical Procedures for Chemical Characterization

Parameter Measured	Analytical Method	MOP/SOP Number
PM mass concentration	Gravimetric analysis	2503
EC/OC	Thermal-optical transmittance	2511
SVOC	Preparation of blank substrates	2501
SVOC	Cleaning of PUF plugs	2509B
SVOC	Solvent extraction of quartz filters	2504
SVOC	Solvent extraction of PUF plugs	2509
SVOC	Extract methylation	2505
SVOC	Silylation of methylated extracts	2506
SVOC	GC/MS analysis	2507
Elemental analysis of Teflon filters	X-ray fluorescence analysis	2515
Water soluble inorganic ions	Extraction of Teflon filters	2513
Water soluble inorganic ions	Ion chromatography analysis	2512
Gas phase air toxics and NMOCs	SUMMA canister cleaning	ERG-MOR-062
Gas phase air toxics and NMOCs	GC/MS and GC/FID analyses	ERG-MOR-005
Gas phase carbonyls	Extraction/analysis of DNPH media by HPLC	ERG-MOR-024
Gas phase carbonyls	High performance liquid chromatography analysis	ERG-MOR-082

MOP = Miscellaneous operating procedure

SOP = Standard operating procedure

HPLC = High performance liquid chromatography

4.5   Sample Preservation and Storage

After returning from the field, all sampling media (Table 4-1) except the SUMMA canisters were stored continuously at -20 °C or below until extraction and analysis. Samples maintained at this temperature in sealed containers with aluminum liners may be safely stored without degradation for long periods of time prior to analysis. Procedures for storing and transporting the samples from the point of collection to EPA's FPCL are described in the approved QAPP for each campaign.

4.6   Post-Test Laboratory Procedures

The samples of fine PM collected during testing by integrated sampling media were transported in a freezer (to minimize sample losses) to the laboratory for chemical analysis. Upon return to the laboratory, sampling information such as date for testing, test ID, test conditions, and sampling location of individual media were collected and recorded into the sample log system. The instruments and procedures for the analyses conducted in the laboratory are described in the following sub-sections.

4.6.1   PM Gravimetric Analysis

The PM gravimetric analysis was performed by weighing the individual Teflon filters before and after sampling on a Sartorius microbalance with a detection limit of ± 3 μg. The filter weighing was done in

accordance with a procedure described by Title 40 of the Code of Federal Regulations (40CFR), Part 53 (EPA, 2008) for ambient sampling. The method requires that the filter samples be conditioned before weighing, by exposure for a minimum of 24 hours to an environmental chamber that is maintained at 20 to 23 °C and a relative humidity of 30 to 40 percent. To eliminate possible electrical charge from accumulating on the surface, both sides of each Teflon filter were exposed to polonium strips for at least 20 seconds before placing on the balance.

Before sampling, the blank Teflon filters were tare weighed and placed in Analyslide dishes purchased from Pall Gelman with individual IDs. The weight change in the same filter after sampling was then used for PM mass emission calculation.

Note that the PM gravimetric analysis for the Teflon filters collected in APEX-2 was not conducted correctly. The laboratory personnel did not follow the procedure to eliminate the static electric charge on the Teflon filter before weighing, making all the tare weight results invalid. Therefore, no Teflon filter data are presented for APEX-2.

4.6.2 Elemental Analysis

After the post-test weighing, the Teflon filters were analyzed using x-ray fluorescence (XRF) to quantitatively determine elements in the PM collected on the filters. In the XRF analyses performed by NRMRL, each Teflon filter was covered with a 4.0-µm thick Prolene film that was attached using glue. The glue was only on the outer rim of the filter and did not interfere with the analysis. This film prevented the PM in the sample from falling off the filter under vacuum analytical conditions. A Philips 2404 wavelength-dispersive XRF spectrometer, running the UniQuant7 program, was used for the analysis. The program provided qualitative and quantitative information for elements greater than atomic number 9 present in the PM sample.

The metal analyses conducted by EPA's National Exposure Research Laboratory (NERL) were conducted using a commercially available Kevex EDX-771energy dispersive x-ray spectrometer (XRF) which utilizes secondary excitation from selectable targets or fluorescers. Teflo filters are easily handled because of the supporting ring. The sample is then placed in a custom designed commercially available two-part sample frame which snaps together holding the filter securely in place. Up to seven spectra are acquired for each sample depending on how many secondary excitation targets are selected. Elements with concentrations below three times the uncertainty are flagged with an asterisk (*) on the printed record. If the true elemental concentration is zero then the fitting procedure implies that negative and positive results are equally probable. Therefore, negative numbers may be reported.

Although the PM mass data from the Teflon filters were lost during APEX-2, the XRF analysis was performed to quantitatively determine elements in the PM collected on these filters.

4.6.3 Analysis of Water-Soluble Inorganic Ions

After non-destructive analyses (weighing and XRF), the Teflon membrane filter samples were further analyzed using a Dionex DX-120 Ion Chromatograph for isocratic ion analysis encompassing K^+, NH_4^+, Mg^{+2}, Ca^{+2}, NO_3^{-2}, SO_4^{-2}, NO_2^-, and Cl^- in the PM samples collected on the filters. During analysis, each individual Teflon filter was first water-extracted by placing it in a vial with 10 mL of HPLC-grade (low conductivity) water. The sample was sonicated for 30 minutes. The extract was then introduced at the head of the ion-exchange resin column of the IC. The ions in the sample were detected by the

conductivity detector and quantified through the use of external standards. The instrument reports the ions in concentrations in the water solution; the concentrations were then converted to the mass of ions on the filter by multiplying the concentrations by the volume of the extraction water (10 mL).

4.6.4   Analysis of Organic and Elemental Carbon

The quartz fiber filter samples were analyzed by a thermal / optical carbon analyzer provided by Sunset Laboratory, Inc., for determination of the OC/EC content before undergoing subsequent analysis for SVOCs. The OC and EC were analyzed based on NIOSH Method 5040 (NIOSH, 2003). The method is a thermal-optical method which proceeds in two stages. First, organic and carbonate carbon are evolved in a helium atmosphere as the temperature is stepped to about 850 °C. The evolved carbon is catalytically oxidized to CO_2 in a bed of granular manganese dioxide (MnO_2) and then reduced to methane in a nitrogen / firebrick methanator. Methane is subsequently quantified by a FID. In the second stage, the oven temperature is reduced, an oxygen-helium mix is introduced, and the temperature is stepped to about 940 °C. As oxygen enters the oven, pyrolytically-generated carbon is oxidized, and a concurrent increase in filter transmittance occurs. The point at which the filter transmittance reaches its initial value is defined as the split between OC and EC. Carbon evolved prior to the split is considered organic (including carbonate), and carbon volatilized after the split is considered elemental. The instrument has a lower detection limit (on the order of 0.2 μg/cm^2) filter for both OC and EC.

The new quartz fiber filters usually have an OC background of 2 to 5 μg/cm^2. To cleanse the purchased quartz filters of this background OC, they were pre-fired in a kiln at 550 °C for 12 hours before use. The clean quartz filters were stored in petri dishes lined with cleaned aluminum foil. Aluminum-foil liners were cut to cover the inside surfaces of the petri dishes so that the filters did not directly touch the dish when placed inside the lined dishes. The aluminum liners were also baked at 550 °C for 12 hours and then compressed into the petri dishes using a plug machined to fit snugly into the dishes. The filters and liners were handled with Teflon forceps to avoid any contamination.

Only a small portion of quartz filter sample was used for OC and EC analysis. To analyze OC and EC content, a 1.45-cm^2 sample was punched from the quartz filter with a tool specially provided by Sunset Lab. The punch from the filter was then placed on the sample holder of the instrument for analysis. The analyzer reports the OC and EC contents in μg per cm^2. Since the actual exposure area of quartz filter was 13.45 cm^2, the OC and EC masses on the filter were calculated by multiplying the reported OC or EC content (μg/cm^2) by 13.45 cm^2.

4.6.5   Analysis of Particle Phase Organic Compounds

The SVOCs in the PM collected on quartz filters were either solvent-extracted and quantified by GC/MS (APEX-2) or thermally desorbed and quantified by GC/MS (APEX-1 and -3). Each of these methods is described below. The thermal desorption (TD) methodology is more sensitive and provides lower detection limits. Table 4-8 details the operating conditions for the GC, MS, and TD components of these systems.

Table 4-8.   GC, MS and TD Operating Conditions

GC Operating Parameter	Solvent Extract GC/MS	TD/GC/MS
GC Column	60 meter HP5 (0.25 mm ID), .25 micron film	30 meter HP5 (0.25 mm ID), .25 micron film
Injection mode	Splitless	Solvent Vent until 0.1 minute using a PTV inlet
Injector Temperature	300 °C	(-100 °C initially, then ramped at 720 °C/min to 300 °C)
GC/MS Interface Temperature	300 °C	300 °C
Initial Oven Temperature	65 °C	65 °C
Initial Oven Hold Time	10 minutes	10 minutes
Oven Temperature Ramp Rate	10 °C /minute	10 °C /minute
Final Oven Temperature	300 °C	300 °C
Final Oven Temperature Hold Time	45 minutes	26.5 minutes
Carrier Gas	helium	helium
Carrier Gas Flow Rate	1.0 ml/minute	1.0 ml/minute
Split Vent Open Time	0.3 minutes	1.5 minutes
Split Vent Flow	50 ml/minute	50 ml/minute
Gas Saver Time	2 minutes	2 minutes
Gas Saver Flow	30 ml/minute	30 ml/minute
MS Operating Conditions	**Solvent Extract GC/MS**	**TD/GC/MS**
Acquisition Mode	Scan	Scan
Solvent Delay	12.95 minutes	6.0 minutes
Low Mass	50	50
High Mass	550	550
Sampling rate	2	2
MS Quad Temperature	150 °C	150 °C
MS Source Temperature	230 °C	230 °C
GERSTEL TDS 2 THERMAL DESORPTION OPERATING CONDITIONS		
Temperature Program	**Solvent Extract GC/MS**	**TD/GC/MS**
Initial Temperature	Not Applicable	25 °C
Initial Time	Not Applicable	0.0 minutes
Delay Time	Not Applicable	1.0 minutes
Ramp rate	Not Applicable	10°C/minute
End Temperature	Not Applicable	300 °C
Hold Time	Not Applicable	5 minutes
TDS Settings	**Solvent Extract GC/MS**	**TD/GC/MS**
Transfer Temperature	Not Applicable	300 °C
Standby Temperature	Not Applicable	50 °C
Vent Time	Not Applicable	1.0
Desorption Mode	Not Applicable	Splitless
Sample Mode	Not Applicable	Standard

4.6.5.1   Solvent Extraction Methodology

Sample Extraction and Concentration
Spiked filters were extracted in five successive 10-min sonication steps. The first two extractions were performed with hexane, and then followed by three extractions with a 2:1 mixture of benzene and isopropyl alcohol. Filters were sonicated for 10 min at ambient temperature. In addition, the second set of quartz filter samples (APEX-2) was extracted in a tertiary solvent mixture of the aforementioned solvents for three separate sonications for times of 40 minutes, 10 minutes and 10 minutes at ambient temperature. The water temperature in the sonicator was monitored and maintained below 32 °C.

Following sonication, the extract was transferred to the flask of the in-line transfer and filtration apparatus, which was thoroughly cleaned before extract transfer. The glass parts, including the quartz wool-packed Pasteur pipette, were solvent rinsed and then baked in aluminum foil at 550 °C for at least 12 hours. Teflon parts were cleaned by sonication with dichloromethane and then air dried. Following assembly, a vacuum system was used to rinse the in-line transfer apparatus with high-purity distilled benzene, which was pulled through the Teflon transfer line and quartz packed pipette, and into the flask. The rinse benzene was discarded, and the flask was then re-rinsed and then reinstalled. The extract was transferred to the flask by connecting a vacuum of approximately 10 cm of mercury via the corrugated Teflon tubing connected to the sidearm. All five extracts were collected together in the same flask.

The extract was then transferred and concentrated in the test tube of the Zymark concentrator instrument. In the instrument, extract was concentrated by passing a gentle stream of pure nitrogen over the surface of the liquid to evaporate the liquid to a total volume of 0.5 to 0.75 mL. The water bath temperature of the concentrator was kept between 35 and 40 °C. After concentration, the extract was quantitatively transferred to a clean amber vial and further concentrated by nitrogen blow-down to approximately 300 µL. Concentrated extract was stored in the vial with a Teflon-lined cap in a freezer until derivatization and analysis.

Extract Methylation
Each concentrated extract was split into two fractions: neutral and methylated. The sample was split by measuring the total volume of the concentrated extract with a thoroughly cleaned gas-tight volumetric syringe and then recording total volume. Half of the sample was returned to the original vial, and the other half was placed in a second cleaned vial and labeled for methylation.

Methylation was performed to yield methyl esters of fatty acids that would otherwise not be eluted from the GC column. The methylation was accomplished by adding approximately 10 µL of high-purity methanol and 100 µL of diazomethane solution to the methylation fraction of extract. After the reaction was complete, the methylated extract was reconcentrated by nitrogen blow-down to the original volume of aliquot before methylation. The methylated extract was stored in the freezer until analysis.

GC/MS Analysis
The extracts were analyzed with a Hewlett-Packard (HP) 6890/5973 GC/MS equipped with a thermal conductivity detector (TCD) (HP-G1530A), autoinjector (HP-G1513A), programmable temperature vaporizing (PTV) inlet, mass selective detection (MSD) interface, and flame ionization detector (FID; HP-G1526A). A 5MS GC column was used to separate the various organic compounds in the sample.

Ultrapurity helium was used as the carrier gas. The GC/MS operating conditions were summarized in Table 4-8 above.

Positive identification of a compound via GC/MS was confirmed when the GC retention time and mass spectrum of the unknown compound matched those of an authentic standard compound under identical instrumental conditions.

For quantification of the target marker compounds by GC/MS, known quantities of deuterated internal standards were included in each quantification standard and were spiked into each sample. Each compound that was quantified by GC/MS is referenced to one or more internal standards so that the response of each compound relative to the appropriate internal standard(s) is fixed with only minor variation in MS detector response, MS tune parameters, GC injection conditions, and GC column conditions.

4.6.5.2 Thermal Desorption Methodology

Sample Preparation
Prior to the TD/GC/MS analysis, each individual quartz filter sample was thawed in a laminar flow clean hood (~10 min), placed in a pre-conditioned (at 350 °C, for 12 hr) glass desorption tube (178 mm long, 6.0 mm outside diameter), and spiked with an appropriate deuterated internal standard suite. Small 0.6-cm^2 sample plugs were taken from each sample rather than attempting to place the entire 47-mm filter inside the desorption tube. Care was taken to use a suitably small sample size (determined by OC/EC analysis) so that the column capacity was not exceeded. The number of sample plugs taken was directly related to the OC/EC value.

Thermal Desorption
Once spiked with internal standard, the glass tube and sample were immediately inserted into a TD system (TDS2, Gerstel Inc., Baltimore, MD). The TD is directly interfaced to a GC/MS (Model 6890/5973; Hewlett Packard; Pal Alto, CA). The thermal extraction was achieved by ramping the TD oven temperature from 25 to 300 °C at 10 °C/min; pyrolytic degradation of organic compounds was minimized by avoiding temperatures greater than 300 °C. Helium (50 mL/min) was passed over the sample throughout the splitless mode desorption. This step facilitated analyte removal from the particle matrix. Desorbed target components passed through a short (152 mm), heated (300 °C) inert steel (SilcoSteel) transfer line and were trapped on a cryogenically cooled (-100 °C, liquid N_2) programmable temperature (PTV-Solvent Vent Mode) inlet system (CIS), also operating in splitless mode. The inlet liner was packed with a glass wool to enhance cryofocussing of the analytes.

GC/MS Analysis
Upon completion of the desorption step, the TD oven was rapidly cooled with liquid nitrogen to ambient temperature (25 °C). The CIS was then ballistically heated (720 °C/min) to 300 °C, to transfer the analytes in plug form to the ultra-low bleed 30-m DB 5 GC capillary column [5% diphenyl / 95% dimethyl siloxane copolymer stationary phase (30-m length, 0.25 μm film thickness, 0.25 mm i.d.)]. The GC oven temperature was held at 65 °C for 10 min, ramped at 10 °C/min to 300 °C, and then held constant for 41.5 min. The MS detector was operated in full scan mode (50-500 amu, 3 scans/sec). Enhanced Chemstation (V. B.01.00, Hewlett Packard) software was used to control the GC/MS and CIS and for data acquisition. Gerstel MASter (Version 1.76x5) software was used to monitor and control the TD operation.

Quantification of target PAHs, alkanes and hopanes was accomplished through comparison with a calibration database of response ratios formed from the certified authentic and isotopically labeled internal standard suites. The GC/MS and TD operating conditions were summarized in Table 4-8 above.

A three-level calibration range was used to quantify sample concentrations. Tube blanks were analyzed prior to every sample to determine the cleanliness of the TD system prior to each sample. Mid-level check standards were analyzed along with the samples to determine system accuracy throughout the analysis period.

4.6.5.3 Analysis of PUFs

Semivolatile organic compounds are partitioned between gas phase and particle phase. The phase distribution depends on the sampling conditions. As a result, there is no clearly defined cut between the gas phase and particle phase. The PUF plugs were installed directly downstream of the quartz filters for collecting the SVOCs that had not been caught by the quartz filters.

The PUF plugs used for the tests were purchased from a plastic product company and contained high backgrounds of various organic compounds. Although these PUF plugs were pre-extracted with solvents, they were still not clean enough to be used for chemical analysis. Therefore, the speciation results of these PUF samples are not reported here.

4.7 Analysis of Gas Phase Samples

4.7.1 Analysis of SUMMA Canister Samples

Analysis of the VOC canister samples was performed by ERG as outlined in SOPs ERG-MOR-005 and ERG-MOR-062. Gaseous samples collected in canisters were analyzed using a GC/MS and GC/FID. This approach is a combination (i.e., the ERG concurrent method) of EPA Method TO-15 (USEPA, 1999a) and EPA's "Technical Assistance Document for Sampling and Analysis of Ozone Precursors" (USEPA, 1998), used to resolve air toxics and hydrocarbon species. The concurrent methodology is performed by simultaneously analyzing an injected aliquot of pre-concentrated whole air sample by two separate techniques. The FID analysis provides a determination of speciated NMOCs (SNMOCs) and allows a calculation of total NMOC concentration. A list of target analytes and their detection limits for Methods TO-15 and CB-4 are provided in Tables B-1 and B-2, respectively, of Appendix B.

4.7.2 Analysis of DNPH-Impregnated Silica Gel Cartridges

Carbonyl samples collected on DNPH-impregnated silica gel cartridges were extracted and analyzed by ERG using a High Performance Liquid Chromatograph (HPLC) with an ultraviolet (UV) detector as outlined in SOPs ERG-MOR-024 and ERG-MOR-082. Analysis of DNPH-impregnated silica gel cartridge samples was performed using a modification of EPA Method TO-11A (USEPA, 1999b) to incorporate additional compounds and generate a value for total unidentified carbonyl species as well as total identified species. Target carbonyl compounds and their detection limits for this program are provided in Table C-1 of Appendix C.

4.8 Determination of Particle Line Losses

Particle losses inside the long sample extraction system between the 30-m probe inlet and the virtual impactor inside the DEAL were a major concern. Therefore, an experiment was designed to create a representative test aerosol that could be sampled using the exact configuration of the DEAL sample

extraction system that was used during each campaign. To determine the particle losses in the system, the particle size distributions and the number concentrations were measured and recorded using the TSI Model 3090 Engine EEPS at two locations: (1) at the probe inlet and (2) inside the DEAL immediately upstream of the virtual impactor. The sample extraction system configuration was set up exactly the same for APEX-2 as it was during APEX-1, except that there was an additional 3 m (10 ft) of tubing added to the configuration.

Note that the line loss experiment could not simulate the exact sampling conditions occurring in the engine exhaust plume during the three APEX campaigns. The experiment also was unable to reproduce any aerosol aging effects in the line which might have been present during emissions sampling.

4.8.1 Experimental Setup and Preparations

The site chosen for the particle loss experiment was the open burn facility that has been used to research emissions from controlled open burns and is located at the NRMRL research facility in RTP, North Carolina. The facility was already equipped with the capability to introduce and mix an exhaust stream and dilution air into an enclosure with inside dimensions of 3 m deep, 3.7 m wide, and 2.4 m high. Figure 4-1 shows the front wall of the open burn facility. The exhaust from the DEAL's Kenworth diesel tractor was introduced using a 7.6-m length of 15-cm flexible stainless steel tubing. One end of the flexible tubing was connected to the tractor exhaust stack and the other end inserted into an existing 20-cm duct through the top right corner of the front wall. The ambient dilution air was introduced with a blower mounted through the left side wall.

Figure 4-1.   Open burn facility.

The sample was extracted through the front wall under the window using a 3-m section of 5-cm tubing connected to a short section of 5-cm stainless steel flex tubing before attaching to a tee and then the sample probe. The EEPS was allowed to draw the necessary sample flow from a bulkhead fitting and a 6-mm tube installed in the branch of the tee immediately upstream of the probe inlet as shown in Figure 4-2.

Figure 4-2.   Line loss sample location at probe inlet.

A small service cart was used as a rolling work surface on which the EEPS and a laptop computer were positioned. A Dell Latitude D400 Laptop equipped with an Intel 1.4 GHz processor and 512 MB of RAM running Windows XP version 2002, SP2, was used to run the EEPS software and to record the data.

All of the 5-cm stainless steel tubing used was cleaned with soap and water then rinsed using a pressure washer prior to each experiment. To prepare the sampling tunnel inside the DEAL for the line loss test, all the small tubing connecting the equipment to the splitters was removed, and all the splitter outlets were plugged.

4.8.2   Sampling Procedures

For all APEX sampling configurations, positive pressure leak checks were performed by pressurizing the system to about 5 psig and allowing the system to maintain this pressure for 15 to 30 min. After establishing that the system was leak free, the diesel tractor was started allowing the exhaust to enter the open burn facility, and the blowers in the DEAL sample extraction system were turned on. The system as a whole was allowed a minimum of 30 min for a conditioning period before sampling was started at the first location. Six 10-min measurements were recorded at five locations as shown in Figure 4-3. Table 4-9 lists the sampling locations and the order in which they were sampled.

Using the EEPS data collected, a series of penetration curves was generated for the APEX-1, -2, and -3 sampling systems. These curves were used during data reduction to correct the PM results for particle losses in the sampling lines. Procedures for derivation of the penetration curves are outlined in Section 5.5 below.
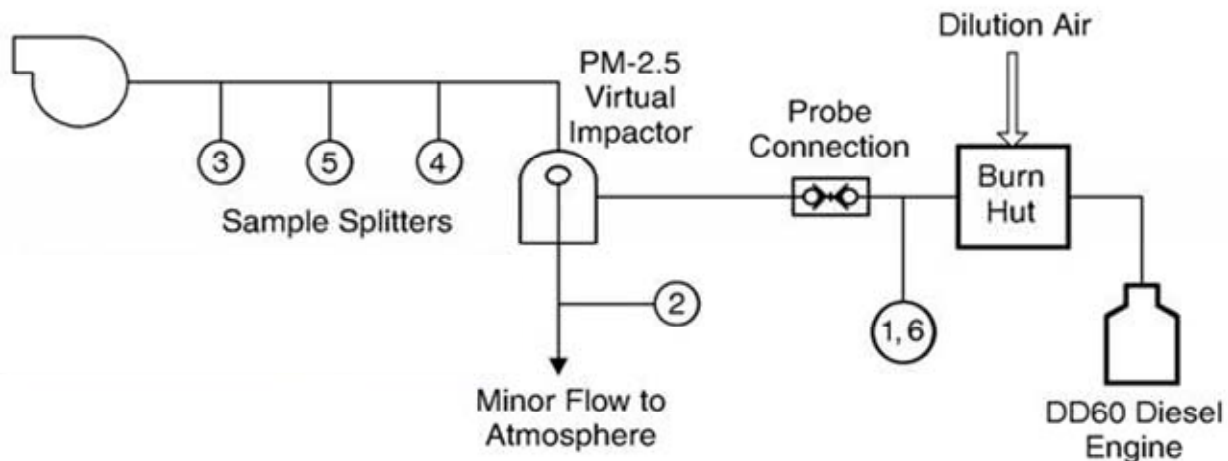
Figure 4-3.   Sampling locations for particle line loss experiments.

Note: the numbers 1-6 indicate EEPS sampling locations.

Table 4-9.   Particle Line Loss Sampling Location Descriptions and Sequence

Location	Location Description	Sampling Sequence
Probe Inlet	Point where exhaust was introduced to the system	1, 6
Splitter # 1	First Splitter in the DEAL sampling system downstream of the virtual impactor major flow outlet	4
Splitter # 2	Middle Splitter in the DEAL sampling tunnel	5
Splitter # 3	Splitter farthest downstream in the DEAL sampling tunnel	3
Virtual Impactor Exit - Minor Flow	Outlet of the minor flow from the virtual impactor	2

This page intentionally left blank.

5.   Data Analysis

The post-test data analysis included the following:

- a series of data reduction procedures;

- calculation of count and mass emission indices for PM, gas-phase and particle-phase compounds;

- determination of particle size distribution;

- calculation of Data Quality Indicator (DQI) goals; and

- calculation of a correction factor for particle losses in sampling lines.

A discussion of the performance of each of these steps is provided below.

5.1   Data Reduction Procedures

The data reduction procedures were applied to the determination of total PM-2.5 mass concentration, EC/OC, and SVOC data. Each procedure is described in the following subsections.

5.1.1   Total PM-2.5 Mass Concentration

Total PM-2.5 mass concentration in jet engine exhaust was measured directly by the TEOM, QCM, and 47-mm Teflon filters. The TEOM and QCM give a continuous measure of PM mass concentration, whereas the Teflon filter provides total time-integrated PM mass concentration.

The TEOM and QCM data processing was straightforward. The average total PM-2.5 mass concentration was calculated by averaging the readings over the sampling time specified for either an individual power condition or the entire test. For the TEOM, there is a set of readings corresponding to each of three times (10, 30, and 60 s). Only the 60-s average data were used.

The PM-2.5 mass collected on a Teflon filter substrate during sampling was determined by weighing the filter before and after sampling. The total PM-2.5 mass concentration is obtained by dividing the PM mass collected on the filter by the total air volume pulled through the filter during sampling. The flow rate of sample gas through the Teflon filters is measured by a mass flow meter with the total volume of sample gas between two consecutive readings calculated by

$$V_i = Q_i \left(t_{i+1} - t_i \right)$$
(5-1)

where

V_i = flow volume over the time between t_i and t_{i+1} (L) and
Q_i = flow rate reading at $t = t_i$ (standard L/min—sLpm).

The total flow volume is then the sum of the time-interval flow volumes over the entire sampling time. Thus, the total PM-2.5 mass concentration is given by

$$C_{PM2.5} = \frac{M_{PM2.5}(1000)}{\sum V_i}$$ (5-2)

where

$C_{PM2.5}$ = total PM-2.5 mass concentration (mg/m^3) and
$M_{PM2.5}$ = PM-2.5 mass collected on the filter (mg).

A background correction is made by subtracting the PM-2.5 concentration determined from the background sampling system from the total PM-2.5 mass concentration obtained above.

5.1.2 *Elemental Carbon/Organic Carbon*

The thermal-optical EC/OC analyzer measures the masses of EC and OC collected on quartz fiber filters in units of μg/cm^2. Thus, the total EC and OC concentrations for each quartz filter are calculated by multiplying the EC or OC reading by the exposed filter area, and then dividing by the total airflow volume passing through the filter during the sampling period as

$$C_{EC} = \frac{M_{EC} A_F}{Q_{inst} t}$$ (5-3)

$$C_{OC} = \frac{M_{OC} A_F}{Q_{inst} t}$$ (5-4)

where

C_{EC} = mass concentration of EC (μg/L),
C_{OC} = mass concentration of OC (μg/L),
M_{EC} = mass of EC per unit area of filter (μg/cm^2),
M_{OC} = mass of OC per unit area of filter (μg/cm^2),
A_F = exposed filter area (cm^2),
Q_{inst} = sample flow rate through the filter (sLpm), and
t = sampling time (min).

The mass ratio of EC to total PM-2.5 (R_{EC}) and the ratio of OC to total PM-2.5 (R_{OC}) are

$$R_{EC} = \left(\frac{C_{EC}}{C_{PM2.5}}\right) 100\%$$ (5-5)

$$R_{OC} = \left(\frac{C_{OC}}{C_{PM2.5}}\right) 100\%$$ (5-6)

and the percentage of OC ($R_{OC/TC}$) in the total carbon (TC) is

$$R_{OC/TC} = \left(\frac{M_{OC}}{M_{EC} + M_{OC}} \right) 100\%$$

(5-7)

where $C_{PM2.5}$ is the total PM-2.5 mass concentration in µg/L.

5.1.3 Semivolatile Organics

For APEX-2, the particulate and gas phase SVOCs collected on quartz filters and PUF plugs were extracted with solvents and concentrated. The concentrated extracts were then analyzed by GC/MS. Before analyzing the samples, calibration was conducted using deuterated internal standards and quantification standards to determine the response factor for each compound. The response factor for a specific compound is calculated from the calibration by

$$RF_x = \frac{Aq_x Cd_x}{Ad_x Cq_x}$$

(5-8)

where

RF_x = response factor of compound x,

Aq_x = area counts of compound x obtained from calibration chromatogram,

Ad_x = area counts for appropriate deuterated internal standard obtained from calibration chromatogram,

Cd_x = concentration of appropriate deuterated internal standard (ng/µL), and

Cq_x = concentration of compound x in quantification standards (ng/µL).

With known response factors, the mass of compound x in the sample extract is calculated from the analytical results by

$$M_x = \frac{Ae_x Cd_x Vd}{Ad_x RF_x}$$

(5-9)

where

M_x = mass of compound x in the sample extract (ηg),

Ae_x = area counts of compound x for the extract obtained from analytical chromatogram,

Ad_x = area counts of the appropriate deuterated internal standard obtained from analytical chromatogram, and

Vd = volume of deuterated internal standards spiked onto the sample (µL)

Once the mass of each compound in the sample is determined from the GC/MS analysis, the mass concentration of compound x in the sample flow is given by

$$C_x = \frac{M_x}{Q_{inst} t}$$

(5-10)

where C_x is the species mass concentration collected by the filter (ng/L).

5.2 Calculation of Count and Mass Emission Indices for PM, Gas-Phase and Particle-Phase Compounds

5.2.1 PM Calculations

The PM-2.5 number emission index (*EI*), expressed in number of particles per kg of fuel burnt, EI_N, was calculated from the background-corrected particle number and carbon dioxide concentrations measured by assuming that the amount of fuel burned can be approximated from the amount of CO_2 produced due to the fuel burning. The equation derivation for EI_N calculation is shown as below.

$$EI_N(particles/kg) = \frac{C_N\left(\frac{particles}{cm^3}\right) \cdot \frac{10^6 cm^3}{m^3} \cdot Q\left(\frac{m^3}{hr}\right)}{\frac{C_{CO2}(\%)}{100} \cdot Q\left(\frac{m^3}{hr}\right) \cdot \frac{kmol}{24.06m^3} \cdot \frac{12.01kg}{kmol} \cdot \frac{1}{f_C}}$$

$$= \frac{200.3 \cdot 10^6 \cdot C_N \cdot f_C}{C_{CO2}} \tag{5-11}$$

where

C_N = background corrected particle number concentration (particles/cm^3),

C_{CO2} = background corrected CO_2 concentration at sampling point C_N (%),

f_C = fraction of carbon in fuel (g/g fuel),

24.06 = volume (m^3) per kg-mol of ideal gas at 20 °C,

12.01 = molecular weight of carbon (kg/kmol),

Q = plume flow rate (m^3/hr), and

200.3 = a combined constant for unit volume and weight corrections

The PM-2.5 mass emission index expressed in particulate mass per kg of fuel burnt, EI_M, was calculated from the loss and background corrected particle mass concentration using

$$EI_M(mg/kg) = \frac{200.3 \cdot C_{PM2.5} \cdot f_C}{C_{CO2}} \tag{5-12}$$

where

$C_{PM2.5}$ = background corrected particle mass concentration (mg/m^3) and

C_{CO2} = background corrected CO_2 concentration at sampling point C_M (%).

The PM-2.5 mass emission rate expressed in mg of particulate mass per second, ER_M, was calculated by multiplying the emission index by the corresponding fuel flow rate using

$$ER_M(mg/\sec) = EI_M \cdot \frac{FF}{3600} \tag{5-13}$$

where

EI_M = PM emission index (mg/kg) and

FF = fuel flow rate (kg/hour) as provided by the aircraft operator.

5.2.2 Gas-Phase Calculations

With one modification, Equation 5-12 could be used to perform the calculations for the gas-phase compounds determined from the time-integrated sampling and consequent GC/MS analyses. The term $C_{PM2.5}$ was replaced with the term C_{gx}, which is the mass concentration of each organic gas-phase compound (Equation 5-14). This substitution allowed the emission indices for individual particulate organic compounds to be calculated.

$$EI_M \, (mg/kg) = \frac{200.3 \cdot C_{gx} \cdot f_C}{C_{CO2}} \tag{5-14}$$

where

C_{gx} = mass concentration of each individual organic gas-phase compound (mg/m^3)

C_{CO2} = background corrected CO_2 concentration at sampling point C_M (%).

5.2.3 Particle-Phase Calculations

With one modification, Equation 5-12 could also be used to perform the calculations for the organic and inorganic particle-phase elements determined from the integrated sampling and consequent analyses (OC/EC analyzer for OC/EC, solvent extraction and TD for organics, and XRF for inorganics). The term $C_{PM2.5}$ was replaced with the term C_{sx}, which is the mass concentration of each particle-phase element (Equation 5-15). This substitution allowed the emission indices for individual organic or inorganic particle-phase elements to be calculated.

$$EI_M \, (mg/kg) = \frac{200.3 \cdot C_{sx} \cdot f_C}{C_{CO2}} \tag{5-15}$$

where

C_{sx} = mass concentration of each individual particle-phase element (mg/m^3)

C_{CO2} = background corrected CO_2 concentration at sampling point C_M (%).

5.3 Determination of Particle Size Distribution

The Nano-SMPS, long SMPS, EEPS, and ELPI were used to determine the particle size distributions under various operating conditions. Both the ELPI and long SMPS were found not to be entirely suitable for measurement of the jet engine particle size distribution due to their instrument size ranges (0.03 to 10 µm for ELPI and 0.01 to 0.4 µm for the long SMPS). Only the Nano-SMPS and EEPS showed the capability of covering the entire particle size range of jet engine PM (primarily between 3 and 100 nm). To obtain an average particle size distribution for an engine power setting, an average was calculated for the dN/dlogDp data for each size bin recorded under the same power level. The average dN/dlogDp data for each power setting was then smoothed over the entire size range by using the "supsmooth" function provided by MathCad 2001 Professional. Once the particle size distribution was determined, the total particle number concentration and particle number geometric mean diameter were calculated for the test using Equations 5-16 and 5-17, respectively.

$$N_T = \sum_{i=1}^{K} \left(dN/d \log Dp \right)_i \times \left(d \log D_P \right)_i \tag{5-16}$$

$$GMD = 10^{\left(\frac{\sum_{i=1}^{K} (dN/d \log Dp)_i \times (d \log Dp)_i \times \log Dp_i}{N_T} \right)} \tag{5-17}$$

where

N_T = total particle number concentration (particles/cm^3),

D_P = particle size (nm),

K = number of size bins, and

GMD = geometric number mean diameter (nm).

In order to determine the particle mass emission index from the measurement of particle number concentrations, Equation 5-18 was used to convert the particle loss and background corrected *dN/dlogDp* into the *dM/dlogDp* for the *i*[th] size bin.

$$(dM / d \log Dp_i) = 0.5236 \times 10^{12} \cdot (dN / d \log Dp_i) \cdot Dp_i^{3} \tag{5-18}$$

where

Dp_i = particle size of the *i*[th] size bin.

The particle mass concentration was then calculated using

$$C_M = \sum_{i=1}^{K} \left[(dM / d \log Dp_i) \cdot (d \log Dp_i) \right]_i \tag{5-19}$$

5.4 Calculation of Data Quality Indicator Goals

The DQI goals are specific criteria used to quantify how well the collected data meet the appropriate data quality objectives. The definitions and calculations for accuracy as expressed in terms of bias, precision, and completeness are described below.

Precision—Precision is the agreement between a set of replicate measurements without assumption of knowledge of the true value. Precision is expressed as percent relative standard deviation (RSD) and can be determined using

$$RSD = \left(\frac{Standard\ Deviation\ of\ Replicate\ Measurements}{Average\ of\ Replicate\ Measurements} \right) 100 \tag{5-20}$$

Bias—The degree of agreement between an average measurement and an accepted reference or true value, expressed as a percentage of the reference or true value. Accuracy DQIs must include systematic errors associated with the sampling process.

$$\% \; Bias = \left[\frac{\left(Averaged \; Measured \; Values\right) - \left(Known \; Value\right)}{Known \; Value} \right] 100 \qquad (5\text{-}21)$$

Completeness—Completeness expresses the percent of acceptable data collected, using

$$\%Completeness = \left(\frac{Amount \; of \; Valid \; Data \; Collected}{Intended \; Collectable \; Data} \right) 100 \qquad (5\text{-}22)$$

5.5 Particle Loss Correction

During the APEX testing, the gas and particulate samples emitted from the jet engines were transported through a long sampling line to the DEAL. The sampling line length, number of bends, etc., were slightly different for each of the three APEX sampling campaigns with the samples subjected to particle losses due to diffusion and inertial impaction during transport. In addition, particle losses could also occur in the DEAL sampling tunnel, though the losses were expected to be much less in comparison to those in the sampling lines. A post-test experiment was conducted to determine the total particle losses for samples travelling from the tip of the sampling probe to the splitters in the DEAL sampling tunnel. By measuring the particle number concentrations at the two locations for each particle size channel, the particle penetration for that particle size was calculated using

$$P(dp) = \frac{C_{N,splitter}(dp)}{C_{N,probe}(dp)} \qquad (5\text{-}23)$$

where

$P(dp)$ = penetration coefficient for particle size dp (dimensionless),

$C_{N,splitter}(dp)$ = particle number concentration for particle size dp measured by EEPS at splitter, particles/cm^3, and

$C_{N,probe}(dp)$ = particle number concentration for particle size dp measured by EEPS at probe, particles/cm^3.

Figure 5-1 shows the particle penetration as a function of particle size for each sample line during APEX-1, -2, and -3. The particle penetration coefficient results were then correlated to particle size. The equations of particle penetration for each of the different sampling lines used in the tests are presented Table 5-1.
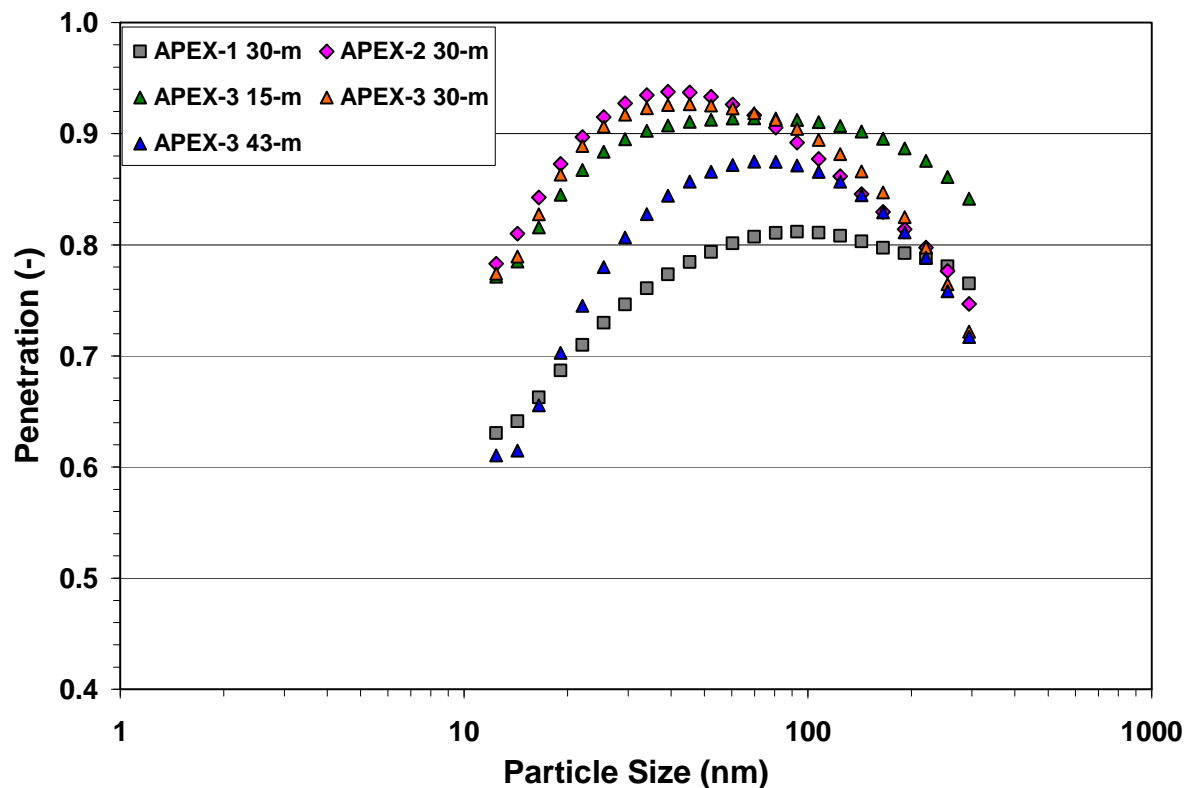
Figure 5-1.   Particle loss experimental results as a function of particle size.

Table 5-1.   Particle Loss Penetration Equations Obtained from the EEPS Measurements[a]

Test	Line	Penetration Equation	R2
APEX-1	30-m	P (-) = 0.0049(logDp)^3 − 0.2518(logDp)^2 + 0.9531(logDp) − 0.1267	0.996
APEX-2	30-m	P (-) = 0.2148(logDp)^3 − 0.7299(logDp)^2 + 3.1391(logDp) − 1.1563	0.997
APEX-3	15-m	P (-) = 0.093(logDp)^3 − 0.7299(logDp)^2 + 1.7312(logDp) − 0.3735	0.984
APEX-3	30-m	P (-) = 0.0612(logDp)^3 − 0.7022(logDp)^2 + 1.8634(logDp) − 0.5062	0.986
APEX-3	43-m	P (-) = 0.0069(logDp)^3 − 0.4979(logDp)^2 + 1.8032(logDp) − 0.7975	0.990

a. Unit of particle diameter (Dp) is nm in the equations. Caution must be taken when the equations are used for particle sizes smaller than 10 nm or greater than 100 nm.

With the penetration equations in Table 5-1, the particle losses were corrected for the plume particle number and mass concentrations measured by various particle instruments. For example, if $C_{N,\ measured}(dp)$ was the particle number concentration measured by an instrument for particle size, dp, the corrected concentration, $C_{N,\ corrected}(dp)$ is

$$C_{N,corrected}(dp) = \frac{C_{N,measured}(dp)}{P(dp)}$$ (5-24)

Note that the penetration coefficient data, shown in Figure 5-1, decreased as particle size increased when the particle size was greater than 30 to 100 nm. This observation is not consistent with the prediction of theoretical particle loss analysis, which predicts that particle losses would not be significantly affected by particle size until the particle size was greater than 800 to 1000 nm. Considering the uncertainty in the particle loss experimental results, the PM emission results in this report are discussed both with and without particle loss correction. NASA has funded research to develop an improved empirical technique to determine particle losses in aircraft engine sampling systems (Liscinsky and Hollick, 2008). If an improved line loss correction scheme becomes available in the future, the experimental data provided in this report may need to be reprocessed to improve data quality.

This page intentionally left blank.

6. Test Matrix, Fuel Composition, and Engine Operation

6.1 Test Matrix and Run Times

A total of 24 tests were conducted during the three APEX campaigns. The CFM56-2C1 jet engine was used throughout the nine APEX-1 tests to investigate the effects of fuel composition on emissions at various power settings. Three types of fuel were used: a base fuel (JP-8, or Jet-A1), a high-sulfur fuel (JP-8 doped to approximately four times the sulfur content of the base fuel), and a higher-aromatic JP-8.

During APEX-2 and -3, the fuel composition was not varied as an experimental parameter. During these tests, each engine was run with the Jet-A fuel normally used during commercial operations. The same engine family used during APEX-1, the CFM56, was also used for all four APEX-2 tests and two of the eleven APEX-3 tests. These tests were used to provide further characterization of the fine particulate emissions from these widely-used jet engines.

During APEX-3, five other jet engines of various sizes were studied. These engines included a General Electric CJ610-8ATJ turbojet (in use on a Lear 25), Rolls Royce AE3007A1E and AE3007A1/1 turbofans (in use on an Embraer ERJ145), a Pratt and Whitney PW4158 turbofan (in use on the A300), and a Rolls Royce RB211-535E4-B turbofan (in use on a B757).

Table 6-1 is the APEX test matrix, which summarizes the details of the 24 tests conducted during APEX-1, -2 and -3, plus the aborted end-of-runway sampling during APEX-3 and the three tunnel blank runs conducted at the end of each campaign to evaluate potential sampling artifacts. The test number designation and run time used for integrated sampling are followed by the aircraft and engine type used in each test. The fuel type is indicated for APEX-1; fleet fuel was used for all other tests. In addition, the individual power settings (percent rated thrust) used during each test are indicated. The individual power settings are approximate values.

6.2 Fuel Type and Composition

Table 6-2 summarizes the composition of the fuels used during the APEX campaigns. Three types of jet fuels were used in the APEX-1 campaign: a base fuel, a higher sulfur fuel, and a higher aromatic fuel. The base fuel, which was a typical JP-8 (Jet-A1) jet engine fuel, was used for EPA-1 and EPA-2, and NASA-1 and -1a. A high-sulfur fuel, with approximately four times the sulfur content of the base fuel, was used for EPA-3 and NASA-2 and -3. A higher aromatic fuel, with approximately 25 percent more aromatics than the base or high-sulfur fuels, was used for NASA-4 and -5.

During APEX-2 and -3, the normal fleet fuels were used for all engines tested. Table 6-2 illustrates that although the sulfur content varied in these fuels (ranging from 132 to 700), these fuels were generally similar to the base fuel used in APEX-1.

Table 6-1.   APEX Test Matrix

APEX	Test No.	Run Time (min)	Aircraft	Engine[a]	Fuel Type	4	5.5	7	8.4	15	30	40	45	60	65	70	76	80	85	100
1	EPA-1	188.53	DC-8	CFM56-2C1	Base			X			X								X	X
	EPA-2	150.7						X			X								X	X
	NASA-1	197.03				X	X	X		X	X	X			X				X	X
	NASA-1a	112.3				X								X	X	X			X	X
	EPA-3	149.58			High Sulfur		X				X							X	X	X
	NASA-2	116.98				X	X	X		X	X	X		X	X	X			X	X
	NASA-3	143.65				X	X	X		X	X	X		X	X	X			X	X
	NASA-4	154.67			High Aromatic	X	X	X		X	X	X		X	X	X			X	X
	NASA-5	155.5				X	X	X		X	X	X		X	X	X			X	X
	Tunnel Blank	N/A	N/A	N/A	N/A															
2	T1	123.8	B737-700	CFM56-7B24	Fleet Fuel	X	X			X	X				X				X	
	T4	142.6				X	X			X	X				X				X	
	T2	135.8	B737-300	CFM56-3B1		X	X			X	X				X				X	
	T3	150.5		CFM56-3B2		X	X			X	X				X				X	
	Tunnel Blank	N/A	N/A	N/A	N/A															
3	T1	115.6	B737-300	CFM56-3B1	Fleet Fuel	X	X			X	X		X		X				X	X
	T11	63.7				X	X			X	X		X		X				X	X
	T2	171.4	NASA Lear	CJ610-8ATJ	Fleet Fuel		X			X	X		X		X				X	X
	T5	146.1	Model 25	(turbojet)			X			X	X		X		X				X	X
	T3	131.48	Embraer	AE3007A1E	Fleet Fuel				X	X	X		X		X				X	X
	T4	112.43	ERJ145						X	X	X		X		X				X	X
	T10	96.75		AE3007A1/1					X	X	X		X		X				X	X
	T6	147.58	A300	P&W 4158	Fleet Fuel		X			X	X		X		X			X		
	T7	76.39					X			X	X		X		X			X		
	T8	103.5	B757	RB211-535E4-B	Fleet Fuel	X	X			X	X		X		X				X	
	T9	122.43				X	X			X	X		X		X				X	X
	End-of-runway (aborted)	N/A	N/A	N/A	N/A															
	Tunnel Blank	N/A	N/A	N/A	N/A															

a. All engines were turbofan except as noted.

Table 6-2.   Composition of Fuel Used in APEX Campaigns

Campaign APEX	Test No.	Aircraft	Engine[a]	Fuel Type	C (fraction)	H (fraction)	S (ppm)	Aromatics (vol%)	Density (mg/cm³)	Heating Value (MJ/kg)
1	EPA-1	DC-8	CFM56-2C1	Base	0.8627	0.1369	409	17.5	0.8199	43.2
	EPA-2									
	NASA-1									
	NASA-1a									
	EPA-3			High Sulfur	0.8617	0.1367	1639	17.3	0.8194	43.3
	NASA-2									
	NASA-3									
	NASA-4			High Aromatic	0.8624	0.1370	553	21.8	0.8114	43.3
	NASA-5									
2	T1	B373-700	CFM56-7B24	Fleet Fuel	0.8569	0.1430	132	19.7	0.8254	NA
	T4				0.8525	0.1470	412	20.3	0.8080	NA
	T2	B737-300	CFM56-3B1		0.8587	0.1411	206	20.4	0.8202	NA
	T3		CFM56-3B2		0.8522	0.1474	352	22.7	0.8169	NA
3	T1	B737-300	CFM56-3B1	Fleet Fuel	0.8613	0.1380	700	17.4	0.8044	43.2
	T11				0.8616	0.1380	400	16.8	0.8109	43.2
	T2	NASA Lear	CJ610-8ATJ	Fleet Fuel	0.8599	0.1401	0[b]	14.5	0.7990	43.3
	T5	Model 25	(turbojet)							
	T3	Embraer	AE3007A1E	Fleet Fuel	0.8637	0.1360	300	19.9	0.8105	43.1
	T4	ERJ145								
	T10		AE3007A1/1		0.8638	0.1360	200	18.6	0.8142	43.1
	T6	A300	P&W 4158	Fleet Fuel	0.8624	0.1370	600	16.5	0.8048	43.2
	T7									
	T8	B757	RB211-535E4-B	Fleet Fuel	0.8637	0.1360	300	19.4	0.8096	43.1
	T9				0.8637	0.1360	300	19.1	0.8090	43.1

a. All engines are turbofan except as noted.

b. Questionable value as reported by NASA. Actual sulfur content should be similar to other APEX-3 tests.

One item of note here is the wide variation in sulfur content of the standard fleet fuels used during the three tests on the same engine model, the CFM563B1. During APEX-2, Test 2, the fuel sulfur content was 206 ppm, whereas for the two APEX-3 tests, the sulfur content was 700 ppm (Test 1) and 400 ppm (Test 11), respectively. This wide variation in fuel sulfur is expected to have a significant effect on the amount and size of the PM generated by the engine due to gas-to-particle conversion occurring in the exhaust. This factor should be kept in mind when comparing test results for these engines.

6.3 Engine Power Settings

In all the APEX tests, the emissions were monitored and studied at different steady-state engine power settings. These steady-state engine power settings are discussed below for each measurement campaign.

6.3.1 APEX-1 Engine Test Cycles

During APEX-1, two engine testing matrices were used for each fuel. The "EPA" test matrix followed the ICAO-defined landing and take-off (LTO) cycle to simulate aircraft emissions at an airport. This matrix consisted of approximately four repetitions of the following power settings: 26 min at idle (7%), 0.7 min at takeoff (100%), 2.2 min at climb (85%), and 4 min at approach (30%). Figure 6-1 presents a graph of the basic jet engine operating cycle that was proposed by NRMRL for the APEX-1 tests. NRMRL's primary emphasis was speciated measurements of the jet engine emissions with the engine operated in repetitive cycles encompassing ICAO LTO power (thrust) settings. These power levels are identical to those used during engine certification, except that the EPA sampling included engine start/stop, transitions between throttle settings, and bleed air extracted from the engine. Note also that large changes in emissions occurred during engine start/stop and power transitions. These large changes in emissions were difficult to characterize due to their short duration.
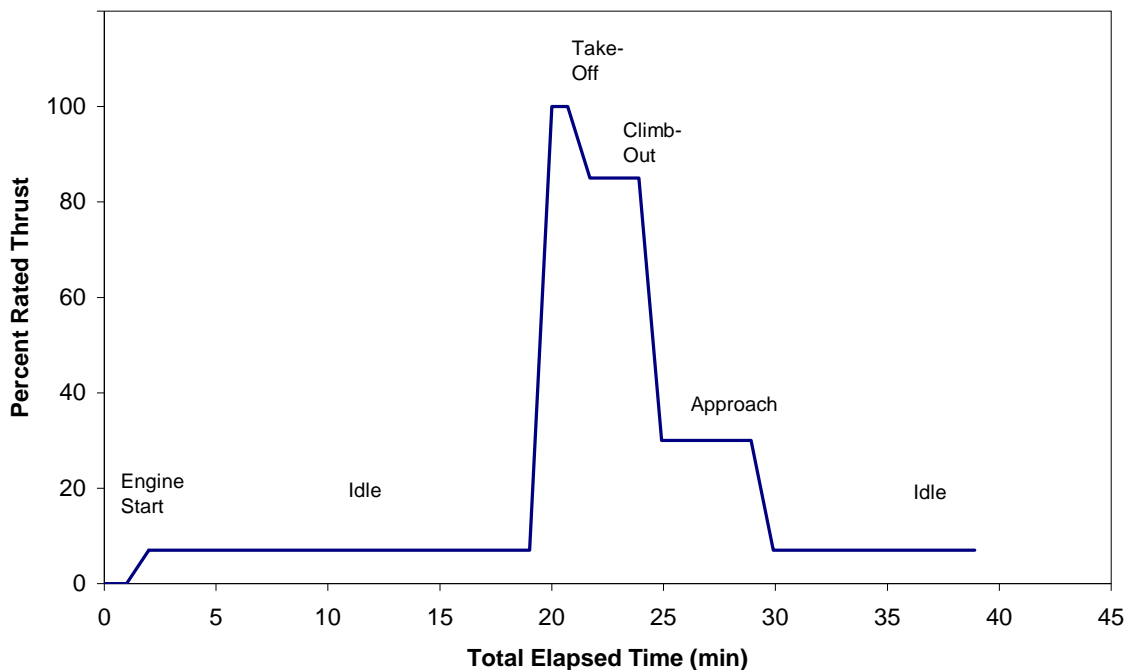
Figure 6-1.   Proposed APEX-1 EPA test cycle.

The "NASA" test matrix was designed to investigate the effects of engine operating parameters on particle emissions. The NASA test matrix included power settings of 4, 5.5, 7, 15, 30, 40, 60, 65, 70, 85 and 100 percent (restricted to about 93%, but considered to be 100%) of rated thrust. Except for the 100 percent thrust level, where run-time was limited to 1.5 min, approximately 10 min were provided at each power setting to allow for samples to be adequately analyzed.

Table 6-1 previously indicated the individual power settings used in each of the APEX-1 tests. Figures 6-2, (EPA tests) and 6-3 and 6-4 (NASA tests) graphically illustrate the sequence of these power settings for each test. Note that the EPA and NASA sampling systems were all time-synchronized, so that the timestamps associated with the different power settings could be related to the instrument data.

For EPA-1, Figure 6-2 shows that the test was burdened with disruptions before 14:30, resulting in several partial cycles. The test was started at the idle (7%), take-off (100%), and climb-out (85%) power settings, followed by a shut-down period from about 12:29 to 13:15 necessitated by a cooling water line leak associated with the 10-m probe. Shortly after the second cycle started, a shifting tailwind violated safety protocols, requiring the power level to be decreased from 100% to idle (7%) at 13:57. The cycle was restarted at the 100% level, but at 14:01, high winds again caused a safety violation that required the power level to be dropped to idle. It was not until 14:30 that two full EPA cycles were completed without any disruptions.

In EPA-2 and -3, the jet engine cycle operating cycle was repeated four times and without any interruption. However, during EPA-3, an additional power setting was introduced at 75% in the first cycle of the test to accommodate the needs of another project participant.

The six NASA tests were conducted at a number of different power levels as shown in Figures 6-3 and 6-4. EPA conducted non-speciated sampling during all of the NASA tests. During NASA-1 and -1a, the DEAL conducted continuous monitoring only. For the remaining NASA tests (NASA-2, -3, -4, and -5), time-integrated sampling was conducted along with the continuous monitoring. For the time-integrated samples (see Tables 3-2 and 3-3), it was necessary to use the same media for two sequential tests (NASA-2 and -3, and NASA-4 and -5) due to the short run times for these tests. NASA-2 and -3 were collected during tests using the high-sulfur fuel and NASA-4 and -5 were collected during tests using the high-aromatic fuel. In both cases, once the first test was completed, the time-integrated sample media holders were placed in the freezer until the subsequent test was ready to be conducted.

6.3.2   APEX-2 Engine Test Cycles

In all four tests of the APEX-2 campaign, the engines were mounted on Boeing 737 airframes owned and operated by Southwest Airlines. A CFM56-7B24 was used in Tests 1 and 4, a CFM56-3B1 for Test 2, and a CFM56-3B2 in Test 3. For tests T2 and T3, the same media were used for the time-integrated sampling (see Tables 3-2 and 3-3), with the exception of the SUMMA canisters, to insure that adequate sample mass was collected.
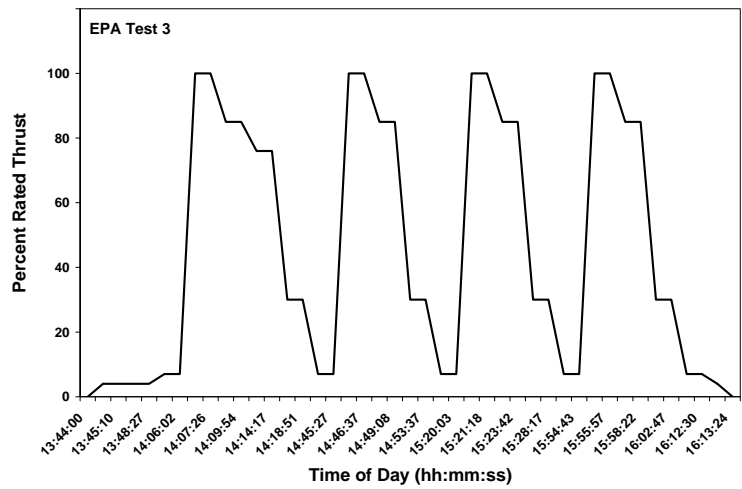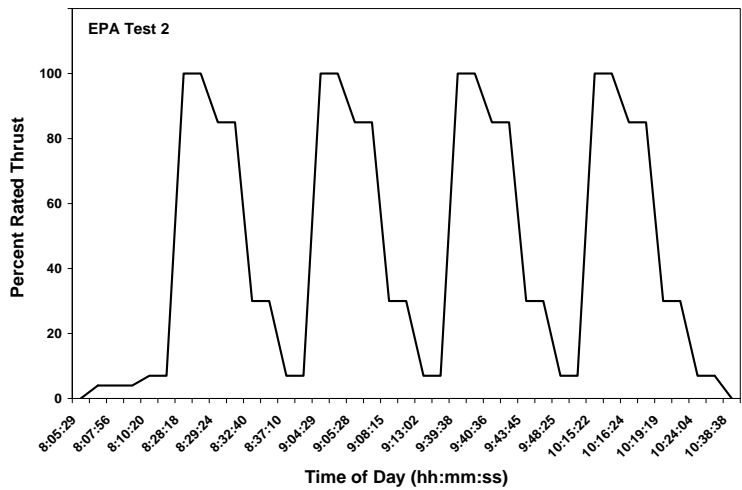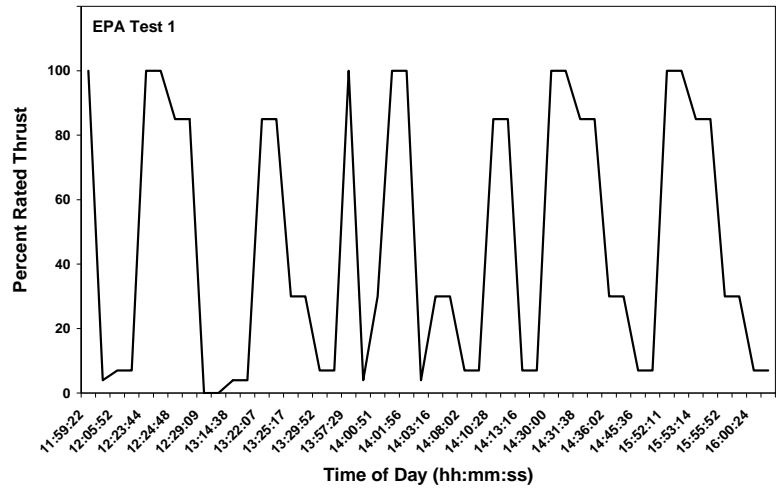
Figure 6-2.   Engine operating cycles for the EPA tests during APEX-1.
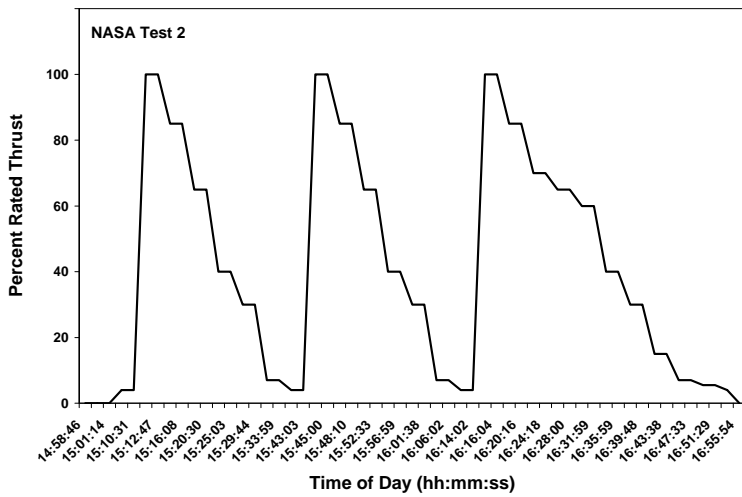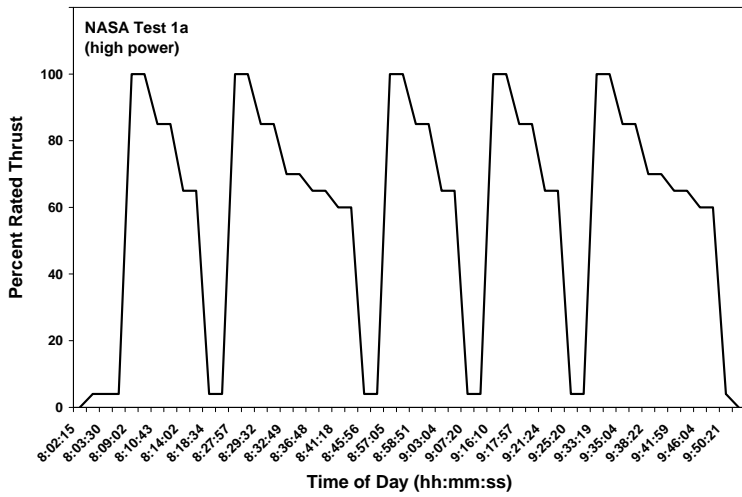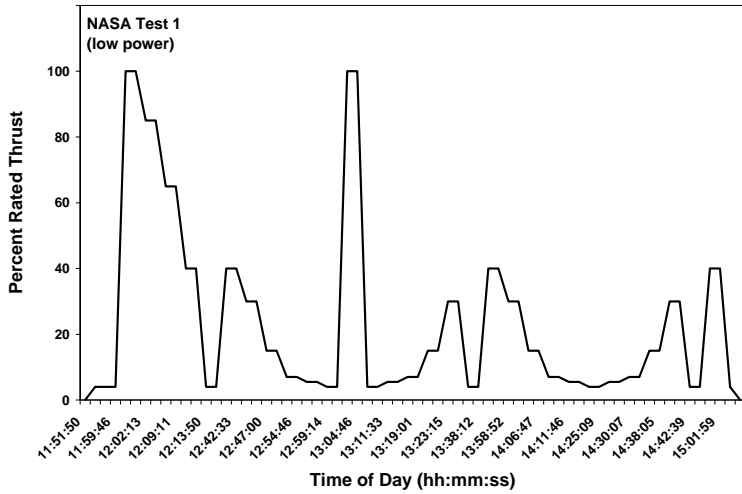
Figure 6-3.   Engine operating cycles for Tests NASA-1, -1a, and -2 during APEX-1.
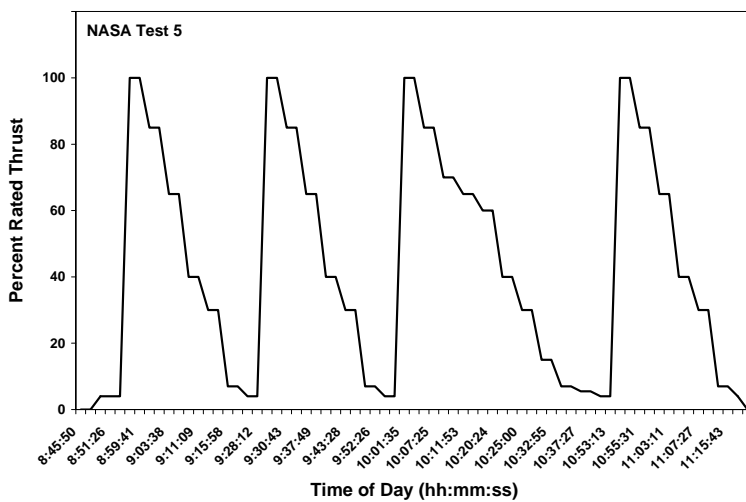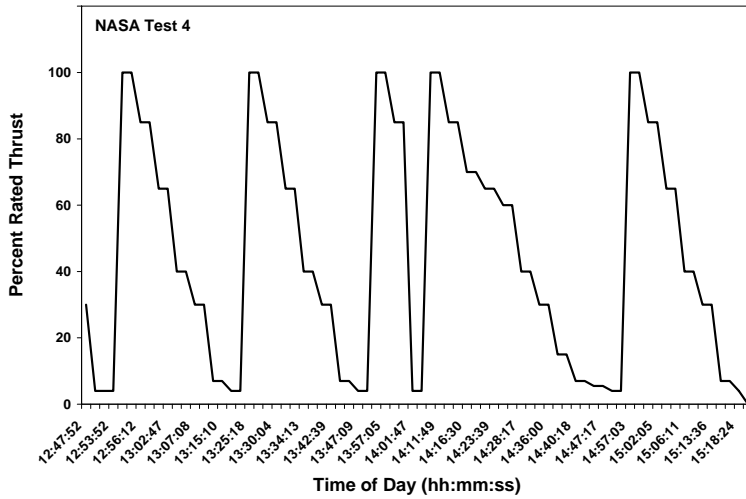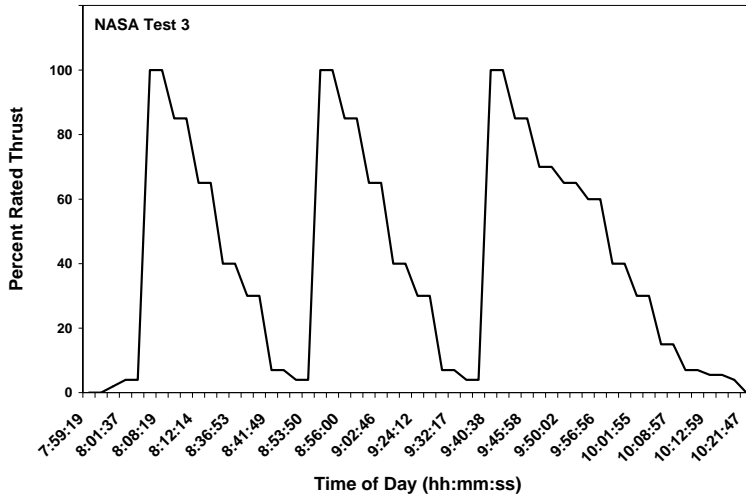
Figure 6-4.   Engine operating cycles for Tests NASA-3, -4, and -5 during APEX-1.

The engines were operated in cycles encompassing a series of steady state power settings. To investigate the effects of engine operating power on particle emissions, the power levels include those used during engine certification (except take-off), cruise, engine start/stop, and transitions between throttle settings. Each test consisted of power settings at 4, 7, 30, 40, 65 and 85 percent of rated thrust. Except for the 85 percent thrust level, where run-time was 8 min, approximately 10 min were provided at each power setting to allow for samples to be adequately analyzed. During the tests, the thrust was changed in a stepwise fashion. The thrust was first increased from the lowest thrust level (4%) to highest level (85%) under "cold" engine condition, and then decreased under "warm" engine condition, as shown in Figure 6-5. Again, the operating cycles used in APEX-2 were similar, but not identical.

6.3.3 APEX-3 Engine Test Cycles

The APEX-3 engine test cycles were similar to those for APEX-2. The emissions were monitored while increasing the rated power thrust from the lowest level to highest level under cold engine conditions, then decreasing the power level from highest to lowest under warm engine conditions. The engine operating cycles for APEX-3 are grouped by engine manufacturer and model. For tests T3 and T4, and tests T6 and T7, the same sampling media were used for some of the time-integrated samples (see Tables 3-2 and 3-3), to insure that adequate mass was collected. In both cases, once the first test was completed, the time-integrated sample media holders were placed in the freezer until the subsequent test was ready to be conducted.

Figure 6-6 presents the engine operating cycles for Tests 1 and 11, which were conducted with the same CFM engine model used during APEX-2, Test 2 (CFM56-3B1). The engines were mounted on a Boeing 737-300 airframe owned and operated by Continental Airlines. The nominal engine power settings were 4, 7, 15, 30, 45, 65, 85, and 100 percent of rated thrust. Note that in Test 11, only half of the usual cycle was completed.

Figure 6-7 presents the engine operating cycles for Tests 2 and 5 of a General Electric CJ610-8ATJ model turbojet engine mounted on a Lear Model 25 airframe owned and operated by NASA. This engine was the smallest and least powerful of all of the engines tested. During these tests, the engine power setting was set at seven levels: 7, 15, 30, 45, 65, 85, and 100 percent of rated thrust. Note that during Test 2, the engine was shut down shortly after reaching maximum power due to high crosswinds. After the crosswinds subsided, the engine operating cycle was restarted from the beginning.

Figure 6-8 shows the operating cycles for AE3007A1E and AE3007A1/1 engines in Tests 3, 4, and 10. In all three of these tests, the exhaust was sampled from the engines mounted on the tail of an Embraer ERJ 145 commuter jet. In Tests 3 and 4, the aircraft was operated by Continental Express and used a Rolls Royce Model AE3007A1E engine. In Test 10, the aircraft was operated by ExpressJet and used a Rolls Royce Model AE3007A1/1 turbofan engine. These tests were conducted at seven nominal power settings: 8.4, 15, 30, 45, 65, 85, and 100 percent.
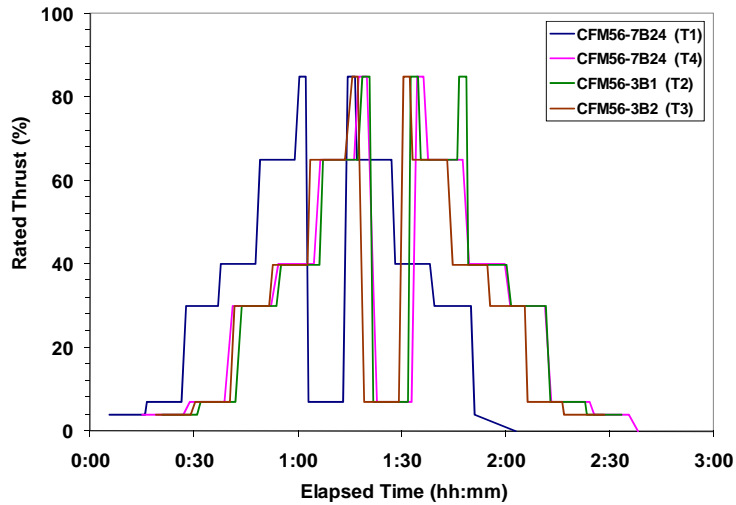
Figure 6-5. **Engine operating cycles for APEX-2.**
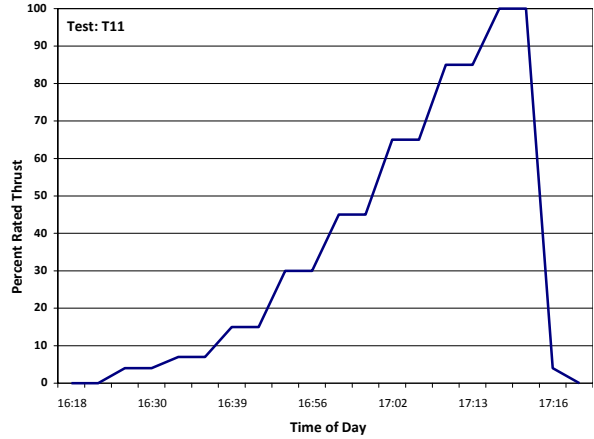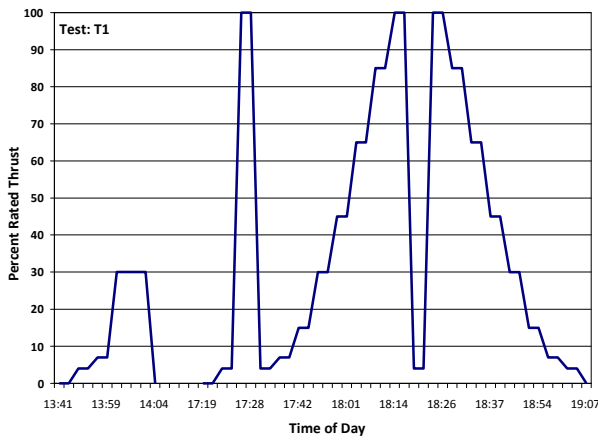
Figure 6-6. **Operating cycles for CFM56-3B1 engines during APEX-3.**
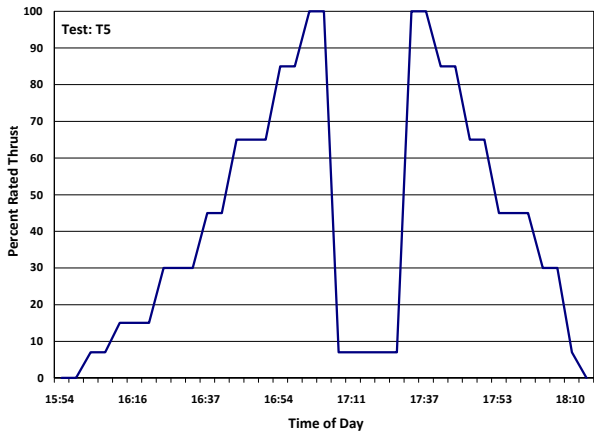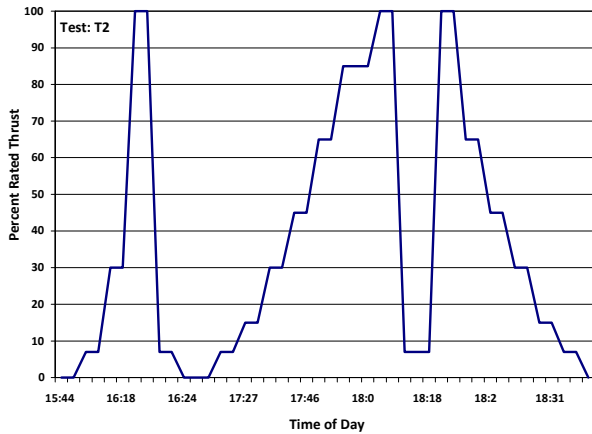
Figure 6-7. **Operating cycles for CJ610-8ATJ engine during APEX-3.**

68
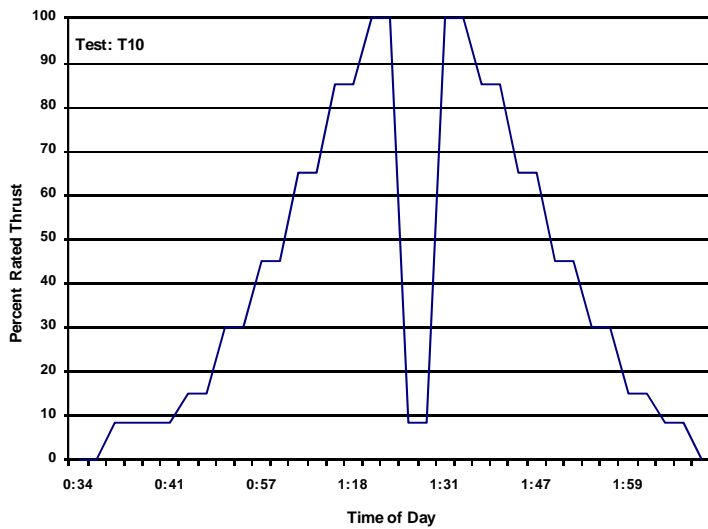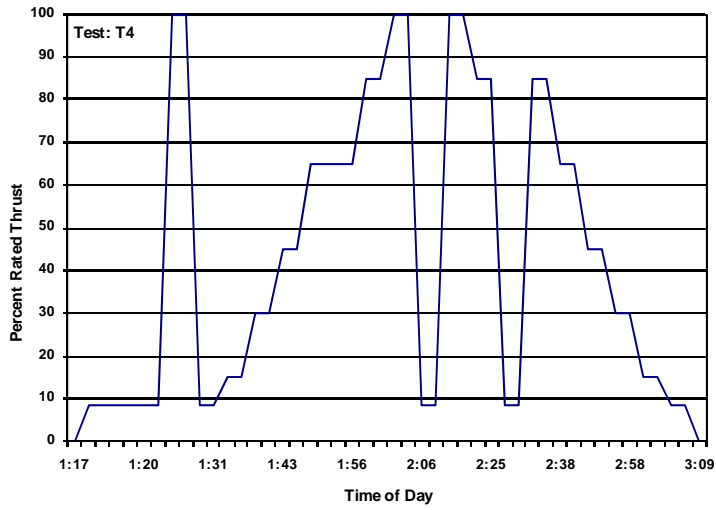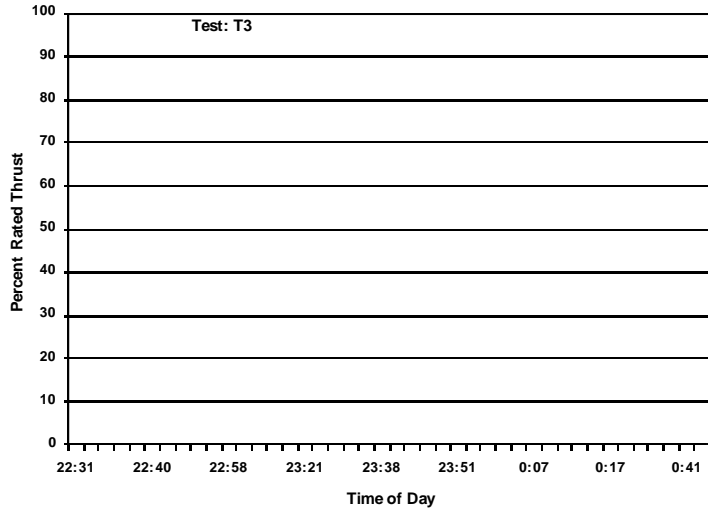
Figure 6-8.   Operating cycles for AE3007A1 engines during APEX-3.

69

Figure 6-9 presents the power cycles for Tests 6 and 7 conducted on the largest and most powerful engine, the Pratt and Whitney Model 4158 turbofan. The engine was wing-mounted on the airframe of an Airbus A300 owned and operated by Federal Express. A wind speed sensor and warning light were used to monitor the exhaust plume velocity on a fence between the engine exit and an adjacent building and tarmac. The warning light was blown off the fence during Test 6 at about 65-percent power. The power level had to be reduced to idle while the light was reattached to the fence. Testing was resumed, but the warning light alarm activated, limiting operation of the engine to about 80-percent power. Therefore, Tests 6 and 7 were actually conducted at six nominal power settings: 7, 15, 30, 45, 65, and 80 percent of rated thrust.
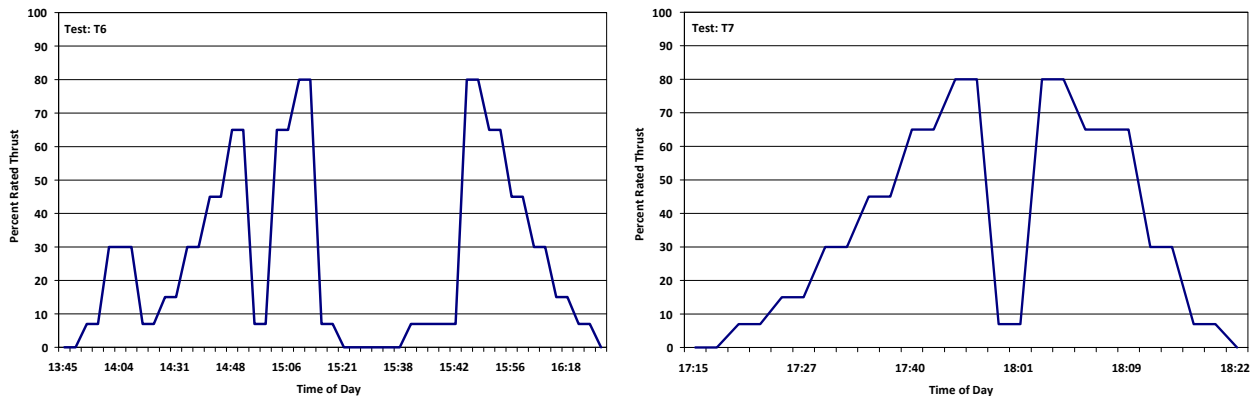
Figure 6-9.   Operating cycles for P&W 4158 engine during APEX-3.

Figure 6-10 shows the engine operating cycles for Tests 8 and 9 of Rolls Royce RB211-535E4-B engines mounted on a Boeing 757 airframe owned and operated by Continental Airlines. The same power settings were used as for Tests 1 and 11; however, the maximum power level in Test 8 was limited to 85 percent because of high crosswinds.

As can be seen from these graphs, no two tests in any of the sampling campaigns had exactly the same operating cycle. This variation in cycles makes it impossible to determine method precision for the time-integrated measurements. In addition, the lack of consistent engine operation hampered the determination of chemical composition for both particle- and gas-phase constituents using methods employed here. It could not be determined whether or not the variations seen from test-to-test were due to different engine technology or were related to changes in engine operation. Therefore, real-time chemical characterization techniques are preferred over time-integrated methods in future tests to allow for variations in engine operation.
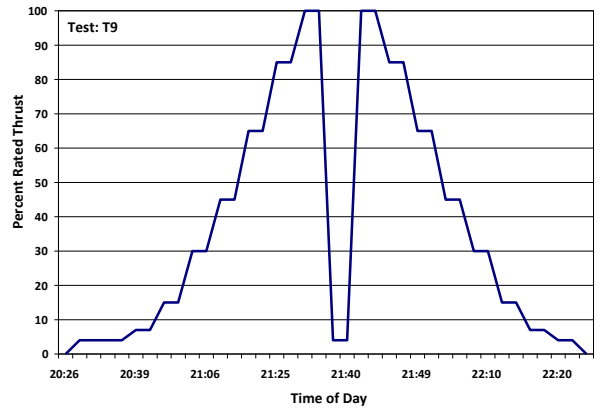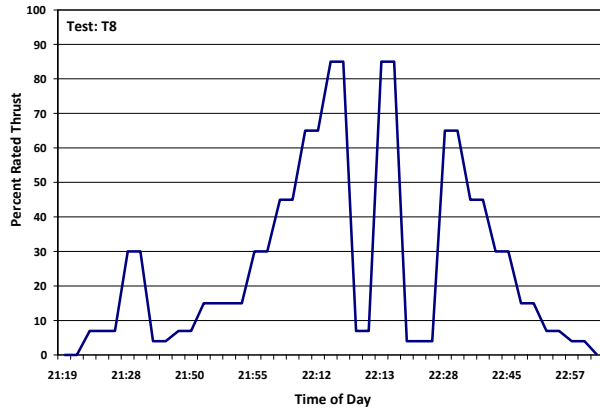
Figure 6-10. Operating cycles for RB211-535E4-B engines during APEX-3.

This page intentionally left blank.

7.   Environmental and Engine Operating Data

7.1   Wind Speed and Direction

Any crosswinds experienced during sampling were expected to have an impact on the emissions measured in the downstream exhaust plume due to contamination of the background samples with engine exhaust and deflection of the plume away from the probe at low engine power. Wind speed and direction were monitored during all three APEX campaigns and averaged over the run time for each test. Table 7-1 presents these results and includes the RSDs in both wind speed and direction. The RSD is a measure of the variation in wind speed and direction experienced during each test.

Table 7-1.   Average and Relative Standard Deviation of Wind Speed and Direction for Individual Tests

Campaign		Wind Speed (km/h)		Wind Direction (degree)	
APEX	Test No	Average	RSD (%)	Average	RSD (%)
1	EPA-1	5	124	133[a]	76
	EPA-2	--	--	288[a]	35
	EPA-3	26	16	270	7
	NASA-1	9	75	109[a]	85
	NASA-1a	2	77	289[a]	40
	NASA-2	11	66	226	28
	NASA-3	23	20	213	5
	NASA-4	37	21	224	5
	NASA-5	7	59	272	37
2	T1	4	36	306	26
	T2	2	75	250	40
	T3	2	60	269	34
	T4	1	66	263	42
3	T1	19	16	198[a]	3
	T2	21	31	233	5
	T3	11	8	224	1
	T4	11	9	222	2
	T5	19	52	245	11
	T6	26	25	282	5
	T7	23	26	276	4
	T8	15	50	283	6
	T9	20	13	225	2
	T10	14	17	230	3
	T11	4	21	237	39

a. Wind direction falls outside of the designated criteria for compressor stall. The data and resulting emissions calculations should be used with caution.

The direction of the wind, when blowing directly toward the nose of the aircraft, was approximately 240° for all of the APEX-1 tests, and 260° for all of the APEX-2 and APEX-3 tests. Based on information from the aircraft flight manual, a variation of ± 45° is allowed to avoid engine compressor stall. If the same minimum criterion is used to determine acceptable crosswinds to avoid background contamination and exhaust plume deflection for the tests, then winds during APEX-1 should fall between 195° and 285°, and between 215° and 305° during APEX-2 and APEX-3.

As shown in Table 7-1, during Test EPA-1 of APEX-1, the average wind direction was 133°. This value indicates that this test was conducted during significant crosswinds. In addition, Test EPA-1 had a very high RSD in wind speed (124%) and wind direction (76%). Based on these data, the EPA-1 test was conducted under poor wind conditions.

There were two other tests where the wind direction fell outside the criteria defined above: the NASA-1 test of APEX-1 and T1 of APEX-3. As was the case for Test EPA-1 of APEX-1, caution should be used with the emissions data resulting from any test conducted during poor wind conditions.

Note also that there were periods during other APEX-3 tests that had poor wind conditions, although the test averages fell within the stated criteria. These tests with poor wind conditions were tests T2 through T5, T8, and T11.

7.2   Fuel Flow Rate

Fuel consumption is directly related to engine power output. In the three APEX campaigns, the fuel flow rate was supplied by either NASA (APEX-1 and -3) or the airline (APEX-2 and -3) and plotted as a function of percent rated thrust for each test. Table 7-2 presents the average fuel flow rates (in kg of fuel per hour) at various power conditions, expressed as percentage of rated thrust, for each test. The table also includes the aircraft, engine, and type of fuel used for each individual test. Note that the fuel flow rate values shown are averages of all the data obtained under the same power condition occurring during a test. In some cases, acceptable data may not be available for all periods at a particular thrust level.

For the APEX-1 campaign, each fuel flow rate is the average value of measurements recorded from cockpit instruments at each specified power level. For the APEX-2 and APEX-3 campaigns, the fuel flow rates were determined under cold (increasing power in a stepwise fashion) and warm (reducing power in a stepwise fashion) engine conditions separately. No fuel flow data were supplied by the airline for T1 of APEX-2. Therefore, the data from T4 (same aircraft and engine) were assumed for T1 in the emission index (EI) calculations.

To investigate the effect of fuel type on fuel consumption, the fuel flow rate measurement results were compared for the APEX-1 campaign, where three types of jet fuels (base, high-sulfur, and high-aromatic) were used. The base fuel was used in EPA-1, EPA-2, NASA-1 and NASA-1a. The high-sulfur fuel was used in EPA-3, NASA-2, and NASA-3, and the high-aromatic fuel was used in NASA-4 and NASA-5. All these tests were conducted with the same aircraft and same CFM56-2C1 engine.

Figure 7-1 plots the APEX-1 fuel flow rate data for these three types of fuels against the percent rated thrust. Their correlation can be expressed by almost identical linear equations, indicating that the higher sulfur and aromatic contents of two of the fuels had no influence on the fuel consumption. This lack of influence is probably because the three tested fuels have approximately the same heating values, even though their sulfur and aromatic contents were different.

Table 7-2. Summary of Fuel Flow Rates Measured at Different Engine Power Levels

APEX	Test No.[a]	Aircraft	Engine	Fuel Type	Engine Conditions	Fuel Flow (kg/h) at Percent Rated Thrust[c]														
						4	5.5	7	8.4	15	30	40	45	60	65	70	76	80	85	100
1	EPA-1	DC-8	CFM56-2C1	Base				436			992								2819	2969
	EPA-2							425			1023								2860	3181
	NASA-1					350	386	427		560	1012	1252			1998				2406	2906
	NASA-1a					336								1922	2098	2252			2898	3127
	EPA-3			High sulfur				438			964							2424	2840	3116
	NASA-2					345	381	413		543	955	1235		1855	2046	2191			2727	2984
	NASA-3					347	382	405		538	986	1255		1846	2053	220			2758	3051
	NASA-4			High aromatic		345	381	401		545	960	1220		1850	2023	2157			2708	2978
	NASA-5					345	395	410		545	989	1292		1930	2131	2247			2894	3176
2[d]	T4	B737-700	CFM56-7B24	Fleet fuel	Cold[b]	336		418			1180	1544			2497				4131	
					Warm	313		381			1135	1498			2497				4086	
					Average	325		400			1158	1521			2497				4109	
	T2	B737-300	CFM56-3B1	Fleet fuel	Cold	341		422			1099	1403			2193				3528	
					Warm	345		418			1067	1367			2184				3559	
					Average	343		420			1083	1385			2188				3543	
	T3	B737-300	CFM56-3B2	Fleet fuel	Cold	372		440			1130	1444			2252				3677	
					Warm	368		422			1108	1412			2261				3650	
					Average	370		431			1119	1428			2256				3664	
3	T1	B737-300	CFM56-3B1	Fleet fuel	Cold	300		397		654	1136		1618		2260				2903	3385
					Warm	300		397		654	1136		1618		2260				2903	3385
					Average	300		397		654	1136		1618		2260				2903	3385
	T11	B737-300	CFM56-3B1	Fleet fuel	Cold	381		431		622	1090		1530		2179				2815	3564
	T2	NASA Lear Model 25	CJ610-8ATJ (turbojet)	Fleet fuel	Cold			182		304	452		568		760				999	1226
					Warm			182		304	454		568		763					1226
					Average			182		304	453		568		762				999	1226
	T5	NASA Lear Model 25	CJ610-8ATJ (turbojet)	Fleet fuel	Cold			227		303	452		567		763				1009	1226
					Warm			227			452		567		763				1009	1226
					Average			227		303	452		567		763				1009	1226
	T3	Embraer ERJ 145	AE3007A1E	Fleet fuel	Cold				174	238	389		555		805				1082	1286
					Warm				173	235	392		563		810				1088	1299
					Average				173	237	391		559		807				1085	1293
	T4	Embraer ERJ 145	AE3007A1E	Fleet fuel	Cold				168	239	385		547		788				1050	1253
					Warm				167	231	384		549		786				1052	1252
					Average				167	235	385		548		787				1051	1252
	T10	Embraer ERJ 145	AE3007A1/1	Fleet fuel	Cold				179	233	372		524		750				971	1171
					Warm				178	231	371		529		767				982	1180
					Average				178	232	371		526		758				976	1175
	T6	A300	P&W 4158	Fleet fuel	Cold			610		1014	2245		3726		5658		7026			
					Warm			368		1097	2465		3834		5658		7026			
					Average			489		1056	2355		3780		5658		7026			
	T7	A300	P&W 4158	Fleet fuel	Cold			600		1035	2230		3688		5702		7100			
					Warm			596			2252				5711		7200			
					Average			598		1035	2241		3688		5706		7150			
	T8	B757	RB211-535E4-B	Fleet fuel	Cold	566		770		1191	2109		3178		4750				6096	
					Warm	437		654		1178	2131		3436		4691				6449	
					Average	501		712		1185	2120		3307		4720				6273	
	T9	B757	RB211-535E4-B	Fleet fuel	Cold	421		690		1221	2004		3068		4479				6233	6966
					Warm	506		668		1173	2037		3111		4551				6307	6987
					Average	464		679		1197	2021		3090		4515				6270	6976

a Note that bleed air was extracted from the engine during tests EPA-1,-2, and -3 in APEX-1. No fuel flows were recorded by the airline during T1 of APEX-2.
b "Cold" refers to increasing power in a stepwise fashion, and "Warm" indicates reducing power in a stepwise fashion. See Section 6.
c Fuel flows provided by aircraft operator.
d Fuel flows for APEX-2, T1, were derived from the same power conditions for T4, since no data were provided by the aircraft operator for this test.
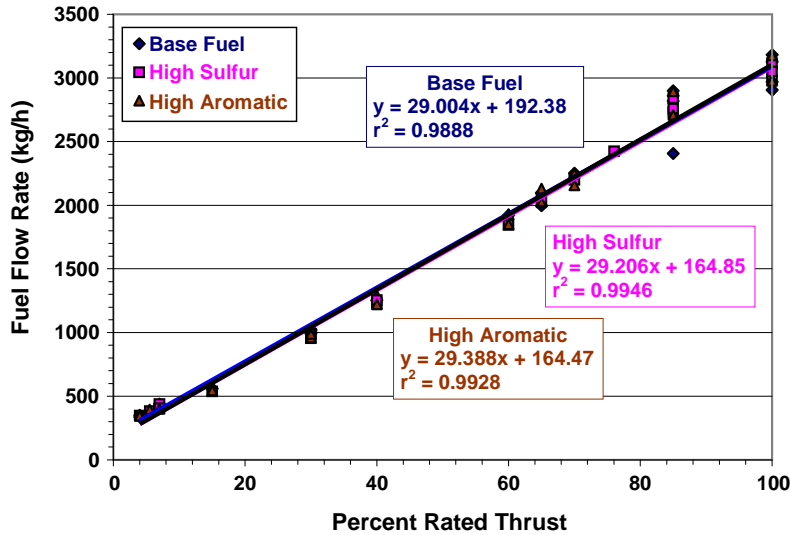
Figure 7-1.   Effect of fuel sulfur and aromatic content on fuel consumption during APEX-1.

The fuel consumption rates for different engine types are compared in Figure 7-2. The three lowest thrust engines in these tests—Models AE3007A1E and AE3007A1/1 mounted on an ERJ 145 express jet, and Model CJ610-8ATJ mounted on a NASA Lear Model 25 airframe—had almost identical fuel consumption rates as a function of rated engine thrust. This trend is somewhat surprising since the AE3007 engines are rated at almost three times the thrust of the smaller CJ610 on the Lear Model 25. For the CFM56 engine family, the -7B engine showed the highest fuel consumption, followed by the -3B engine. The -2C engine had the lowest fuel flow consumption rate of the CFM56 engines tested. The P&W 4158 turbofan engine mounted on an Airbus A300 was the most powerful engine, and operation of this engine resulted in the highest fuel consumption rate. The second highest fuel consumer was the RB211-535E4-B mounted on a B757 airframe.
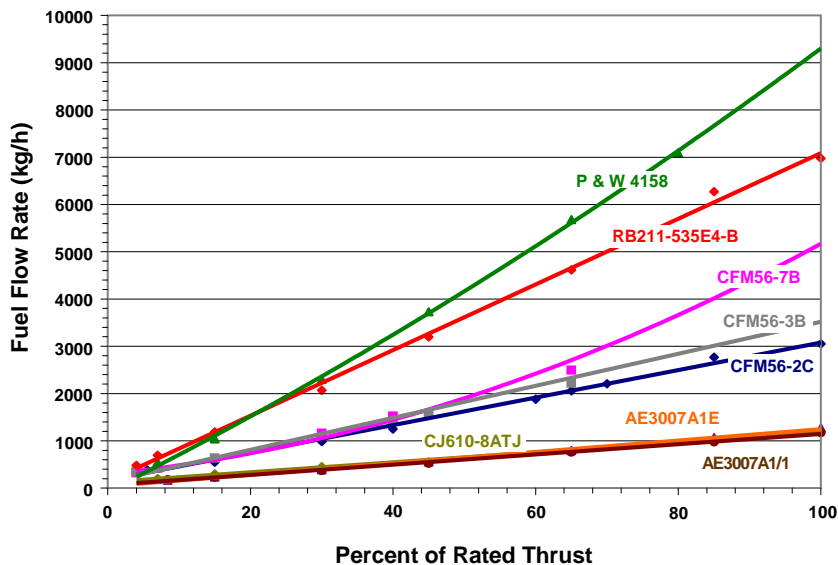
Figure 7-2.   Effect of engine type on fuel consumption during APEX-3.

The effects of the engine operating condition (cold and warm) on fuel consumption were investigated by plotting the APEX-2 and -3 measurement results obtained under cold engine conditions against the measurement results obtained under warm operation conditions and are shown in Figure 7-3. Cold conditions were the step-wise increasing of power levels to maximum, whereas warm engine conditions were the step-wise decreasing of power levels after the engine had been run at maximum power (refer to Figure 6-5 for APEX-2 and Figures 6-6 through 6-10 for APEX-3). The diagonal line represents the data that have identical measurement results under both cold and warm conditions. The majority of measurement points are closely grouped around the diagonal. Therefore, fuel consumption is not affected by whether the engine is operated under cold or warm conditions although differences in emissions were consistently observed as discussed below.
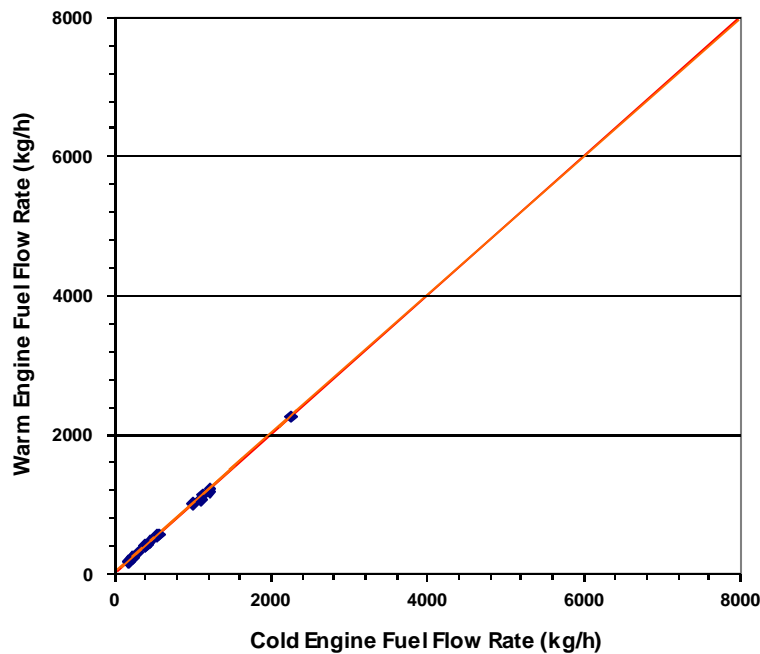
Figure 7-3. **Effect of cold and warm engine operating conditions on fuel consumption during APEX-2 and -3.**

7.3 Carbon Dioxide Monitoring

As discussed in Section 5, the EI calculation requires knowledge of the CO_2 concentration at the emission sampling location, and both plume and background CO_2 concentrations are needed to obtain a background-corrected concentration for the EI calculation. For the APEX-1 and APEX-2 campaigns, the plume CO_2 sampling, as well as other PM sampling, was performed along the plume centerline 30 m downstream from the engines. No CO_2 measurements were obtained for T1 of APEX-2 due to an instrument malfunction. Since there were also no fuel flow data for this test, these parameters were assumed to be identical to T4 (same aircraft and engine). During APEX-3, samples were collected at 15, 30, and 43 m behind the testing engines to investigate the effect of dilution on emissions results.

As expected, the CO_2 concentration was found to be closely correlated with engine rated thrust, which, in turn, is related directly to the fuel flow rate. Figure 7-4 is a typical result for the NASA-1 test of APEX-1. The background-corrected CO_2 concentration and fuel flow rate are plotted with the run time in blue (dark)

and red (light) lines, respectively — showing that the CO_2 concentration corresponded closely with the fuel flow rate during the test.
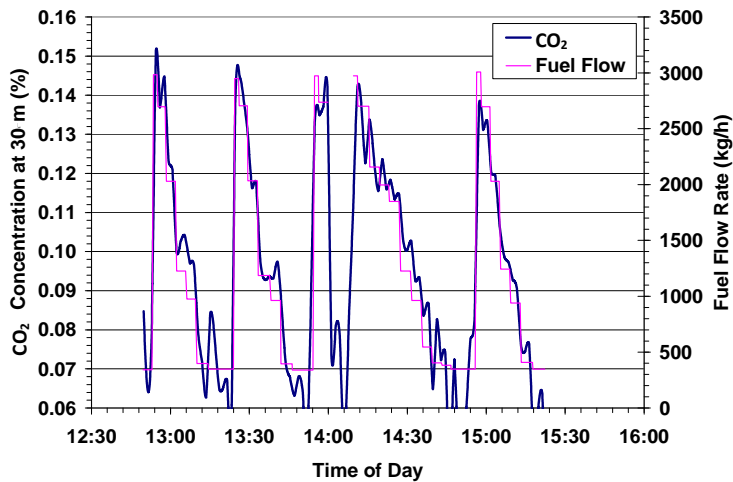
Figure 7-4.   Correlation between CO_2 concentration and fuel flow rate during Test NASA-1 of APEX-1.

Table 7-3 summarizes the different power settings used for each APEX-1 and -2 test, along with the corresponding background-corrected average CO_2 concentration and standard deviation (SD). In these campaigns, the sampling was done at the same location, 30 m downstream of the engine. As discussed previously, three possible sampling locations were used during the APEX-3 campaign. Table 7-4 presents data for APEX-3, similar to the data shown in Table 7-3 for APEX-1 and -2, along with the location where the CO_2 emissions were sampled for each APEX-3 test.

The CO_2 emissions for the different fuels tested during APEX-1 were studied by plotting the CO_2 concentration data as a function of fuel flow rate. Figure 7-5 shows very similar trends for all three fuel types. The CO_2 emissions increased as the fuel flow rate increased from 300 kg/hr. The CO_2 concentration reached its maximum when the fuel flow rate was at about 2,800 to 2,900 kg/hr, after which the CO_2 concentration decreased as the fuel flow rate continued increasing to its maximum. Note that this decrease at the highest fuel flow rates (which correspond to the takeoff mode, or 100% thrust) may possibly be an artifact of the short run times at this setting. Because the instrumentation experiences a slight response lag time, these results may actually be an average of the transition results, and not a true reflection of CO_2 concentrations at these highest thrust ratings. Whether this observation is an artifact or an indication of the actual chemistry occurring at 100 percent thrust, the data collected by APEX-1 collaborators showed similar trends (Wey et al., 2006).

To investigate airport CO_2 emissions, the APEX-1 results at different engine operation cycles were compared. In Figure 7-6, the CO_2 concentrations measured were compared at four engine power settings: idle (7% rated thrust), takeoff (100% rated thrust), climb-out (85% rated thrust), and approach (30% rated thrust) for the three fuel types. Two conclusions can be drawn from these comparisons:

78

Table 7-3. **Average Background Corrected CO_2 Concentrations at Different Power Settings for APEX-1 and -2**

APEX	Test No.	Parameter	The values for APEX-1 are the average at each thrust of all the cycles of that test shown in Figures 6-2 through 6-4[a]										
1	EPA-1	% of Rated Thrust	7	30	85	100							
		Average CO_2 (ppm)	573	590	1048	983							
		SD (ppm)	41	35	41	116							
	EPA-2	% of Rated Thrust	7	30	85	100							
		Average CO_2 (ppm)	449	573	1073	956							
		SD (ppm)	57	46	17	172							
	EPA-3	% of Rated Thrust	7	30	76	85	100						
		Average CO_2 (ppm)	181	370	787	1026	740						
		SD (ppm)	74	59		70	250						
	NASA-1	% of Rated Thrust	4	5.5	7	15	30	40	65	85	100		
		Average CO_2 (ppm)	542	448	462	533	596	692	901	1025	926		
		SD (ppm)	155	47	97	61	25	38	--	--	288		
	NASA-1a	% of Rated Thrust	4	60	65	70	85	100					
		Average CO_2 (ppm)	462	812	882	880	1059	944					
		SD (ppm)	56	29	50	--	23	100					
	NASA-2	% of Rated Thrust	4	5.5	7	15	30	40	60	65	70	85	100
		Average CO_2 (ppm)	536	249	346	310	599	715	862	922	941	1088	1021
		SD (ppm)	50	--	177	--	66	18	--	26	--	38	30
	NASA-3	% of Rated Thrust	4	5.5	7	15	30	40	60	65	70	85	100
		Average CO_2 (ppm)	454	427	460	503	632	699	880	903	921	1107	872
		SD (ppm)	45	--	8	--	22	13	--	25	--	7	34
	NASA-4	% of Rated Thrust	4	5.5	7	15	30	40	60	65	70	85	100
		Average CO_2 (ppm)	307	274	372	479	583	640	795	833	877	1010	1000
		SD (ppm)	56	--	16	--	28	34	--	13	--	43	71
	NASA-5	% of Rated Thrust	4	5.5	7	15	30	40	60	65	70	85	100
		Average CO_2 (ppm)	414	510	418	389	597	634	841	903	999	1081	1111
		SD (ppm)	124	--	132	--	32	76	--	21	--	24	86

APEX	Test No.	Parameter	The values for APEX-2 are the average at each thrust in the cycles shown in Figure 6-5[b]													
2	T2	% of Rated Thrust	4	7	30	40	65	85	7	85	65	85	40	30	7	4
		Average CO_2 (ppm)	459	510	702	818	1054	1430	496	1495	1047	1461	816	697	539	530
		SD (ppm)	51	51	45	43	53	59	41	75	50	55	42	44	50	57
	T3[c]	% of Rated Thrust	4	7	30	40	65	85	7	85	65		40	30	7	4
		Average CO_2 (ppm)	600	552	712	822	1050	1457	530	1464	1059		792	699	513	547
		SD (ppm)	65	59	49	48	57	71	54	78	53		44	46	57	62
	T4	% of Rated Thrust	4	7	30	40	65	85	7	85	65		40	30	7	4
		Average CO_2 (ppm)	307	350	515	624	852	1110	301	1120	848		604	510	316	272
		SD (ppm)	41	28	30	33	34	39	35	43	35		34	34	33	43

a 100% thrust at this test site actually represents 93% rated thrust at standard sea level conditions.

b 85% thrust is maximum take-off power at this airport.

c Based on an analysis of the criteria gas data by the manufacturer's representative, this engine may not have been operating per specifications.

Table 7-4. Average Background Corrected CO_2 Concentrations at Different Power Settings for APEX-3

The values for APEX-3 are the average at each thrust in the cycles shown in Figures 6-6 to 6-10

T1 — Power Cycle Reference Figure 6-6
Sampling Location: 30 m
Sampling Times: 17:31 to 19:07

Parameter																	
% of Rated Thrust	4	7	15	30	45	65	85	100	4	100	85	65	45	30	15	7	4
Average CO_2 (ppm)	102	117	137	199	243	315	359	396	99	378	323	265	202	164	115	94	88
SD (ppm)	13	13	12	10	16	13	14	11	12	13	13	12	9	7	9	10	9

T2 — Power Cycle Reference Figure 6-8
Sampling Location: 15 m (17:23 to 17:57) | 30 m (17:57 to 18:16) | 15 m (18:16 to 18:33)

Parameter																
% of Rated Thrust	7	15	30	45	65	85	85	100	7	7	100	65	45	30	15	7
Average CO_2 (ppm)	19	645	906	1031	1183	1430	870	982	42	360	1633	1272	1051	877	682	39
SD (ppm)	3	83	49	41	47	40	55	57	27	185	42	51	39	59	78	2

T3 — Power Cycle Reference Figure 6-10
Sampling Location: 15 m
Sampling Times: 22:41 to 00:41

Parameter															
% of Rated Thrust	8.4	15	30	45	65	85	100	8.4	100	85	65	45	30	15	8.4
Average CO_2 (ppm)	78	142	181	228	274	295	313	87	319	272	207	164	160	151	85
SD (ppm)	50	50	45	37	41	56	55	54	53	52	33	35	33	34	51

T4 — Power Cycle Reference Figure 6-10
Sampling Location: 15 m
Sampling Times: 01:24 to 03:09

Parameter																	
% of Rated Thrust	8.4	15	30	45	65	85	100	8.4	100	85	8.4	85	65	45	30	15	8.4
Average CO_2 (ppm)	59	66	101	154	268	358	439	54	387	342	52	297	230	120	64	52	50
SD (ppm)	16	17	32	48	54	56	38	3	71	50	5	57	54	41	21	5	3

T5 — Power Cycle Reference Figure 6-8
Sampling Location: 15 m (15:55 to 17:03) | 30 m (17:11 to 18:20)

Parameter														
% of Rated Thrust	7	15	30	45	65	85	100	7	100	85	65	45	30	7
Average CO_2 (ppm)	115	496	650	654	817	958	1042	190	565	529	488	449	457	177
SD (ppm)	42	95	58	55	31	22	23	72	49	42	25	29	25	7

T6 — Power Cycle Reference Figure 6-9
Sampling Location: 30 m
Sampling Times: 14:14 to 15:20 then 15:38 to 16:26

Parameter																
% of Rated Thrust	7	15	30	45	65	7	65	80	7	7	80	65	45	30	15	7
Average CO_2 (ppm)	453	512	823	1099	1513	409	1505	1752	426	425	1703	1470	1111	808	531	434
SD (ppm)	31	26	21	28	33	46	35	29	39	87	32	37	26	27	28	35

T7 — Power Cycle Reference Figure 6-9
Sampling Location: 30 m
Sampling Times: 17:16 to 18:22

Parameter											
% of Rated Thrust	7	15	30	45	65	80	7	80	65	30	7
Average CO_2 (ppm)	491	580	852	1133	1522	1755	482	1759	1515	864	477
SD (ppm)	20	30	26	31	36	32	19	29	43	23	29

T8 — Power Cycle Reference Figure 6-7
Sampling Location: 30 m (21:37 to 22:20) | 43 m (22:20 to 23:03)

Parameter																	
% of Rated Thrust	4	7	15	30	45	65	85	7	85	4	4	65	45	30	15	7	4
Average CO_2 (ppm)	134	140	590	820	1039	1346	1563	340	1567	433	350	1022	875	660	475	349	292
SD (ppm)	5	3	40	23	25	30	56	56	54	29	36	24	26	29	23	33	40

T9 — Power Cycle Reference Figure 6-7
Sampling Location: 30 m
Sampling Times: 20:29 to 22:25

Parameter																	
% of Rated Thrust	4	7	15	30	45	65	85	100	4	100	85	65	45	30	15	7	4
Average CO_2 (ppm)	298	419	484	684	855	1091	1365	1469	374	1391	1330	1105	880	688	495	378	344
SD (ppm)	67	41	48	43	31	36	41	48	50	50	44	31	37	33	32	46	49

T10 — Power Cycle Reference Figure 6-10
Sampling Location: 30 m
Sampling Times: 00:35 to 02:10

Parameter															
% of Rated Thrust	8.4	15	30	45	65	85	100	8.4	100	85	65	45	30	15	8.4
Average CO_2 (ppm)	127	205	282	318	391	444	491	138	500	451	361	326	265	193	156
SD (ppm)	80	41	21	35	27	33	29	48	21	23	56	21	39	41	53

T11 — Power Cycle Reference Figure 6-6
Sampling Location: 30 m
Sampling Times: 16:20 to 17:15

Parameter								
% of Rated Thrust	4	7	15	30	45	65	85	100
Average CO_2 (ppm)	352	444	641	840	979	1130	1290	1405
SD (ppm)	34	43	54	48	31	38	49	55
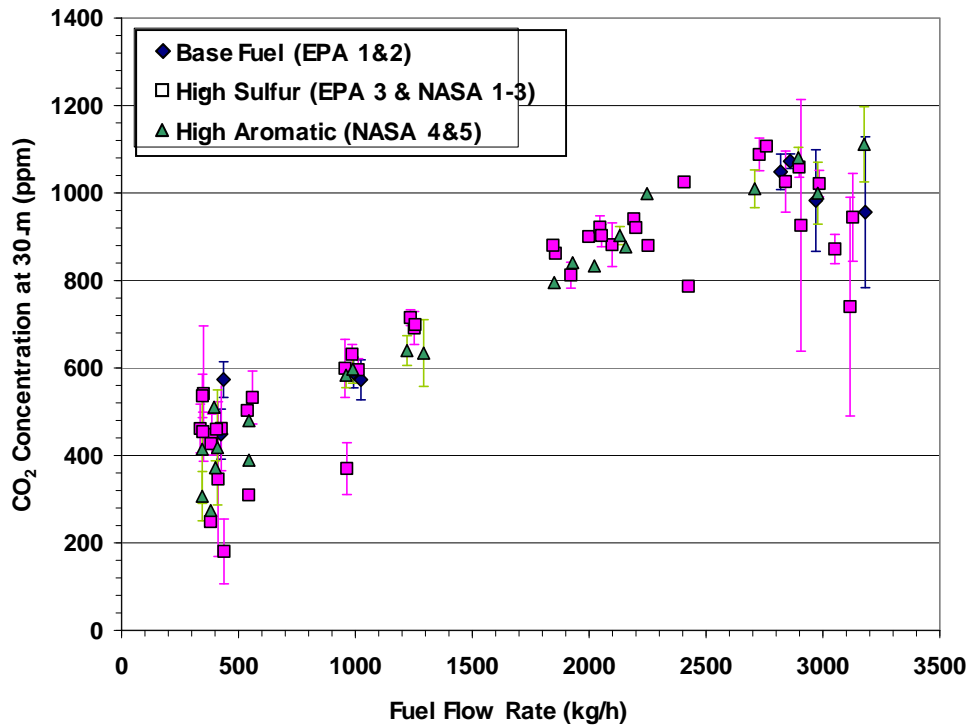
Figure 7-5. Effects of fuel type on CO_2 emissions for CFM56-2C1 engine during APEX-1.
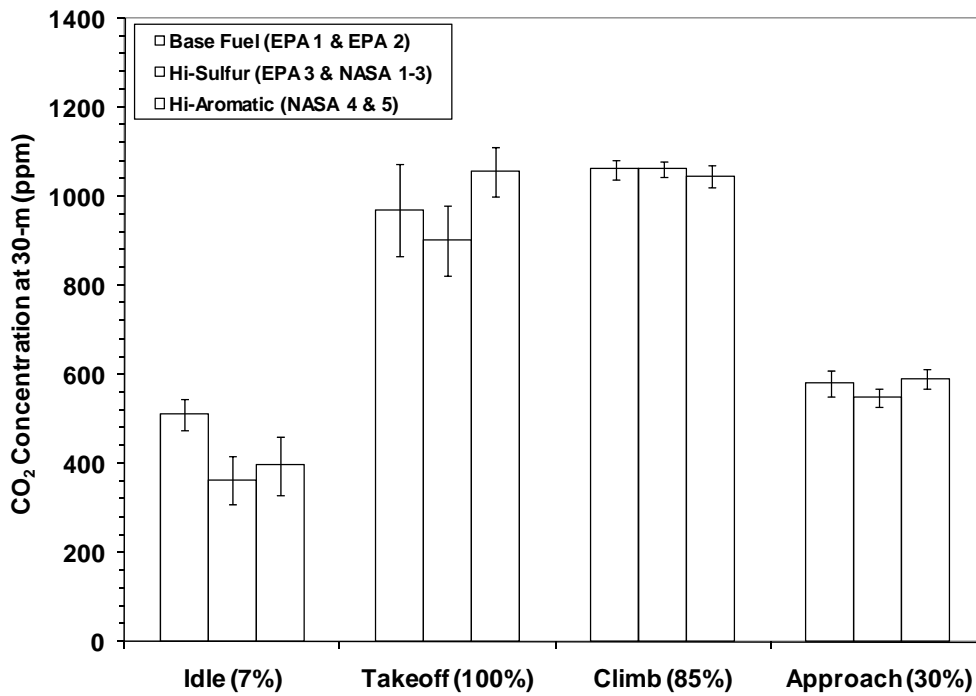
Figure 7-6. Effects of engine operation cycle on CO_2 emissions for CFM56-2C1 engine during APEX-1.

1. Except for idle condition, where the base fuel showed a slightly higher CO_2 concentration, the difference in the average CO_2 concentrations for the three different fuels was negligible in comparison to the experimental errors.

2. For all three fuel types, the CO_2 emissions were low when the engine was under idle condition. As the engine power setting was increased from 7 to 100 percent, the CO_2 emissions increased significantly. The emissions were highest when the engine moved to climb-out power, and then reduced sharply when the engine was changed to approach mode. As discussed above, the slightly lower concentrations seen during takeoff (100%) as compared to climb condition may be an artifact of the short duration sampling time at the maximum power setting. This result is slightly different from the results for fuel flow rate. The fuel consumption was observed to reach the maximum when the aircraft was at takeoff power.

The effects of engine operating temperature (cold or warm) on the CO_2 concentration measurements were also investigated. In Figure 7-7, the CO_2 concentration data measured under cold and warm conditions were plotted against the fuel flow rate for selected engines tested during the APEX-3 campaign. This figure shows that these engines, when warm, had an approximately equal or slightly lower CO_2 concentration compared to the CO_2 concentration that was measured under cold conditions.

The CO_2 concentration data recorded for each of the individual tests were averaged over the run time of the test and are presented in Table 7-5 for the three campaigns. This table also includes the corresponding standard deviations (SDs). Large SDs shown in the table for all the tests are believed to be attributed to the various engine power levels used for each test. The test-average CO_2 concentration data were used in the calculation of PM EI's from the integrated samples and will be presented in Sections 8 (PM Mass Emissions) and 13 (PM-Phase Chemical Composition).
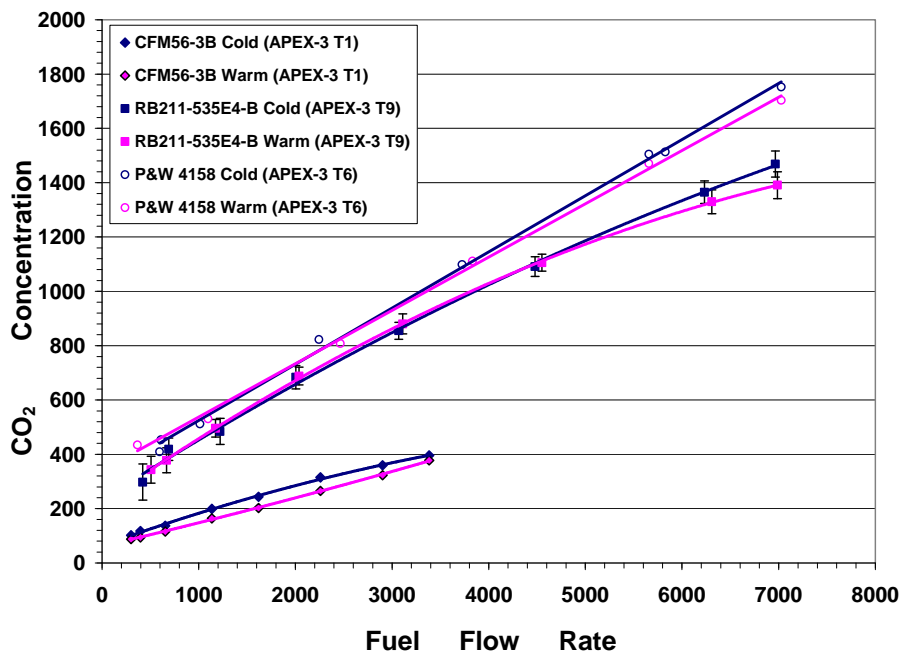
Figure 7-7. **Effects of cold and warm engine conditions on CO_2 emissions for multiple engine types.**

Table 7-5.   Test-Average Background Corrected CO_2 Concentrations for Each Test

Campaign	Test	CO_2 (ppm)	
		Test Average	**Standard Deviation**
APEX-1	EPA-1	605	179
	EPA-2	527	192
	EPA-3	294	269
	NASA-1	601	170
	NASA-1a	730	264
	NASA-2	659	269
	NASA-3	676	212
	NASA-4	583	282
	NASA-5	647	266
APEX-2	T2	739	265
	T3	738	233
	T4	518	233
APEX-3	T1	204	99
	T2	647	501
	T3	179	101
	T4	172	138
	T5	461	282
	T6	802	440
	T7	947	486
	T8	563	448
	T9	710	362
	T10	301	126
	T11	752	353

This page intentionally left blank.

8.   Particulate Matter Mass Emissions

The PM-2.5 mass emissions were investigated by converting the PM number concentration data measured by the Nano-SMPS and EEPS into the PM mass concentrations assuming unit density and spherical morphology using Equations 5.18 and 5.19 The PM number concentration data measured by the ELPI were not used for this mass emission conversion because the ELPI measurements did not represent the entire particle size distribution and, without correct particle size distribution information, the mass concentrations could not be appropriately converted from the particle number concentration. Also note that the Nano-SMPS or EEPS were only operated in the plume sampling system of the DEAL. Therefore, for the Nano-SMPS, the ambient background was determined before and after each test and averaged to correct the data. The EEPS data were not background corrected since the background had been determined to have a negligible effect on the experimental results.

From the PM-2.5 mass concentration, the mass emission index was calculated using the CO_2 concentration and carbon in the fuel according to Equation 5.12. The particle mass emission rate was then calculated by multiplying the mass emission index with the corresponding fuel flow rate using Equation 5.13. Thus, from the particle number concentrations corrected and uncorrected for line loss, the mass emission results before and after line loss corrections were calculated. The mass emission indices and emission rates obtained from the Nano-SMPS and EEPS are shown in Tables D-1 and D-2, respectively, in Appendix D. In this section, the Nano-SMPS was used as the primary instrument to determine EI_M.

The TEOM and QCM were also used in this study to directly monitor the PM mass emissions from the various jet engines. The TEOM was installed in both the plume and background sampling systems to allow for background correction in the calculation of the PM mass emission indices from measurements. The QCM was only employed in the plume monitoring, and therefore its results are not background-corrected. The TEOM measurements were conducted for all three APEX campaigns. The QCM was only employed in the APEX-2 and APEX-3 campaigns. Due to the experimental difficulty of this study, the readings recorded by the TEOM and QCM were extremely unstable in some of the tests. Negative readings of PM mass concentration were recorded under some of the power conditions, and these tests showed very poor correlations between the measured PM mass concentrations and engine power (fuel flow rate). In the APEX-1 campaign, the TEOM measurements failed in all of the tests except NASA-2. In the APEX-3 campaign, TEOM measurements failed for tests T2, T3, T4, T8, and T9, and QCM measurements failed for tests T2, T4, T5, T8, and T9. Therefore, these data are not reported here.

The data recorded by the TEOM and QCM were the mass concentrations for all sizes of particles. Since particle losses are particle size dependent, the correction of line particle losses for the data collected by these two instruments becomes difficult. To correct particle losses from the TEOM and QCM measurements, a particle loss correction coefficient was used. The particle loss coefficient is a ratio of the

test-averaged particle mass concentration after line loss correction to the test-averaged concentration before line loss correction calculated from the Nano-SMPS measurements. The loss correction coefficient derived from Nano-SMPS data is assumed to apply equally well to TEOM and QCM data. Table 8-1 presents the particle loss correction coefficient for each test in this study.

Table 8-1.   Particle Loss Correction Coefficient Determined from Nano-SMPS Measurements for Each Test

APEX	Test	Nano-SMPS Mass Concentration (mg/m^3)		Loss Correction Coefficient
		Before Loss Correction	After Loss Correction	
1	EPA-1	0.00620	0.00858	1.38
	EPA-2	0.0102	0.0142	1.40
	EPA-3	0.0103	0.0144	1.40
	NASA-1	0.0098	0.0132	1.35
	NASA-1a	0.0178	0.0240	1.35
	NASA-2	0.0135	0.0187	1.38
	NASA-3	0.0247	0.0355	1.44
	NASA-4	0.00918	0.0120	1.31
	NASA-5	0.0169	0.0226	1.34
2	T1	0.00923	0.0104	1.12
	T2	0.00877	0.00982	1.12
	T3	0.0154	0.0172	1.11
	T4	0.00851	0.00962	1.13
3	T1	0.0251	0.0278	1.11
	T2	0.0908	0.0997	1.10
	T3	0.00496	0.00553	1.11
	T4	0.00434	0.00481	1.11
	T5	0.0822	0.0901	1.10
	T6	0.0389	0.0429	1.10
	T7	0.0522	0.0576	1.10
	T8	0.0406	0.0461	1.13
	T9	0.0407	0.0446	1.10
	T10	0.00692	0.00774	1.12
	T11	0.0592	0.0647	1.09

The ratio for each test in the table is an average over the entire test and is assumed to be constant regardless of the variation of the engine power load. Therefore, the line loss correction for an uncorrected mass emission index measured for a certain power level of a jet engine was made by multiplying the mass emission index with a corresponding loss correction coefficient. The TEOM and QCM results before

and after sampling line particle loss correction, including the emission indices and emission rates under various power levels for different jet engines, are summarized in Tables D-3 and D-4, respectively, in Appendix D.

Finally, the mass emission indices for different jet engines were determined on a test-average basis from the Teflon filter sampling. The gravimetric analysis of Teflon filters for the APEX-2 campaign failed, and results are not reported for that campaign. The PM mass emission index obtained from a filter sample was an average value over various engine power settings for an entire test. These test-average mass emission results will also be discussed in this section.

The discussion of particle mass emissions will be based primarily on the measurement results made with the sampling probe located 30 m downstream of the tested engines. The effect of the probe position on the PM emissions will be discussed in Section 10.

8.1   Effect of Fuel Flow Rate and Engine Thrust

The mass emission index is expected to be correlated to the rated engine thrust as a function of fuel flow rate. Figure 8-1 shows the typical relationships between the particle mass emission index and the fuel flow rate obtained by the Nano-SMPS for the CFM56-2C1 engine powered with different jet fuels: base fuel (top left), high sulfur fuel (top right), and high aromatic fuel (bottom left). The data used in the graphs were obtained from the NASA-1a, NASA-2 and NASA-5 tests of the APEX-1 campaign, respectively.

Figure 8-1 shows that the particle mass emission indices (EI_M) under these test conditions ranged from ~20 to 160 mg/kg. Unlike the particle number emission index, the value of EI_M decreased when the fuel flow rate increased from around 300 kg/h. At 1000-2000 kg/h, the EI_M reached the minimum and then increased with the fuel flow rate. Similar trends of the EI_M with fuel flow rate for the CFM56-2C1 engine were also reported by other participants of the APEX-1 campaign (Anderson et al., 2006). Wey et al. (2006) reported that their line-loss-corrected mass-based emission indices derived from SMPS-type measurements for the APEX-1 campaign were typically 10 to 30 mg/kg in the low power ranges (less than 65%) and more than 200 mg/kg at climb and takeoff thrust. The EI_M value first decreased as the power load increased from idle, and the value reached the lowest at the middle range of rated thrust, after which EI_M increased with the power load. Lobo et al. (2006) reported from their APEX-1 measurements that the EI_M values ranged from 1 to 370 mg/kg fuel, values which are close to what was obtained by EPA during the same tests.

The PM particle mass emission indices for the CFM56-3B1 (T2 of APEX-2) and CFM56-7B24 (T4 of APEX-2) jet engines as derived from the Nano-SMPS are presented as a function of fuel flow rate in Figure 8-2. The figure shows a similar trend in the EI_M of varying with the fuel flow rate for both engines. In general, the value of EI_M always showed the minimum at mid-range fuel flow rates of 1000–1500 kg/h, corresponding to the operation of engines near approach power (30%).
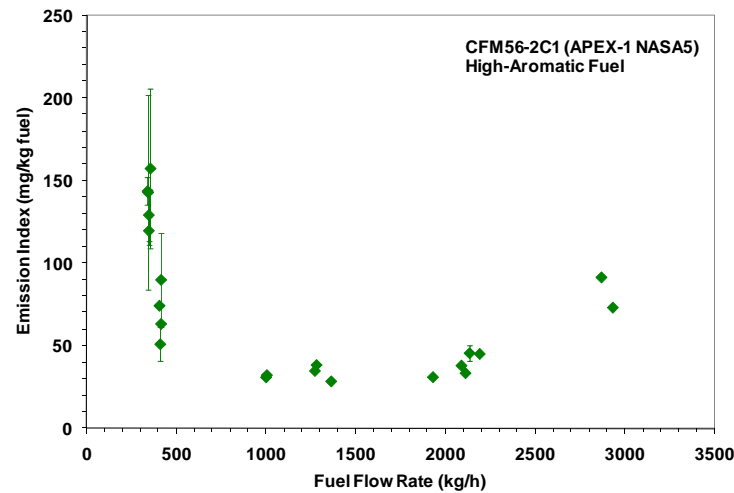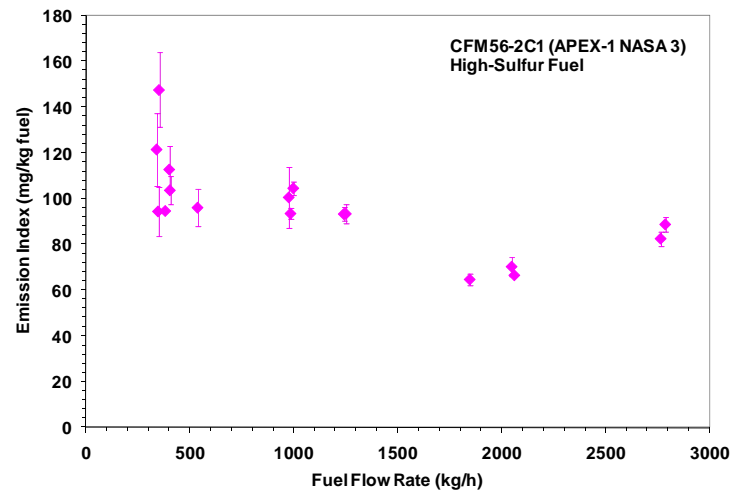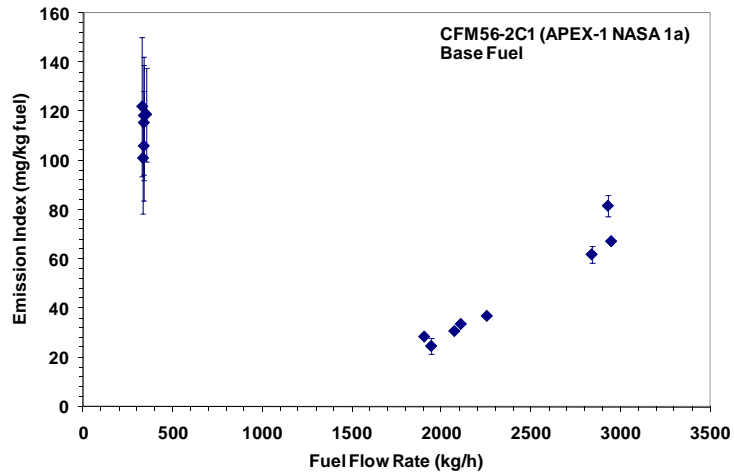
Figure 8-1. PM-2.5 emission index as a function of fuel flow rate by Nano-SMPS for the CFM56-2C1 engine. Data shown are corrected for sampling line particle losses.
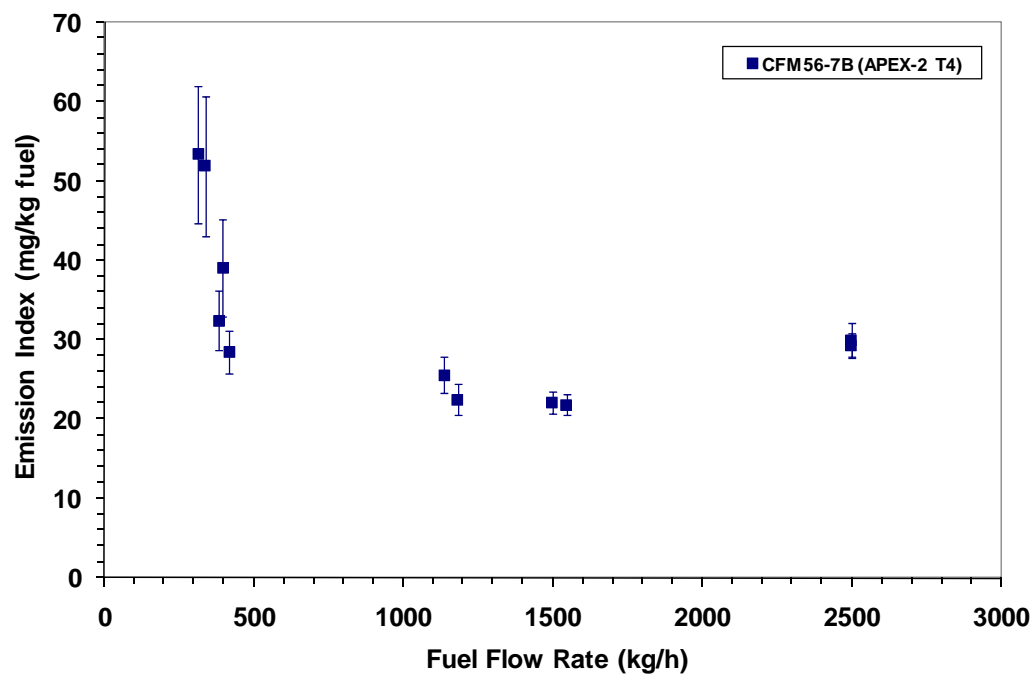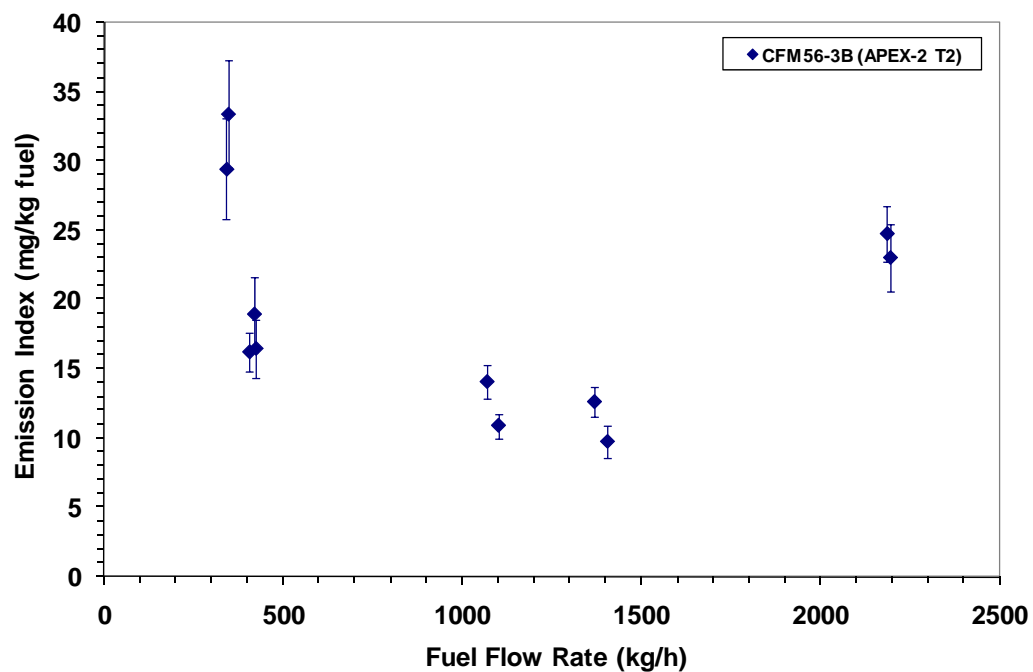
Figure 8-2. PM-2.5 mass emission index as a function of fuel flow as determined by the Nano-SMPS for: (a) APEX-2 T2; and (b) APEX-2 T4. Data corrected for sampling line loss.

Figure 8-3 shows the particle mass emission indices as a function of fuel flow rate for the CJ610-8ATJ turbojet engine. The data were derived from the Nano-SMPS measurements from the 30-m probe in test T5 of the APEX-3 campaign. Like the results of particle number emissions discussed in Section 9.1 for this engine, the variation of the particle mass index with the fuel flow rate did not show the same pattern as that for the turbofan engines in this study. Figure 8-3 shows that, unlike the characteristic U-shaped curve, the EI_M value monotonically increases with fuel flow rate.
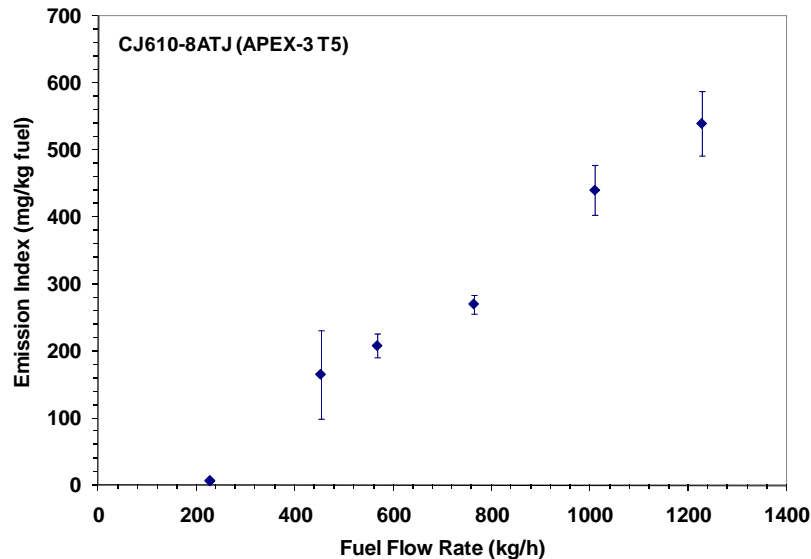
Figure 8-3. PM-2.5 mass emission index as a function of fuel flow rate as determined by the Nano-SMPS for the CJ610-8ATJ jet engine in APEX-3 T5. Data shown are corrected for sampling line particle losses.

Test T10 from APEX-3 is the only test that conducted sampling at 30-m for the AE3007 series jet engine. Figure 8-4 presents the emission indices obtained from this 30-m sampling by the Nano-SMPS. The values of EI_M derived from the measurements of the Nano-SMPS show a trend of the EI_M with the engine load such that the value of EI_M reached the minimum at fuel flow rates around 300 kg/h where the engine was operated in approach mode.

The Nano-SMPS measurements during APEX-3 tests T6 and T7 for the P&W 4158 jet engine are presented in Figure 8-5. A trend similar to the CFM56 is shown with the values of EI_M decreasing with an increase in engine load and reaching the minimum at fuel flow rates around 1000 to 2000 kg/h, after which the EI_M increased with the fuel flow rate.

The results for the RB211-535E4-B jet engine obtained from tests T8 and T9 from APEX-3 are shown in Figure 8-6 as derived from the Nano-SMPS measurements. There were no valid data available from the TEOM and QCM for this engine. The figure shows that the EI_M of the RB211 varied with the fuel flow rate in a trend similar to that observed for the P&W 4158 engine below ~5000 kg/h. However, as the fuel flow rate increased above ~4,600 kg/h, the EI_M for the RB211 started to decrease rather than to continuously increase as was seen for the P&W 4158 and the other turbofan engines tested. Note that the RB211 is an internally mixed-flow engine, unlike the P&W 4158 and CFM56.
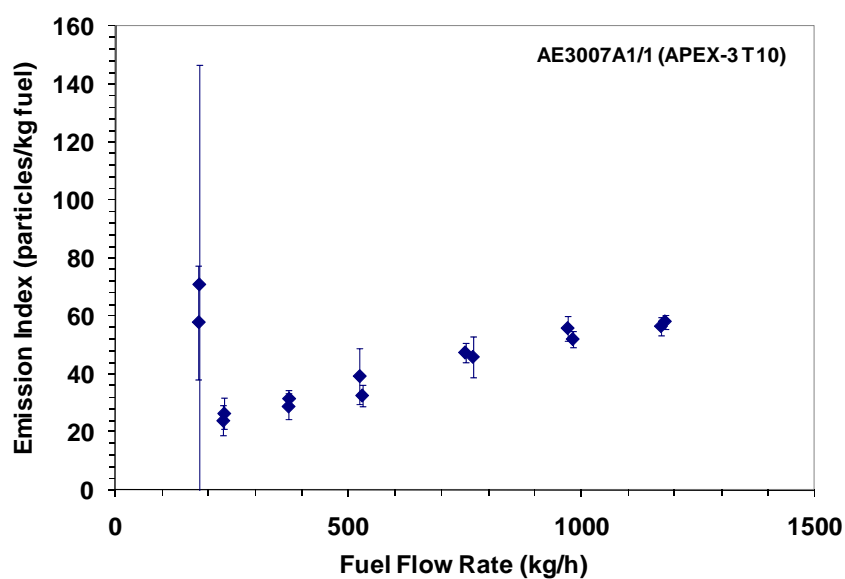
Figure 8-4. PM-2.5 mass emission index as a function of fuel flow rate as determined by the Nano-SMPS for the AE3007A1/1 jet engine in APEX-3 T10. Data shown are corrected for sampling line particle losses.
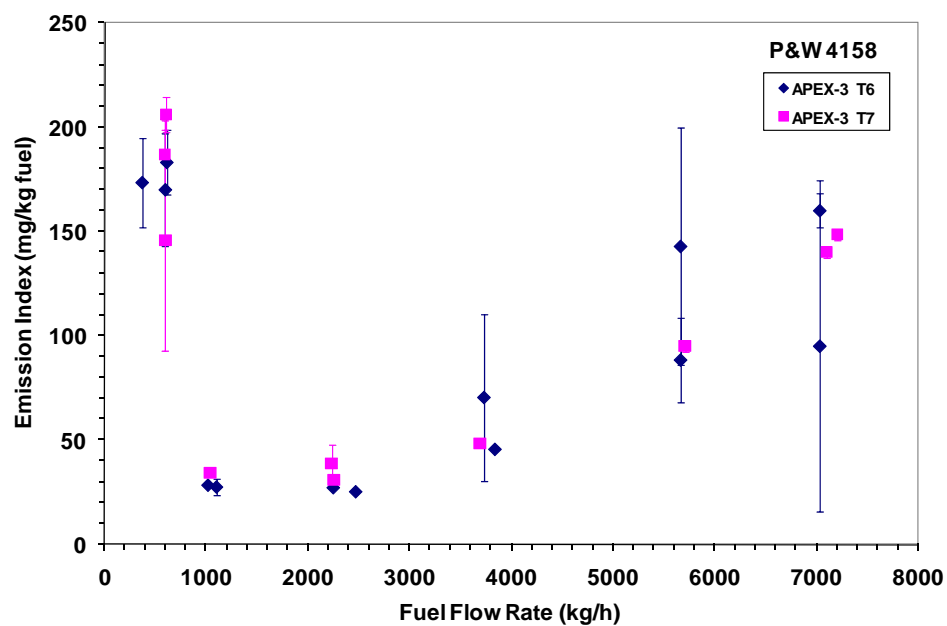
Figure 8-5. PM-2.5 mass emission index as a function of fuel flow rate as determined by the Nano-SMPS for P&W 4158 jet engine in APEX-3 T6 and T7. Data shown are corrected for sampling line particle losses.
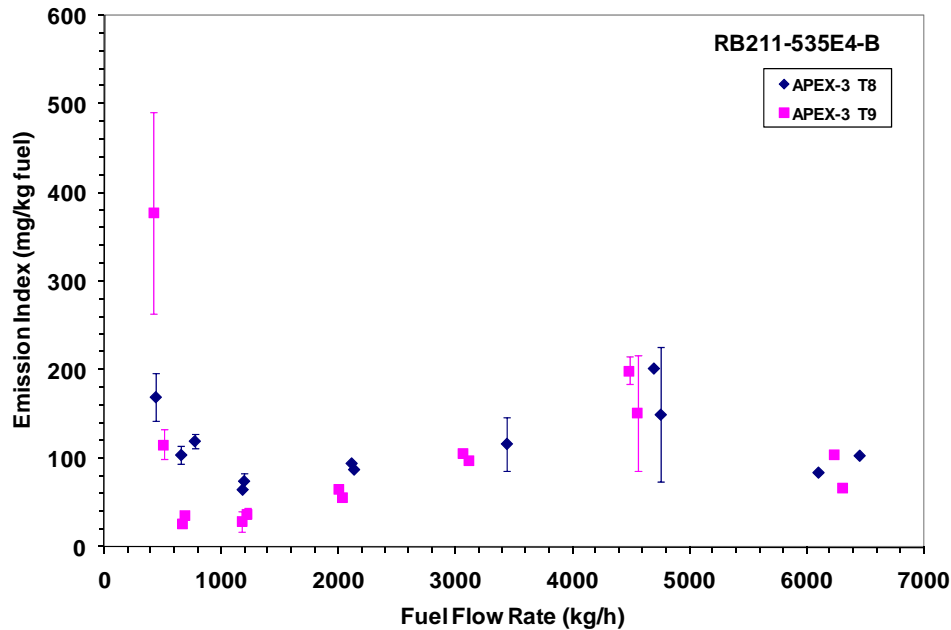
Figure 8-6. **PM-2.5 mass emission index as a function of fuel flow rate as determined by the Nano-SMPS for RB211-535E4-B jet engine in APEX-3 T8 and T9. Data shown are corrected for sampling line particle losses.**

The particle mass emissions for the ICAO landing and take-off (LTO) thrust levels were also evaluated. Only four engine types had particle mass emission data collected at 30 m during all four ICAO-defined engine operating modes of idle (7%), takeoff (100%), climb (85%) and approach (30%). These four engines, tested during the APEX-3 campaign, were the CFM56-3B1, CJ610-8ATJ, AE3007A1/1 and RB211-535E4-B, which will be used as examples of the entire APEX data set. The lowest-rated thrust for the AE3007A1E engine was 8.4 percent, and the data collected under this rated thrust were used to represent the idle engine condition to compare with the other engines at 7 percent rated thrust. Although tests EPA-1, EPA-2, and EPA-3 from the APEX-1 campaign were specifically designed for investigating the ICAO engine cycle, the Nano-SMPS measurements for the takeoff and climb modes were inadequate for this analysis. Also, the four tests conducted during the APEX-2 campaign did not include 100 percent takeoff thrust. The average particle mass emission index results derived from the Nano-SMPS measurement under the four modes for these engines are summarized in Table 8-2.

Figure 8-7 presents the average emission indices at the four power conditions for the CFM56-3B engine. As shown, the highest PM mass emissions were observed at takeoff power, followed by climb, idle, and approach, respectively. Thus the CFM56-3B engine had the best combustion efficiency when it was operated at approach power, and emitted the most PM-2.5 mass per kilogram of fuel at 100 percent takeoff power.

Table 8-2.   Effect of Engine Power on Average Emission Index for Different Engines

Engine	APEX-3 Test	Engine Cycle	Emission Index	
			Average	SD[a]
			(mg/kg)	(mg/kg)
CFM56-3B1	T11	Idle (7%)	146	21.3
		Takeoff (100%)	256	10.0
		Climb (85%)	215	8.21
		Approach (30%)	110	8.25
CJ610-8ATJ	T5	Idle (7%)	6.28	1.128
		Takeoff (100%)	540	47.5
		Climb (85%)	441	37.3
		Approach (30%)	166	65.8
AE3007A1/1	T10	Idle (8.4%)	64.4	55.4
		Takeoff (100%)	57.3	2.89
		Climb (85%)	53.9	3.53
		Approach (30%)	30.2	3.63
RB211-535E4-B	T9	Idle (7%)	31.6	3.87
		Takeoff (100%)	67.1	2.18
		Climb (85%)	101	3.22
		Approach (30%)	60.7	4.34

[a] SD = standard deviation.
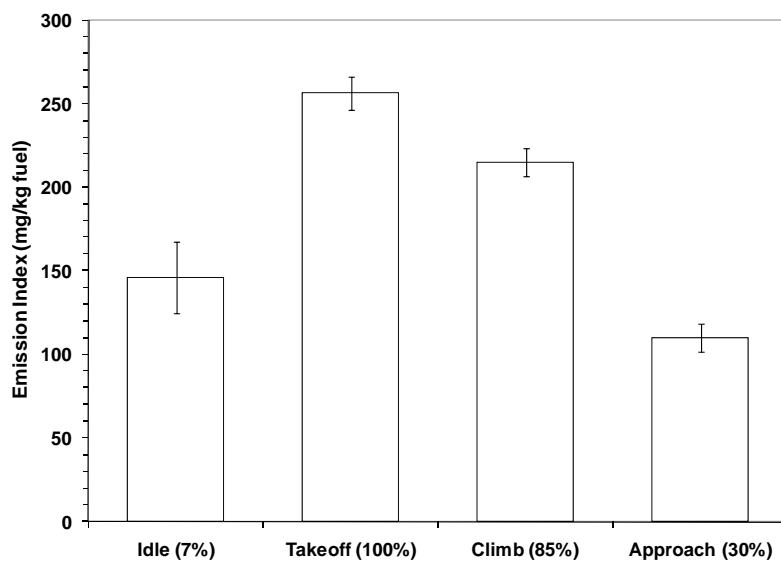
Figure 8-7.   Effect of engine operating mode on PM-2.5 mass emissions for a CFM56-3B1 engine. Based on Nano-SMPS loss corrected data.

For the CJ610-8ATJ turbojet engine, shown in Figure 8-8, the emission index was the highest at takeoff, similar to the CFM56-3B engine. The climb mode ranked the second, with the lowest value of EI_M at idle.

The mass emission indices for the internally mixed flow AE3007A1/1 engine tested in APEX-3 are shown in Figure 8-9. Unlike the other three engines, the AE3007A1/1 engine had the highest EI_M value at idle. The EI_M at takeoff ranked second and was the lowest under the approach mode.
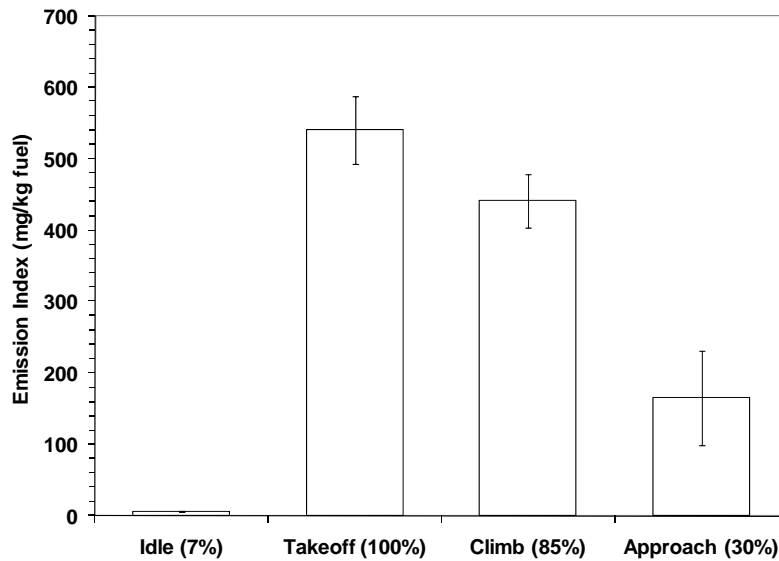
Figure 8-8. **Effect of engine operating mode on particle mass emissions for a CJ610-8ATJ turbojet engine. Based on Nano-SMPS loss-corrected data.**
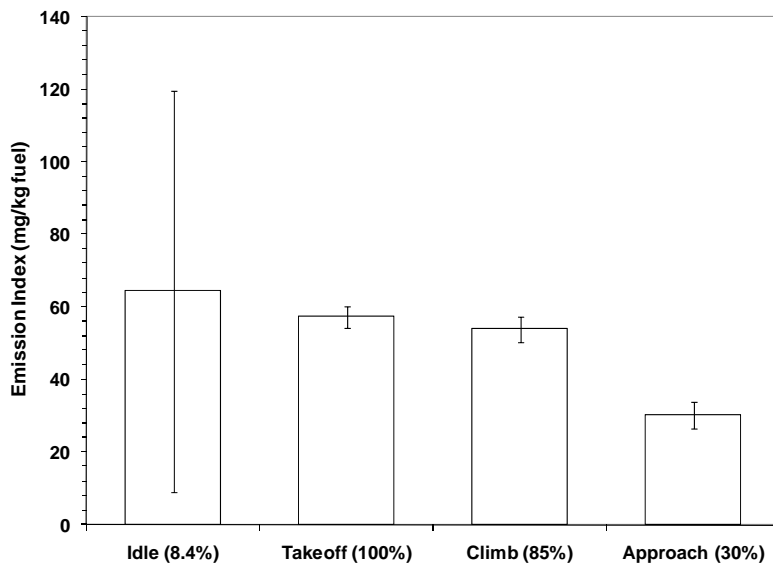
Figure 8-9. **Effect of engine operating mode on particle mass emissions for an AE3007A1/1 engine. Based on Nano-SMPS loss-corrected data.**

94

The PM mass emission index derived from the Nano-SMPS measurements for the RB211-535E4-B engine are presented in Figure 8-10. The emission index was the highest when the engine was operating at climb-out power, unlike the other three engines. This observation was also verified by the EEPS measurement results available for this test. In the order of their magnitude, climb > takeoff > approach > idle.
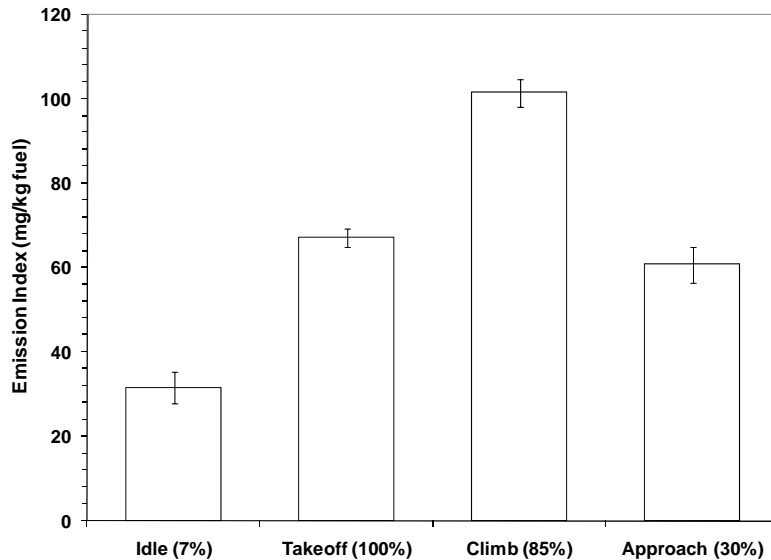
Figure 8-10. Effect of engine operating mode on particle mass emissions for a RB211-535E4-B engine. Based on Nano-SMPS loss corrected data.

8.2 Effect of Fuel Composition

The effects of fuel composition on PM particle mass emission index were investigated based on the results obtained in the APEX-1 campaign. The average emission indices at individual power levels derived from the Nano-SMPS measurements are summarized in Table 8-3. The data were collected from three tests with different fuels: EPA-2 and NASA-1a using the base fuel, NASA-3 using the high-sulfur fuel, and NASA-4 using the high-aromatic fuel.

Figure 8-11(a) compares the mass emission indices as a function of fuel flow rate between these different types of fuels. This figure shows that high-sulfur fuel emits more mass of particles per kg of fuel at all the tested power conditions. Like the particle number emissions, the high particle mass emissions from the high-sulfur fuel are believed attributable to the formation of additional sulfate particles. Although the base fuel showed slightly lower particle number emissions in comparison to the high-aromatic fuel, as will be discussed in Section 9, Figure 8-11(a) shows no obvious difference between these two fuels in terms of the particle mass emission index.

To further illustrate the effect of fuel sulfur on the particle mass emissions, the particle mass emission indices obtained by the Nano-SMPS were plotted against the sulfur content in the fuel for idle and approach power as shown in Figure 8-11(b). The CFM56 jet engine results were used, including the data obtained from the -2C, -3B, and -7B models tested in the three APEX campaigns. The mass emission

95

indices for the same level of engine rated thrust and the same sulfur content were averaged and presented in this figure. Although the Nano-SMPS data were only adequate for 7 and 30 percent power levels, all of the data show linear relationships between the mass emission index and the sulfur content in fuel. The particle mass emission index increased with the sulfur content. The linear equations and corresponding correlation coefficients are also shown in the figure.

Table 8-3.   Comparison of Emission Indices by Different Type of Fuels (Based on Nano-SMPS particle loss-corrected results)

Fuel Type	Power (%)	Fuel Flow (kg/h)	Loss Corrected Emission Index (mg/kg Fuel)	
			Average	SD*
Base Fuel	4	336	108	24.6
	7	425	45.0	12.8
	30	1023	22.6	2.69
	60	1922	26.6	2.47
	65	2088	32.2	1.21
	70	2252	36.9	1.11
	85	2904	70.2	3.39
High-Sulfur	4	356	115	12.7
	7	403	108	8.33
	15	538	96.1	8.21
	30	986	100	7.98
	40	1246	93.4	3.54
	60	1846	64.7	2.49
	65	2054	68.4	3.08
	85	2774	85.7	3.06
High-Aromatic	4	344	53.0	16.7
	5.5	381	33.1	15.5
	7	401	33.3	5.60
	30	962	23.6	0.941
	40	1218	21.7	1.11
	60	1850	19.9	0.402
	65	2019	23.6	1.37
	85	2700	59.4	2.66

*SD = Standard Deviation
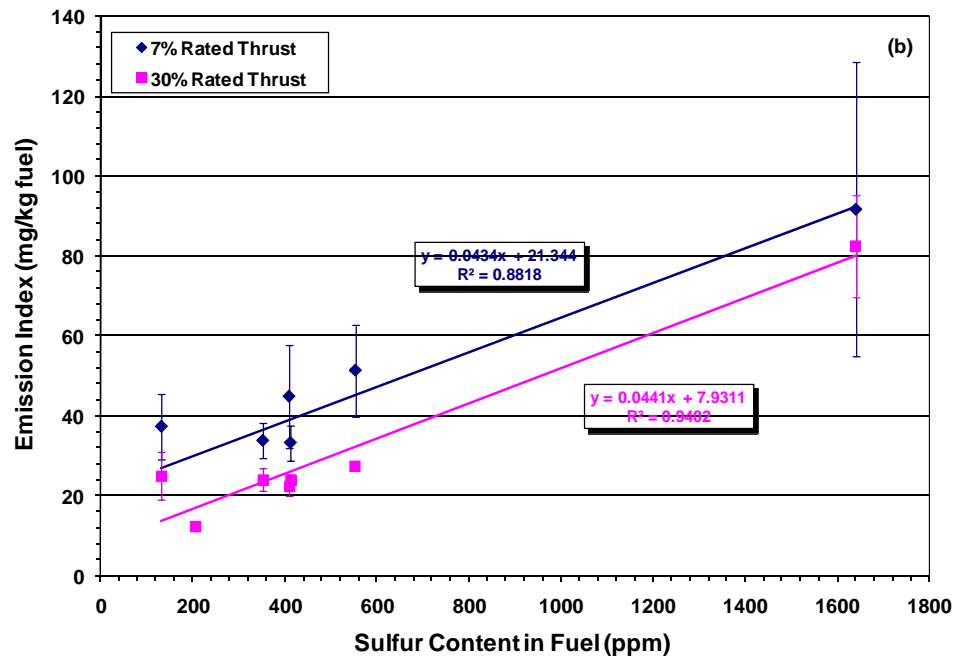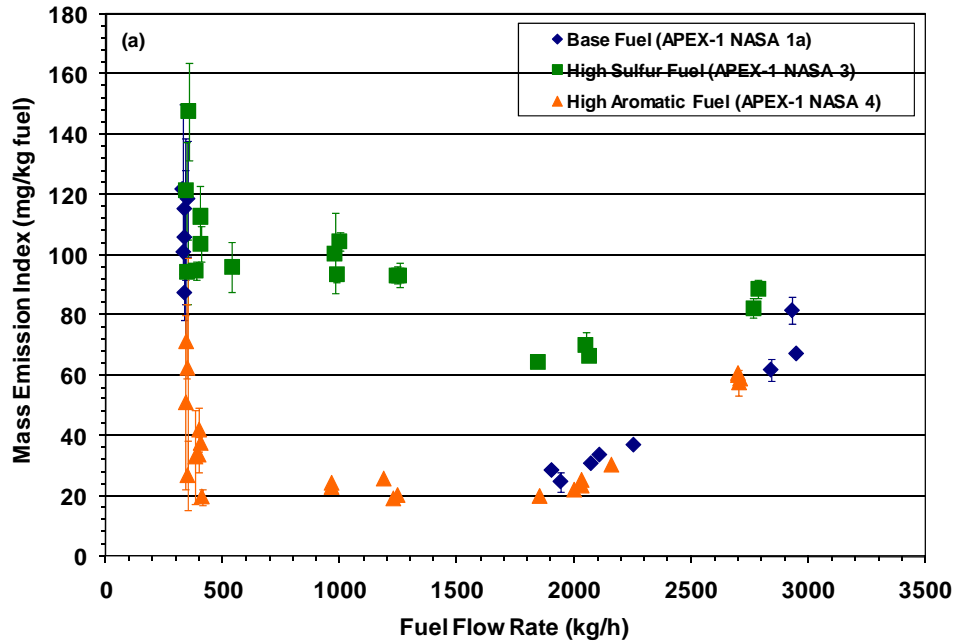
Figure 8-11. Effects of fuel type on: (a) mass emission index (CFM56-2C1) and (b) mass EI as a function of fuel sulfur (all CFM56 derivatives). Based on Nano-SMPS loss-corrected results.

The effect of jet fuel sulfur content on particle mass emissions as discussed in this report is also consistent with the findings presented in the NASA APEX-1 report. Wey et al. (2006) reported that the high-sulfur fuel generated both more number and mass of particles in comparison to the other two types of fuel tested. A discussion of fuel sulfur conversion efficiency is provided in Section 13.1.

8.3   Effect of Engine Type

In Section 8.1, the effects of engine power on PM emission index were shown to depend on the type of engine studied. Different types of engines can have different relationships of EI_M with power. For example, in the order of the particle number emission indices (see Section 9.1) for the CFM56-3B engine, approach is greater than idle which is greater than climb which, in turn, is greater than takeoff. This order is exactly the opposite of that obtained for the mass emission indices, indicating that the emitted particle sizes were different under the different engine operating modes.

The effect of engine type on the particle mass emissions was investigated using the results derived from the Nano-SMPS measurements. The average mass emission indices obtained from the different types of engine tested are compared in Figure 8-12. The figure consist of plots representing the four ICAO LTO engine thrust modes of idle, take-off, climb and approach. All of the data were obtained with the base fuel or fleet fuel and were measured at the 30-m sampling location. In Figure 8-12, the emission indices of different engines are presented as bars with the average EI_M value of each engine is written at the bottom of each bar.

The data for tests EPA-1 and NASA-1 from APEX-1 and test T1 from APEX-3 were not used due to the consideration of possible background interference as discussed previously. The data were averages from the different tests of the same engines under each of the four engine operating modes during all three test campaigns. As indicated earlier, the lowest rated thrust for the AE3007A1E engine was 8.4 percent, which was used for the idle condition for comparison with the other engines at 7 percent rated thrust. For the P&W 4158 engine, the data available at 80 percent thrust were averaged and compared with the other engines under climb condition at 85 percent thrust. There were no data available at engine take-off (100% thrust) for the CFM56-2C, CFM56-7B and P&W 4158 engines.

Because the fuel flow rate is related to both the engine rating and operating power, the fuel flow rates measured at the same power setting for the same engines were averaged and are also included in Figure 8-12 as the second y-axis. The fuel flow rate data in the figure (pink points with values above them) indicate that the P&W 4158 and the Rolls-Royce RB211-535E4-B were two of the largest engines in this study. The CJ610-8ATJ turbojet and AE3007A1/1 engines were the smallest, and the CFM56 derivatives were mid-sized in terms of thrust and fuel flow rate (also see Table 2-1 for engine specifications). Note that the average fuel flow rates shown in Figure 8-12 for each thrust setting were obtained only from those test periods that also had valid Nano-SMPS measurements. Therefore, some of the fuel flow values shown in the figure may not match those presented previously in Table 7-2.

A number of observations can be made from Figure 8-12. First, the smallest engine tested (CJ610-8ATJ turbojet) had the lowest EI_M under 7 percent idle power, whereas the largest engine evaluated (P&W 4158) exhibited the highest. The CJ610-8ATJ turbojet also displayed the largest EI_M for 100 percent take-off, 85 percent climb-out, and 30 percent approach, which is probably a function of its older combustor design. In addition, relatively good agreement in EI_M was shown for the three CFM56 variants tested, with the exception of climb-out. In this case, the EI_M varied over an order of magnitude for the three CFM56 models tested.
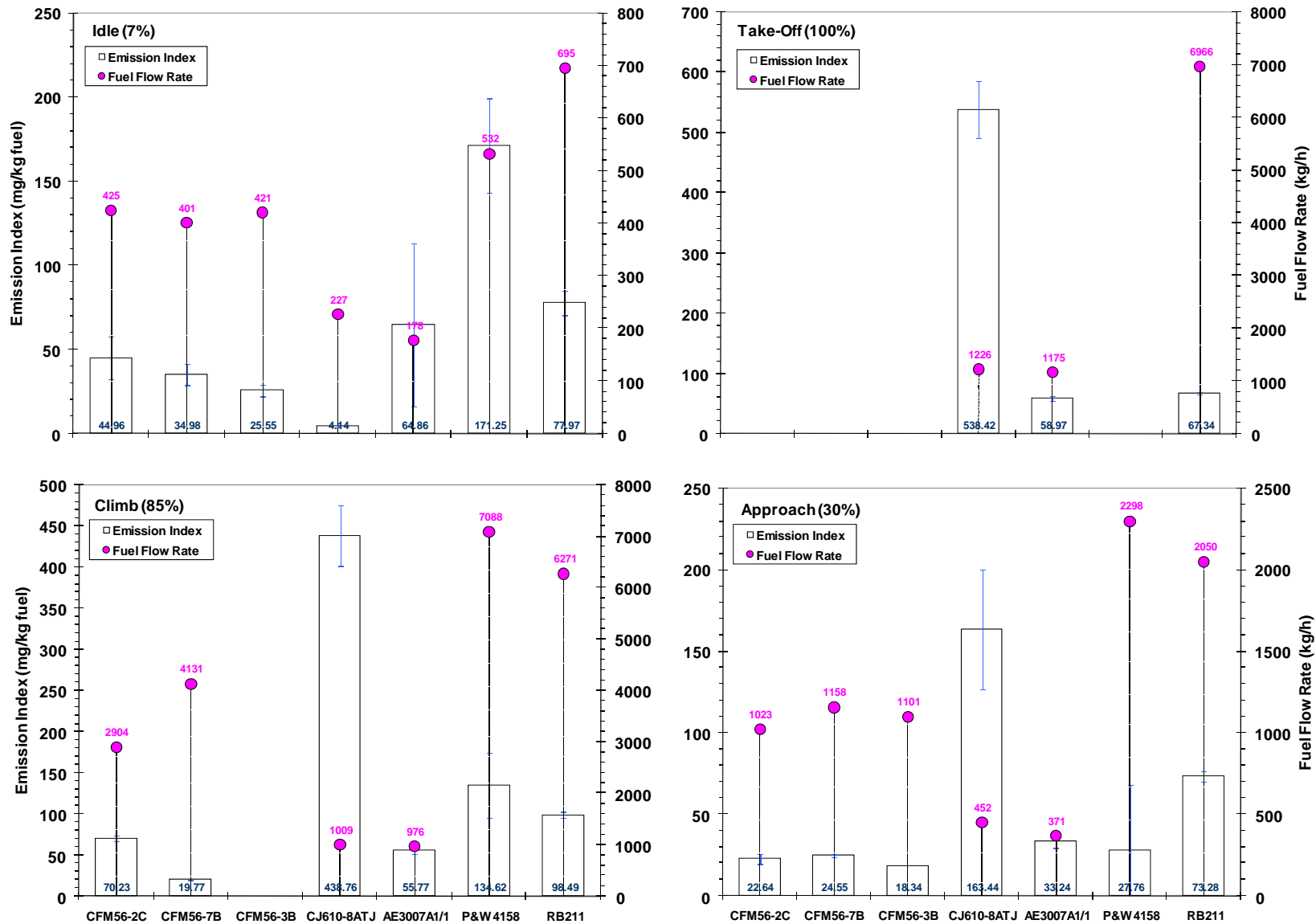
Figure 8-12. Effect of engine type on the PM-2.5 mass emission index for ICAO LTO power conditions. Based on the line loss corrected Nano-SMPS results.

8.4 Effect of Cold and Warm Engine Conditions

The particle mass emission results obtained by Nano-SMPS were used to investigate the effect of engine operating temperature on the mass emission index. Recall that "cold" refers to going stepwise up in power, whereas "hot" is the opposite. In Figure 8-13, the particle mass emission indices obtained under the cold condition were plotted against the emission indices obtained under the warm operating condition measured by the Nano-SMPS for the same engine. The diagonal line in the figure represents where the emission indices under cold and warm conditions would be identical.

The data obtained under the warm engine condition were linearly correlated with the data obtained for the cold condition. The correlation line had a slope of 0.92 with a correlation coefficient of 0.94. A slope less than one indicates that the engine had the higher efficiency and produced ~8 percent less PM mass at the warm condition than at the cold condition. Engine performance is expected to improve as it gets warmer. This trend is consistent with Lobo et al. (2007), and was also observed in terms of particle number, which will be discussed in Section 9.
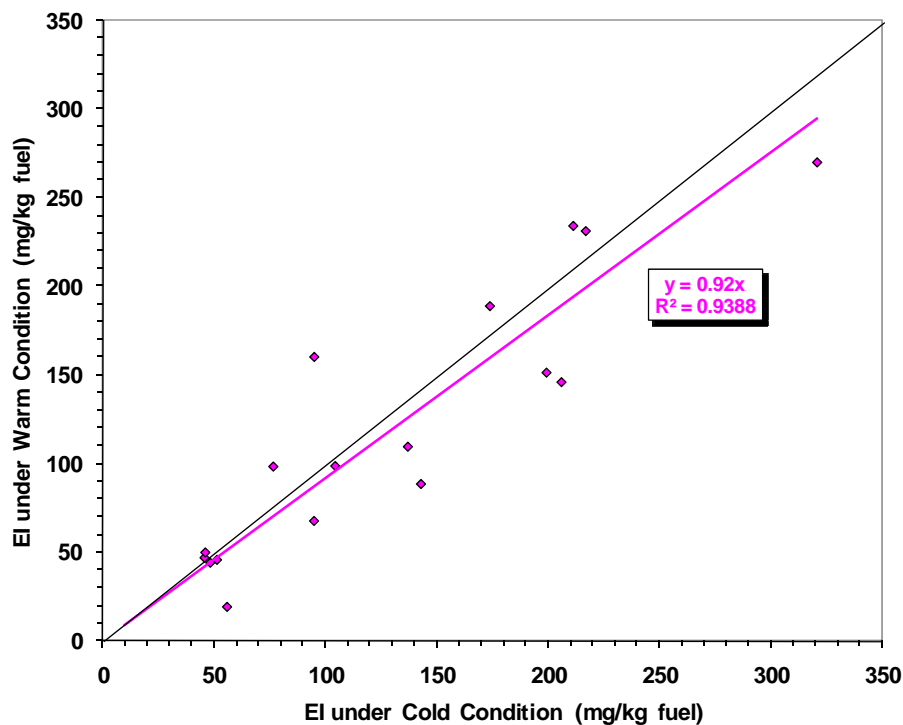
Figure 8-13.   Effect of cold and warm engine temperature on PM mass emission index.

8.5 Comparison of Particle Mass Emission Indices Obtained from Different Instruments

Since the ELPI could not produce appropriate particle size distributions for this jet engine study as discussed previously, the particle number emission data collected cannot be used to calculate the mass emission indices. The instruments that provided continuous mass emissions data were the Nano-SMPS, EEPS, TEOM and QCM. The EEPS was only used in the APEX-2 and APEX-3 campaigns.

Figure 8-14 is the comparison between the measurement results by the Nano-SMPS and EEPS. Mass emission indices derived from the particle number concentrations collected by the two instruments correlate very well for tests T2, T3, T10, and T11 from APEX-3, with a correlation coefficient (r^2) greater than 0.93. The linear correlation between the Nano-SMPS and EEPS results was even better for tests T4 and T5 from APEX-3 ($r^2 = 0.97$). However, the slope from the T4 and T5 tests was different from the slope for the other APEX-3 tests. A linear correlation between the mass emissions results of the two instruments for the four tests of APEX-2 was also observed, but with a relatively weak correlation coefficient ($r^2 = 0.74$). Figure 8-14 indicates that the EEPS had systematically higher measurement results than the Nano-SMPS in tests T1 to T4 from APEX-2 and tests T4 and T5 of APEX-3, but had lower measurements in T2, T3, T10, and T11 from APEX-3. The EEPS mass emission results for tests T6, T7, T8, and T9 during APEX-3 did not show linear correlations with the Nano-SMPS results, although their number emission results did.
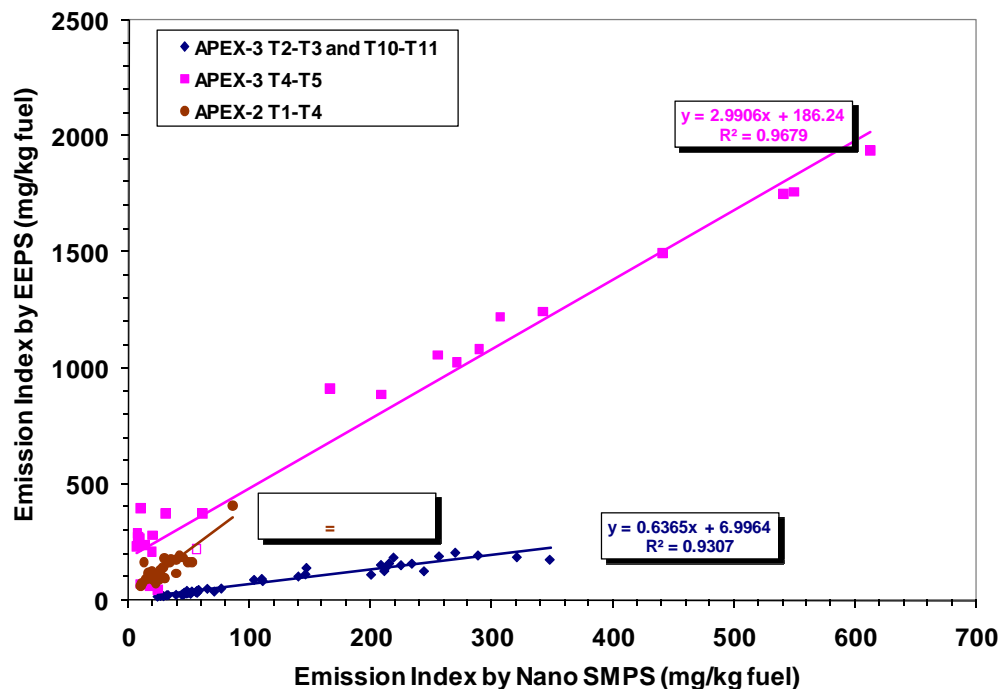
Figure 8-14. Comparison of the mass emissions indices between the Nano-SMPS and EEPS for different tests.

The TEOM and QCM were used in the study to directly monitor the particle mass emissions. However, their data were unstable and were useful only for some of the tests. The linear correlations between the Nano-SMPS and the TEOM measurements of successful tests are presented in Figure 8-15. Figure 8-16 shows the results from the Nano-SMPS with the successful QCM measurements. The lower correlation coefficients shown in these two figures indicate that the mass emissions data collected by TEOM and QCM were relatively scattered as compared to the number emissions data collected by the EEPS and ELPI (see Section 9). The higher slopes of the correlation lines in the figures mean that the measurements by TEOM and QCM were systematically higher than that obtained by Nano-SMPS in most of the cases in this study.
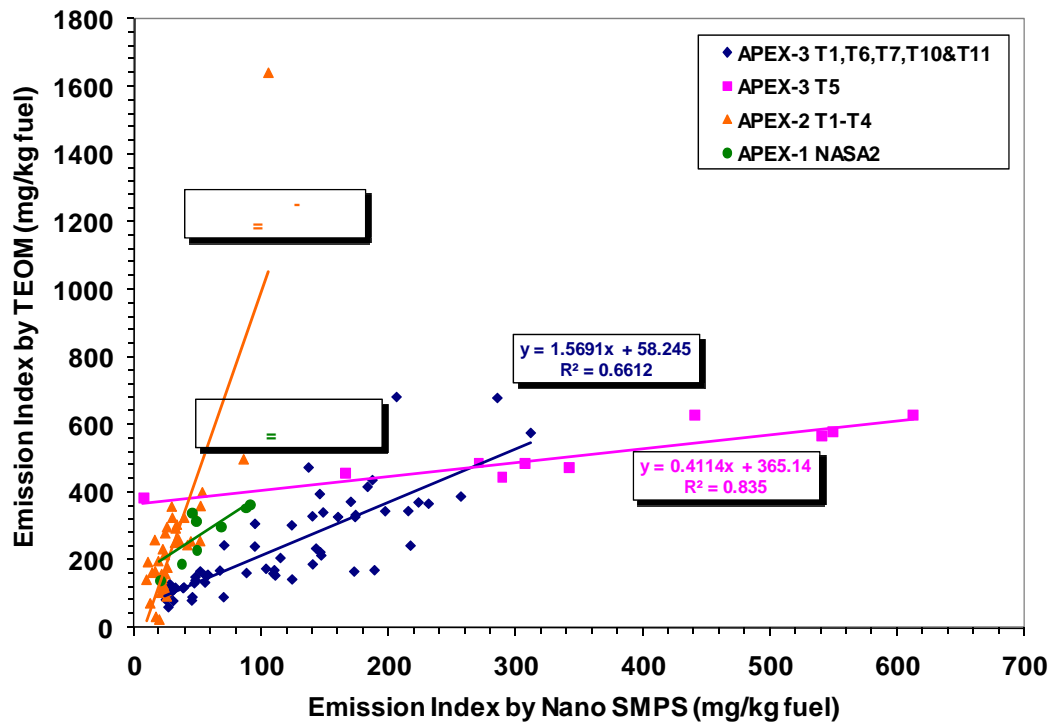
Figure 8-15. Comparison of the mass emissions indices between the Nano-SMPS and TEOM for different tests in APEX-2 and -3.
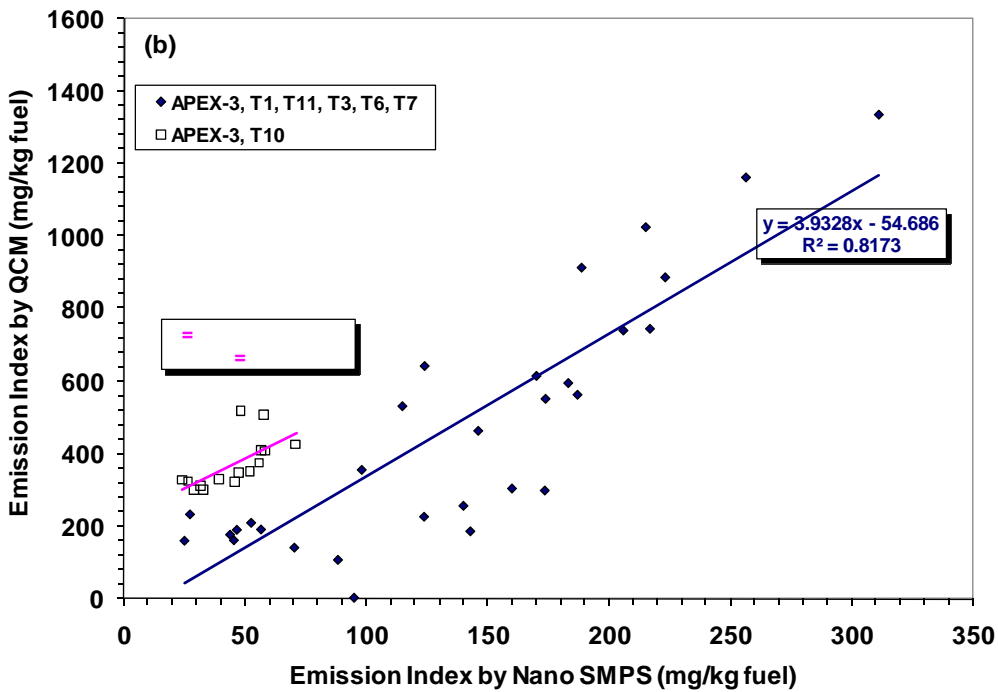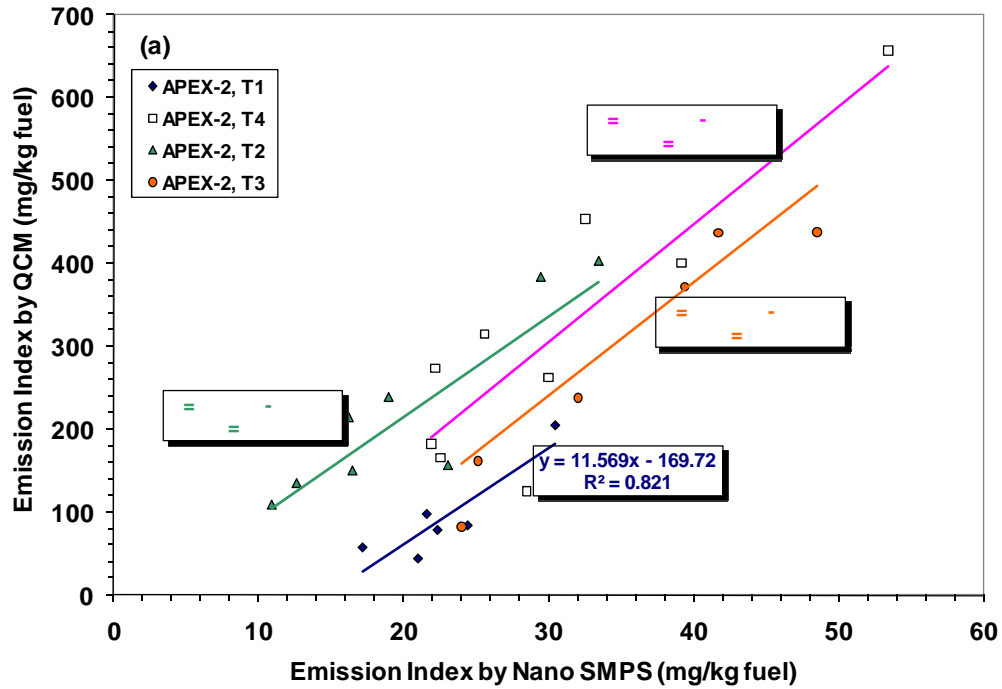
Figure 8-16. Comparison of the mass emissions indices between the Nano-SMPS and QCM for: (a) APEX-2 tests and (b) APEX-3 tests.

Table 8-4 summarizes how well the different instruments performed during all APEX tests. The M in the table indicates acceptable measurements where the correlation coefficients between the measurements of the EEPS, TEOM and QCM instruments and the measurements obtained from the Nano-SMPS were above 0.5. The (") sign represents tests during which the particular instrument failed to track with engine power and the correlation coefficient was less than 0.3.

Table 8-4.   Comparison of Instruments Used for Mass Emissions Measurements

Campaign		Airframe	Engine	Instrument[b]			
APEX	Test No.			Nano SMPS	EEPS	TEOM	QCM
1	EPA-1[a]	DC-8	CFM56-2C1	M	NA	"	NA
	EPA-2			M	NA	"	NA
	NASA-1[a]			M	NA	"	NA
	NASA-1a			M	NA	"	NA
	EPA-3			M	NA	"	NA
	NASA-2			M	NA	M	NA
	NASA-3			M	NA	"	NA
	NASA-4			M	NA	"	NA
	NASA-5			M	NA	"	NA
2	T1	B737-700	CFM56-7B24	M	M	M	M
	T4			M	M	M	M
	T2	B737-300	CFM56-3B1	M	M	M	M
	T3		CFM56-3B2	M	M	M	M
3	T1[a]	B737-300	CFM56-3B1	M	M	M	M
	T11			M	M	M	M
	T2	NASA Lear Model 25	CJ610-8ATJ turbojet	M	M	"	"
	T5			M	M	M	"
	T3	Embraer ERJ 145	AE3007A1E	M	M	"	M
	T4			M	M	"	"
	T10		AE3007A1/1	M	M	M	M
	T6	A300	P&W 4158	M	"	M	M
	T7			M	"	M	M
	T8	B757	RB211-535E4-B	M	"	"	"
	T9			M	"	"	"

a. Test with high cross wind in the background.

b. M = instrument measurements were acceptable.
    NA = not applicable.
    " = instrument's measurements were not linearly correlated with the Nano-SMPS.

8.6   Teflon Filter Integrated Sampling Results

In this study, the Teflon filters were used to collect the PM-2.5 samples in both the plume and background sampling systems. However, the gravimetric analysis of the Teflon filters obtained from the APEX-2 integrated sampling failed, and their results are not reported here. In APEX-1, integrated sampling was conducted for tests EPA-1, EPA-2, EPA-3, NASA-2&3, and NASA-4&5. The test called "NASA-2&3" represents the integrated sampling in which the same Teflon filters were used to collect samples during tests NASA-2 and NASA-3. The same qualification applies to NASA-4&5. For APEX-3, the tests conducting Teflon filter sampling included T3&4, T6&7, T9, and T11. All the Teflon filter data were background and line-loss corrected. The line-loss correction was done by using the loss correction coefficients obtained from the Nano-SMPS measurements as discussed previously.

The PM mass emission index derived from the Teflon filter integrated sampling is an average value over the entire test including start-up, shut down and transitions. The percentage of volatile matter in the PM collected by a Teflon filter for each test was estimated by dividing the PM mass concentration from the filter after the thermal denuder by that from the plume filter. The mass emission indices thus obtained by the Teflon filters for various tests, together with the test-average EI_M values derived from the measurements of other instruments, are summarized in Table 8-5.

The table shows that almost the same PM mass emission indices were obtained from tests EPA-3 and NASA-2&3 with the same high sulfur fuel, although their engine operation was different. The time-weighted thrust level and fuel flow rate were 20.4 percent and 797 kg/h for EPA-3 and 38.5 percent and 1278 kg/h for NASA-2&3, respectively. By averaging the results with the same fuels, the PM mass emissions and volatile contents for different fuels for the APEX-1 campaign were compared and are shown in Figure 8-17. The figure shows that the high sulfur fuel had the highest PM mass emission index and volatile fraction (79.3%) among the three types of fuels. This observation is generally consistent with the results obtained from the Nano-SMPS data. The volatile content in the PM emissions from the use of the base fuel and high-aromatic fuel ranged from ~62 to 66 percent.

The test-average mass emission index obtained by filter sampling for the CFM56-2C engine fueled with base fuel is compared to the indices for the other engines in Figure 8-18. The figure shows that the large, internally mixed flow RB211-535E4-B engine produced the most mass of particles per kg of fuel and the smallest volatile fraction, while the smallest engine, the AE3007A1/1 (also internally mixed) had the lowest mass emission index. The PM emitted from all engines contained 40–80 percent volatile matter. The CFM56 engines appeared to emit more volatile matter (62–80%) compared to the others shown.

Figure 8-19 compares the test-average emission indices derived from Teflon filter integrated sampling with the results derived from the Nano-SMPS measurements. The figure shows that the test average EI values were much higher from the Teflon filter sampling than from the Nano-SMPS measurements. The figure also shows that there was no linear correlation of results between two measurements. This lack of correlation is probably at least partially due to a slow instrument response time, which caused gaps in collecting sufficient data points for high thrust runs and transition from one thrust level to another in very short periods of time. Regardless of the cause, the large difference in EI_M obtained by the Teflon filter sampling compared to traditional SMPS measurements certainly warrants further investigation.

Table 8-5.   Test-Average PM Mass Emission Indices Derived from Measurements of Various Instruments

APEX	Test	Run Time (min)	Aircraft	Engine	Fuel	Emission Index (mg/kg fuel)		Nano-SMPS	EEPS	TEOM	QCM
						Teflon Filter					
						Total	% of Volatile				
1	EPA-1	188.53	DC-8	CFM56-2C1	Base	*	*	*	*	*	*
	EPA-2	150.7				305	62.0	35.2	nc	cc	nc
	NASA-1	197.03				*	*	*	*	*	*
	NASA-1a	112.3				nc	-	54.8	nc	cc	nc
	EPA-3	149.58			Hi-Sulfur	447	69.3	42.0	nc	cc	nc
	NASA-2	116.98				443	79.3	57.0	nc	cc	nc
	NASA-3	143.65						90.8	nc	cc	nc
	NASA-4	154.67			Hi-Aromatic	219	65.5	31.2	nc	cc	nc
	NASA-5	155.5						59.4	nc	cc	nc
2	T1	123.8	B737-700	CFM56-7B24	Fleet	gv	-	34.4	132	262	89.9
	T4	142.6				gv	-	31.7	131	244	117
	T2	135.8	B737-300	CFM56-3B1		gv	-	22.9	113	215	207
	T3	150.5		CFM56-3B2		gv	-	39.6	167	272	326
3	T1	115.6	B737-300	CFM56-3B1	Fleet	*	*	*	*	*	*
	T11	63.7				267	79.4	148	125	248	576
	T2	171.4	NASA Lear Model 25	CJ610-8ATJ turbojet		nc	-	266	153	cc	cc
	T5	146.1				nc	-	337	1221	532	cc
	T3	131.48	Embraer EMB145	AE3007A1E		116	61.8	53.6	83.5	cc	172
	T4	112.43						48.3	278	cc	cc
	T10	96.75		AE3007A1/1		nc	-	44.5	38.2	129	350
	T6	147.58	A300	P&W 4158		268	53.6	92.3	cc	178	cc
	T7	76.93						105	cc	243	cc
	T8	103.5	B757	RB211-535E4-B		384	40.9	142	cc	cc	cc
	T9	122.43						109	cc	cc	cc

*   High background interference (crosswinds) during the test.
nc   Not collected.
gv   Gravimetric analysis of Teflon filters failed.
cc   Poor correlation coefficient.
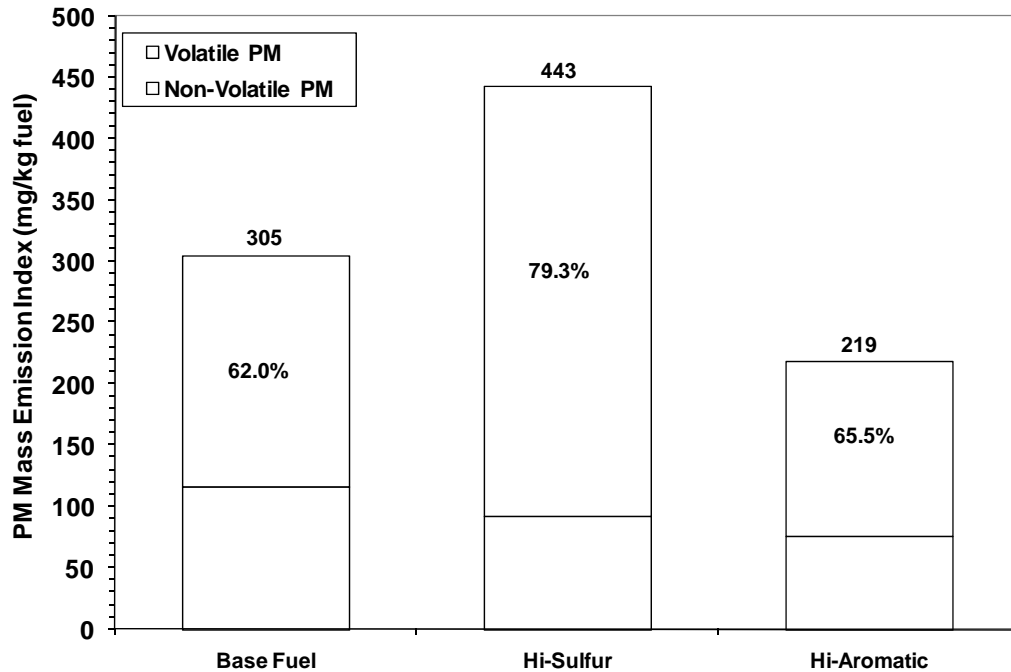
Figure 8-17. Effects of fuel type on test-average PM mass emission index from the Teflon filter for APEX-1 tests. Note that the percent volatile fraction is also shown in the figure.
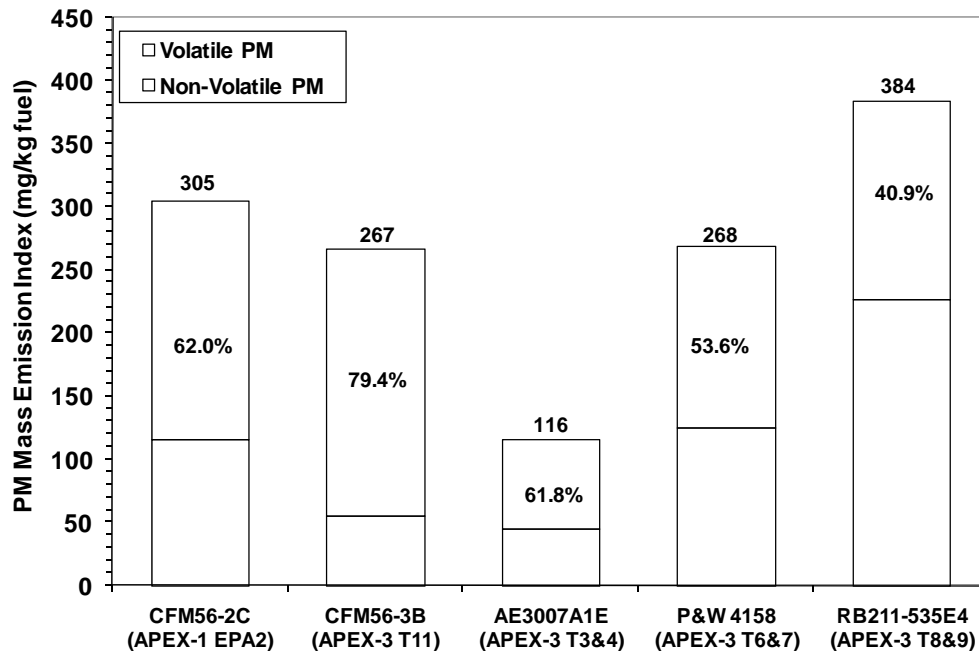
Figure 8-18. Effects of engine type on test-average PM mass emission index from the Teflon filter integrated sampling. Note that the percent volatile fraction is also shown in the figure.
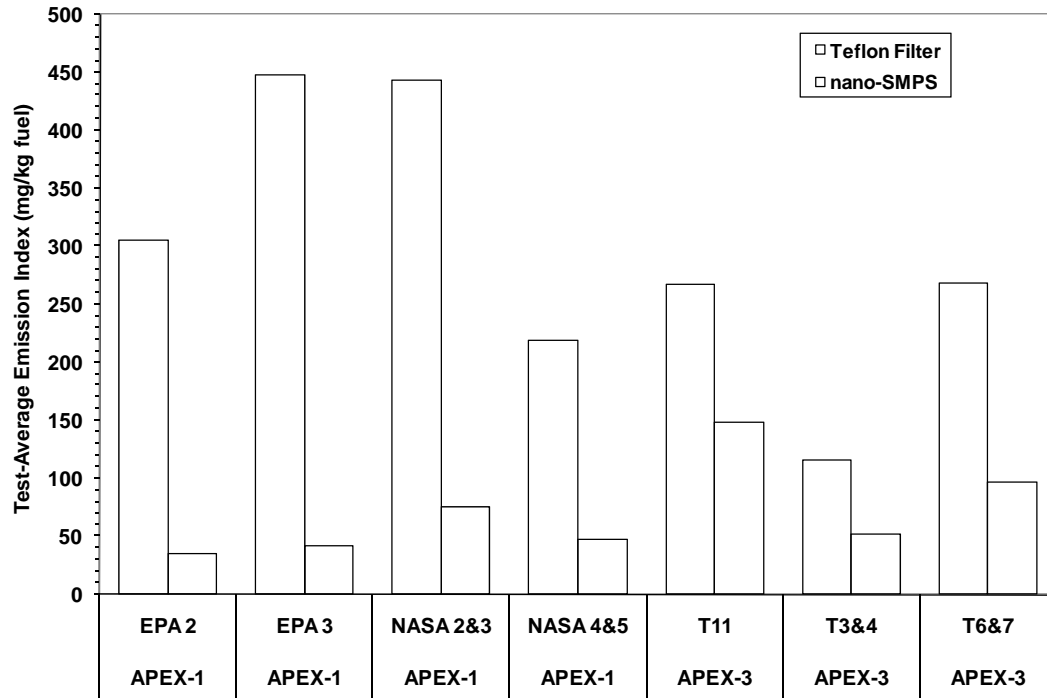
Figure 8-19. Comparison of the test-average emission indices between Teflon filter and Nano-SMPS measurements.

9.   PM Number Emissions

The PSD measurements made by the Nano-SMPS, EEPS and ELPI provided the particle number concentrations under various test conditions. The PM number emissions in this study were quantified by emission index (EI_N), which was expressed by the number of particles emitted from burning one kg of fuel. Although the ELPI was not useful in this study for the PSD determination due to the relatively large cut-off size of its lowest channel (see Section 10), the use of a filter stage enabled the instrument to measure the total particle number concentration for the jet engine PM emissions. Therefore, the PM number emissions data obtained from all three instruments are discussed in this section.

The ELPI was installed in both the plume and background sampling systems to allow for background correction in the calculation of PM number emission indices. However, the Nano-SMPS and EEPS were only used in the plume sampling system. Therefore, the PM number emission indices obtained from the Nano-SMPS were corrected for background using data collected before/after each test. A similar correction was not applied to the EEPS, however, since background had little effect on the EI_N values obtained.

The PM particle number emission indices and their SDs under various test conditions, both before and after sampling line particle-loss correction, are summarized in Table E-1 for the Nano-SMPS, in Table E-2 for the EEPS, and in Table E-3 for the ELPI as found in Appendix E. Note that the EEPS was not available during the APEX-1 campaign. In addition, the ELPI data were not available for some APEX-1 tests (NASA-1 and NASA-5) and APEX-3 tests (T2, T5, T8 and T10) due to sample recovery. Thus, these results are not reported in the tables. Because of the effects of the crosswind on the emission measurements during tests EPA-1 and NASA-1 from APEX-1, and test T1 from APEX-3 (as indicated in Table 7-1), the emission results from these tests were not used in the particle emission analysis and are not presented in the tables. Note also that the ELPI is subject to small particle artifacts, thus further limiting its usefulness.

It was difficult to run the jet engines under high power settings (e.g., 100% takeoff) for long periods of time. Therefore, few data points are available from the Nano-SMPS measurements at high power settings due to the slow instrument response.

In this section, the effects of the fuel flow rate, fuel type, engine type, engine cycle, engine temperature, and sampling probe location were studied based on the particle number emissions results corrected for sampling line particle losses, except where noted. The discussion in the following subsections will primarily be based on the results obtained from the measurements made by the 30-m probe with the Nano-SMPS.

9.1   Effect of Fuel Flow Rate

The particle number emission indices from the jet engines were found to strongly correlate to the fuel flow rate, which in turn is a function of rated engine thrust. Figure 9-1 shows the typical relationship between the particle number emission index and the fuel flow rate observed by the Nano-SMPS for the CFM56-2C1 engine burning three different jet fuels: base, high sulfur and high aromatic. The data used for these three fuels were obtained from the NASA-1a, NASA-2 and NASA-5 tests from the APEX-1 campaign, respectively. The average particle number emission indices range between 2×10^{15} to 8×10^{16} kg^{-1} with the value of EI_N decreasing with increasing fuel flow rate. The decrease in particle number emission index was much steeper at a fuel flow rate <1000 kg/h. The emission indices were below 1×10^{16} particles/kg when the fuel flow rates were greater than approximately 2000 kg/h for the base fuel, 1000 kg/h for the high-sulfur fuel, and 2500 kg/h for the high-aromatic fuel.

The above observation is consistent with the results reported in the NASA APEX-1 report for the 30-m probe (Wey et al., 2006). NASA found that the EI_N values at 30 m were typically 5 to 20 times greater than in comparable samples drawn from the 1-m probe, with the EI_N decreasing with increasing engine power. The EI_N values obtained for the APEX-1 test ranged from 2×10^{15} to 4×10^{16} kg^{-1}, which are close to the NASA results. NASA reported that the number-based emission indices varied from 1 to 5×10^{15} kg^{-1}.

Figure 9-2 presents the PM particle number emission indices as a function of fuel flow rate for the CFM56-3B1 and CFM56-7B24 engines. The CFM56-3B1 data are taken from the T2 test from APEX-2 and the T11 test from APEX-3, whereas the CFM56-7B24 emission indices were obtained from the T4 test from APEX-2. All models of the jet engine CFM56 show similar trends: the particle number emission index decreased with increases in fuel flow rate, except for the T11 test from APEX-3. In this case, the EI_N increases slightly above idle, then decreases in a fashion similar to the other CFM56 engines tested. Note, however, that APEX-3 T11 only included the cold portion of the engine operating cycle which could have influenced these results. A steep reduction was also observed in the particle number emission index with fuel flow rates less than 500 kg/h.

Figure 9-3 presents the particle number emission index as a function of fuel flow rate for the CJ610-8ATJ turbojet engine. This engine was evaluated in both the T2 and T5 tests from APEX-3. The emissions were sampled primarily by the 15-m probe, with only part of the data in the T5 test being measured by 30-m probe. Figure 9-3 shows the data for the T5 test as measured at the 30-m probe. These data do not follow the same trend that was observed for the CFM56 model engines shown above. This engine also exhibited a different trend in the EI_M with fuel flow compared to the other engines which were previously described in Section 8.

With the exception of engine CJ610-8ATJ, the relationship between the particle number emission index and the fuel flow rate for all the other types of engines tested in the three APEX campaigns was similar to the relationship observed for the CFM56 engines. For example, the results from the APEX-3 campaign for the AE3007 series engines are presented in Figure 9-4, the P&W4158 engine in Figure 9-5, and the RB211-535E4-B engine in Figure 9-6.
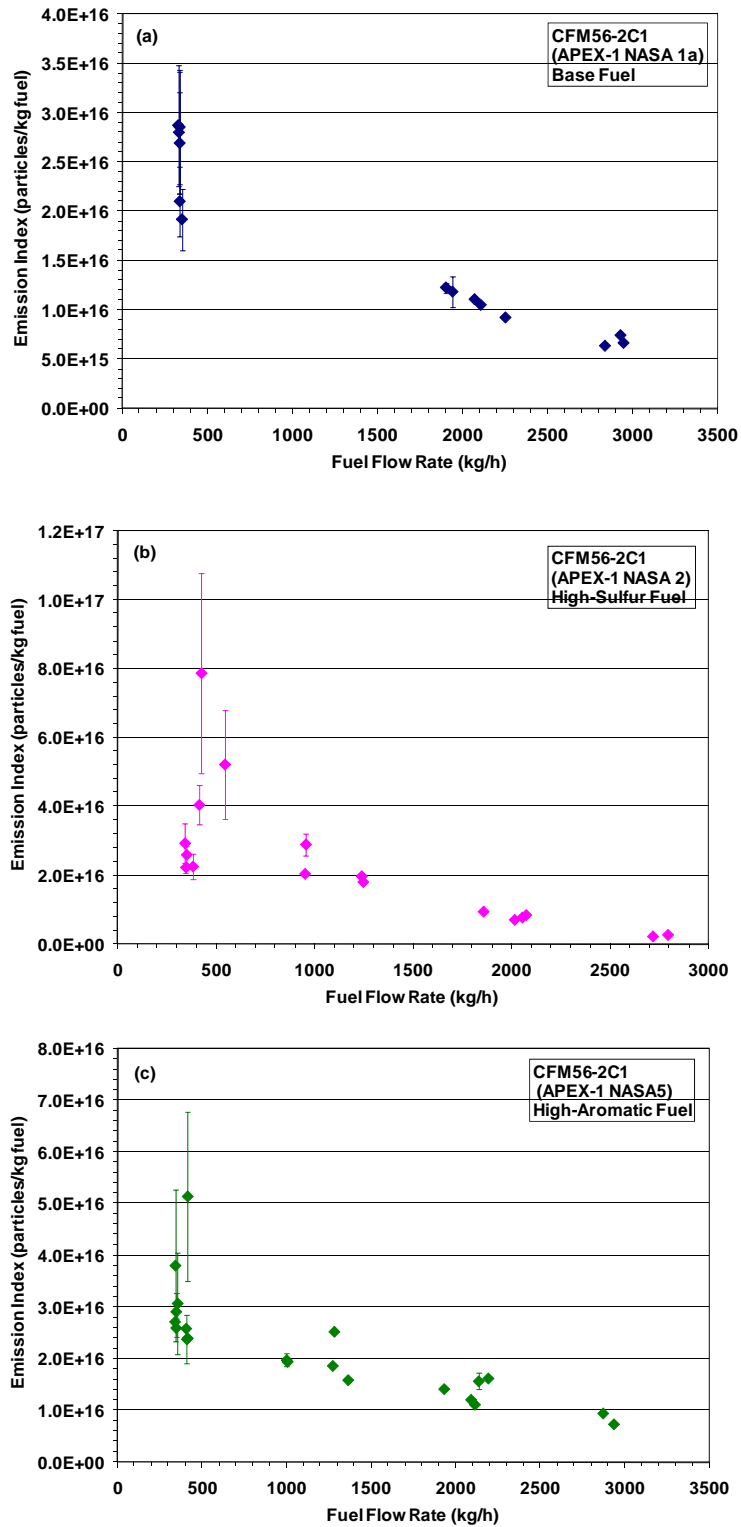
Figure 9-1. Particle number emission indices as a function of fuel flow as determined by the Nano-SMPS during APEX-1 for: (a) base fuel; (b) high-sulfur fuel; and (c) high-aromatic fuel.
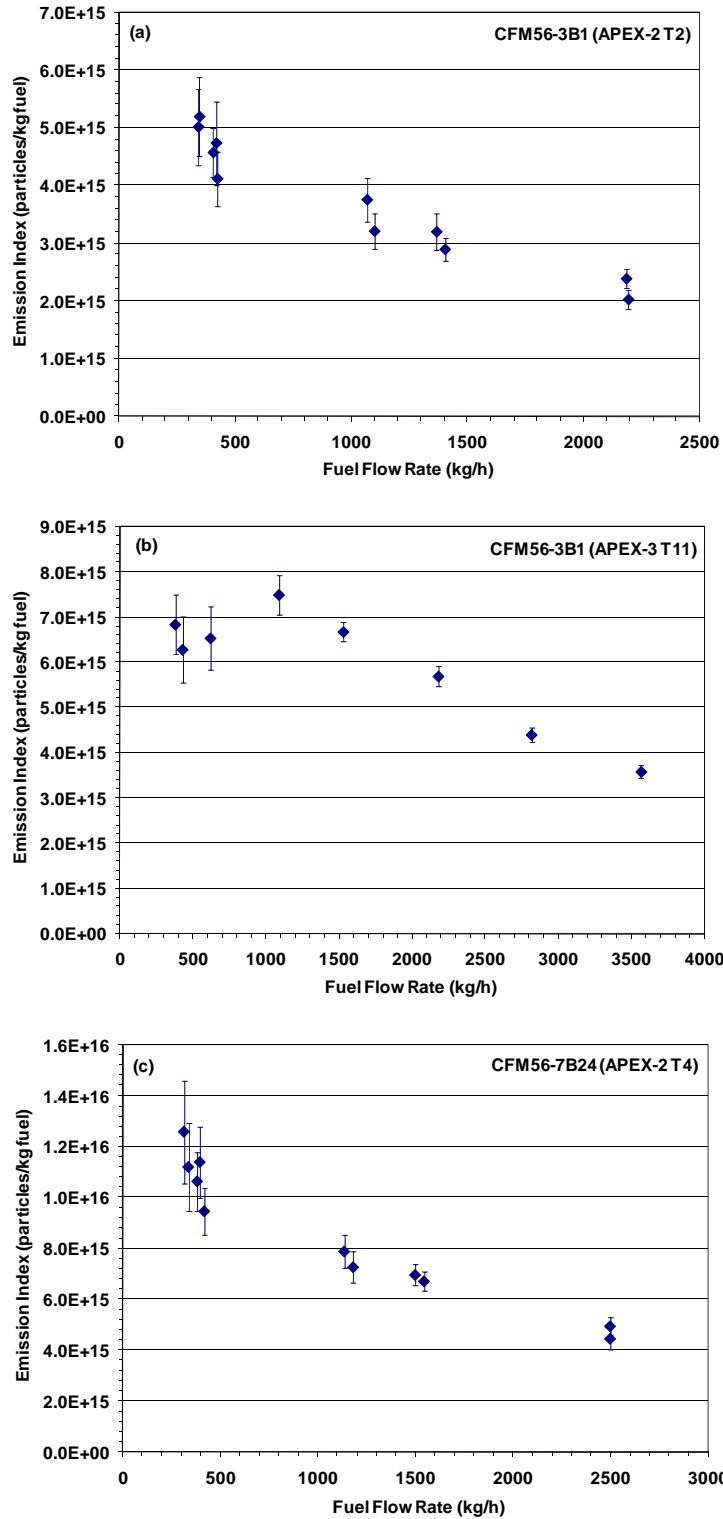
Figure 9-2. Particle number emission indices as a function of fuel flow as determined by the Nano-SMPS for two CFM56 engine models during: (a) APEX-2 T2; (b) APEX-3 T11; and (c) APEX-2 T4. Data shown are corrected for line losses.
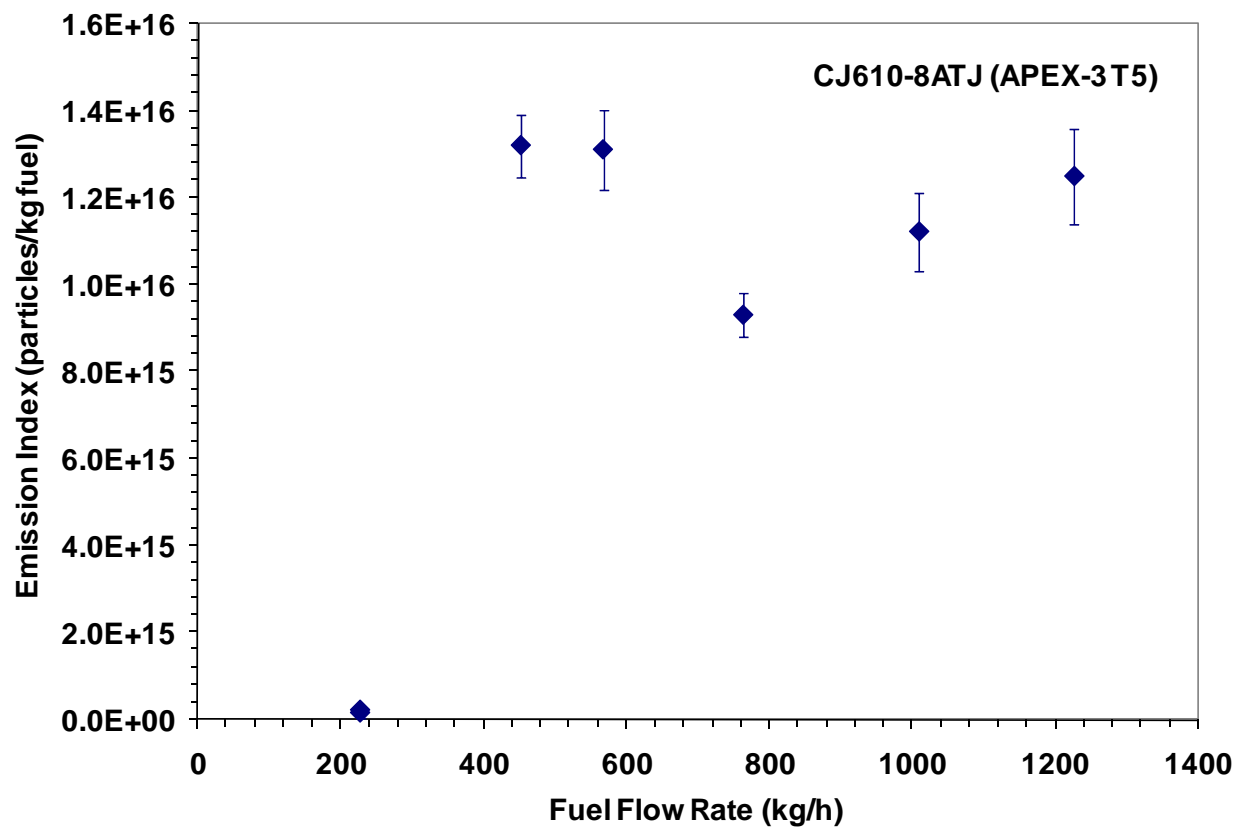
Figure 9-3. Particle number emission index as a function of fuel flow rate as determined by the Nano-SMPS for the CJ10-8ATJ turbojet engine. Data shown are corrected for sampling line particle losses.
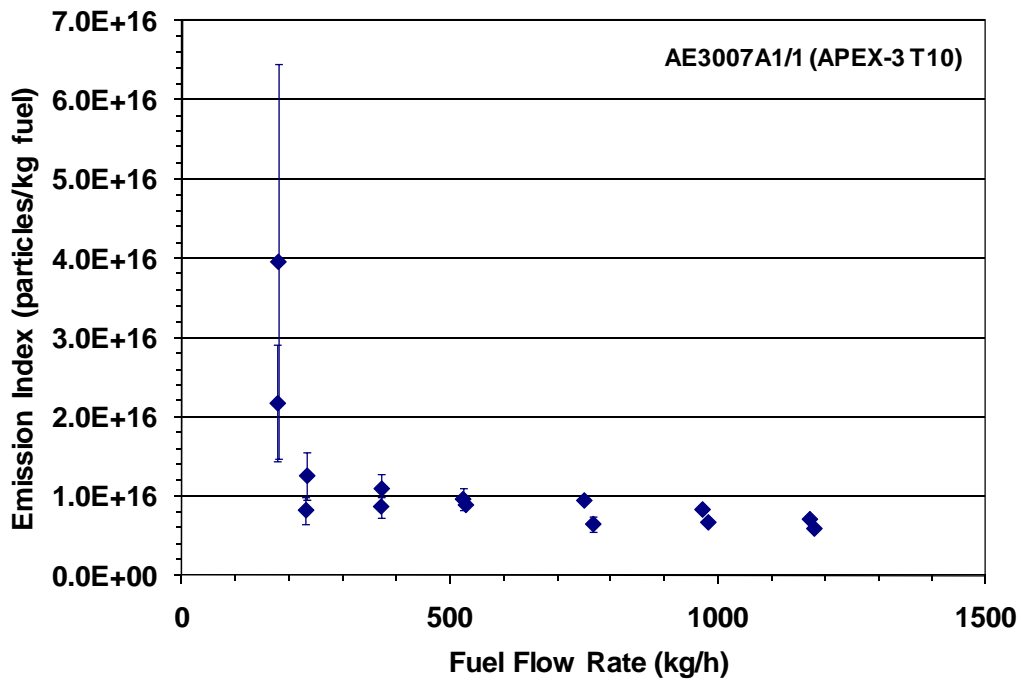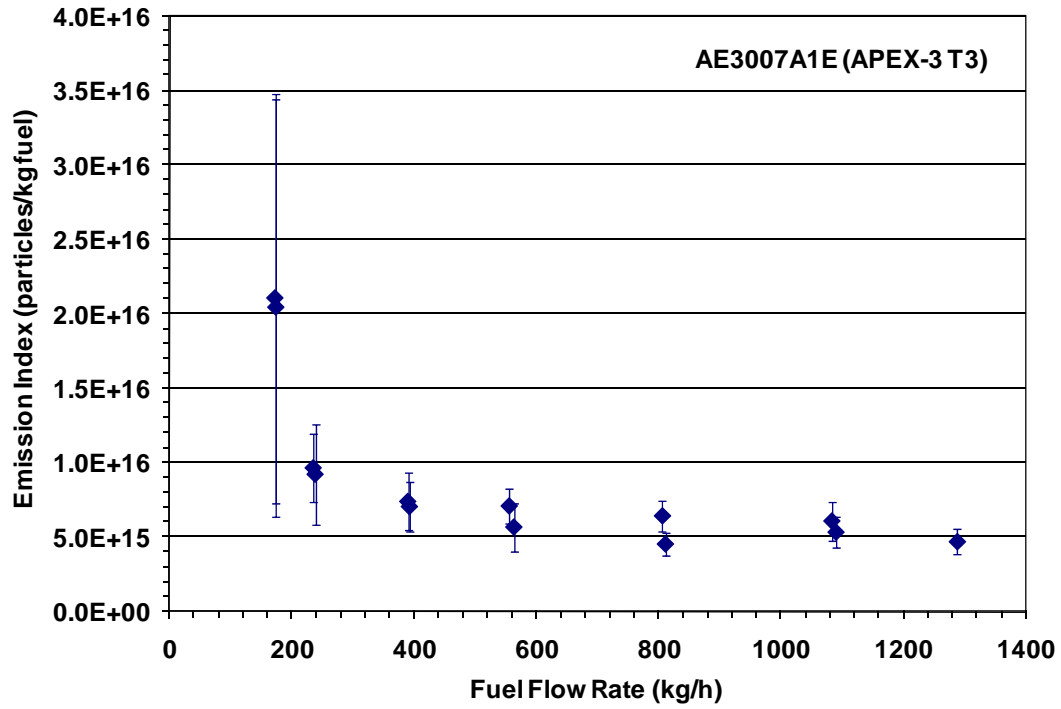
Figure 9-4. Particle number emission index as a function of fuel flow as determined by the Nano-SMPS for: AE3007A1E; and AE3007A1/1 engines. Data are corrected for particle line losses.
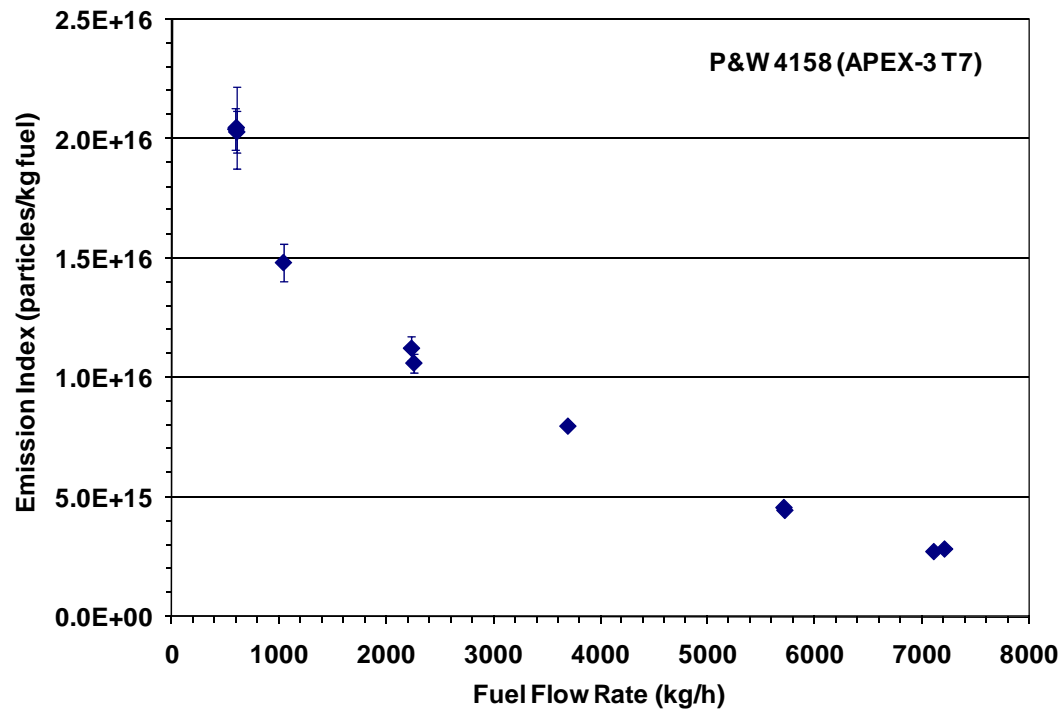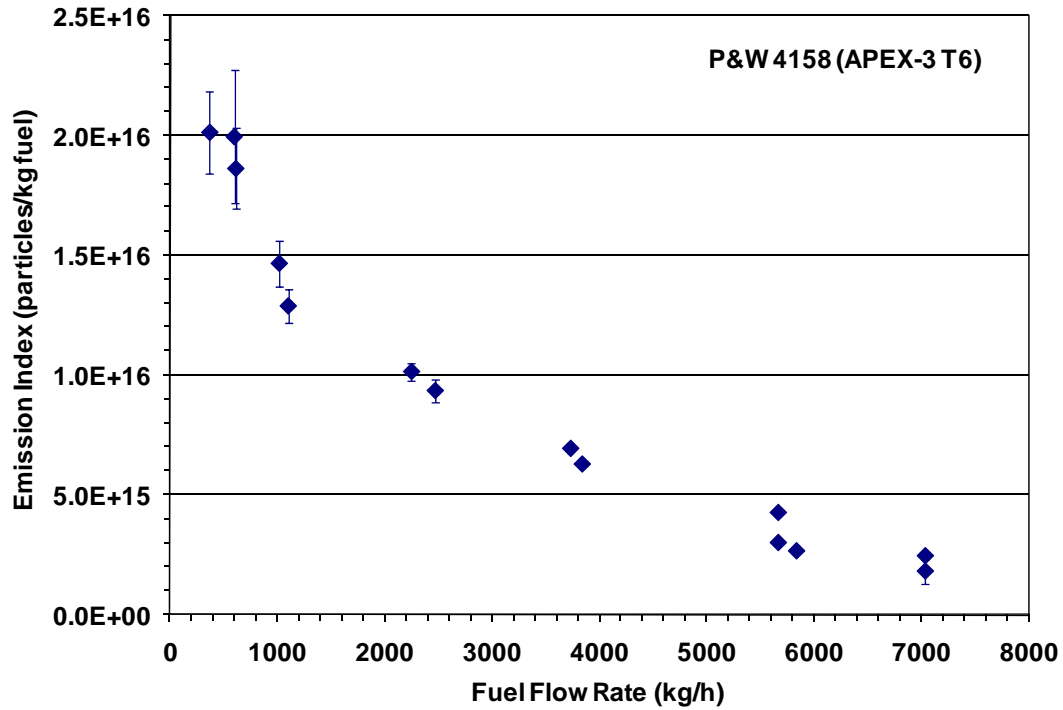
Figure 9-5. Particle number emission index as a function of fuel flow as determined by the Nano-SMPS for a PW4158 engine during: Test 6; and Test 7 of APEX-3. Data are corrected for particle line losses.
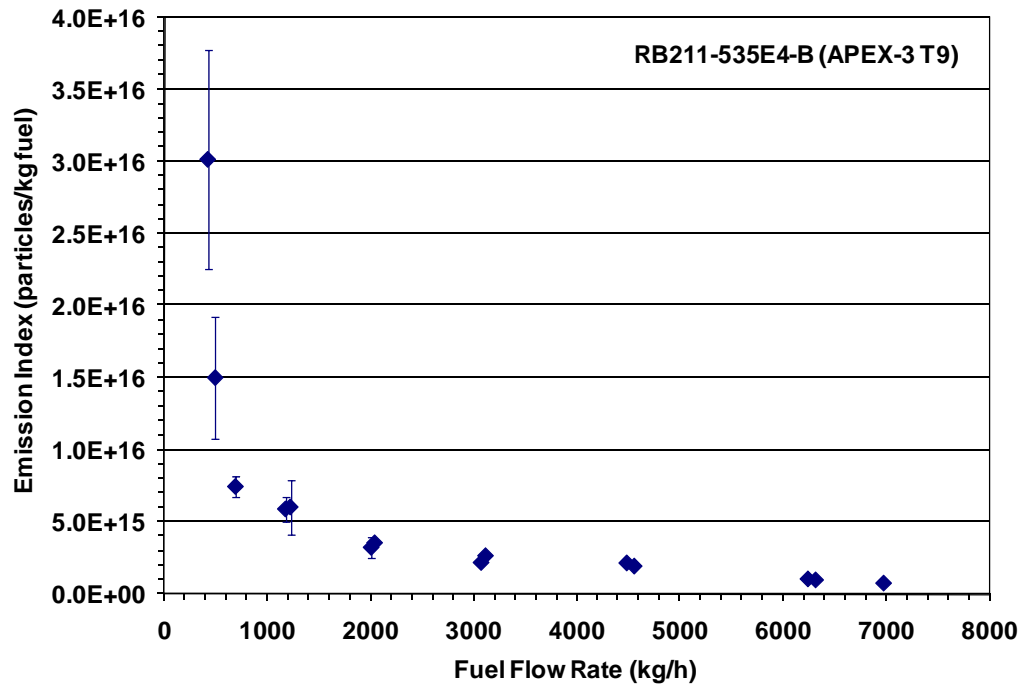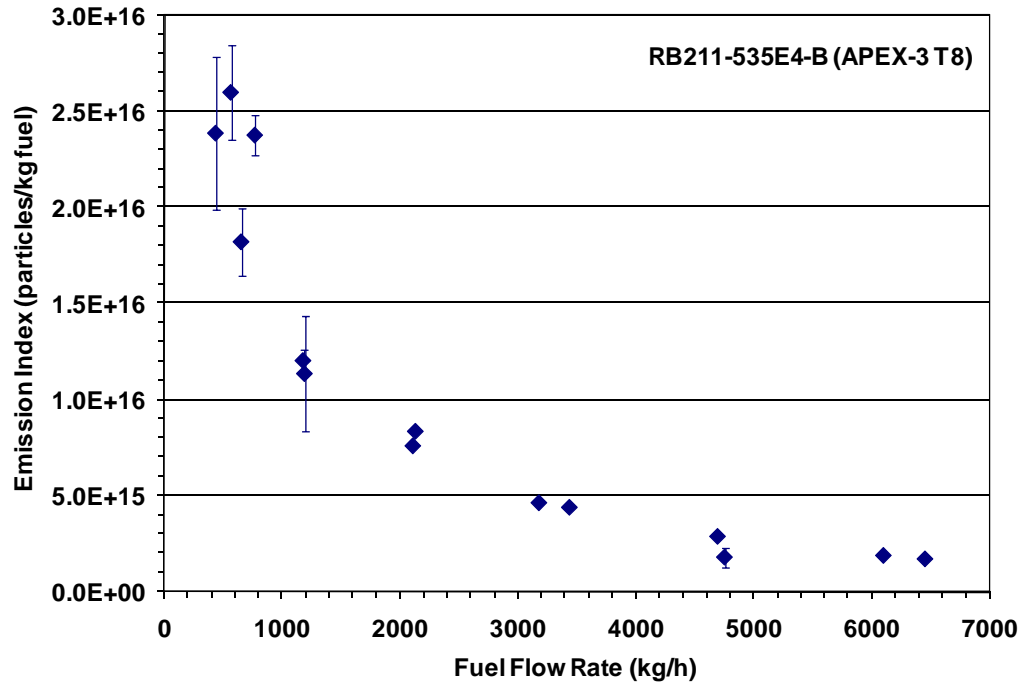
Figure 9-6. Particle number emission index as a function of fuel flow as determined by the Nano-SMPS for two different RB211-535E4B engines during: Test 8; and Test 9 of APEX-3. Data are corrected for particle line losses.

A predictive model was found capable of approximately describing the relationship between the particle number emission index and the fuel flow rate obtained in this study. Figure 9-7 is an example of the results obtained from the EEPS measurements, showing that, in general, the emission indices obtained for five types of engines were logarithmically correlated to the fuel flow rate (power).
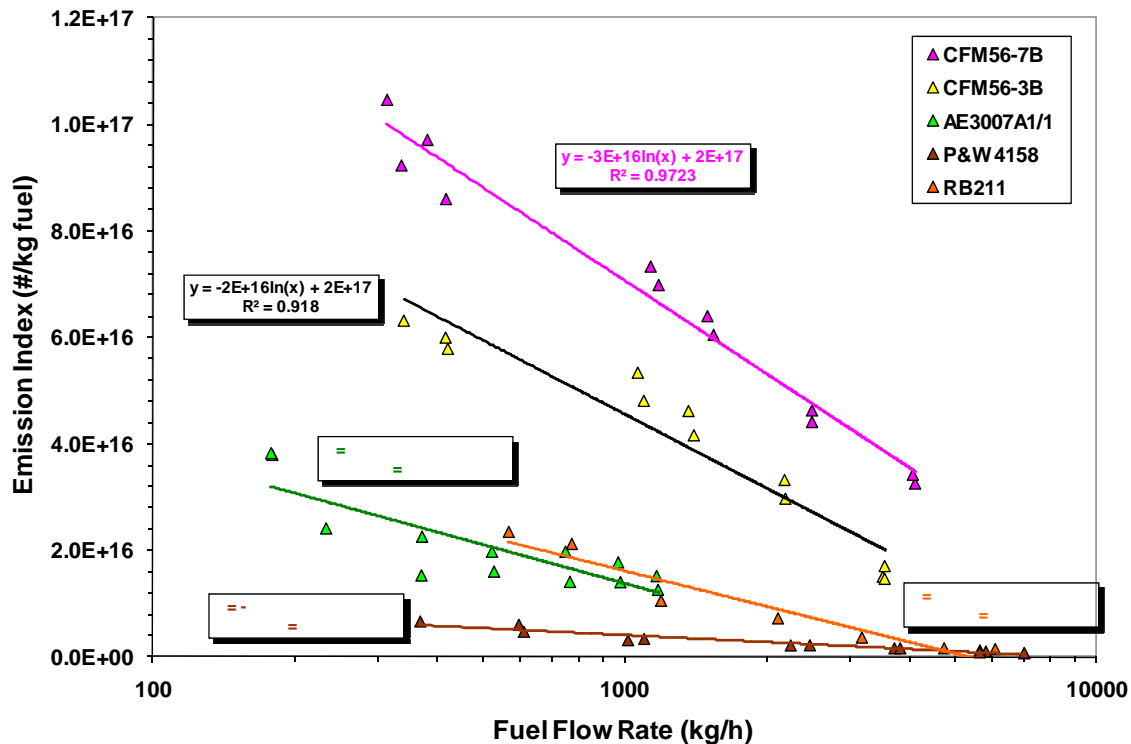
Figure 9-7.   Logarithmic correlation between particle number emission index measured by EEPS and fuel flow rate.

9.2   Effect of Fuel Composition

The effects of fuel composition on the PM particle number emission index were investigated based on the results of the Nano-SMPS and ELPI obtained in the APEX-1 campaign. Figure 9-8 compares the emission indices as a function of fuel flow rate obtained from the three tests with different fuels: test NASA-1a with the base fuel, test NASA-3 with the high-sulfur fuel, and test NASA-4 with the high-aromatic fuel.

The Nano-SMPS results in Figure 9-8 show that high-sulfur fuel produced higher particle counts at all tested fuel flow rates. The higher particle number emissions from the high-sulfur fuel may be attributable to the formation of sulfate particles or sulfate coatings on particles. A small portion of the sulfur in jet fuel was converted into sulfuric acid. The sulfuric acid could either form nucleates or condense onto the existing aerosol surfaces as the plume cooled. Sulfur content in the PM and its contribution will be further discussed in Sections 10 and 13.
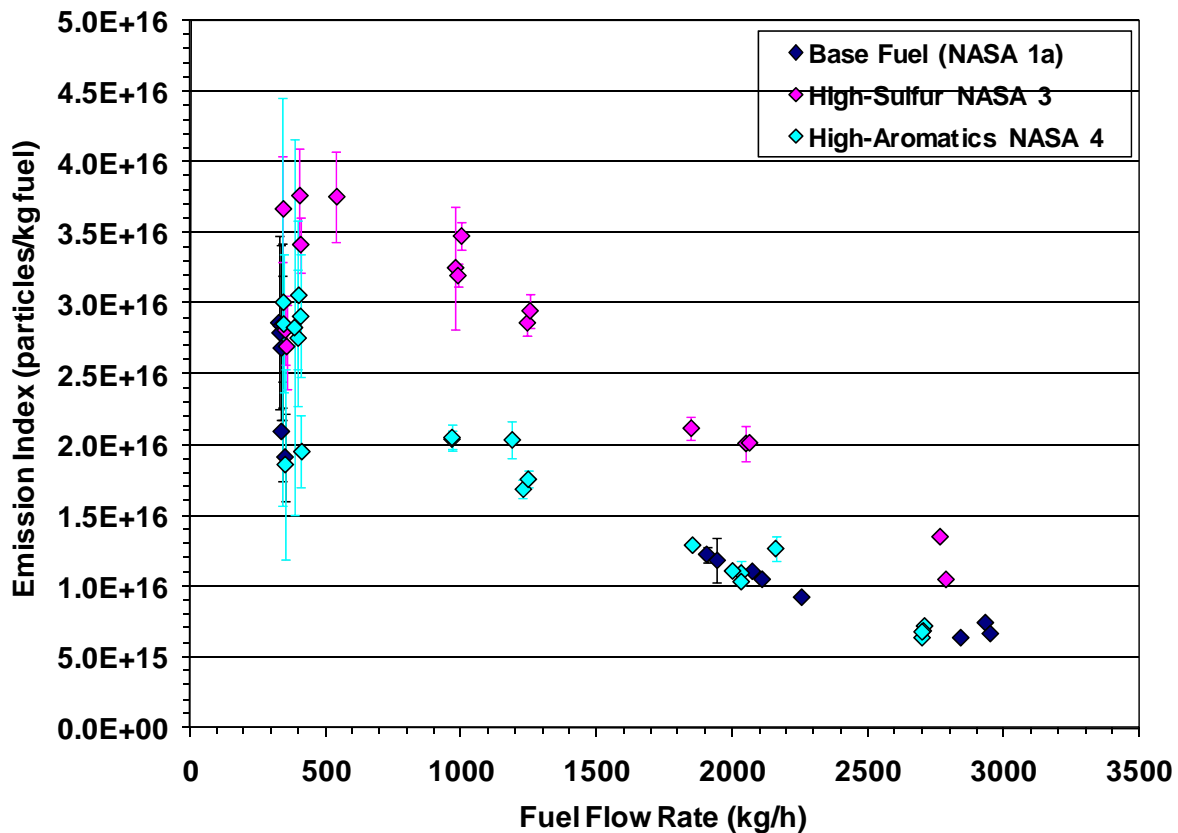
Figure 9-8. Effects of fuel type on particle number emissions index as determined during APEX-1 (Nano-SMPS).

Figure 9-8 also shows that the base fuel had the lowest particle number emissions in comparison with the other fuel types tested. The slightly higher particle number emissions observed from the high-aromatic fuel over the base fuel can also be attributed to a combination of a slight increase in sulfur content (553 ppm for the high-aromatic fuel and 409 ppm for the base fuel) as well as the higher aromatic content of the fuel tested. These trends are also consistent with those reported previously by other APEX-1 investigators (Wey et al., 2006).

Anderson et al. (2006) found that the values of particle number emission index varied in rough proportion to fuel sulfur content, with values at any given power setting following the trend that high sulfur fuel > high aromatic fuel > base JP8 fuel. Petzold and Schroder (1998) also found from their jet engine exhaust aerosol study that the SO_2 emitted from a jet engine was oxidized by OH or O to SO_3, which then reacted with H_2O to form gaseous H_2SO_4. Nucleation and condensation of the low volatility sulfuric acid and hydrocarbons were the primary sources for the increase in number of particles in the exhaust plume.

To further illustrate the effect of fuel sulfur on the particle number emissions, the Nano-SMPS particle number emission indices obtained with fuels of same sulfur content for the CFM56 series engine (including models -2C1, -3B1 and 2 and -7B24 used in APEX-1 and APEX-2 campaigns) were averaged under two levels of engine thrust: 7 and 30 percent. The results were then plotted as a function of fuel

sulfur content as shown in Figure 9-9. The figure shows that the particle number emission index increased with fuel sulfur. However, the emission indices at 132 ppm sulfur were higher than those at 206 and 352 ppm sulfur. The reason for this observation is not currently known. One possible explanation is associated with differences in technology used in the three variants of the CFM56 jet engine used in this comparison. The CFM56-7B24 engine was tested with the fuel of 132 ppm sulfur, while the CFM56-3B engine used the fuels with 206 ppm and 352 ppm sulfur. The CFM56-3B seemed to produce a smaller number of particles.
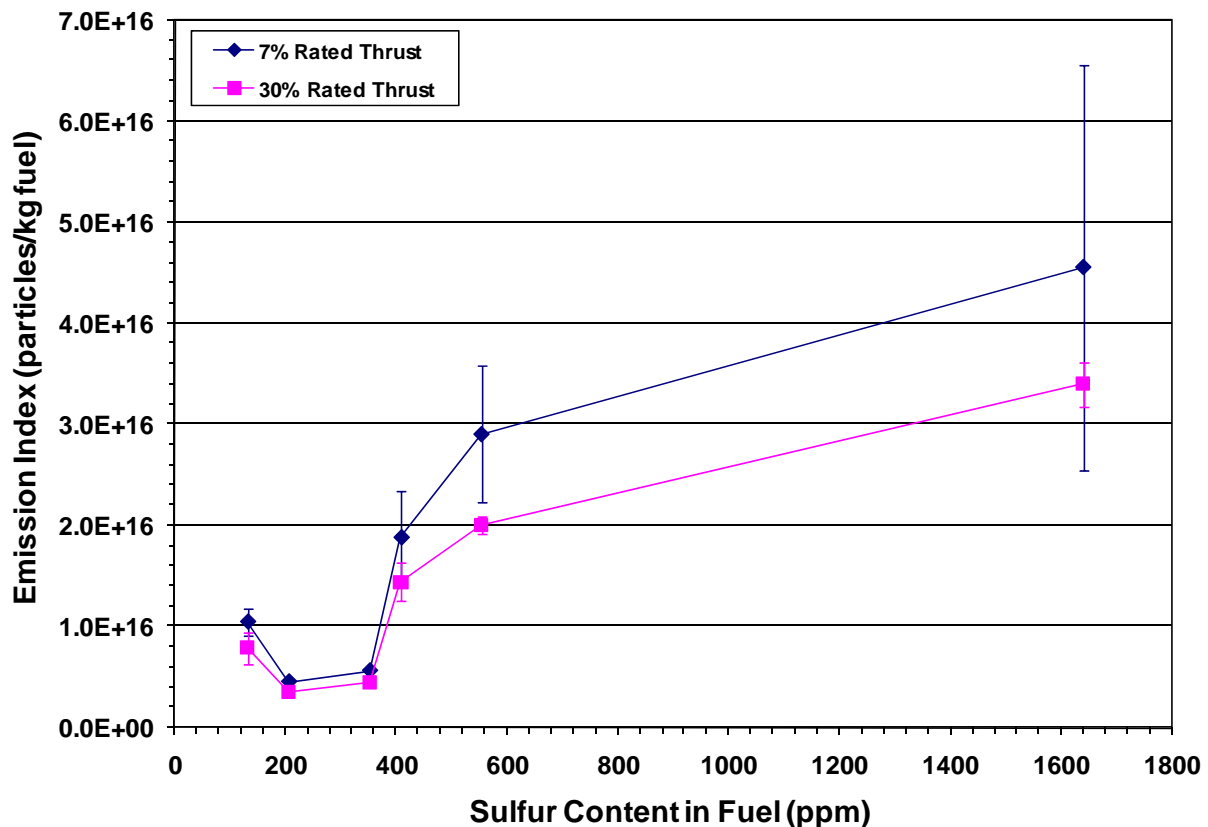
Figure 9-9.   Particle number emission index as a function of fuel sulfur for all CFM56 variants.

9.3   Effect of Engine Type

To investigate the effect of engine type on the particle number emissions, only the data obtained with the base fuel or fleet fuel measured at 30 m were used. Considering the possible interference of strong crosswinds, the results for the tests EPA-1 and NASA-1 from APEX-1, and test T1 from APEX-3, were discarded. For comparison, the particle number emission indices obtained by the same jet engines in different tests were averaged under the four engine power settings that simulate the ICAO airport LTO cycle.

The lowest rated thrust for the tests with jet engine AE3007A1E was 8.4 percent, and this value was treated as the idle engine condition and compared with the other engines at 7 percent thrust. Similar treatment was used for the P&W 4158 engine, where data at 80 percent thrust were averaged and

compared with the other engines under climb-out condition (85% thrust). The fuel flow rates corresponding to each engine power setting were also averaged to obtain the averaged fuel flow rate under that engine cycle for each different engine.

The results of averaged EI_N values for different engines as a function of fuel flow rates are compared in Figure 9-10. These results indicate that, in general, the P&W4158 had the highest particle number emission index. Since the value of EI_N is also engine-power-dependent, the comparison of particle number emission index between different engines was made under the same engine operation mode.

Table 9-1 and Figure 9-11 show the comparisons of the EI_N values obtained by the Nano-SMPS for different engines at the four designated LTO engine power settings (idle, takeoff, climb and approach). The data at engine takeoff mode were not available for the CFM56-2C1, CFM56-7B24 and P&W 4158 engines. The data show that, at engine takeoff and climb modes, the CJ610-8ATJ turbojet produced the highest particle number emissions per kg of fuel burned among the seven engines shown. The reason for the low emissions for the CJ610-8ATJ turbojet engine at idle is unknown. It seems unlikely that this discrepancy was attributable primarily to the measurement errors, because this trend was also shown by the EI_N results derived from the EEPS measurement, as shown in Figure 9-12.

It is also interesting to note from Figure 9-11 that, among the CFM56 engine variants, the EI_N at climb-out power for model -7B was significantly lower than the comparable value for the older technology -2C and -3B models (also see Lobo et al., 2007). At idle and approach, however, the model -3B had the lowest EI_N, followed by -7B, and -2C models, respectively.

9.4   Effect of Cold and Warm Engine Conditions

The particle number emission results derived from the Nano-SMPS measurements were used to investigate the effect of engine cold and warm operating conditions on the particle number emission index. In Figure 9-13, the particle number emission indices obtained under the cold engine condition were plotted against the emission indices obtained for the same engines under the warm operating condition. The diagonal line in the figure represents the situation where the emission index results obtained under cold and warm conditions are identical. The linear regression results are also provided in the figure (see the pink line) showing a slope of 0.92. This slope would indicate that the PM number emission indices are approximately 8 percent lower with warm engines.
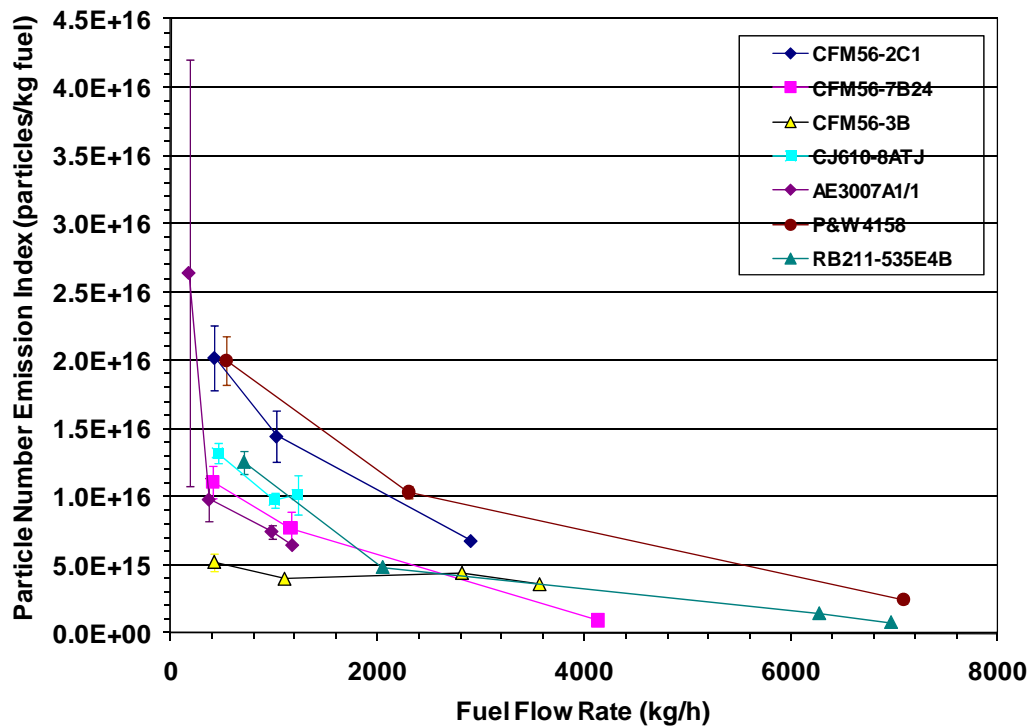
Figure 9-10. Particle number emission index as a function of fuel flow (power) for different engines (Nano-SMPS).

Table 9-1. Particle Number Emission Indices at Each of Four Engine Power Settings for Different Engines (Nano-SMPS results)

Engine	Idle		Takeoff		Climb		Approach	
	Ave	**SD**	**Ave**	**SD**	**Ave**	**SD**	**Ave**	**SD**
CFM56-2C1	2.02E+16	2.40E+15			6.79E+15	3.24E+14	1.44E+16	1.89E+15
CFM56-7B24	1.11E+16	1.18E+15			9.56E+14	3.38E+13	7.70E+15	1.21E+15
CFM56-3B	5.20E+15	6.53E+14	3.58E+15	1.40E+14	4.40E+15	1.68E+14	3.98E+15	4.34E+14
CJ610-8ATJ	2.03E+14	1.48E+14	1.01E+16	1.41E+15	9.76E+15	5.53E+14	1.32E+16	7.28E+14
AE3007A1/1	2.64E+16	1.56E+16	6.45E+15	3.37E+14	7.45E+15	5.03E+14	9.79E+15	1.59E+15
P&W 4158	2.00E+16	1.79E+15			2.45E+15	2.77E+14	1.03E+16	4.37E+14
RB211-535E4-B	1.25E+16	8.51E+14	7.59E+14	2.46E+13	1.41E+15	6.33E+13	4.80E+15	4.37E+14

Ave = arithmetic average; SD = standard deviation.
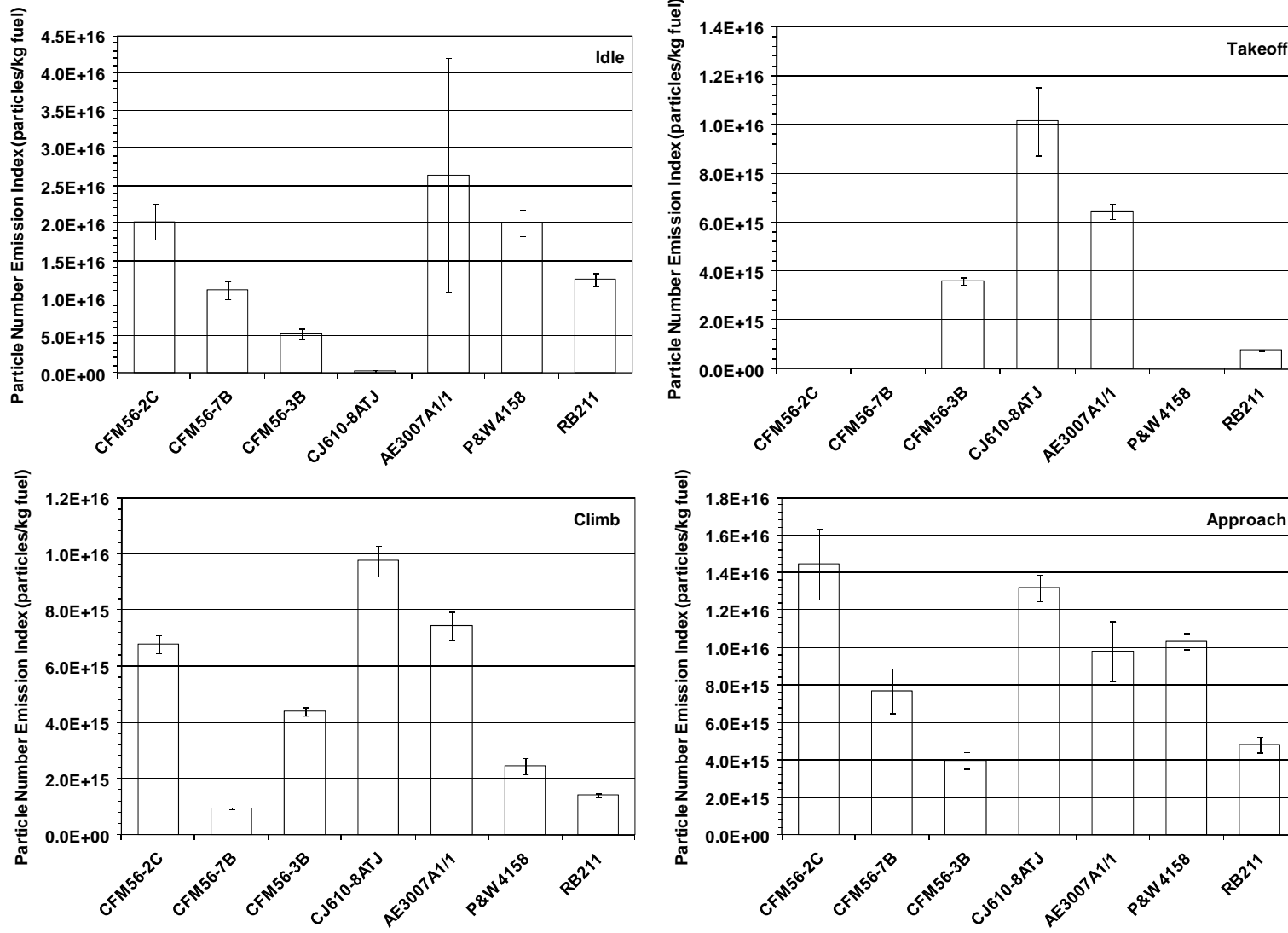
Figure 9-11. Comparison of particle number emission indices for different engines at: idle; take-off; climb-out; and approach power (Nano-SMPS).
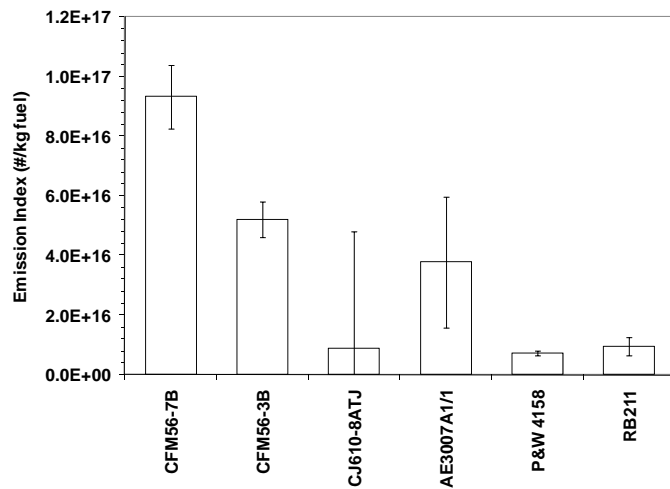
Figure 9-12. Comparison of particle number emission indices by EEPS for different engines under the idle power condition.
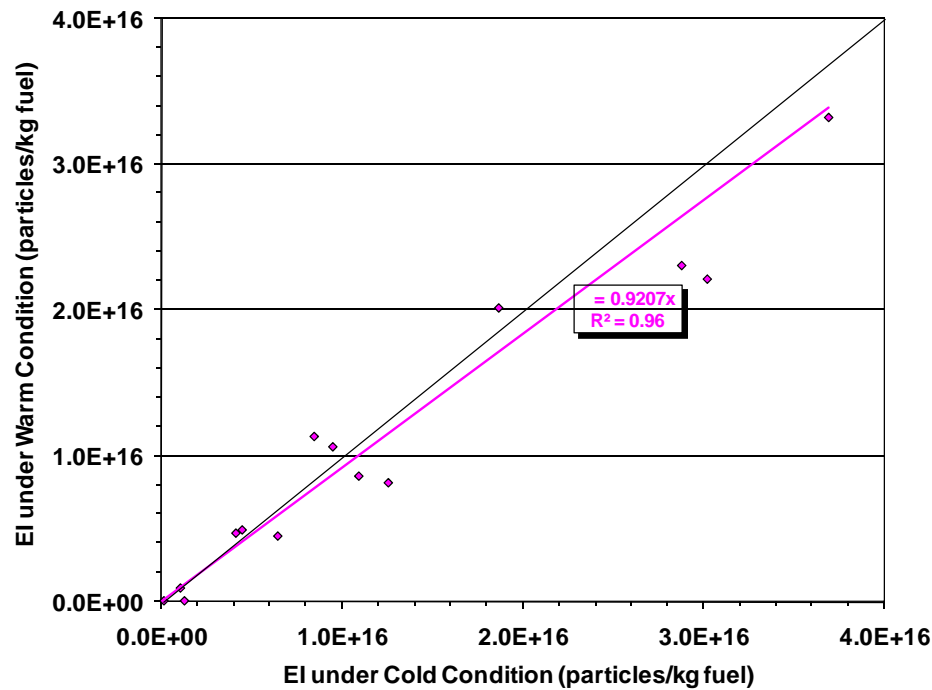
Figure 9-13. Effect of engine operating temperature on particle number emission index.

9.5 Comparison of Particle Number Emission Indices Obtained from Different Instruments

Four different instruments were used in the APEX campaigns for the measurement of particle number concentration in the plume. The Nano-SMPS was used for plume sampling during all three APEX campaigns, a SMPS equipped with a long DMA for both plume and background sampling during APEX-1, an EEPS for plume sampling during APEX-2 and APEX-3, and an ELPI for both plume and background sampling during all three APEX campaigns.

The comparison between Nano-SMPS and EEPS was made based on the test results obtained from the APEX-2 and APEX-3 campaigns. The EI_N results obtained by the EEPS were plotted against the data obtained with the Nano-SMPS under the same test conditions. The two straight lines shown in Figure 9-14 were obtained, indicating a linear relationship between the Nano-SMPS and EEPS measurements. These lines represent the two groups of APEX tests: (1) APEX-3: T1-T3 and T6-T11, and (2) APEX-3: T4-T5 and APEX-2: T1-T4. It is not clear why the results obtained by Nano-SMPS and EEPS were linearly correlated in the separate groups, as this observation could not be explained by engine type or test conditions. The explanation may be related either to the characteristics of the PM emissions, differences in instrument design, or both.
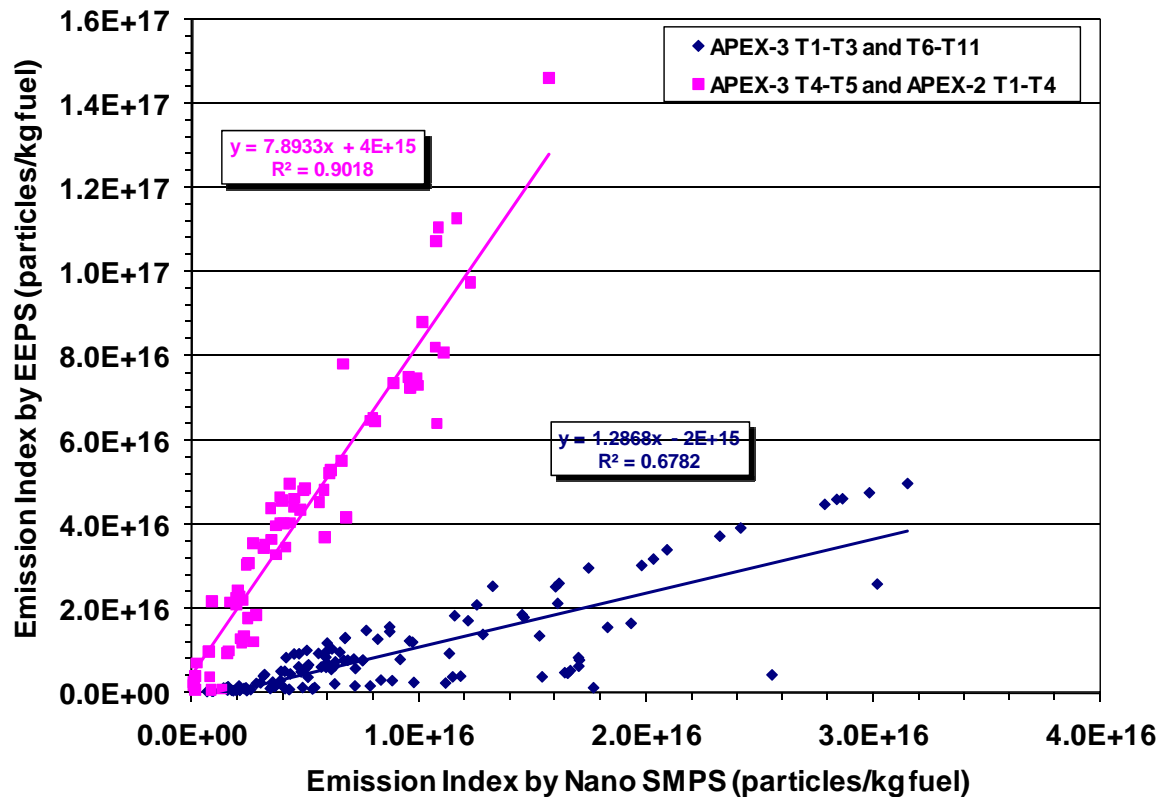
Figure 9-14. Comparison of particle number emission indices as obtained from the Nano-SMPS and EEPS instruments.

The EI_N results from APEX-1, obtained by the long DMA SMPS, were compared with those obtained by Nano-SMPS in Figure 9-15. The figure shows that measurements from two instruments can be correlated approximately in two linear groups: (1) tests EPA-1, EPA-2, NASA-1, NASA-1a, NASA-2, NASA-3 and EPA-3; and (2) NASA-4 and NASA-5. This observation again suggests that the characteristics of the PM might affect the comparison of instrument measurements since the group (1) data were obtained with base jet fuel or high sulfur fuel, and group (2) data were from the high aromatic fuel. Both lines in the figure have slope values of less than 0.7, probably due to the difference in the effect of line loss correction on the results from these two instruments. The long DMA SMPS did not collect particles smaller than 10 nm, so the line losses of the particles in the 3 to 10 nm size range were counted by the Nano-SMPS but were not compensated for by the long DMA SMPS.
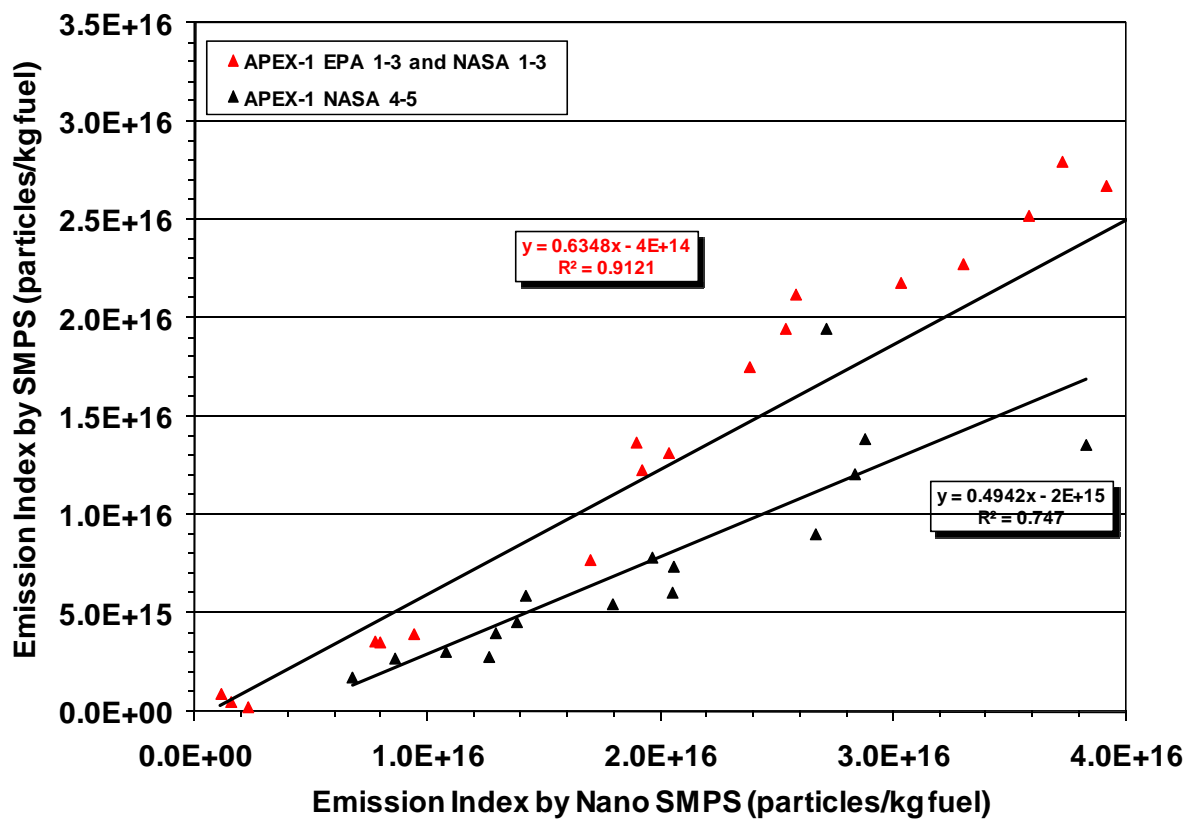
Figure 9-15. Comparison of particle number emission indices as obtained from the Nano-SMPS and long DMA SMPS.

This page intentionally left blank.

10. Particle Size Distribution and Geometric Mean Diameter

The PM emissions from jet engines were monitored by various instruments for investigations of the effects of fuel type, fuel flow rate, engine type and operating condition (cold or warm) on particle size distribution (PSD). In APEX-1, the PM PSDs were measured with a long DMA SMPS, the Nano-SMPS, and the ELPI. PM emitted from the jet engines contained a large portion of particles with diameters below the sizes of the lowest instrument channel for either the long DMA SMPS or the ELPI. Only the Nano-SMPS was capable of providing a complete PSD for the jet engine PM emissions. However, the Nano-SMPS had a data recording frequency of approximately 2.5 minutes. In contrast, the engine run time for the 100 percent power setting was usually maintained for less than 1.5 minutes. This relatively slow instrument response made it difficult for the Nano-SMPS to obtain the PSD information under the highest power settings. Therefore, no PSDs for the 100 percent power setting (take-off) are reported for Nano-SMPS, and limited data are reported for the 85 percent power setting (climb). After the APEX-1 campaign, an EEPS was used to replace the long DMA SMPS for PM emissions measurements in both APEX-2 and APEX-3. The EEPS had a fast instrument response and was able to record data points at 1 second intervals.

The differential number PSD, dN/dlogDp at a specified power setting, was obtained by averaging the particle numbers recorded under the same engine operating condition from the same instrument size bins and then plotting them against the particle size. Both the Nano-SMPS and EEPS were only used in the plume emissions measurement system. Therefore, the PM emission results obtained by the Nano-SMPS were background-corrected using measurements obtained before and after each test. No background correction was needed for the EEPS, as discussed earlier. Also, the PSD data both before and after particle line loss-correction are presented in the following discussion with the differences also investigated.

The geometric mean diameter (GMD) and geometric standard deviation (GSD) were calculated as a function of fuel flow rate from the PSD for each individual test of the three APEX campaigns. Table F-1, included in Appendix F, summarizes the results obtained from the Nano-SMPS and EEPS measurements. The GMD and GSD data, both before and after particle loss correction, are presented in the table.

10.1 Particle Size Results for APEX-1

During APEX-1, all tests were conducted on a CFM56-2C1 engine using two different engine testing matrices. The "EPA" test matrix followed the ICAO-defined LTO cycle to simulate aircraft emissions at an airport and consisted of approximately four repetitions of the following power settings: 26 min at idle (7%), 0.7 min at takeoff (100%), 2.2 min at climb (85%), and 4 min at approach (30%). The "NASA" test matrix was designed to investigate the effects of engine operating parameters on particle emissions and encompassed steady-state power settings of 4, 5.5, 7, 15, 30, 40, 60, 65, 70, 85 and 100 percent

(restricted to about 93% actual thrust, henceforth, 100%). Except for the 100 percent thrust level, which was limited to a run-time of 1.5 min, approximately 10 min were provided at each power setting to allow for samples to be adequately analyzed.

The PSD at a specified experimental condition was obtained by averaging the dN/dlogDp data recorded from the instrument in the same size bins and then plotting those averages against the particle size. To investigate the effects of fuel type and engine operation cycle on PSD, the dN/dlogDp data were then averaged for the same fuel type and operation cycle. Since only the Nano-SMPS was able to cover the entire particle size range of the jet engine PM emissions, this section is restricted to the results obtained from the Nano-SMPS measurements. Also, no PSD data for the 100 percent power setting (as well as the 85% power setting for EPA-2) are reported here as discussed above.

The particle size results for the EPA test series conducted during APEX-1 are shown in Figures 10-1 to 10-3. Note that both the loss-corrected (a) and uncorrected (b) PSDs are provided in these figures. Figures 10-4 to 10-9 provide similar information for the NASA test series. The figures show that for most tests a unimodal and log-nomal PSD was obtained regardless of experimental conditions.

10.2 Particle Size Results for APEX-2

During the APEX-2 campaign, two additional models of the CFM56 engine, the -7B24 and -3B1 and 2, were tested. The engine-rated power thrust was varied in a stepwise fashion at six thrust levels (4, 7, 30, 40, 65, and 85%) as discussed in Section 6. Except for the 85 percent thrust level where run-time was 8 min, approximately 10 min were provided at each power setting to allow for samples to be adequately analyzed. The power setting was first increased from the lowest thrust level to highest level under cold engine conditions, and then decreased under warm engine conditions to investigate the effects of engine temperature on particle emissions.

Figures 10-10, 10-11, 10-12 and 10-13 present the average PSDs under different power settings obtained from the Nano-SMPS, with (a) and without (b) particle loss correction for tests T1, T2, T3 and T4, respectively. Again these figures show that the PSDs of the PM emissions from jet engines were generally unimodal and followed a log-normal function.

10.3 Particle Size Results for APEX-3

In APEX-3 campaign, six different engines were tested for emissions at various power settings. Like APEX-2, the engine tests in APEX-3 were conducted by increasing the thrust power in a stepwise fashion from idle (4 or 7%) to climb (100%) under cold engine conditions and then decreasing through the same power settings under warm engine conditions.

Figures 10-14 to 10-24 present the Nano-SMPS results of the average PSD with (a) and without (b) particle loss correction under different power settings for each of individual tests T1 through T11, respectively. All the data were measured with the 30 m sampling probe. The PSDs shown in these figures were log-normal and consistent with the results of APEX-1 and APEX-2. However, in some cases, the PSDs were bimodal with an additional accumulation mode present at higher fuel flows.
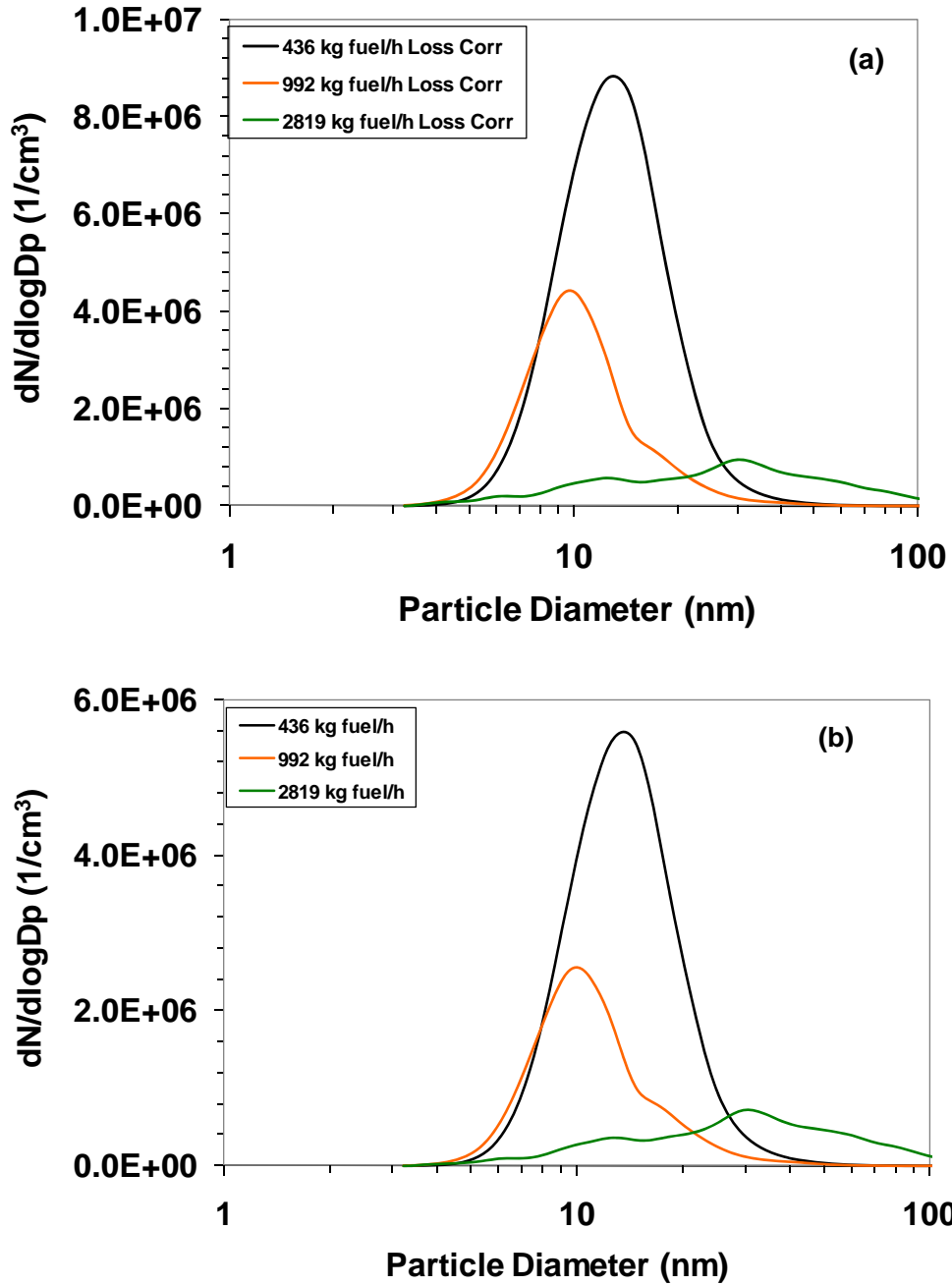
Figure 10-1. Average PSD measured by the Nano-SMPS during APEX-1, Test EPA-1, (a) <u>with</u> line loss correction; and (b) <u>without</u> line loss correction.

Note: unable to collect PSD for 2969 kg fuel/h (100%) power.
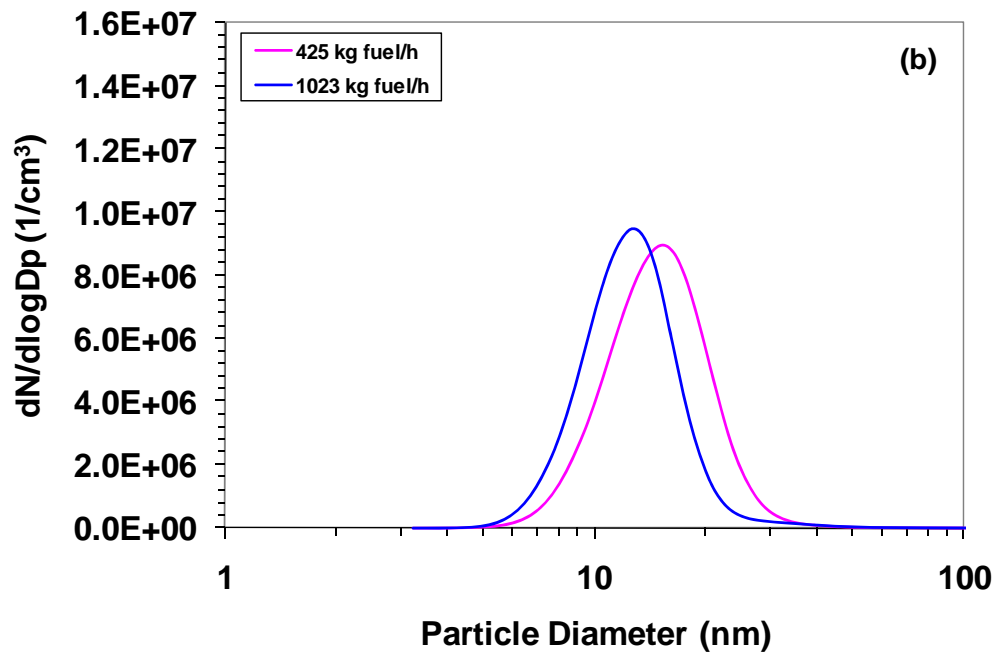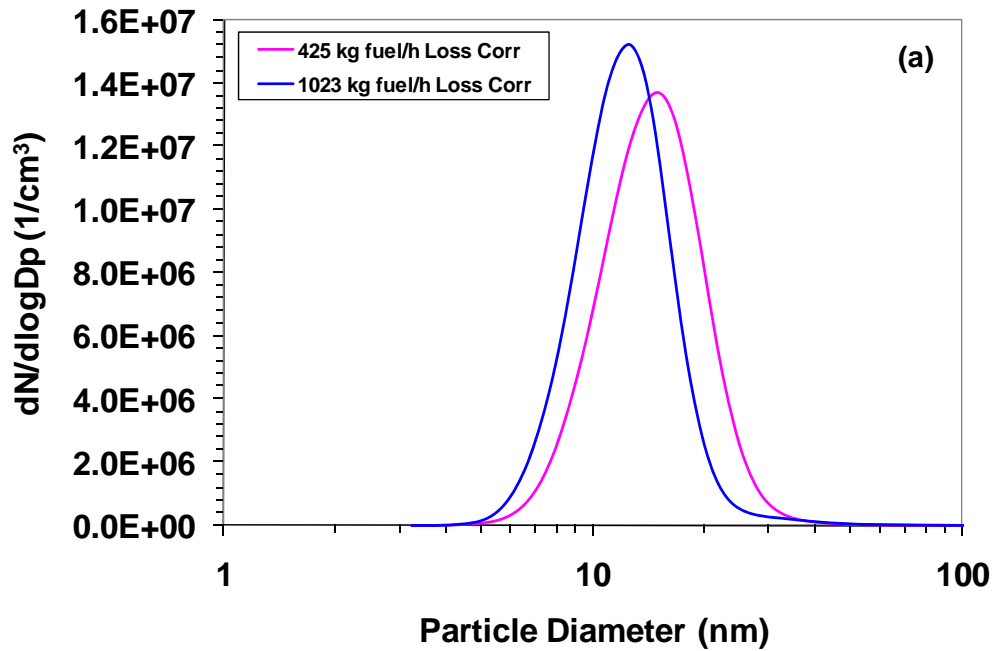
Figure 10-2. Average PSD measured by the Nano-SMPS during APEX-1, Test EPA-2, (a) <u>with</u> line loss correction; and (b) <u>without</u> line loss correction.

Note: unable to collect PSD for 2860 kg fuel/h (85%) and 3181 kg fuel/h (100%) power.
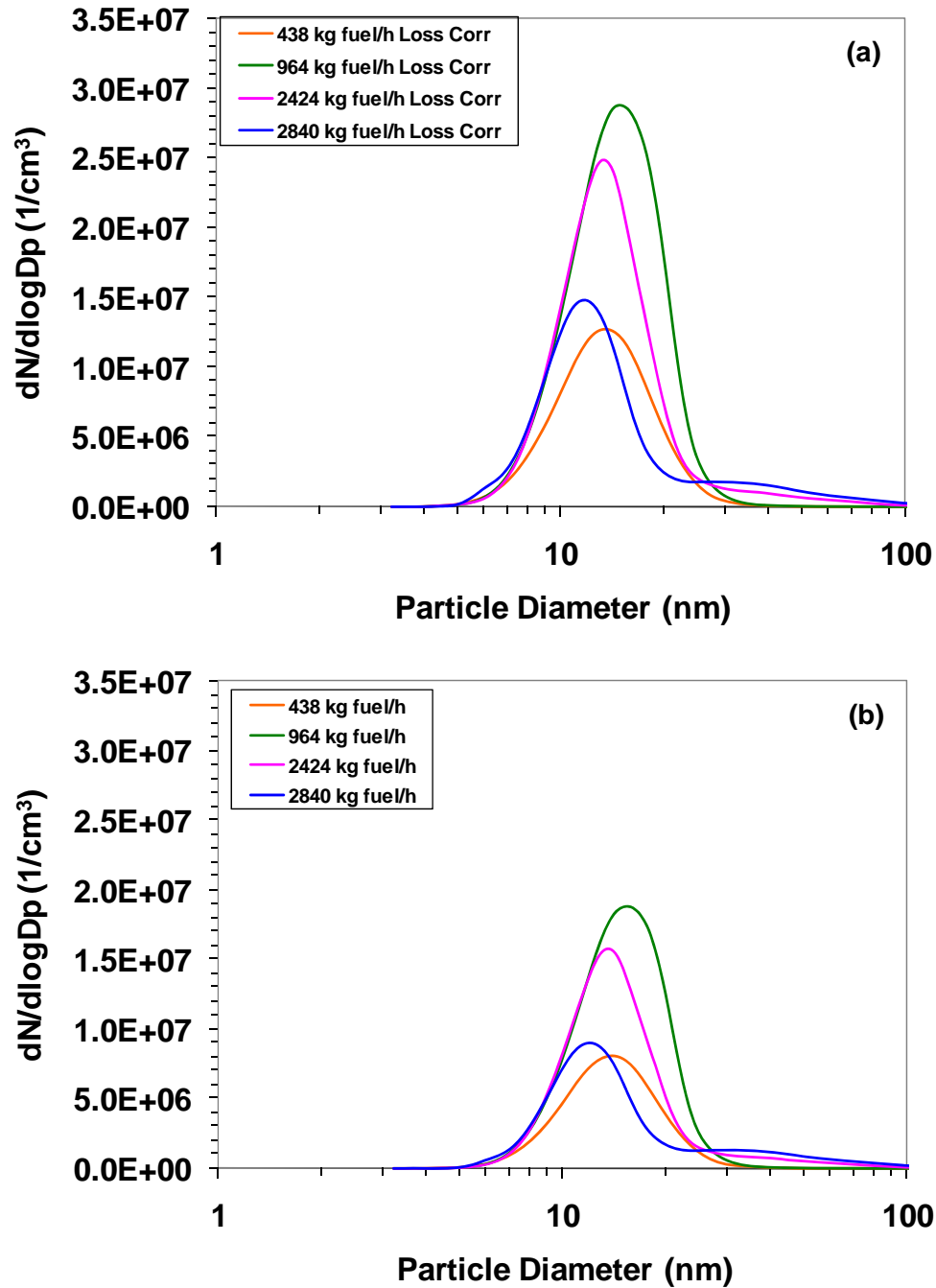
Figure 10-3. Average PSD measured by the Nano-SMPS during APEX-1, Test EPA-3, (a) <u>with</u> line loss correction; and (b) <u>without</u> line loss correction.

Note: unable to collect PSD for 3116 kg fuel/h (100%) power.
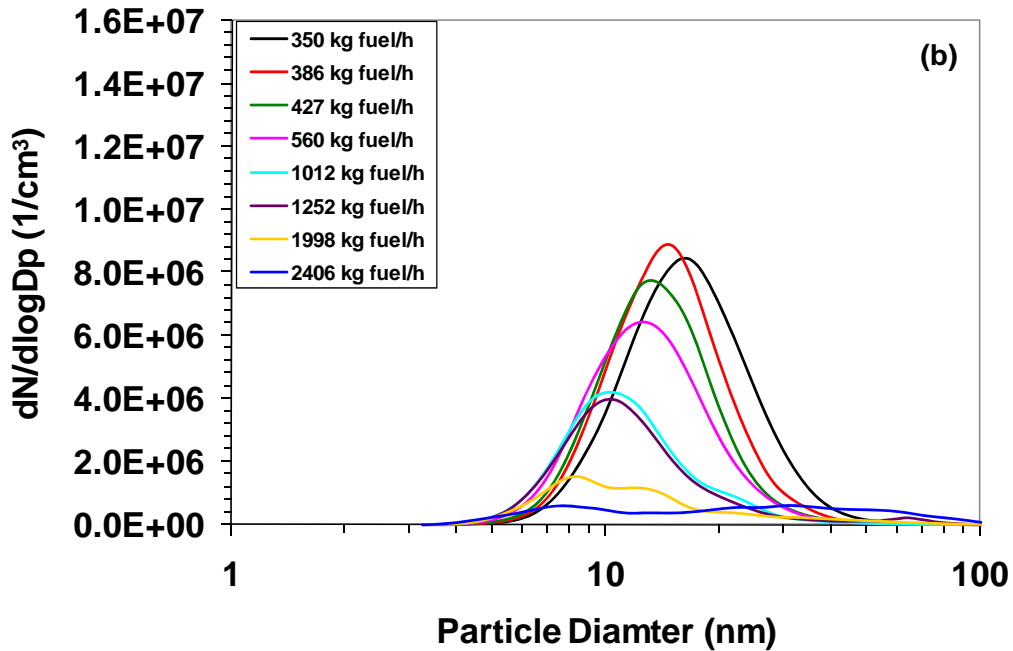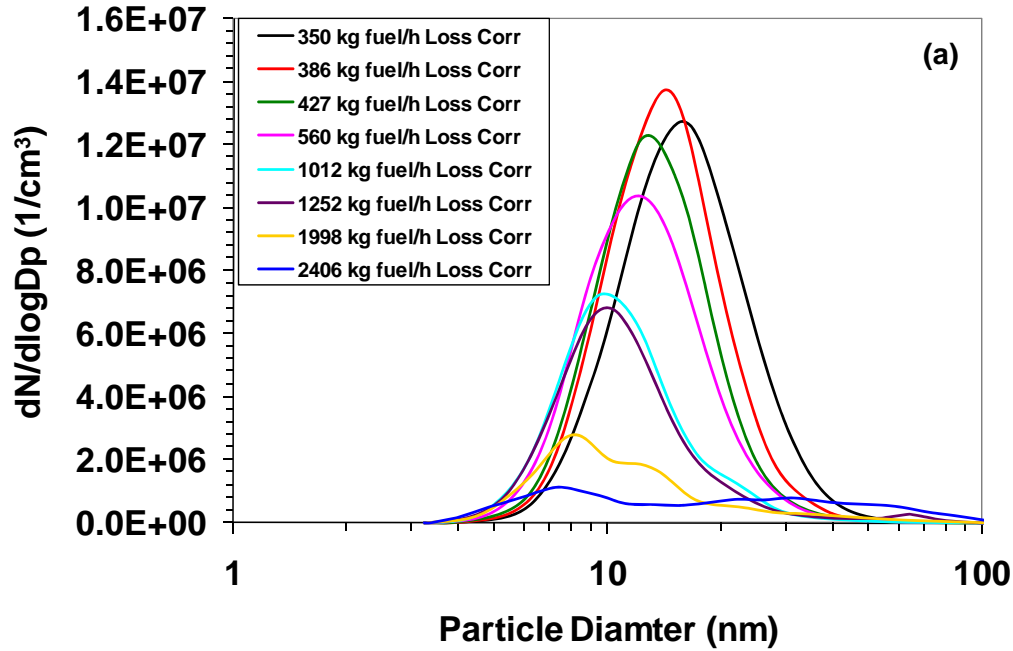
Figure 10-4. Average PSD measured by the Nano-SMPS during APEX-1, Test NASA-1, (a) <u>with</u> line loss correction; and (b) <u>without</u> line loss correction.

Note: unable to collect PSD for 2906 kg fuel/h (100%) power.
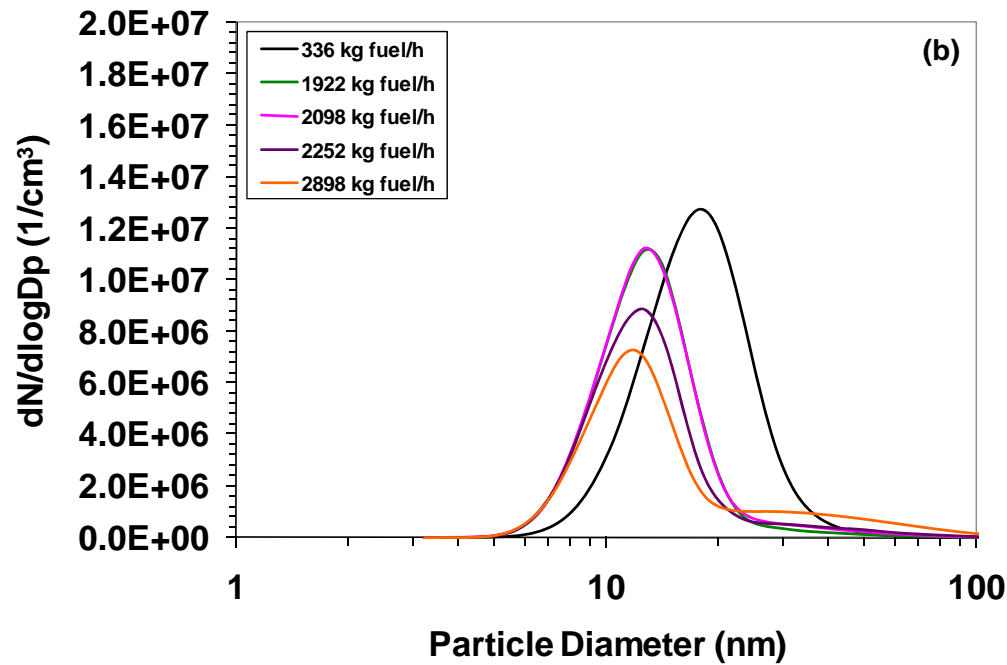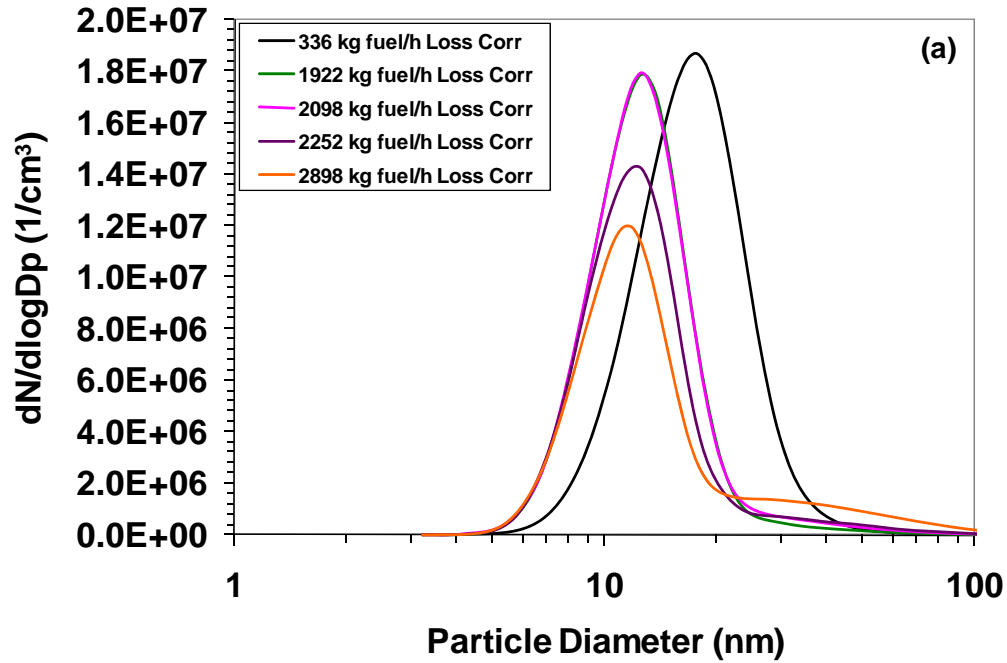
Figure 10-5. Average PSD measured by the Nano-SMPS during APEX-1, Test NASA-1a, (a) <u>with</u> line loss correction; and (b) <u>without</u> line loss correction.

Note: unable to collect PSD for 3127 kg fuel/h (100%) power.
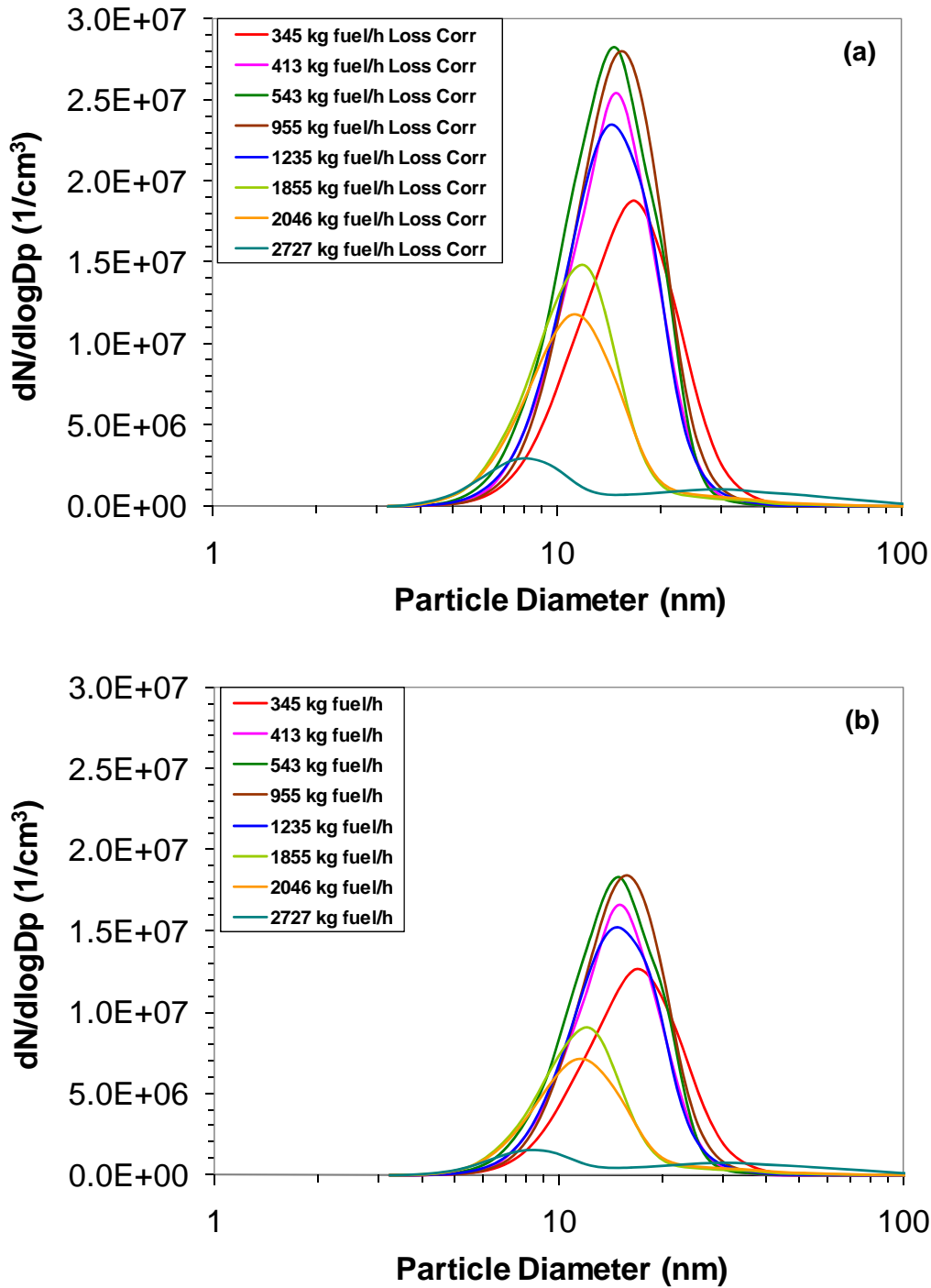
Figure 10-6. Average PSD measured by the Nano-SMPS during APEX-1, Test NASA-2, (a) <u>with</u> line loss correction; and (b) <u>without</u> line loss correction.

Note: unable to collect PSD for 3116 kg fuel/h (100%) power.
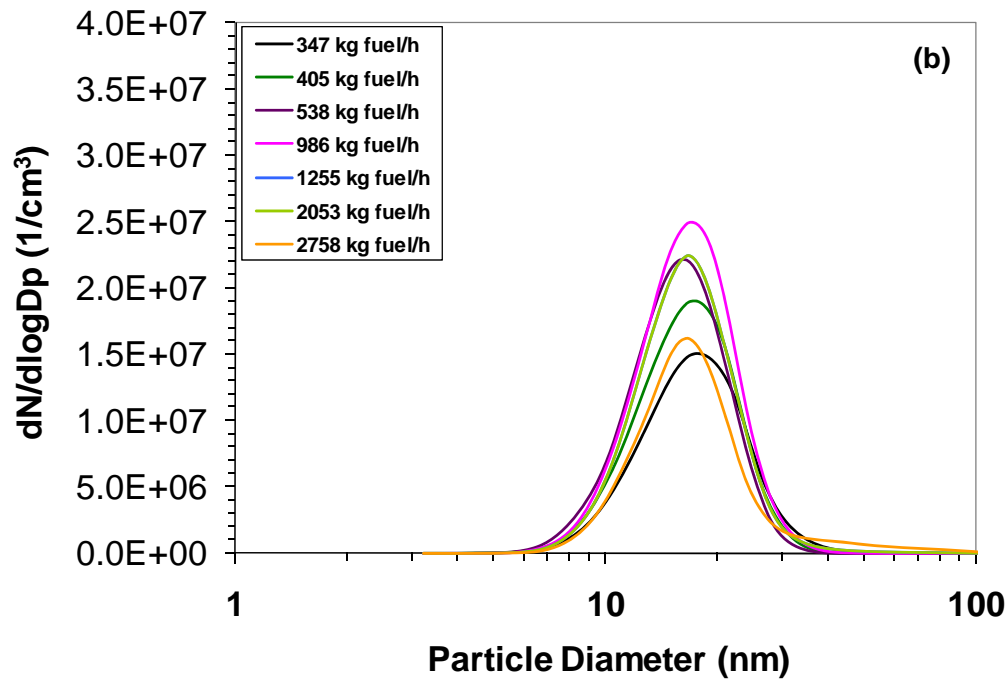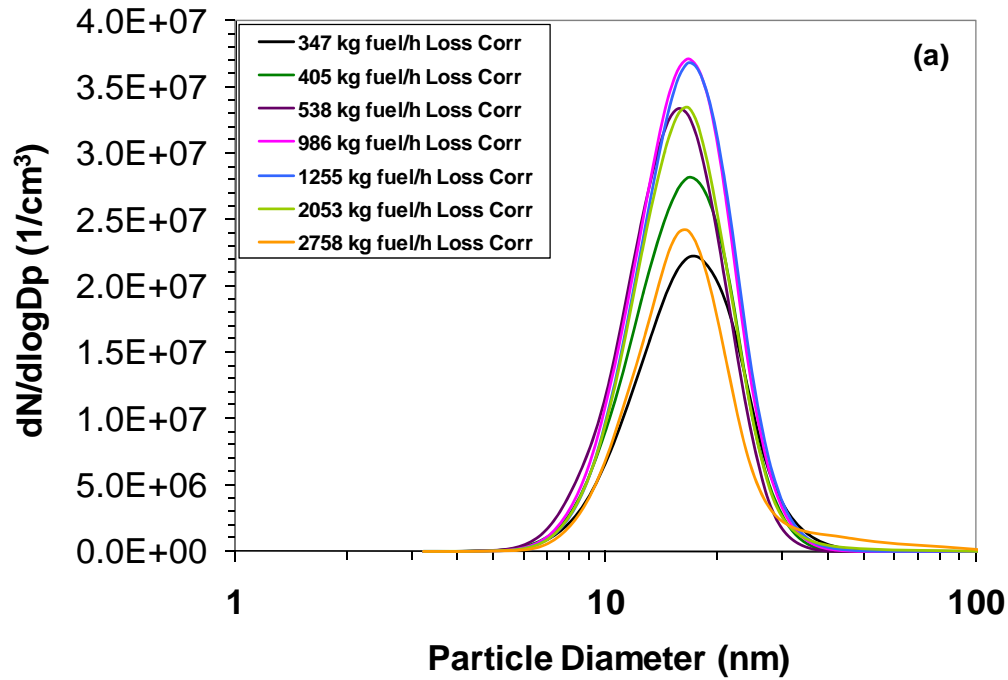
Figure 10-7. Average PSD measured by the Nano-SMPS during APEX-1, Test NASA-3, (a) <u>with</u> line loss correction; and (b) <u>without</u> line loss correction.

Note: unable to collect PSD for 3051 kg fuel/h (100%) power.
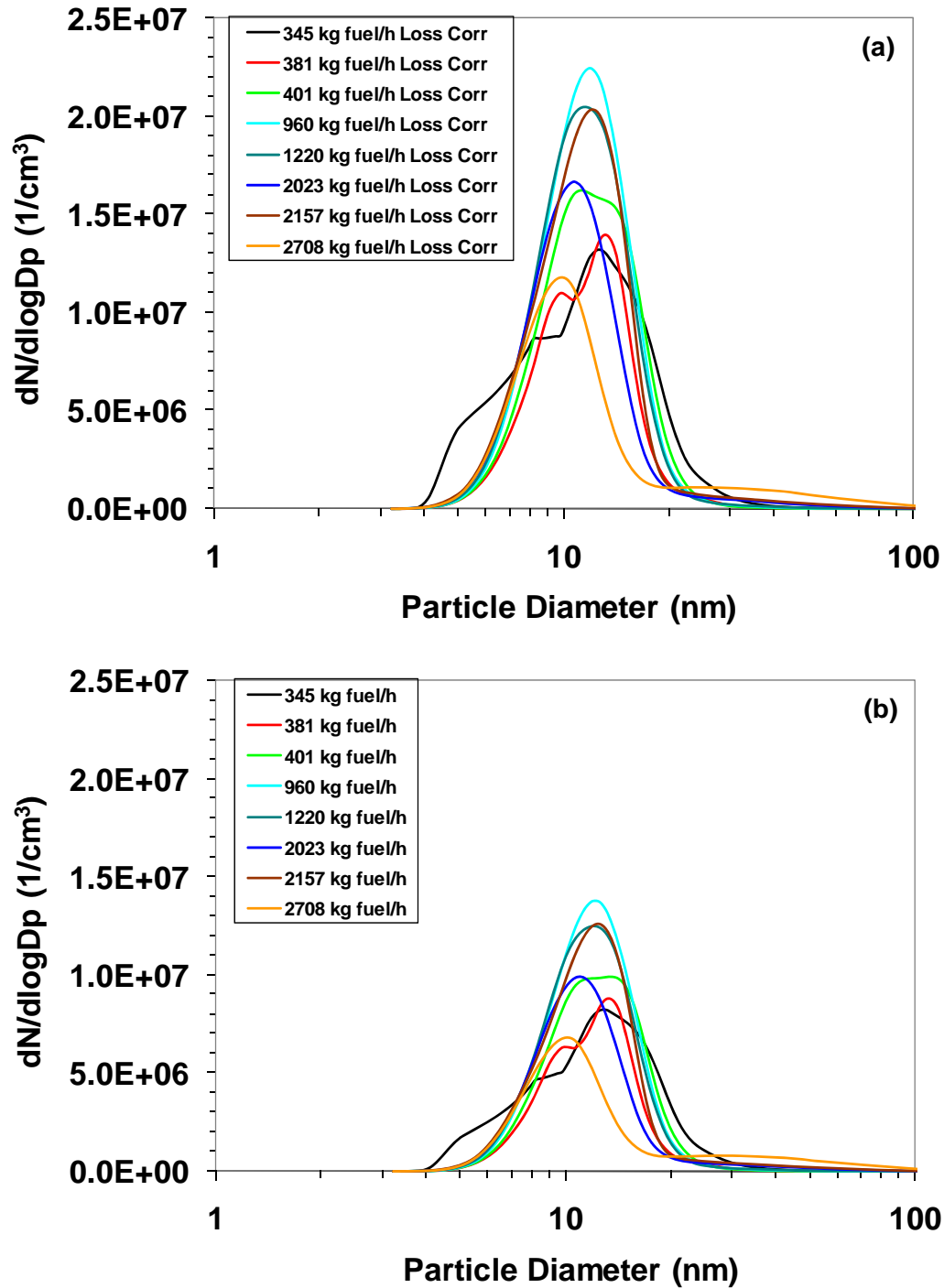
Figure 10-8. Average PSD measured by the Nano-SMPS during APEX-1, Test NASA-4, (a) <u>with</u> line loss correction; and (b) <u>without</u> line loss correction.

Note: unable to collect PSD for 2978 kg fuel/h (100%) power.
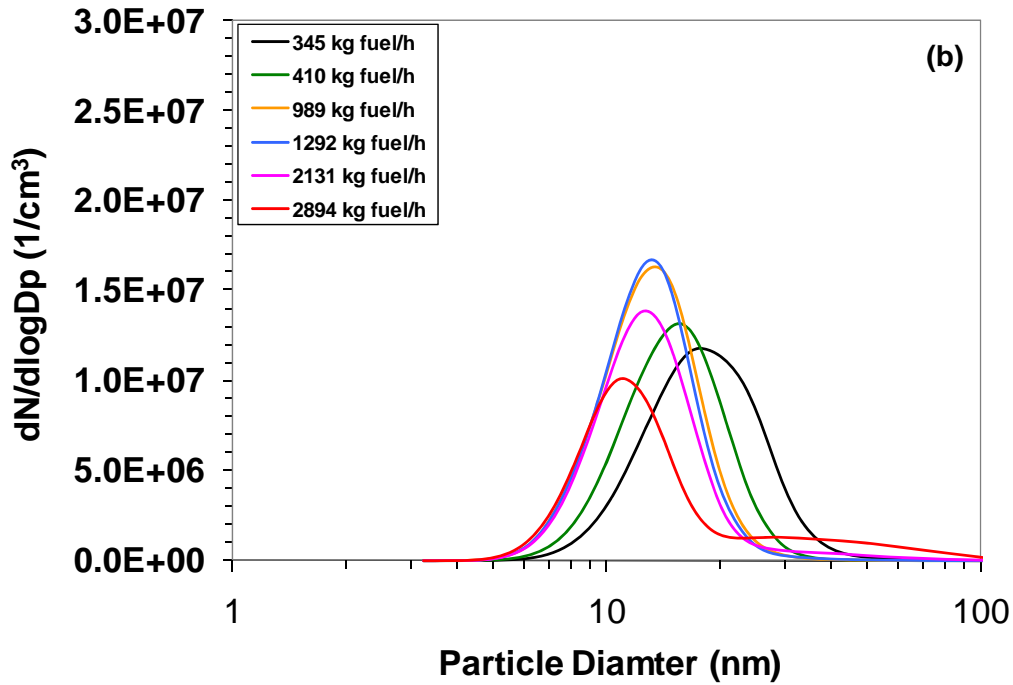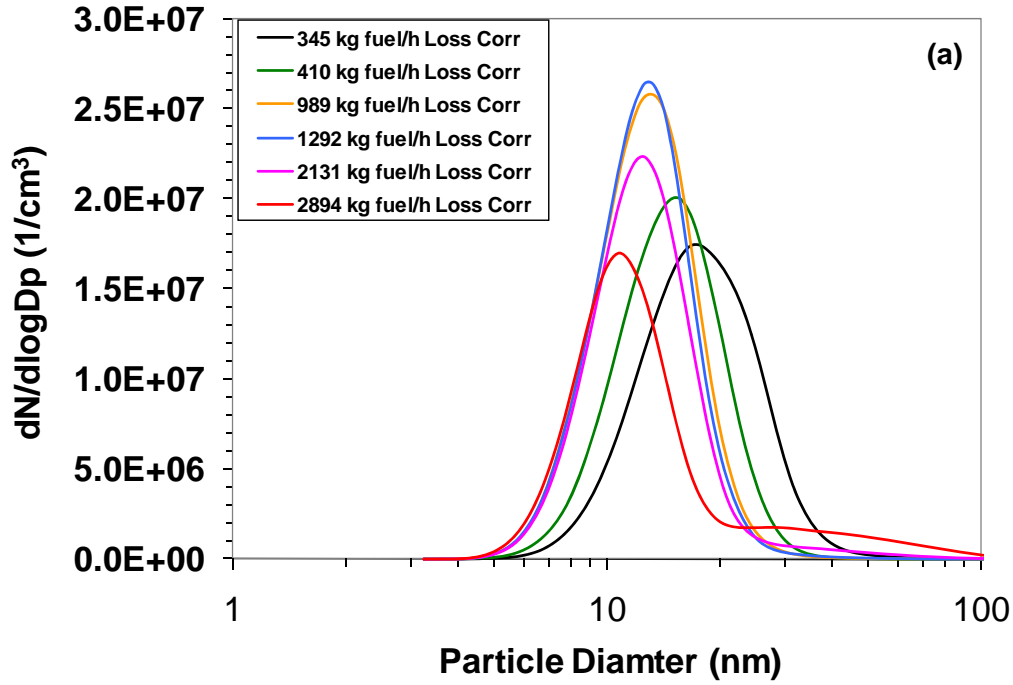
Figure 10-9. Average PSD measured by the Nano-SMPS during APEX-1, Test NASA-5, (a) <u>with</u> line loss correction; and (b) <u>without</u> line loss correction.

Note: unable to collect PSD for 3176 kg fuel/h (100%) power.
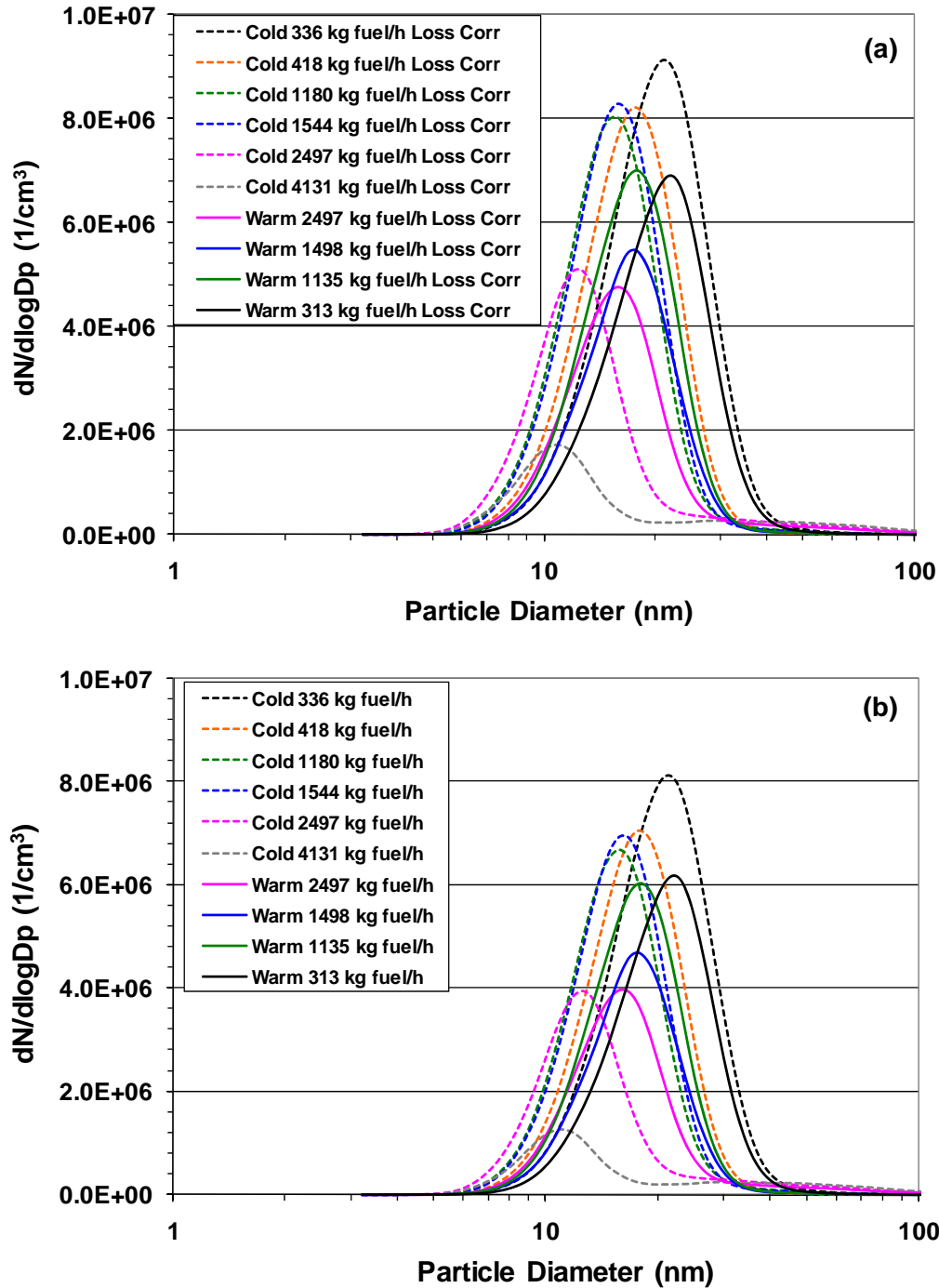
Figure 10-10. Average PSD for a CFM56-7B24 engine measured by the Nano-SMPS during APEX-2, Test T1, (a) <u>with</u> line loss correction; and (b) <u>without</u> line loss correction.
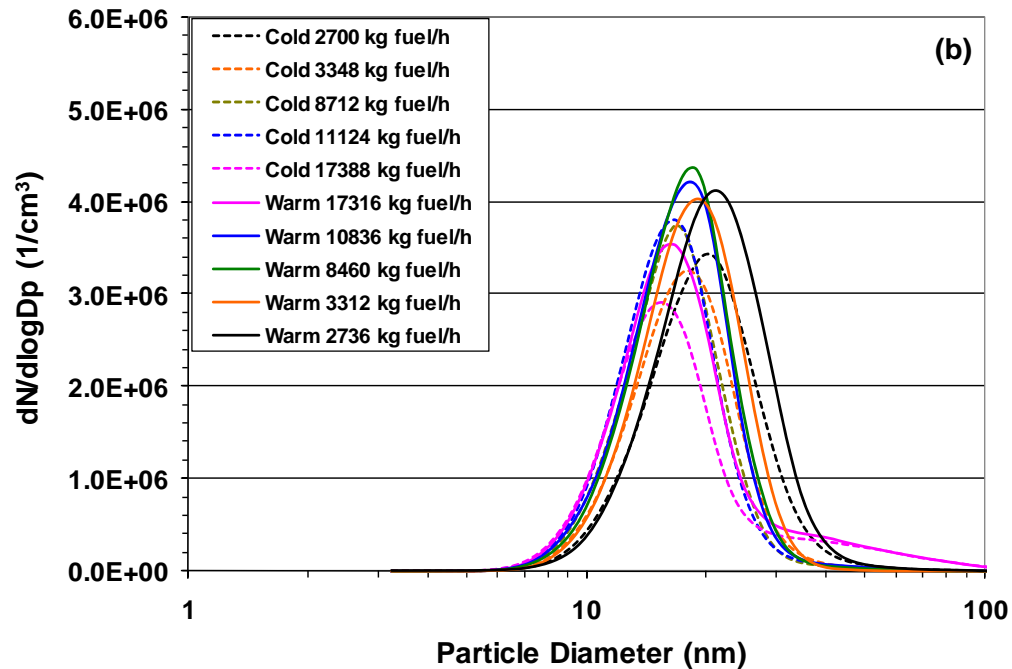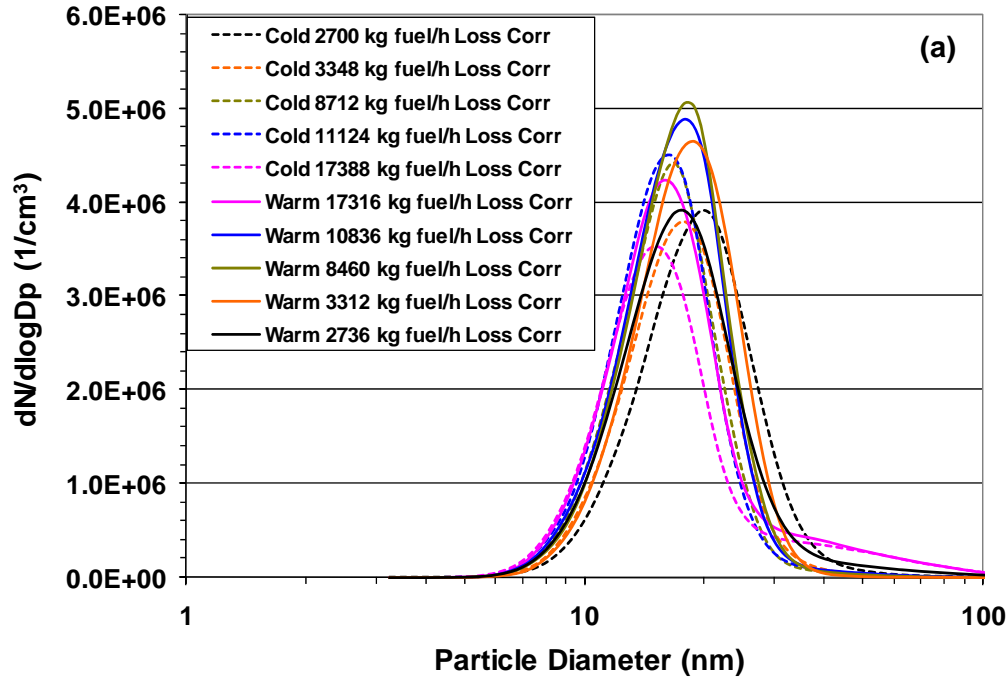
Figure 10-11. Average PSD for a CFM56-3B1 engine measured by the Nano-SMPS during APEX-2, Test T2, (a) <u>with</u> line loss correction; and (b) <u>without</u> line loss correction.
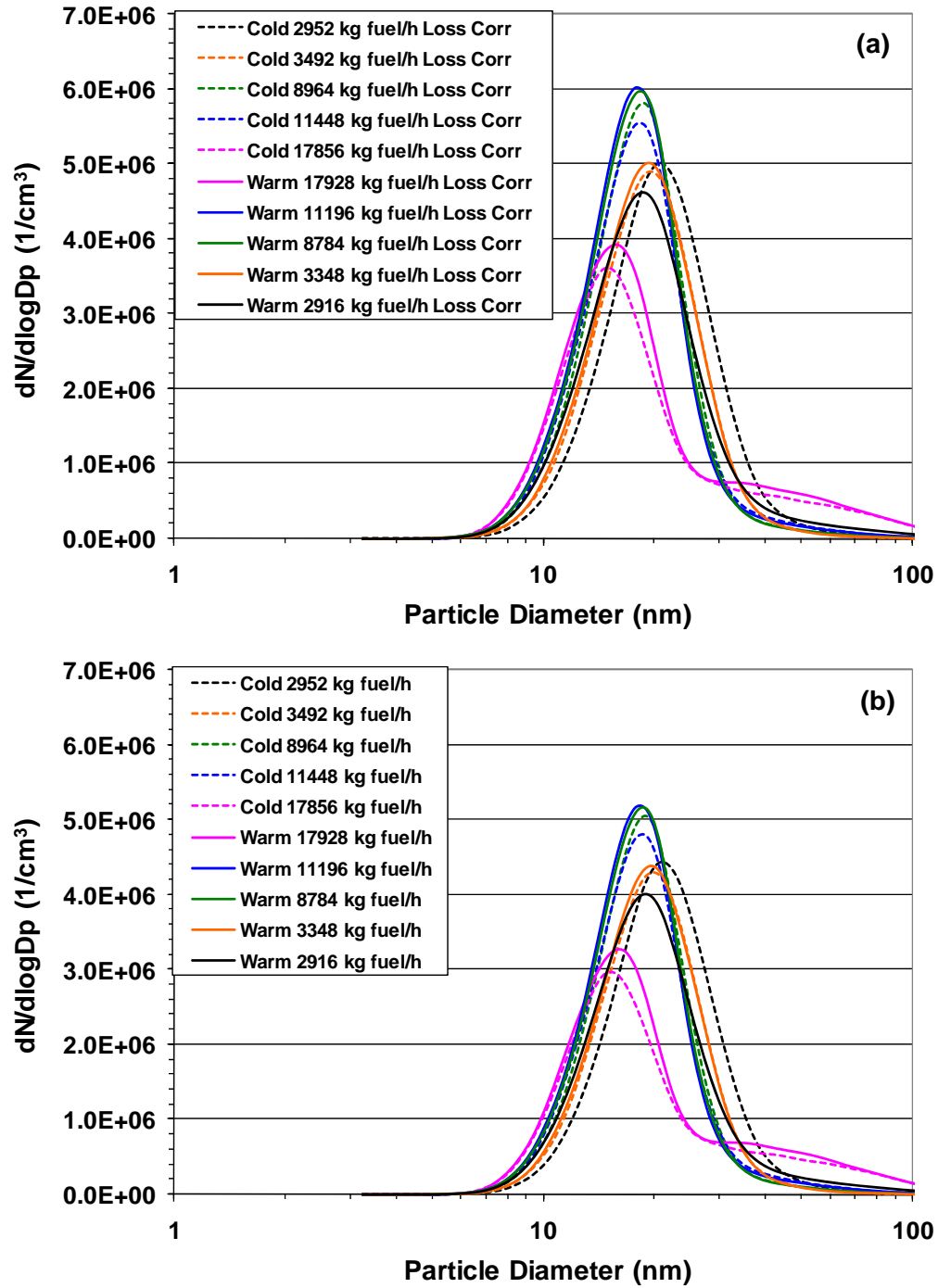
Figure 10-12. Average PSD for a CFM56-3B2 engine measured by the Nano-SMPS during APEX-2, Test T3, (a) <u>with</u> line loss correction; and (b) <u>without</u> line loss correction.
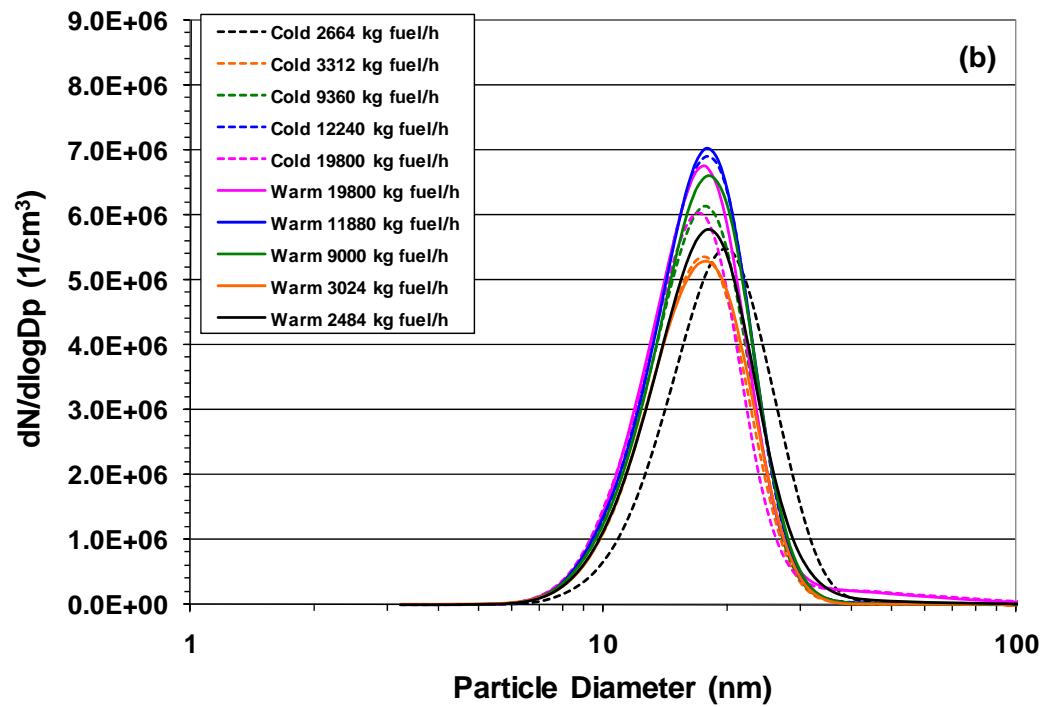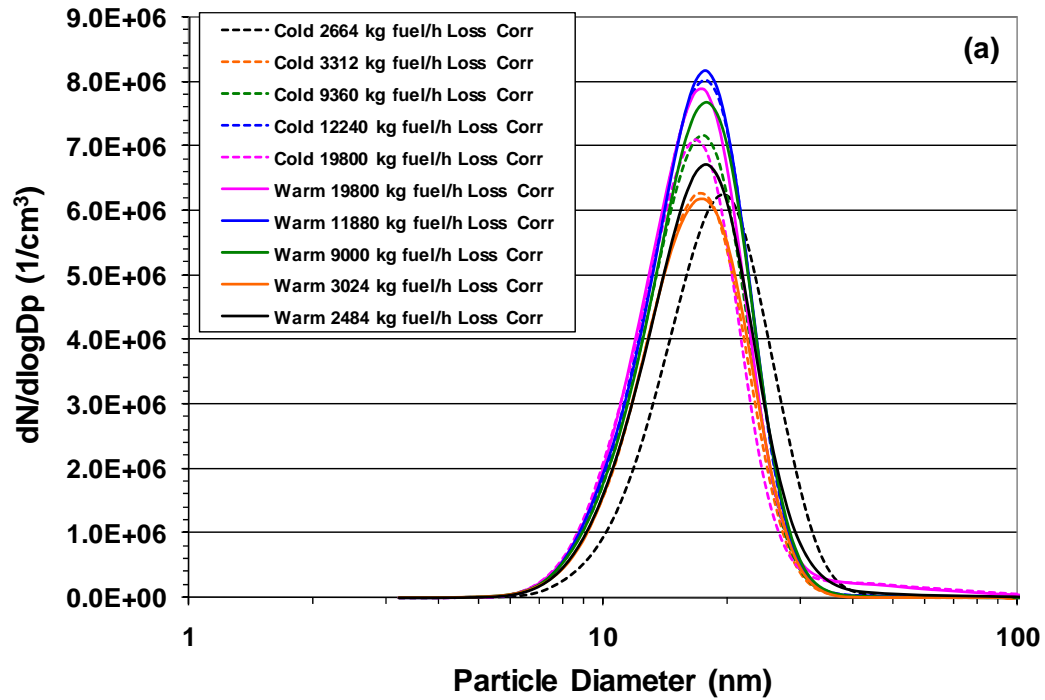
Figure 10-13. Average PSD for a CFM56-7B24 engine measured by the Nano-SMPS during APEX-2, Test T4, (a) <u>with</u> line loss correction; and (b) <u>without</u> line loss correction.
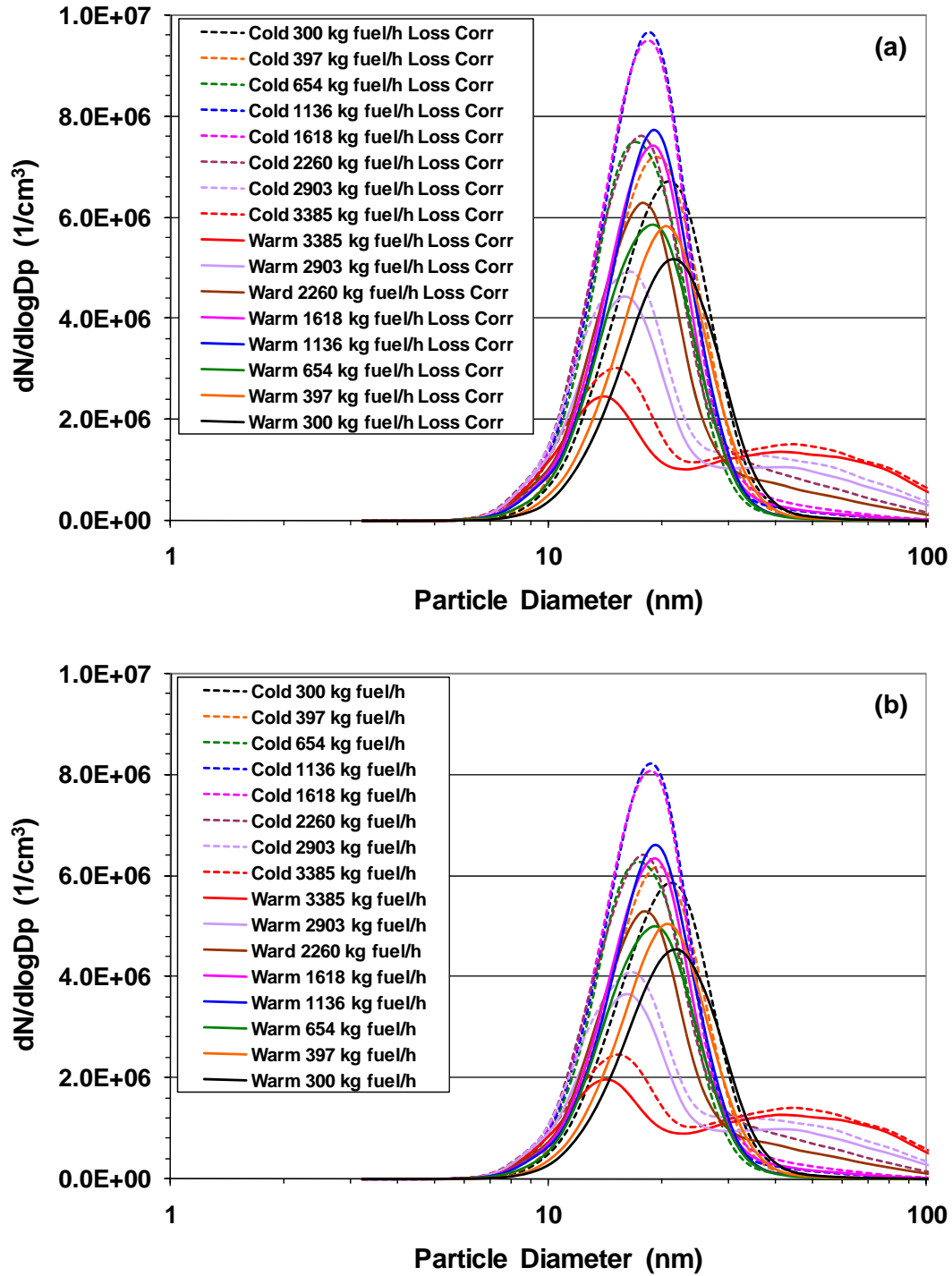
Figure 10-14. Average PSD for a CFM56-3B1 engine measured by the Nano-SMPS during APEX-3, Test T1, (a) <u>with</u> line loss correction; and (b) <u>without</u> line loss correction.
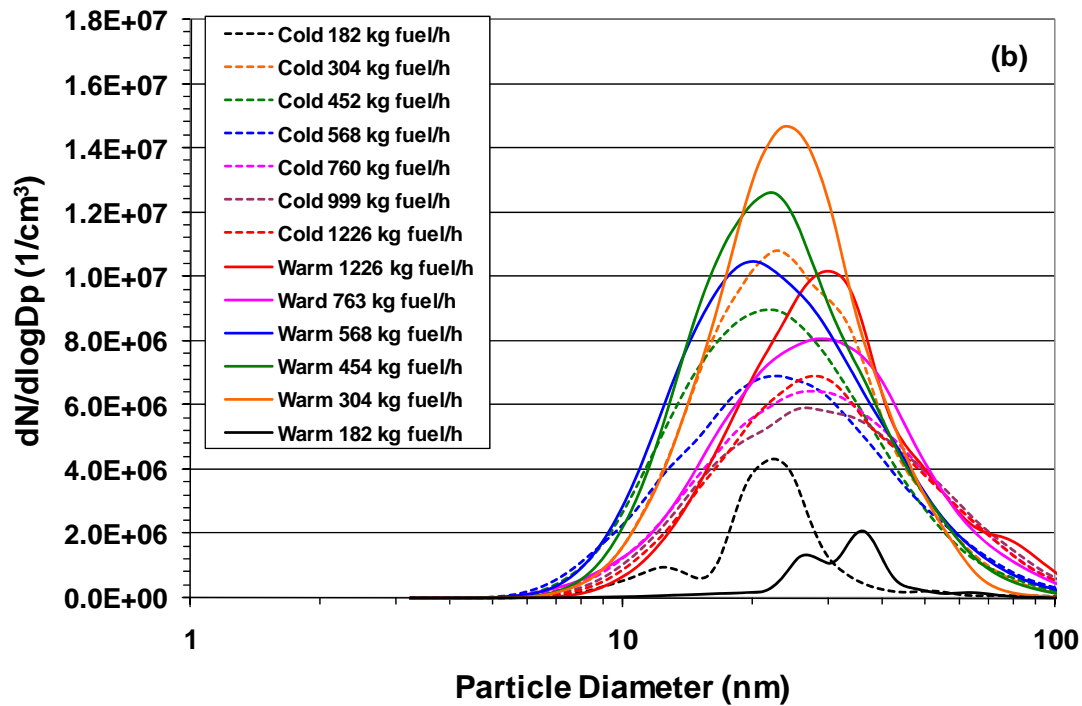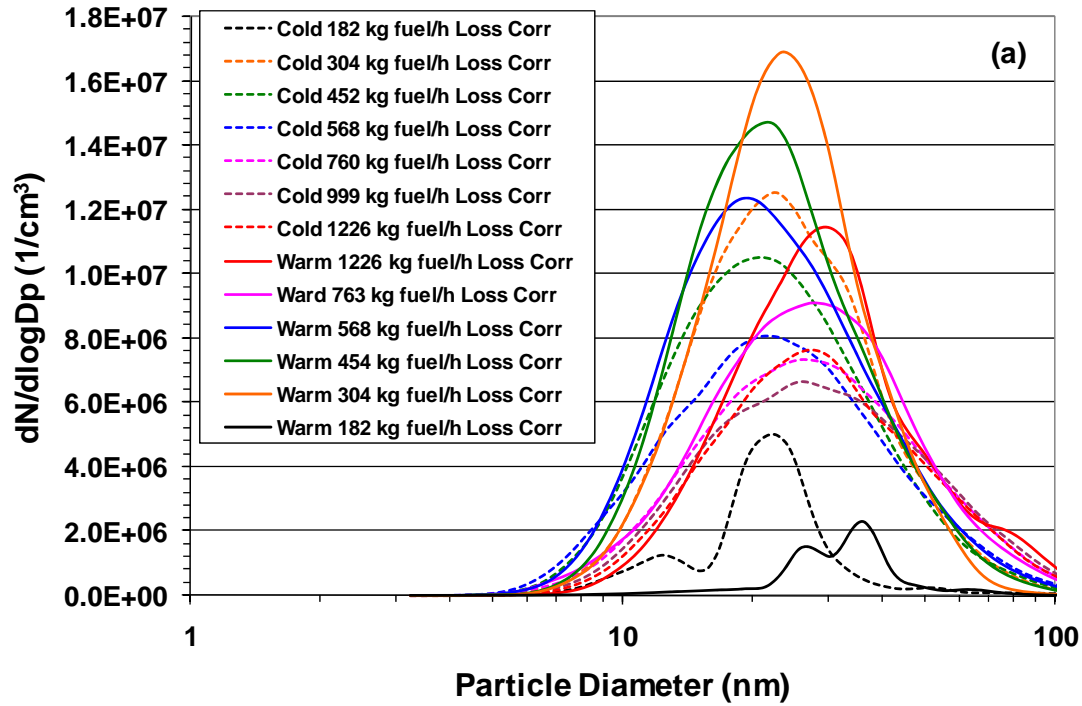
Figure 10-15. Average PSD for a CJ610-8ATJ turbojet engine measured by the Nano-SMPS during APEX-3, Test T2, (a) <u>with</u> line loss correction; and (b) <u>without</u> line loss correction.
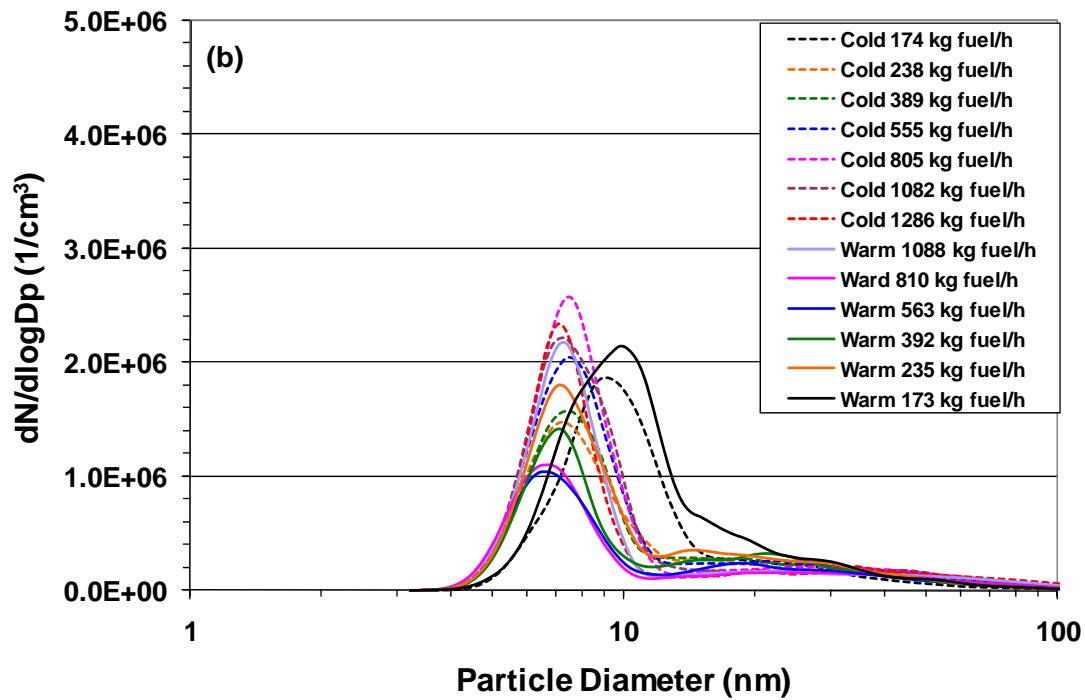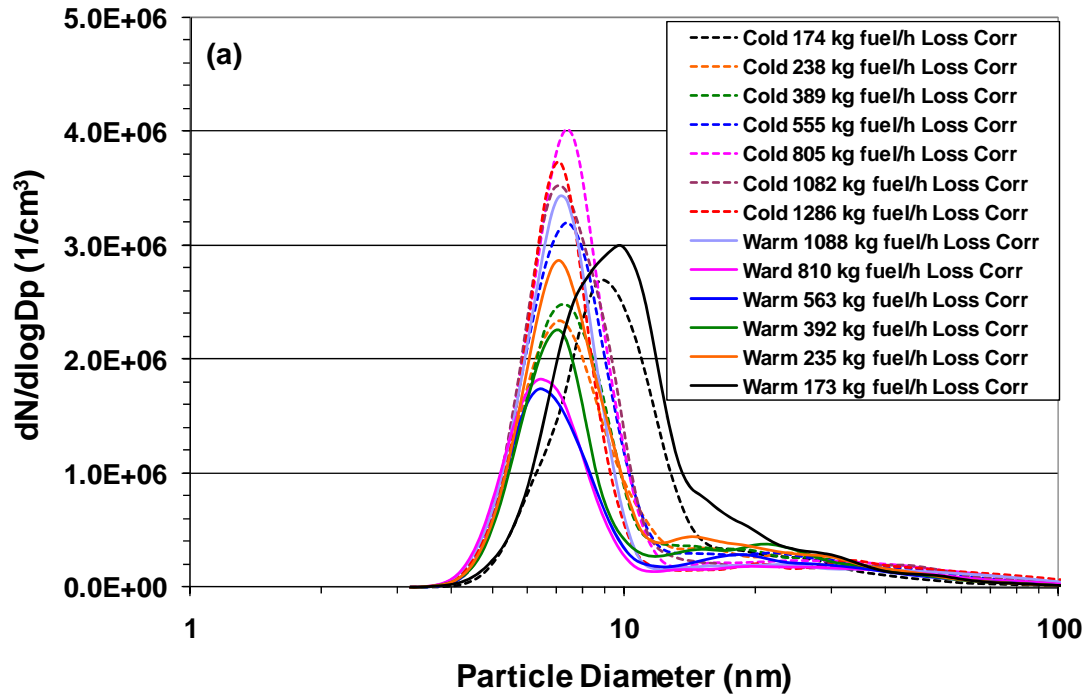
Figure 10-16. Average PSD for an AE3007-A1E engine measured by the Nano-SMPS during APEX-3, Test T3, (a) <u>with</u> line loss correction; and (b) <u>without</u> line loss correction.
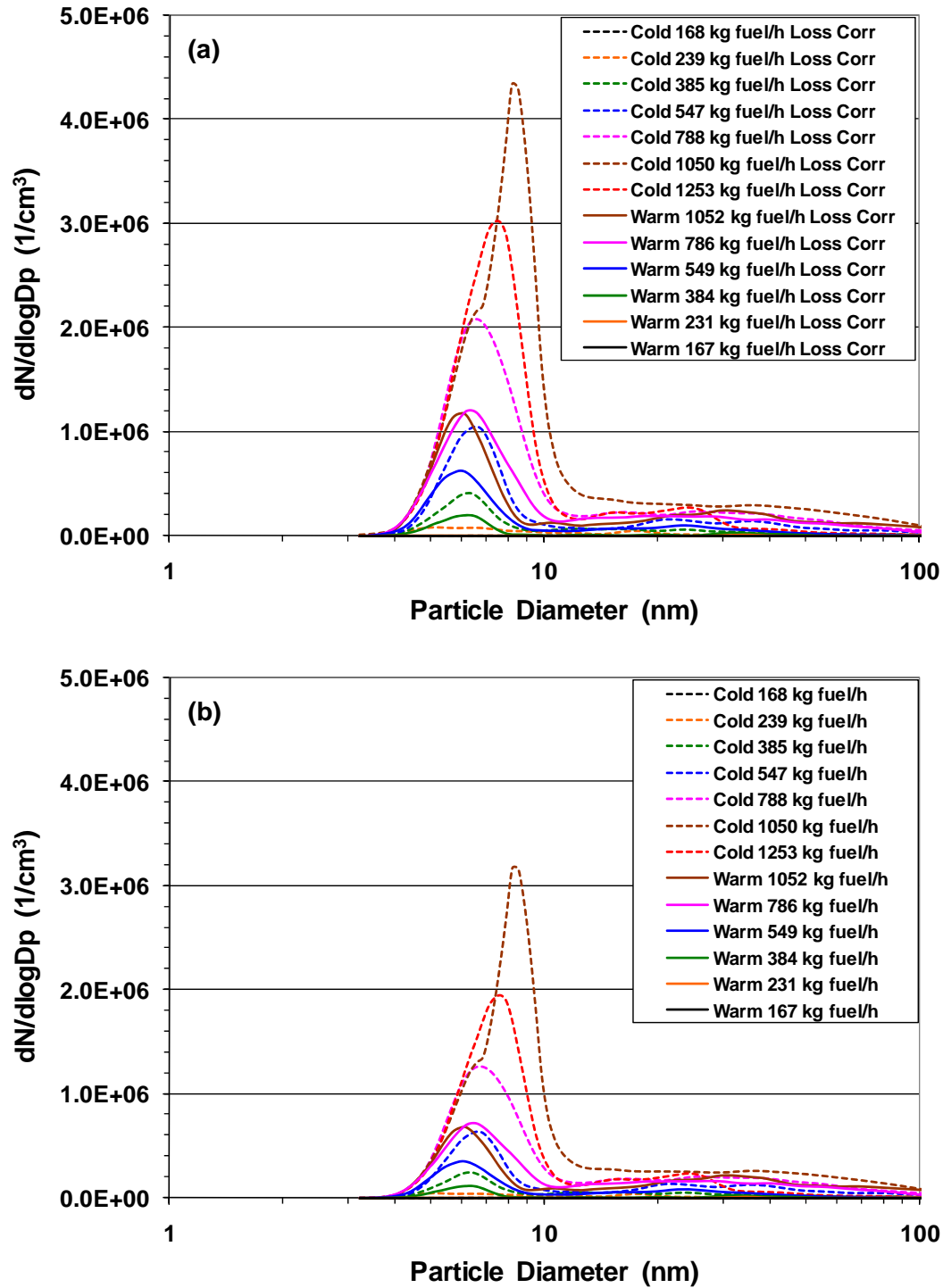
Figure 10-17. Average PSD for an AE3007-A1E engine measured by the Nano-SMPS during APEX-3, Test T4, (a) <u>with</u> line loss correction; and (b) <u>without</u> line loss correction.
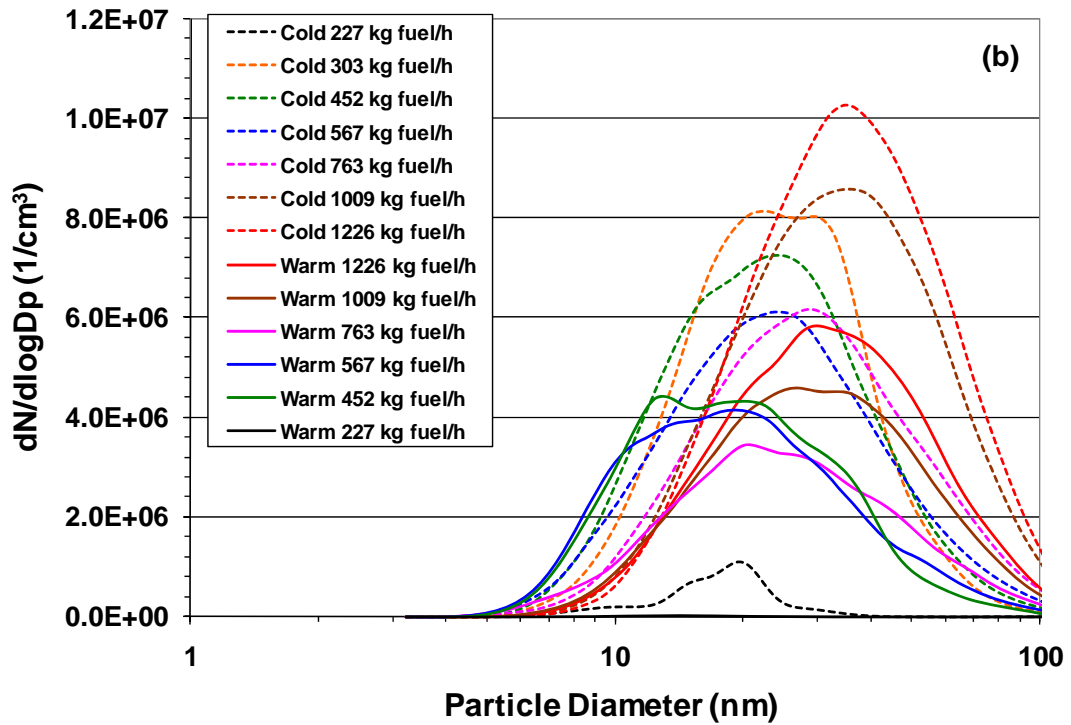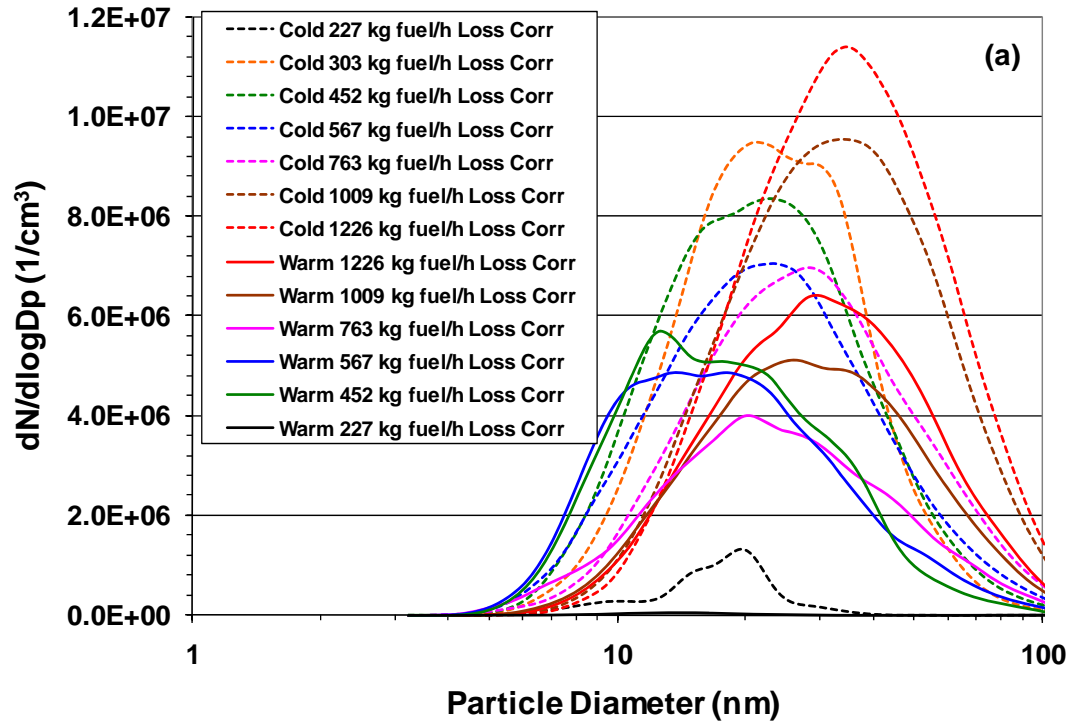
Figure 10-18. Average PSD for a CJ610-8ATJ turbojet engine measured by the Nano-SMPS during APEX-3, Test T5, (a) <u>with</u> line loss correction; and (b) <u>without</u> line loss correction.
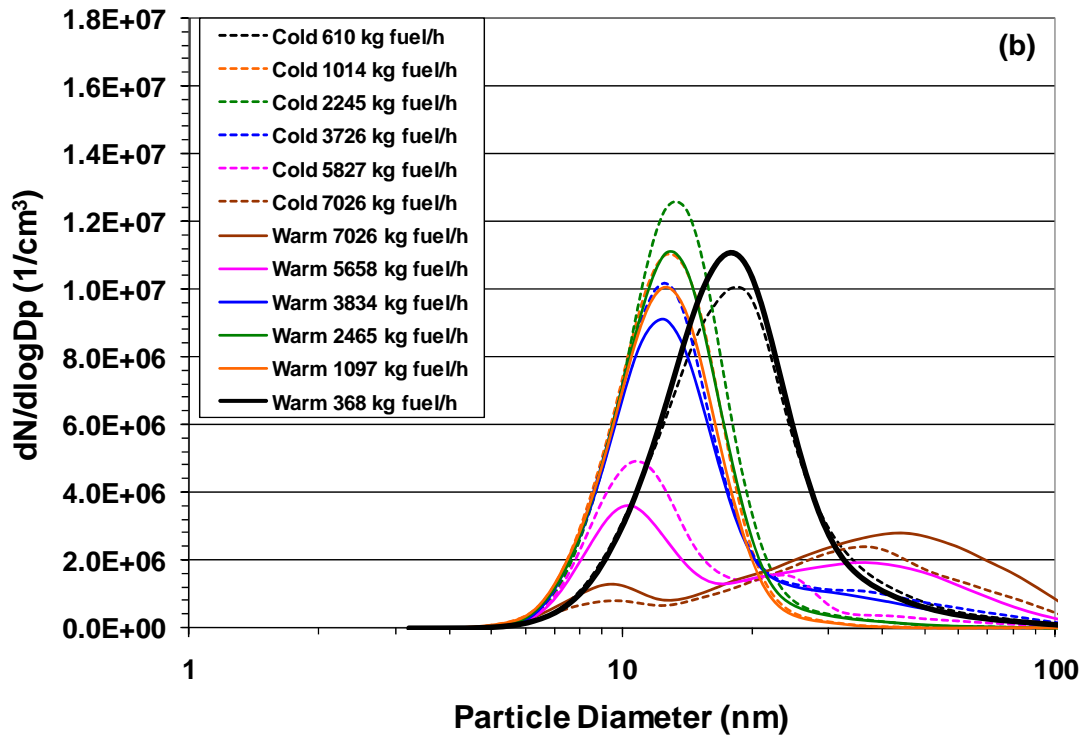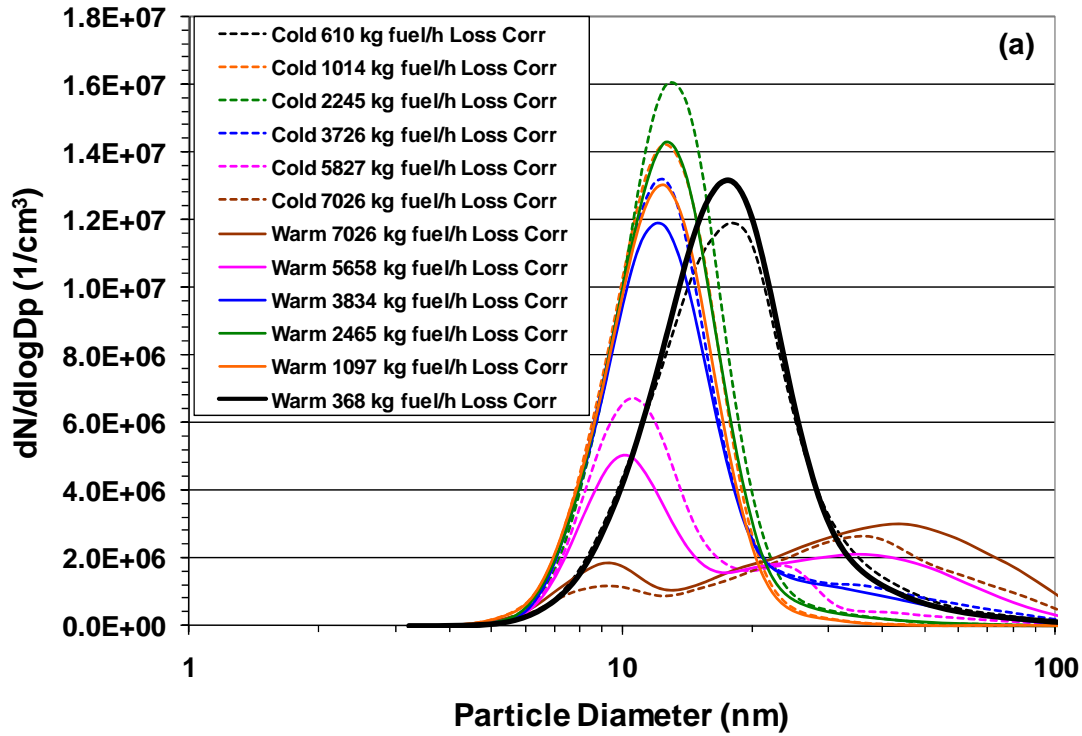
Figure 10-19. Average PSD for a PW4158 engine measured by the Nano-SMPS during APEX-3, Test T6, (a) <u>with</u> line loss correction; and (b) <u>without</u> line loss correction.
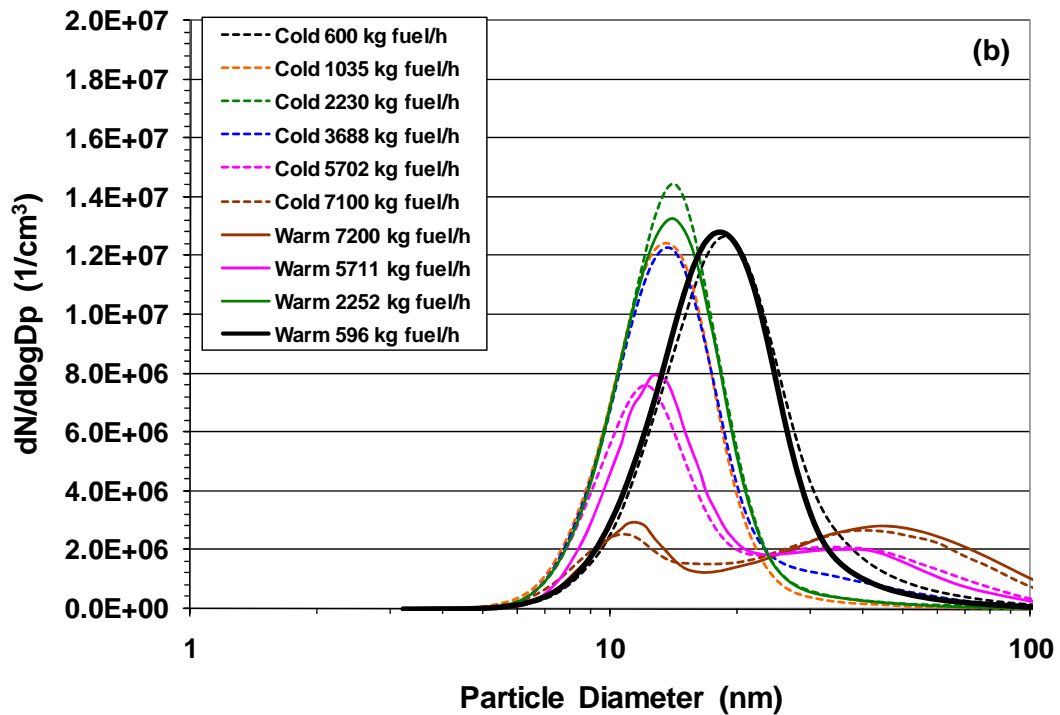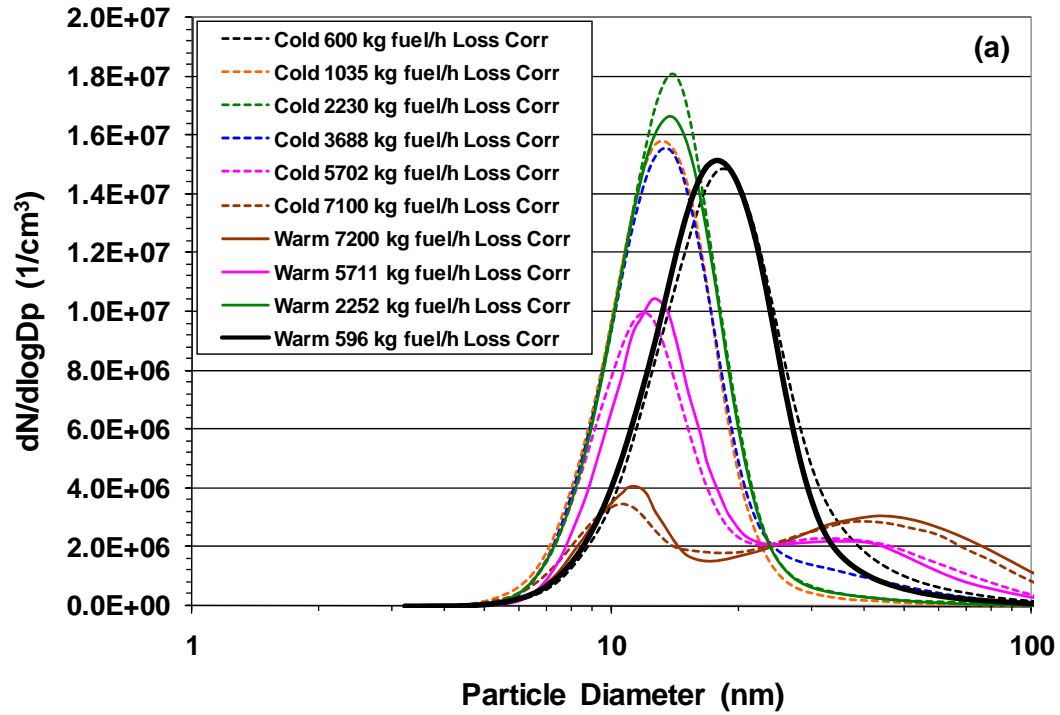
Figure 10-20. Average PSD for a PW4158 engine measured by the Nano-SMPS during APEX-3, Test T7, (a) <u>with</u> line loss correction; and (b) <u>without</u> line loss correction.
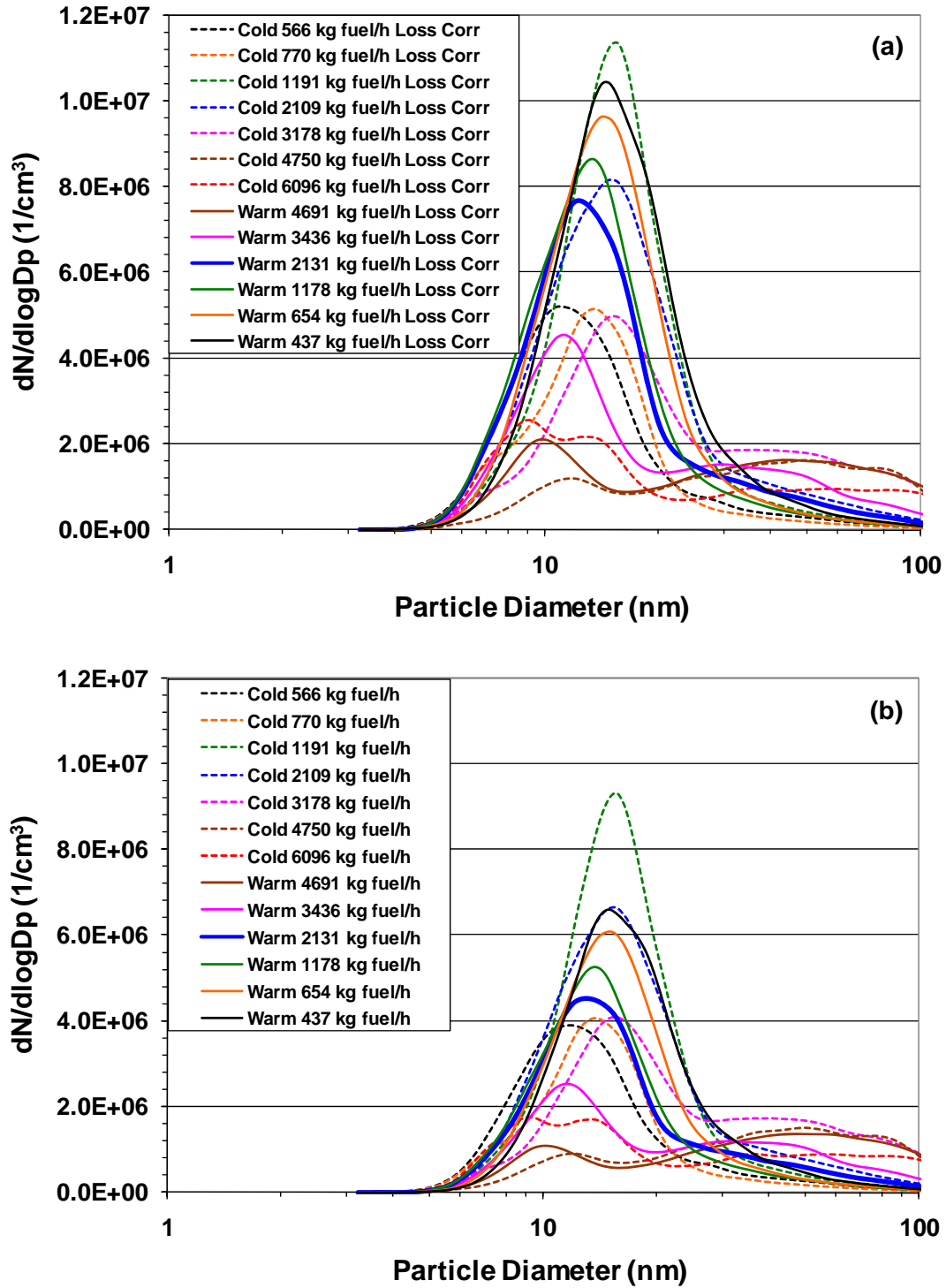
Figure 10-21. Average PSD for a RB211-535E4B engine measured by the Nano-SMPS during APEX-3, Test T8, (a) <u>with</u> line loss correction; and (b) <u>without</u> line loss correction.
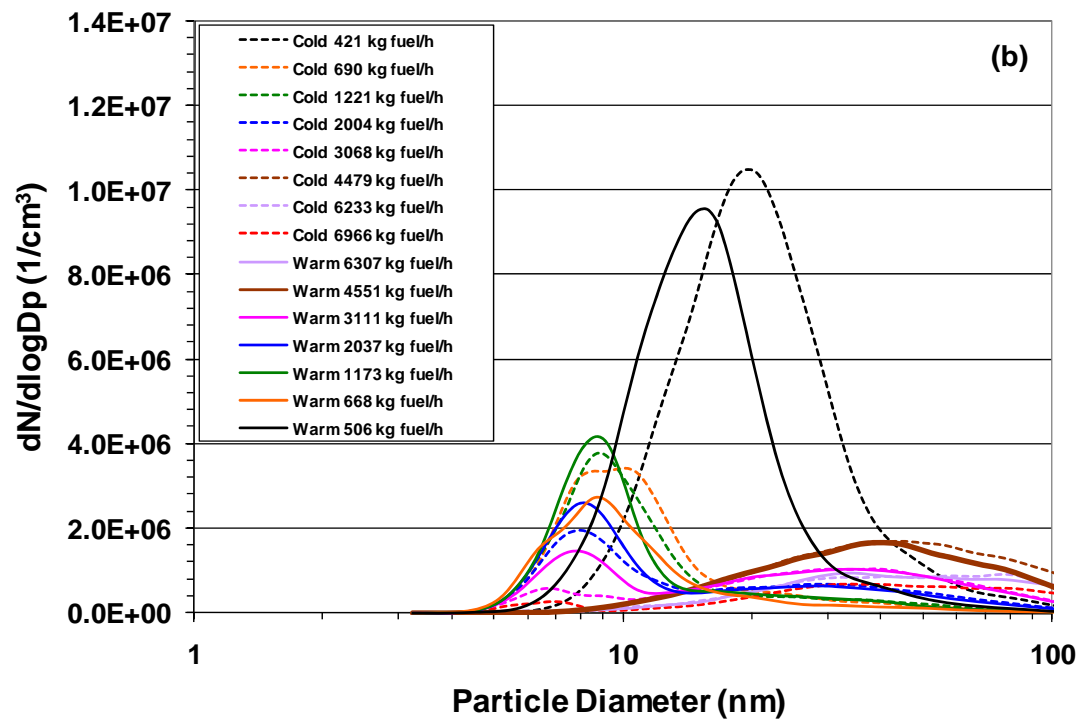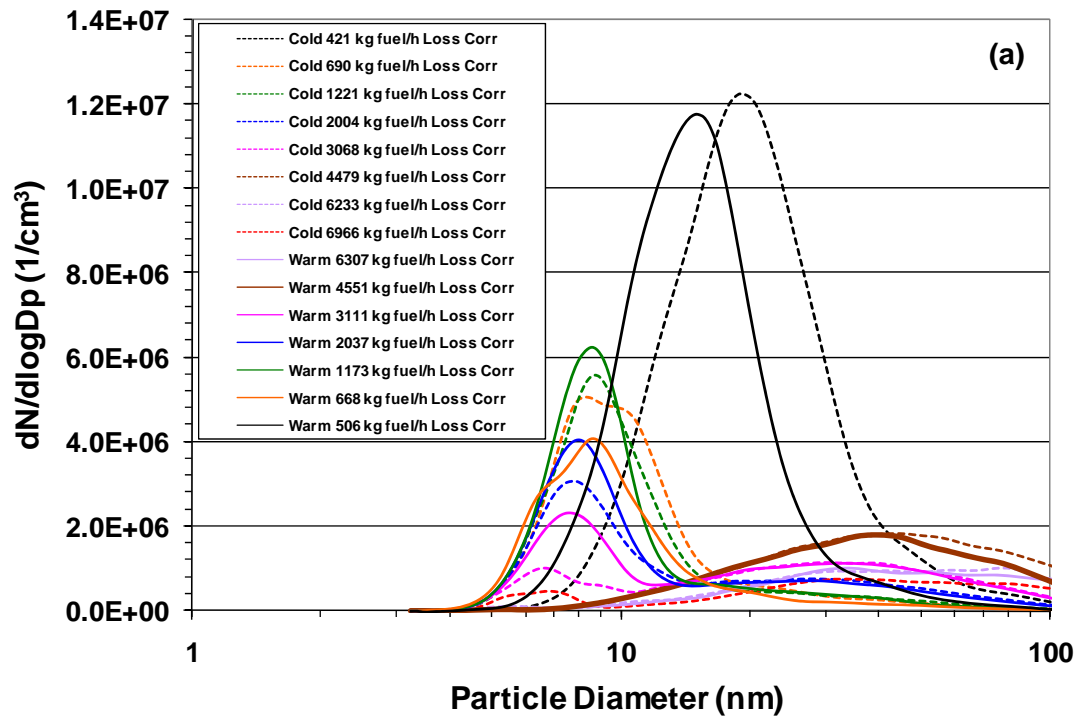
Figure 10-22. Average PSD for a RB211-535E4B engine measured by the Nano-SMPS during APEX-3, Test T9, (a) <u>with</u> line loss correction; and (b) <u>without</u> line loss correction.
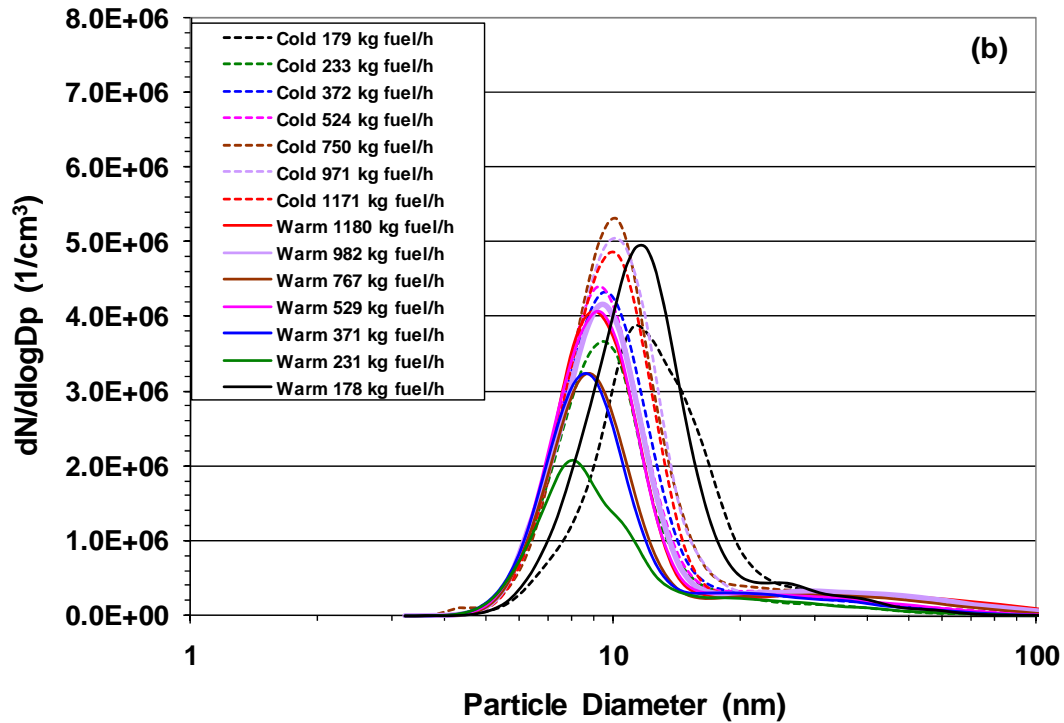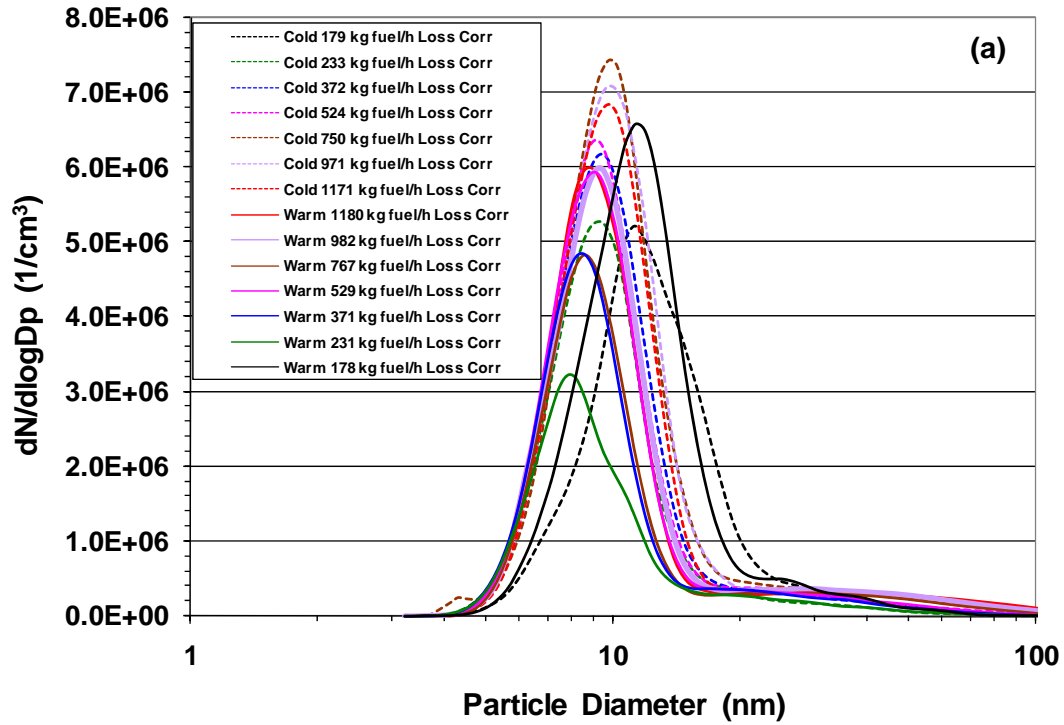
Figure 10-23. Average PSD for an AE3007-A1/1 engine measured by the Nano-SMPS during APEX-3, Test T10, (a) <u>with</u> line loss correction; and (b) <u>without</u> line loss correction.
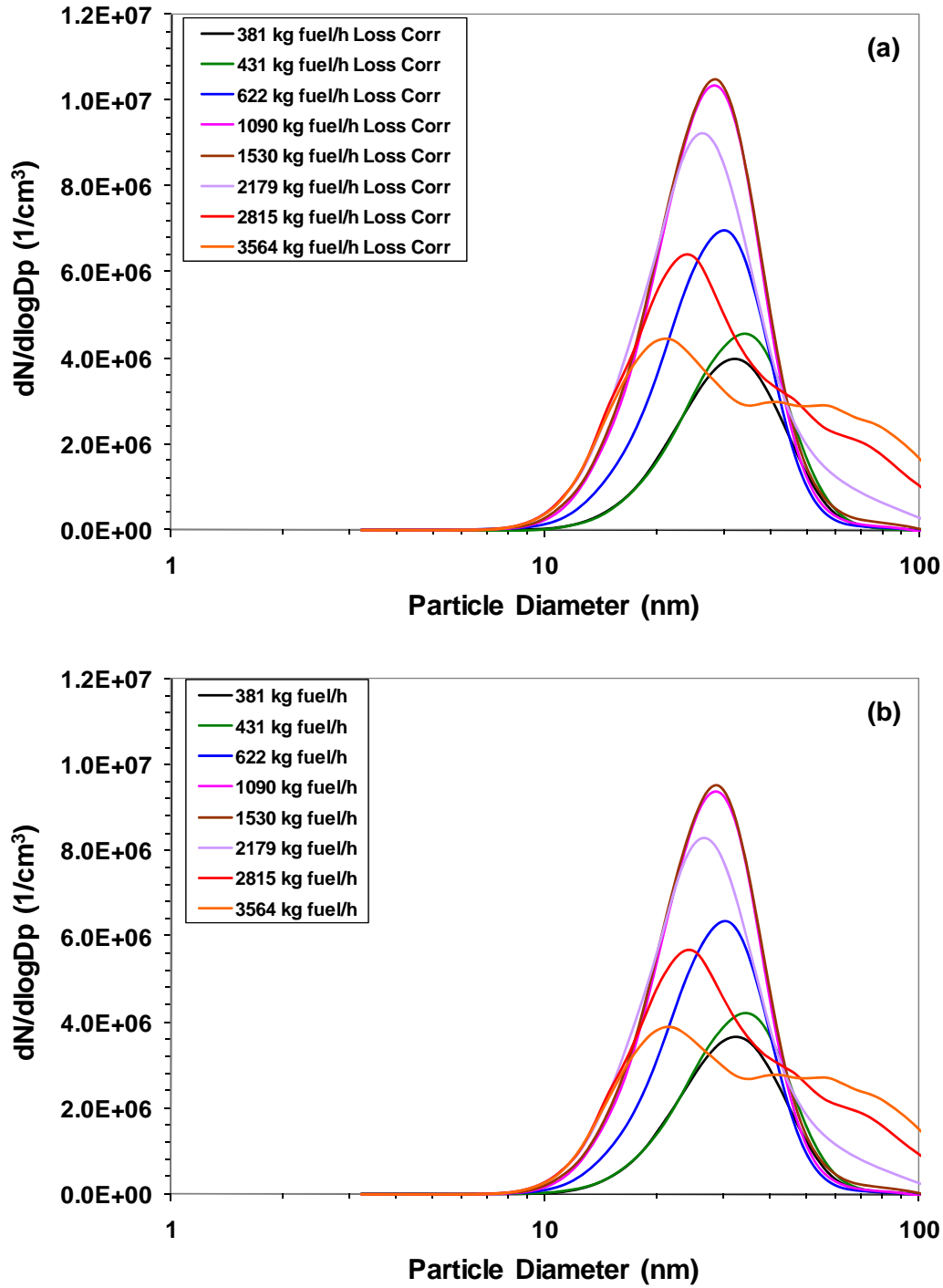
**Figure 10-24.** Average PSD for a CFM56-3B1 engine measured by the Nano-SMPS during APEX-3, Test T11, (a) <u>with</u> line loss correction; and (b) <u>without</u> line loss correction.

10.4 Effects of Particle Loss Correction on PSD Results

To examine the effect of particle loss correction on the PSD results, the PSDs under the idle condition (7% power), before and after loss correction, were plotted in Figure 10-25 for APEX-1. Shown in this figure are Test EPA-2 for base fuel, NASA-2&3 for high sulfur fuel, and NASA-4&5 for high aromatic fuel. The six PSD curves in this figure represent the three different fuels: the blue lines show the base fuel, the pink lines the high-sulfur fuel, and the green lines the high-aromatic fuel. The PSD curves before particle loss correction are shown as fine lines with open dots, and the results after loss correction are shown as solid lines. The particle loss correction in this study did not alter the shape of the PSD over the entire particle size range. However, this correction did change the results for number of particles emitted.
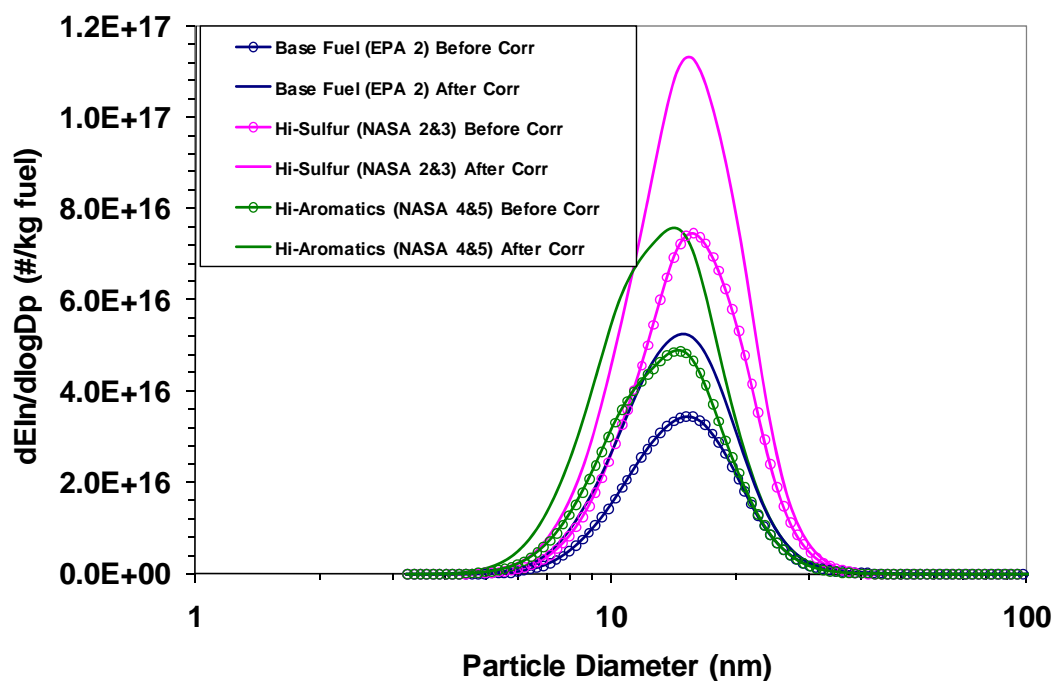
Figure 10-25. Effects of line particle loss correction on PSD for a CFM56-2C1 during APEX-1 (Nano-SMPS results).

The effects of particle loss correction can also be evaluated by comparing the total particle number data, GMDs and GSDs of the PSD, before and after line loss correction as obtained by the Nano-SMPS measurements. The results of this comparison for all three APEX campaigns are shown in Figure 10-26. In Figure 10-26(a), the total particle number concentrations before and after line loss correction show that the concentrations after loss correction increased by about a factor of 1.6 for APEX-1, and about 1.2 for APEX-2 and APEX-3. The different increases for the three APEX campaigns are considered to be due to differences in the sampling line configurations used for these three APEX campaigns. Figure 10-26(b) shows that the GMD data after line loss correction were linearly correlated with the data before loss correction with a correlation coefficient of approximately 0.99. The straight line had a slope of 0.95, indicating that the average particle size was reduced by about 5 percent after sampling line loss correction due to the loss of fine particles by diffusion in the sampling line. Figure 10-26(c) indicates that the line loss correction had little effect on the GSD results as the slope of the correlation line is close to unity.
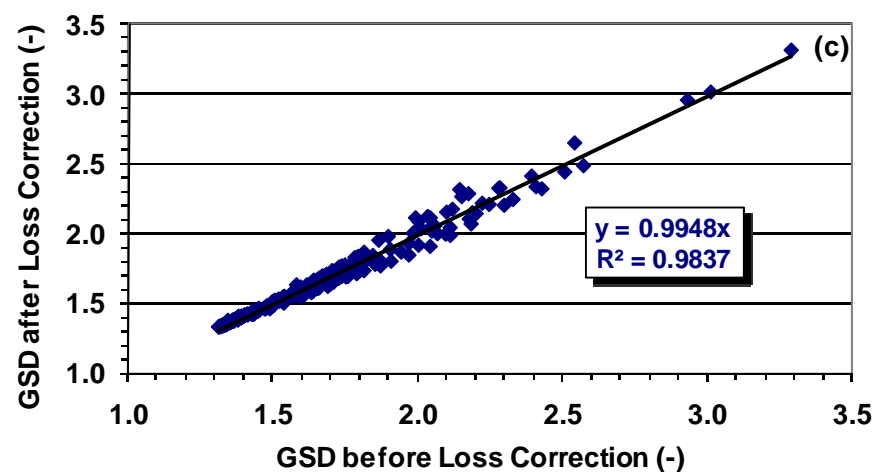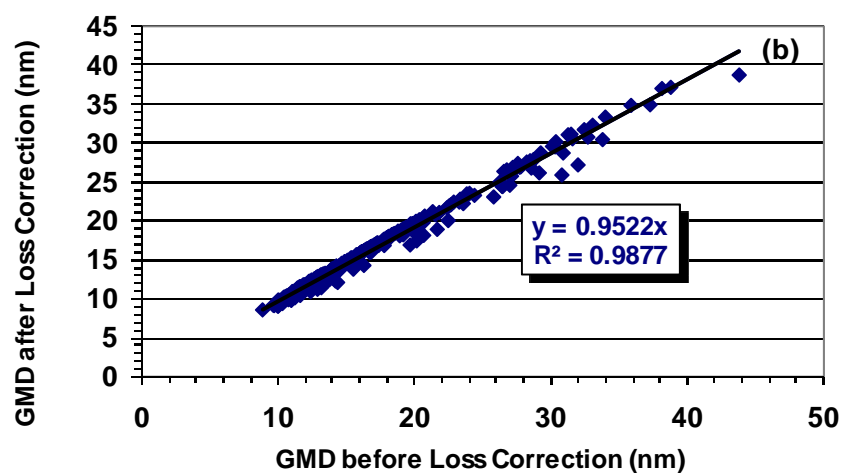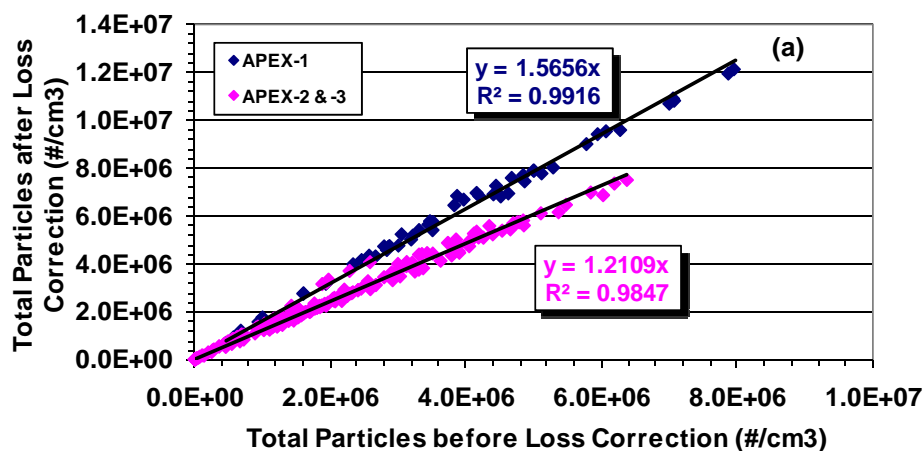
Figure 10-26. Comparison of total particle number, GMD and GSD before and after loss correction for all tests conducted based on: (a) total particle concentration and (b) GMD and (c) GSD.

Thus, in summary, the sampling line loss correction increased the total particle number (mass) and slightly reduced the GMD. No effect on the GSD was observed.

10.5 Effect of Engine Power and Fuel Flow Rate

The particle GMD was found to track closely with engine fuel flow rate and, in turn, thrust. Figure 10-27 shows the typical GMD time-series results of two tests: EPA-2 of APEX-1 and T1 of EPA-3. The GMD data were obtained by Nano-SMPS and are presented both with and without line loss correction. The fuel flow rate data are represented by the red line (refer to the second y-axis on the right).

To investigate the effect of engine power thrust or fuel flow rate on PSD, the time series GMD and GSD data measured by the Nano-SMPS in each APEX test were averaged at the same power settings and then plotted against the fuel flow rate as shown in Figure 10-28 for APEX-1, Figures 10-29 and -30 for APEX-2, and Figures 10-31 to -34 for APEX-3. The data for APEX-2 and -3 are broken down by engine size and cold or warm operation. Since the sampling line particle loss does not affect the overall trend of PSD with engine operation conditions, only the results with particle loss correction are presented here.

These figures show that, in general, the GMD was larger at idle (lowest fuel flow rate), decreased as fuel flow rate increased until the minimum value was reached, and then increased again with fuel flow. Notable exceptions to this U-shaped pattern include the AE3007 series engines which exhibited an almost consistent GMD of ~10 nm across all fuel flow (thrust) levels as indicated in Figures 10-31(a) and 10-33(a). Most of the GMD values in the figures were obtained from the measurement probe 30 m downstream of the engines, which show variation with fuel flow between 10 to 30 nm. Note that in Figure 10-31(a), the cold engine data for APEX-3 tests T2, T3, T4 and T5 were measured by the 15-m probe, and the cold engine data for T8 in Figure 10-32(a) were measured by the 43-m probe.

The GSD values in Figures 10-29 to -34 were usually near 1.4 at idle, then gradually increased to greater than 2 as the fuel flow increased. As shown in Figure 10-31(b) and 10-33(b) for T2 and T3 of APEX-3, the GSDs measured at 15 m varied with fuel flow in a pattern different from the other engines tested.

Figure 10-35(a) and (b) compare the GMDs and GSDs measured by the Nano-SMPS for the four ICAO-specified engine operation modes of idle, takeoff, climb-out, and approach power for different jet engines in the three test campaigns. The data in the figures are particle-loss-corrected, and only data from the 30-m probe are presented.

The figure shows that, in general, the PM emissions for the approach power condition (30% power) had the smallest GMD for all of the engines tested. The largest GMDs and GSDs were obtained during the takeoff (100% power) and climb-out (85% power) conditions. These observations suggest that the PSDs of PM emissions from the jet engines under both idle (7% power) and approach (30% power) conditions were unimodal and consisted of primary nuclei particles. When the engines were operated under the takeoff (100% power) and climb (85% power) conditions, accumulation mode particles were formed (by either homogeneous nucleation, condensational growth, and/or coagulation to form larger particles) and the PSD curves became broader.
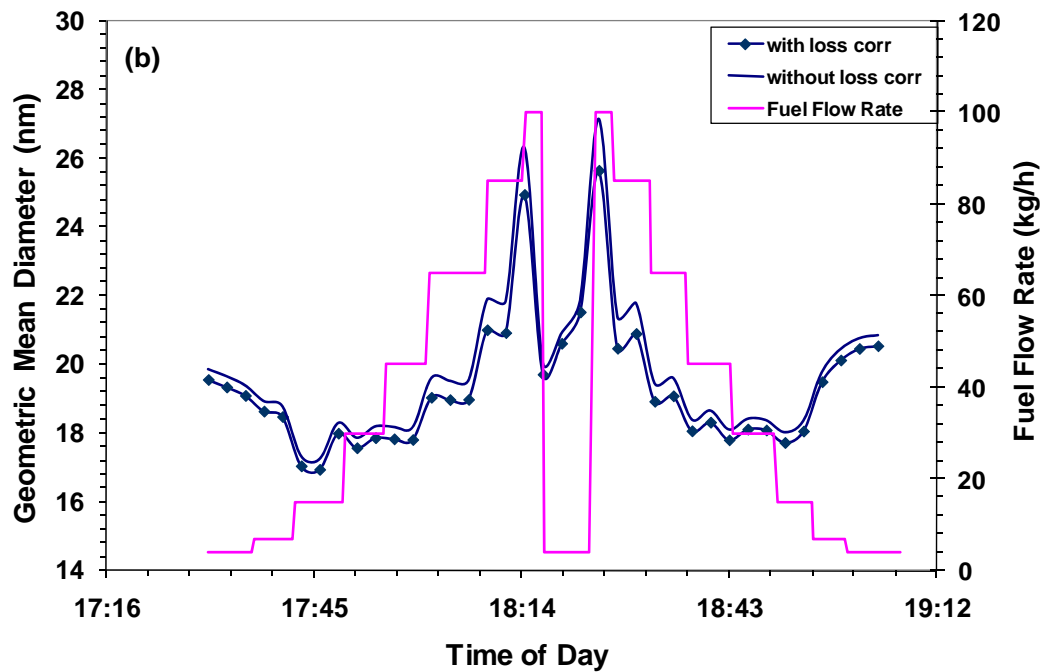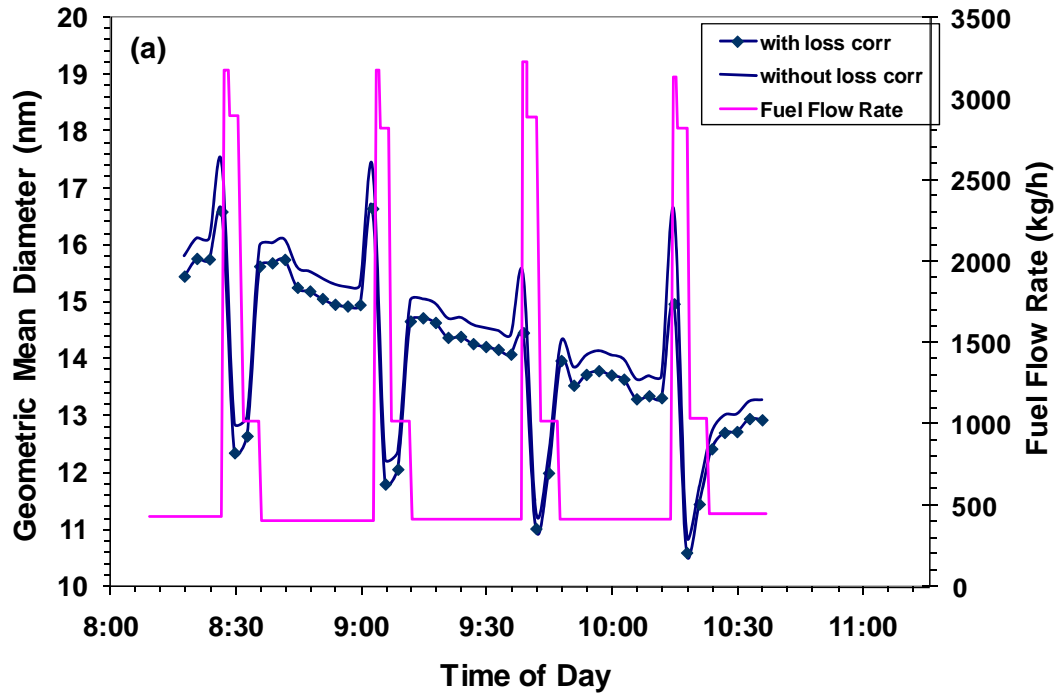
Figure 10-27. Two typical results of GMD as a function of fuel flow rate for (a) a CFM56-2C1 engine during APEX-1, Test EPA-2; and (b) for a CFM56-3B1 engine during APEX-3, Test T1.
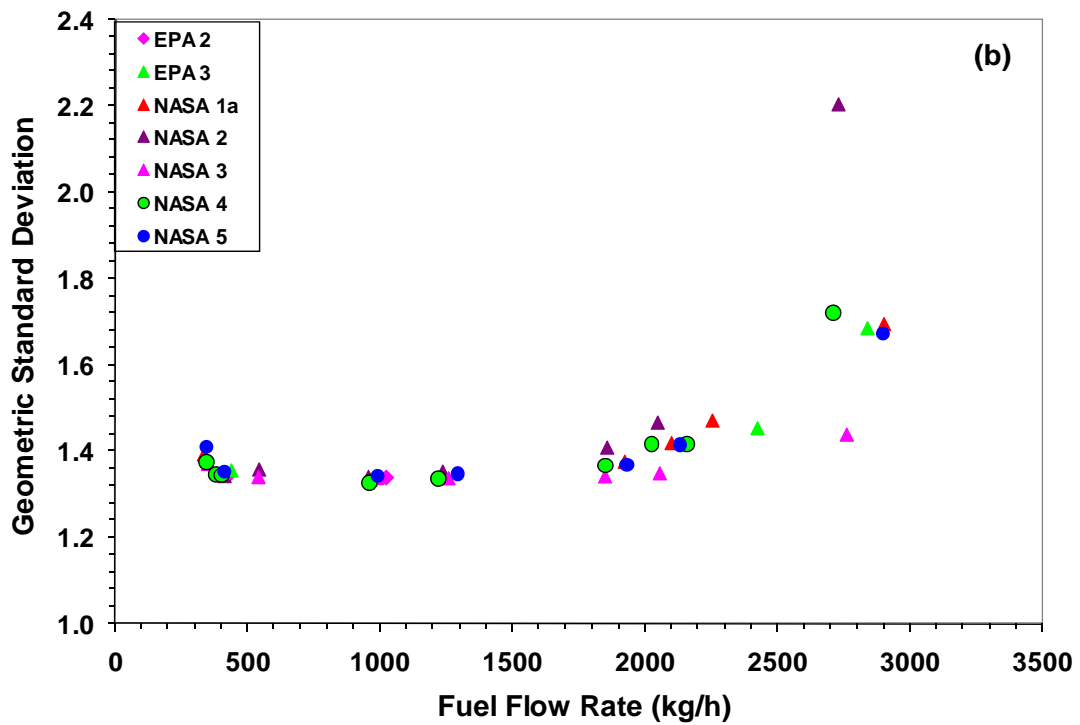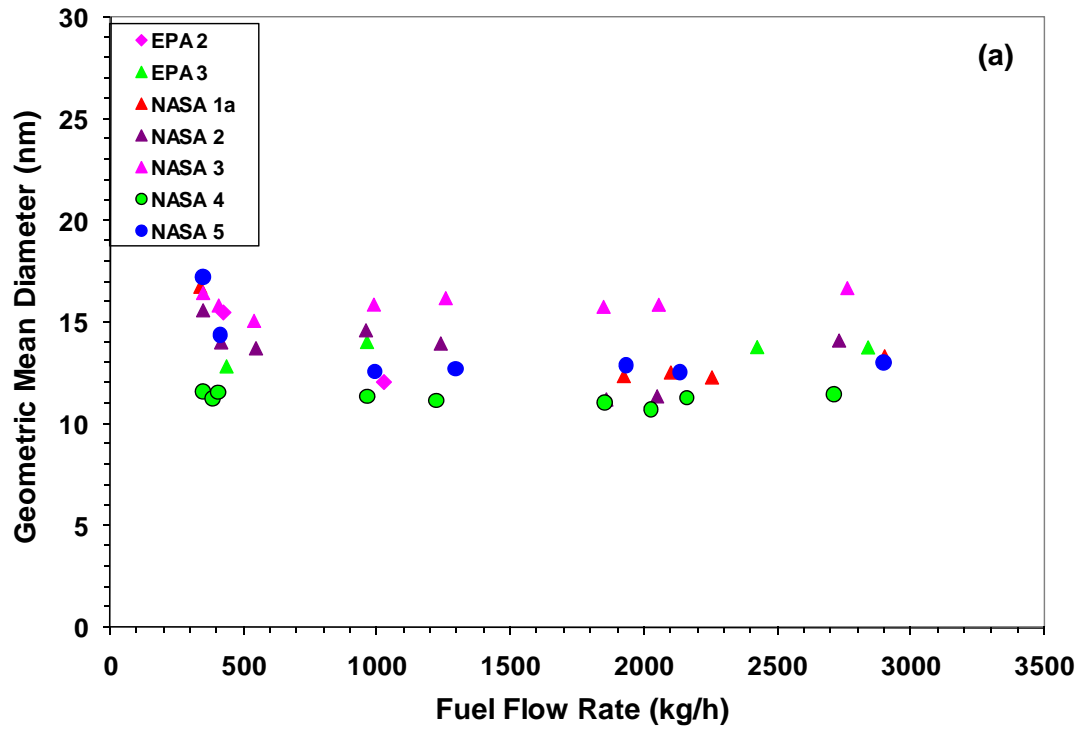
Figure 10-28. The (a) GMD and (b) GSD of the PM emissions measured during APEX-1 for a CFM56-2C1 engine as a function of fuel flow.
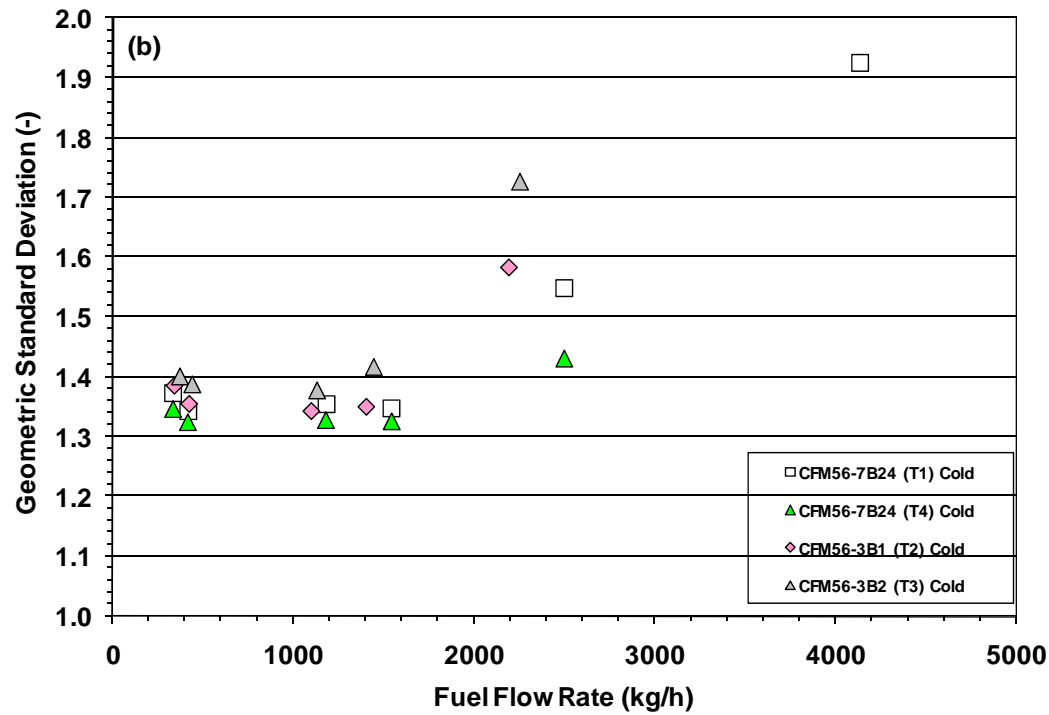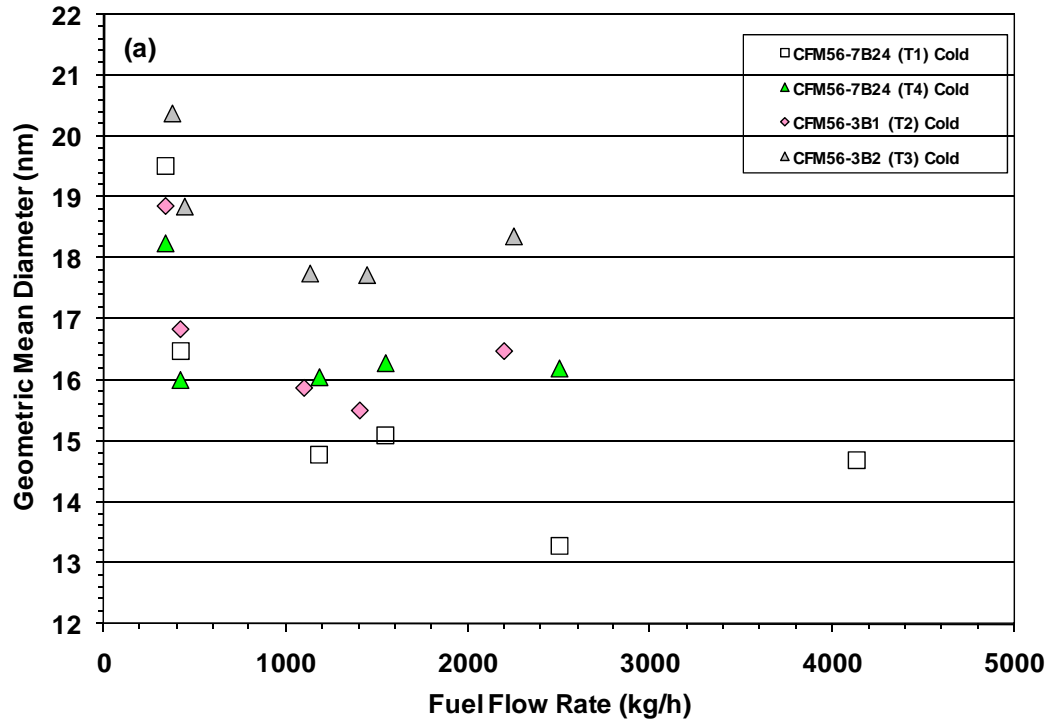
Figure 10-29. The (a) GMD and (b) GSD of the PM emissions measured for three derivatives of the CFM56 engine during APEX-2 as a function of fuel flow. Engines operated during <u>cold</u> portion of test cycle.
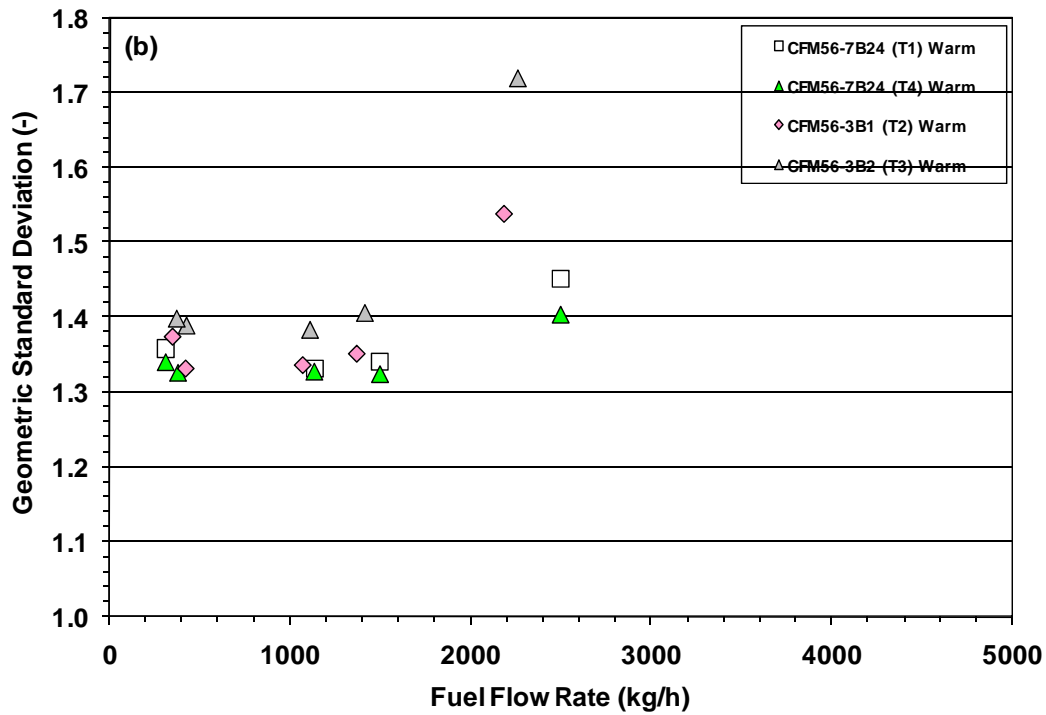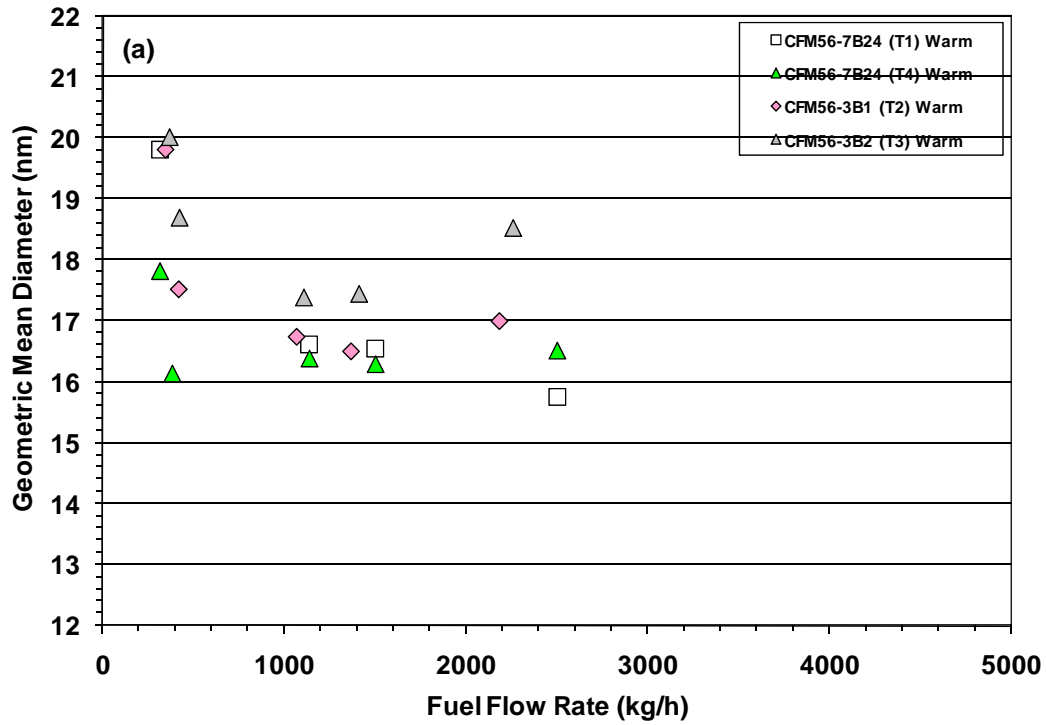
Figure 10-30. The (a) GMD and (b) GSD of the PM emissions measured for three derivatives of the CFM56 engine during APEX-2 as a function of fuel flow. Engines operated during <u>warm</u> portion of test cycle.
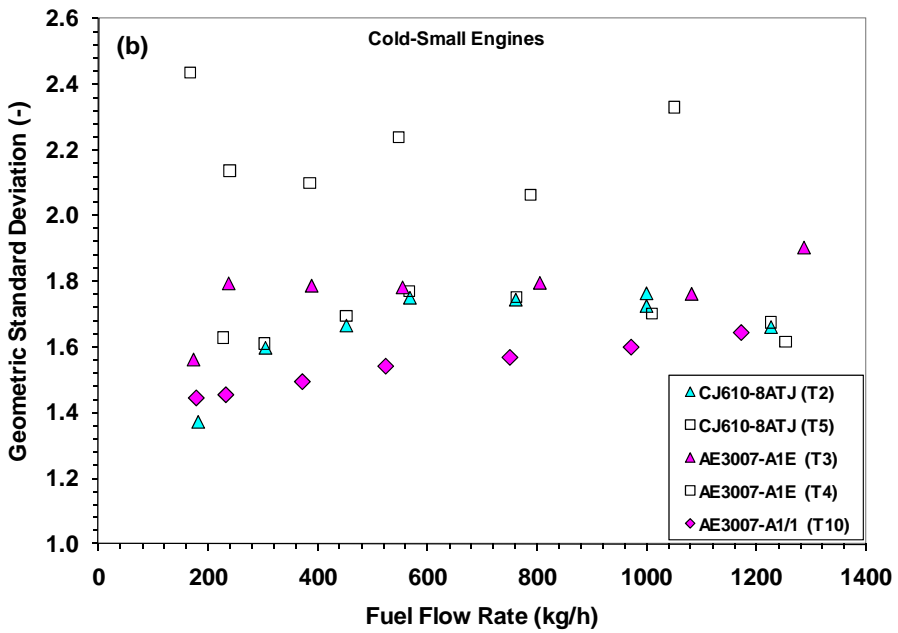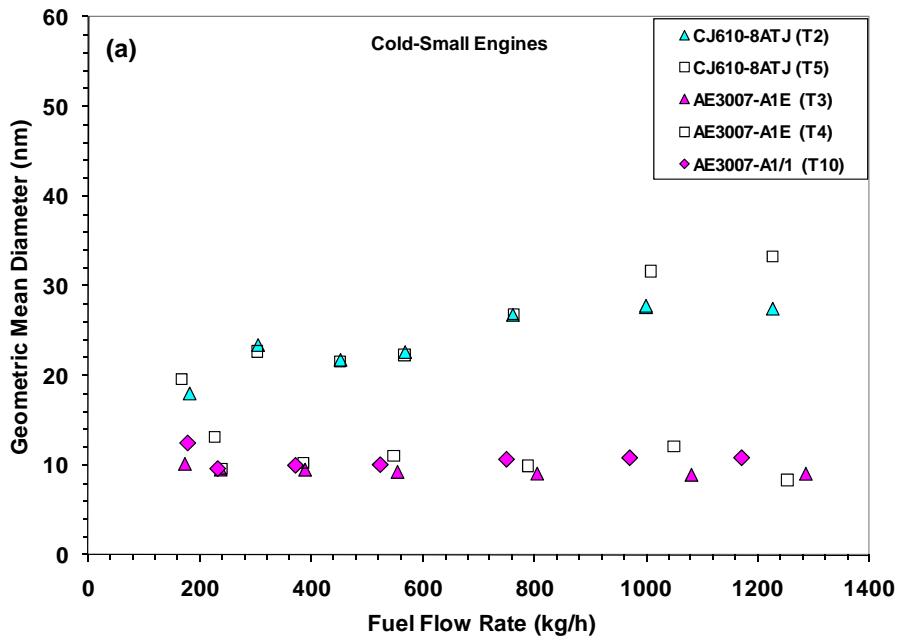
Figure 10-31. The (a) GMD and (b) GSD of the PM emissions measured for the small engines during APEX-3 as a function of fuel flow. Engines operated during the <u>cold</u> portion of the test cycle.
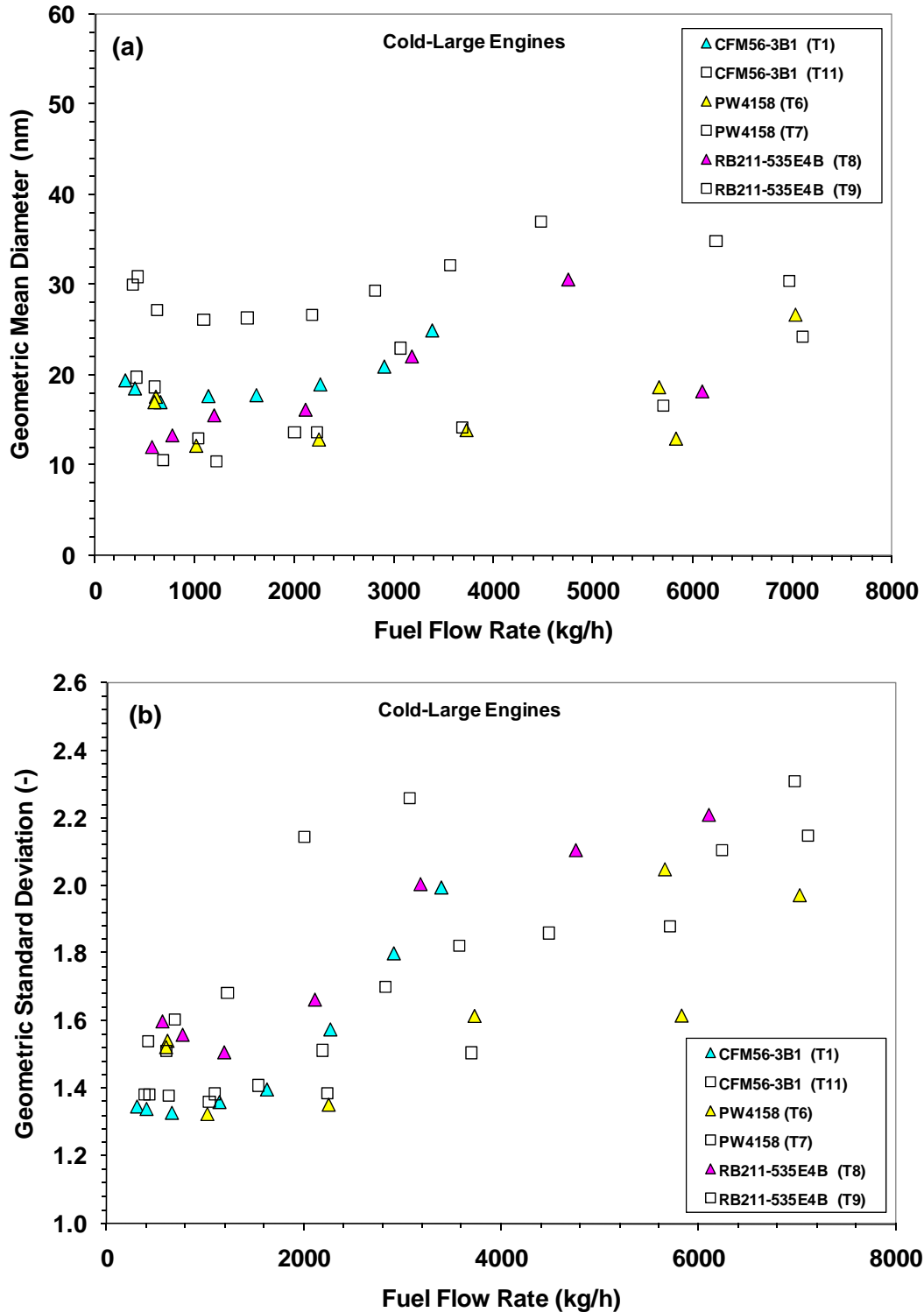
Figure 10-32. The (a) GMD and (b) GSD of the PM emissions measured for the large engines during APEX-3 as a function of fuel flow. Engines operated during the <u>cold</u> portion of the test cycle.
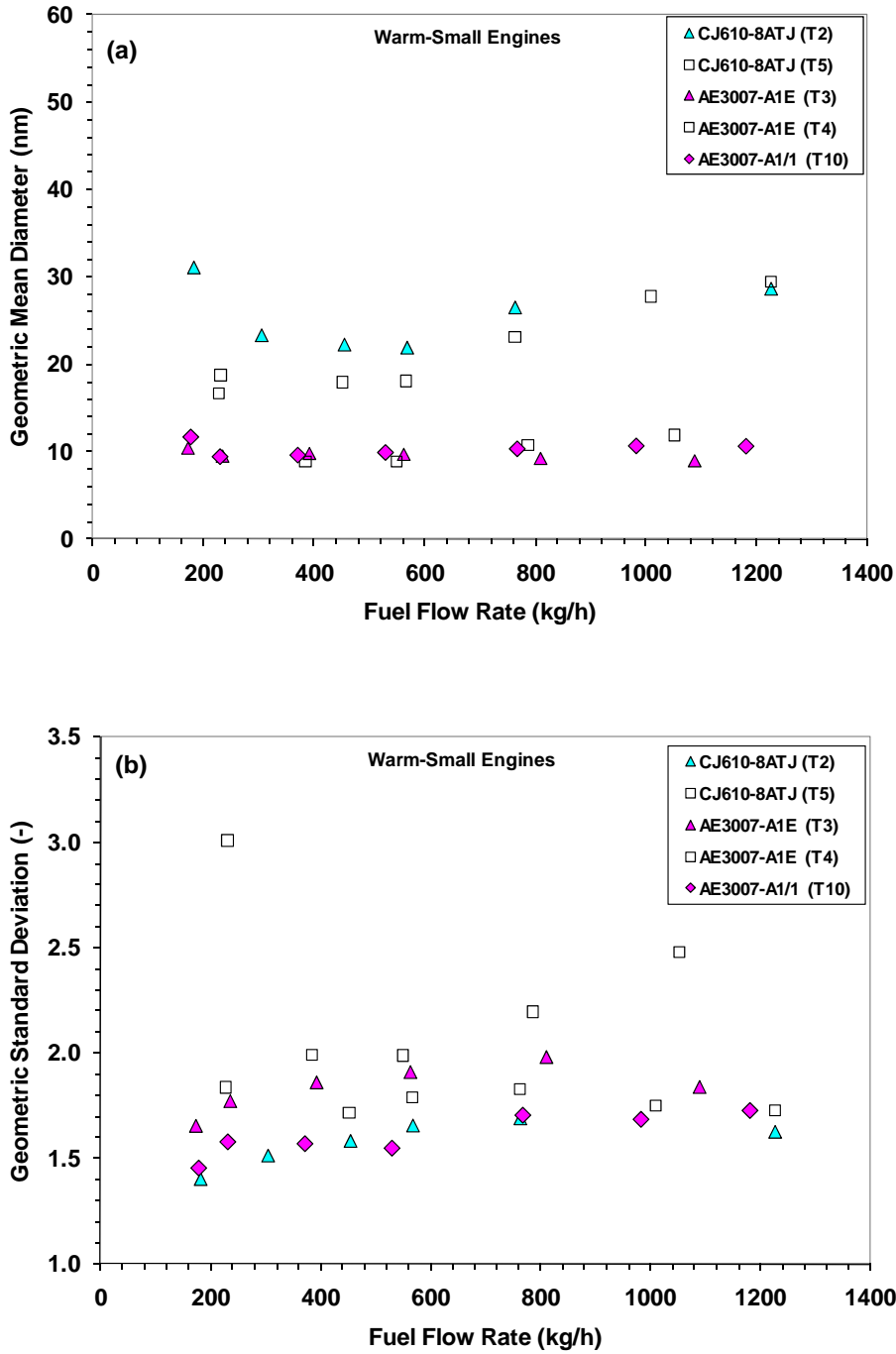
Figure 10-33. The (a) GMD and (b) GSD of the PM emissions measured for the small engines during APEX-3 as a function of fuel flow. Engines operated during the <u>warm</u> portion of the test cycle.
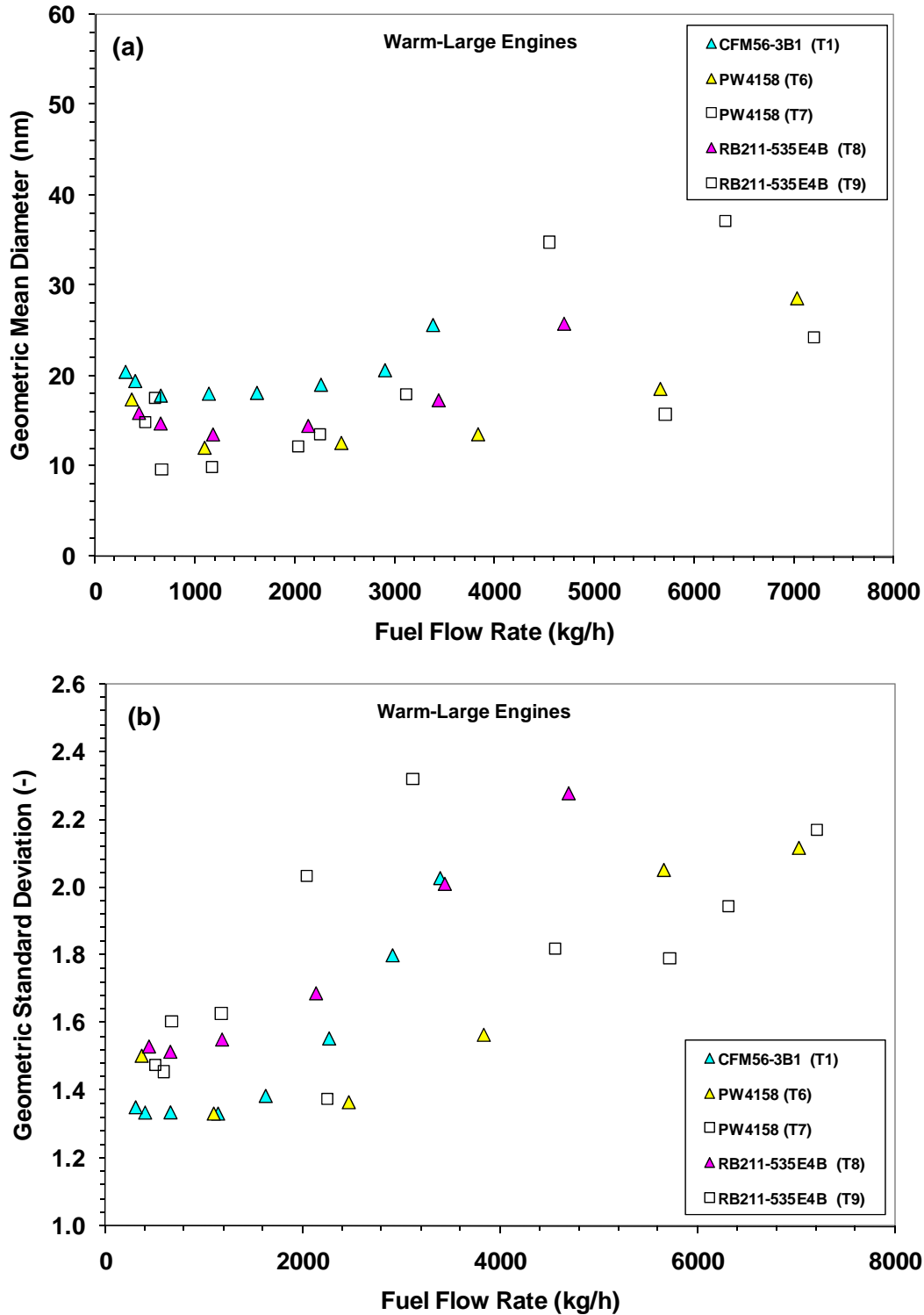
Figure 10-34. The (a) GMD and (b) GSD of the PM emissions measured for the large engines during APEX-3 as a function of fuel flow. Engines operated during the <u>warm</u> portion of the test cycle.
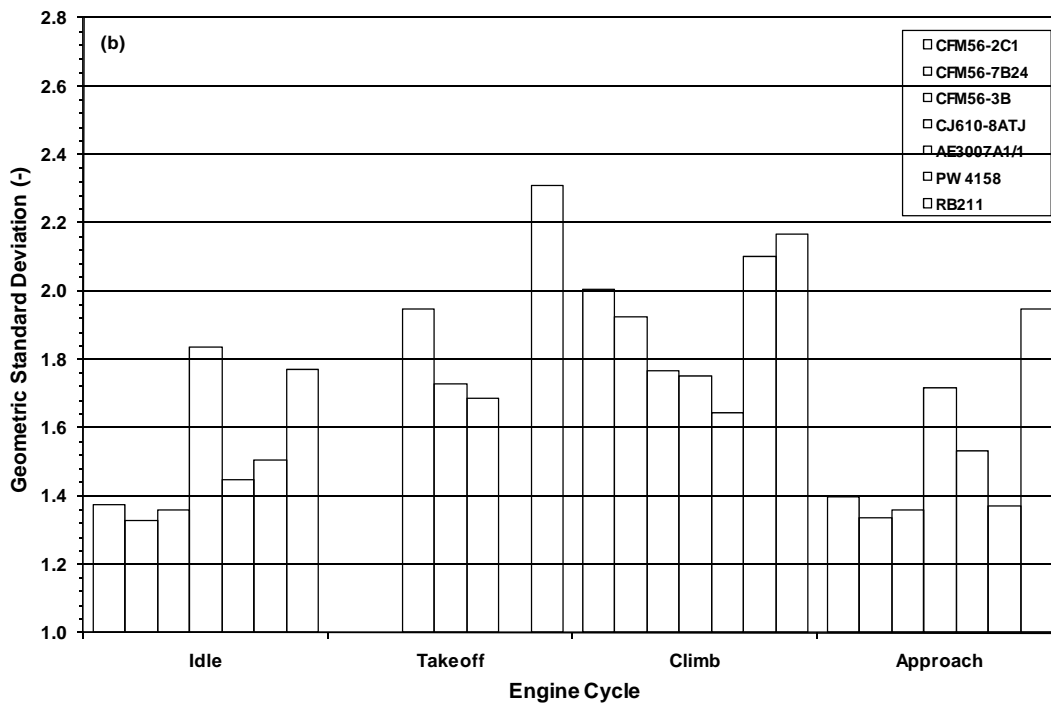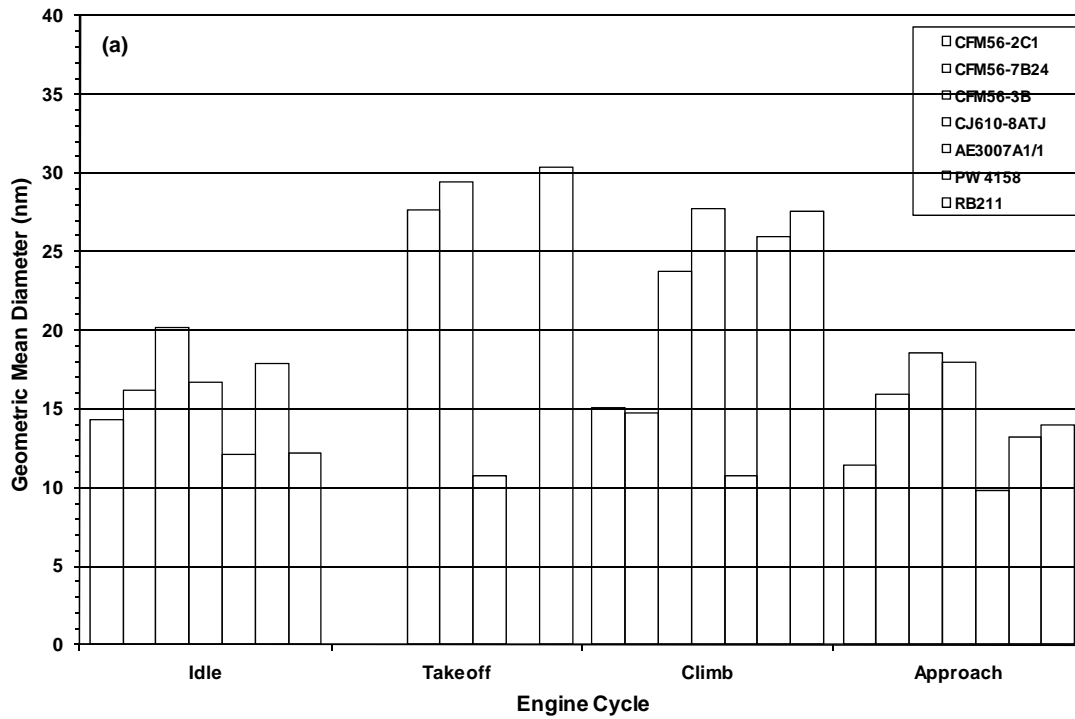
Figure 10-35. Comparison of: (a) GMD and (b) GSD under four ICAO power conditions for different engine types.

10.6   Effects of Fuel Type

To investigate the effects of fuel type on particle size distribution, the differential number PSDs (dN/dlogDp) obtained from APEX-1 for different fuels were compared. Figure 10-36 shows the comparisons of the PSDs obtained by the Nano-SMPS for the three different jet fuels (base, high-sulfur and high-aromatic) under three engine power levels representative of (a) idle, (b) climb and (c) approach, respectively. The three test results used were NASA-1 for base fuel, NASA-3 for high-sulfur fuel, and NASA-4 for high-aromatic fuel. Take-off data could not be obtained by the Nano-SMPS due to its slow instrument response and relatively short run time under the 100 percent rated thrust condition. Note that the test NASA-1 of APEX-1 was run under higher crosswind conditions as discussed previously. This test is being used for the discussion here because the NASA-1 test was the only test with all three power levels for the base fuel measured by Nano-SMPS.

Under all three power levels, a unimodal and log-normal PSD was observed regardless of the difference in fuel type and power setting. In Figure 10-36, under all three power settings, the base fuel produced the smallest number of particles, followed by the high-aromatic fuel and the high-sulfur fuel. This trend is due to the conversion of a small fraction of the sulfur in jet fuel to sulfate during combustion. The sulfate then becomes part of the PM emissions. The PSD for the high-sulfur fuel peaked at approximately 17 nm regardless of the power setting, while the peaks for the PSDs of base and high-aromatic fuels were at slightly smaller particle size. Measurement of higher PM emissions from high-aromatic fuel than from base fuel is most likely due to unburned hydrocarbons in the high-aromatic fuel being condensed and forming additional nuclei particles in the emissions.

In Figure 10-36(c), the PSD curves under the climb-out power (85%) shows notable "tails" in the larger particle size channels (>30 nm) indicative of the formulation of a minor accumulation mode. Under approach conditions (30% power), as shown in Figure 10-36(b), the number of particles emitted from all three fuels sharply increased, but the particles were still not as numerous as was the case at idle. Again, like idle, a higher particle count resulted from the high-sulfur fuel.

Figure 10-37 also provides a comparison of the average GMDs and GSDs obtained for selected APEX-1 tests at idle and at 30 and 85 percent rated thrust. The data presented in the figure were particle-loss-corrected. As Figure 10-37 shows, the GMDs of the particles produced using high sulfur fuel tend to be greater than those for the other two fuel types tested. Also, the GMDs obtained with either high-sulfur or high-aromatic fuel showed little effect from changes in engine power. The GMD for high-sulfur fuel was in the range of 16-17 nm, the GMD for high-aromatic fuel was between 11-12 nm, and, in contrast, the GMD for base fuel varied significantly from ~11 to 17 nm as the engine power changed. Figure 10-37(b) also shows that the GSD obtained with base fuel varied by a factor of 1.7 between idle and climb-out power, where the GSD exceeded 2.3.

10.6 Effects of Engine Type

To investigate the effects of engine type on particle size distribution, Figure 10-38 compares the GMDs obtained by the different engines tested during the three APEX campaigns. The results, measured by Nano-SMPS at 30 m behind the engines, are presented in the figure. The PSDs for the CJ610-8ATJ (Test 2 and 5 from APEX-3) and AE3007-A1E (Test 3 and 4 from APEX-3) engines were measured 15 m downstream of the engines, and are therefore not presented here. The effect of probe position on the PM emission from jet engines is discussed in Section 10.9 below.

3.0E+07

2.5E+07

2.0E+07

1.5E+07

1.0E+07

5.0E+06

0.0E+00

dEln/dlogDp (#/kg fuel)

Base Fuel (NASA1)

Hi-Sulfur (NASA3)

Hi-Aromatic (NASA4)

(a)

1   10   100

Particle Diameter (nm)

3.0E+07

2.5E+07

2.0E+07

1.5E+07

1.0E+07

5.0E+06

0.0E+00

dEln/dlogDp (#/kg fuel)

(b)

1   10   100

Particle Diameter (nm)

4.0E+07

3.5E+07

3.0E+07

2.5E+07

2.0E+07

1.5E+07

1.0E+07

5.0E+06

0.0E+00

dEln/dlogDp (#/kg fuel)

(c)

1   10   100

Particle Diameter (nm)
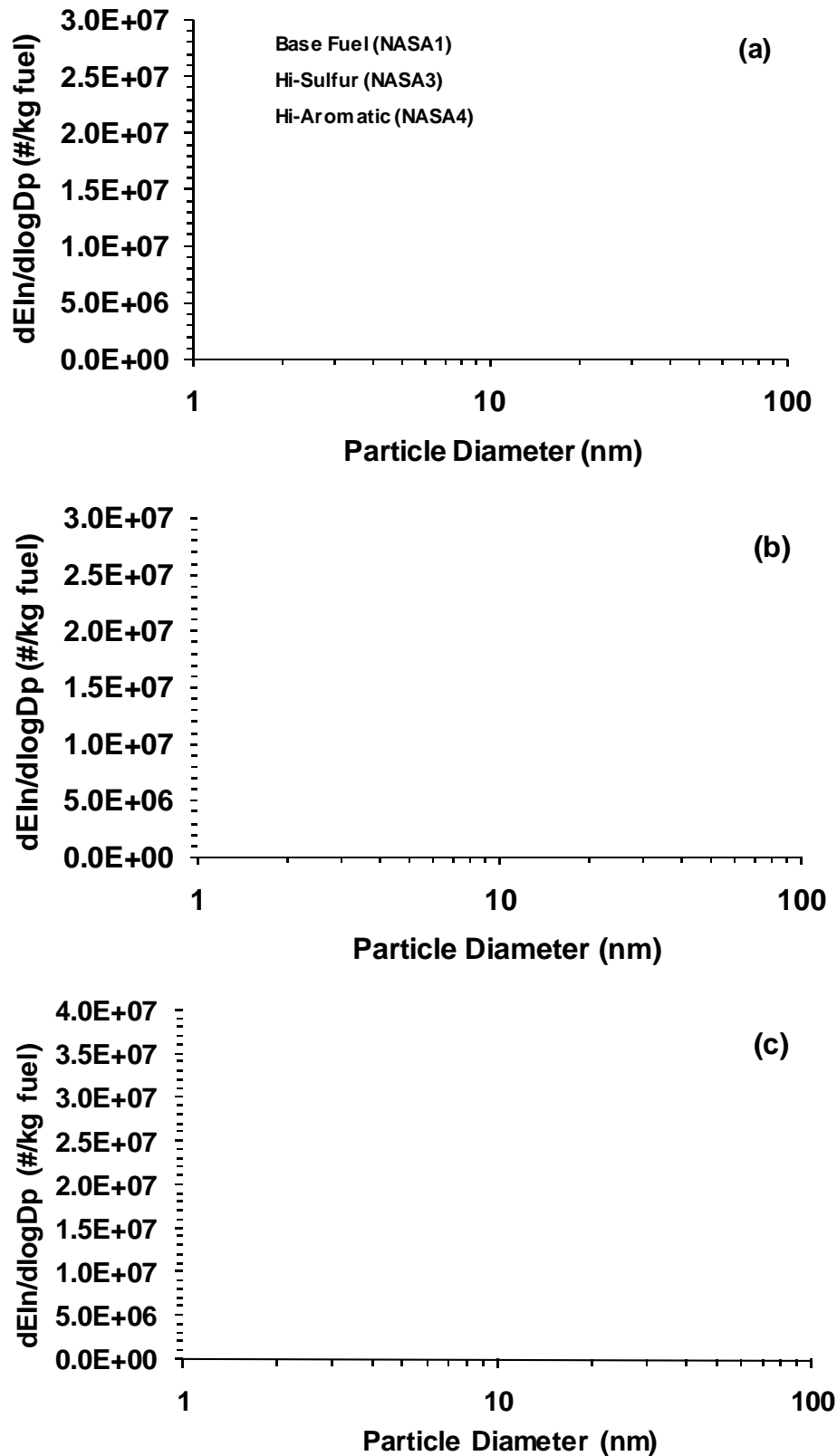
Figure 10-36. Effects of fuel type on PSD for different engine power conditions during APEX-1 for: (a) idle (7%), (b) climb-out (85%), and (c) approach (30%).
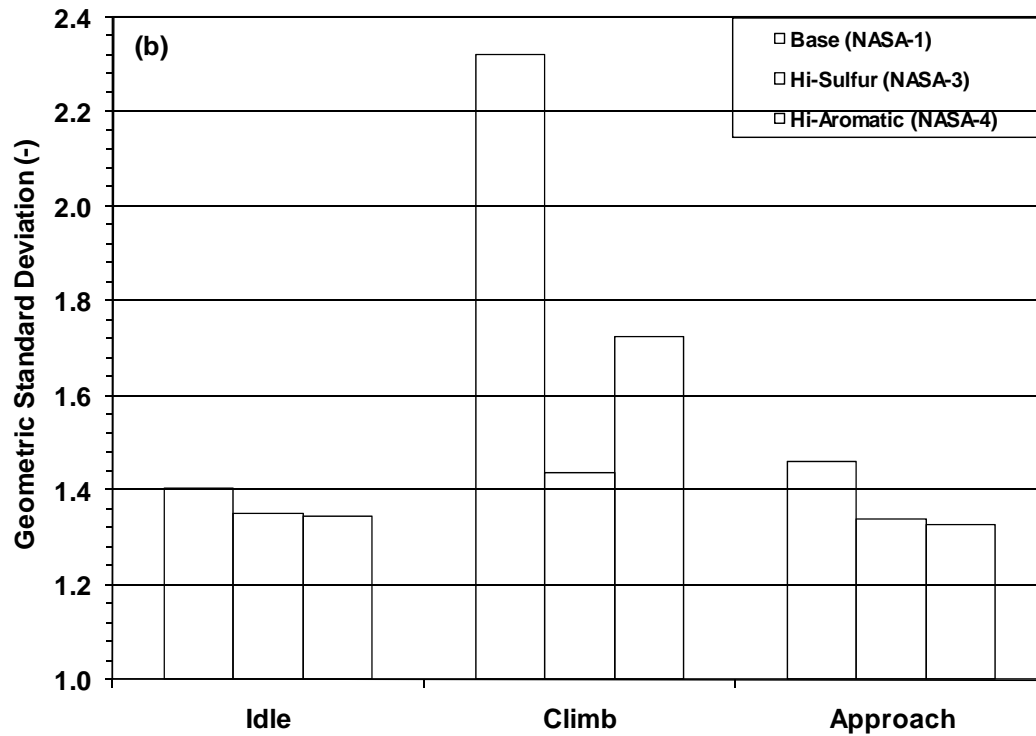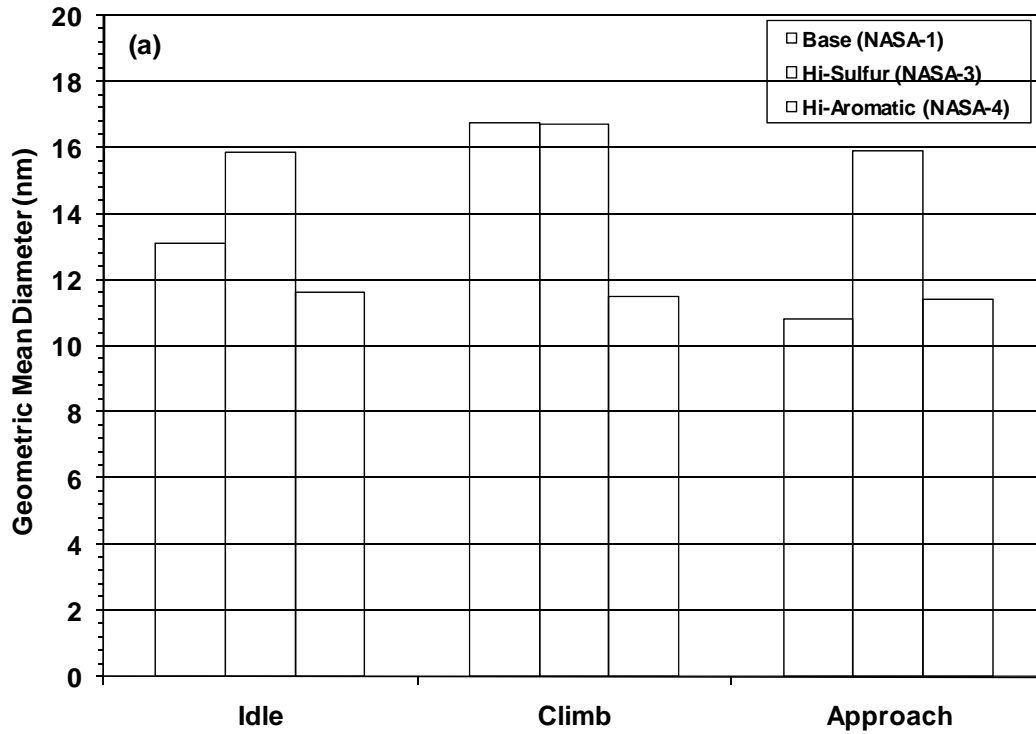
Figure 10-37. Comparison of the loss-corrected: (a) GMDs; and (b) GSDs for different power conditions and fuels during APEX-1.
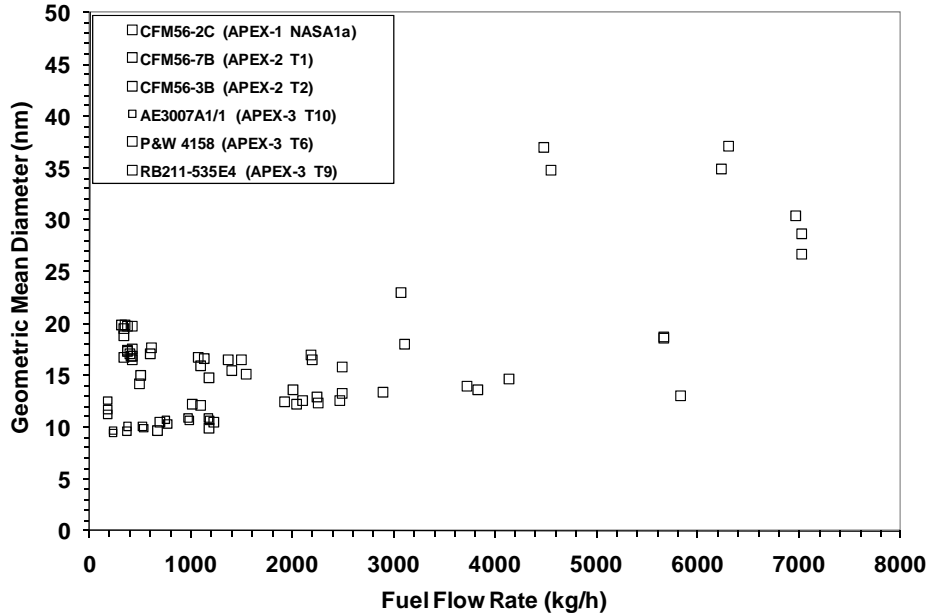
Figure 10-38. Comparison of GMDs for different engines.

Figure 10-38 shows that at low fuel flow rates, all the engines had a GMD of about 10-20 nm, which first decreased and then increased as the fuel flow rate increased. For most of these engines, the GMD was smallest at the fuel flow rate ranging below ~2,000 kg/h. Also, in comparison to the P&W 4158 engine, the GMD of the RB211 engine increased more sharply as the fuel flow rate increased beyond ~3,000 kg/h.

The GSD data for different engines can be compared as shown in Figure 10-39. The GSD results showed a trend similar to the GMD. All of these observed trends suggest that more accumulation mode particles were present in the PM emissions when the engines were operated under the higher power settings (higher fuel flow rate). Figures 10-38 and 10-39 also show that the P&W 4158 and RB211 engines, which were the largest tested in the APEX campaigns, also had larger GMD and GSD at higher fuel flow rates.

The GMDs of the PM emissions obtained from the six different engines were also compared under the four ICAO-specified engine operation modes of takeoff, climb-out, approach and idle, as shown in Figure 10-40(a) – (d). The data in the figure are particle-loss-corrected, and only 30-m data are presented for APEX-3. In Figure 10-40(a), only three engines − CFM56-3B1, AE3007-A1/1 and RB211-535E4-B − have Nano-SMPS data at 100 percent power thrust for comparison. At takeoff, the GMD of the PM emissions generally increased with engine size. The larger RB211-535E4-B engine had a GMD of about 30 nm, followed by 28 nm for the medium-sized CFM56-3B1 engine, with the smaller AE3007-A1/1 engine having the smallest GMD (11 nm). When the engines operated at climb mode, Figure 10-40(b) shows that the GMD of the RB211-535E4-B engine decreased to ~28 nm and was the largest among all the engines tested. The larger P&W 4158 engine ranked second at climb-out with a GMD of 26 nm.
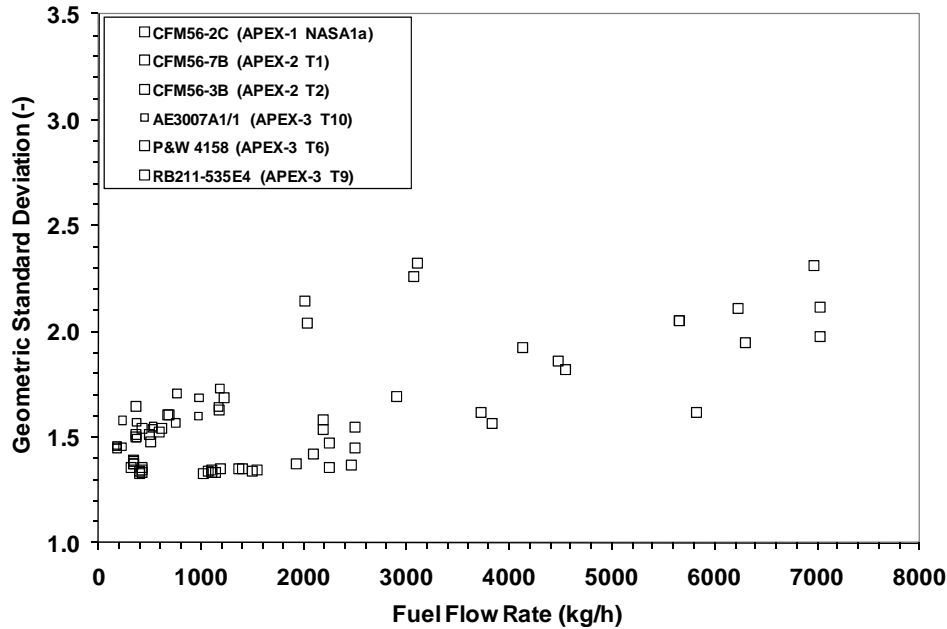
Figure 10-39. Comparison of GSDs for different engines.

When the engines switched to approach mode, the GMD for all of the engines was significantly reduced as shown in Figure 10-40(c). Figure 10-40(d) shows that the engines at idle also had small GMDs, but the GMDs measured at idle were slightly larger than those measured at approach mode.

The GSDs obtained by different engines operated under four modes were compared in Figure 10-41(a) – (d). Regardless of engine type, the PM emissions at approach and idle modes generally had lower GSD values, in the 1.3 to 1.5 range, except for the RB211-535E4-B engine, which had a GSD of 1.9 at approach power. As was the case for GMD, the GSDs increased during takeoff and climb modes. The only exception to the GSD increase during takeoff and climb modes was for the small AE3007-A1/1 engine, which showed little change in GSD value when the engine operated at climb-out power.

These observations again suggest that the PSDs of PM emissions from the jet engines under both idle (7% power) and approach (30% power) conditions were unimodal and consisted of primary nuclei particles. When the engines operated under the takeoff (100% power) and climb (85% power) conditions, accumulation mode particles were formed and the PSD curves became broader.
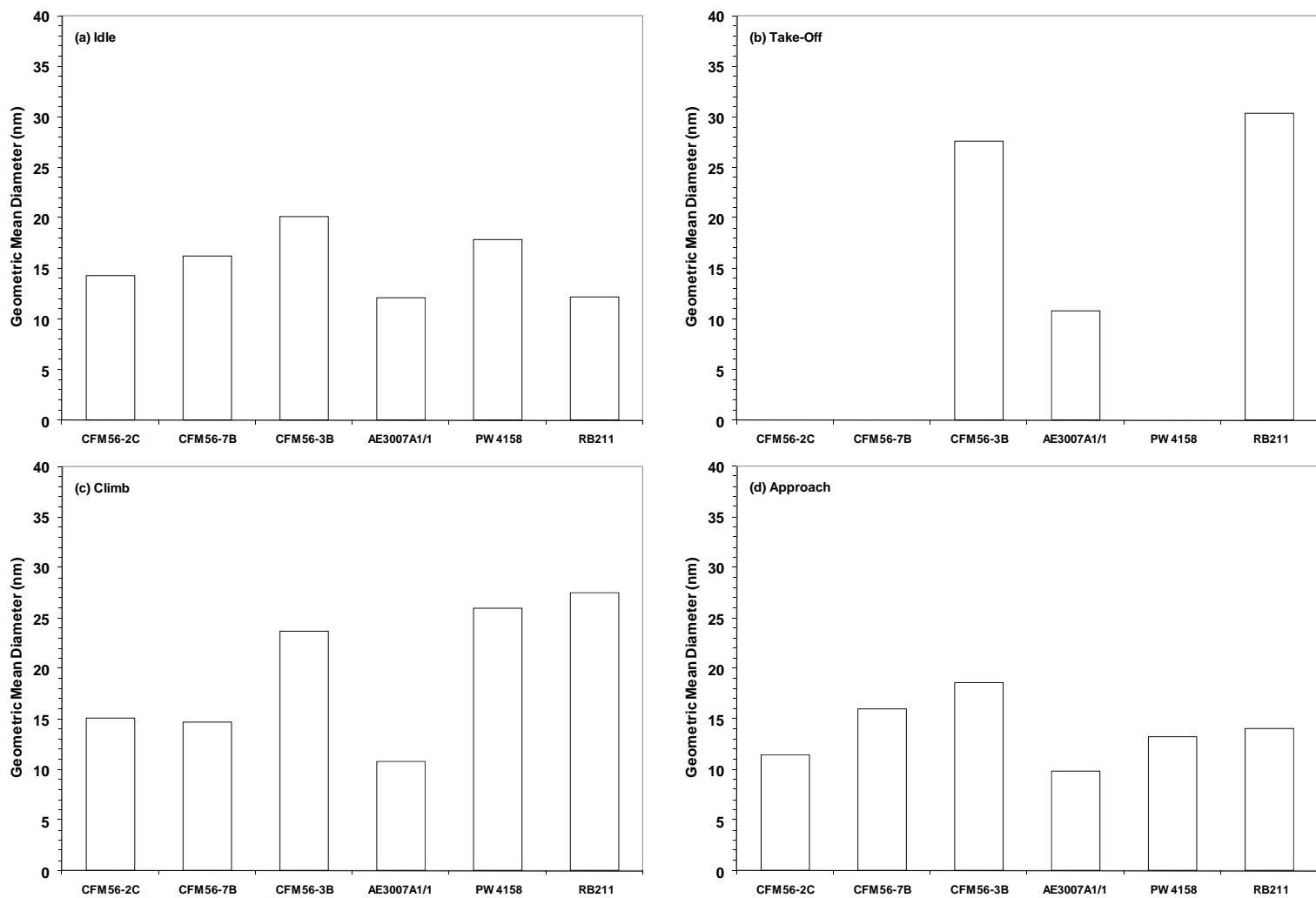
Figure 10-40. Comparison of GMD produced by different engines at: (a) idle, (b) takeoff, (c) climb, and (d) approach power.
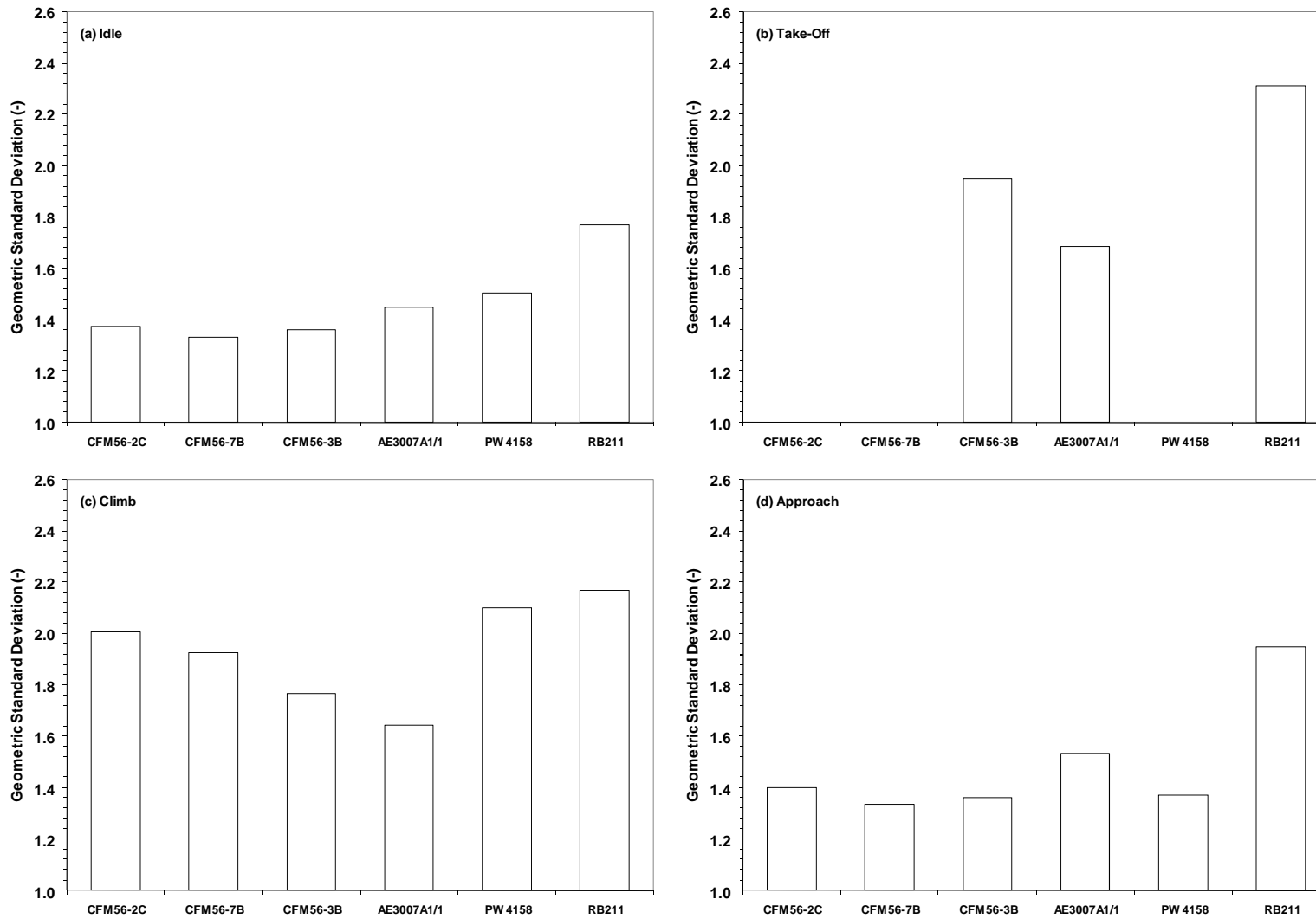
Figure 10-41. Comparison of GSD produced by different engines at: (a) idle, (b) takeoff, (c) climb, and (d) approach power.

10.7 Effects of Cold and Warm Engine Conditions

In APEX-2 and APEX-3, the PM emissions were measured under both increasing (cold) and decreasing (warm) engine power. Figures 10-10 through 10-13 (for APEX-2) and Figures 10-14 through 10-24 (for APEX-3) show that slight differences were observed in the PSD between cold and warm engine conditions. To investigate the magnitude of these differences, particle number concentration, GMD and GSD obtained at different power settings under cold engine conditions were plotted against the corresponding data under warm engine conditions in Figure 10-42(a), (b) and (c), respectively. Figure 10-42(a) shows that the particle number concentration data obtained from cold engines were linearly correlated with the data obtained from warm engines, with a correlation coefficient of 0.91. The straight line had a slope of 0.925, indicating that the particle number concentrations were ~7 percent lower with warm engines than they were with cold engines. Figures 10-42(b) and (c) show that the correlation lines between cold and warm engine conditions have slopes equal to 1 for both GMD and GSD. Engine warm-up results in fewer particles being emitted, but does not markedly change the particle size distribution.

10.8 Effect of Probe Position on PSD

During the APEX-3 campaign, the effect of sampling probe location on the PM emissions was investigated in tests T5 and T8. In test T5, the emissions from the CJ610-8ATJ turbojet engine were sampled at two locations. The data were first collected by the 15-m sampling probe as the engine power increased step-by-step at the rated thrust levels of 7, 30, 45, 65, 85, and 100 percent. Samples were then collected by the 30-m probe while the engine power setting was switched in opposite order from 100 to 7 percent. The same procedure was used to compare the results between the 30-m and 43-m probes in test T8 for the RB211-535E4-B engine. However, the data were comparable only at the power setting levels of 4, 7, 15, 30, 45 and 65 percent. The engine was tested at up to 85 percent thrust, but the emissions were only measured at 30 m.

The probe position effects on PM emissions were first investigated by comparing the three characteristic parameters of the PSDs measured by Nano-SMPS at different distances from the tested engines. Figure 10-43(a) – (c) shows the particle number concentration, GMD and GSD, respectively, plotted against the engine thrust as measured by the 30-m and 15-m probes during APEX-3 test T5. Figure 10-43(b) shows that the GMD measured by the 30-m probe was lower than the GMD measured by the 15-m probe under all the engine power settings, with the exception of 7 percent idle. The GSD measured by 30-m probe, on the other hand, was greater than the GSD measured by 15-m probe at all power levels. As the plume moved from 15-m to 30-m downstream of the engine, more nuclei mode particles were formed in the plume, which reduced the average particle size and widened the size distribution. The exception at idle seen in Figure 10-43(b) shows that smaller GMDs were obtained from the 15-m probe, indicating compositional differences in the particles produced at lower power settings. At higher power settings (i.e., fuel flow), the engine seems to produce more volatiles, which formed additional nuclei mode particles from the gas phase as the plume traveled farther downstream of the engine.
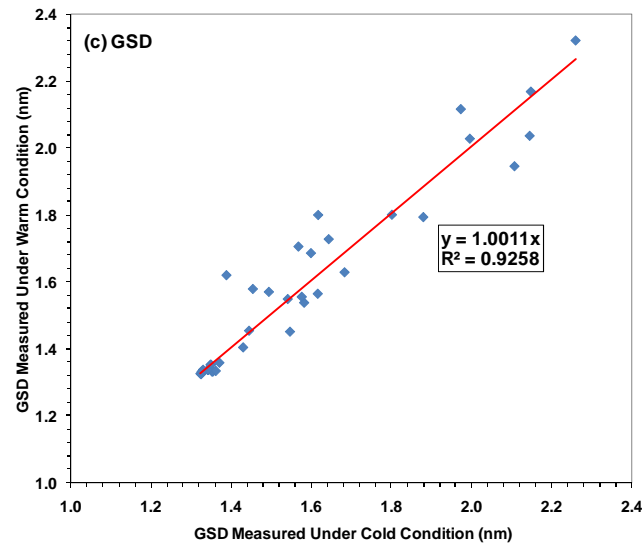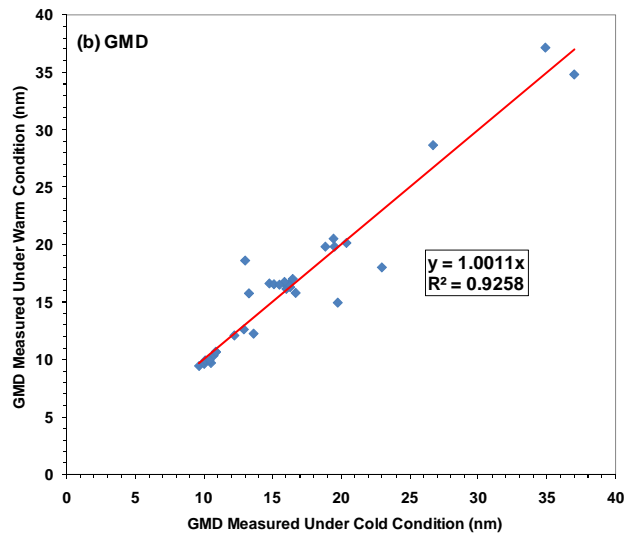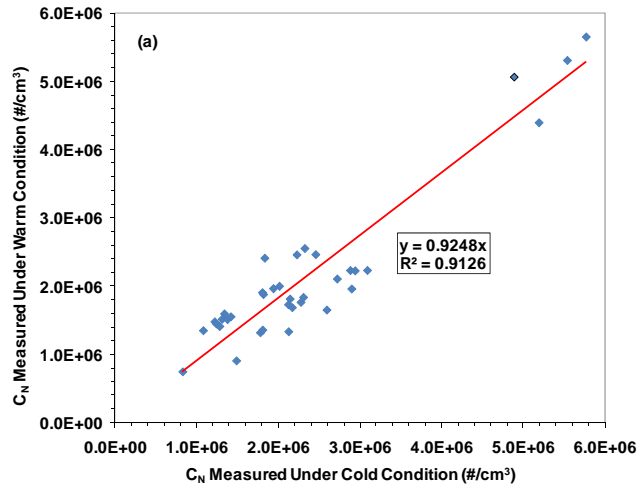
Figure 10-42. Effect of engine operating temperature on: (a) PM number concentration; (b) GMD; and (c) GSD.
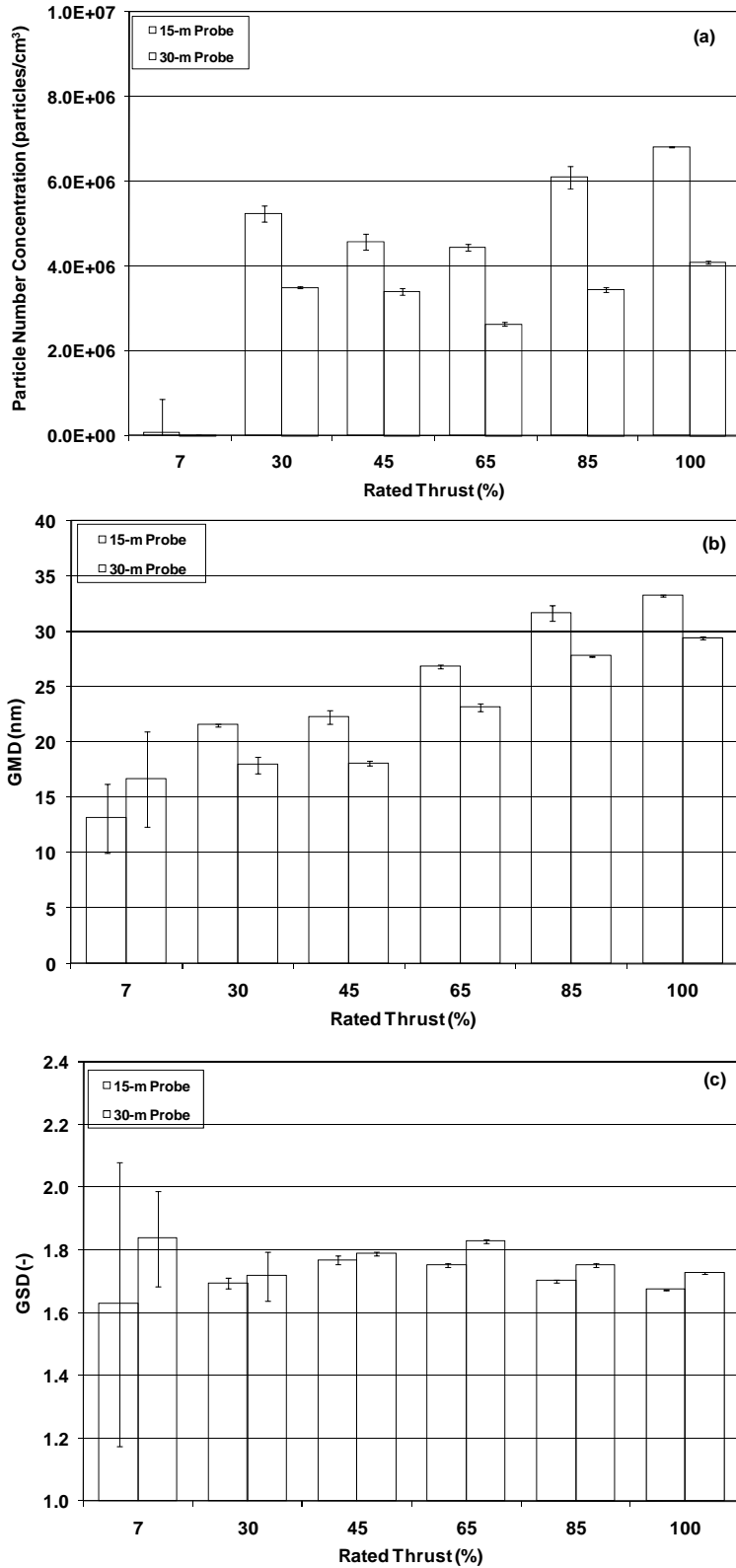
Figure 10-43. Comparisons of: (a) particle number concentration; (b) GMD; and (c) GSD measured by the 15- and 30-m probes during APEX-3 T5 (Nano-SMPS; line-loss corrected).

Figure 10-44(a) - (c) show the particle concentration, GMD and GSD measured using the 30-m and 43-m probes from APEX-3 test T8 for the RB211-535E4-B engine. The comparison shows similar trends to those observed in APEX-3 test T5. Figure 10-44(b) shows that the GMDs measured at 43-m were lower than the GMDs measured at 30 m at power levels greater than 15 percent, again indicating that, at higher power settings, the formation of fine particles by the nucleation and condensation of volatiles continued to dominate as the plume moved from the 30- to 43-m probe location. At lower power settings, as was seen in test T5 for the 15-m and 30-m comparison, the GMD was larger at 43-m than that at 30-m. The GSD measured by the 43-m probe at power settings above 7 percent was greater than the GSD measured by the 30-m probe, as shown in Figure 10-44(c), consistent with the observation in APEX-3 test T5. This result is considered to be mainly a result of the formation of additional sulfate particles from the gas phase as reported by Wey et al. (2006).

Both Figures 10-43(a) and 10-44(a) show that, at higher power settings, the particle number concentration decreased as the plume traveled farther downstream of the engine, possibly because of the dilution of the plume by ambient air during transit.

The effects of probe position on particle number and mass were further investigated using the number- and mass-based EIs derived from the Nano-SMPS measurements in the APEX-3 T5 and T8 tests. Figure 10-45 shows the comparison between the particle number emission indices (EI_N) measured by the 15-m and 30-m probes for test T5 with the CJ610-8ATJ engine and T8 of the RB211-535E4-B engine. Although the particle number EIs varied differently with power settings for these two engines, at lower power settings the EI_N decreased as the probe moved farther from the engine and, at higher power settings, the EI_N increased with distance. The increase in EI_N at higher power settings as the plume traveled farther is probably attributable to the nucleation of volatiles, while the EI_N decrease at engine idle may imply some different mechanism for particle transformation under lower power conditions.

For particle mass emissions, Figure 10-46 compares the mass emission indices (EI_M) measured at different probe positions for APEX-3 test T5 for the CJ610-8ATJ engine and APEX-3 test T8 for the RB211-535E4-B engine. The figure shows that, for both engines, the EI_M values decreased with travel distance of the plume, and that the trends were consistent for most power setting levels. The only exception was for the RB211 engine at 4 and 65 percent thrust, where the EI_M was higher at the 43-m probe position than that at 30-m. The decrease in EI_M observed here is in conflict with the EI_N results discussed above. This decrease may be partly attributed to the EI_M results being converted from the Nano-SMPS number measurements, which were affected by the PSDs measured. Note also that in APEX-3 test T5 and T8, the first measurements were made at the probe location closer to the engine when the engine was operating under the cold condition, resulting in the measurements at the more distant probe position always being collected under warm engine conditions. The engine condition may have also affected these results. Additional research would be needed to help explain the above experimental results.
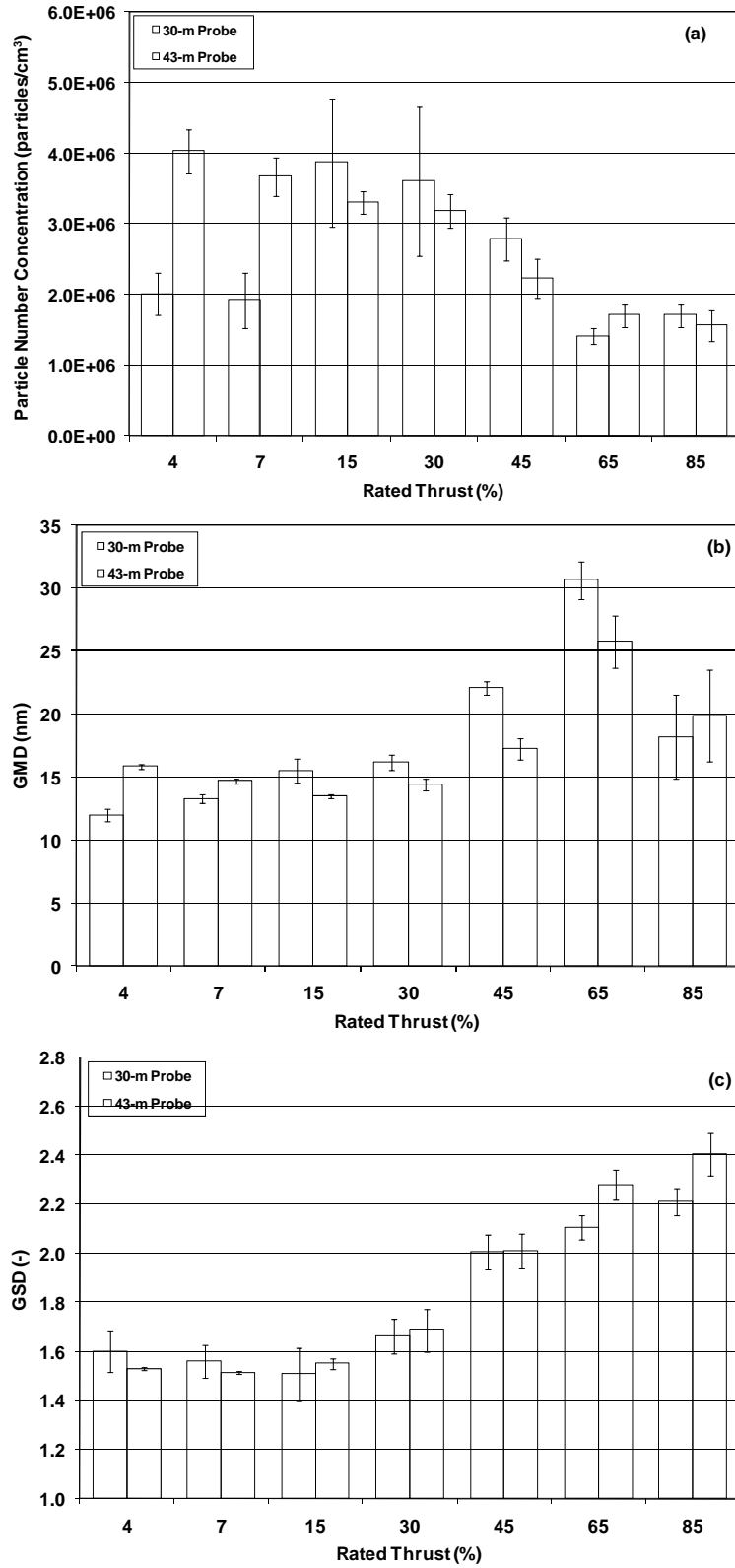
Figure 10-44. Comparisons of: (a) particle number concentrations; (b) GMD; and (c) GSD measured by the 30- and 43-m probes during APEX-3 T8 (EEPS; line-loss corrected).
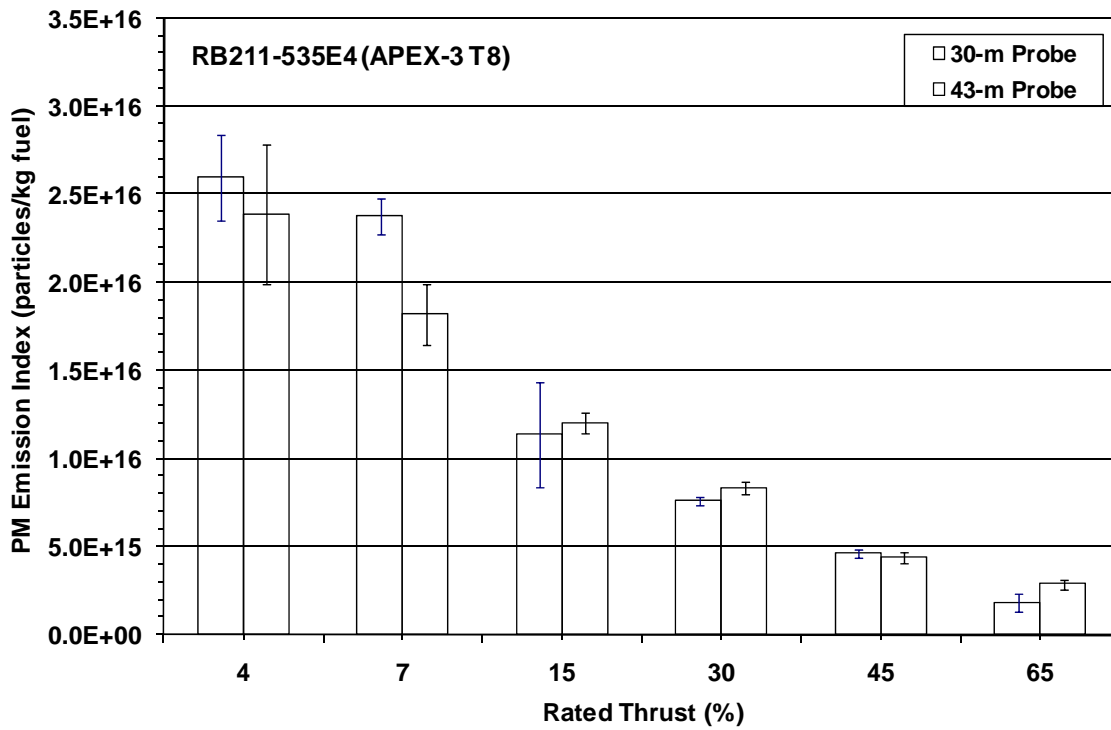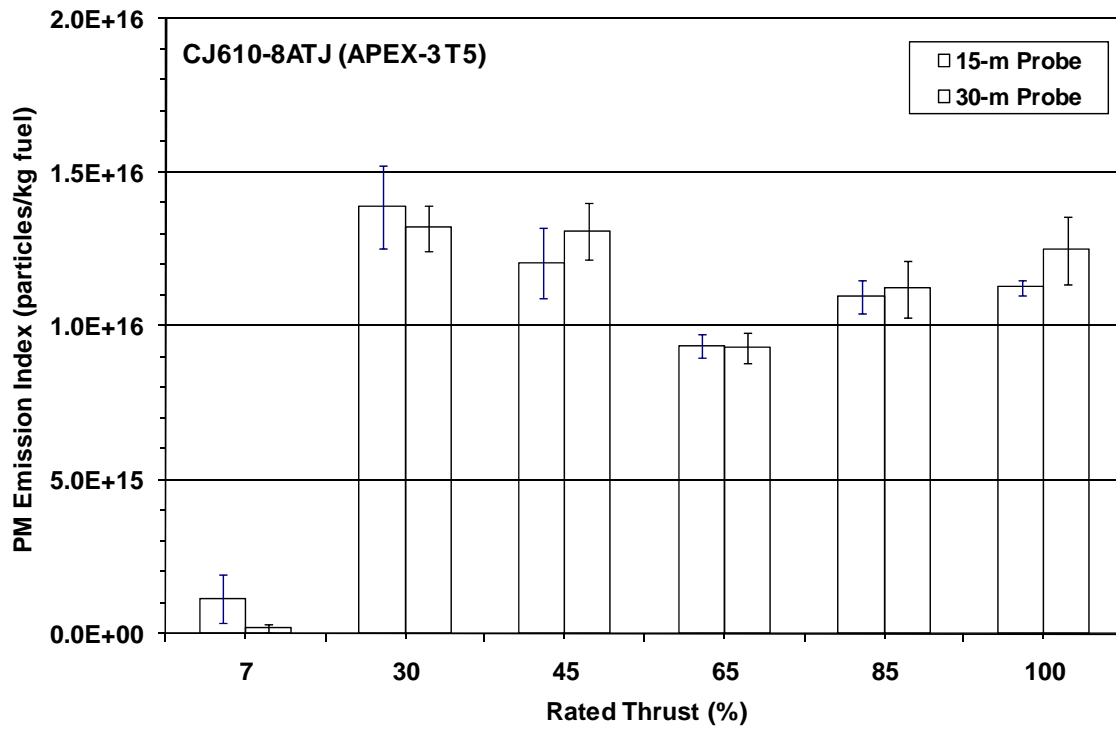
Figure 10-45. Effects of probe position on particle number emission indices for a: CJ610-8ATJ turbojet; and RB211-535E4B turbofan engine.
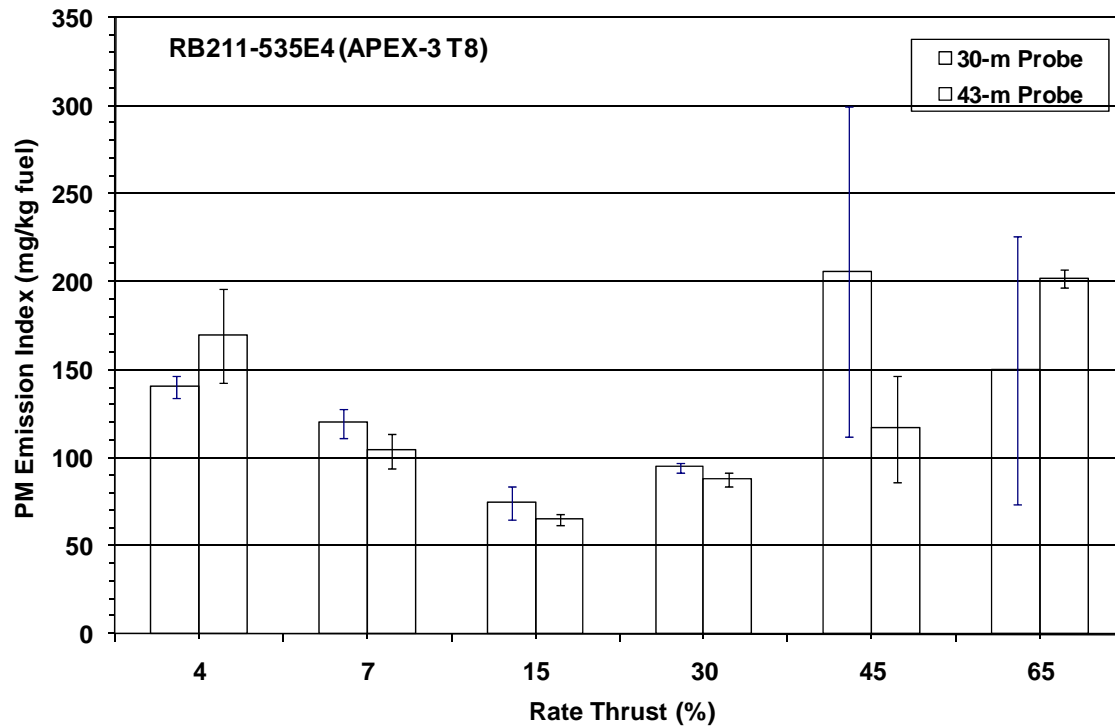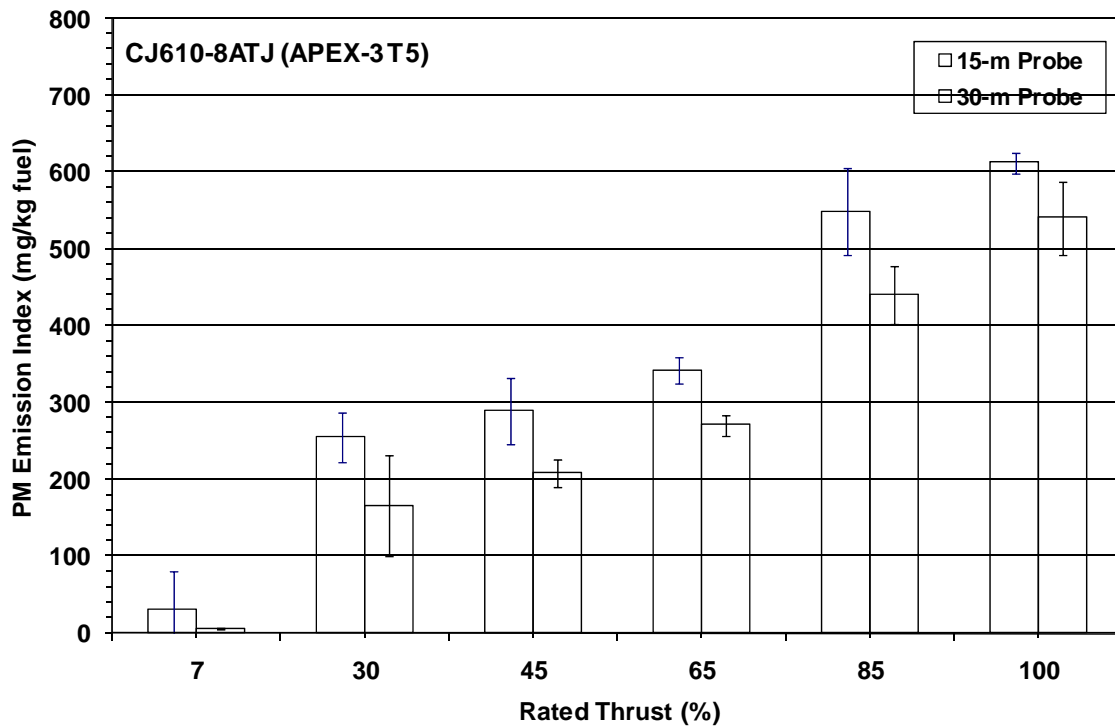
Figure 10-46. Effects of probe position on particle mass emission indices for a: CJ610-8ATJ turbojet; and RB211-535E4B turbofan engine.

10.9 Comparison of PSDs Measured by Different Instruments

The GMD and GSD data of the particle size distributions, as measured by Nano-SMPS and EEPS, were compared. The comparison of particle number emission indices measured by different instruments was discussed previously in Section 9 (PM Number Emissions). Figure 10-47 plots the results from the Nano-SMPS against those of the EEPS under the same test conditions for all APEX-2 and APEX-3 tests. Therefore, these graphs show the average of tests T1 to T4 from APEX-2 for the CFM56-7B24, -3B1, and -3B2 engines; and tests T1 to T11 from APEX-3 for the CFM56-3B1, CJ610-8ATJ, AE3007-A1E and – A1/1, P&W 4158 and RB211-535E4-B engines.

Figure 10-47(a) shows the comparison of GMD results measured by the two instruments. The correlation line in the figure shows a slope of 0.84, indicating that the GMDs measured by the EEPS were ~16 percent smaller than those measured by the Nano-SMPS. For most of the measurement results, a weak linear correlation between the two instruments can be observed, with a correlation coefficient of ~0.6. The GSD comparison is shown in Figure 10-47(b), where the weak linear correlation between the two instrument measurements can again be observed (correlation coefficient is ~0.5). The slope of the correlation line is 0.98, indicating that the PSD measurements by the two instruments had nearly the same standard deviations.
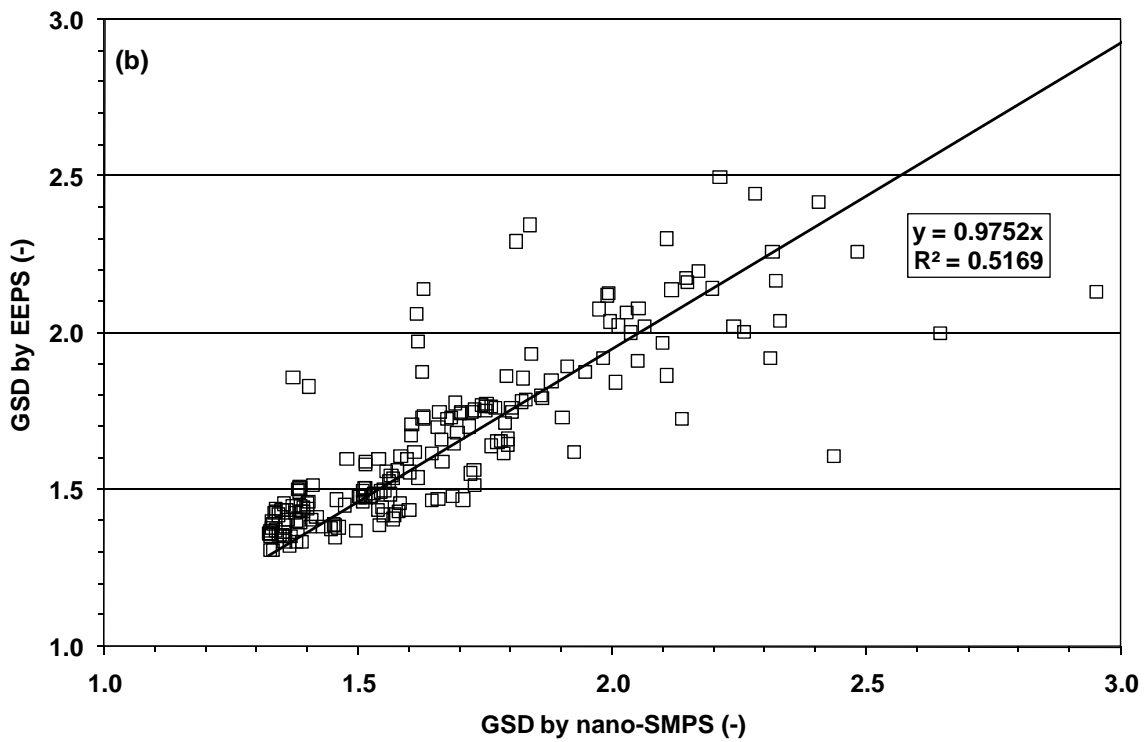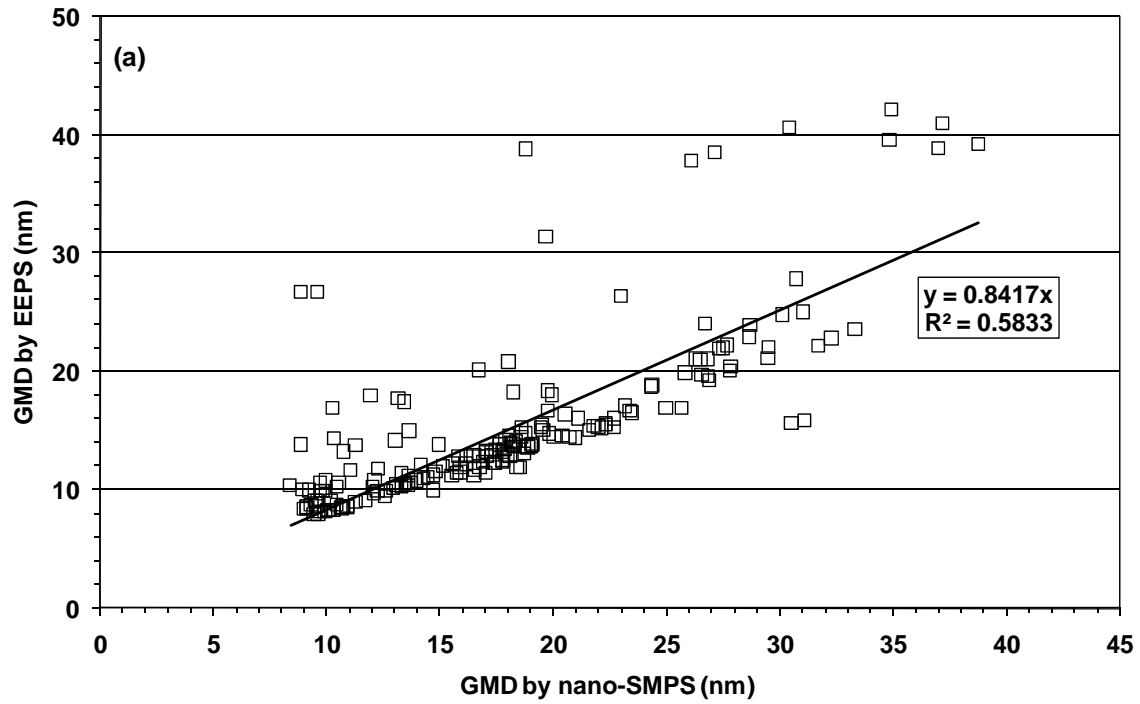
Figure 10-47. Comparison of the GMD and GSD as obtained from Nano-SMPS and EEPS measurements during all tests conducted during APEX-2 and -3.

11.   Black Carbon and PAH Emissions

The PM emissions from aviation gas turbine engines consist of a number of components including black carbon (BC) as well as other organic compounds, inorganic acids and salts, etc., which are generated during the combustion process. In the APEX test series, black carbon was continuously monitored using a Magee Aethalometer and particle surface-bound PAHs were continuously monitored by a PAS 2000 instrument. The data collected from these two analyzers are summarized in this section with details provided in Appendix G. All results provided were background-corrected using data collected before/after each test.

However, the quality of the data collected by the aethalometer and PAH analyzer was generally poor. The data were highly variable and often did not respond to changes in engine power. Therefore, only selected data are being presented here for the sake of completeness and the analysis of trends. All continuous BC and PAH results should be used with extreme caution and certainly should not be used in absolute terms.

11.1 Black Carbon Emissions

The black carbon (BC) content in PM emissions was continuously monitored by the Magee Aethalometer for all the three APEX campaigns. The data were recorded every second. The time-series BC concentration data for individual tests are presented in Figures 11-1 to 11-8. In the figures, the black lines represent the recorded black carbon concentration and the rated power thrust was plotted using the second y-axis. Also note the very high degree of variability in the data produced by the aethalometer.

Figure 11-1 consists of the results of four tests: EPA-1, EPA-2, NASA-1, and NASA-1a of APEX-1 campaign. These tests were conducted with the same CFM56-2C1 engine and base jet fuel. The BC concentrations measured for EPA-2 and NASA-1a were well correlated to the variation in engine power thrust. The responses for the EPA-1 and NASA-1 tests were poor and may have been caused by the crosswind background interference.

The CFM56-2C1 engine was also tested with high-sulfur fuel during APEX-1 tests EPA-3, NASA-2 and NASA-3. The BC concentrations recorded for NASA-2 were found to be unrealistically high during some of the test period, and the BC data for EPA-3 and NASA-3 did not correlate well with the power settings. Therefore, these tests were not used in the data analysis.

Figure 11-2 shows the BC concentrations measured for the CFM56-2C1 engine with high-aromatic fuel. The two APEX-1 tests, NASA-4 and NASA-5, are presented in the figure. The data show some correlation between the BC concentration and the rated power thrust, though there was large fluctuation in these tests.

The BC concentration results of APEX-2 T1 and T4 tests for the CFM56-7B24 engine are shown in Figure 11-3, with the results of the T2 and T3 of APEX-2 and the T1 and T11 of APEX-3 presented in Figure 11-4. As shown, there is some correlation of the BC measurements with power changes.

Figure 11-5 presents the results of APEX-3 T2 and T5 for the CJ610-8ATJ engine. The discrepancy between the BC concentration change with ascending and descending power variation were believed to be caused primarily by the probe position change. The probe position was changed during these two tests. This change in the probe position will be discussed further in a later subsection.

Figures 11-6, 11-7, and 11-8 are the results for the AE3007-A series, P&W 4158 and RB211 engines, respectively, during APEX-3. The BC concentrations recorded in these tests show good correlation with power change. The results of the test T8 of APEX-3 in Figure 11-8 were obtained from the two probe positions. The effect of probe position will be discussed later.

The tests during which the black carbon monitoring results were not correlated to engine power are indicated in Table 11-1. Also note that all data presented are uncorrected for losses in the sampling lines since this parameter was not measured during the line loss determination.
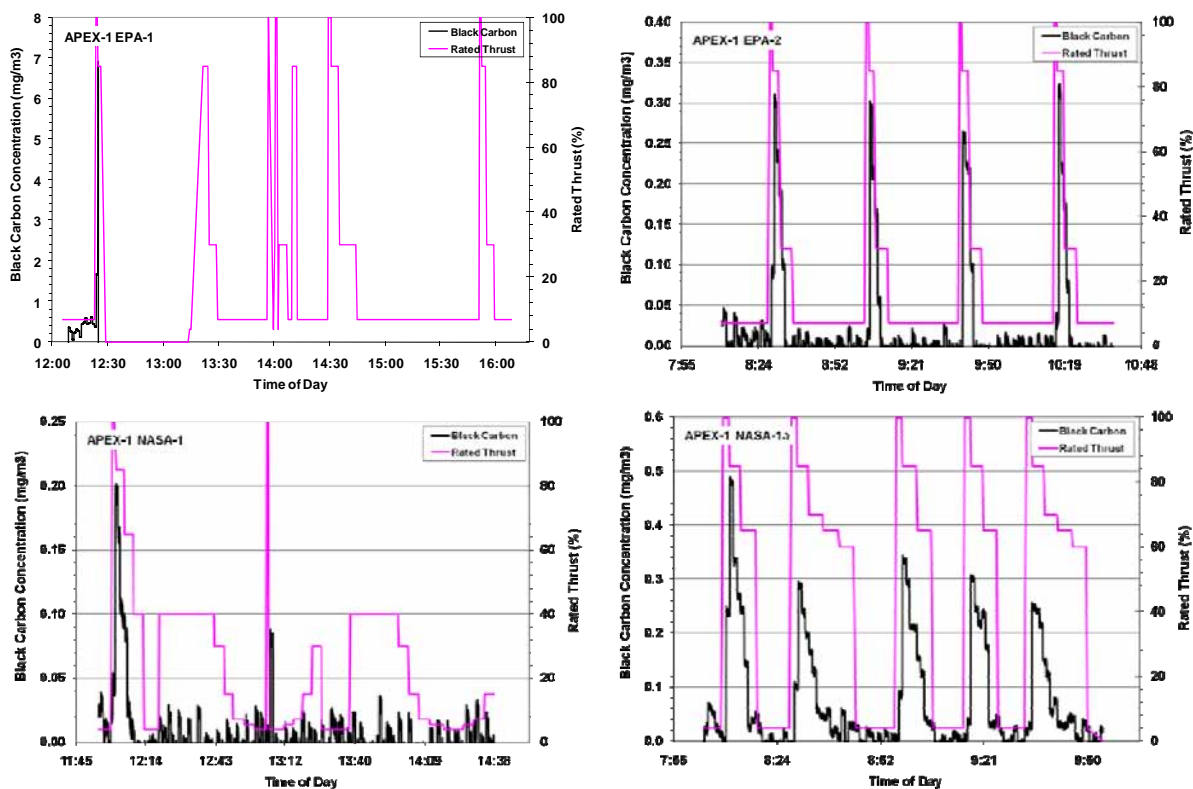
Figure 11-1.   Time-series black carbon concentration data for the tests EPA-1, EPA-2, NASA-1, and NASA-1a of APEX-1 campaign for the CFM56-2C1 engine with base fuel.
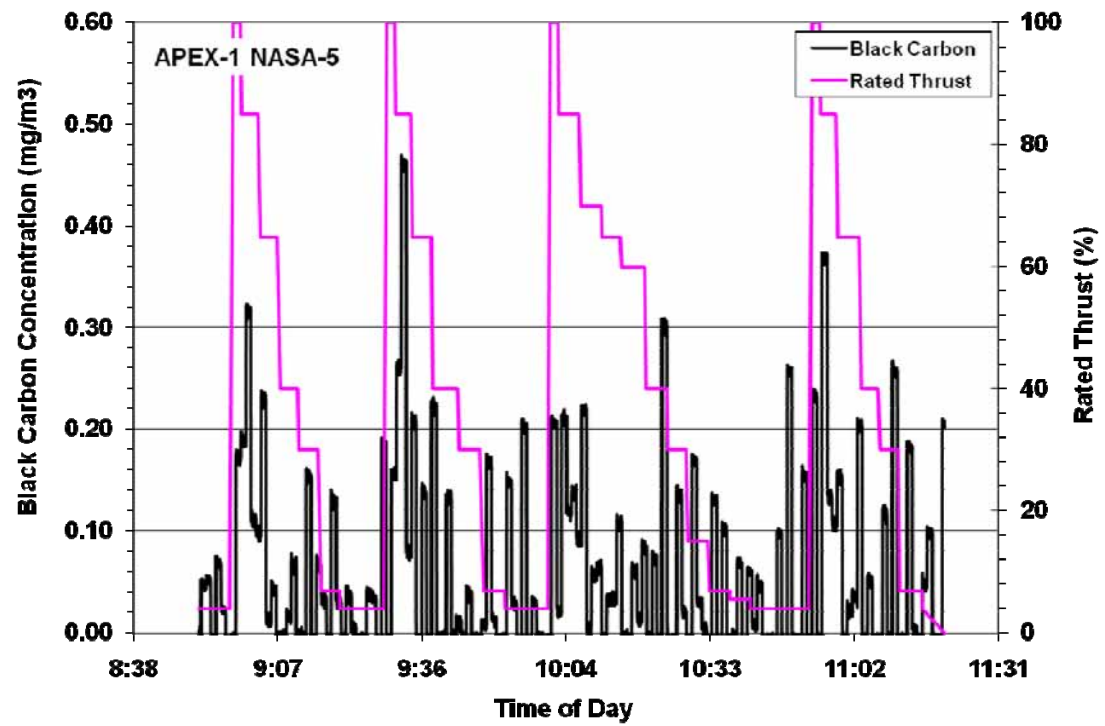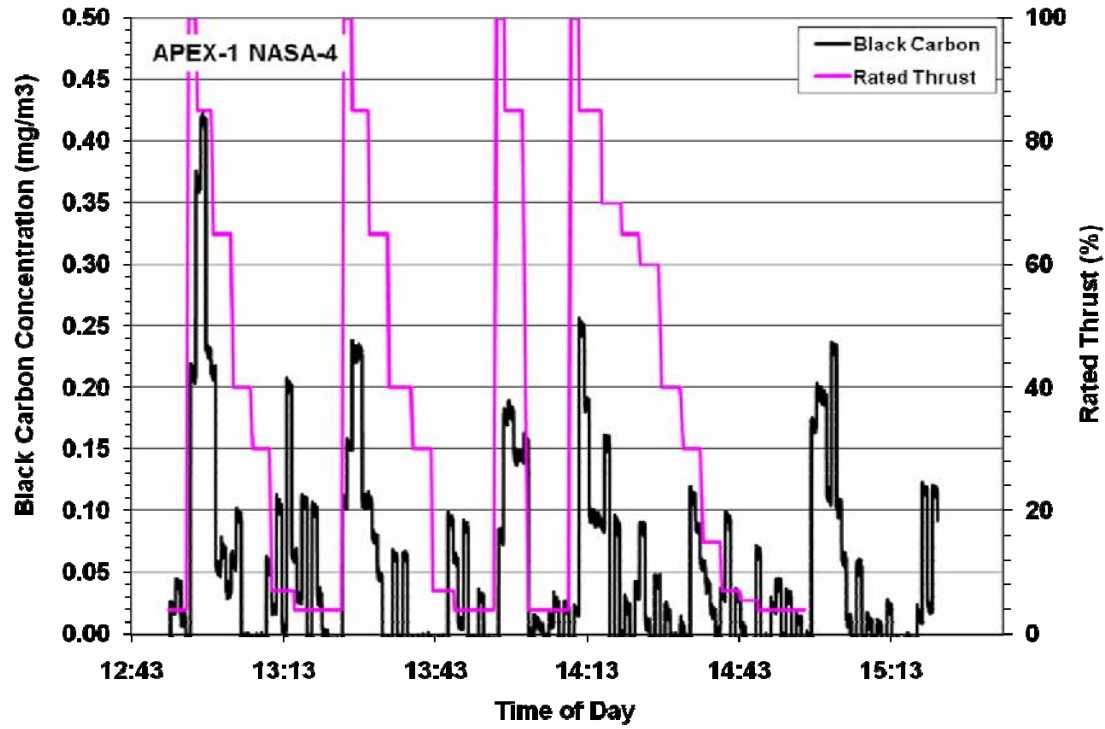
Figure 11-2. Time-series black carbon concentration data for the tests NASA-4 and NASA-5 of APEX-1 campaign for the CFM56-2C1 engine with high-aromatic fuel.
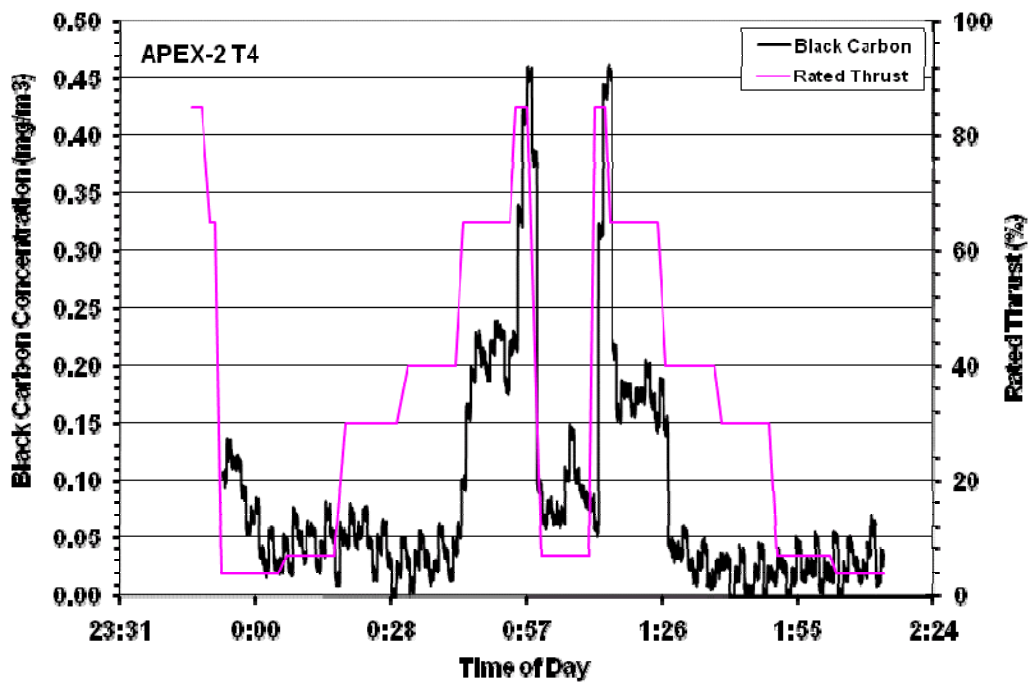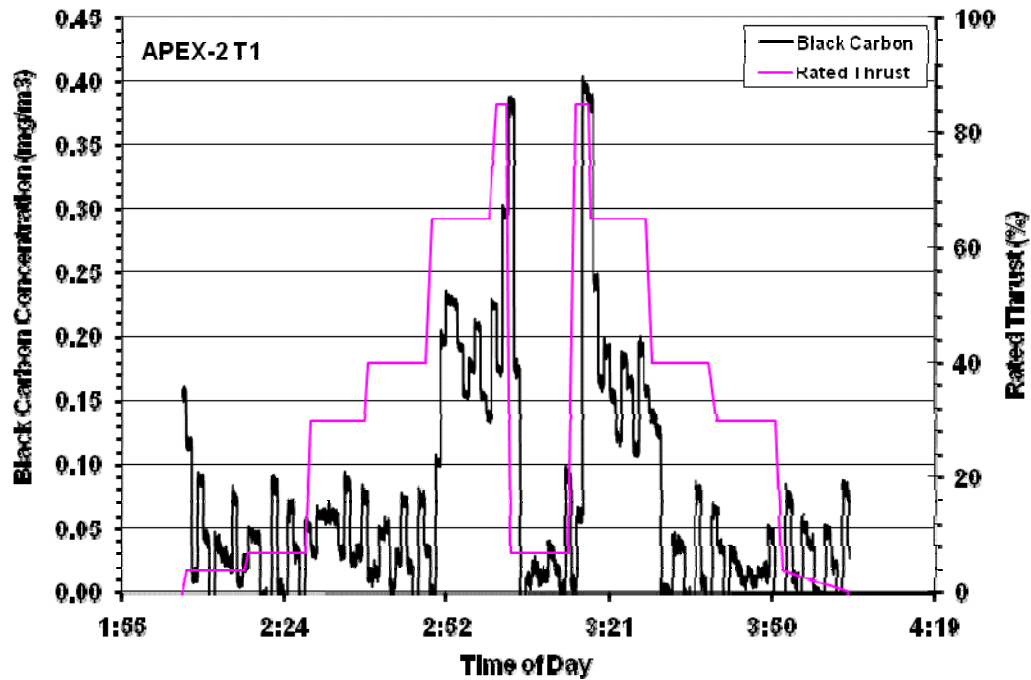
Figure 11-3.   Time-series black carbon concentration data for the tests T1 and T4 of APEX-2 campaign for the CFM56-7B24 engine.
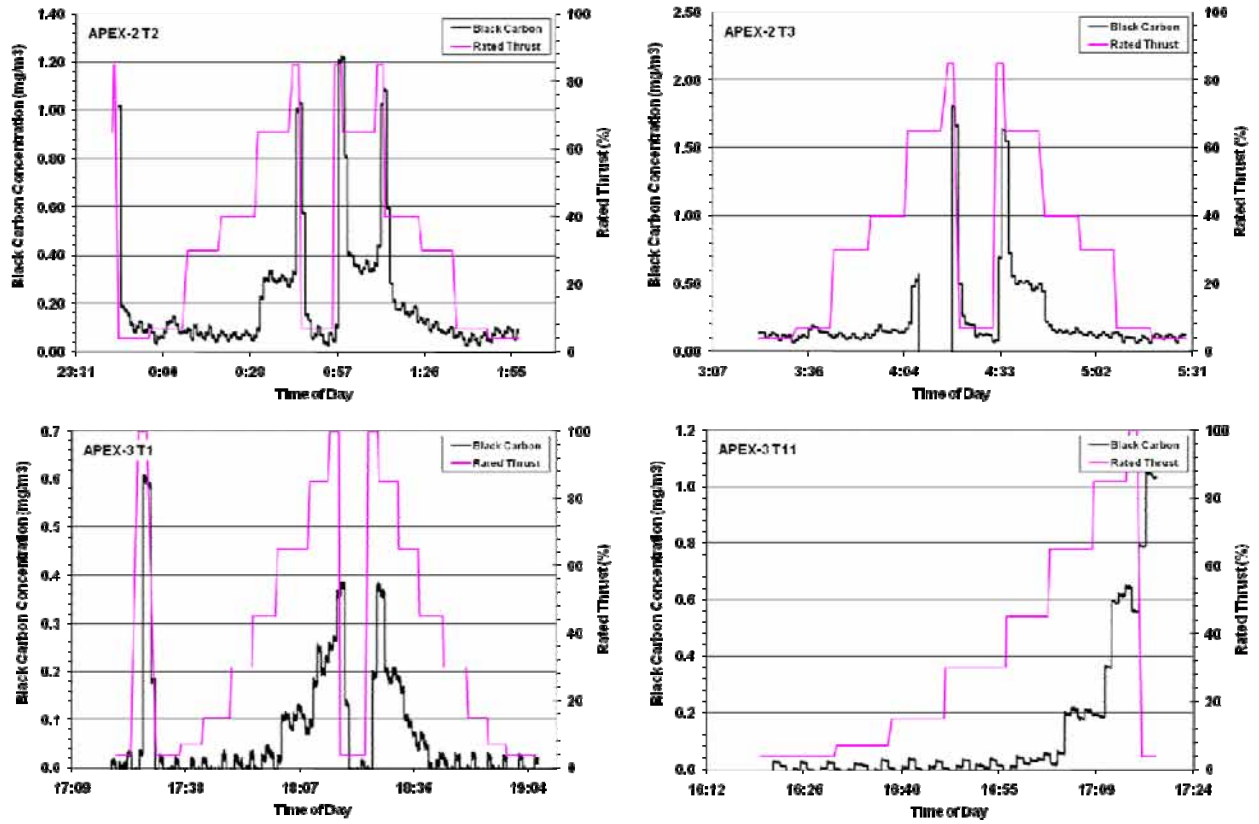
Figure 11-4. Time-series black carbon concentration data for the tests T2 and T3 of APEX-2 and T1 and T11 of APEX-3 for the CFM56-3B series engine.
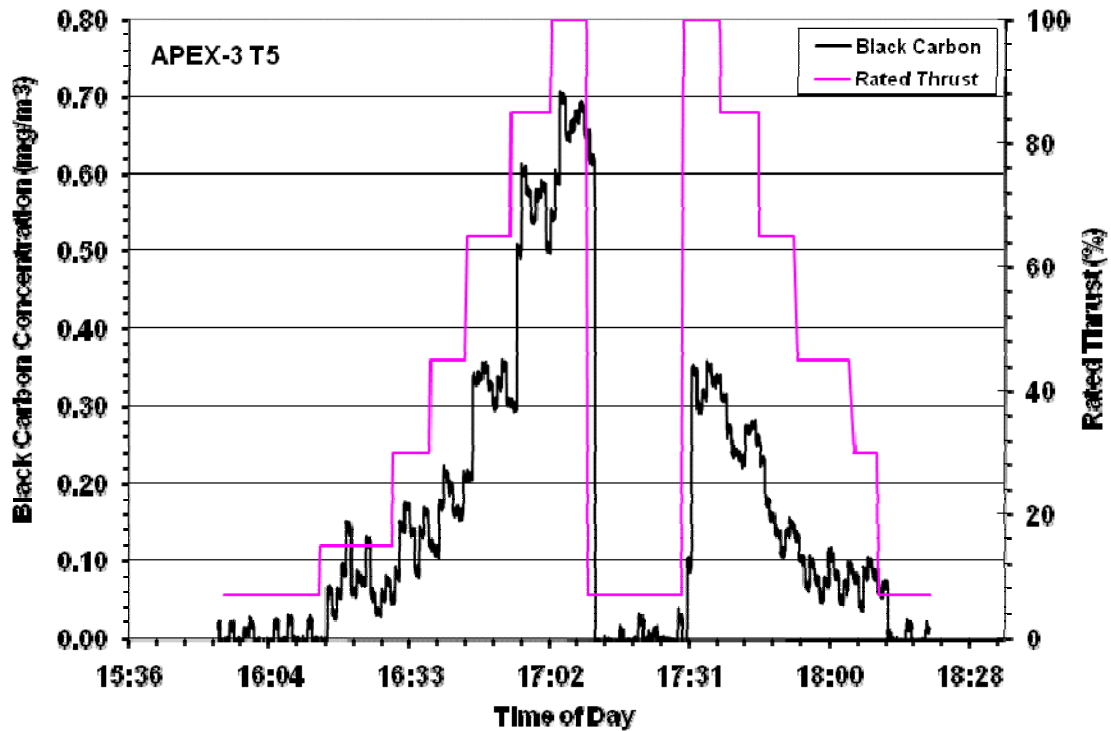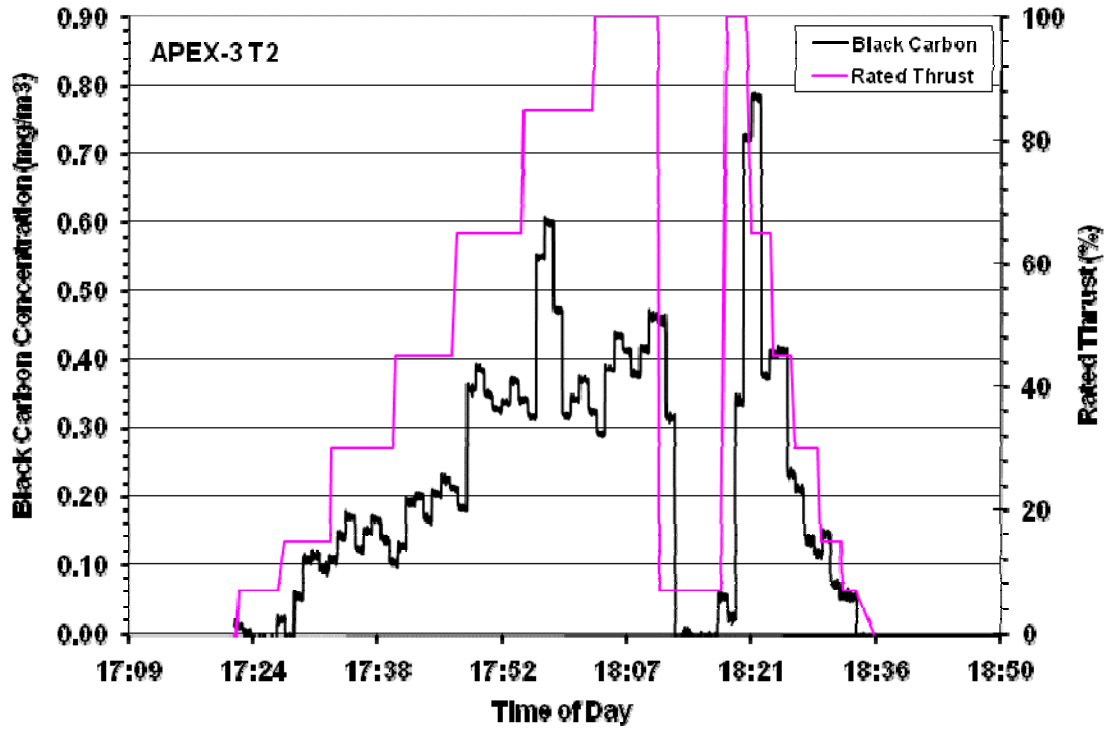
Figure 11-5. Time-series black carbon concentration data for the APEX-3 T2 and T5 for the CJ610-8ATJ turbojet engine.
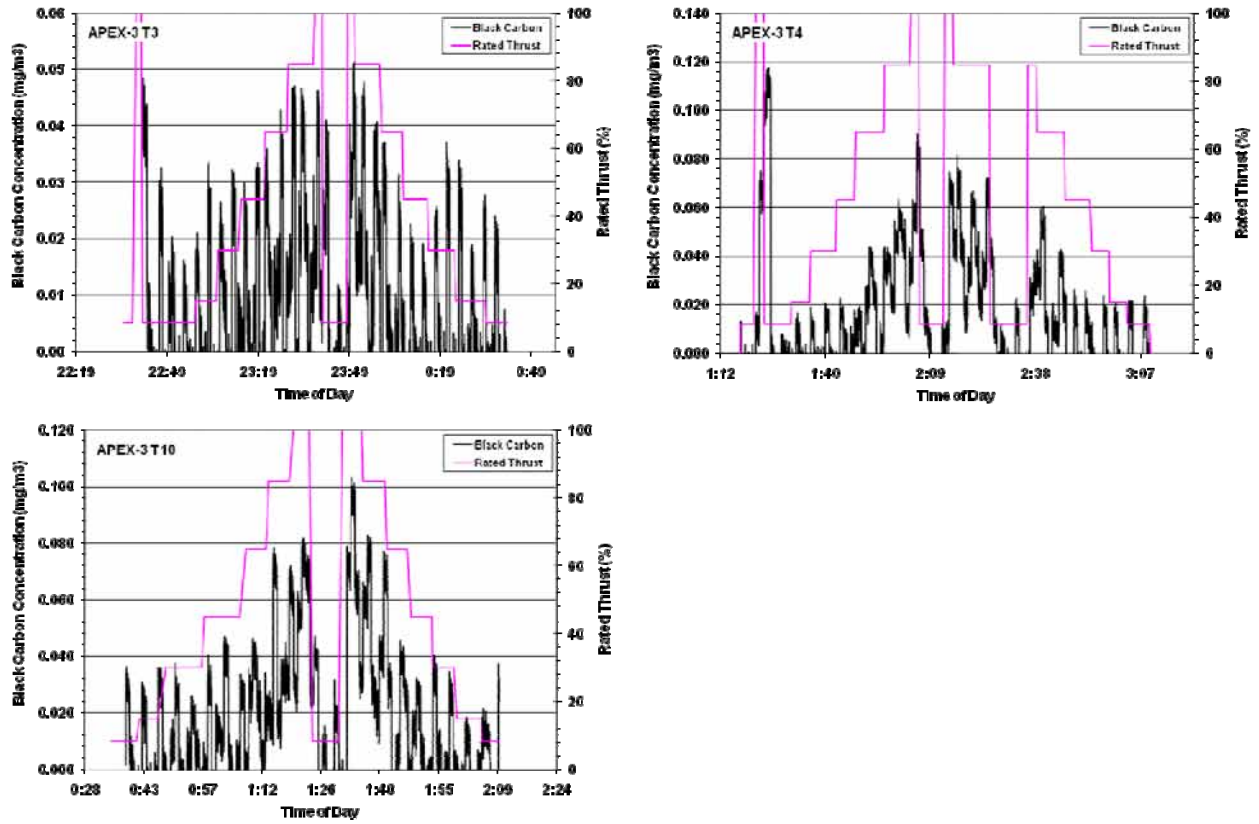
Figure 11-6. Time-series black carbon concentration data for the APEX-3 T3 and T4 for the AE3007A1E engine and T10 for the AE3007A1/1 engine.
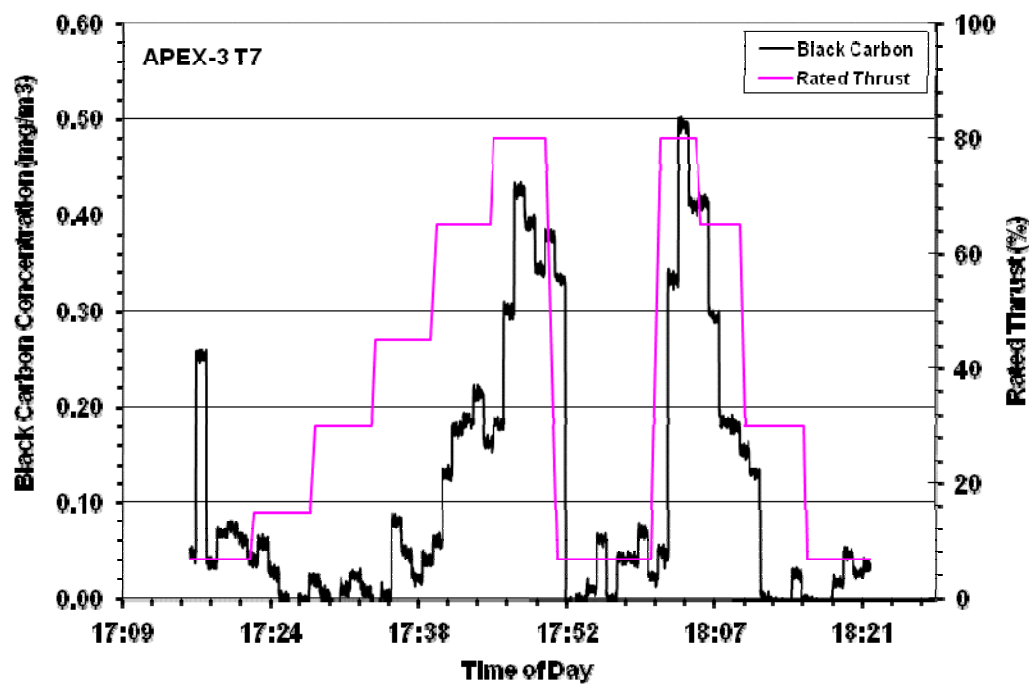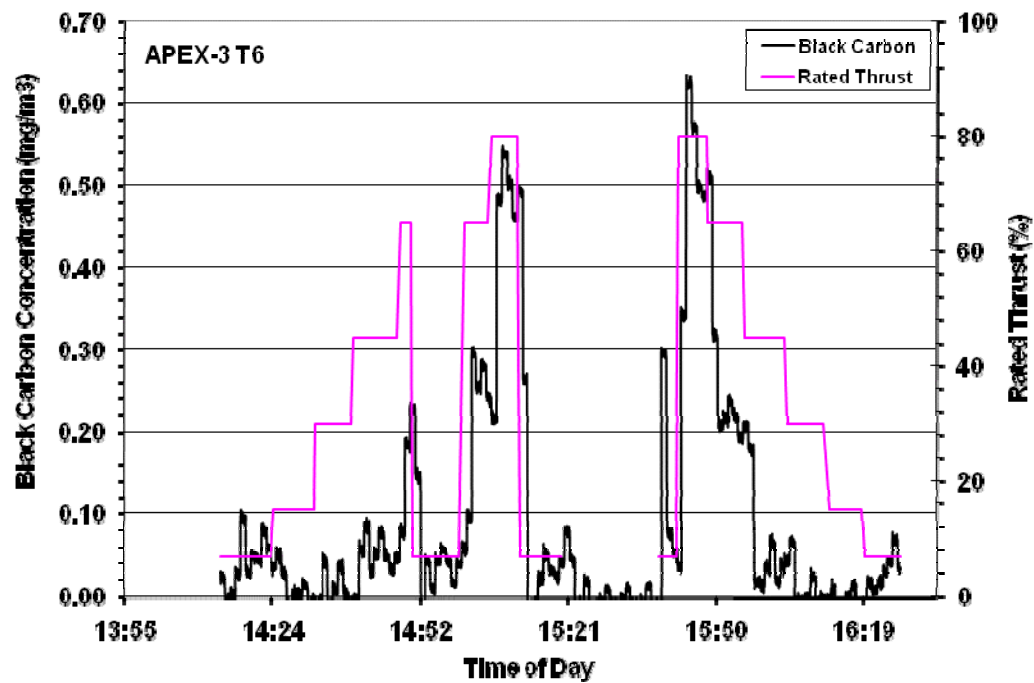
Figure 11-7. Time-series black carbon concentration data for the APEX-3 T6 and T7 for the P&W 4158 engine.
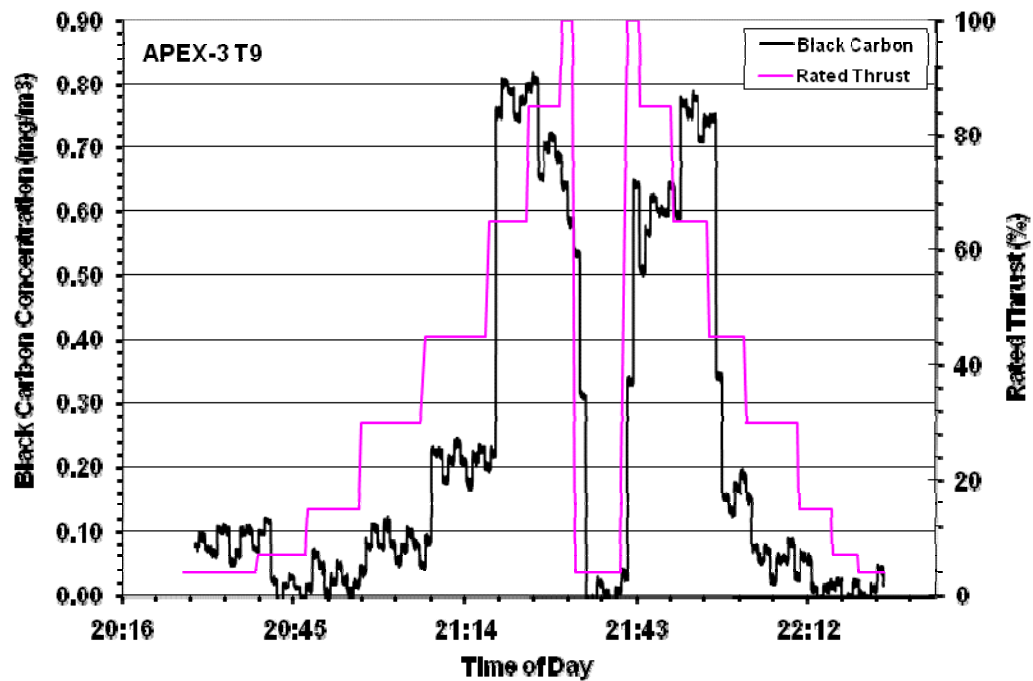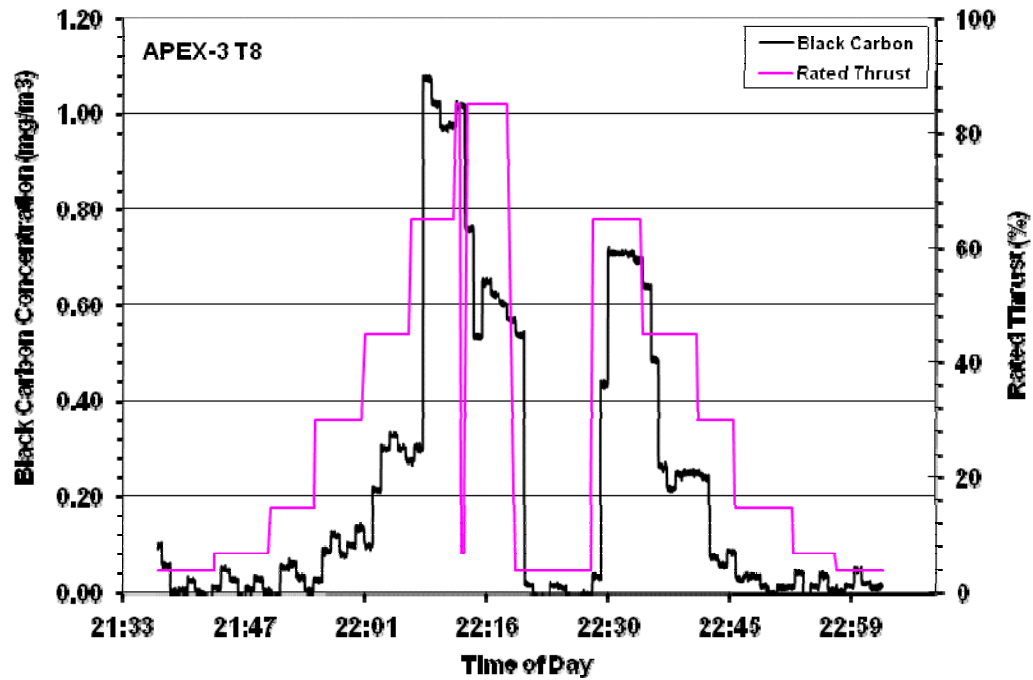
Figure 11-8. Time-series black carbon concentration data for the APEX-3 T8 and T9 for the RB211-535E4-B engine.

Table 11-1.   Black Carbon Monitoring in APEX Tests

Campaign		Aircraft	Engine	Fuel Type	Probe Position	Concentration correlated with engine power?[b]
APEX	Test No.					
1	EPA-1[a]	DC-8	CFM56-2C1	Base	30-m	N
	EPA-2				30-m	Y
	NASA-1[a]				30-m	N
	NASA-1a				30-m	Y
	EPA-3			Hi-S	30-m	N
	NASA-2				30-m	N
	NASA-3				30-m	N
	NASA-4			Hi-A	30-m	Y
	NASA-5				30-m	Y
2	T1	B737-700	CFM56-7B24	Fleet	30-m	Y
	T4				30-m	Y
	T2	B737-300	CFM56-3B1		30-m	Y
	T3		CFM56-3B2		30-m	Y
3	T1[a]	B737-300	CFM56-3B1	Fleet	30-m	N
	T11				30-m	Y
	T2	NASA Lear Model 25	CJ610-8ATJ turbojet		15-m	Y
	T5				30-m/15-m	Y
	T3	Embraer EMB145	AE3007A1E		15-m	Y
	T4				15-m	Y
	T10		AE3007A1/1		30-m	Y
	T6	A300	P&W 4158		30-m	Y
	T7				30-m	Y
	T8	B757	RB211-535E4-B		30-m/43-m	Y
	T9				30-m	Y

[a] Indicates the tests with high cross wind in background.

[b] N = no; Y = yes.

11.1.1 Effect of Fuel Flow Rate and Engine Thrust

The effect of fuel flow rate on the BC emission index was investigated. By averaging the fuel flow rates and BC concentration readings that were recorded under the same rated power within a test, the average BC concentrations as well as the corresponding average fuel flow rates at various power levels were calculated for each test. The average BC emission indices were then calculated from the average CO_2 concentration and summarized in Table G-1 in Appendix G. Figures 11-9 to 11-15 plot the BC emission index as a function of fuel flow rate. Note that only the results obtained from the 30-m probe are discussed here. The effect of probe position will be discussed later.

In these figures, the results of different tests with the same engine and fuels were plotted for comparison. Figure 11-9 shows the large uncertainty in the APEX-1 black carbon measurement. In comparison, the BC measurements for the APEX-2 and APEX-3 campaigns, shown in Figures 11-10 to 11-15, were much better. These figures show that the fuel flow rate had effects on the BC emission index similar to those observed for the PM mass emission index. A U-shaped curve of EI vs. fuel flow was determined where the emissions are slightly elevated near idle, decreases to a minimum at mid-range power, and then increases to the maximum at climb-out or take-off power.

Five engines in this study had black carbon emission data collected at 30-m for the four ICAO- specified engine powers: idle (7%), takeoff (100%), climb (85%), and approach (30%). These five engines are CFM56-2C1, CFM56-3B series, CJ610-8ATJ, AE3007A1/1, and RB211-535E4-B. The data for the AE3007A1/1 engine collected at 8.4 percent rated thrust were used to represent the results of the idle engine condition and were compared with the data of the other engines at seven percent rated thrust. The emission indices derived from the black carbon measurements under the same engine thrust were averaged and summarized in Table 11-2.

The effects of the LTO engine cycle on the BC emission index for different engines are illustrated in Figure 11-16. This figure shows the same trend of BC EI with the change in engine power, although the absolute EI values were different for the different engines at the same engine power. In general the BC emission indices were the highest at takeoff and climb and became the lowest when the engine was at idle and approach modes. The engines operated under approach mode emitted slightly more or less black carbon than under idle. These results are consistent with those reported by Wey et al. (2006) and Lobo et al. (2007) for APEX-1 and -2. The reported results indicate that the BC emissions are generally greater at higher engine power.
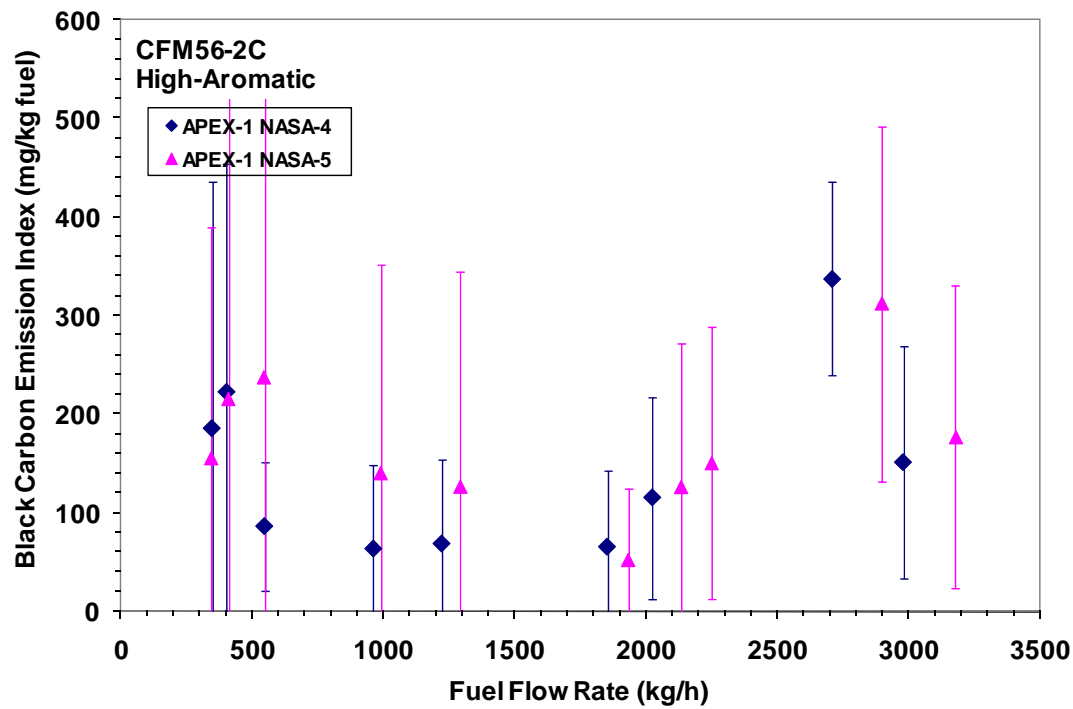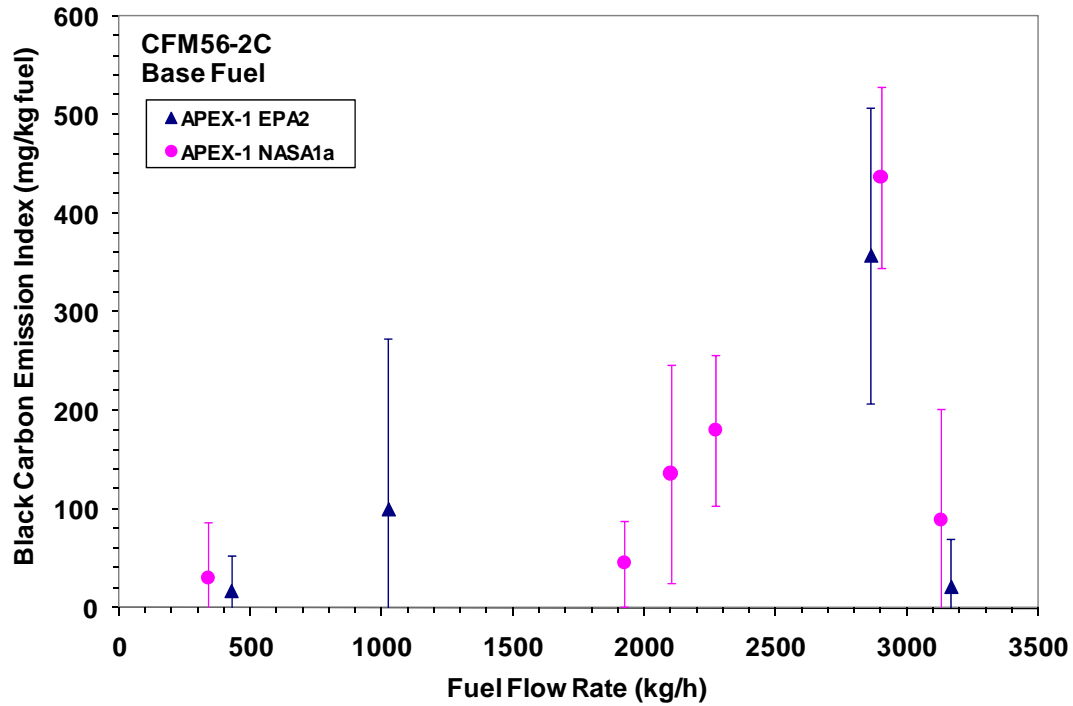
Figure 11-9. Black carbon emission index as a function of fuel flow rate for the CFM56-2C1 engine during APEX-1.
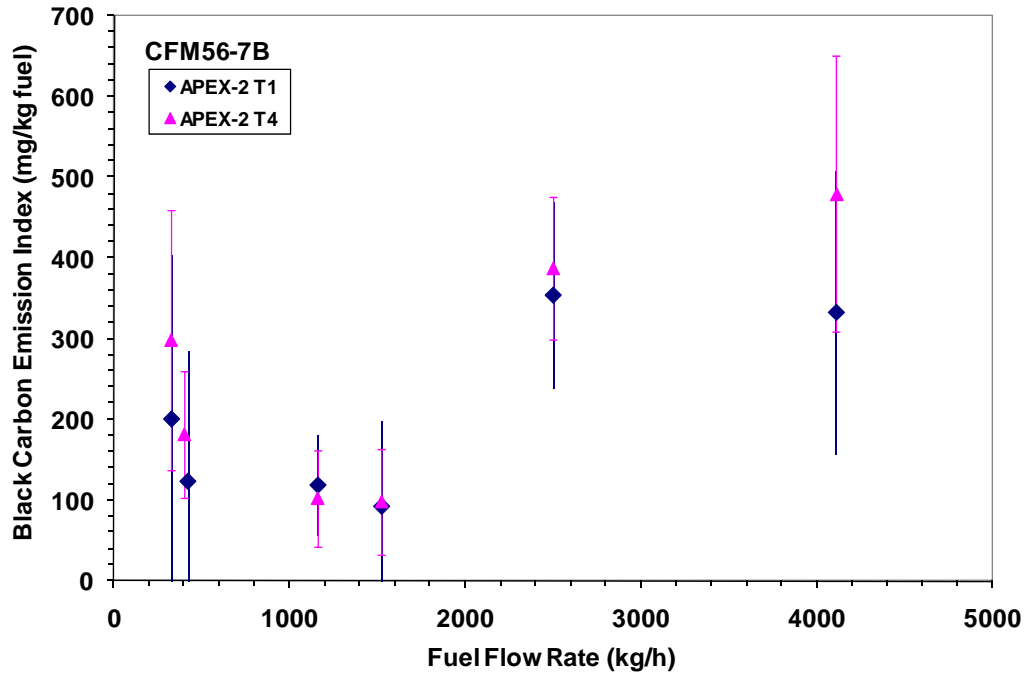
Figure 11-10. Black carbon emission index as a function of fuel flow rate for the CFM56-7B24 engine.
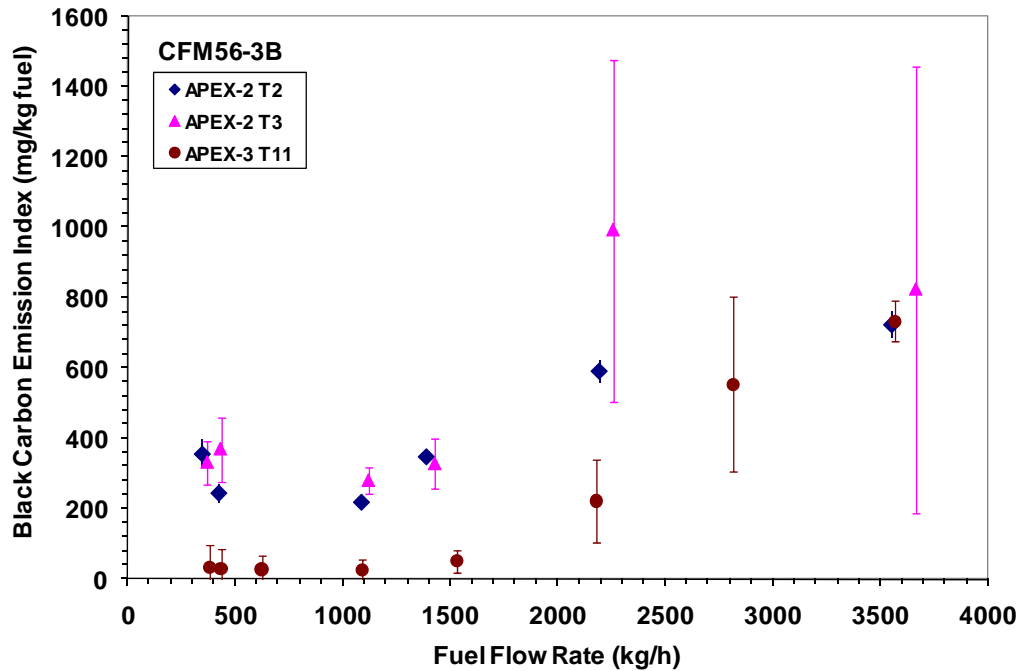
Figure 11-11. Black carbon emission index as a function of fuel flow rate for the CFM56-3B series engine.

193
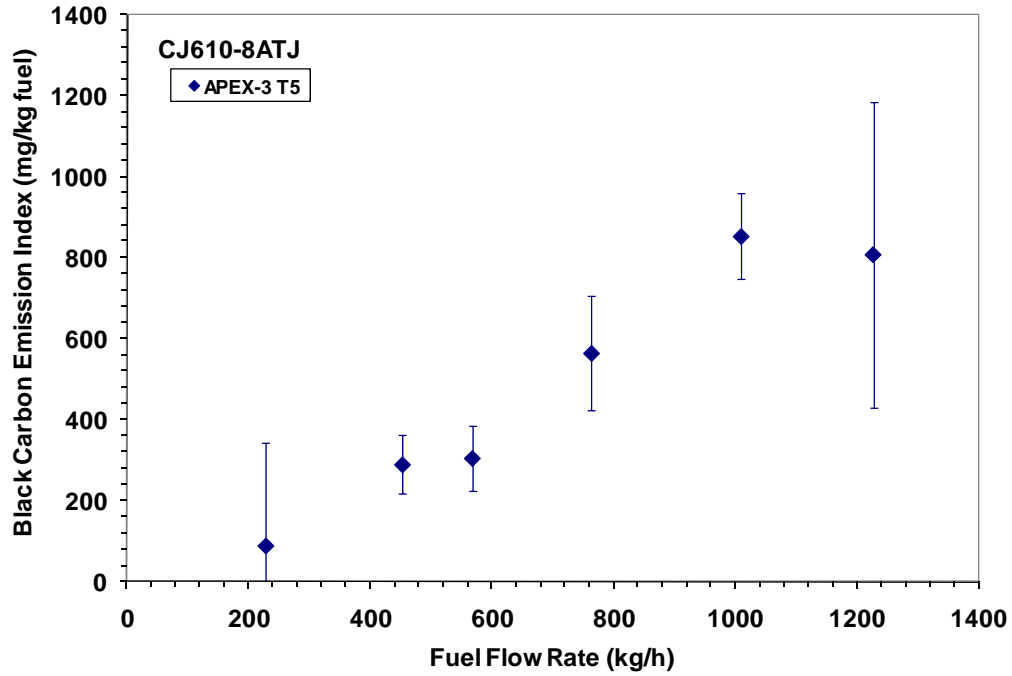
Figure 11-12. Black carbon emission index as a function of fuel flow rate for the CJ610-8ATJ turbojet engine.
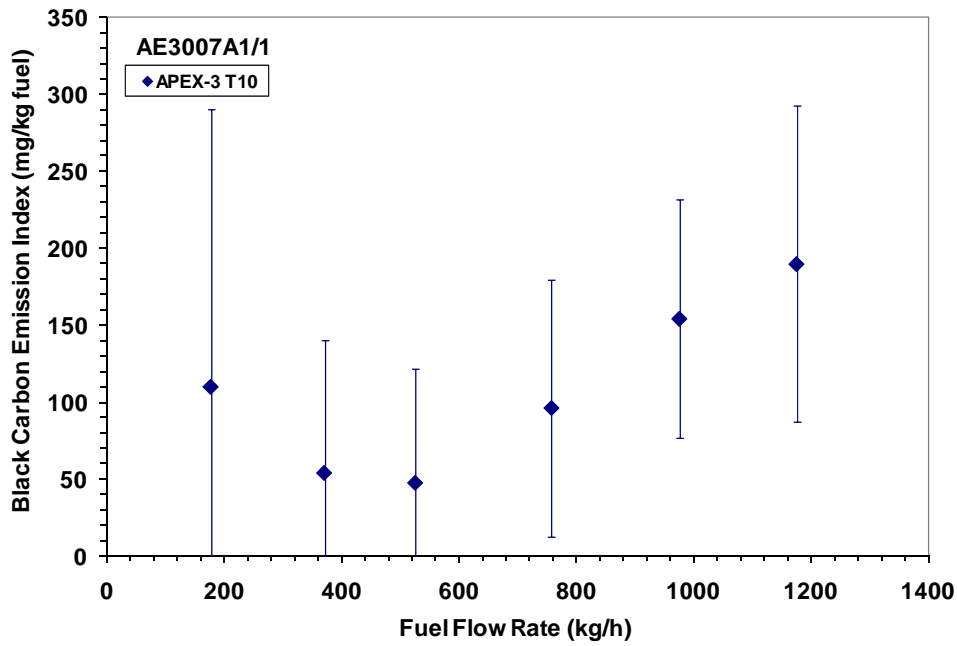
Figure 11-13. Black carbon emission index as a function of fuel flow rate for the AE3007A1/1 engine.
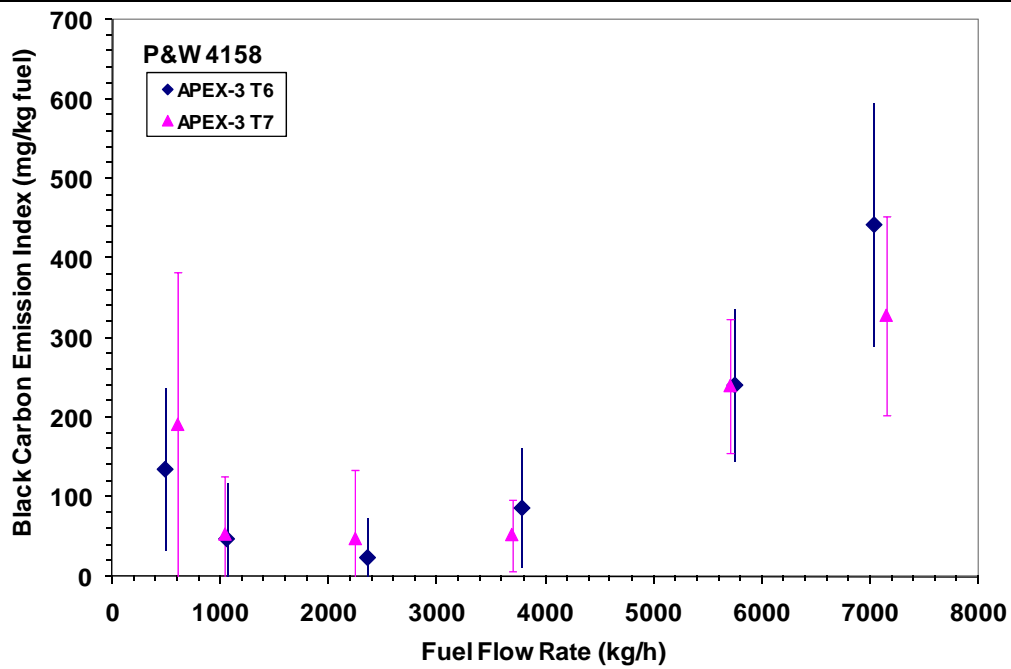
Figure 11-14. Black carbon emission index as a function of fuel flow rate for the P&W 4158 engine.
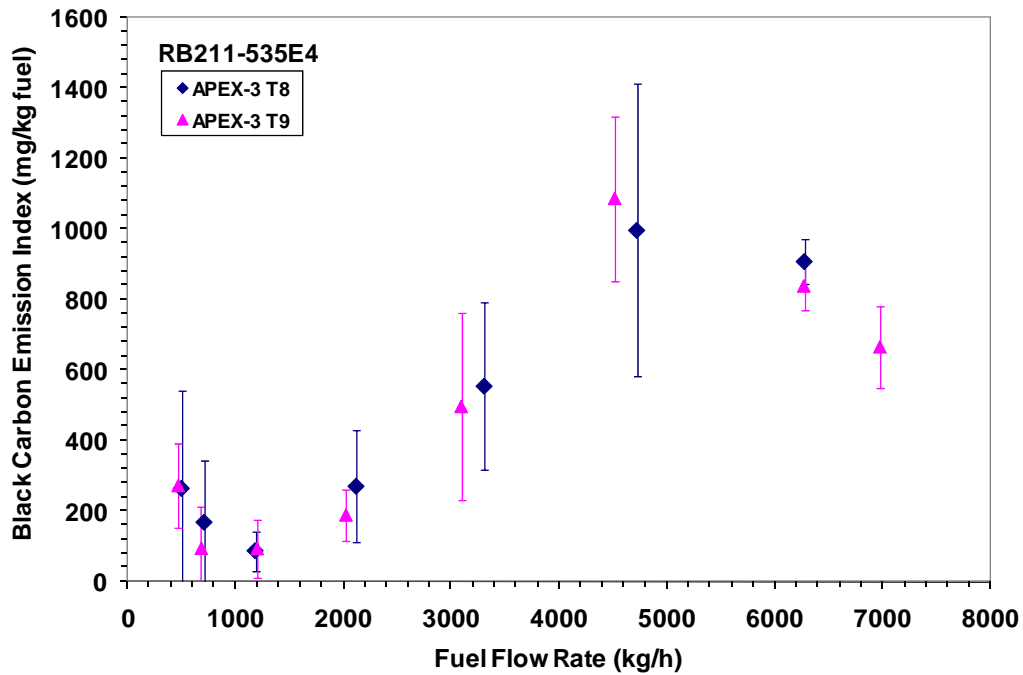
Figure 11-15. Black carbon emission index as a function of fuel flow rate for the RB211-535E4B engine.

Table 11-2.   BC Emission Indices at the LTO Power Levels for Different Engines

Engine	Test Average	Engine Cycle	BC EI mg/kg	BC SD mg/kg
CFM56-2C1	APEX-1 EPA-2 & NASA-1a	Idle (7%)	33.6	46.2
		Takeoff (100%)	71.2	81.6
		Climb (85%)	402	113
		Approach (30%)	99.5	174
CFM56-7B24	APEX-2 T1&T4	Idle (7%)	260	204
		Takeoff (100%)	-	-
		Climb (85%)	406	168
		Approach (30%)	111	60.9
CFM56-3B series	APEX-2 T2&T3 APEX-3 T11	Idle (7%)	333	92.6
		Takeoff (100%)	734	58.5
		Climb (85%)	718	236
		Approach (30%)	205	27.1
CJ610-8ATJ	APEX-3 T5	Idle (7%)	137	651
		Takeoff (100%)	808	378
		Climb (85%)	853	106
		Approach (30%)	289	72.3
AE3007A1/1	APEX-3 T10	Idle (8.4%)	108	192
		Takeoff (100%)	190	97.3
		Climb (85%)	154	77.4
		Approach (30%)	53.6	85.1
P&W 4158	APEX-3 T6&T7	Idle (7%)	209	229
		Takeoff (100%)	-	-
		Climb (80%)	386	135
		Approach (30%)	35.4	60.5
RB211-535E4-B	APEX-3 T8&T9	Idle (7%)	142	172
		Takeoff (100%)	665	140
		Climb (85%)	873	65.9
		Approach (30%)	191	72.6
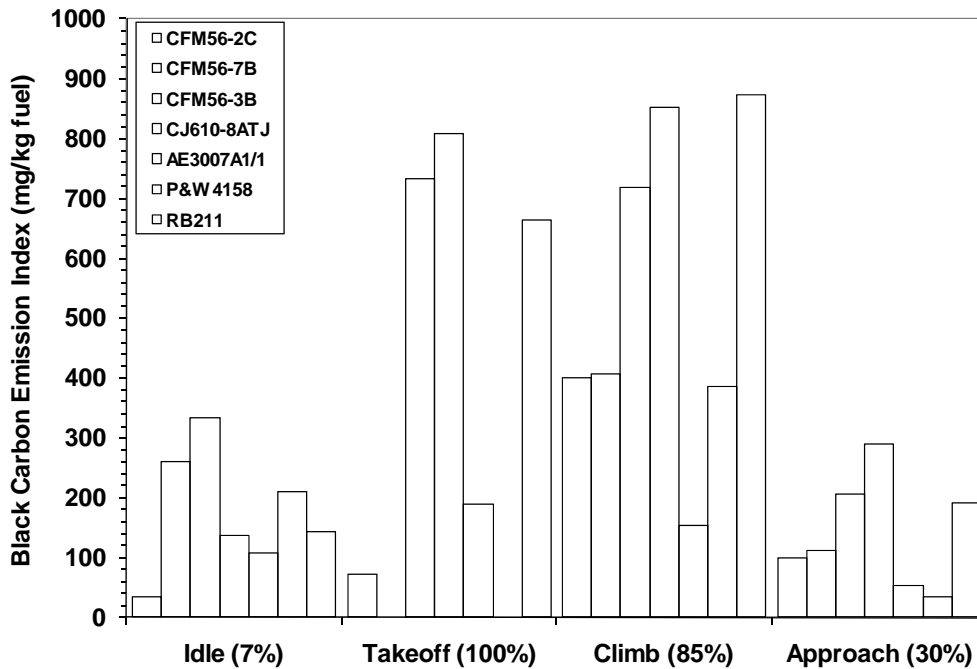
Figure 11-16. Effect of engine cycle on BC emission index for multiple engine types.

11.1.2 Effect of Fuel Composition

To investigate the effects of fuel type on the BC emissions, the APEX-1 test results with different types of fuels were evaluated. Figure 11-17 compares the BC emission indices for the base and high-aromatic fuels. The BC emission indices in the figure are the average values obtained from the data at the same rated thrust levels for the same fuel. For the base fuel, the data from the APEX-1 test NASA-1a were averaged, and the data for the high-aromatic fuel were from the test NASA-5. There were no BC data for the high-sulfur fuel tests in the comparison because, as discussed previously, the BC measurements for tests EPA-3, NASA-2 and NASA-3 were not reliable. The BC emission index data for each fuel type were plotted against fuel flow rate. The fuel type appeared to have little effect on the BC emission index. The difference in BC emission indices between the base fuel and the high-aromatic fuel was insignificant in comparison to the experimental errors.

To assess the effect of sulfur content, the black carbon emission indices obtained from all the tests with the CFM56 engine were plotted in Figure 11-18 against the sulfur content in the fuel, including the data obtained from the -2C1, -3B, and -7B24 models in all the three APEX campaigns. The BC emission indices are the averages at the same engine rated thrust level and fuel sulfur content. The figure shows that, unlike the PM mass emission index, the BC emission index was not directly correlated to the sulfur content of the jet fuel. Our finding that BC EI is independent of fuel type is consistent with the observations of other APEX investigators (Lobo et. al., 2007).

197
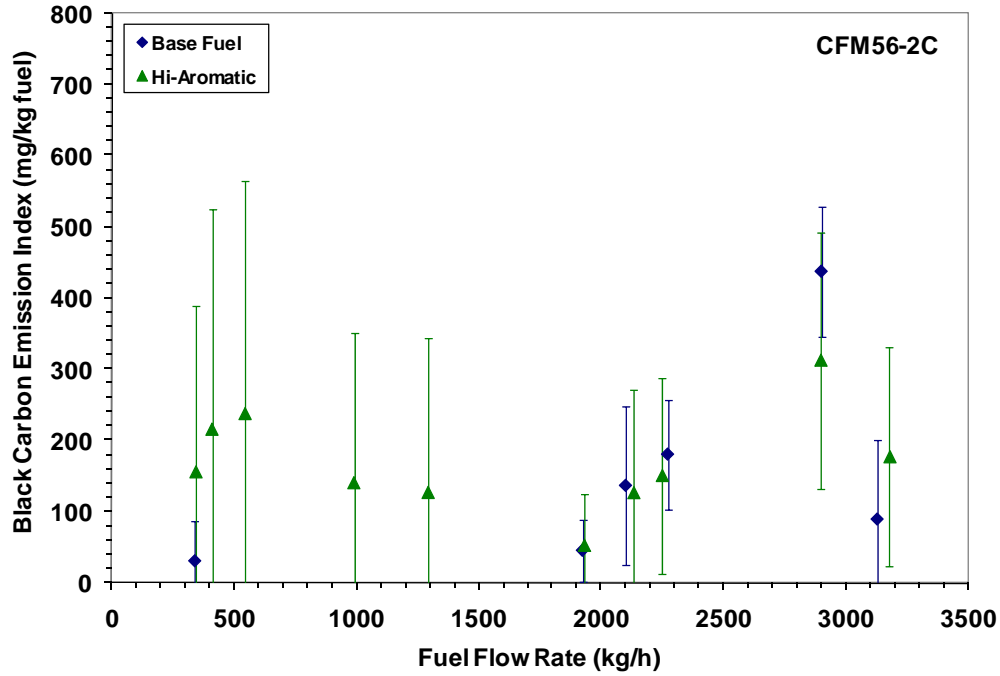
Figure 11-17. Comparison of black carbon emission indices obtained from different types of fuel for the CFM56-2C1 engine during APEX-1.
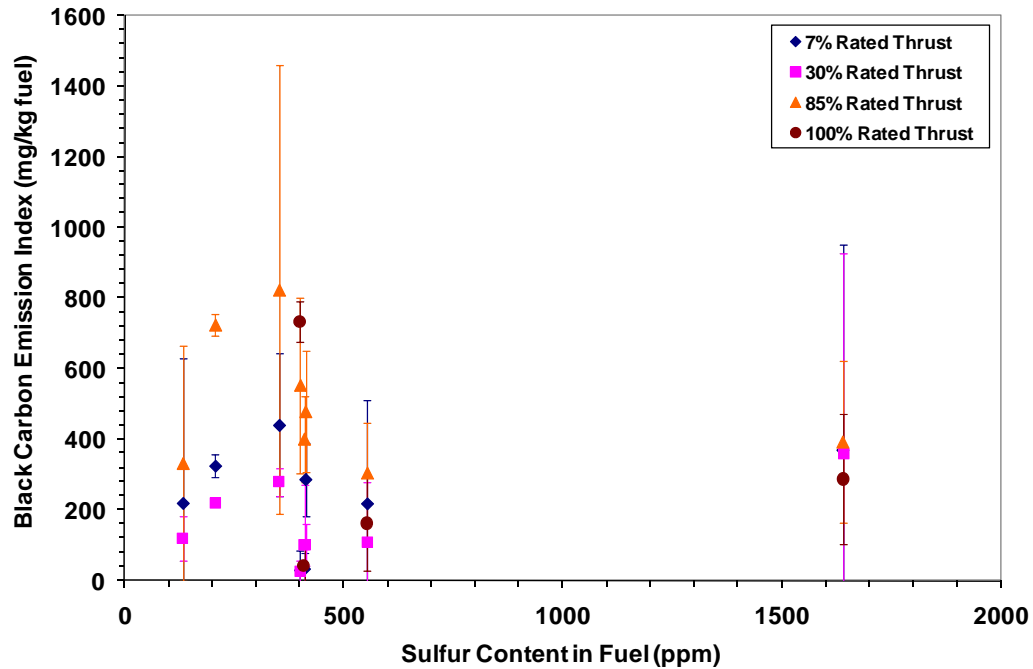
Figure 11-18. Effect of sulfur content in fuel on BC emission index for all CFM56 engines tested.

11.1.3 Effect of Engine Type

The average BC emission indices obtained from the different engine types tested were compared in Figures 11-19 for the four ICAO engine power levels: idle, take-off, climb, and approach. Only the data with the base fuel or fleet fuel and measured at the 30-m sampling location were presented here. The data for the tests EPA-1 and NASA-1 of APEX-1 and the test T1 of APEX-3 were not used as discussed previously. The data are averages from the different tests with the same engines. The lowest rated thrust, 8.4 percent, for the AE3007-A1/1 engine, was used as the idle condition and compared with the other engines at 7 percent rated thrust. For the P&W 4158 engine, the data available at 80 percent rated thrust were averaged and compared with the other engines at 85 percent rated thrust. There were no data available at engine take-off (100%) thrust for the CFM56-7B24 and P&W 4158 engines. The fuel flow rate is also presented in the figure using the second y-axis. Again note that the fuel flows provided are averages for only those test periods where valid BC data were available and may not match those shown earlier in Table 7-2.

The figure shows that the larger engines did not always produce the most BC. In fact, the CJ610-8ATJ turbojet, which is the smallest engine with older combustor technology, had highest BC emission indices except for idle. The large error bars in the figure indicate that the BC emission data measured in this study were highly variable. It is therefore difficult to make any clear conclusion from the above observations. More accurate data than can be provided by the aethalometer are needed to reach clear conclusions.

11.1.4 Effect of Cold and Warm Engine Conditions

In Figure 11-20, all of the BC emission index data under the cold engine condition were plotted against the equivalent indices obtained for the same engine type and the same engine power but under the warm condition. The black diagonal line in the figure represents the 1:1 relationship where the emission indices under cold and warm conditions are identical. The figure also shows the linear regression results (see the pink line). The correlation line has a slope of 0.947, indicating that the BC emission indices were approximately 5 percent lower after engine warm-up. Therefore, the warm-up of engines can improve carbon burn-off.

11.1.5 Effect of Probe Position

In the APEX-3 campaign, the effect of the sampling probe distance from the test engine was investigated. The emissions were collected at both 15 m and 30 m in test T5 for the CJ610-8ATJ engine and at 30 m and 43 m in test T8 for the RB211-535E4-B engine. In the test T5, the data were first collected at 15 m while the engine power increased in five steps from 7, 30, 45, 65, 85 to 100 percent rated thrust, and then collected at 30 m with the engine power setting varied stepwise downward from 100 to 7 percent. The same experimental procedure was used in Test T8, but the rated thrust settings were between 4 and 85 percent in six steps.
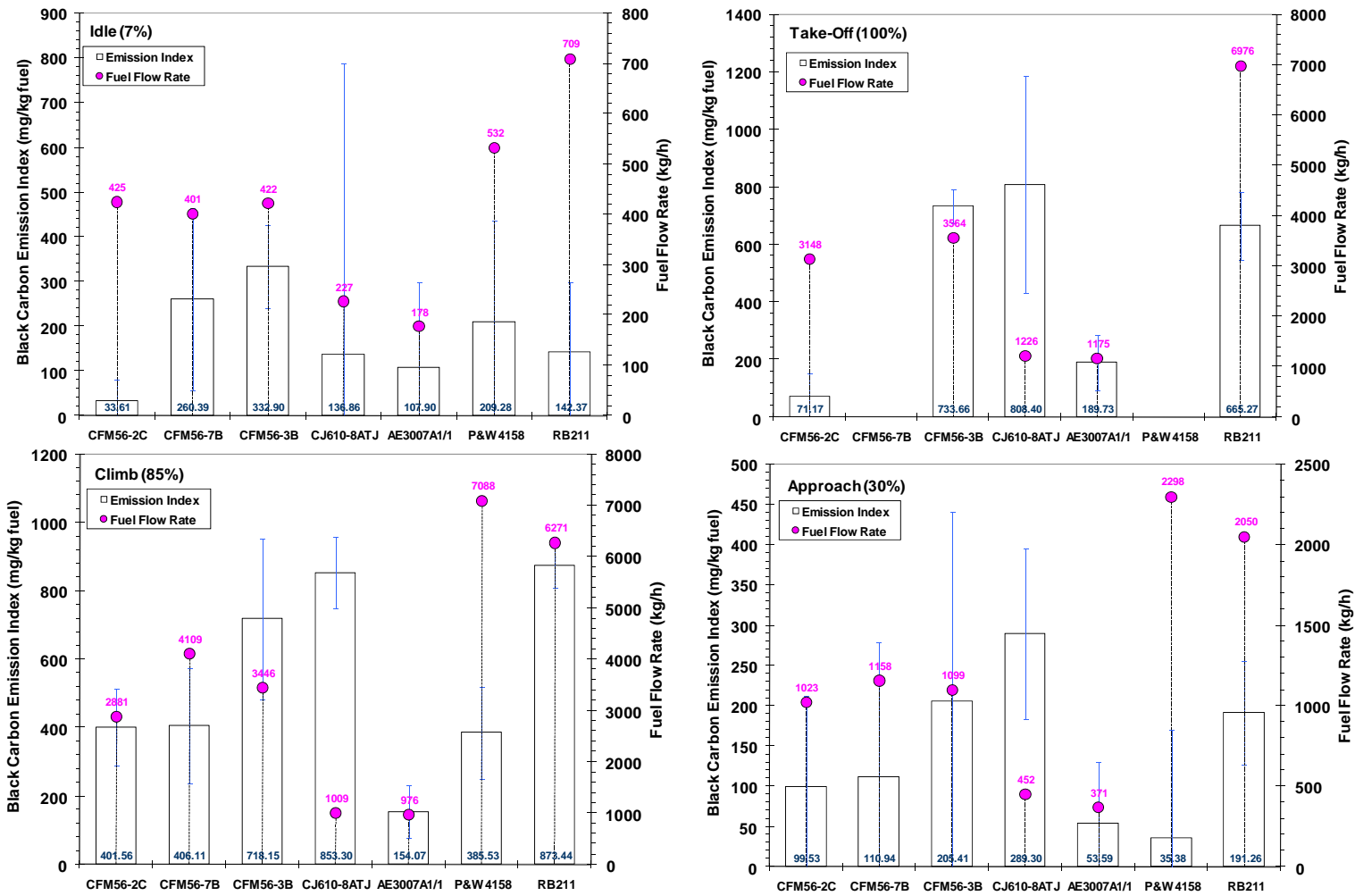
Figure 11-19. Effect of engine type on BC emission index for multiple engine types.
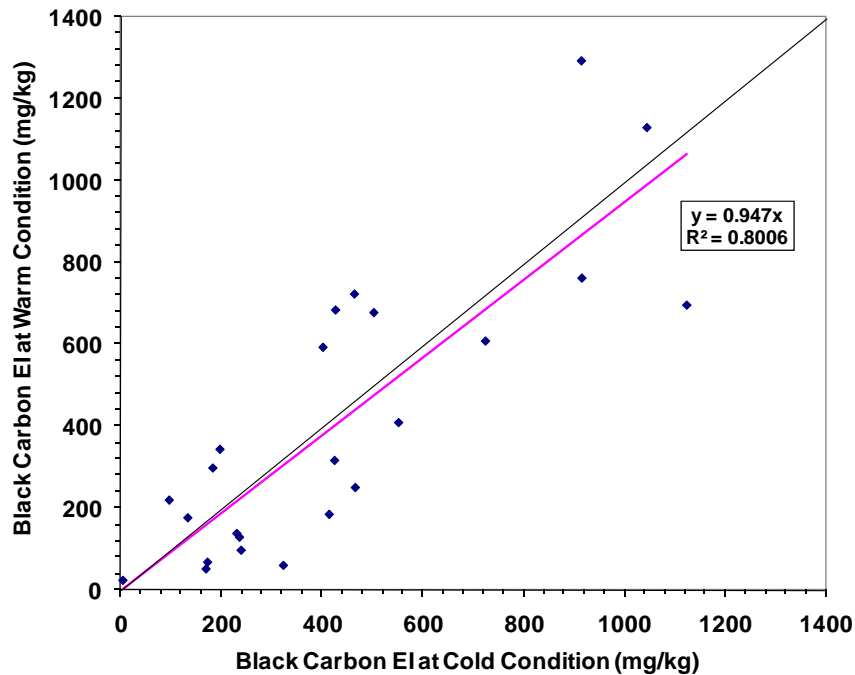
Figure 11-20. Effect of engine cold and warm condition on BC emission index.

The BC emission indices obtained from the different sampling positions for these two engines are compared in Figure 11-21. The results show that the BC emission indices of the CJ610-8ATJ engine obtained at 15 m were always higher than the indices obtained at 30 m except for idle. For the RB211-535E4-B engine, the BC emission index was lower at idle and at a rated thrust >65 percent but was higher at 30 or 45 percent rated thrust when the sampling probe changed from 30 m to 43 m. The reason for higher BC emissions when the probe was closer to the engine is currently unknown. However, this result is consistent with the results of measurements of particulate mass based emission indices discussed in Section 10, where EI_M decreased as the probe distance increased. Since the BC EI should not be affected by probe distance, further study without complication by engine cold and warm operating condition is required.

11.1.6 Test-Average Black Carbon Emission Index

The test-average black carbon emission indices are summarized in Table 11-3. The available test-average PM mass emission indices and the percentage non-volatile PM obtained from the Teflon filter sampling are also presented in the table. The percentage black carbon in PM as shown in the table for each test was obtained by dividing the BC EI by the PM EI. The comparison shows that the percentage black carbon in PM for most of the APEX tests was higher than the percentage non-volatile PM measured from the Teflon filter/thermal denuder sampling. This result implies that there were significant non-volatile PM losses in the thermal denuder. The test-average rated power and fuel flow rate for each test shown in Table 11-3 were evaluated by taking account of both the time at each power setting and the time for transition from one power setting to another.
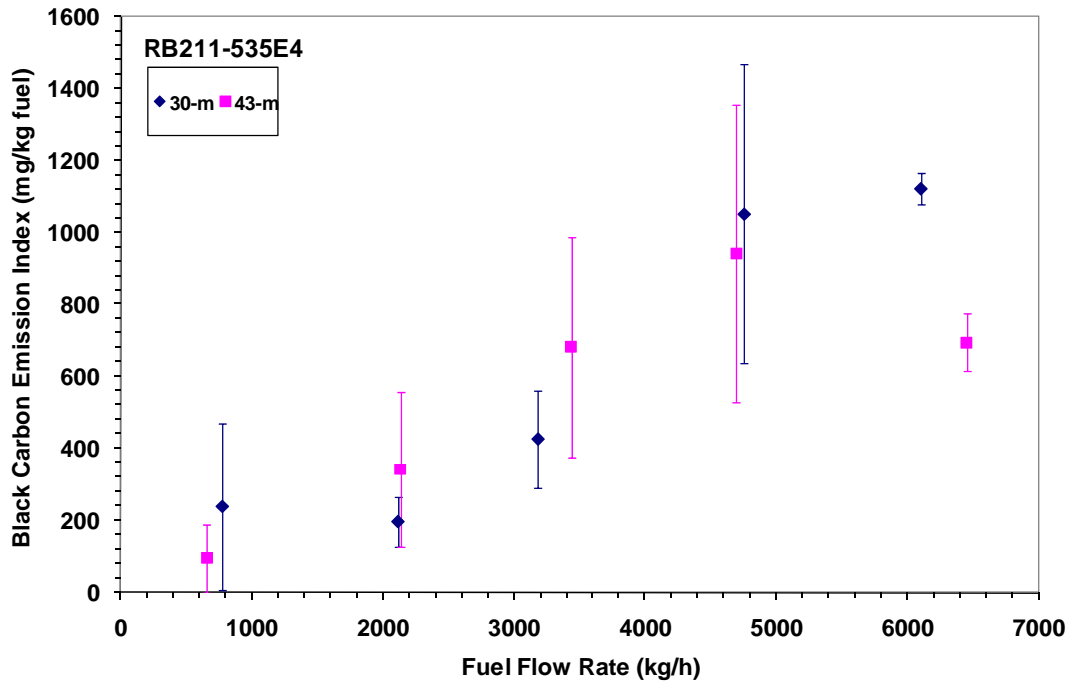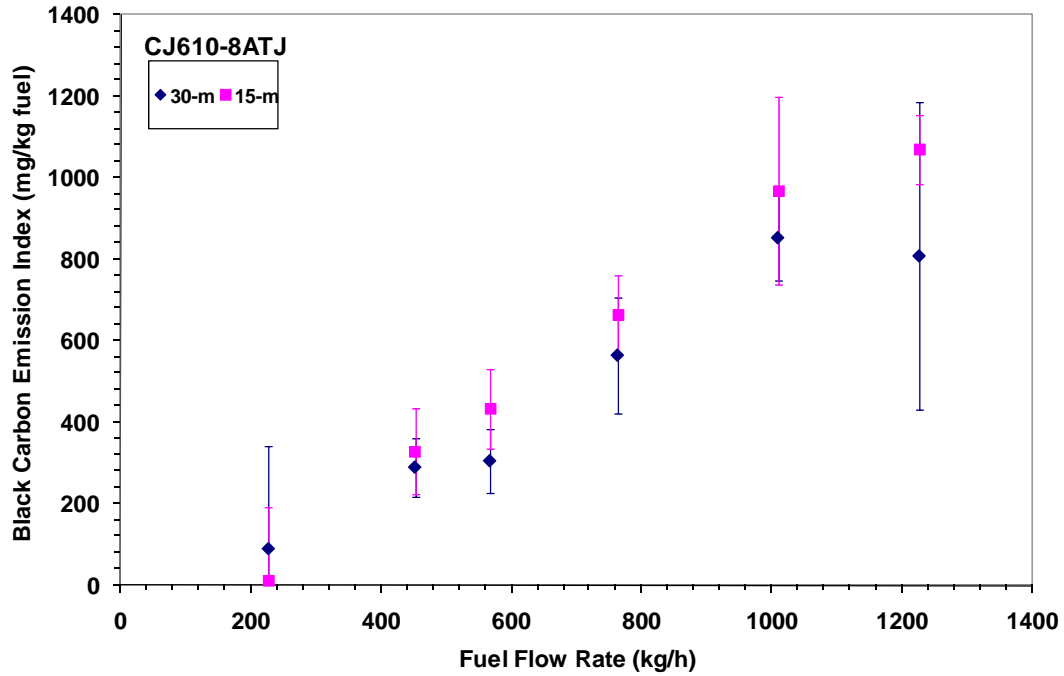
Figure 11-21. Effect of probe position on BC emission index for the CJ610-8ATJ and RB211-535E4B engines.

Table 11-3.   Test-average PM and BC EIs and BC Fraction in PM

APEX	Test	Engine	Fuel	Rated Thrust	Fuel Flow	Teflon Filter		Black Carbon	
						PM EI	Non-Volatile	EI	BC/PM
				%	kg/h	mg/kg	%	mg/kg	%
1	EPA-1	CFM56-2C1	Base Fuel	19.5	785	107	32.0	Fail	
1	EPA-2			18.8	770	305	38.0	71.3	23.4
1	NASA-1			22.6	635	N/A		Fail	
1	NASA-1a			45.1	1559	N/A		166	
1	EPA-3		Hi-Sulfur	20.4	797	447	30.7	301	67.4
1	NASA-2			38.4	1279	443	20.7	Fail	
1	NASA-3			38.6	1277			Fail	
1	NASA-4		Hi-Aromatic	36.2	1197	219	34.5	153	70.0
1	NASA-5			35.3	1244			168	77.0
2	T1	CFM56-7B24	Fleet Fuel	30.1	1264	Fail		237	
2	T4			30.1	1264	Fail		282	
2	T2	CFM56-3B series		31.5	1201	Fail		464	
2	T3			30.4	1199	Fail		288	
3	T1			36.7	1352	N/A		Fail	
3	T11			31.1	1161	267	20.6	275	§
3	T2	CJ610-8ATJ		47.4	618	N/A		592	
3	T5			41.0	566	N/A		584	
3	T3	AE3007A1E		39.3	523	116	38.2	62.5	53.9
3	T4			43.1	554			137	§
3	T10	AE3007A1/1		45.0	550	N/A		101	
3	T6	P&W 4158		28.5	2344	268	46.4	198	73.7
3	T7			35.0	2968			198	73.7
3	T8	RB211-535E4-B		27.5	2087	N/A		667	
3	T9			34.2	2473	384	59.1	559	§

§ BC/PM percentage exceeds 100%.

11.2 PAH Emissions

The particle surface-bound PAH was monitored by the PAS 2000 during all the APEX tests. The data were recorded every second. The time-series PAH concentration data for each test are presented in Figures 11-22 to 11-29. In these figures, the PAH concentrations were plotted as black lines. The rated thrust for each test was plotted as a pink color line using the second y-axis. Again note the variable, and sometimes erratic, data produced by the PAH analyzer which were difficult to analyze and significantly impacted the resulting EIs.

Figure 11-22 shows the results of four tests: EPA-1, EPA-2, NASA-1, and NASA-1a of APEX-1 campaign. These tests were conducted with the same CFM56-2C1 engine and the same base jet fuel. The PAH concentrations measured for the tests EPA-2 and NASA-1a generally tracked with changes in engine power. The EPA-1 and NASA-1 tests may have been influenced by the strong crosswind.

PAH concentration data for the CFM56-2C1 engine with high-sulfur fuel were collected during APEX-1 Tests EPA-3, NASA-2, and NASA-3. However, as was the case for BC with these tests, the data were found to be unreliable and were not used in the data analysis.

Figure 11-23 shows the PAH concentrations measured for the CFM56-2C1 engine with high-aromatic fuel. The NASA-4 and NASA-5 tests of APEX-1 are presented here. The data show some correlation between the PAH concentration and the percentage thrust, though large fluctuations were observed.

The PAH concentration results for APEX-2 T1 and T4 tests for the CFM56-7B24 engine are shown in Figure 11-24 and the results of the T2 and T3 of APEX-2 and the T1 and T11 of APEX-3 are presented in Figure 11-25. Figure 11-26 presents the results of APEX-3 T2 and T5 for the CJ610-8ATJ engine and Figures 11-27, 11-28, and 11-29 are the results for the AE3007A, P&W 4158 and RB211 engines, respectively. The tests during which the PAH monitoring results were not correlated to engine power for all the APEX tests are summarized in Table 11-4. Also note that all data presented are uncorrected for sampling line losses.
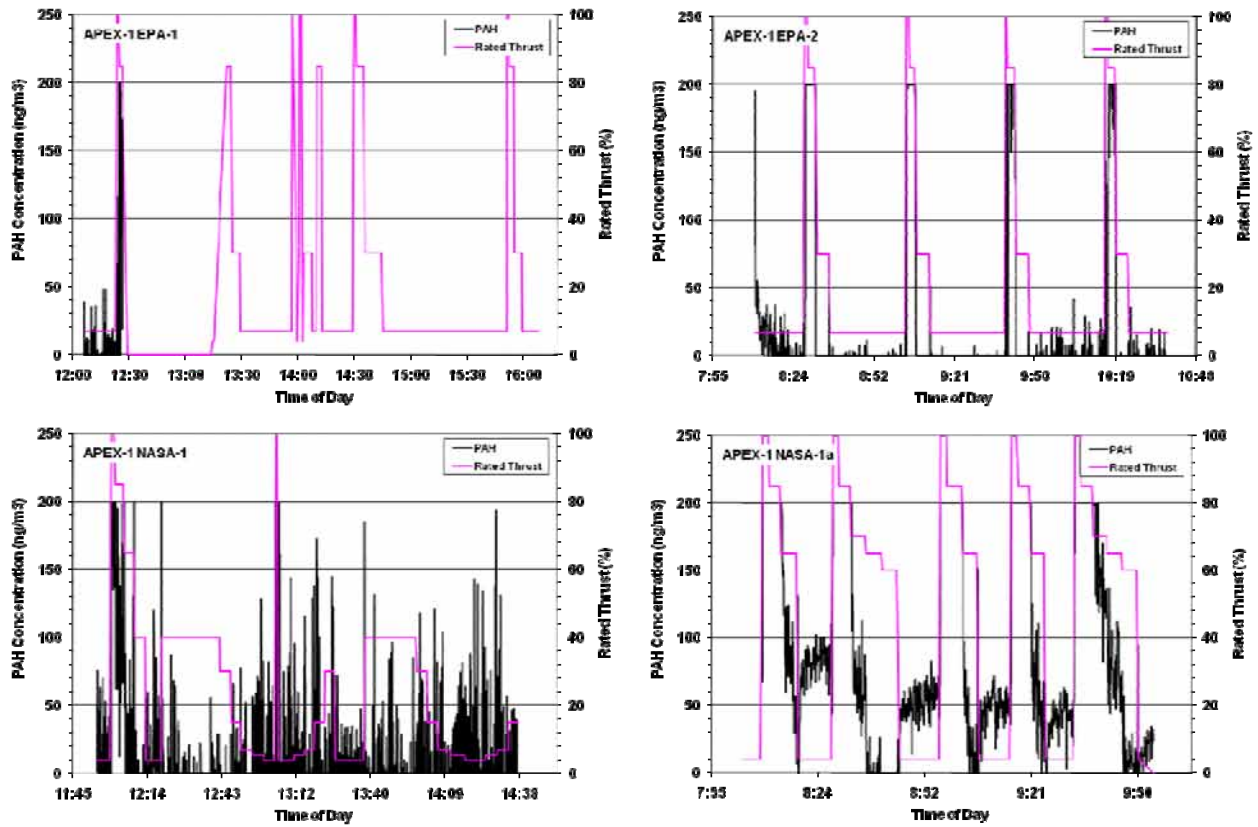
Figure 11-22. Time-series PAH concentration data for tests EPA-1, EPA-2, NASA-1, and NASA-1a of APEX-1 campaign for the CFM56-2C1 engine with base fuel.
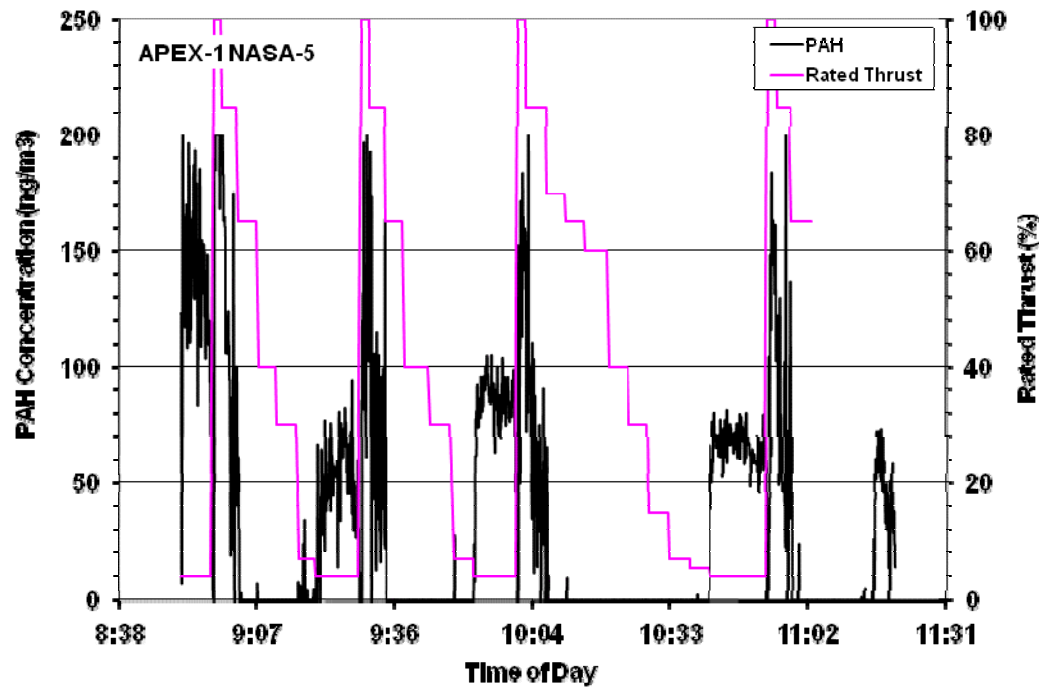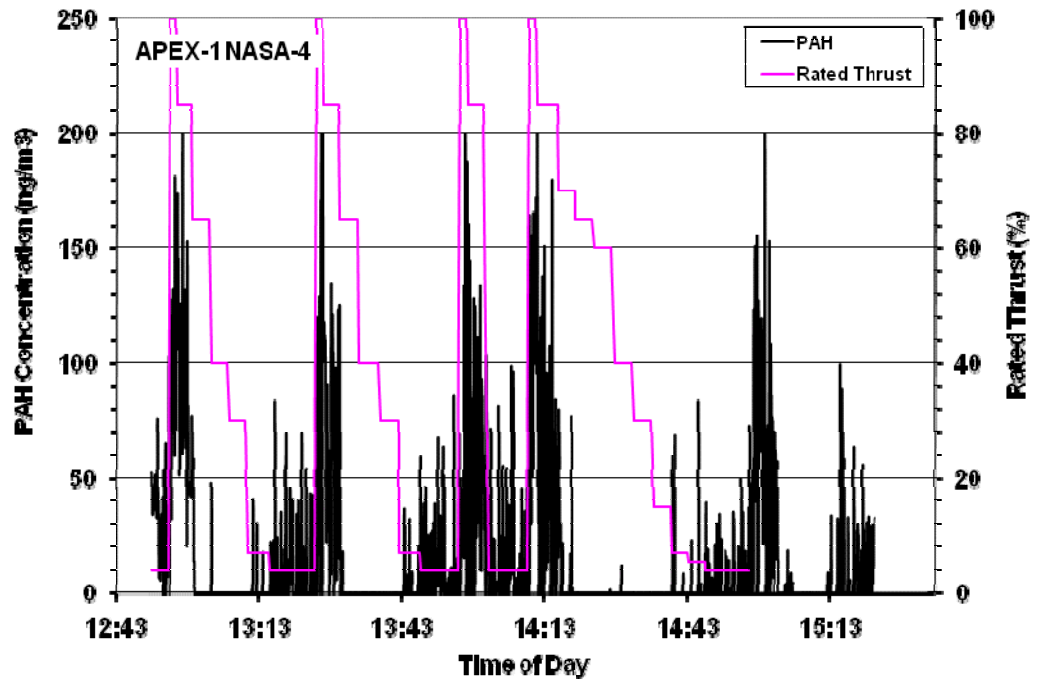
Figure 11-23. Time-series PAH concentration data for tests NASA-4 and NASA-5 of APEX-1 campaign for the CFM56-2C1 engine with high-aromatic fuel.
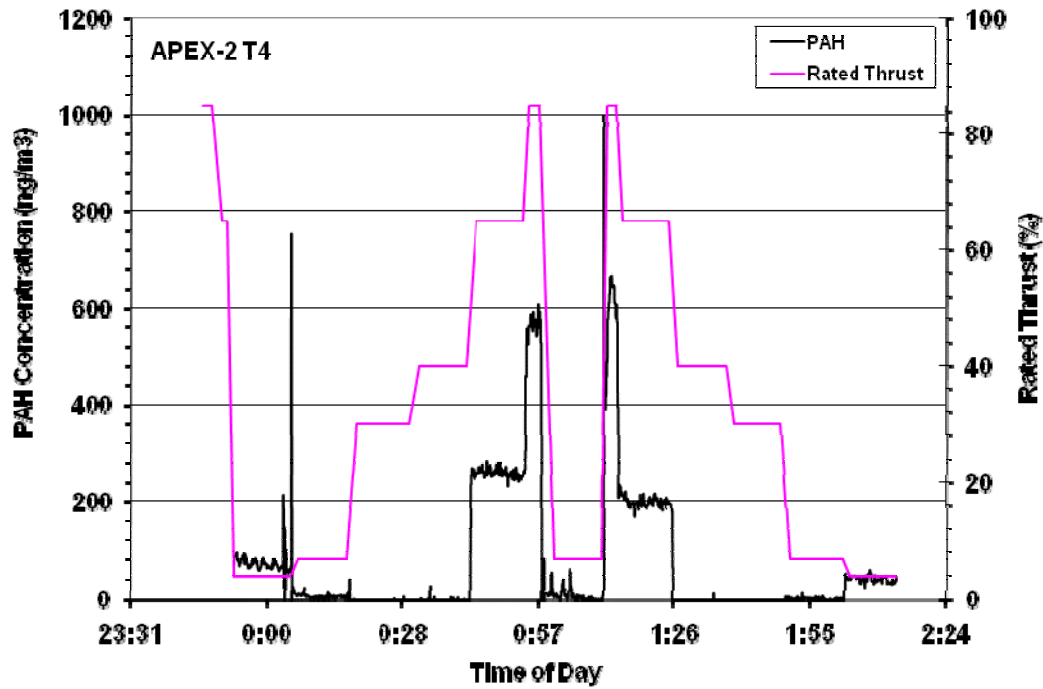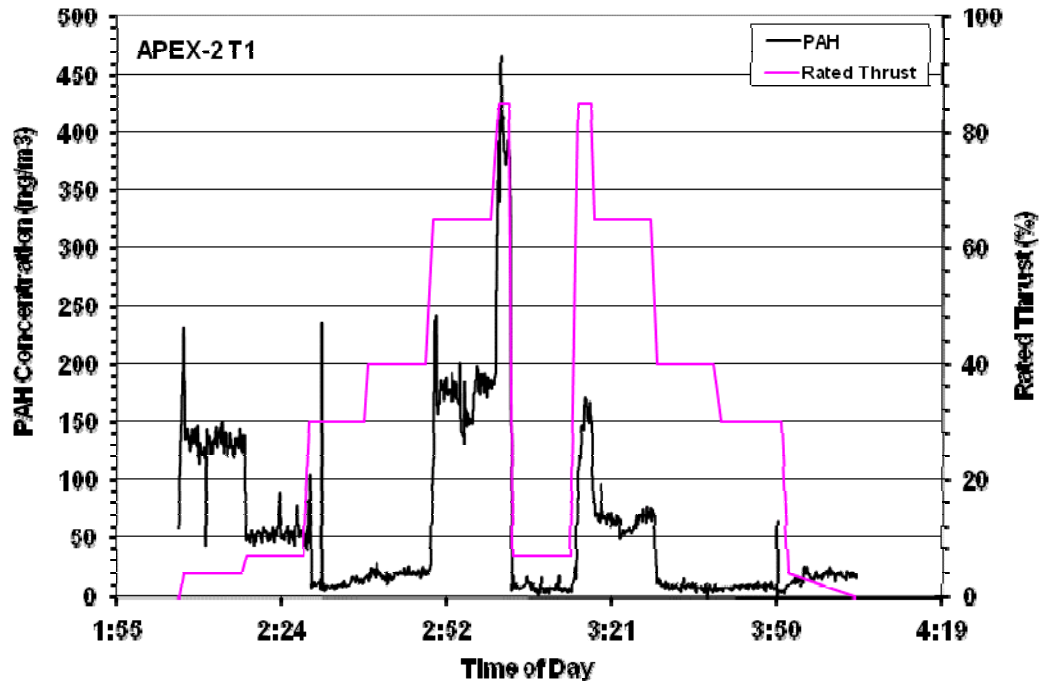
Figure 11-24. Time-series PAH concentration data for tests T1 and T4 of APEX-2 campaign for the CFM56-7B24 engine.

207
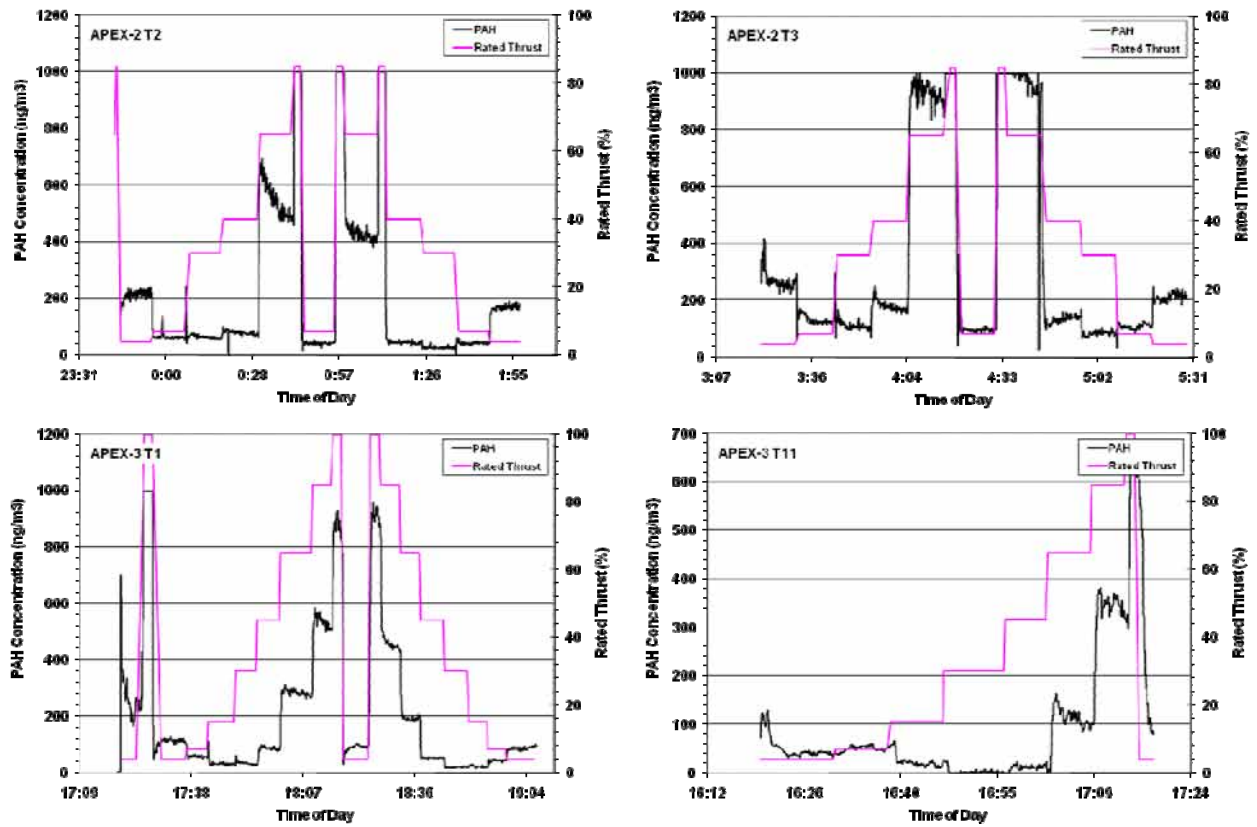
Figure 11-25. Time-series PAH concentration data for tests T2 and T3 of APEX-2 and T1 and T11 of APEX-3 for the CFM56-3B series engines.
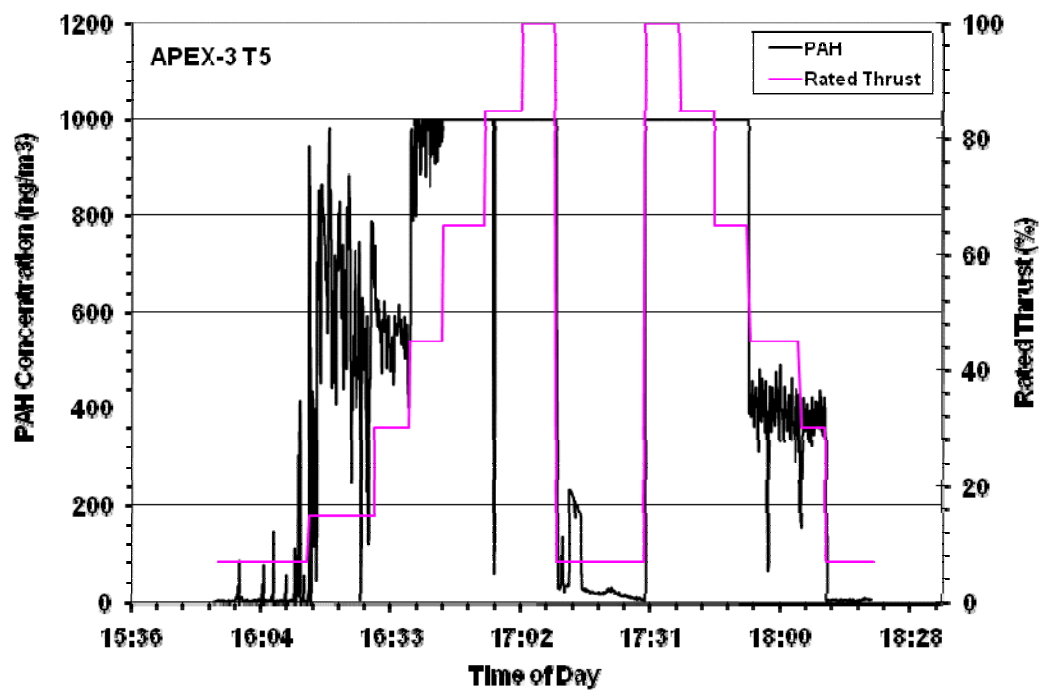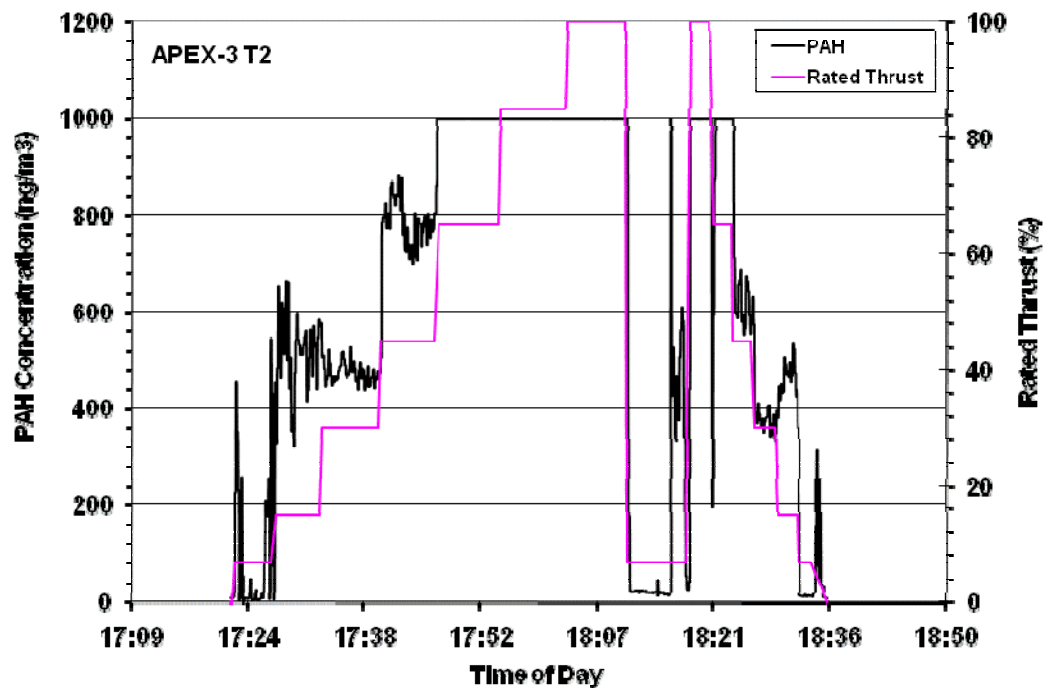
Figure 11-26. Time-series PAH concentration data for the APEX-3 T2 and T5 for the CJ610-8ATJ turbojet engine.
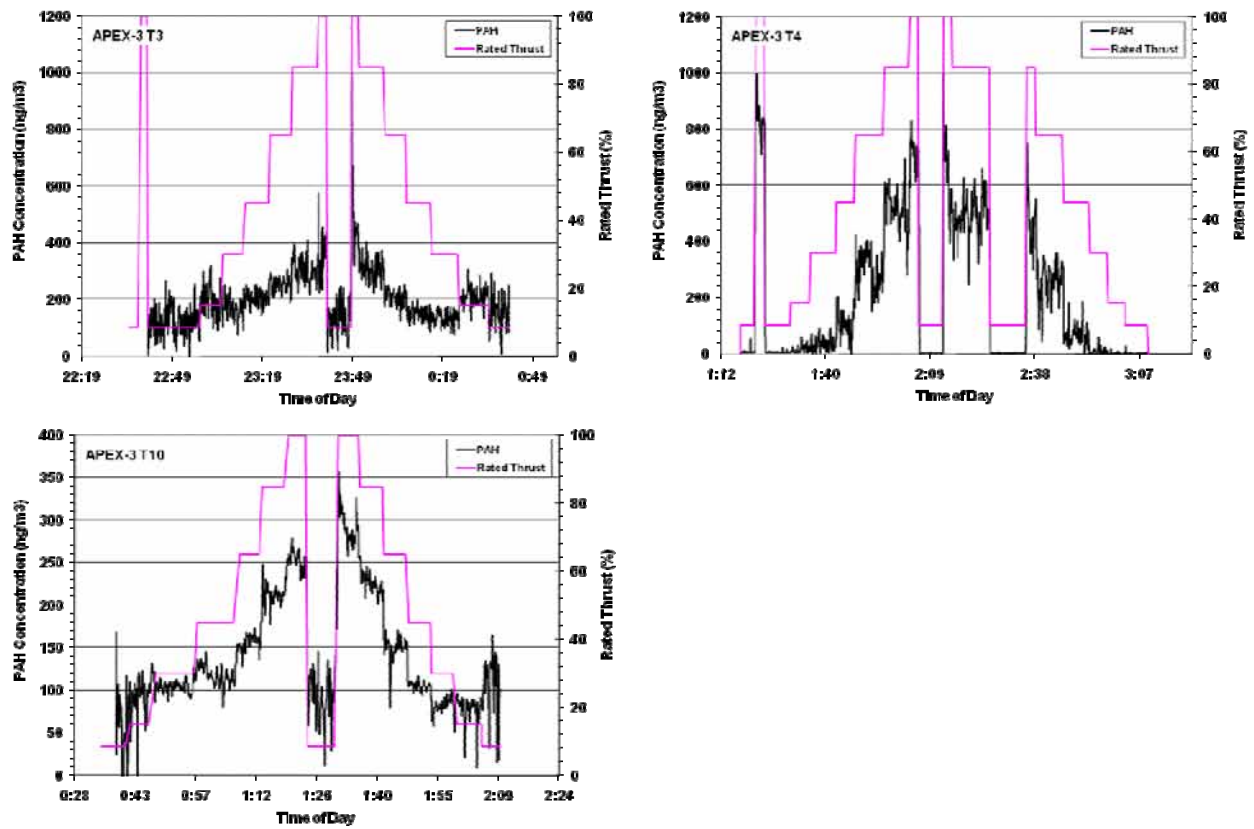
Figure 11-27. Time-series PAH concentration data for the APEX-3 T3 and T4 for the AE3007A1E engine and T10 for the AE3007A1/1 engine.
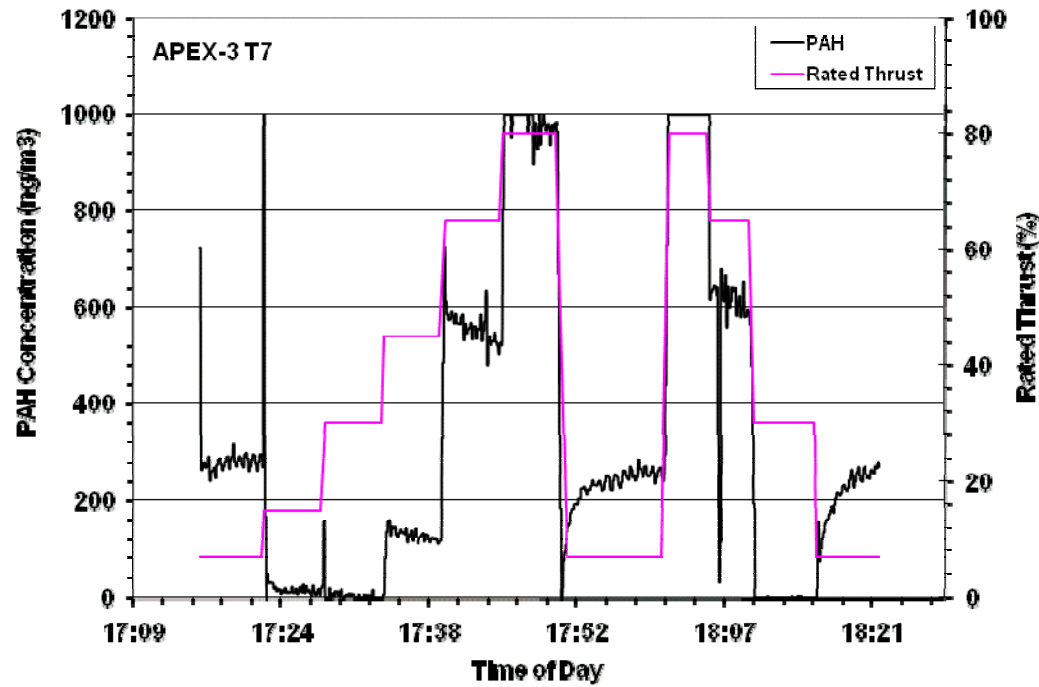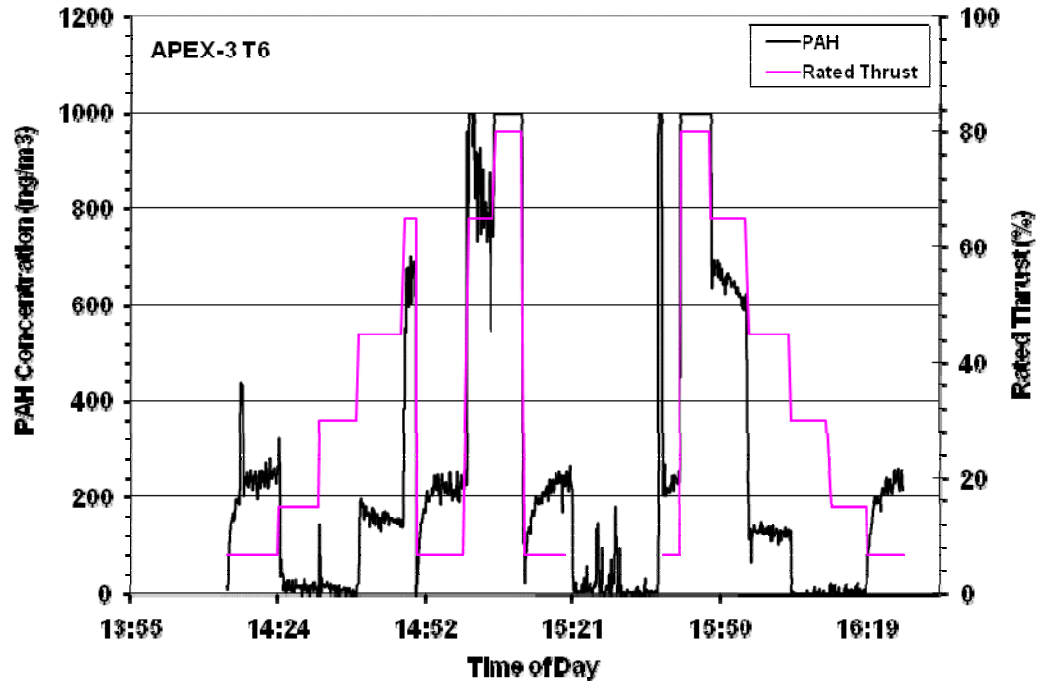
Figure 11-28. Time-series PAH concentration data for the APEX-3 T6 and T7 for the P&W 4158 engine.
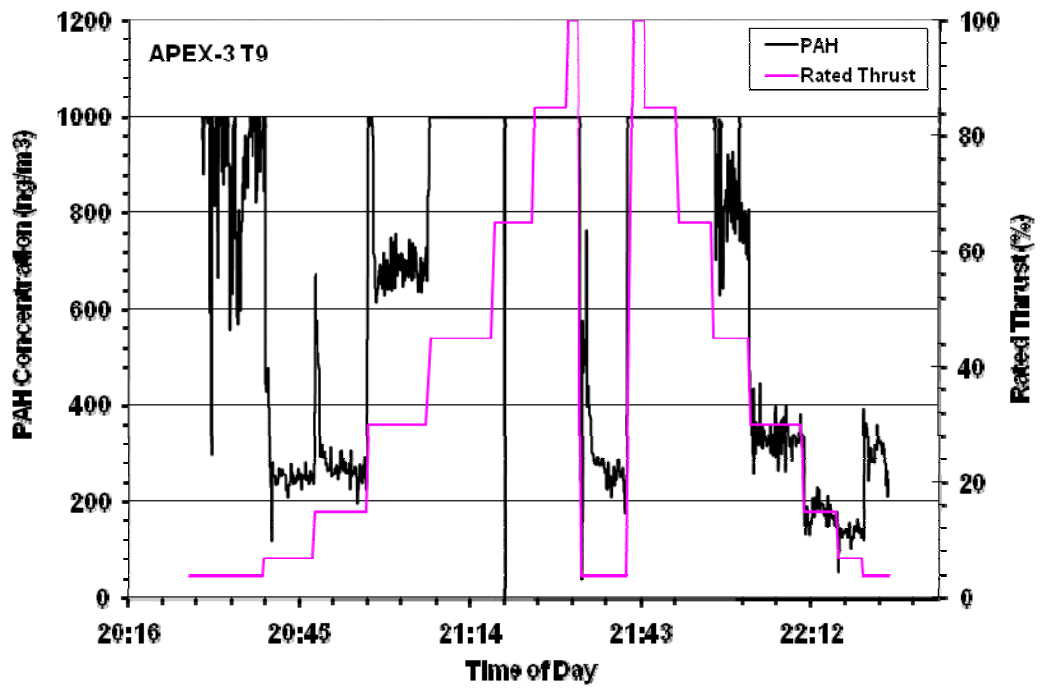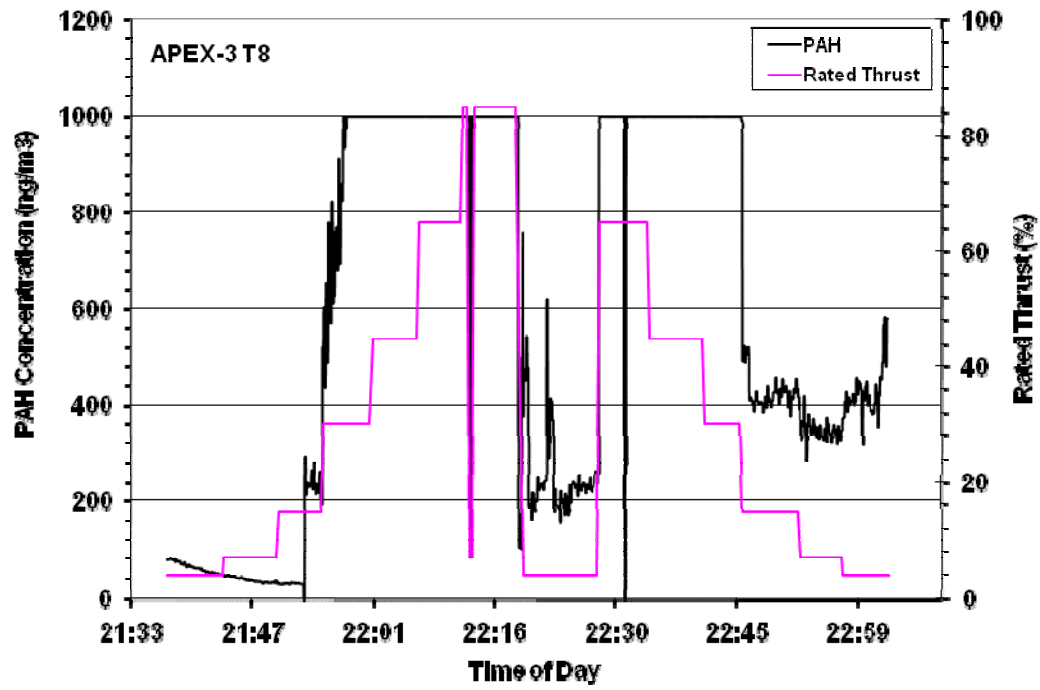
Figure 11-29. Time-series PAH concentration data for the APEX-3 T8 and T9 for the RB211-535E4-B engine.

Table 11-4. PAH Monitoring in APEX Tests

Campaign		Aircraft	Engine	Fuel Type	Probe Position	Concentration Correlated with Engine Power?[b]
APEX	Test No.					
1	EPA-1	DC-8	CFM56-2C1	Base	30-m	N[a]
	EPA-2				30-m	Y
	NASA-1a				30-m	N
	NASA-1				30-m	Y[a]
	EPA-3			Hi-S	30-m	N
	NASA-2				30-m	N
	NASA-3				30-m	N
	NASA-4			Hi-A	30-m	Y
	NASA-5				30-m	Y
2	T1	B737-700	CFM56-7B24	Fleet	30-m	Y
	T4				30-m	Y
	T2	B737-300	CFM56-3B1		30-m	Y
	T3		CFM56-3B2		30-m	Y
3	T1	B737-300	CFM56-3B1		30-m	Y[a]
	T11				30-m	Y
	T2	NASA Lear Model 25	CJ610-8ATJ turbojet		15-m	Y
	T5				30-m/15-m	Y
	T3	Embraer EMB145	AE3007A1E		15-m	Y
	T4				15-m	Y
	T10		AE3007A1/1		30-m	Y
	T6	A300	P&W 4158		30-m	Y
	T7				30-m	Y
	T8	B757	RB211-535E4-B		30-m/43-m	N
	T9				30-m	N

a. indicates tests not used due to high cross wind in background.

b. N = no; Y = yes.

11.2.1 Effect of Fuel Flow Rate

The relationship between the PAH concentration and fuel flow rate was investigated. The PAH concentration readings and corresponding fuel flow rate data under the same rated thrust were averaged within the test and the results summarized in Table G-2 in Appendix G. The PAH emission indices for various tests were then calculated from average CO_2 and plotted as a function of fuel flow rate as shown in Figures 11-30 to 11-35. Only the results obtained from the 30-m probe are presented in the figures. The results of different tests for the same engine and same fuel were plotted together for comparison. These figures show that the PAH emission index varied with the fuel flow rate in a pattern similar to that observed for black carbon. The PAH EI was slightly elevated at low fuel flow (engine power), reached a minimum at mid-range fuel flow (500-2000 kg/h, depending on the type of engine), and increased with fuel flow at high engine power.

11.2.2 Effect of Fuel Composition

The effects of fuel composition on the PAH emissions were investigated using the data available from the APEX-1 campaign. The base fuel data were from the Tests EPA-2 and NASA-1a and the high aromatic fuel were from the NASA-4 and NASA-5 tests. The high sulfur fuel results for Test EPA-3 were not used for the reasons discussed above. For each type of fuel, the PAH EI values and corresponding fuel flow rate at the same rated thrust levels were averaged and compared in Figure 11-36. The figure shows that the base fuel had highest PAH emission index. This observation seems to suggest that the PAH emissions are primarily determined by factors other than just the aromatic content of the fuel. However, this preliminary finding needs further investigation.
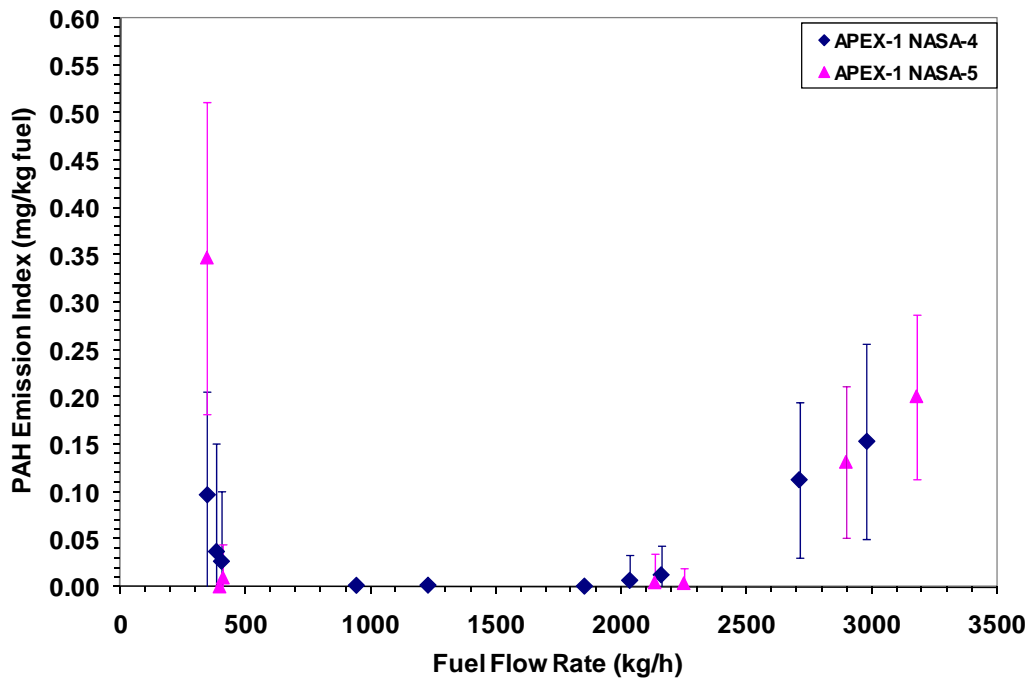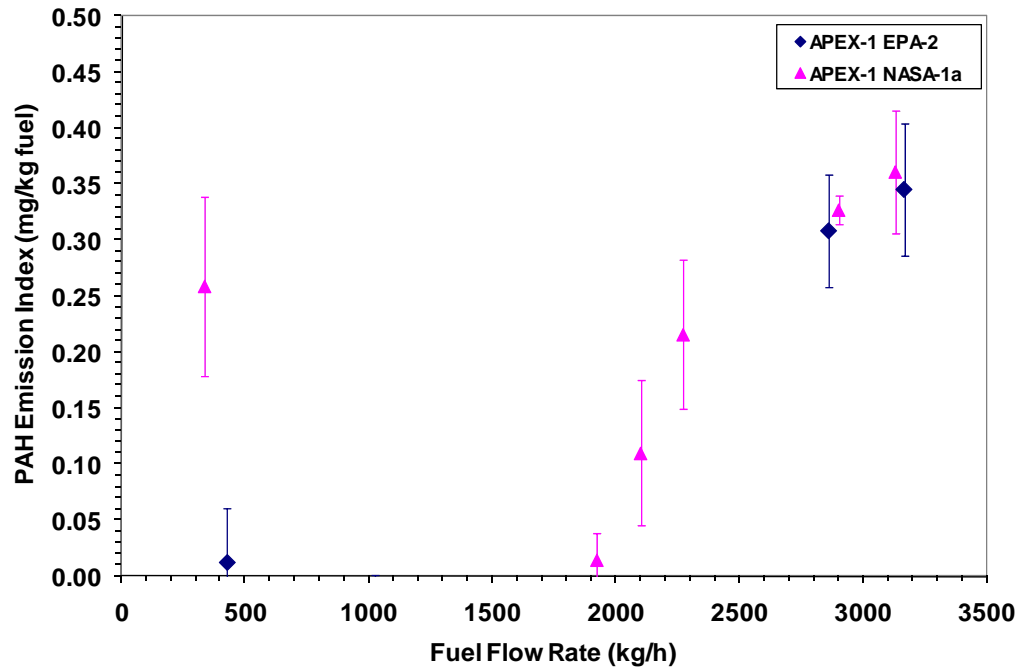
Figure 11-30. PAH emission index as a function of fuel flow for the CFM56-2C1 engine while burning: (a) base fuel; and (b) high-aromatic fuel.
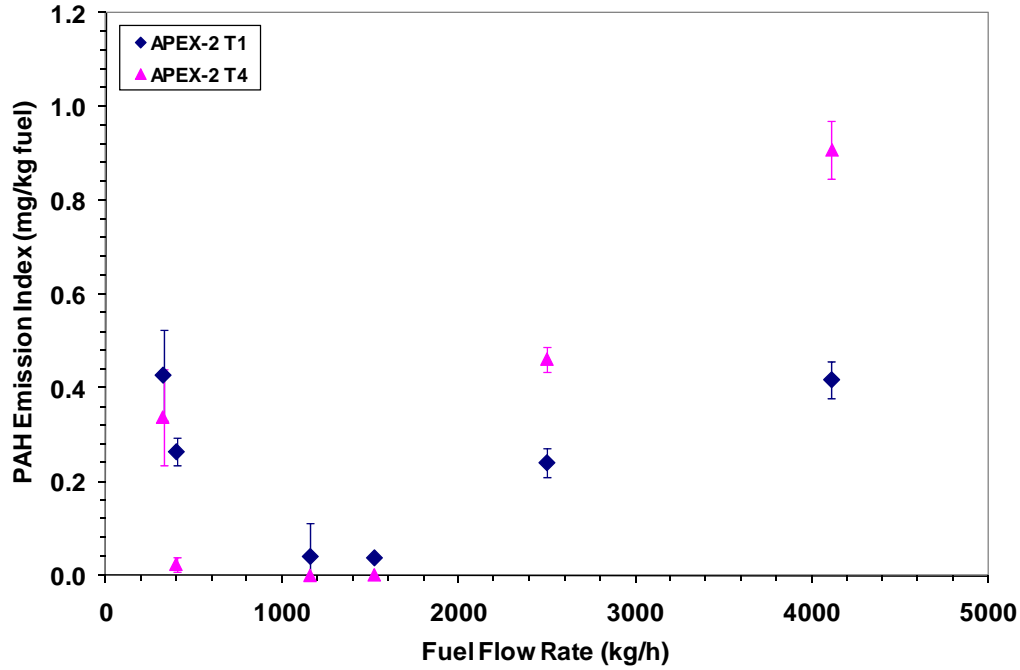
Figure 11-31. PAH emission index as a function of fuel flow for CFM56-7B24 engines.
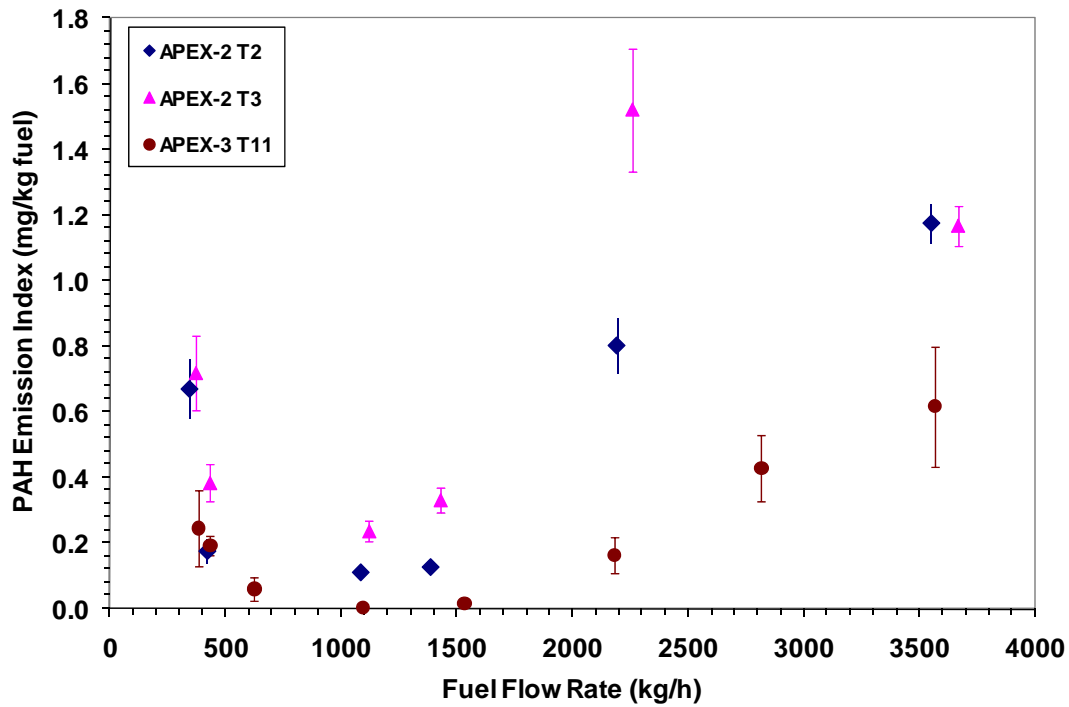
Figure 11-32. PAH emission index as a function of fuel flow for CFM56-3B series engines.
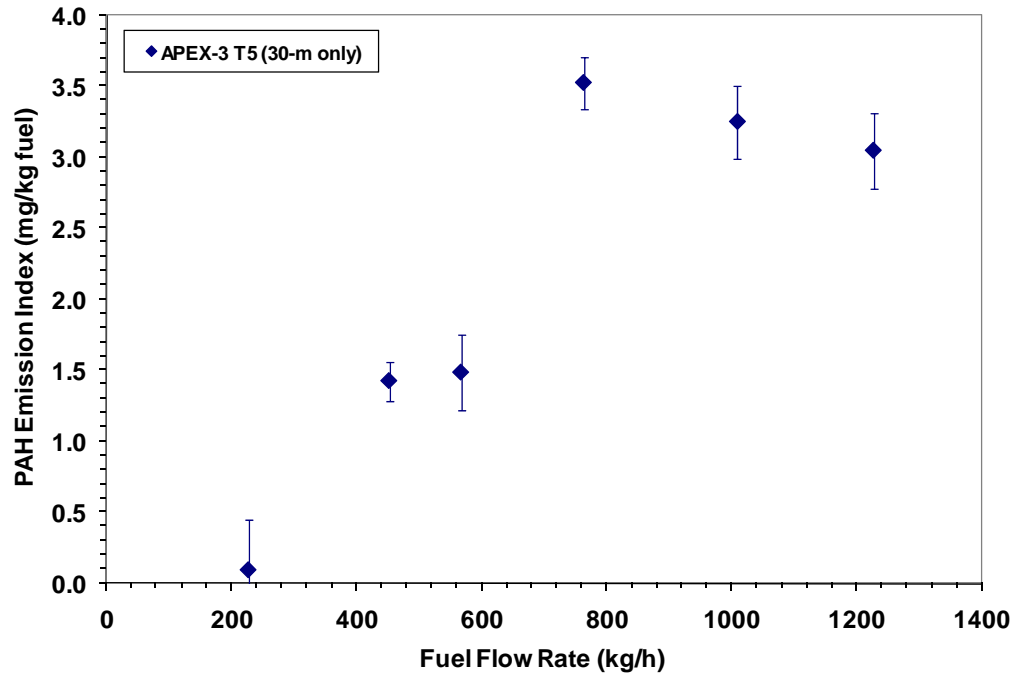
Figure 11-33. PAH emission index as a function of fuel flow for the CJ610-8ATJ turbojet engine.
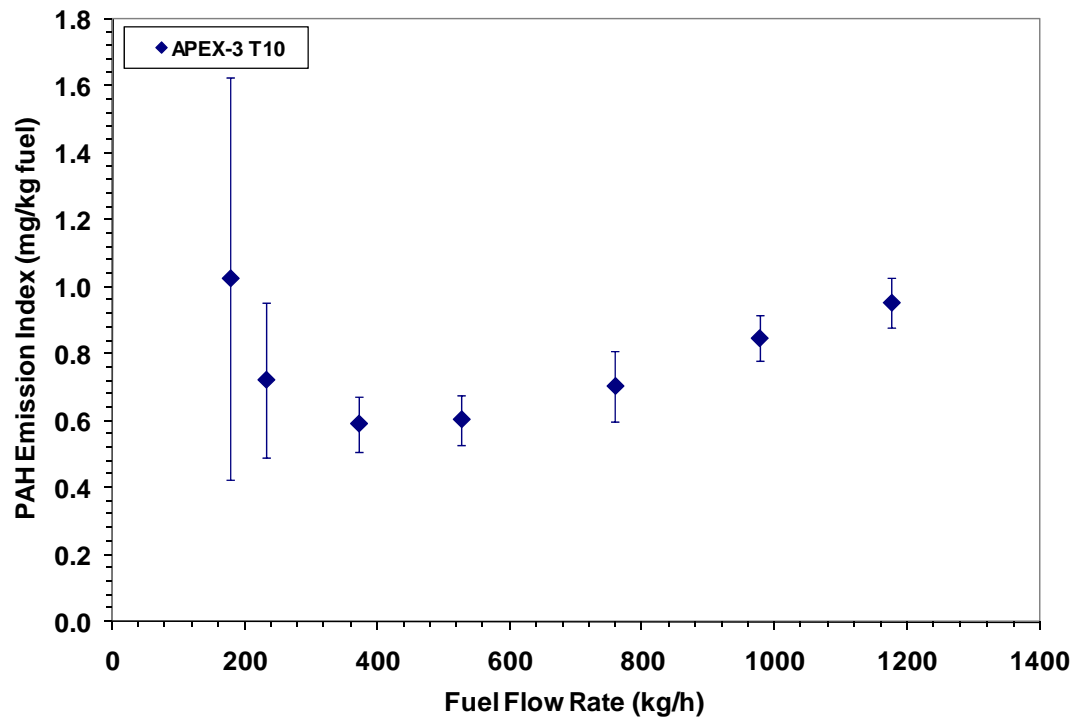
Figure 11-34. PAH emission index as a function of fuel flow for the AE3007-A1/1 engine.

217
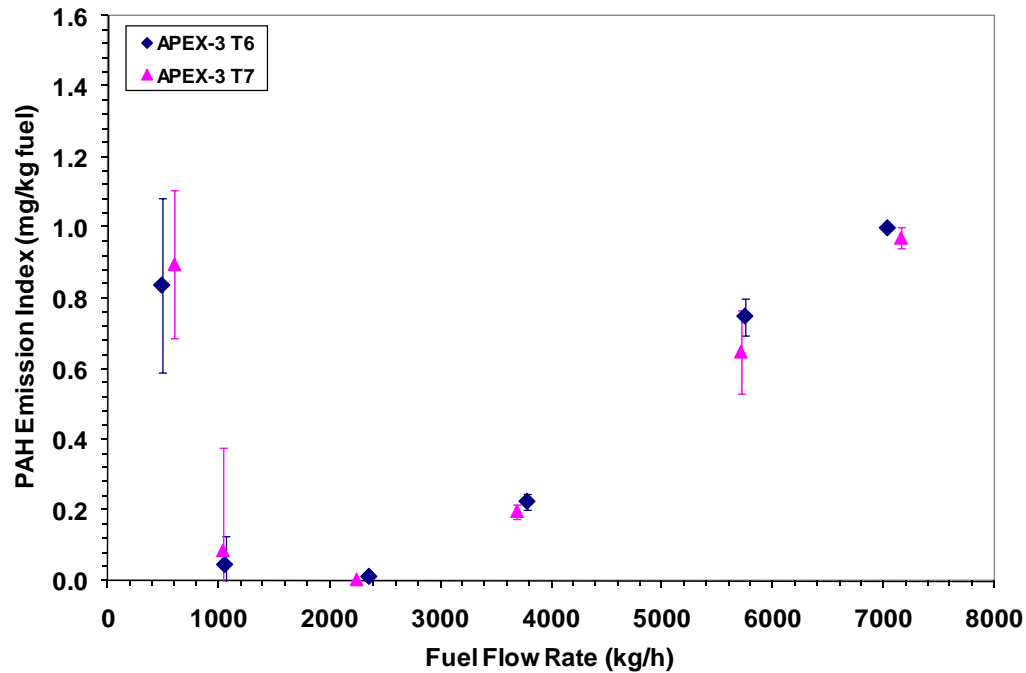
Figure 11-35. PAH emission index as a function of fuel flow for the PW4158 engine.
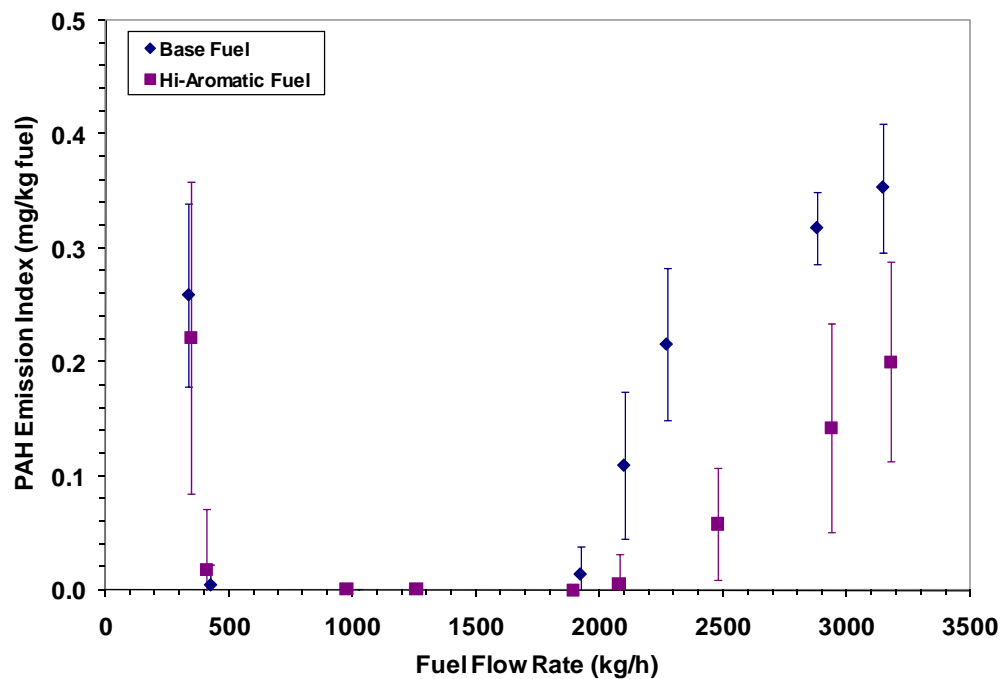
Figure 11-36. Comparison of PAH emission indices for different fuel types during APEX-1.

11.2.3 Effect of Engine Cycle

Like black carbon discussed previously, the PAH emission data collected at 30 m from the CFM56-2C1, CFM56-3B series, CJ610-8ATJ, AE3007A1/1 and RB211-535E4-B engines under the four ICAO-specified engine thrusts representing idle (7%), takeoff (100%), climb (85%) and approach (30%) were used to investigate the effects of the LTO engine cycle. The data for the AE3007A1/1 engine collected at a rated thrust of 8.4 percent were used to represent the results of idle engine condition and compare with the data of the other engines at 7 percent rated thrust. The average emission index results derived from the PAH measurements were averaged for each of the four power levels and summarized in Table 11-5 for the individual engine types.

The PAH emission indices derived from the measurement data for the CFM56-2C, CFM56-3B, CFM56-7B24 and CJ610-8ATJ engines had a trend similar to the trend shown in Figure 11-37(a)-(c). The engines all showed lower PAH EI values when engine was at idle and approach and higher PAH EI values when the engines were at take-off and climb-out. Also, the CJ610-8ATJ had the highest PAH EI except at idle. Figure 11-37 also shows the PAH emissions from the AE3007A1/1 and PW4158 were affected differently by engine power. The AE3007A1/1 and PW4158 engines had the highest PAH emission index at idle, comparable to the PAH emission index observed at climb-out and take-off. The differences observed could have been caused by differences in engine technology or may simply be experimental errors as the large error bars in the figure suggest.

11.2.4 Effect of Engine Type

The average PAH emission indices obtained from the different engine types tested were compared in Figure 11-38. Only the data with the base fuel or fleet fuel and measured at the 30-m sampling location were presented here. The data for the Tests EPA-1 and NASA-1 of APEX-1 and Tests T1, T8 and T9 of APEX-3 were not used due to lack of response to changes in engine power as mentioned previously in Table 11-4. The data were the averages from the different tests of the same engines under each of the four ICAO engine power levels. The lowest rated thrust, 8.4 percent, for the engine AE3007A1E was used as idle condition and compared with the other engines at 7 percent rated thrust. For the P&W 4158 engine, the data available at 80 percent rated thrust were averaged and compared with the other engines at 85 percent rated thrust. No data were available at engine take-off (100% thrust) for the CFM56-7B24 and P&W 4158 engines. The PAH EI value for each engine was presented at the bottom of the bars. The fuel flow rate is also presented in the figure using the second y-axis. As before, the fuel flows shown only represent those periods with valid PAH data.

As was the case for BC, the figure shows that the CJ610-8ATJ turbojet which is the smallest engine had the highest PAH emission indices when this engine was run at approach, climb-out and take-off power. The CFM56-2C engine, on the other hand, had the lowest PAH emission indices at all thrust levels.

11.2.5 Effect of Cold and Warm Engine Conditions

The PAH emission index data under the cold engine condition were plotted against the indices obtained for the same engine type and the same engine power but under warm condition in Figure 11-39. The black dashed line in the figure represents where the emission indices under cold and warm conditions are identical. The figure also shows the linear regression results (see the pink line), indicating a slight reduction in the PAH emission indices after the engine was warmed up. These results are consistent with most of the other emission parameters measured during the APEX campaigns, such as the mass and BC EIs, which tended to be lower after engine warm up.

Table 11-5. PAH Emission Indices at the Four ICAO Engine Power Levels for Different Engines

Engine	Campaign and Tests	Engine Power	Average Fuel Flow	PAH	
				EI	SD
			(kg/h)	(mg/kg)	(mg/kg)
CFM56-2C1	APEX-1 EPA-2 & NASA-1a	Idle (7%)	419	0.0127	0.0325
		Takeoff (100%)	3151	0.319	0.0858
		Climb (85%)	2881	0.319	0.0366
		Approach (30%)	1023	0.00	0.000736
CFM56-7B24	APEX-2 T1 & T4	Idle (7%)	401	0.0814	0.0389
		Takeoff (100%)			
		Climb (85%)	4109	0.663	0.0514
		Approach (30%)	1158	0.0208	0.0502
CFM56-3B series	APEX-2 T2 &T3 APEX-3 T11	Idle (7%)	419	0.226	0.0361
		Takeoff (100%)	3564	0.617	0.184
		Climb (85%)	3465	1.05	0.0649
		Approach (30%)	1099	0.141	0.0228
CJ610-8ATJ	APEX-3 T5	Idle (7%)	227	0.0944	0.352
		Takeoff (100%)	1226	3.05	0.267
		Climb (85%)	1009	3.25	0.256
		Approach (30%)	452	1.43	0.137
AE3007A1/1	APEX-3 T10	Idle (8.4%)	178	1.03	0.601
		Takeoff (100%)	1175	0.954	0.0749
		Climb (85%)	976	0.847	0.0689
		Approach (30%)	371	0.591	0.0830
PW 4158	APEX-3 T9	Idle (7%)	532	0.946	0.492
		Takeoff (100%)			
		Climb (80%)	7088	0.985	0.0241
		Approach (30%)	2298	0.00853	0.0144
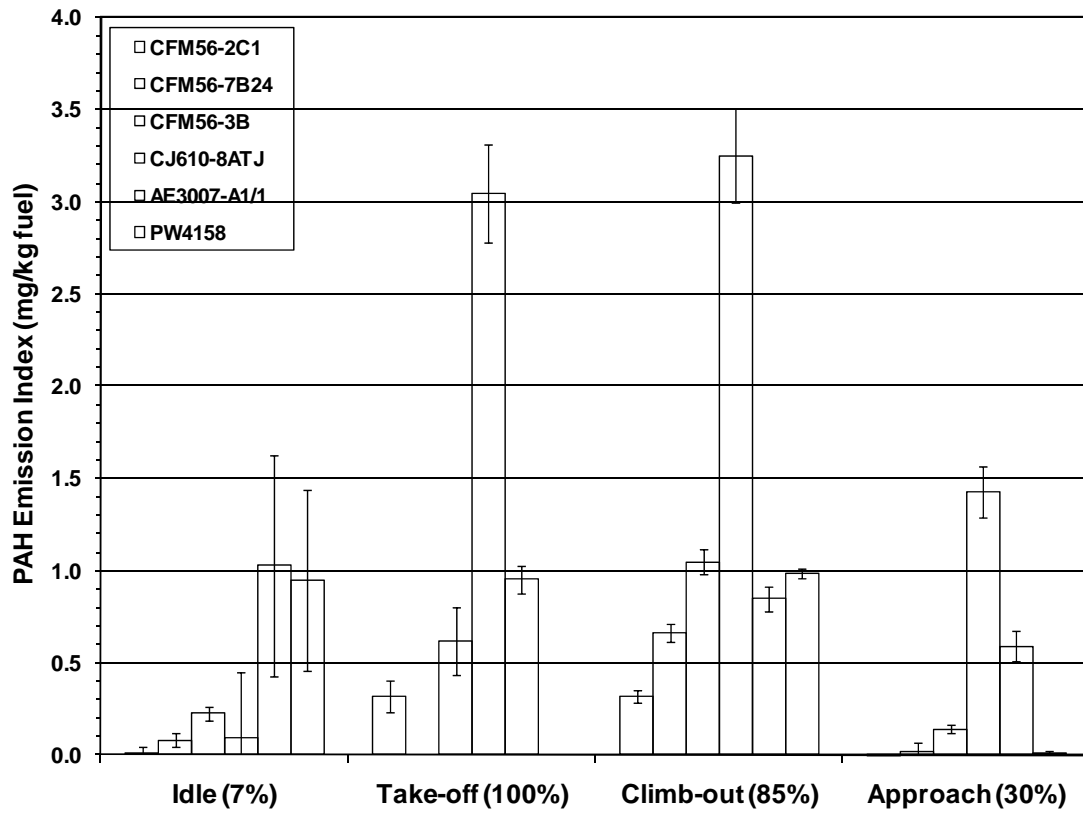
Figure 11-37. Effect of engine power on the PAH emission index for different engine types.
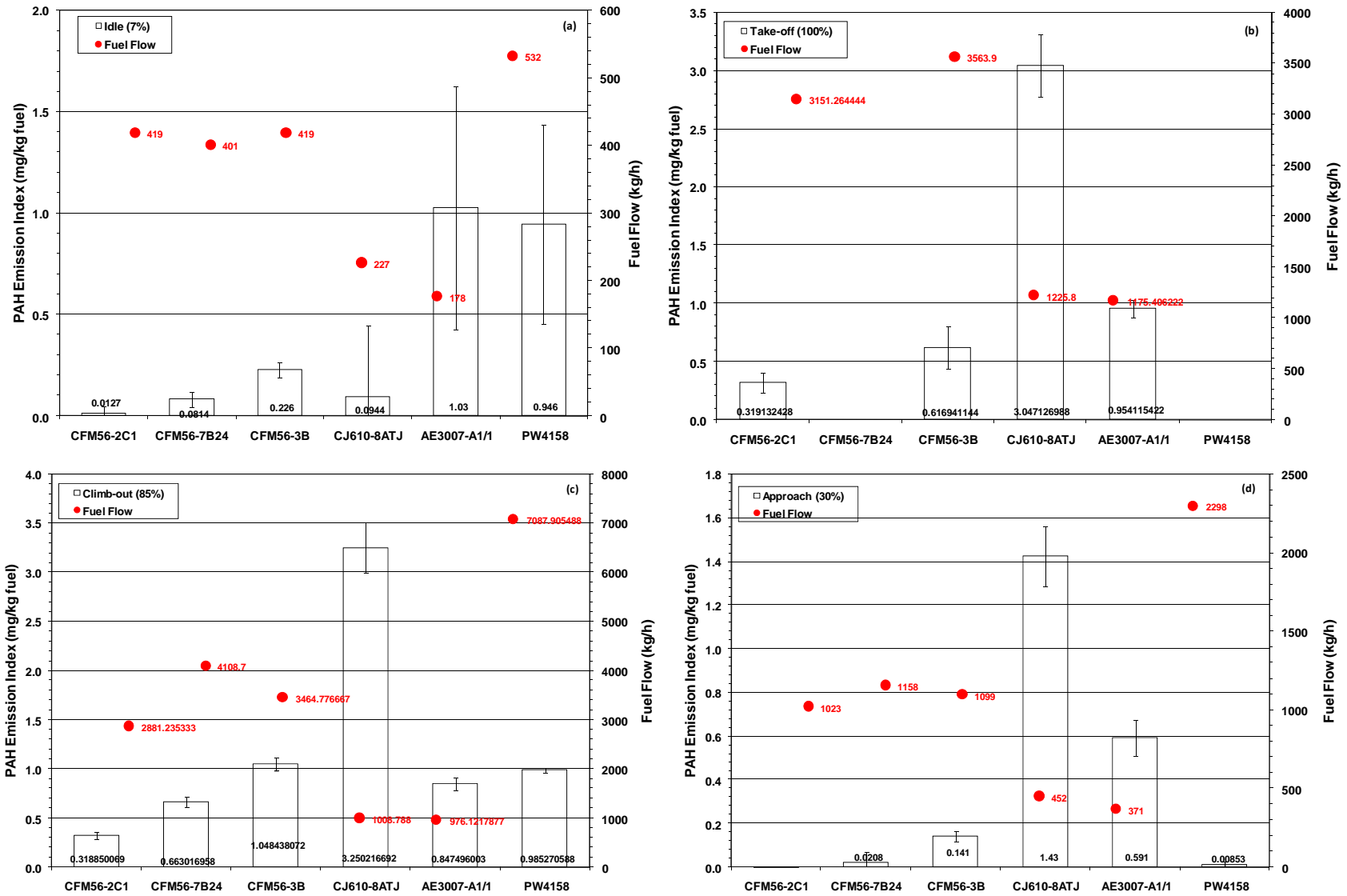
Figure 11-38. Effect of engine type on (a) idle, (b) take-off, (c) climb-out and (d) approach PAH emissions.
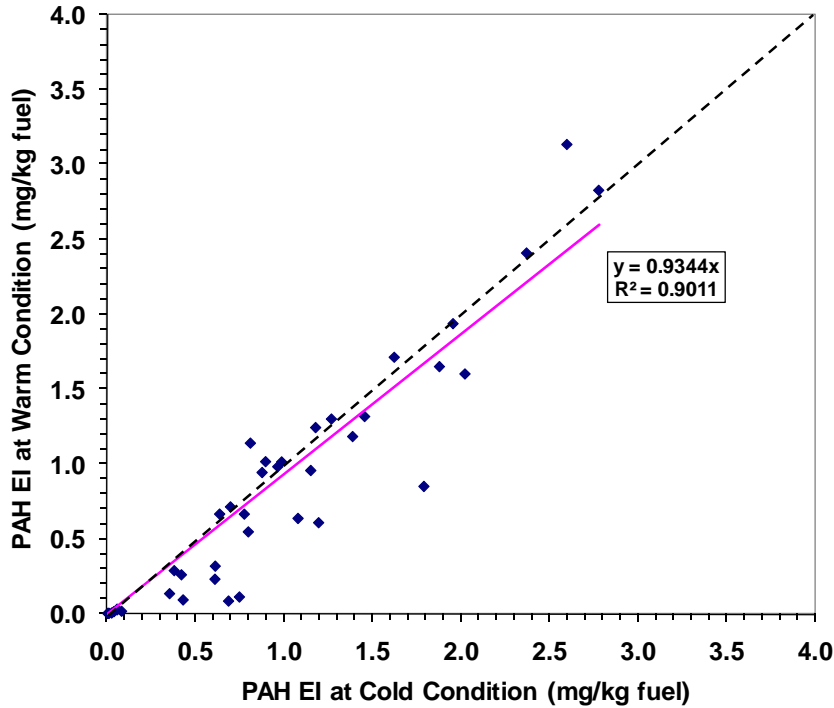
Figure 11-39. Effect of engine operating temperature on PAH emissions.

11.2.6 Effect of Probe Position

Emissions data were collected at both 15 m and 30 m locations in Test T5 of APEX-3 for the CJ610-8ATJ engine and at 30 m and 43 m in Test T8 of APEX-3 for the RB211-535E4-B engine. In the Test T5, the data were first collected at 15 m while the engine power increased step by step from 7, 30, 45, 65, 85 to 100 percent rated thrust, and then collected at 30 m with the engine power setting varied stepwise downward from 100 to 7 percent. The same experimental procedure was used in Test T8, but the rated thrust settings were 4, 7, 15, 30, 45, 65 and 85 percent. Again, the data for RB211 were deemed unreliable and are not presented here.

The PAH emission indices obtained from the different sampling positions for the CJ610-8ATJ engine were compared as shown in Figure 11-40. The results show that the PAH emission index obtained from the probe position farther from the engine was generally higher at higher fuel flows (thrust), suggesting that more particles with surface-bound PAHs were formed during plume transport from the gas phase. This observation is consistent with the previous discussion about more nuclei size particles being formed as the plume moves away from the engines. As discussed in Section 10, the GMD decreased and the GSD increased with probe distance due to the formation of more nuclei particles during plume processing in the near-field atmosphere.
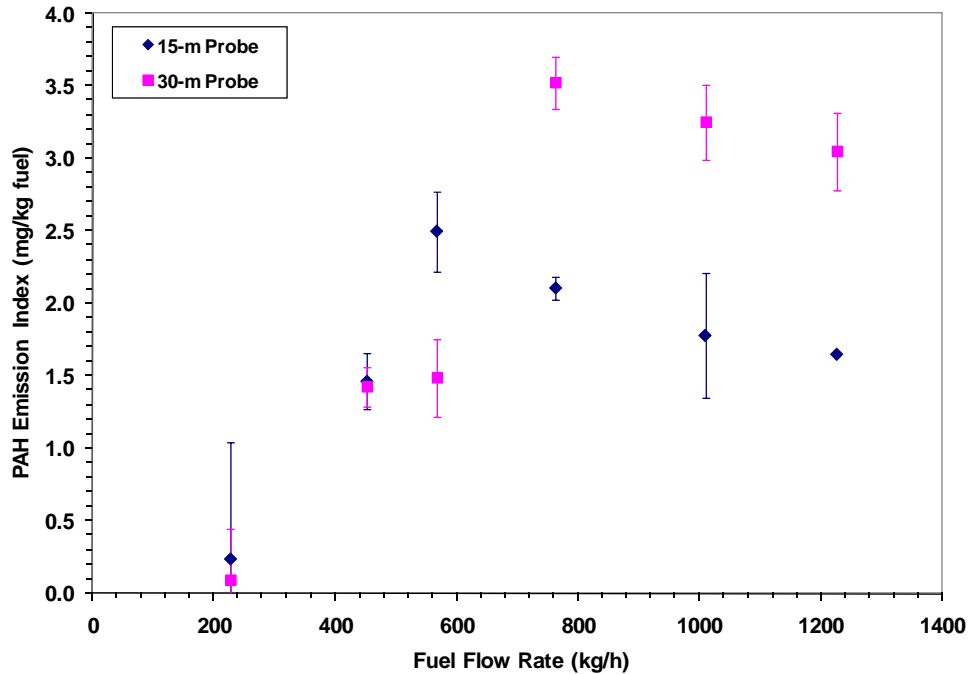
Figure 11-40. Effect of probe position on PAH emission index for the CJ610-8ATJ engine during APEX-3.

11.2.7 Test-Average PAH Emission Index

The test-average PAH emission indices for all the APEX tests are summarized in Table 11-6. By averaging the results of the same engines from different tests, Figure 11-41 compares the PAH emission indices of different engines when the base fuel or fleet fuels were used. The figure shows that the CJ610-8ATJ and AE3007A1 series engines had highest PAH emission indices. The CFM56 model engines, on the other hand, emitted the least particles with surface-bound PAHs. Note that the test-average emission index is an overall measure of the emissions for all power conditions. The red color points in the figure are the test-averaged fuel flow rates for individual tests, which were determined by the power log during the tests. A higher test-average PAH emission index with lower test-average fuel flow rate implies a poorer combustion efficiency for an engine over the range of power conditions evaluated.

Also shown for comparison in Table 11-6 are the equivalent PAH EIs obtained from the quartz filter time-integrated sampling. Table 11-6 shows that the two data sets somewhat agree for the CFM56 series engines during some tests, but not for the others. Of the data presented, the quartz filter data are considered to be underestimated due to the lack of information on the unresolved compounds by the GC-MS analysis, as discussed in Section 13.

Table 11-6. Comparison between the PAH Emission Indices Obtained by the PAS 2000 Measurements and the Quartz Filter Integrated Sampling

APEX	Test	Engine Model	Fuel	Average Fuel Flow (kg/h)	PAH Emission Index (mg/kg fuel)	
					PAS 2000[a]	Quartz filter analysis[b]
1	EPA-1*	CFM56-2C1	Base Fuel	785	Fail	
	EPA-2			770	0.0650	0.0696
	NASA-1*			635	Fail	
	NASA-1a			1559	0.225	
	EPA-3		Hi-Sulfur	797	Fail	0.104
	NASA-2			1279	Fail	
	NASA-3			1277	Fail	
	NASA-4		Hi-Aromatic	1197	0.0560	
	NASA-5			1244	0.0927	
2	T1	CFM56-7B24	Fleet	1264	0.196	0.00997
	T4			1264	0.253	
	T2	CFM56-3B series		1201	0.479	0.0243
	T3			1199	0.752	
3	T1*			1352	1.53	
	T11			1161	0.205	0.154
	T2	CJ610-8ATJ		618	1.67	
	T5			566	1.93	
	T3	AE3007A1E		523	1.94	0.123
	T4			554	1.94	
	T10	AE3007A1/1		550	0.802	
	T6	P&W 4158		2344	0.564	0.00807
	T7			2968	0.598	
	T8	RB211-535E		2087	Fail	
	T9			2473	Fail	0.179

* indicates the tests with high cross wind in background

a. The PAH EI data shown here were obtained from the measurement by the PAS 2000 with no background correction.

b. The quartz filter data shown here were after background and backup-filter correction.
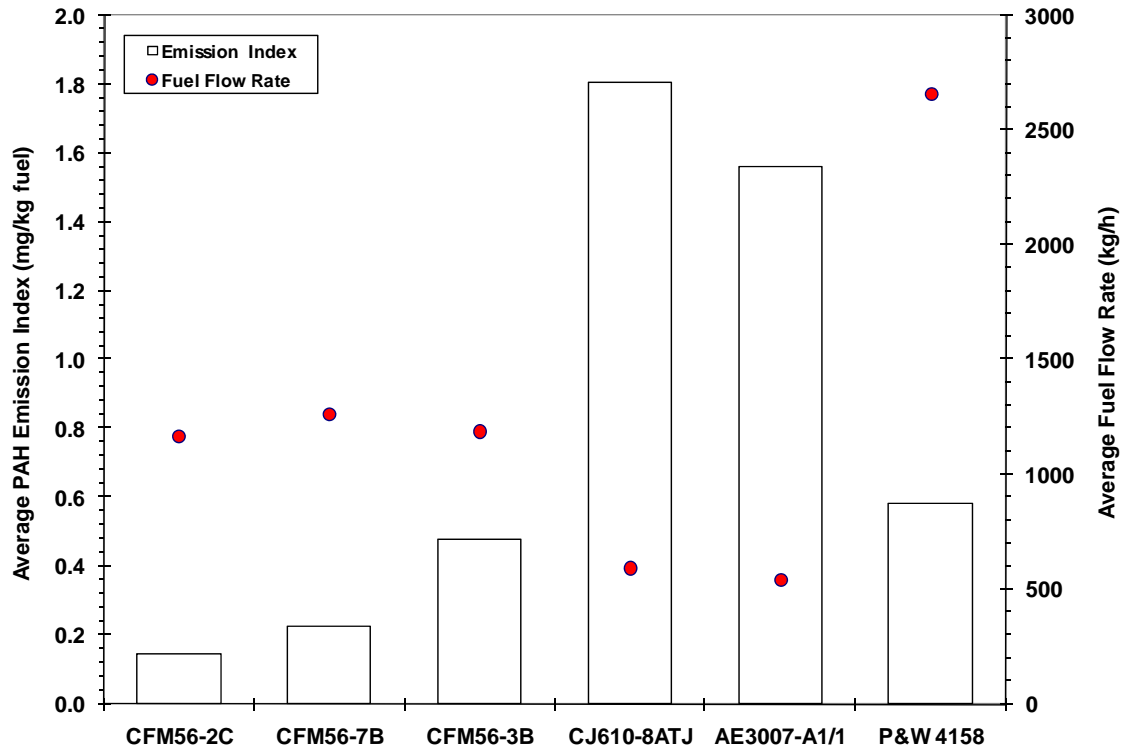
Figure 11-41. Comparison of the average PAH emission indices obtained from the tests with different types of jet engines.

12. Gas-Phase Chemical Composition

The gaseous emission samples were collected in both the plume and background sampling system during the APEX tests on a time-integrated basis using SUMMA canisters and DNPH cartridges. The samples were then analyzed by EPA Method TO-15 for analysis of the SUMMA samples and Method TO-11A for the DNPH samples. The analytical results from these plume and background samples were used to derive the background corrected EIs for the individual non-methane volatile organic compounds (NMVOCs) and carbonyls in the gaseous engine emissions. The test results used in investigating gaseous emissions from different engines in this section were: EPA-2 of APEX-1 for the CFM56-2C1, T1&4 of APEX-2 for the CFM56-7B24, T2&3 of APEX-2 for the CFM56-3B series, T3&4 of APEX-3 for the AE3007-A1E, T6&7 of APEX-3 for the P&W 4158, and T9 of APEX-3 for the RB211-535E4-B engine. The gaseous emissions from a total of six different engine types were studied here.

The emission indices of individual NMVOCs and carbonyl compounds obtained from the SUMMA and DNPH sampling for different engines are summarized in Table 12-1 and Figure 12-1, and Table 12-2 and Figure 12-2, respectively. Table 12-3 and Figure 12-3 compare the EI sums of VOCs and carbonyls for the different engines. The tables show that the P&W 4158 engine had emission indices of 703 mg/kg for NMVOCs and 729 mg/kg for carbonyls. These values are the highest among all the engines tested. The AE3007A1E engine produced the least amount of speciated gaseous pollutants and its emission indices were 258 mg/kg for NMVOCs and 287 mg/kg for carbonyls. Note that the ratio of NMVOCs to carbonyls was close to 1 for the CFM56-2C1, CFM56-7B24, CFM56-3B, AE3007-A1E, and P&W 4158 engines despite the difference in engine technology. The RB211-535E4-B engine, on the other hand, had higher NMVOC pollutants compared to carbonyls. The NMVOCs accounted for 57 percent of the total speciated gas phase pollutants for the CFM56-3B and 69 percent of the total gaseous pollutants for the RB211.

The individual gaseous compounds emitted from the six different engines are compared in Figure 12-4. The figure shows that the gaseous emissions primarily consisted of formaldehyde (EI = 120-360 mg/kg or 16-28 percent of total gaseous emissions), ethylene (41-246 mg/kg, 8-23%), acetaldehyde (38-126 mg/kg, 5-13%), acetylene (28-128 mg/kg, 5-15%), propylene (9-86 mg/kg, 2-8%), and glyoxal (0-112 mg/kg, 3-8%), with significant quantities of acrolein (0-38 mg/kg, <4%), benzene (0-25 mg/kg, <3%), 1,3-butadiene (2-31 mg/kg, <3%), and toluene (3-10 mg/kg, <1%). A slight difference in the speciated gaseous emissions was seen for the AE3007-A1E engine, which had no glyoxal in the emissions, but instead contained 15 percent acetone (82 mg/kg) and 6 percent ethane (33 mg/kg). Formaldehyde, acetaldehyde, benzene, acrolein, toluene, and 1,3-butadiene are some of the compounds considered as hazardous air pollutants by EPA in the Clean Air Act.

The above discussion was based on the gaseous compounds that were identified and quantified by the analytical instruments. Unresolved compounds made up about 16-42 percent of the total NMVOC (as

227

ppmC) and carbonyl (as formaldehyde) compounds shown by gas chromatography, depending on the engine tested.

Table 12-1. **Emission Indices of Individual VOCs Obtained by SUMMA Sampling for Different Engines**

Engine	CFM56-2C1	CFM56-7B24	CFM56-3B	AE3007A1E	P&W 4158	RB211-535E4B
APEX	APEX-1	APEX-2	APEX-2	APEX-3	APEX-3	APEX-3
Test	EPA-2	T1&4	T2&3	T3&4	T6&7	T9
Gaseous Compound	mg/kg	mg/kg	mg/kg	mg/kg	mg/kg	mg/kg
Ethylene	219	92.7	123	40.6	246	194
Acetylene	103	107	119	28.3	105	128
Ethane		9.05	10.8	32.8	15.0	10.7
Propylene	66.4	75.4	86.3	8.99	86.8	61.7
Propane		2.53	2.09	25.9	0.944	1.10
Isobutane		0.0778	0.265	6.23		
Isobutene/1-Butene	18.1	23.3	31.1		32.1	20.9
n-Butane			0.316	15.4		
trans-2-Butene	1.44	2.53	2.67		2.68	1.86
cis-2-Butene	1.15	1.62	1.95		2.63	2.01
3-Methyl-1-butene		0.453	0.845		2.99	1.98
Isopentane		2.94	2.12	8.28		
1-Pentene	6.62	5.53	8.08		11.4	6.05
2-Methyl-1-butene	2.69	2.61	1.38		3.04	1.91
n-Pentane		2.90		5.48	0.270	0.539
Isoprene		3.81	2.44		0.274	
trans-2-Pentene	1.31	0.978	0.880		1.51	1.00
cis-2-Pentene		0.731	0.867		0.844	0.613
2-Methyl-2-butene		0.453	0.786		0.328	
2,2-Dimethylbutane	2.82	0.908	2.96		0.109	
Cyclopentene	0.655	1.28	1.49			
4-Methyl-1-pentene	1.15	1.30			1.73	1.52
Cyclopentane			0.0564	0.547	0.0912	
2,3-Dimethylbutane		0.0362	0.0113			
2-Methylpentane	0.884			2.98		
3-Methylpentane				2.63		
2-Methyl-1-pentene	0.917	0.435	0.421		0.698	0.466
1-Hexene	2.88	4.99	5.08	0.145	7.98	5.34

228

Engine	CFM56-2C1	CFM56-7B24	CFM56-3B	AE3007A1E	P&W 4158	RB211-535E4B
APEX	APEX-1	APEX-2	APEX-2	APEX-3	APEX-3	APEX-3
Test	EPA-2	T1&4	T2&3	T3&4	T6&7	T9
Gaseous Compound	mg/kg	mg/kg	mg/kg	mg/kg	mg/kg	mg/kg
n-Hexane				2.41		
trans-2-Hexene		0.398	0.475		0.567	0.441
cis-2-Hexene			0.452	3.62	34.6	58.6
Methylcyclopentane				1.01	0.301	
2,4-Dimethylpentane	0.557					
Benzene		25.5	22.5	5.54	24.7	21.9
Cyclohexane					0.483	
2-Methylhexane			0.0564	1.23	0.604	0.588
2,3-Dimethylpentane			0.564		0.310	
3-Methylhexane			1.03	1.21		
1-Heptene		3.31	3.27		4.07	2.33
n-Heptane		0.290	0.684	4.68	2.61	2.13
Methylcyclohexane		0.409	0.391	0.994	2.52	0.809
2,3,4-Trimethylpentane			0.285			
Toluene	2.88	8.19	9.80	2.87	9.57	6.30
2-Methylheptane		0.525	0.933		1.52	
3-Methylheptane		1.03	1.11		0.766	
1-Octene		1.83	1.24			
n-Octane	0.0655	1.69	1.86		4.11	0.882
Ethylbenzene		2.22	2.36	0.603	2.57	1.25
Styrene	3.47	4.59	4.49		3.34	2.23
o-Xylene		2.95	2.72	0.704	2.49	0.34
1-Nonene	1.41	2.02	1.92		2.50	1.40
n-Nonane	0.197	1.65	2.02	0.905		
Isopropylbenzene			0.27			
α-Pinene	0.917	0.416	2.99			
n-Propylbenzene		1.06	1.38		1.20	0.466
m-Ethyltoluene	0.622	2.22	2.57	0.402	4.60	2.03
p-Ethyltoluene		1.15	1.49		2.33	0.294
1,3,5-Trimethylbenzene	0.557	0.49	1.39	0.402	3.45	
o-Ethyltoluene		1.79	2.15	0.453	1.32	
1,2,4-Trimethylbenzene	1.08	5.57	6.05		9.46	3.63
n-Decane	0.557	4.17	1.48			

Engine	CFM56-2C1	CFM56-7B24	CFM56-3B	AE3007A1E	P&W 4158	RB211-535E4B
APEX	APEX-1	APEX-2	APEX-2	APEX-3	APEX-3	APEX-3
Test	EPA-2	T1&4	T2&3	T3&4	T6&7	T9
Gaseous Compound	mg/kg	mg/kg	mg/kg	mg/kg	mg/kg	mg/kg
1,2,3-Trimethylbenzene		2.00	2.36		2.84	0.809
m-Diethylbenzene		0.779	0.508		1.07	1.27
p-Diethylbenzene		0.435	0.582		1.41	0.466
1-Undecene					1.84	0.882
n-Undecane	2.10	3.60	2.81		10.1	3.82
1-Dodecene		1.68			3.08	1.20
n-Dodecane		2.37	1.42		5.49	1.89
n-Tridecane					2.06	
Dichlorodifluoromethane		0.272	0.0564	18.7		
Chloromethane		0.349	0.182	6.34		
Dichlorotetrafluoroethane				0.704		
1,3-Butadiene	7.11	24.6	30.6	1.69	25.3	18.4
Acrolein		30.0	37.6			
Trichlorofluoromethane		0.109		10.8		
Acrylonitrile		0.634				
Dichloromethane		0.836	0.0790	1.06		
Trichlorotrifluoroethane				5.03		
1,1,1-Trichloroethane				0.805		
Carbon Tetrachloride	1.87	0.198		5.67	0.147	0.294
m,p-Xylene		4.90	7.15	1.56	8.08	2.25
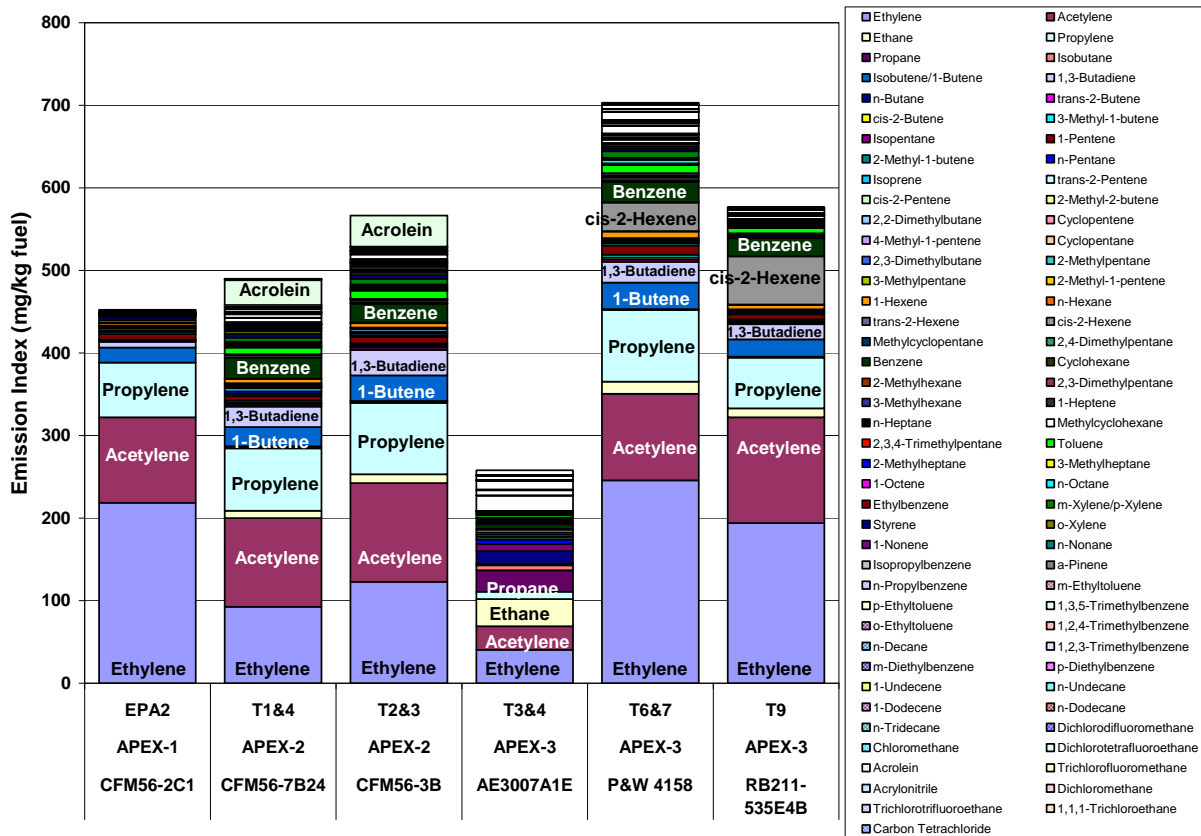
Figure 12-1.   Mass EIs of individual NMVOCs from SUMMA canister sampling.

Table 12-2. Emission Indices of Individual Carbonyl Compounds Obtained by DNPH Sampling for Different Engines

Engine	CFM56-2C1	CFM56-7B24	CFM56-3B	AE3007A1E	P&W 4158	RB211-535E4B
APEX	APEX-1	APEX-2	APEX-2	APEX-3	APEX-3	APEX-3
Test	EPA-2	T1&4	T2&3	T3	T6&7	T9
Gas Compound	mg/kg	mg/kg	mg/kg	mg/kg	mg/kg	mg/kg
Formaldehyde	268	232	231	117	357	130
Acetaldehyde	90.3	95.8	76.4	69.8	126.4	38.3
Acetone	11.4	16.8	1.61	82.4		
Propionaldehyde	7.37	10.4	9.55	7.81	16.6	6.64
Crotonaldehyde	21.7	19.7	20.7		26.8	10.41
Butyraldehyde	3.11	5.26	4.22	4.86	2.70	
Benzaldehyde	13.5	10.2	10.0		14.0	7.18
Isovaleraldehyde	2.14	0.670	0.811		2.43	
Valeraldehyde	6.94	3.48	4.57		6.13	3.01
o-Tolualdehyde		3.57	4.77		6.45	2.60
m-Tolualdehyde	7.04	3.85	5.42		9.33	3.01
p-Tolualdehyde	3.24	1.20	1.30		3.14	
Hexaldehyde	0.118	1.92	2.41		4.72	2.09
2,5-Dimethylbenzaldehyde	4.72	0.986				
Diacetyl	1.71					
Methacrolein	11.8	9.73	7.56		11.4	3.06
2-Butanone		5.35	3.86	5.12	4.36	
Glyoxal	29.8	44.8	40.2		112	40.7
Acetophenone	12.4					3.95
Methylglyoxal	25.2	7.00	5.01		23.7	9.80
Octanal		1.57	2.63		0.811	
Nonanal		3.83			0.568	2.65
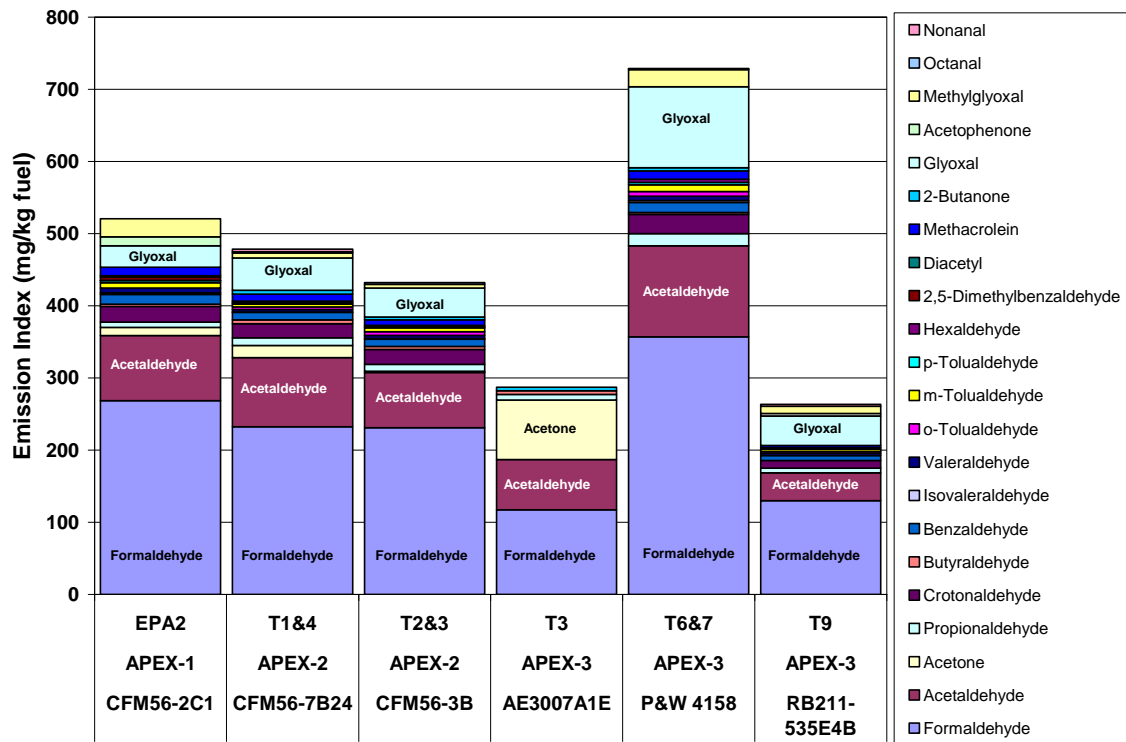
Figure 12-2. Mass EIs of individual carbonyl compounds from DNPH cartridge sampling.

Table 12-3. Comparison of NMVOC and Carbonyl Emission Indices for Different Engines

Test		EPA-2	T1&4	T2&3	T3&4	T6&7	T9
APEX		APEX-1	APEX-2	APEX-2	APEX-3	APEX-3	APEX-3
Engine		CFM56-2C1	CFM56-7B24	CFM56-3B	AE3007A1E	P&W 4158	RB211-535E4B
NMVOCs	mg/kg	452	490	567	258	703	577
Carbonyls	mg/kg	521	479	432	287	729	263
NMVOCs	%	46.5	50.6	56.7	47.3	49.1	68.7

233
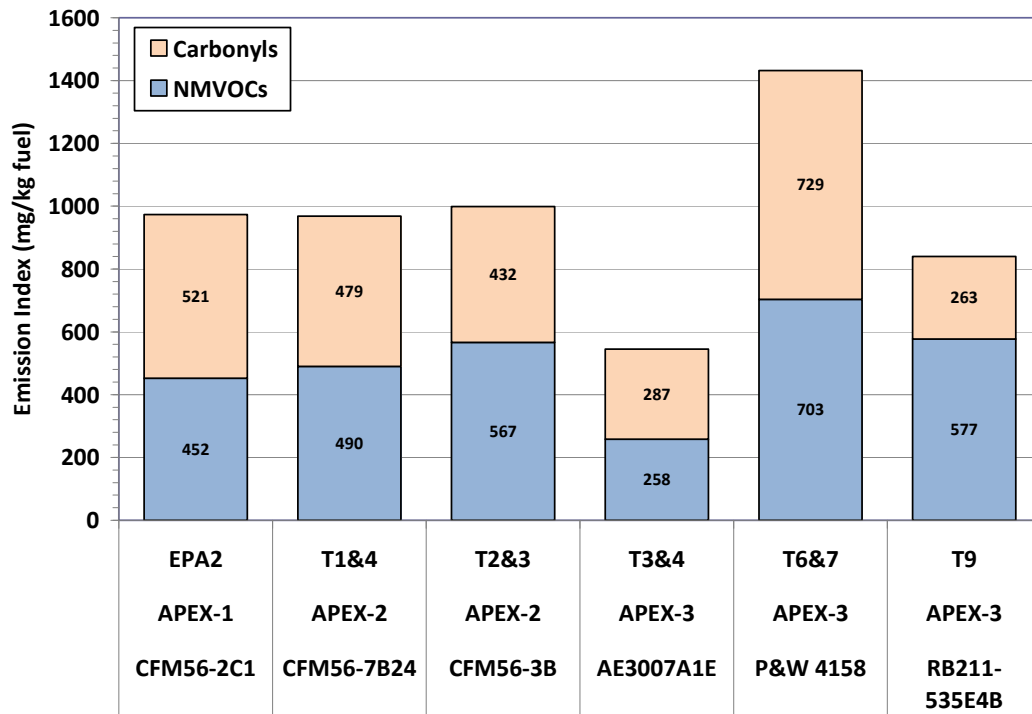
Figure 12-3. Emission indices of total NMVOCs and carbonyls for different engines.
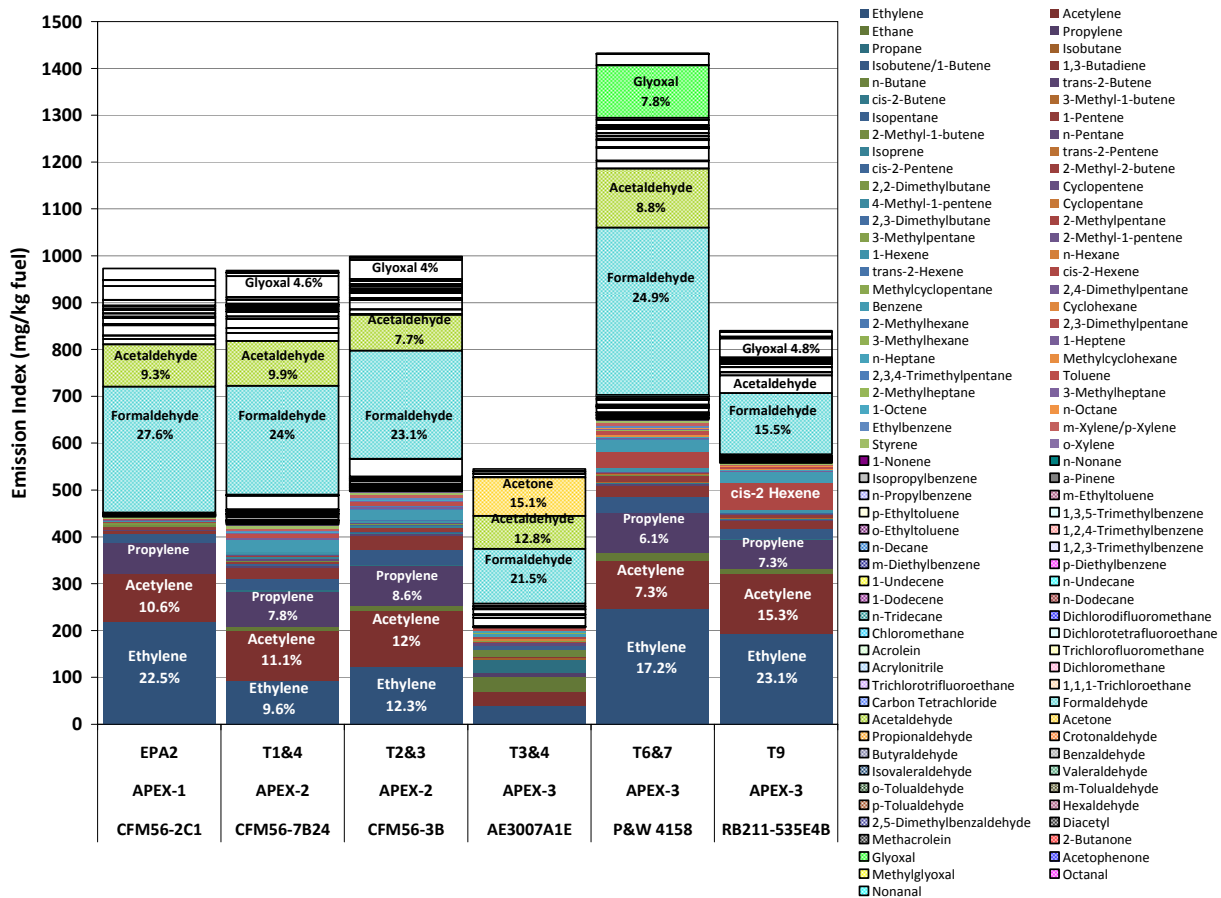
Figure 12-4. Comparison of EIs for individual gas phase species as produced by different engine types.

This page intentionally left blank.

13. Particle-Phase Chemical Composition

The PM-phase chemical composition discussed in this study includes the inorganic elements and ions, elemental carbon, organic carbon, and organic compounds determined by analyzing the Teflon and quartz filter samples collected from the time-integrated sampling. Like the discussion of black carbon and PAH emissions, the emission indices reported here are without correction for sampling line particle losses because the fraction of species of the PM lost in the sampling line could not be determined from available data. Summary tables of experimental results for PM speciation and element EI can be found in Tables H-1 and H-2, respectively, in Appendix H.

13.1 Element and Ion Emissions

The Teflon filter samples were first subjected to trace elemental analysis by X-ray fluorescence (XRF). The samples were then extracted with HPLC-grade deionized water and the extracts were analyzed by ion chromatography (IC) for determination of sulfate, nitrate, and chloride in the PM collected on the filters. The Teflon filters were installed in both plume and background sampling systems, so that the background-corrected concentrations and emission indices for individual elements and ions were obtained for each test. The tests in this study for which the XRF and IC analyses were conducted are EPA-1, EPA-2, EPA-3 and NASA-4&5 of APEX-1, T1 to T4 of APEX-2, and T3&4, T6&7, T9, and T11 of APEX-3. In calculation of the element emission indices from the XRF analytical results, the reported uncertainties were used. Thus, the elements which had detected concentrations either less than their detection limits or less than three times their uncertainties were not reported.

Although integrated filter sampling was conducted in the APEX-1 EPA-1 test, the results from this test were not used in the discussion of this section because of high background interference by crosswinds during this test. Furthermore, the total element and ion concentrations on the background Teflon filter for the APEX-3 T6&7 were extremely high. Since the PM mass collected on the background Teflon filter for this test was low (-0.016 mg), that filter may have been contaminated either in the field or in the laboratory. Therefore, this test was also excluded in the element and ion emission discussion.

Various trace elements in the PM emissions are considered to originate from the presence of these elements in fuels, lubricating oils, engine wear and corrosion, sampling line, and fugitive dust. Table 13-1 summarizes the total emission index of elements derived from the XRF analysis for each test. The engine type, fuel sulfur content, and test-average rated thrust and fuel flow rate are also presented in the table. The emission indices for individual elements are presented in stacked column format for each test in Figure 13-1. The blue columns in the figure represent the sulfur in PM, which clearly was the most abundant element for all the tests. The samples of APEX-2 T1 test contained notable amounts of Si, probably due to dust contamination resulting from the resuspension of concrete cuttings left over from the drilling of holes in the tarmac.

Table 13-1.   Total Elemental Emission Index Derived from the XRF Analyses

APEX	Test	Engine	Fuel Sulfur (ppm)	Time-weighted Engine Power[a] (%)	Fuel Flow (kg/h)	Total Metal Emission Index (mg/kg fuel)
1	EPA-2	CFM56-2C1	409	18.8	770	10.8
	EPA-3		1639	20.4	797	27.5
	NASA-4&5		553	35.7	1221	12.0
2	T1	CFM56-7B24	132	30.1	1264	6.33
	T4		412	30.1	1264	13.5
	T2&3	CFM56-3B series	279	31.0	1200	10.1
3	T11		400	31.1	1161	12.8
	T3&4	AE3007A1E	300	41.1	537	7.51
	T9	RB211-535E4-B	300	34.2	2473	6.92

[a] Time-weighted average (TWA) thrust calculated over entire test period.
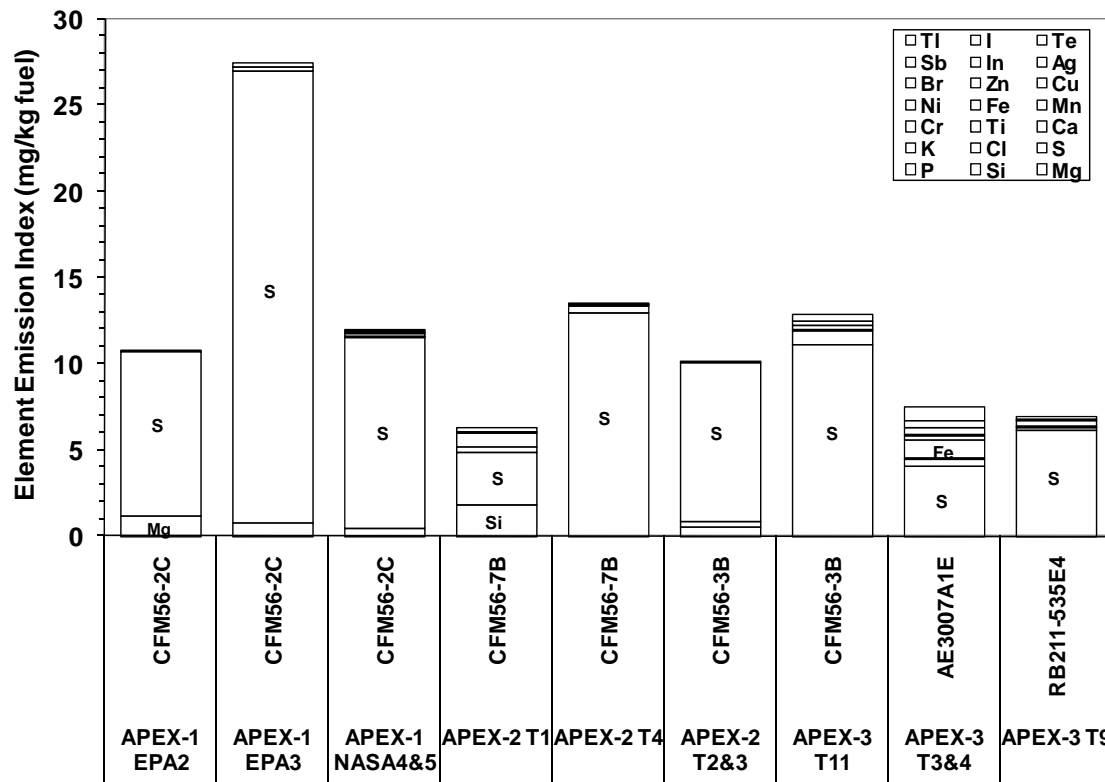
Figure 13-1.   Elemental emission indices for each test.

The results of the tests with the same engine and same fuel were averaged and the elemental emissions from different engines compared in Table 13-2 and Figure 13-2. The element emission indices for different engines were obtained with base fuel or fleet fuel and were plotted in stacked columns in the figure. The results show that the total element emissions produced from the CFM56 engines were relatively higher than the total element emissions from the AE3007-A1E and RB211-535E4-B engines. The table shows that about 2 to 7 percent of the total PM mass were the elements for these engines. The mass percentage of sulfur in the total elements detected for each test was also provided in the figure, indicating that over 80 percent of the elemental mass was sulfur for all five engines compared except for the AE3007A1E engine (54% sulfur).

Table 13-2. Elemental Emission Indices for Different Engines

Engine	Time-Weighted Engine Power[a] (%)	Fuel Flow (kg/h)	PM EI (mg/kg)	Total Metal EI (mg/kg)	Metal/PM (%)	Sulfur EI (mg/kg)	S/Metal (%)
CFM56-2C1	18.8	770	305	10.8	3.54	9.54	88.3
CFM56-7B24	30.1	1264		9.94		8.05	81.0
CFM56-3B	31.0	1200	267	11.5	4.30	10.1	88.4
AE3007A1E	41.1	537	116	7.51	6.48	4.03	53.7
RB211-535E4-B	34.2	2473	384	6.92	1.80	6.15	88.9

a. TWA calculated for all tests conducted.
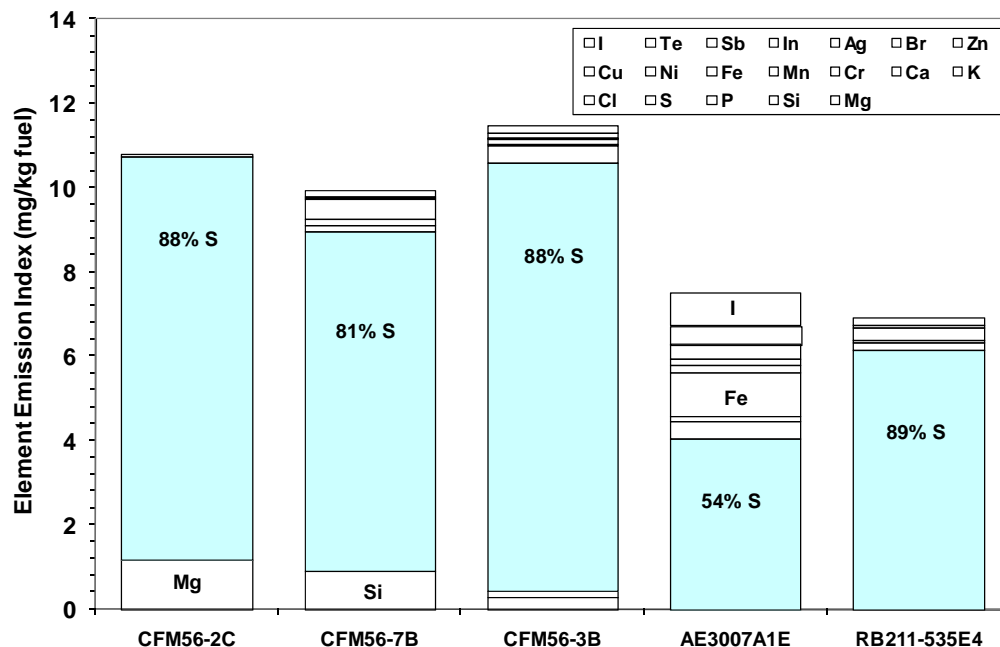
Figure 13-2.   Comparison of elemental emission indices for different engines.

239

The sulfur detected in PM samples originated from the jet fuels used in the tests. Therefore the high-sulfur fuel was expected to produce a higher elemental sulfur emission index. Table 13-3 provides the sulfur emission index results and the sulfur contents in the fuels. Table 13-3 indicates that the primary element in the PM emissions was sulfur regardless of fuel type. The sulfur content in the total detected elements was 88 percent for base fuel (APEX-1 EPA2), 95 percent for high sulfur fuel (APEX-1 EPA3), and 93 percent for high aromatic fuel (APEX-1 NASA-4&5). The sulfur emission index for high sulfur fuel was 26.2 mg/kg, which was 2.3 times as much for high aromatic fuel and 2.7 times as much for base fuel. It is not surprising that the high sulfur fuel had the highest sulfur emission index. The conversion of fuel sulfur into particulate was also calculated and presented in the table, indicating that about 2 to 3 percent of fuel sulfur was converted into sulfate as part of particulate matter emissions. By plotting the sulfur emission indices derived from the XRF analytical results for the CFM56 engines as a function of fuel sulfur content, Figure 13-3 shows that the correlation between the emission index of sulfur in PM and the fuel sulfur content can be approximately expressed by a linear equation with a correlation coefficient (r^2) of 0.93.

The water soluble ion emission indices derived from the IC analysis of the Teflon filter samples for various tests are presented in Table 13-4 and Figure 13-4. Four ions, K^+, NH_4^+, Cl^-, and SO_4^{-2}, were reported, of which SO_4^{-2} and NH_4^+ were the two primary inorganic ions comprising 90 percent of the total ion mass. The table also presents the S(IV) to S(VI) conversion calculated from the known amount of sulfur in fuel and the measured sulfate EI. Also shown for comparison in Table 13-4 are similar results from the European PartEmis program (Katragkou et al., 2004) and the landmark study by Schumann et al. (2002). The IC results show that approximately two to four percent of the sulfur in the fuel was converted to water soluble particulate sulfate, consistent with the data of Katragkou et al. (2004) and Schumann et al. (2002). Also, comparing this value to the sulfur conversion values shown in Table 13-3, the fuel sulfur conversion efficiency determined by IC was either slightly more or less than that measured by XRF, indicating differences in the two analytical methods.

Table 13-5 and Figure 13-5 compare the average EIs of individual ions among five different engines. The total ion emission indices for all five engines range from 30-40 mg/kg fuel. For the three CFM56 engines, SO_4^{-2}, had about 71 percent of total ion mass. The AE3007-A1E and RB211-535E4-B engines had 63 and 53 percent SO_4^{-2}, respectively.

Table 13-6 presents the SO_4^{-2} ion EIs obtained for the CFM56 engine with different fuel compositions. Like sulfur detected by XRF, the emission index of SO_4^{-2} was linearly correlated to the sulfur content in fuel as shown in Figure 13-6. The relation between SO_4^{-2} EI and fuel sulfur content can be approximately described by a linear equation with an r^2 of 0.90.

Table 13-3. **Sulfur Emission Indices for Individual Tests as Determined from the XRF Analyses and Their Associated Fuel Sulfur Contents**

APEX	Test	Engine	Sulfur in Fuel (ppm)	Sulfur EI (mg/kg)	S/Metal (%)	Sulfur Conversion (%)
1	EPA2	CFM56-2C1	409	9.54	88.3	2.33
	EPA3		1639	26.2	95.3	1.60
	NASA-4&5		553	11.2	93.3	2.02
2	T1	CFM56-7B24	132	3.11	49.1	2.35
	T4		412	13.0	95.9	3.15
	T2&3	CFM56-3B series	279	9.21	91.2	3.30
3	T11		400	11.1	86.3	2.77

$y = 0.0136x + 4.4952$
$R^2 = 0.9258$
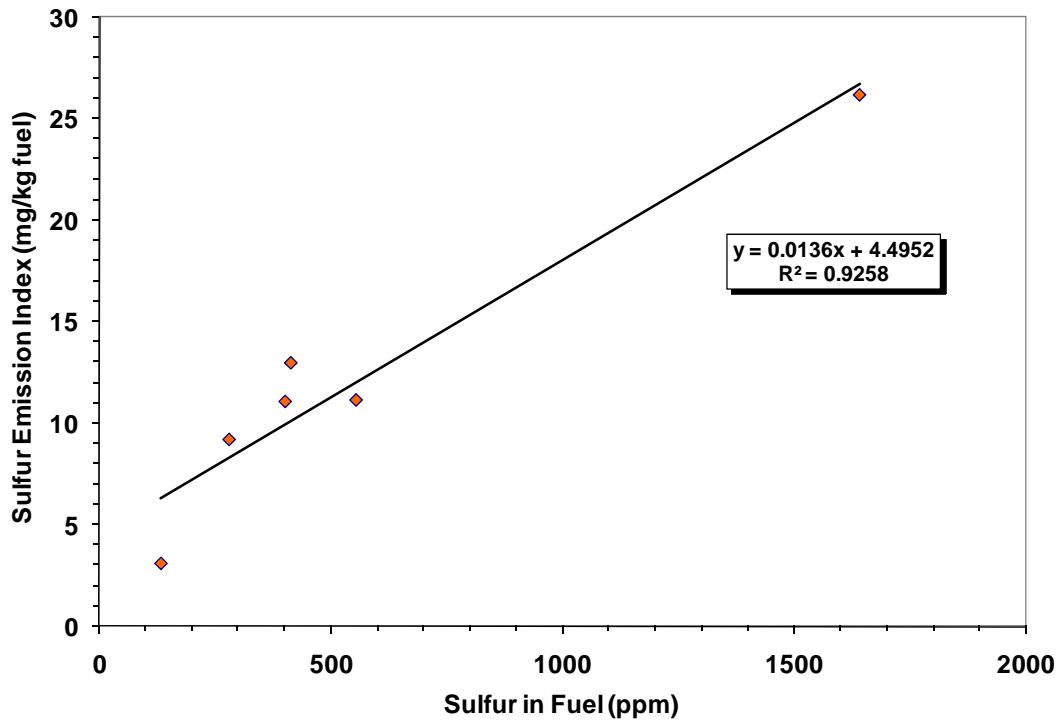
Figure 13-3. **Correlation of sulfur emission index with fuel sulfur content for CFM56 engines.**

Table 13-4. Water Soluble Ion Emission Indices Derived from the IC Analyses for Each Test

APEX	Test	Engine	Fuel Sulfur (ppm)	Time-Weighted Engine Power (%)	Time-Weighted Fuel Flow (kg/h)	Emission Indices					Sulfur Conversion (%)
						Total Ions (mg/kg)	K (mg/kg)	NH$_4$ (mg/kg)	Cl (mg/kg)	SO$_4$ (mg/kg)	
1	EPA2	CFM56-2C1	409	18.8	770	29.4	2.98	5.46		20.9	1.71
	EPA3		1639	20.4	797	86.0	5.54	10.5		69.9	1.42
	NASA-4&5		553	35.7	1221	40.0	1.91	5.69		32.4	1.95
2	T1	CFM56-7B24	132	30.1	1264	25.8		8.51		17.3	4.37
	T4		412	30.1	1264	53.0		13.8		39.2	3.17
	T2&3	CFM56-3B series	279	31.0	1200	36.5	2.38	6.69		27.4	3.28
3	T11		400	31.1	1161	42.0		13.6		28.4	2.37
	T3&4	AE3007-A1E	300	41.1	537	40.7		15.1		25.6	2.85
	T9	RB211-535E4-B	300	34.2	2473	31.8	3.85	8.24	3.01	16.7	1.86
PartEmis (Katragkov et al., 2004)											2.30[a]
Schumann et al., 2002											3.30[b]

[a] Low pressure stage of combustor + hot end simulator at modern cruise power.

[b] CFM56-3B1 engine at cruise altitude.
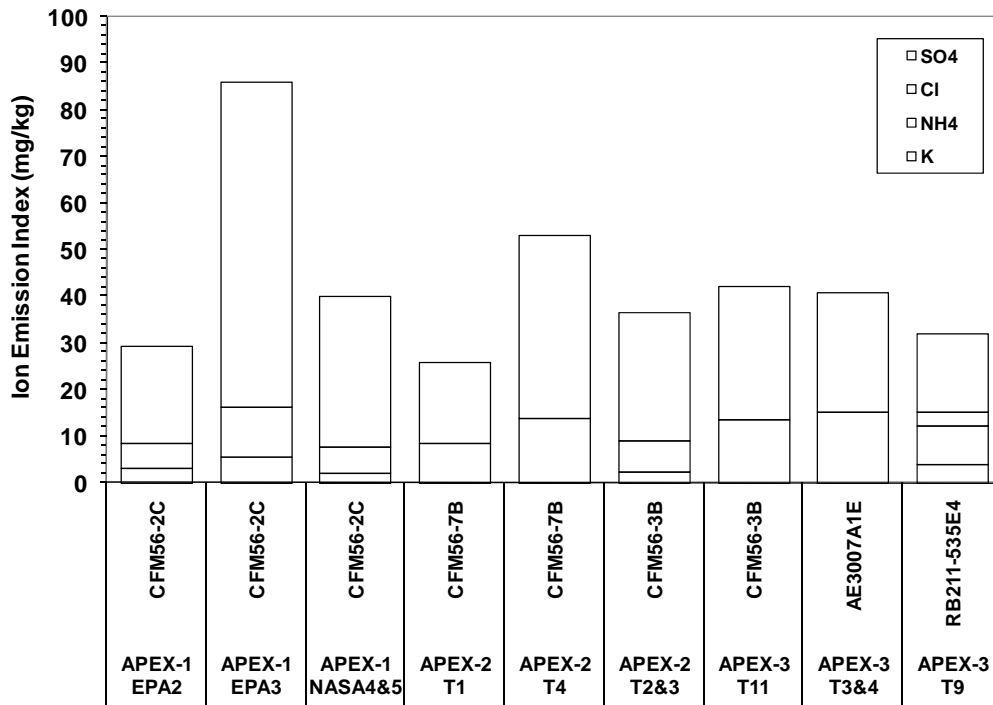
Figure 13-4.   Water-soluble ion emission indices for each test.

Table 13-5.   Water Soluble Ion Emission Indices for Different Engines

Engine	Power[a] (%)	Fuel Flow[a] (kg/h)	PM EI (mg/kg)	Total Ion EI (mg/kg)	Ions/PM (%)	SO$_4$ EI (mg/kg)	SO$_4$/Ions (%)
CFM56-2C1	18.8	770	305	29.4	9.64	20.9	71.3
CFM56-7B24	30.1	1264		39.4		28.3	71.7
CFM56-3B	31.0	1200	267	39.3	14.7	27.9	71.2
AE3007-A1E	41.1	537	116	40.7	35.2	25.6	62.9
RB211-535E4-B	34.2	2473	384	31.8	8.29	16.7	52.6

[a] TWA calculated for all tests conducted.
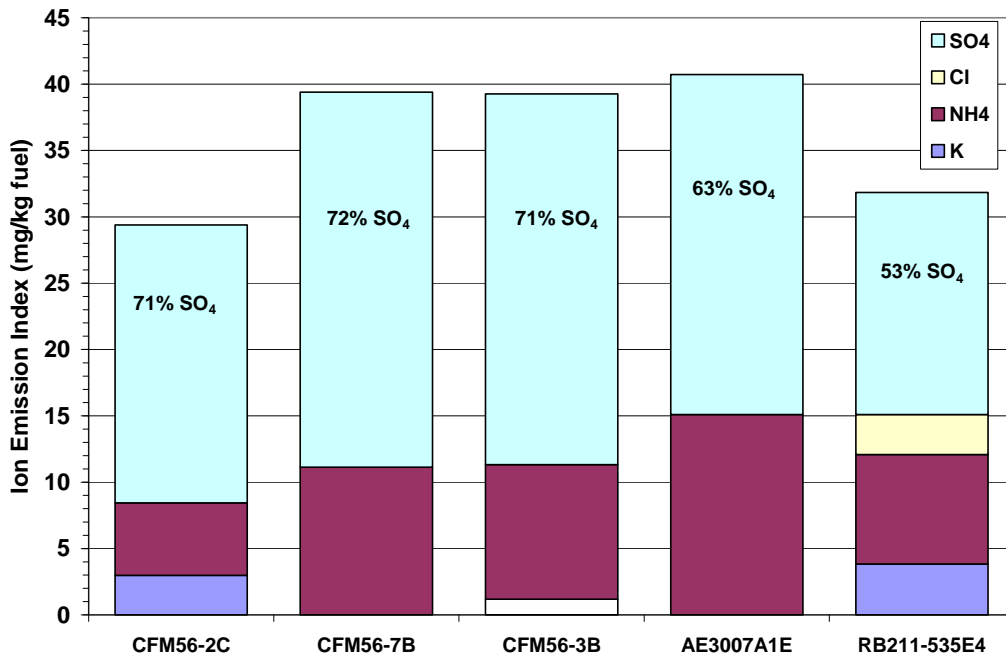
Figure 13-5.   Comparison of water-soluble ion emission indices for different engines.

Table 13-6.   Sulfate Emission Indices from the IC Analyses and Their Fuel Sulfur Contents

APEX	Test	Engine	Fuel Sulfur (ppm)	SO_4 EI (mg/kg)	S/Ions (%)
1	EPA2	CFM56-2C1	409	20.9	71.3
	EPA3		1639	69.9	81.3
	NASA-4&5		553	32.4	81.0
2	T1	CFM56-7B24	132	17.3	67.0
	T4		412	39.2	74.0
	T2&3	CFM56-3B series	279	27.4	75.2
3	T11		400	28.4	67.7
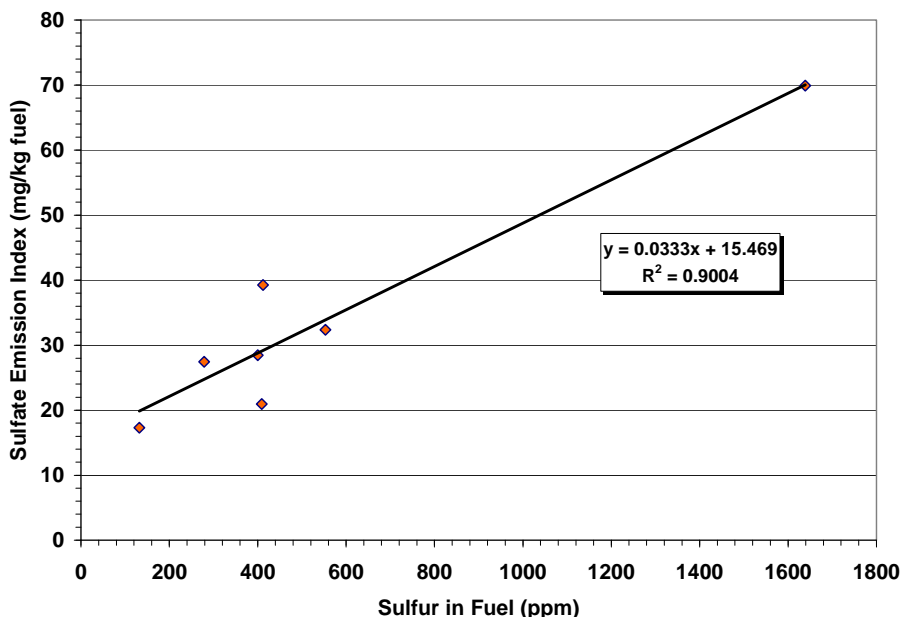
Figure 13-6.   Correlation of SO_4 emission index with fuel sulfur content for CFM56 engines.

13.2 Organic and Elemental Carbon Emissions

The quartz filters collected from the integrated sampling were first analyzed by the EC/OC analyzer to determine the organic and elemental carbon content in the PM samples, and then analyzed by GC/MC to determine the semivolatile organic compounds in PM. Accurate collection and determination of particulate organic material on quartz filters was complicated by the fact that gas phase organic compounds may be adsorbed by the quartz filters during sampling, resulting in overestimate of the actual concentrations. This sampling artifact was accounted for by placing a backup quartz filter(s) behind the Teflon filter in the sampling array using an approach developed by Turpin et al. (1994). No artifact correction was made for

the Teflon filters. The organic carbon was then obtained by subtracting the amount of OC found on the quartz filter located downstream of the Teflon filter from the amount found on the primary quartz filter. The elemental carbon is always considered as non-volatile particulate, and therefore no backup filter correction was needed in the elemental carbon emission index calculation. Like Teflon filter sampling, the quartz filters were installed in both the plume and background systems so that the background could be corrected. For comparison, the emission indices of OC and semivolatile organic compounds were reported both with background and backup correction and with only the background corrected.

Table 13-7 summarizes the results of organic and elemental carbon emission indices derived from the analysis of quartz filter samples. The tests shown are EPA-3, NASA-2&3, and NASA-4&5 for APEX-1; T1, T4 and T2&3 for APEX-2; and T3&4, T9 and T11 for APEX-3. For the EPA-2 test, both plume front and background quartz filters were found broken. Therefore the EPA-2 plume quartz filter samples were not analyzed for organic and elemental carbon content. However, these samples were solvent-extracted and analyzed by GC/MS for organic speciation which will be discussed later. High background OC and EC content was also found for APEX-3 T3&4. As a result, only the uncorrected OC EI was reported. For backup and background-corrected samples, the emission indices obtained in this study ranged from 37-83 mg/kg of fuel burned for OC and 21-98 mg/kg of fuel burned for EC, depending on the test conditions. The EC/OC ratio ranged from 0.3 to 2.

Table 13-7.   Organic and Elemental Carbon Emission Indices for Each Test

APEX	Test	Engine	Time-Weighted Engine Power (%)	Time-Weighted Average Fuel Flow (kg/h)	Background and Backup Corrected			Background Corrected Only		Without Any Correction	
					OC (mg/kg)	EC[a] (mg/kg)	EC/OC Ratio	OC (mg/kg)	EC[a] (mg/kg)	OC (mg/kg)	EC (mg/kg)
1	NASA-2&3	CFM56-2C1	18.8	770	83.2	21.1	0.253	100	21.1	179	27.9
	EPA-3		20.4	797	37.1	26.1	0.703	21.1	26.1	188	40.2
	NASA-4&5		35.7	1221	50.7	32.4	0.640	80.7	32.4	137	48.2
2	T1	CFM56-7B24	30.1	1264	82.0	28.1	0.342	132	28.1	225	37.4
	T4		30.1	1264	42.2	25.1	0.595	76.8	25.1	176	33.5
	T2&3	CFM56-3B series	31.0	1200	50.4	91.9	1.82	69.3	91.9	120	95.4
3	T11		31.1	1161	54.7	98.4	1.80	77.5	98.4	113	98.4
	T3&4	AE3007-A1E	41.1	537	-	39.2	-	-	39.2	118	63.4
	T9	RB211-535E4-B	34.2	2473	39.2	27.5	0.700	57.0	27.5	89.9	27.5

a. Quartz filters will not adsorb EC, therefore the EC data before and after backup correction should be the same.

By averaging the emission indices of the tests with the same engine type, the OC and EC EIs for different engine models are compared in Table 13-8. The EI results for the CFM56-2C1 are not shown in the table due to the high background effect of crosswinds. For APEX-3 T3&4 for the AE3007-A1E engine, the background quartz filter had high OC contamination, resulting in zero OC EIs after backup and/or background corrections.

Table 13-8.   Organic Carbon and Elemental Carbon Emission Indices for Different Engines

Engine	Time-Weighted Engine Power[a] (%)	Time-Weighted Fuel Flow (kg/h)	Background and Backup Corrected		Background Corrected Only		Without Any Correction	
			OC (mg/kg)	EC[b] (mg/kg)	OC (mg/kg)	EC[b] (mg/kg)	OC (mg/kg)	EC (mg/kg)
CFM56-7B24	30.1	1264	62.1	26.6	105	26.6	200	35.4
CFM56-3B	31.0	1200	52.5	95.2	73.4	95.2	116	96.9
AE3007-A1E	41.1	537	-	39.2	-	39.2	118	63.4
RB211-535E4-B	34.2	2473	39.2	27.5	57.0	27.5	89.9	27.5

a. TWA was calculated from all the power levels tested for each test.

b. Quartz filters do not adsorb EC, therefore the EC data before and after backup filter correction should be the same.

Figure 13-7 compares the OC and EC emission indices obtained from different engines. Figure 13-7(a) shows that, among the engines tested, the newer CFM56-7B24 engine produces the highest organic carbon emissions and the RB211-535E4 engine had lowest OC EI. The figure also shows that the effects of backup and background correction on the emission index were different from one engine to another. For elemental carbon emissions as shown in Figure 13-7(b), the highest EI was obtained from the CFM56-3B engine and the CFM56-2C had lowest EC EI.

13.3 Particle-Phase Organic Compounds

The identification and quantification of trace organic compounds collected on the APEX quartz filter samples were done using two approaches. After the APEX-1 campaign, the amount of organic carbon collected on each individual quartz filter ranged between 0.01 and 0.16 mg, much below 1 mg of OC required in order to use the solvent-extraction and GC/MS method for appropriate organic compound speciation. As a result, the quartz filter samples obtained during APEX-2 from the same engines were composited to increase the amount of OC for solvent extraction analysis. Thus, the corresponding samples from T2 and T3 tests for the CFM56-3B tests were composited and labeled as T2&3. Also the composite samples from T1 and T4 for the -7B24 model CFM56 were labeled as T1&4. In the case of APEX-3, the more sensitive thermal desorption GC/MS (TD/GC/MS) method was used in lieu of solvent extraction for all samples collected.

The emission indices of individual organic compounds were calculated for the different tests. Both the quartz-filter artifact correction (backup correction) and background correction were conducted during the emission index calculation. The results of emission indices with both backup and background correction and the results that were background corrected but without backup-quartz-filter correction are all summarized in Table H-1 in Appendix H. The total emission indices for individual organic groups and for all the organic compounds detected are also presented in the tables.
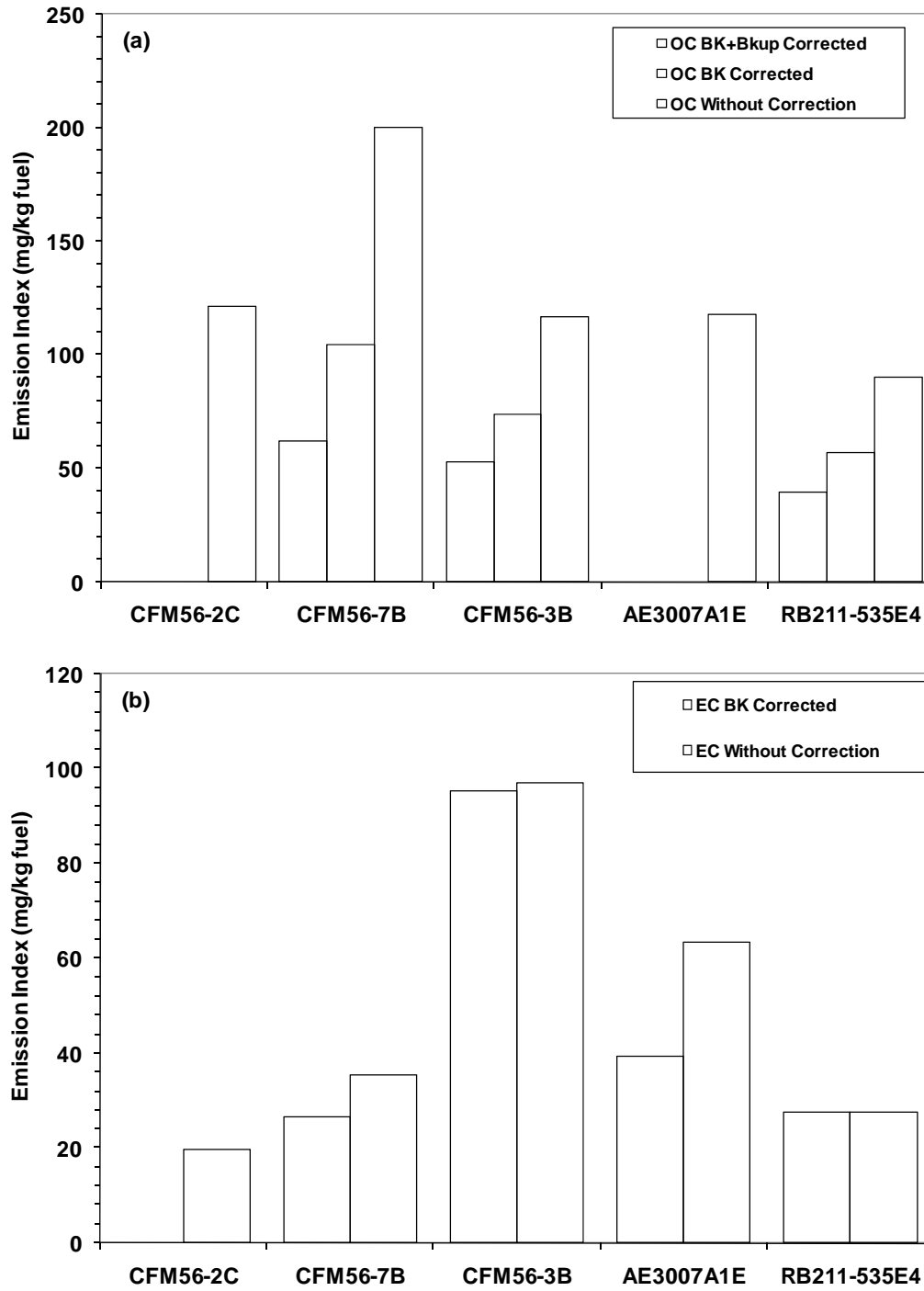
Figure 13-7. Comparison of OC and EC emission indices for: (a) organic carbon; and (b) elemental carbon.

Figure 13-8 shows the contribution of individual organic compounds to the total speciated particle-phase EI for different engines. The results were corrected for both quartz filter sampling artifact and background. The test number and sampling campaign are presented in the figure. In general, the figure shows that AE3007-A1E and CFM56-3B were the two engines having the highest emission indices of total speciated organics. Both the P&W 4158 and CFM56-7B24 produced the lowest EI for semi-volatile organic compounds. However, the samples from APEX-2 T1&4 for the CFM56-7B24 engine were analyzed by solvent extraction, which is considered less sensitive than the thermal desorption analysis used for the APEX-3 engine samples. Therefore, the lower emission indices of speciated organic compounds for APEX-2 T1&4 could be attributable to the method of analysis used.

Figure 13-9 compares the emission indices of classes of organic compounds for different engines. The percentage value for each group is also presented in the figure. Regardless of the difference in engine type, the *n*-alkanes and PAHs were the primary compounds observed. For the AE3007-A1E engine, the total emission index of organic compounds was 293 ug/kg of fuel burned, of which about 58 percent was *n*-alkanes and 42 percent was PAHs.
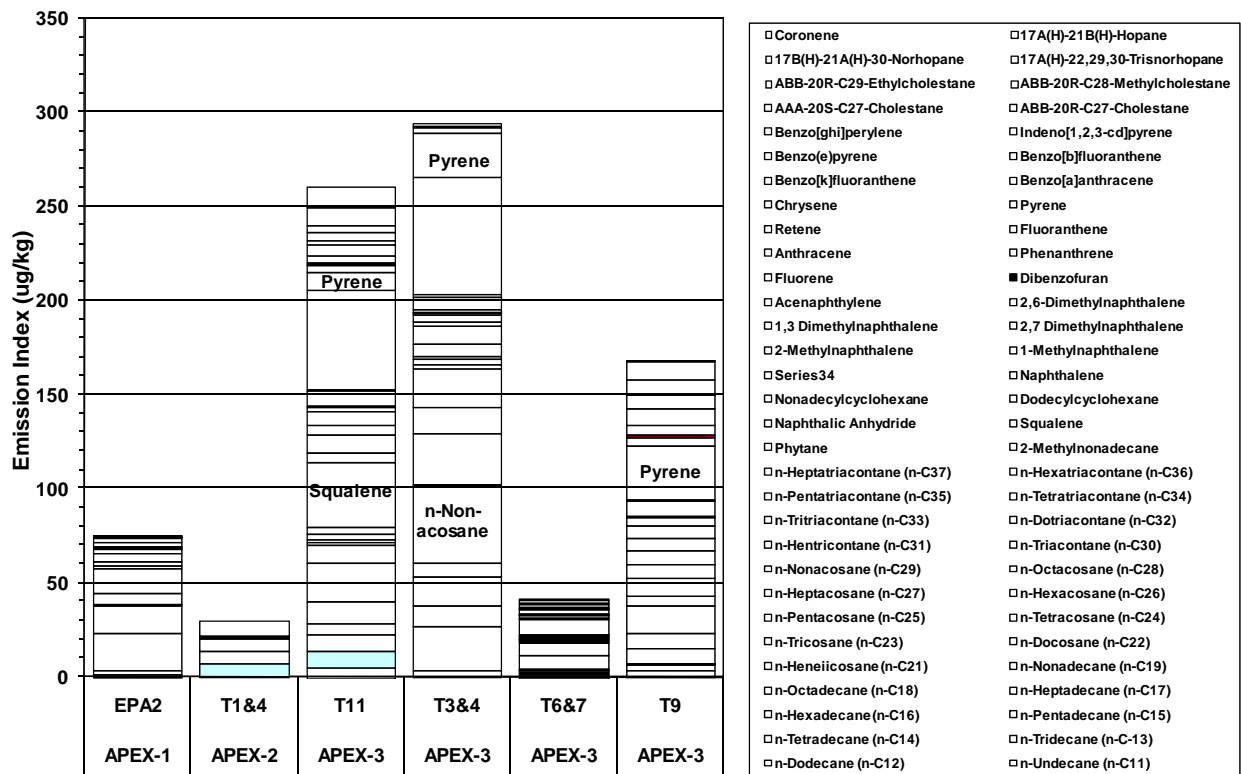
Figure 13-8. Relative contribution of individual organic compounds to the total speciated particle-phase EI.

248
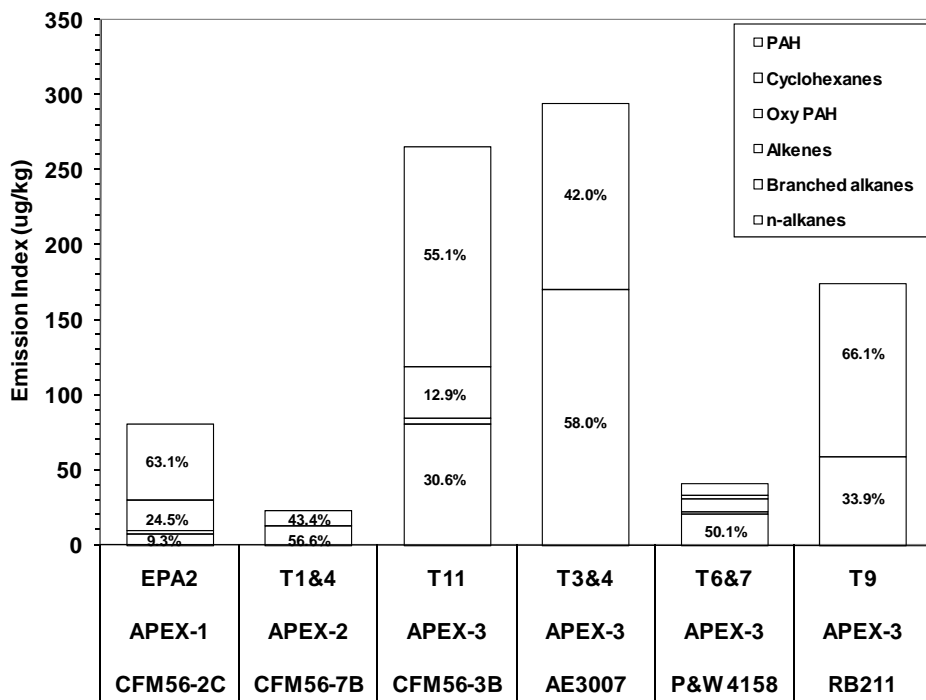
Figure 13-9.   Relative contribution of classes of organic compounds to the total speciated particle-phase EI.

The effects of the correction for quartz filter sampling artifact on the emission indices of individual organic compounds were investigated by comparing the emission index results of individual organic groups before and after backup correction as presented in Figure 13-10(a) and (b), respectively. After correction, most oxy PAH and phthalates on the plume front quartz filters were significantly reduced or even eliminated for all engines.

The effect of background correction was further investigated in Figure 13-11, where the emission index results of *n*-alkanes and PAH obtained without any correction, with background correction only and with both backup and background correction were compared. The results for *n*-alkanes are presented in Figure 13-11(a) and Figure 13-11(b) provides the PAH results. The figures show that the background quartz filters contained high *n*-alkanes, and therefore the EI values for alkanes were substantially reduced by background correction. For the PAHs, only the APEX-3 T3&4 and T9 tests had a high background. Both Figure 13-10 and 13-11 underscore the need for a valid ambient background correction for these types of chemical analyses.
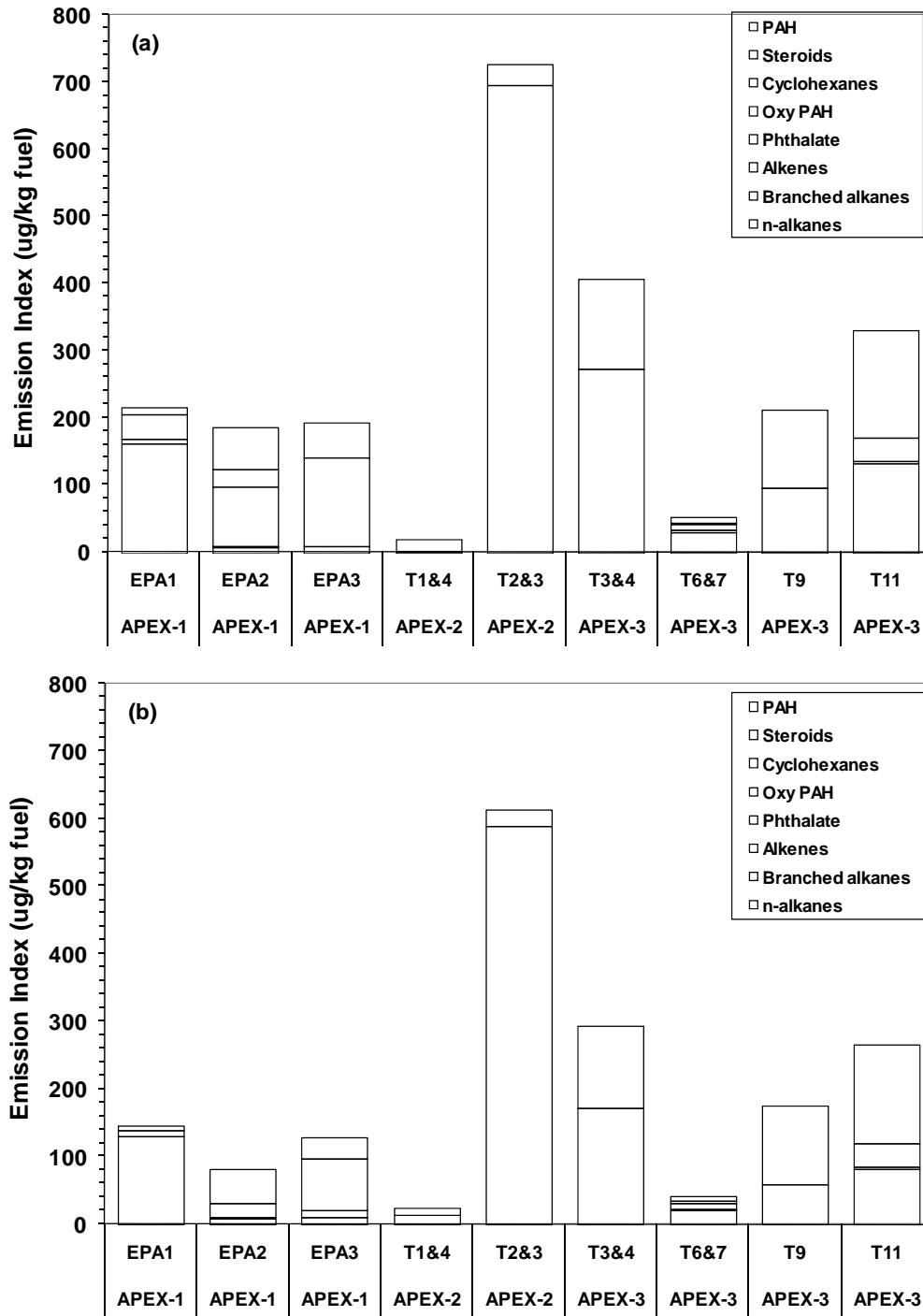
Figure 13-10. Effects of quartz-filter sampling-artifact correction on emission indices of individual organic groups: (a) before backup correction; and (b) after backup correction.
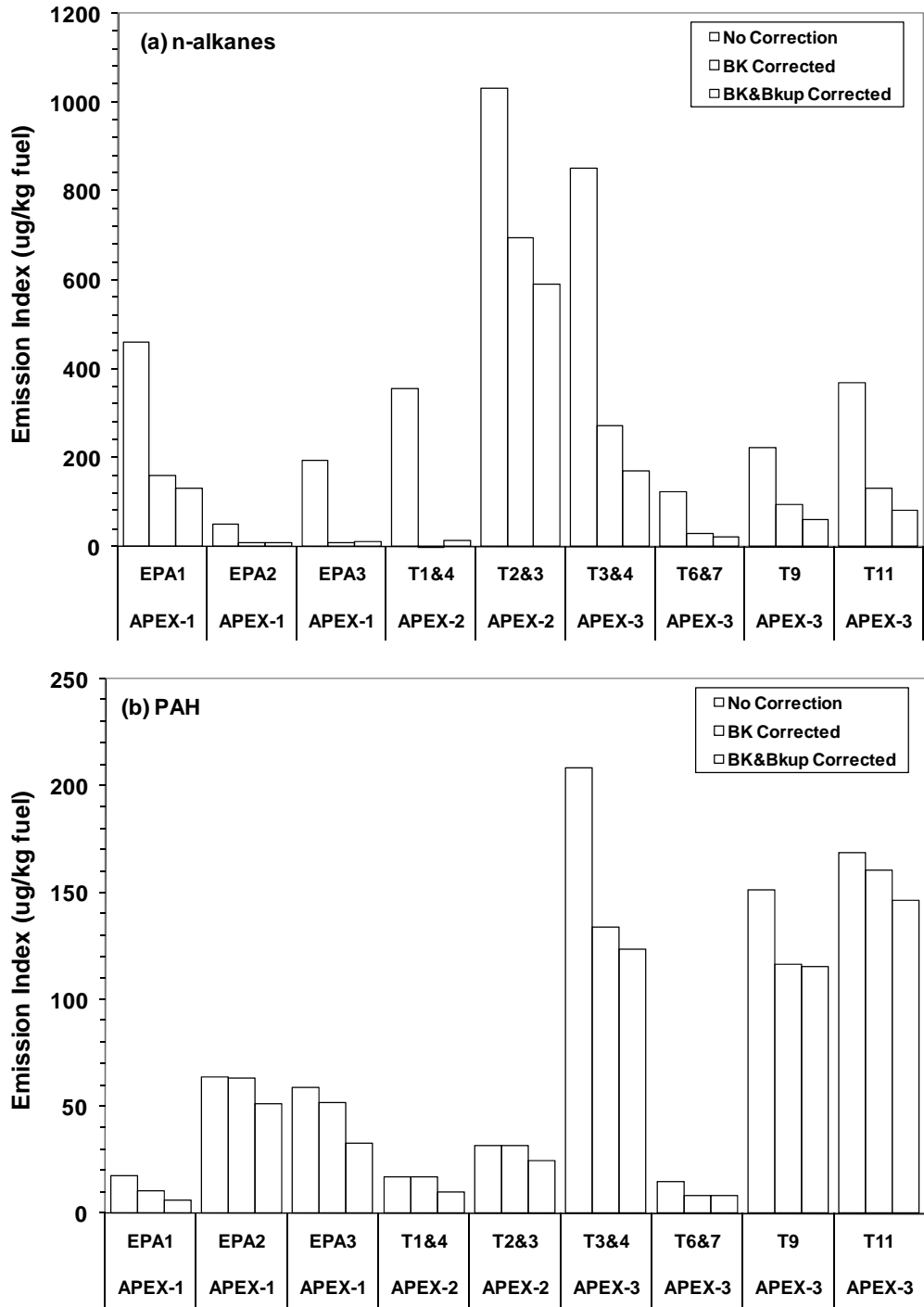
Figure 13-11. Effects of background correction on emission indices of individual organic groups for: (a) *n*-Alkanes; and (b) PAHs.

This page intentionally left blank.

14.   Quality Assurance

14.1   Data Quality Indicator Goals

The DQI (Data Quality Indicator) goals that were established prior to the three testing campaigns and referenced in the respective QAPPs are presented in Table 14-1.

Table 14-1.   DQI Goals for DEAL Instrumentation

Experimental Parameter	Measurement Method	Precision[a]	Accuracy[b]	Completeness	Detection Limit or Range
[APEX-1]:Gas phase measurements (CO_2, CO, THC)	Photoacoustic analyzer	± 5%	± 5%	95%	CO_2: 3.4 ppmv CO: 0.2 ppmv THC (as hexane): 0.008 ppmv
[APEX-2 and APEX-3]: Gas phase measurements (CO_2) [c]	Infrared analyzer	± 5%	± 5%	95%	0 to 800 ppm[c] 0 to 2000 ppm
[APEX-3]: Gas phase measurements (CO_2) [d]	Infrared analyzer	± 5%	± 5%	95%	0- to 10,000 ppm
Temperature	Thermocouple	5%	± 5%	95%	K-type: -200°C-1250°C J-type: 0 °C-750°C T-type: -250 °C – 350 °C
Volumetric air flow rate	Mass flow controllers[e]	5%	± 10%	95%	0-2 Lpm; 0-15 Lpm; 0-50 Lpm; 0-112 Lpm; 0-1120 Lpm
Differential pressure	Transducers	5%	± 10%	95%	0-17.5 inches H_2O
PM mass[f]	Gravimetric analysis	3 µg[g]	± 15 µg	90%	1 µg

[a] Calculated as the RSD of the reference measurements obtained at a constant instrument set point.

[b] Average variation between the reference measurements and instrument readings as determined over the entire operating range.

[c] 0 to 800 ppm used for APEX-2; 0 to 800 ppm and 0 to 2000 ppm used in APEX-3.

[d] Horiba Model AIA 210.

[e] Includes all on-line and time-integrated instruments as well as sampling tunnels.

[f] For time-integrated sampling only.

[g] Determined as the standard deviation of the results of multiple analyses of the same filter on the same microbalance.

All of the instruments used were calibrated before and after APEX-1 and before the APEX-2 field campaign. APEX-3 followed shortly thereafter. Although not all of the instrumentation was calibrated following APEX-3, all measurements were taken within the annual calibration window and, therefore, there should be no resulting impact on data quality.

14.1.1 Photoacoustic Analysis (APEX-1)

Table 14-2 lists the optical filters and the calibration gas concentrations used with the B & K Photoacoustic Multigas Analyzer during APEX-1. The analyzer was set up and calibrated for each of the three gas channels before departing for the test campaign.

Table 14-2.   INNOVA 1314 Photoacoustic Multigas Analyzer Calibrations

Optical Filter	Gas Name	Span Gas Concentration
UA0983	Carbon Dioxide (CO_2)	924 ppm
UA0984	Carbon Monoxide (CO)	41.8 ppm
UA0987	Total Hydrocarbons (THC) as *n*-Hexane	5.37 ppm
Water	Water (H_2O)	N/A

Quality control checks for the three gas compounds (CO_2, CO and *n*-hexane) measured by the photoacoustic analyzer were performed before each test during APEX-1 per the QAPP. Post-test calibration checks were not possible due to physical and time constraints that restricted access to the test site. Therefore, span and zero calibration checks for the photoacoustic analyzer were performed once each day. Summaries of all the daily calibration checks are included in the paragraphs below and are summarized in Table 14-3.

Table 14-3.   DQI Values for Photoacoustic Analyzer Gas Measurements for All Tests

Gas Compound	Calibration Check Range (ppm)	Accuracy (% bias)	Precision (% RSD)	Percent Complete
CO_2	891– 960	3.6 – 3.9	<2	100
CO	39.8 – 41.3	1.2 – 4.8	<2	100
THC	4.95 – 5.58	3.9 – 7.8	<2	88

Calibration checks for CO_2 ranged from 891 ppm to 960 ppm. This range represents an accuracy range of 3.6 to 3.9 percent, which meets the 5 percent DQI goal. Precision for all CO_2 measurements was <2 percent, which also meets the 5 percent DQI goal. CO_2 measurements during APEX-1 were 100 percent complete.

Measured calibration checks for CO ranged from 39.8 ppm to 41.3 ppm. This range represents an accuracy range of 1.2 to 4.8 percent, which meets the 5 percent DQI goal. Precision for all CO measurements was <2 percent, which also meets the 5 percent DQI goal. CO measurements for APEX-1 were 100 percent complete.

THC calibration checks ranged from 4.95 ppm to 5.58 ppm. This range represents an accuracy range from 3.9 to 7.8 percent, which falls slightly above the 5 percent DQI goal. Precision for all THC measurements was <2 percent, which meets the 5 percent DQI goal. Of the 26 measurements made, three were below 5.1 ppm, a value which represents the lowest acceptable value. This number of measurements results in a completeness of 88 percent, which falls below the 95 percent completeness goal.

14.1.2 Infrared CO_2 Gas Analyzers (APEX-2 and APEX-3)

Two identical Milton Roy 3300A infrared gas analyzers were used to measure the CO_2 gas concentration during APEX-2 and APEX-3. One analyzer was installed to measure a sample from the plume tunnel and the second to measure a sample from the background tunnel per the equipment configuration diagrams included in the QAPP. The analyzers were equipped with three selectable ranges of 0-800, 0-1600, and 0-2000 ppm. Calibrations for both analyzers were performed on August 2, 2005, before departing for the APEX-2 field campaign. Calibrations were performed on October 10, 2005, for the 0 to 2000 ppm range before departing for APEX-3.

One Horiba Model AIA 210 infrared gas analyzer was used in APEX-3 only and was calibrated in the DEAL on October 17, 2005, prior to departing for the field campaign.

These calibrations, summarized in Table 14-4, generated a linear relationship between the voltage output of the analyzers and the calibration gases.

Daily calibration checks performed during the APEX-2 and APEX-3 campaigns are summarized in the following paragraphs and in Table 14.5.

Table 14-4.   Carbon Dioxide Analyzer Calibrations

Gas Analyzer	Gas Name	Span / Mid Gas Concentrations
Milton Roy 3300A – Plume (APEX-2 only)	CO_2	710 ppm / 454 ppm
Milton Roy 3300A – Background (APEX-2 and APEX-3)	CO_2	710 ppm / 454 ppm
Milton Roy 3300A – Plume Low Range Analyzer (APEX-3 only)	CO_2	1730 ppm / 1103 ppm
Horiba AIA 210 – Plume High Range Analyzer (APEX-3 only)	CO_2	5610 ppm / 8570 ppm

Table 14.5   DQI Values for Infrared CO_2 Gas Analyzer Measurements for All Tests

Gas Compound	Plume	Background	Accuracy (% bias)	Precision (% RSD)	Percent Complete
	Daily Calibration Check Range (ppm)				
CO_2 Span Gas (APEX-2)	709.5 – 734	705 – 716	−0.7 to 3.4	<3	100*
CO_2 Mid-range (APEX-2)	439 – 467	429 – 461	−3.3 to 2.9 (P) −5.5 to 2.9 (B)*	<3	
CO_2 Span Gas, High Range (APEX-3)	8319 – 8807	---	−3 to 3	0 – 1	100
CO_2 Span Gas, High mid-range (APEX-3)	5613 – 5905	---	0 to 5	1 –3	
CO_2 Span Gas, Low Range (APEX-3)	1719 – 1786	---	−1 to 3	0 – <1	90
CO_2 Span Gas, Low mid-range (APEX-3)	1104	---	0 to 6	0 – <1	
CO_2 Span Gas (APEX-3)	---	699 – 736	−2 to 4	0 – 1	100
CO_2 Mid-range (APEX-3)	---	438 – 474	−4 to 4	0 – 2	

* With the exception of one low reading of 429 ppm in the analyzer used to sample background.

Daily calibration checks for the CO_2 span gas concentration during the APEX-2 campaign ranged from 709.5 to 734 ppm for the analyzer used to sample the plume, and from 705 to 716 ppm for the analyzer used to sample the background. This range represents an accuracy range for both analyzers of −0.7 to 3.4 percent to meet the DQI goal of ± 5 percent.

Daily calibration checks for the CO_2 mid-gas concentration during APEX-2 ranged from 439 to 467 ppm for the analyzer used to sample the plume. This range represents an accuracy range of −3.3 to 2.9 percent for the plume analyzer to meet the DQI goal of 5 percent. The analyzer used to sample background ranged from 429 to 461 ppm, a range which represents an accuracy range of −5.5 to 2.9 percent. This range failed to meet the DQI goal of ± 5 percent for one reading of 429 ppm. This value is the only reading that failed to meet the accuracy DQI goal and there is no explanation for the low value. The same instrument performed exceptionally well the day before and the day after for the mid-calibration checks, with readings of 460.7 and 450.1 ppm, respectively. These values represent accuracy values of 1.5 and −0.7 percent, respectively. Precision for all CO_2 measurements taken with both analyzers was less than 3 percent to meet the DQI goal of 5 percent. With the exception of the one low reading, CO_2 measurements were 100 percent complete.

During the APEX-3 campaign, three gas analyzers were used to measure CO_2 concentrations. Two analyzers were used to sample from the "plume tunnel" with ranges of 0 to 2000 ppm and 0 to 10,000 ppm. One analyzer was used to sample from the "background tunnel" at a range from 0 to 800 ppm.

The span gas calibration checks for the Plume High Range CO_2 Anlayzer ranged from 8319 ppm to 8807 ppm, with an average of 8559 ppm. These values represent an accuracy range of −3 to 3 percent and a precision ranging from 0 to 1 percent. The mid-range gas calibration checks for the same analyzer ranged from 5613 ppm to 5905 ppm, with an average overall reading of 5742 ppm. The accuracy values ranged from 0 to 5 percent and the precision ranged from 1 to 3 percent. Plume High Range CO_2 measurements were 100 percent complete.

The span gas calibration checks for the Plume Low Range CO_2 Analyzer ranged from 1719 ppm to 1786 ppm, with an average of 1742 ppm. These values represent an accuracy range of −1 to 3 percent, and a precision range from 0 to <1 percent. The mid-range gas calibration checks for the same analyzer ranged from 1104 ppm to 1159 ppm, with an average overall reading of 1133 ppm. The accuracy values ranged from 0 to 6 percent (highest value slightly exceeded the DQI goal of 5 percent) and the precision ranged from 0 to <1 percent. Plume Low Range CO_2 measurements were 90 percent complete, a level which fell slightly below the 95 percent goal.

The span gas calibration checks for the Background CO_2 Analyzer ranged from 699 ppm to 736 ppm, with an average of 713 ppm. These values represent an accuracy range of −2 to 4 percent and a precision ranging from 0 to 1 percent. The mid-range gas calibration checks for the same analyzer ranged from 438 ppm to 474 ppm, with an average overall reading of 450 ppm. The accuracy values ranged from −4 to 4 percent and the precision ranged from 0 to 2 percent. These measurements were 100 percent complete.

14.1.3 DQI Measurements for Volumetric Air Flow Rates

For APEX-1, APEX-2 and APEX-3, calibrations for the filter sampler mass flow meters and mass flow controllers were completed annually by the EPA Metrology Laboratory. The calibration files will be archived as part of the permanent record of the study. The DQIs can be assessed using the Metrology Laboratory reports and the information they provide. The reports include a "combined expanded uncertainty" value that is applicable over the calibration range of the particular device. All volumetric flows were recorded on the DAS and were monitored closely before, during, and after testing. No unexpected behavior was observed during the field campaigns, and it is therefore assumed that the true value is ± the uncertainty of the recorded value. These measurements were 100 percent complete.

During the APEX-1 campaign, the major and minor sampling tunnel flows were measured using thermal dispersion mass flow transmitters that provided feedback to a pair of variable speed blowers. The ability of this system to precisely control the flow rate was impractical to test prior to the system being subjected to the ram effects from the jet engine exhaust. The blowers functioned properly in providing a sample flow into the DEAL that was sufficient for the particle measurement instruments to draw a slipstream via their own internal or external pump. Since isokinetic sampling was not a requirement and a sufficient sample was delivered, the quality of the data does not appear to have been compromised as a result of these imprecise measurements. The only compromise that could be a result of these imprecise measurements would be having an unknown cutpoint for the virtual pre-separator. However, the main function of the virtual impactor was to remove the larger particles that were not of interest and that could result in the need for more frequent instrument cleaning. The EPA Metrology Laboratory performed calibrations of these devices. The calibration files will also be archived.

For the APEX-2 and APEX-3 campaigns, new centrifugal blowers, each controlled by variable frequency drives, were installed in the DEAL to replace the sample extraction system used in APEX-1. The new blowers substantially improved flow stability in the plume sampling tunnel.

14.1.4 Temperature (Thermocouples)

The DEAL thermocouples are calibrated annually by the EPA Metrology Laboratory. The calibration files will be archived as part of the permanent record of the study. The thermocouple DQIs can be assessed using the Metrology Laboratory reports and the information they provide. The reports include a "combined expanded uncertainty" value that is applicable over the calibration range of that thermocouple. As long as there were no observations of a thermocouple responding with unexpected values, it can be assumed that the true value is ± the uncertainty of the recorded value. Metrology Laboratory experience has determined that thermocouple results are consistent and reliable within one year of the calibration date. No measurements were made during the field campaigns that fell outside of the calibration range of the thermocouples; therefore, these measurements were 100 percent complete.

14.1.5 DQI Measurements for Differential Pressure

The Validyne PD55 and the Modus R12 differential pressure transducers were calibrated by the EPA Metrology Laboratory so that the field campaigns took place within a year of the calibration date. The Validyne PD55 was used in APEX-1 and the Modus R12 was used in APEX-2 and APEX-3. The calibration files will be archived. The differential pressure transducer DQIs can be assessed using the Metrology Laboratory report and the information this report provides. The report includes a "combined expanded uncertainty" value that is applicable over the calibration range of the pressure transducer. As long as there were no observations of the transducer responding with unexpected values, it can be assumed that the true value is ± the uncertainty of the recorded value. No measurements were made during the field campaigns that fell outside of the calibration range of the differential pressure transducers; therefore, these measurements were 100 percent complete.

14.2 Post-Test Laboratory Analysis

14.2.1 Gravimetric Analysis of Teflon Filter Samples

As described by MOP-2503 for filter gravimetric analysis (see Table 4-7), sample weighing was conducted at specified ranges of room temperature and relative humidity. The balance stability was controlled by checking the variations of the standard weights before and after analysis. A control Teflon filter was used to monitor the long-term balance stability.

Table 14-6 shows the results of a QC check of the variations in these parameters during the gravimetric analysis that was conducted for the APEX-3 samples. The balance exhibited good stability with RSDs of less than 0.002 percent. The RSD was 0.8 percent for weighing room temperature and 1.2 percent for weighing room relative humidity, indicating that the gravimetric analysis was done under the required strictly controlled environmental conditions. Table 14-6 also includes replicate weights obtained for 100 mg and 200 mg standards used to assess accuracy/bias. All of the weights obtained met the DQI accuracy goal of ± 0.015 mg.

Table 14-7 documents the standard deviation of replicate tare weights observed for individual APEX-3 Teflon filters. These standard deviations were equal to 0.003 mg or less, a value which also met the QA precision requirement.

The replicate final weights of APEX-3 Teflon filter samples are shown in Table 14-8. The values in the table were measured on three different days: 1/16, 1/18 and 1/20/06. The standard deviation in replicate sample weight measurement was less than 0.05 mg. By comparing the weights measured on 1/16 and 1/20, consistent losses were observed for almost all the samples as shown in Figure 14-1. This weight reduction is considered to be primarily attributable to slight sample losses by vaporization of volatile materials during the sample measurement procedure (in particular, during the 24-hour equilibrium prior to weighing). The detection limit of this sampling technique was limited due to the low mass of PM collected on the filters. Therefore, the usability of these data is limited.

Table 14.6   Variations in Environmental Conditions and Balance Stability for APEX-3 Teflon Filter Gravimetric Analysis

Date	Time	Temp (F)	RH (%)	Control TF (mg)	Blank TF (mg)	Standard Weight (100 mg)	Standard Weight (200 mg)
10/17/05		69.5	36.0	172.627	174.773	99.994	199.993
				172.627			199.993
				172.627			199.993
				172.627			199.992
	14:57	70.0	36.3	172.629	174.772	99.995	199.990
	17:15	70.0	36.3				
10/18/05	14:50	69.9	36.0				
	16:48	70.5	36.5				
10/19/05		71.0	37.0				
		71.0	37.0				
10/21/05		70.0	37.0	172.633	174.780	99.993	199.993
				172.634	174.769	99.996	199.993
				172.632	174.774		
Standard Deviation		**0.54**	**0.44**	**0.003**	**0.004**	**0.001**	**0.001**
Relative SD (%)		**0.77**	**1.19**	**0.002**	**0.002**	**0.001**	**0.001**

Table 14-7. **Standard Deviation of Replicate Tare Weight Measurement for Each of APEX-3 Teflon Filters**

Filter ID	Tare Weight (mg)								Standard Deviation
	1	2	3	4	5	6	7	8	mg
T101305A	152.394	152.393							0.001
T101305B	150.436	150.437							0.001
T101305C	151.785	151.786							0.001
T101305D	148.281	148.284	148.280	148.280					0.002
T101305E	147.762	147.761							0.001
T101305F	148.521	148.523	148.519	148.524	148.523	148.522			0.002
T101305G	149.070	149.071							0.001
T101305H	149.312	149.309	149.311	149.312					0.001
T101305I	149.999	149.998							0.001
T101305J	151.229	151.226	151.228	151.229					0.001
T101305K	151.106	151.101	151.099	151.103	151.103	151.103			0.002
T101305L	144.638	144.637							0.001
T101305M	148.034	148.034							0.000
T101305N	146.045	146.043	146.047	146.044	146.046	146.041	146.039	146.041	0.003
T101305O	146.488	146.487							0.001
T101305P	147.761	147.761							0.000
T101305Q	149.349	149.349							0.000
T101305R	147.470	147.470							0.000
T101305S	146.170	146.169							0.001
T101305T	146.722	146.718	146.720	146.715	146.718	146.717			0.002
T101305U	147.734	147.730	147.734	147.733					0.002
T101305V	147.462	147.464	147.462	147.465	147.465	147.465			0.001
T101305W	149.207	149.209	149.206	149.210	149.208	149.208			0.001
T101305X	145.766	145.767							0.001
T101305Y	147.371	147.374	147.370	147.375	147.377	147.371	147.376		0.003

Table 14-8.   Replicate Final Weight Measurement for Each APEX-3 Teflon Filter

Filter ID	1/16/06 (mg)	1/16/06 (mg)	1/18/06 (mg)	1/18/06 (mg)	1/20/06 (mg)	1/20/06 (mg)	SD (mg)
T101305A	152.547	152.542			152.531		0.008
T101305B	150.489	150.468			150.467		0.012
T101305C	151.838	151.804			151.798		0.022
T101305D	148.352	148.318			148.265		0.044
T101305E	148.345	148.332	148.325	148.324	148.323	148.320	0.009
T101305F	148.635				148.587	148.584	0.029
T101305G	149.444		149.435	149.437	149.432		0.005
T101305H	149.324				149.315		0.006
T101305I	150.067				150.060		0.005
T101305J	151.276	151.247	151.239		151.241		0.017
T101305K	151.258				151.250	151.247	0.006
T101305L	144.696		144.659		144.656		0.022
T101305N	146.070				146.064		0.004
T101305O	146.749				146.743		0.004
T101305P	147.794				147.772		0.016
T101305Q	149.374				149.351	149.351	0.013
T101305S	146.204	146.187			146.181		0.012
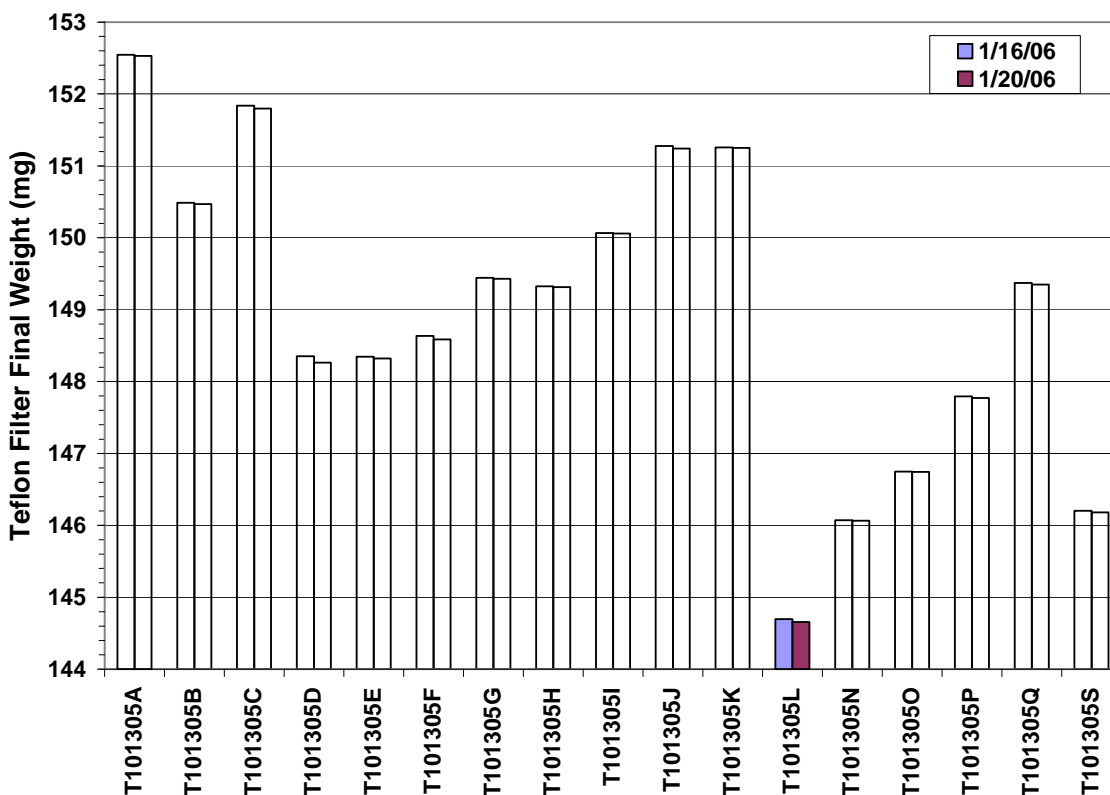
Figure 14-1.   Sample losses from the comparison of weights measured on 1/16/06 and 1/20/06.

14.2.2 PM Organic Speciation Analysis

14.2.2.1 Solvent Extraction - GC/MS

The speciation of APEX-2 quartz filter samples was conducted by solvent extraction and GC/MS analysis. Five-level standard calibration curves were prepared and injected onto the GC/MS system prior to analysis of all quartz filter samples. These calibration curves consisted of aromatic PAHs (NIST1491 and NIST 2260 standards), the second calibration curve of semivolatile alkanes (NIST 1494), and the third calibration curve of methyl esters of organic acids [Quantitative Standard #3 (QS#3) from University of Wisconsin]. The standard deviations for all calibration components were below 30 percent (most below 15%) for nearly all target compounds.

A method detection limit (MDL) study was also conducted prior to sample analysis. The lowest calibration level (the practical quantitation limit, or PQL) was chosen to be the level that was replicated seven times in accordance with EPA's SW-846 guidelines (Test Methods for Evaluating Solid Waste, Physical/Chemical Methods) for determination of an MDL. The standard deviation was multiplied by 3.14 (chart values for seven replicates) to determine each MDL. Sample values that fell below the MDL were not used.

Some compounds were not present in the standard and were quantified using relative response factors from closely eluting similar compounds. The qualitative determination of these non-target components

was facilitated using retention times gathered from an extracted wax resin and also by using fragmentation library matching.

Due to the punches taken from the quartz filter samples for OC/EC analysis before solvent extraction, a compensation was required to account for sample losses. Since the exposed area of each quartz filter was 13.45 cm^2 and each punch had a known area of 1.45 cm^2, the total nanogram (ng) value of the filter was multiplied by a factor of 1.12 if one punch was taken from the filter.

Overall target analyte validity was determined by the presence of the target ion plus the molecular ion (alkanes)/qualifier ions. Comparison of isotopic ratios and retention times with daily standards as well as known mass spectral libraries assisted greatly in this process. Since the GC/MS system used was equipped with an electronically programmable control (EPC), retention times did not shift appreciably throughout the analysis period. This stability of retention times was critical for accurate determination of target analyte components, especially when good isotopic ratio comparisons/lack of molecular ion (alkanes) were not a viable option. In certain cases, the levels of interfering ions were judged to be significant, and these particular components were deemed invalid. These results were not used.

Spikes were performed to determine the recoveries of individual components. Excellent recoveries were found for most of the targets as shown in Table 14-9.

14.2.2.2 Thermal Desorption – GC/MS

The quartz filter samples collected during APEX-1 and APEX-3 were analyzed using the thermal desorption (TD) system with GC/MS. Quantitative analysis was performed for semivolatile alkanes and PAHs.

Due to the known low organic content in the quartz filter samples, a single level (high level 1) calibration was used to quantify the data set. A lower calibration level (mid level 2) was used as the closing standard and laboratory acceptance criterion. The standard had 83 percent of the components fall within 20 percent of the actual values. More than 75 percent of the target components meet the acceptance criteria, meaning the calibration was valid. A valid calibration ensured that all of the samples and blanks analyzed were bracketed by a successful stable calibration.

Blanks were analyzed prior to the analysis of each sample to determine cleanliness of the TD/GC/MS system. Cleanliness of the TD/GC/MS system was of particular importance due to the nature of the TD methodology and the relative inefficiency of system cleansing for the components with higher boiling points in complex matrices. A method was specifically designed to purge the system of all residual target components. This purging method allowed the TDS split vent to open and purge the system at 90 ml/min for 10 minutes under high heat. This procedure was conducted prior to each sample run. An additional intensive rinsing procedure was developed to minimize target contamination.

Maximum sample load was determined by a pre-study. The pre-study demonstrated that a maximum of three quantitative slivers (2 mm × 30 mm) could be contained within the critical 79 mm "optimal heat zone." Loading more sample slivers would have proved more difficult and could have potentially resulted in adverse affects such as poor thermal transfer and internal standard biasing. The methodology proved to have enough organic material present for each sample to acquire meaningful data without jeopardizing thermal transfer to the GC/MS.

Table 14-9. Recoveries of Individual Components by Solvent Extraction Analysis

Compound	% Recovery	Compound	% Recovery
Napthalene	78%	Squalene	110%
1-Methylnaphthalene	91%	*n*-Heptacosane	130%
2-Methylnaphthalene	91%	Pristane	86%
2,6-Dmethylnaphthalene	94%	*n*-Octacosane	131%
Acenapthylene	93%	*n*-Nonacosane	128%
Acenapthene	95%	*n*-Triacontane	128%
Dibenzofuran	92%	*n*-Hentricontane	123%
Fluorene	103%	*n*-Dotriacontane	116%
Methylfluorene	96%	*n*-Tritriacontane	116%
Phenanthrene	101%	*n*-Tetratriacontane	113%
Anthracene	114%	*n*-Pentatriacontane	120%
9-Methylanthracene	99%	*n*-Hexatriacontane	112%
Fluoranthene	110%	*n*-Heptatriacontane	107%
Retene	113%	*n*-Octatriacontane	106%
n-Decane	26%	Pyrene	93%
n-Undecane	66%	Benzo(ghi)fluoranthene	114%
n-Dodecane	86%	Cyclopenta(cd)pyrene	95%
n-Tridecane	96%	Benz(a)anthracene	101%
n-Tetradecane	99%	Chrysene	98%
n-Pentadecane	102%	1-Methylchrysene	108%
n-Hexadecane	104%	Benzo(b)fluoranthene	101%
n-Heptadecane	105%	Benzo(k)fluoranthene	100%
n-Octadecane	106%	Benzo(e)pyrene	108%
Phytane	110%	Benzo(a)pyrene	115%
Dodecylcyclohexane	111%	Perylene	122%
n-Nonadecane	113%	Indeno(1,2,3-cd)pyrene	99%
2-Methylnonadecane	126%	Dibenzo(a,h)anthracene	99%
3-Methylnonadecane	127%	Benzo(ghi)perylene	113%
n-Eicosane	102%	Coronene	87%
n-Heneicosane	108%	ABB-20R-C27-Cholestane	74%
Pentadecylcyclohexane	114%	AAA-20S-C27-Cholestane	91%
Docosane	111%	ABB-20R-C28-Methylcholestane	98%
Tricosane	118%	ABB-20R-C29-Ethylcholestane	95%
Tetracosane	122%	17A(H)-22,29,30-Trisnorhopane	82%
Pentacosane	120%	17B(H)-21A(H)-30-Norhopane	115%
Hexacosane	125%	17A(H)-21B(H)-Hopane	96%
Nonadecylcyclohexane	98%		

14.2.2.3 IC Analyses

The quality of the inorganic water-soluble ion analysis was evaluated by comparing the results of three replicate injections of the sample extracts. Table 14-10 provides the RSD for some of the filter samples analyzed, all of which met the measurement acceptance criterion of ± 15 percent established for the IC analyses.

14.2.2.4 XRF Analyses

In the XRF analytical report, the concentrations of elements were reported together with their uncertainties. To insure the quality of the emissions data calculated accordingly, a criterion was set to discriminate the data reported. Only an element with a concentration three times greater than its uncertainty was considered acceptable for further emission factor estimation.

Table 14-10. Relative Standard Deviation in IC Measurements

Sample ID	NH_4	Cl	SO_4	NO_3
	%	%	%	%
T032204O	0.990		3.95	
T032304U	3.08		0.747	
T032403A			2.64	
T032204Q	1.13		3.44	
T080105B	0.845		1.25	
T080105F	1.77		2.97	0.941
T080105G		2.98		
T080105E			3.57	7.75
T108105I	7.72		2.25	
T101305E	5.30		0.784	
T101305F			1.10	
T101305D	5.68		2.82	
T101305G	14.0		0.669	
T101305K	3.27		0.340	
T101305J		1.92		
T101305N		1.30	1.10	
T101305O		2.04		

14.2.2.5 EC/OC Analyses

Single point calibrations were performed daily prior to analysis of samples using a known amount of sucrose solution spiked into a filter cut. If the results of this calibration check were within ± 5 percent of the known value, the sample analysis was performed. If results of the calibration were outside the ± 5 percent criterion, the instrument was recalibrated and analysis of the spike was repeated until an acceptable value was achieved. Instrument blanks were also performed with each batch of samples and at least one sample was analyzed in duplicate. All accuracy and precision objectives were met and the analyses were 100 percent complete.

This page intentionally left blank.

15. Conclusions and Recommendations

A number of conclusions were reached as a result of the APEX testing program. These conclusions are as follows:

- The testing of aircraft turbine engine emissions is difficult, requiring long sampling lines with their associated high residence time and particle losses. Corrections were made for particle losses, but the impact of the long residence time has yet to be established.

- The PM mass emission index ranged from approximately 10 to 550 mg/kg of fuel burned, depending on engine and fuel type, operating power, and environmental conditions.

- For the turbofan engines tested, the relationship of EI_M to fuel flow (engine power) followed a characteristic U-shape with the emissions high at idle, dropping off to a minimum at mid-range power, and rising again at high engine thrust.

- The particle number emission indices observed in the program ranged from approximately $1(10)^{15}$ to $1(10)^{17}$ particles/kg of fuel burned, again depending on engine and fuel type, operating power, and environmental conditions.

- For most of the turbofan engines tested, a logarithmic relationship of EI_N to fuel flow (engine power) was determined in the general form:

$$EI = m(ln\ fuel\ flow) + b \tag{15-1}$$

where
  m = slope of the regression line = $-2(10)^{15}$ to $-3(10)^{16}$
  b = intercept of the regression line = $2(10)^{16}$ to $2(10)^{17}$

- Both EI_M and EI_N were found to increase with increasing fuel sulfur content. For EI_M, the PM emission increased linearly with fuel sulfur, whereas for EI_N, the increase appears to be more of an exponential function.

- Engine operating temperature had a measurable effect on both EI_M and EI_N. In both cases, the emissions were slightly lower (i.e., ~8%) when the engine was warm.

- The particle size distributions of the emissions found in the study were generally unimodal and lognormally distributed with electrical mobility diameters ranging from ~3 to slightly larger than 100 nm. At higher power levels, a small accumulation mode was also observed.

- Both the GMD and GSD of the PSD also varied with engine and fuel type, thrust, and environmental conditions. The GMD ranged from approximately 10 to 30 nm (electrical mobility diameter) and the GSD ranged from 1.4 to 2.

- In general, the largest GMDs and GSDs were obtained at high power conditions. The observations suggest that the PSDs produced by the engines tested under power conditions of <30% rated thrust were unimodal and consisted of primary nuclei particles, whereas for thrust levels >85%, accumulation mode particles were formed, and the PSD curves became broader.

- A comparison of measurement techniques for PM mass, number, and size indicated significant discrepancies between instruments. Of particular note is a comparison of the EI_M obtained by the Nano-SMPS and the time-integrated Teflon filter sampling. The filter-based method always produced higher values than the SMPS-based method and there was no linear correlation between the two techniques.

- Of the various instruments used to measure PM mass, number, and size, the SMPS appears to be the most reliable. The lack of correlation with the filter-based technique is disturbing, however, and an area worthy of further investigation.

- The emission indices for BC and particle surface-bound PAHs generally follow trends similar to EI_M discussed above, except that: (1) BC was always highest at high power, and (2) fuel composition had no measureable effect on either BC or PAH emissions. However, the BC and PAH on-line measurements were highly variable and oftentimes did not track well with power changes.

- The chemical composition of the gas-phase NMVOCs and carbonyls varied by engine type as measured on a time-integrated basis over all power conditions. However, significant quantities of a number of compounds listed in the Clean Air Act as HAPs were found in some or all engines including formaldehyde, acetaldehyde, benzene, acrolein, toluene, and 1,3-butadiene.

- The elemental composition of the PM samples collected on Teflon filters was dominated by sulfur. In some samples, however, significant amounts of crustal elements such as silicon were also found due to the resuspension of concrete cuttings generated during installation of the sampling probes and lines.

- Sulfate was by far the most abundant water-soluble ion determined from the Teflon filter samples. Calculations of the transformation of S(IV) in the fuel to S(VI) indicate conversion rates in the range of 2 to 4%, a conversion rate which compares favorably to the rates obtained by other investigators.

- The emission indices determined in the program for OC and EC as determined from quartz filter sampling ranged from 37 to 83 mg/kg fuel for OC and 21 to 98 mg/kg fuel for EC, respectively. The ratio of EC to OC ranged from 0 to almost 2 depending on the engine type and fuel being tested.

- Over 70% of the particle-phase organic compounds, also determined from the quartz filters, consisted of *n*-alkanes and PAHs. Also, of the engines tested, the CFM56-3B1 and AE3007A1E had the highest emission indices of total speciated organic compounds, whereas the P&W 4158 and CFM56-7B24 had the lowest.

- The results obtained in the study are at least generally comparable to those of other APEX investigators. However, a report of the APEX-3 results from the other groups has not as yet been released.

Based on the above conclusions, the following recommendations for future research are offered for consideration by funding agencies:

- One major issue to be resolved in future work is the effect of the sampling system on the experimental results. This effect includes both particle losses in the sampling lines as well as the potential transformation of the aerosol from the point of collection to the point of measurement. A standardized sampling system with well-characterized performance should be employed in all future testing. Also, the issue of representative plume sampling should be addressed.

- The lack of good agreement between instruments is also a significant issue warranting additional research. Of particular importance is the lack of correlation between on-line SMPS and filter-based methods for determining EI_M.

- Although particle losses through the sampling system can be characterized using traditional aerosol science techniques (e.g., NaCl aerosol), a reliable soot calibration source is needed that is both reproducible and stable. Although work is underway under both NASA and EPA Office of Transportation and Air Quality sponsorship to develop the necessary calibration equipment, additional research and development is definitely needed in this regard.

- A reliable on-line method for the direct determination of PM mass emissions is needed. Neither the TEOM nor the QCM appears capable of conducting these measurements in a reliable manner. The TEOM is generally not sensitive enough and the QCM produces values higher than other methods and QCM sampling times are limited due to crystal saturation.

- The effect of fuel composition is also an area worthy of additional investigation. In particular, the further examination of the influence of sulfur and aromatics on sulfate and organic emissions is needed to assess the impact of future aviation fuels on local air quality and global climate change.

- Further work is needed in the characterization of plume aging. To date, all measurements have been performed in the near-field plume < 50 m from the engine exit. There are many issues related to fence-line and neighborhood air quality that need to be addressed at distances far greater than 50 m and multiple points downstream. For the plume aging tests, the instrumentation should be positioned directly in the plume to avoid problems with long sampling lines.

- Additional chemical characterization of both the gas- and particle-phase emissions by power condition is needed. The data provided above are representative of all thrust levels during a particular test. However, specific data for at least the four ICAO-specified power conditions are needed in order to make a determination of the local air quality impacts from airports.

This page intentionally left blank.

16.   References

Anderson, B. E., E. L. Winstead, C. H. Hudgins, and K. L. Thornhill (2006). Concentrations and physical properties of particles within the exhaust of a CFM-56 engine. In *Aircraft Particle Emissions eXperiment*, Report No. NASA/TM-2006-214382, National Aeronautics and Space Administration, Glenn Research Center, Cleveland, OH.

EPA (2008). Ambient air monitoring reference and equivalent methods. Title 40 Code of Federal Regulations, Part 53, available at: http://www.gpoaccess.gov/cfr/index.html.

EPA (2005a). Characterization of fine particulate emissions from commercial jet aircraft engines during JETS (Jet Emissions Testing for Speciation). Quality Assurance Project Plan, Category III/Applied Research, Revision 0, QTRAK # 3056, August.

EPA (2005b). Characterization of fine particulate emissions from commercial jet aircraft engines during the Aircraft Particle Emissions eXperiment 3 (APEX3) Program. Quality Assurance Project Plan, Category III/Applied Research, Revision 0, QTRAK # 3056, October.

EPA (2004). Testing of a CFM-56 commercial aircraft engine. Quality Assurance Project Plan, Category III/Applied Research, Revision 0, QTRAK # 3056, April.

EPA (1999a). Compendium Method TO-15: Determination of Volatile Organic Compounds (VOCs) In Air Collected in Specially-Prepared Canisters and Analyzed By Gas Chromatography/Mass Spectrometry (GC/MS). Center for Environmental Research Information, Office of Research and Development, U.S. Environmental Protection Agency, Cincinnati, OH. January 1999. Available at: http://www.epa.gov/ttn/amtic/files/ambient/airtox/to-15r.pdf.

EPA (1999b). Compendium of Methods for the Determination of Toxic Organic Compounds in Ambient Air, Second Edition, Compendium Method TO-11A: Determination of Formaldehyde in Ambient Air Using Adsorbent Cartridge Followed by High Performance Liquid Chromatography (HPLC) [Active Sampling Methodology]. Center for Environmental Research Information, Office of Research and Development, U.S. Environmental Protection Agency, Cincinnati, OH. January 1999. Available at: http://www.epa.gov/ttn/amtic/files/ambient/airtox/to-11ar.pdf.

EPA (1998). Technical Assistance Document for Sampling and Analysis of Ozone Precursors, EPA/600-R-98/161; National Exposure Research Laboratory, U.S. Environmental Protection Agency, Research Triangle Park, NC. September 1998. Available at: http://www.epa.gov/ttn/amtic/files/ambient/pams/newtad.pdf.

Hildemann, L. M., G. R. Markowski, M. C. Jones, and G. R. Cass (1991). "Submicrometer aerosol mass distributions of emissions from boilers, fireplaces, automobiles, diesel trucks, and meat cooking operations," *Aerosol Sci. Technol.*, 14, 138-152.

Katragkou, E., S. Wilhem, and F. Arnold (2004). First gaseous S(VI) measurements in the simulated internal flow of an aircraft gas turbine engine. *Geo. Res. Letters*, 31, L02117, doi: 10.1029/2003GL018231.

Kinsey, J. S., W. A. Mitchell, W. C. Squier, A. Wong, C. D. Williams, R. Logan, and P. H. Kariher (2006a). Development of a new mobile laboratory for characterization of the fine particulate emissions from heavy-duty diesel trucks," *J. Auto. Eng.*, D3, Vol. 220, 335-345.

Kinsey, J. S., W. A. Mitchell, W. C. Squier, K. Linna, F. G. King, R. Logan, Y. Dong, G. J. Thompson, N. N. Clark (2006b). "Evaluation of methods for the determination of diesel-generated fine particulate matter: Physical characterization results," *J. Aero. Sci.*, 37, 63-87.

Liscinsky, D. and H. Hollick (2008). Effect of particle sampling technique and transport on particle penetration at the high temperature and pressure conditions found in gas turbine combustors and engines. Summary Report of Year 1 Activities, NASA Contract No. NNC07CB03C, United Technologies Research Center, East Hartford, CT, February 29.

Lobo, P., P. D. Whitefield, D. E. Hagen, S. C. Herndon, J. T. Jayne, E. C. Wood, W. B. Knighton, M. J. Northway, D. Cocker, A. Sawant, H. Agrawal, and J. W. Miller (2007). The development of exhaust speciation profiles for commercial jet engines. Final Report, Contract No. 04-344, California Air Resources Board, Sacramento, CA, October 31.

Lobo, P., D. E. Hagen, and P. D. Whitefield (2006). Physical characterization of aerosol emissions from a commercial gas turbine engine—Project APEX. In *Aircraft Particle Emissions eXperiment*, Report No. NASA/TM-2006-214382, National Aeronautics and Space Administration, Glenn Research Center, Cleveland, OH.

NIOSH (2003). Diesel particulate matter (as elemental carbon). Method 5020:Issue 3, available at: http://198.246.98.21/niosh/nmam/pdfs/5040.pdf.

Petzold, A. and F. P. Schröder (1998). "Jet engine exhaust aerosol characterization, *Aerosol Sci. Technol.,* 28, 63-77.

Schumann, U., F. Arnold, R. Busen, J. Curtius, B. Karcher, A. Kiendler, A. Petzold, H. Schlager, F. Schroder, and K.-H. Wohlfrom (2002). Influence of fuel sulfur on the composition of aircraft exhaust plumes: The experiments SULFUR 1-7. *J. Geo. Res.*, 107, D15, 4247, doi: 10.1029/2001JD000813.

Turpin, B.J.; Huntzicker, J.J.; Hering, S.V. (1994). Investigation of organic aerosol sampling artifacts in the Los Angeles Basin, *Atmos. Environ.* 28, 3061-3071.

Wey, C. C. et al., (2006). Aircraft particle emissions experiment (APEX). NASA/TM-2006-214382, ARL-TR-3903, National Aeronautics and Space Administration, Glenn Research Center, Cleveland, OH., September. Available at: http://gltrs.grc.nasa.gov.